SISSA
Scuola
Internazionale
Superiore di
Studi Avanzati

Physics Area - PhD course in
Statistical Physics

Entanglement and symmetries in many-body quantum systems

Candidate:
Sara Murciano

Advisor:
Prof. Pasquale Calabrese

Academic Year 2021-22

Contents

List of Publications

1. Luca Capizzi, S. M. and Pasquale Calabrese, *Rényi entropy and negativity for massless complex boson at conformal interfaces and junctions,* arXiv:2208.14118.

2. Filiberto Ares, S. M. and Pasquale Calabrese, *Entanglement asymmetry as a probe of symmetry breaking*, arXiv:2207.14693.

3. S. M., Pasquale Calabrese and Lorenzo Piroli, *Symmetry-resolved Page curve*, Phys. Rev. D **106**, 046015 (2022).

4. Filiberto Ares, Pasquale Calabrese, Giuseppe Di Giulio and S. M., *Multi-charged moments of two intervals in conformal field theory* , JHEP **09** 051 (2022).

5. Luca Capizzi, S. M. and Pasquale Calabrese, *Rényi entropy and negativity for massless Dirac fermions at conformal interfaces and junctions,* JHEP **08** (2022) 171.

6. Filiberto Ares, S. M. and Pasquale Calabrese, *Symmetry-resolved entanglement in a long-range free-fermion chain*, J. Stat. Mech. (2022) 063104.

7. S. M., Vittorio Vitale, Marcello Dalmonte and Pasquale Calabrese, *The Negativity Hamiltonian: An operator characterization of mixed-state entanglement,* Phys. Rev. Lett. **128**, 140502 (2022).

8. S. M., Pasquale Calabrese and Robert M. Konik, *Generalized entanglement entropies in two-dimensional conformal field theory*, JHEP **05**, 152 (2022).

9. S. M., Pasquale Calabrese, and Robert M. Konik, *Post-Quantum Quench Growth of Renyi Entropies in Low Dimensional Continuum Bosonic Systems*, Phys. Rev. Lett. **129**, 106802 (2022).

10. S. M., Vincenzo Aba and Pasquale Calabrese *Quench dynamics of Rényi negativities and the quasiparticle picture,* arXiv:2110.14589 (2021).

11. Pasquale Calabrese, Jérome Dubail, and S. M., *Symmetry-resolved entanglement entropy in Wess-Zumino-Witten models*, JHEP **10** (2021) 067.

12. S. M., Riccarda Bonsignori and Pasquale Calabrese, *Symmetry decomposition of negativity of massless free fermions*, SciPost Phys. **10**, 111 (2021).

13. S. M., Giuseppe Di Giulio, and Pasquale Calabrese, *Entanglement and symmetry resolution in two dimensional free quantum field theories*, JHEP **08** (2020) 073.

14. S. M., Paola Ruggiero and Pasquale Calabrese, *Symmetry resolved entanglement in two-dimensional systems via dimensional reduction*, J. Stat. Mech. (2020) 083102.

15. Pasquale Calabrese, Mario Collura, Giuseppe Di Giulio and S. M., *Full counting statistics in the gapped XXZ spin chain*, EPL **129**, 60007 (2020).

16. S. M., Giuseppe Di Giulio and Pasquale Calabrese, *Symmetry resolved entanglement in gapped integrable systems: a corner transfer matrix approach*, SciPost Phys. **8**, 046 (2020).

17. S. M., Paola Ruggiero and Pasquale Calabrese, *Entanglement and relative entropies for low-lying excited states in inhomogeneous one-dimensional quantum systems,* J. Stat. Mech. 034001 (2019).

Chapter 1

Introduction

In classical statistical physics, the concept of entropy is related to the lack of knowledge about a subsystem since it quantifies the uncertainty on its exact microscopic state due to thermal fluctuations. The definition of entropy of a subsystem in terms of the number of allowed microstates Ω is $S = k_B \log \Omega$. At zero temperature, thermal fluctuations vanish and $S = 0$. At quantum level, if we consider the ground state of a quantum many-body Hamiltonian and we restrict to a region of this system, the entropy of the region does not vanish. This is due to a fundamental property of quantum mechanics, *entanglement*, and such entropy is known as *entanglement entropy*. Indeed, the quantum correlations between the region and the rest of the system are such that we cannot exactly describe its state, which causes a lack of knowledge. Said otherwise, the uncertainty about the subsystem, i.e. its entropy, is not anymore due to thermal fluctuations but to quantum correlations. Entanglement generally provides a deeper understanding of a quantum theory.
This example is one of many showing that entanglement is *the* most fundamental characteristic distinguishing the quantum from the classical world [1–3].

First meeting with Alice and Bob

Over the last decades, the point of view of the scientific community about entanglement has changed dramatically. At first, it was seen as the wart of quantum mechanics to the point that Einsein, Podolsky and Rosen tried to surgically remove it. This "spooky action at a distance" [4] appeared to go against the idea that nothing, not even information, can travel faster than the speed of light [5]. On the other hand, entanglement creates correlations between the parts of a quantum system, even if they are separated by an arbitrary distance.
This paradox can be illustrated with a simple example that will give also the opportunity to introduce two characters, Alice and Bob, who will help us in understanding the intricate world of quantum mechanics. Let us suppose that we have a system of two spins, labelled A and B, that are initially prepared in the singlet state

$$|\psi\rangle = \frac{1}{\sqrt{2}}(|\uparrow_A\downarrow_B\rangle - |\downarrow_A\uparrow_B\rangle).$$

The spins are then sent in opposite directions to Alice and Bob. If Alice observes that her spin is in the state $|\uparrow_A\rangle$, the axioms of quantum mechanics imply that the wave function has collapsed to the state $|\uparrow_A\downarrow_B\rangle$ and hence the outcome of Bob's measurement will be, or was, the state $|\downarrow_B\rangle$. This instantaneous effect, independent of the physical distance between Alice and Bob, seems to be in contradiction with the principles of relativity and the finite velocity of light and information [6].
This paradox led different authors to argue that quantum states are simply an incomplete characterisation of a quantum system, supporting the existence of the hidden-variable theories.

After about 30 years, Bell showed that such surgery cannot be performed without destroying some fundamentals of physical reality [7]. He considered a setup in which Alice and Bob perform independent measurements on a one-particle system prepared in a fixed state. Each observer has a detector to make measurements. On each trial, Alice and Bob can independently choose between various detector settings, whose outcome of each measurement can be ± 1, depending on the state of the particle. If we assume that the particles' properties are fully determined prior to the measurement, and that Alice's measurements do not influence those of Bob, we end up into correlations between observables which must satisfy some inequalities (Bell inequalities) that are violated by entangled states, such as the singlet $|\psi\rangle$. This implies that quantum mechanics cannot be secretly just some classical theory where everything has a definite state before the measurement. The inconsistency of local hidden-variable theories was also supported by strong experimental evidences [8], e.g. by the group of Aspect [9].

Entanglement in many-body systems

Once the existence of entanglement has been at least accepted despite its puzzling nature, it has become one of the main characters of the Physics scene (and not only, see e.g. the cartoon of Martin Mystere (Num. 368, April 2020)) and the most popular and useful of its measures is the *von Neumann entanglement entropy*. During the 90s, entanglement became a resource for quantum technology, communication and information in general [10], the crucial ingredient to perform tasks that are impossible or extremely inefficient in a pure classical setting, such as quantum teleportation [11] or quantum error correction [12]. Around 2000, the progress made in quantum information for quantifying entanglement has led to further insights into other areas of physics such as statistical mechanics and quantum field theory, in particular in the analysis of extended quantum systems [13–16], i.e. with infinitely many degrees of freedom. For example, it can be useful to detect and describe phase transitions, even when a conventional order parameter is unavailable. In fact, its behaviour as a function of the subsystem size allows us to distinguish if the system is in a gapped or gapless phase and what are the universal features of critical systems [17–21]. It turns out that in the former case, the entanglement follows the *area law*, i.e. it is proportonal to the border of the subsystem, unlike the thermal entropy which is characterised by a *volume law*. This idea was firstly put forward and explored in the context of black hole physics [22, 23], where it was suggested that this property of entanglement could be at the origin of the black hole entropy, given by the Bekenstein-Hawking formula [24,25], which is in fact proportional to the area of the boundary surface of the black hole. This is one of the reasons for which the high-energy communities have always showed a great interest in the physics of the entanglement. For example, in the framework of the AdS/CFT correspondence, which argues that a theory of quantum gravity in an Anti-de Sitter (AdS) space is equivalent to a Conformal Field Theory (CFT) defined on the boundary of the former, we have to mention the celebrated Ryu-Takayanagi formula [26–29]. Inspired by the Bekenstein-Hawking formula for the entropy of a black hole, it states that the entanglement of a region can be computed in the classical regime from the area of certain minimal surfaces in the bulk, anchored to the entangling surface in the boundary. Another important contribution from the high-energy community was given by Page [30], who took the first steps towards a systematic characterisation of entanglement in random quantum states, with important applications in different fields, ranging from the black hole information paradox [31–35] to the foundations of statistical mechanics [36, 37]. We will come back to the behaviour of the Page curves in the presence of symmetries in Chapter 10.

Let us go further in the exploration of the research fields in which entanglement plays a prominent role. In two dimensions, a very interesting class of systems are the ones displaying topological phases. The first correction to the area law is called topological entropy [38, 39] because it is a

topological invariant directly related to the total quantum dimension. Hence, by computing the entanglement entropy and isolating the constant term in the size of the subsystem, we have a tool to detect topological order. Prototypical examples in which this situation occurs are the Kitaev model [40] and two-dimensional ($2d$) electron gases in large magnetic fields in the fractional quantum Hall regime [41].

Up to this point, we have shown some examples concerning the area law of entanglement, typical of gapped systems (see also Chapter 2 for a field theoretical approach to the subject, while Chapter 7 for a formulation of the problem on the lattice) and its connections with black hole physics and the topological order of matter. However, for the ground state of gapless local Hamiltonians in one dimension, the area law is corrected by a logarithmic term [20]. One practical implication is that the presence of entanglement makes difficult to deal with quantum many-body systems using a classical computer. For example, the Density Matrix Renormalization Group (DMRG) algorithm [42] works well in non critical $1d$ systems, but it becomes less efficient (and practically useless in $2d$) when we approach a quantum critical point. In this case, the growth of the entanglement originates long-range correlations that increase the complexity of simulating the system. As a consequence, it is necessary to construct algorithms that try to capture the essential properties of the state's entanglement and they are usually based on tensor network techniques [43]. We have already mentioned the most prominent examples of logarithmic area-law violations, which are critical $1d$ models [17, 19–21], for which the mass gap becomes zero, the correlation length diverges and the ground state correlation functions decay algebraically. The low-energy properties of such corrections are captured by CFT and, besides signaling criticality, the logarithmic term turns out to be universal. Indeed it is proportional to the corresponding central charge, which does not depend on the microscopic details of the model but only on the universality class associated with a given fixed point of the renormalization group (RG). This kind of systems will be the core of the Chapters 3, 4, 5, 12, 13 and 15, where we try to unveil some universal properties of the systems through the study of entanglement-related quantities, such as their symmetry resolution, to characterise the properties of the group generating the symmetry itself. We mention that the ground state correlations can display algebraic decay even with non-zero mass gap, e.g. for fermionic chains with long-range couplings, as we are going to study in Chapter 9. With respect to higher dimensions, to our knowledge, there are no rigorous and general proofs for the area law as it happens in one dimension [50]. It is known that for non-critical, local systems of free fermions the entanglement entropy of the ground state fulfils an area law. The same occurs if we consider bosons instead of fermions. On the other hand, for critical fermions with a finite, non-zero Fermi surface, the entanglement entropy of the ground state presents logarithmic corrections to the area law. This will be the subject of Chapter 8.

We close this broad introduction about entanglement in extended systems by mentioning another question that has been addressed in the last years, i.e. the connection between entanglement and thermodynamics in the framework of the out-of-equilibrium dynamics of quantum correlations. The simplest and most broadly studied protocol is the quantum quench [44, 45]: a system is prepared in the ground state of a $1d$ translationally invariant Hamiltonian, and at a given time a sudden change modifies the Hamiltonian. In integrable systems, the entanglement dynamics after a quench is captured by a well-known quasiparticle picture [46–49]. The key tenet of the quasiparticle picture is that the entanglement dynamics is described by the ballistic propagation of pairs of entangled excitations, which are produced after the quench (see Fig. 1.1). We will study the entanglement dynamics in many-body systems in Chapters 6, 11, 14 and 16.

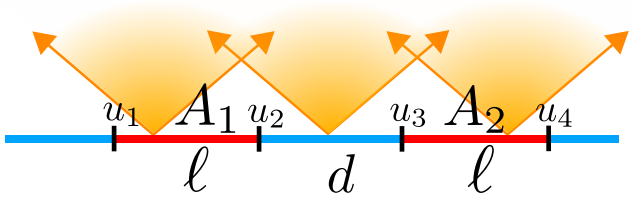

Figure 1.1: Quasiparticle picture for the time evolution after a quench of the entanglement between two disjoint intervals ($A_1 = [u_1, u_2]$ and $A_2 = [u_3, u_4]$) embedded in the infinite line. Pairs of entangled quasiparticles are emitted from every point in space at $t = 0$. At a given time t the entanglement between $A = A_1 \cup A_2$ and the remainder is proportional to the number of pairs shared between A and its complement.

1.1 Walking with Alice and Bob through quantum information

Let us consider a quantum system made up of two parts. The first one, A, is owned by Alice, and the second one, B, by Bob. This corresponds to a bipartition of the total Hilbert space as $\mathcal{H} = \mathcal{H}_A \otimes \mathcal{H}_B$. Any normalised pure state $|\psi\rangle \in \mathcal{H}$ has a Schmidt decomposition [51]

$$|\psi\rangle = \sum_{i=1}^{r} \sqrt{\lambda_i}\, |\psi_{A,i}\rangle \otimes |\psi_{B,i}\rangle\,, \quad \sum_{i=1}^{r} \lambda_i = 1, \tag{1.1.1}$$

where $\{|\psi_{A,i}\rangle\}$ and $\{|\psi_{B,i}\rangle\}$ are, respectively, an orthonormal basis of $\mathcal{H}_A$ and $\mathcal{H}_B$. Here r denotes the Schmidt rank and it cannot be larger than $\min(\dim\mathcal{H}_A, \dim\mathcal{H}_B)$. If $r = 1$, Eq. (1.1.1) reduces to

$$|\psi\rangle = |\psi_A\rangle \otimes |\psi_B\rangle\,, \tag{1.1.2}$$

and we say that the state $|\psi\rangle$ is separable (or product state). The definition of separable states means that $|\psi_A\rangle$ and $|\psi_B\rangle$ are uncorrelated. Contrarily to the example we have done in the previous section, if Alice measures any observable in A and Bob measures it in B, the probabilities of the different outcomes factorise. Thus, the measurement outcomes for Alice do not depend on the outcomes on Bob's side. If $r > 1$, the state is entangled.
In a more general situation, the full system is not in a pure state $|\psi\rangle$, but in a mixed state described by a density matrix

$$\rho = \sum_j p_j\, |\psi_j\rangle \langle\psi_j|\,, \tag{1.1.3}$$

being p_j the probability that the state is $|\psi_j\rangle \in \mathcal{H}$. For mixed states, ρ is a product state if $\rho = \rho_A \otimes \rho_B$, as it also occurs for pure states, while it is separable if

$$\rho = \sum_j p_j \rho_{A,j} \otimes \rho_{B,j}. \tag{1.1.4}$$

Otherwise the state is called entangled. Therefore, we have found three different scenarios. First, a product state is an uncorrelated state, where Alice and Bob own each a separate state. For non-product states, we can distinguish two types of correlations. Separable states are classically correlated, i.e. they can be produced only through local operations and classical communication (LOCC) [52, 53]. In this case, Alice and Bob share a random number generator that produces the outcomes j with probabilities p_j and for each of them they can build the state $\rho_{A,j} \otimes \rho_{B,j}$, and, as a consequence, ρ. These states only share classical correlations while if a state is entangled, the correlations cannot originate from the classical procedure described above. In this sense, entangled

states are a typical feature of quantum mechanics. We specify that, if the state is pure, it can only be either a product state or entangled.

Let us come back to the original problem of quantifying the entanglement in a pure state of the bipartite system $A \cup B$. This is provided by a family of functions known as Rényi entanglement entropies (REEs).
Starting from the density matrix $\rho = |\psi\rangle \langle\psi|$, the key object to study the bipartite entanglement is the reduced density matrix (RDM) of A, $\rho_A = \mathrm{Tr}_B \rho$, where Tr_B denotes the partial trace. If $r \neq 1$, now ρ_A describes a mixed state. The Rényi entropies are defined as (throughout the Chapters of this thesis we will specify the superscript denoting the subsystem only if necessary, otherwise we omit it for simplicity)

$$S_n^A \equiv \frac{1}{1-n} \log \mathrm{Tr} \rho_A^n, \tag{1.1.5}$$

where n is an integer number. After an analytic continuation to complex values of n, the limit $n \to 1$ provides the von Neumann entanglement entropy (vNEE)

$$S_1^A \equiv -\mathrm{Tr} \rho_A \log \rho_A. \tag{1.1.6}$$

If we now apply the Schmidt decomposition of Eq. (1.1.1) in the definition of the entropies, we obtain

$$S_n^A = \frac{1}{1-n} \log \left(\sum_{i=1}^{r} \lambda_i^n \right), \quad S_1^A = -\sum_{i=1}^{r} \lambda_i \log(\lambda_i). \tag{1.1.7}$$

From the Schmidt decomposition, it also follows that if we take the partial trace over A, rather than B, $S_n^A = S_n^B$ for a pure state. The entanglement entropy (1.1.6) satisfies all the requirements to be considered a good entanglement measure. In particular, it vanishes when it is separable and it is an "entanglement monotone", meaning that it does not not grow on average under operations that do not increase the degree of entanglement (the LOCC) [54].
Given two spatial subsystems A_1 and A_2 (not necessarily one the complement of the other), the vNEE satisfies two important inequalities [55, 56], namely the subadditivity

$$S_1^{A_1 \cup A_2} \leq S_1^{A_1} + S_1^{A_2}, \tag{1.1.8}$$

and the strong subadditivity

$$S_1^{A_1 \cup A_2} + S_1^{A_1 \cap A_2} \leq S^{A_1} + S_1^{A_2}. \tag{1.1.9}$$

On the other hand, the REEs do not satisfy subadditivity.

For a mixed state, the entanglement entropies are no longer good measures of entanglement because both quantum and classical correlations contribute to the von Neumann and Rényi entropies. A situation usually considered is when A is further divided into two parts, $A = A_1 \cup A_2$. In general, the RDM ρ_A is mixed and, therefore, entanglement between two non-complementary subsystems A_1 and A_2 is not provided by $S_n^{A_1}$. In this case, a useful quantity to consider is the Rényi mutual information

$$I_n^{A_1:A_2} \equiv S_n^{A_1} + S_n^{A_2} - S_n^{A_1 \cup A_2}, \tag{1.1.10}$$

which is not a measure of the entanglement between A_1 and A_2, but for $n \to 1$ it quantifies the amount of global correlations between the two subsystems (we mention that for $n \neq 1$, $I_n^{A_1:A_2}$ can be also negative [57] and a more complicated definition of mutual information must be employed [58]).

Let us introduce a more convenient way to deal with entanglement in mixed states. Assume that we know the joint density matrix of two particles belonging to Alice and Bob, respectively. We carry out the following mathematical operation: we apply a matrix transposition to that part of the

density matrix which corresponds to Bob's particle and leave Alice's part unchanged. Physically this *partial transposition* would correspond to a time reversal transformation in Bob's lab. If the state is unentangled then its partial transpose is again an admissible density matrix. However, the partial transposition may lead to negative and hence unphysical eigenvalues of the density matrix if the state is entangled. Looking at whether or not the density matrix has a "positive partial transpose" (PPT) can in this way help us to answer whether a given state is entangled. Now we can formalise this condition, also known as Peres criterion [59, 60]. It states that given a system described by the density matrix $\rho_{A=A_1\cup A_2}$, a sufficient condition for the presence of entanglement between A_1 and A_2 is that the partial transpose $\rho_A^{T_1}$ with respect to the degrees of freedom in A_1 (or equivalently A_2) has at least one negative eigenvalue. We can introduce the partial transpose operation as follows. We write down the density matrix as

$$\rho_A = \sum_{ijkl} \langle e_i^1, e_j^2|\rho_A|e_k^1, e_l^2\rangle \, |e_i^1, e_j^2\rangle \, \langle e_k^1, e_l^2| \, , \tag{1.1.11}$$

where $|e_j^1\rangle$ and $|e_k^2\rangle$ are orthonormal bases in the Hilbert spaces $\mathcal{H}_{A_1}$ and $\mathcal{H}_{A_2}$ corresponding to the A_1 and A_2 regions, respectively. The partial transpose of a density matrix for the subsystem A_1 is defined by exchanging the matrix elements in the subsystem A_1, i.e.

$$\rho_A^{T_1} = \sum_{ijkl} \langle e_k^1, e_j^2|\rho_A|e_i^1, e_l^2\rangle \, |e_i^1, e_j^2\rangle \, \langle e_k^1, e_l^2| \, . \tag{1.1.12}$$

In terms of its eigenvalues λ_i, the trace norm of $\rho_A^{T_1}$ can be written as

$$\mathrm{Tr}|\rho_A^{T_1}| = \sum_i |\lambda_i| = \sum_{\lambda_i>0} |\lambda_i| + \sum_{\lambda_i<0} |\lambda_i| = 1 + 2\sum_{\lambda_i<0} |\lambda_i|, \tag{1.1.13}$$

where in the last equality we used the normalisation $\sum_i \lambda_i = 1$. Here $\mathrm{Tr}|O| \equiv \mathrm{Tr}\sqrt{O^\dagger O}$ denotes the trace norm of the operator O. Therefore, starting from the Peres criterion, two measures of the bipartite entanglement for a general mixed state can be naturally defined as [62, 63]

$$\mathcal{N} = \frac{\mathrm{Tr}|\rho_A^{T_1}| - 1}{2}, \quad \mathcal{E} \equiv \log \mathrm{Tr}|\rho_A^{T_1}|, \tag{1.1.14}$$

which are known as *negativity* and *logarithmic negativity*, respectively. The expression in Eq. (1.1.13) makes evident that the negativity measures "how much" the eigenvalues of the partial transpose of the density matrix are negative, a property which is the reason for the name negativity.

1.2 Entanglement in the lab

Heretofore, we have discussed the relevance of entanglement from a theoretical point of view, while the aim of this section is to give some insights about how it can impact the physics from a more practical perspective, i.e. in the realm of experiments. Of course, this discussion is far from being comprehensive, but the goal is to give further motivations on the importance of the theoretical study of entanglement properties of quantum many-body systems. As we already pointed out, entanglement is the heart of quantum information and computation. Let us illustrate this with the help of our friends. Alice wants to send quantum information to Bob. Specifically, suppose she wants to send the qubit state $|\psi\rangle = \alpha\,|0\rangle + \beta\,|1\rangle$, i.e. passing on information about α and β to Bob. There exists a theorem in quantum mechanics which states that you cannot simply make an exact copy of an unknown quantum state. This is known as the no-cloning theorem [61]. As a

result, we can see that Alice cannot simply generate a copy of $|\psi\rangle$ and give it to Bob. However, with the assistance of two classical bits and an entangled qubit pair, Alice can transfer her state $|\psi\rangle$ to Bob. This is known as quantum teleportation because, at the end, Bob will get $|\psi\rangle$ and Alice will eventually have a different state. We do not enter into the description of this protocol, but as a sample of the rapid development of this research field we can mention the experiment [64] of Zeilinger's group in 2012 in which they were able to teleportate a state between two entangled photons separated 143 km.

Let us move on to review some of the main proposed techniques to detect and measure entanglement itself. One of the first proposal was given in [65–68], exploiting special relations between the RDM of a subsystem and quantum noise in free-systems. Such relations, however, are not valid in the presence of interactions. An alternative way to detect entanglement in a generic system is given by quantum state tomography [10], i.e. a measurement of all the density matrix elements. Its drawback is that is scales exponentially with the system size, so it has been applied to trapped ions [69, 70] and superconducting qubits [71] up to, at most, 10 qubits [72].

Going further in the review, in the lab, it is easier to have access to REEs by preparing n identical copies of the system and letting them interact in such a way that it is then possible to extract the expectation value of the shift operator $V^{(n)}$, whose action is to cyclically permute the n copies $V^{(n)} |\psi_1\rangle \dots |\psi_n\rangle = |\psi_n\rangle |\psi_1\rangle \dots |\psi_{n-1}\rangle$ [73]. This shift operator allows to estimate $\mathrm{Tr}(\rho^n)$ as $\mathrm{Tr}(V^n \rho^{\otimes n})$, i.e. from the expectation values of the shift operator on the replicated system.

There exist two possible ways to implement the shift operation experimentally: the first one was proposed by Cardy in [74] and also later exploited by Abanin and Demler in [75] and it consists in performing a quantum quench on the n copies of the system. The second, proposed for $n = 2$ by Alves and Jaksch in [76] and extended to general n by Daley et al. in [77, 78], is based on an optical lattice where the copies interfere by switching on the tunneling among them in a controlled way. By observing the system after this controlled interference, it is possible to have access to the value of the shift operator for any desired subsystem. This technology has been used in Greiner's group at Harvard to calculate the quantum purity of a subsystem, i.e. $\mathrm{Tr}\rho_A^2$, in a Bose-Hubbard system [79]. The advantage of using this quantity is that it is connected to an observable depending on the number of particles, which is the parity. When two pure and identical quantum states are inferred on a beam splitter, the interference of odd outcomes is destructive and the output state has an even number of particles in each copy. As a consequence, the measurement of entanglement simply reduces to the measure of a single operator.

A recent toolbox which has been firstly introduced to measure entanglement entropies are the randomised measurements [80]. The idea is to apply local random unitary operators, extracted from the circular unitary ensemble, on the L-qubit state of the system ρ and store the bit-string outcomes of the measurements. From the bit-strings and the unitaries it is possible to construct the classical-shadows, which are an estimator of the density matrix of the measured quantum state. The use of this protocol has been extended to estimate many physical properties of a quantum state as state fidelities, out-of-time ordered correlators, topological invariants and other nonlinear functions of the density matrix.

Let us now conclude this section by mentioning an experiment which allows us to introduce another crucial subject of this thesis, the *entanglement resolution*. We refer to the recent experiment by Lukin et al. [81] about the time evolution of a many-body localised system through particle fluctuations and correlations. This has shed the light on the internal symmetry structure of the total entanglement, that can be better understood in terms of two quantities in which the total entanglement can be split, i.e. the configurational and the number entropy. In the presence of both disorder and interaction, the dynamics of configurational and number entanglement occur over different time scales: the number entanglement quickly saturates to an asymptotic value while

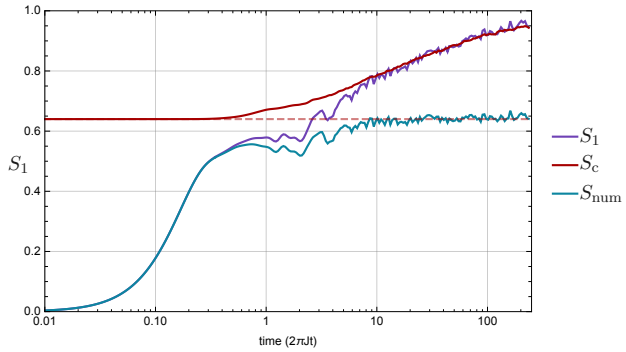

Figure 1.2: The results obtained in [81] for the temporal evolutions of the vNEE (S_1), the configurational (S_c) and the number (S_{num}) entropy (see eq. (1.3.5) for their definitions). They system is a half-chain in a one-dimensional interacting bosonic chain with disorder, where J parametrises the interaction strength. The configurational entropy is vertically shifted with respect to its initial value. Figure taken from [81].

the configurational one exhibits a slow logarithmic growth [81]. This is shown in Fig. 1.2, where a plot with the results of Ref. [81] has been reported. As we will find out, this experiment has opened a fruitful reasearch activity about the symmetry resolved entanglement measures.

1.3 Alice and Bob meet symmetries

Following the conclusion of the previous section, a question that has recently attracted much attention is how entanglement decomposes into the different symmetry sectors in the presence of global conserved charges [84–86]. Various reasons have motivated the interest in this problem. The fact that the effect of symmetries on entanglement can be investigated experimentally [81, 87–89] and, moreover, understanding how entanglement arises from the symmetry sectors is crucial to better grasp some quantum features, for example in non-equilibrium dynamics [81]. Also at more practical level, it can help to speed-up the numerical algorithms to simulate quantum many-body systems [85]. All that has been the breeding ground for a plethora of works that analyse the resolution of entanglement from different perspectives: spin chains [86, 88–100, 102, 106–110], integrable quantum field theories [103, 104, 111–115], CFTs [84, 85, 101, 116–127], holography [128–131], out-of-equilibrium [132–137] and disordered systems [138–141] or topological matter [142–147] to mention some of them.

Let us define the problem starting with an example. Alice and Bob share three boxes with only one quantum chocolate inside one of them and this is described by a pure state $|\Psi\rangle = \frac{1}{\sqrt{6}}(|100\rangle + |010\rangle + 2\,|001\rangle)$. The chocolate number is fixed to be $N = 1$. Alice is curious to know the probability of finding it in two of them. The RDM of Alice is $\rho_A = \mathrm{Tr}_B|\psi\rangle\langle\psi| = \frac{1}{6}(4\,|00\rangle\langle 00| + (|10\rangle + |01\rangle)(\langle 10| + \langle 01|)$, i.e.

$$\rho_A = \frac{1}{6}\begin{pmatrix} 4 & 0 & 0 & 0 \\ 0 & 1 & 1 & 0 \\ 0 & 1 & 1 & 0 \\ 0 & 0 & 0 & 0 \end{pmatrix}, \tag{1.3.1}$$

in the basis $\{|00\rangle, |01\rangle, |10\rangle, |11\rangle\}$. This matrix is block diagonal with respect to the occupation number N_A, i.e. the chocolate number in Alice's boxes. Let us observe that the total charge

N is fixed to be 1, while the possible outcomes for N_A are $0, 1, 2$ (even though, as we will see, finding 2 chocolates is, unfortunatly, impossible). From Eq. (1.3.1), we can read the probabilities $p(N_A = 0) = 2/3$, $p(N_A = 1) = 1/3$, $p(N_A = 2) = 0$ and quantify the information stored in the three boxes by computing $-\sum_{N_A} p(N_A) \log p(N_A) = \log(3/4^{1/3})$, which is known as *Shannon entropy* or, as we mentioned, number entropy. Poor Alice, the probability of eating one chocolate is not on her side!

The example above has showed to us that the presence of a conserved charge, i.e. the number of chocolate in this case, is reflected into a block-diagonal structure of the RDM and one can compute the entanglement corresponding to the RDM in only one charge sector. Thus, $N_A = 0, 1, 2$ is a good quantum number in which the total entanglement between A and B can be *resolved*. Let us formally define this concept. We take a spatial bipartition $A \cup B$ of an extended quantum system in a pure state $|\Psi\rangle$. We assume that the system is endowed with a global $U(1)$ symmetry generated by a local charge $Q = Q_A \otimes \mathbb{1}_B + \mathbb{1}_A \otimes Q_B$. If $|\Psi\rangle$ is an eigenstate of Q, the density matrix $\rho = |\Psi\rangle\langle\Psi|$ commutes with Q, i.e. $[Q, \rho] = 0$, and, by taking the trace over B, we find that $[Q_A, \rho_A] = 0$. This implies that the reduced density matrix ρ_A presents a block diagonal structure, in which each block corresponds to an eigenvalue $q \in \mathbb{Z}$ of Q_A. That is,

$$\rho_A = \bigoplus_q \Pi_q \rho_A = \bigoplus_q \left[p(q) \rho_A(q) \right], \tag{1.3.2}$$

where Π_q is the projector onto the eigenspace associated to the eigenvalue q and $p(q) = \mathrm{Tr}\left(\Pi_q \rho_A\right)$ is the probability of obtaining q as the outcome of a measurement of Q_A. Notice that Eq. (1.3.2) guarantees the normalisation $\mathrm{Tr}[\rho_A(q)] = 1$ for any q.

The amount of entanglement between A and B in each symmetry sector can be quantified by the *symmetry resolved Rényi entropies* (SRRE), defined as

$$S_n^A(q) \equiv \frac{1}{1-n} \log \mathrm{Tr}[\rho_A(q)^n]. \tag{1.3.3}$$

Taking the limit $n \to 1$ in this expression, we obtain the *symmetry resolved entanglement entropy* (SREE),

$$S_1^A(q) \equiv -\mathrm{Tr}[\rho_A(q) \log \rho_A(q)]. \tag{1.3.4}$$

According to the decomposition of Eq. (1.3.2), the total entanglement entropy in Eq. (1.1.6) can be written as

$$S_1^A = \sum_q p(q) S_1^A(q) - \sum_q p(q) \log p(q) \equiv S_{\mathrm{c}}^A + S_{\mathrm{num}}^A, \tag{1.3.5}$$

where S_{c} is known as *configurational entropy* and quantifies the average contribution to the total entanglement of all the charge sectors [81, 93–95], while S_{num} is called *number entropy* (or *fluctuation entanglement* [90]) and takes into account the entanglement due to the fluctuations of the value of the charge within the subsystem A [81, 139, 140, 143, 148–150]. The origin of the latter name is inspired by the case when the conserved charge is the particle number (see also Fig. 1.2).

If $A = A_1 \cup A_2$, the total charge in A is the sum of the charge in A_1 and A_2, $Q_A = Q_{A_1} + Q_{A_2}$, and the RDM ρ_{A_1}, ρ_{A_2} of A_1 and A_2, can be independently decomposed in charged sectors as we did for ρ_A in Eq. (1.3.2). Therefore, we can define the SRREs $S_n^{A_1}(q_1)$, $S_n^{A_2}(q_2)$ for the regions A_1 and A_2 analogous to Eq. (1.3.3) for A, with $q = q_1 + q_2$. This leads to the definition of the *symmetry resolved mutual information* as [133]

$$I^{A_1:A_2}(q) = \sum_{q_1=0}^{q} p(q_1, q - q_1) \left[S_1^{A_1}(q_1) + S_1^{A_2}(q - q_1) \right] - S_1^A(q). \tag{1.3.6}$$

The quantity $p(q_1, q-q_1)$, normalised as

$$\sum_{q_1=0}^{q} p(q_1, q-q_1) = 1, \tag{1.3.7}$$

is the probability that a simultaneous measurement of the charges Q_{A_1} and Q_{A_2} yields q_1 and $q-q_1$, respectively, while the charge of the whole system A is fixed to q. Although Eq. (1.3.6) is a natural definition, $I_1^{A_1:A_2}(q)$ is not in general a good measure of the total correlations between A_1 and A_2 within each charge sector since, in some cases, it can be negative [133]. Nevertheless, it provides a decomposition for the total mutual information (1.3.6) similar to the one reported in Eq. (1.3.5) for the entanglement entropy,

$$I^{A_1:A_2} = \sum_q p(q) I^{A_1:A_2}(q) + I^{A_1:A_2}_{\text{num}}, \tag{1.3.8}$$

where $I^{A_1:A_2}_{\text{num}} \equiv S^{A_1}_{\text{num}} + S^{A_2}_{\text{num}} - S^{A}_{\text{num}}$ is the *number mutual information*.

Another entanglement measure with an interesting symmetry decomposition is the negativity. The first question to answer is whether the partial transposed RDM admits a block-diagonal structure. Performing a partial transposition of the relation $[\rho_A, Q_{A_1} + Q_{A_2}] = 0$ yields [116]

$$[\rho_A^{T_1}, Q_2 - Q_1^{T_1}] = 0, \tag{1.3.9}$$

from which we can do a block matrix decomposition according to the eigenvalues q_{imb} of the imbalance operator $Q_{\text{imb}} = Q_2 - Q_1^{T_1}$. Let $\Pi_{q_{\text{imb}}}$ denote the projector onto the subspace of eigenvalue q_{imb} of the operator Q_{imb}. We define the *normalised charge imbalance partially transposed density matrix* as

$$\rho_A^{T_1}(q_{\text{imb}}) = \frac{\Pi_{q_{\text{imb}}} \rho_A^{T_1} \Pi_{q_{\text{imb}}}}{\text{Tr}(\Pi_{q_{\text{imb}}} \rho_A^{T_1})}, \qquad \text{Tr}(\rho_A^{T_1}(q_{\text{imb}})) = 1, \tag{1.3.10}$$

such that

$$\rho_A^{T_1} = \oplus_{q_{\text{imb}}} p(q_{\text{imb}}) \rho_A^{T_1}(q_{\text{imb}}). \tag{1.3.11}$$

Here, $p(q_{\text{imb}}) = \text{Tr}(\Pi_{q_{\text{imb}}} \rho_A^{T_1})$ is the probability of finding q_{imb} as the outcome of a measurement of Q_{imb} and corresponds to the sum of the diagonal elements of $\rho_A^{T_1}(q_{\text{imb}})$. Although the eigenvalues of $\rho_A^{T_1}$ can be negative, the partial transpose leaves invariant all the elements on the diagonal and so they remain the same as those of ρ_A which are non-negative. Hence $p(q_{\text{imb}})$ satisfies $p(q_{\text{imb}}) \geq 0$ and $\sum_{q_{\text{imb}}} p(q_{\text{imb}}) = 1$, as it should be for a probability measure.

We can thus define the (normalised) *charge imbalance resolved negativity* as

$$\mathcal{N}(q_{\text{imb}}) = \frac{\text{Tr}|(\rho_A^{T_1}(q_{\text{imb}}))| - 1}{2}. \tag{1.3.12}$$

If in the q_{imb} sector there are no negative eigenvalues, according to Eq. (1.3.12), $\mathcal{N}(q_{\text{imb}}) = 0$. Hence, this definition not only provides a resolution of the negativity, but also tells us in which sectors the negative eigenvalues are, i.e. where the entanglement is. The total negativity, $\mathcal{N}$, is resolved into (normalised) contributions from the distinct imbalance sectors as

$$\mathcal{N} = \sum_{q_{\text{imb}}} p(q_{\text{imb}}) \mathcal{N}(q_{\text{imb}}). \tag{1.3.13}$$

We stress that the imbalance decomposition of the negativity as in Eq. (1.3.13) cannot be performed for the logarithmic negativity in Eq. (1.1.14), because of the nonlinearity of the logarithm.

1.4 From field theoretical tools to the lattice computation of the entanglement

In the context of extended quantum systems, the calculation of the vNEE is not an easy task. The difficult point lies in the computation of $\log \rho_A$. One of the most successful strategies to avoid this problem is the *replica approach*, firstly used in this context by Holzey et al. in [17] and then by Calabrese and Cardy [20]. The idea of this technique is the following: calling λ_i a Schmidt eigenvalue and starting from the identities

$$\begin{aligned} \log \lambda_i &= \lim_{m\to 0} \frac{\lambda_i^m - 1}{m}, \\ \frac{\partial}{\partial n}\lambda_i^n\Big|_{n\to 1} &= \lim_{m\to 0} \frac{\lambda_i^{m+1} - \lambda_i^1}{m}, \end{aligned} \tag{1.4.1}$$

we can derive the following relation

$$\lambda_i \log \lambda_i = \frac{\partial}{\partial n}\lambda_i^n\Big|_{n\to 1}. \tag{1.4.2}$$

Since $\mathrm{Tr}\rho_A^n = \sum_i \lambda_i^n$, if we are able to evaluate $\mathrm{Tr}\rho_A^n$ for n integer and then analytically continue it as a function of n to complex values, we can compute the vNEE in (1.1.6) (assuming that the analytical continuation is unique) as

$$S_1^A = -\lim_{n\to 1}\frac{\partial}{\partial n}\mathrm{Tr}\rho_A^n. \tag{1.4.3}$$

A generalisation of this replica trick (1.4.3) has been then introduced in Refs. [151,152] for the negativity. In this case, we must distinguish the two cases

$$\begin{aligned} \mathrm{Tr}(\rho_A^{T_1})^{n_e} &= \sum_{\lambda_i>0}\lambda_i^{n_e} + \sum_{\lambda_i<0}\lambda_i^{n_e} \quad n_e = 2m, \\ \mathrm{Tr}(\rho_A^{T_1})^{n_o} &= \sum_{\lambda_i>0}\lambda_i^{n_o} - \sum_{\lambda_i<0}|\lambda_i|^{n_o} \quad n_o = 2m+1. \end{aligned} \tag{1.4.4}$$

with $m \in \mathbb{N}$. The limit from the odd sequence of replicas would give $\mathrm{Tr}|\rho_A^{T_1}| = 1$, therefore, in order to properly reproduce the absolute value in the definition of negativity, it is given by the limit

$$\mathcal{N} = \lim_{n_e\to 1}\mathrm{Tr}(\rho_A^{T_1})^{n_e}. \tag{1.4.5}$$

Below we review some of the most powerful techniques to deal with entanglement measures in the context of many-body quantum systems, focusing on the main ones used throughout the thesis.

1.4.1 Path-integral formalism

The replica trick turns out to be a powerful strategy to compute the REEs using the path-integral approach. We focus on the ground state of a $2d$ quantum field theory (QFT) parameterised by the complex coordinate $w = x + i\tau$, where x denotes the spatial coordinate, whose support is on a finite segment of length L. The path integral representation of the density matrix ρ is given by [20,21]

$$\begin{aligned} \langle\Phi'|\,\rho\,|\Phi''\rangle = Z^{-1}\int \mathcal{D}\phi e^{-S(\phi)}\prod_x(\delta(\phi(x,\tau=0^-)-\Phi'(x))) \\ \times\prod_x(\delta(\phi(x,\tau=0^+)-\Phi''(x))), \end{aligned} \tag{1.4.6}$$

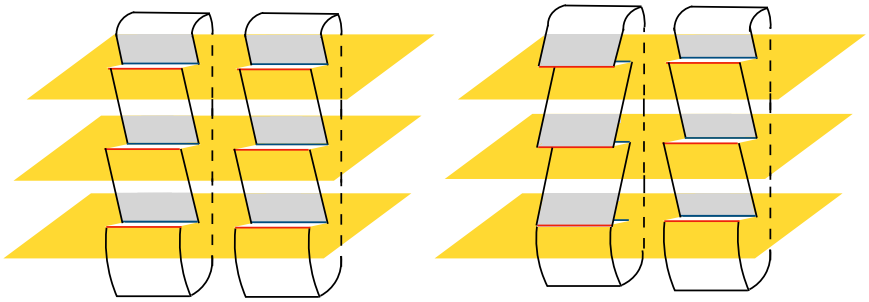

Figure 1.3: Left panel: Representation of the n-sheeted Riemann surface $\mathcal{R}_n$ for $n = 3$ and $A = [u_1, v_1] \cup [u_2, v_2]$. The blue edge of each cut is identified with the red edge of the corresponding cut in the upper copy. Right panel: Path-integral representation of $\mathrm{Tr}(\rho_A^{T_1})^3$: the geometry is different as compared with $\mathcal{R}_n$.

where the geometry of the integration surface is an infinite cylinder with a discontinuity of the field configurations at $\tau = 0$, $S(\phi)$ is the Euclidean action of the theory and Z is a normalisation factor. Let us now compute the RDM by tracing over the subsystem B

$$\langle \Phi' | \, \mathrm{Tr}_B(\rho) \, | \Phi'' \rangle = Z^{-1} \int \mathcal{D}\phi e^{-S(\phi)} \prod_{x \in A} (\delta(\phi(x, \tau = 0^-) - \Phi'(x))) \times \prod_{x \in A} (\delta(\phi(x, \tau = 0^+) - \Phi''(x))). \quad (1.4.7)$$

Then we replicate n times ρ_A and we glue the copies together along the cuts in a cyclical way. The last and the first copy are also sewed together in the same form (see the left-hand-side of Fig. 1.3 for a graphical representation when $L \to \infty$). We eventually obtain an n-sheeted Riemann surface $\mathcal{R}_n$ of genus $(n-1)(p-1)$, with p the number of intervals, which is symmetric under the $\mathbb{Z}_n$ cyclic permutation of the sheets. The moments of ρ_A^n are given by the partition function on $\mathcal{R}_n$, denoted by $Z_n(A)$, as

$$\mathrm{Tr}\rho_A^n = \frac{Z_n(A)}{Z_1^n}. \quad (1.4.8)$$

If we deal with a CFT, the path integral formalism easily generalises to a state different from the ground state [153, 154]: the excess of the REEs of the excited state with respect to the vacuum can be expressed as a correlator of the operators corresponding to the excited states by using the state-operator correspondence. We will provide an explicit example for this in Chapter 5.

Alternatively, instead of replicating the space-time where the theory is defined, one can take n copies of the QFT on one single worldsheet, and quotient it by the $\mathbb{Z}_n$ symmetry under the cyclic exchange of the copies. We then get the orbifold theory $\mathrm{QFT}^{\otimes n}/\mathbb{Z}_n$ [155]. Specifically, for a subsystem A consisting of p disjoint intervals, $A = \bigcup_{i=1}^{p} [u_i, v_i]$, $\mathrm{Tr}\rho_A^n$ can be expressed as a $2p$-point correlation function of twist and antitwist fields, $\mathcal{T}_n$ and $\bar{\mathcal{T}}_n$, respectively, [21, 156]

$$\mathrm{Tr}\rho_A^n = \langle \prod_{i=1}^{p} \mathcal{T}_n(u_i) \bar{\mathcal{T}}_n(v_i) \rangle. \quad (1.4.9)$$

The (anti)-twist fields implement in the orbifold the multivaluedness of the correlation functions on the surface $\mathcal{R}_n$ when we go around its branch points [155, 157]. In fact, the winding around the

point where $\mathcal{T}_n$ ($\bar{\mathcal{T}}_n$) is inserted maps a field $\mathcal{O}_k$ living in the copy k of the orbifold into the copy $k+1$ ($k-1$), that is

$$\mathcal{T}_n(u)\mathcal{O}_k(e^{2\pi i}(z-u)) = \mathcal{O}_{k+1}(z-u)\mathcal{T}_n(u). \tag{1.4.10}$$

This approach is particularly fruitful when dealing with a CFT, where the twist felds are spinless primaries with conformal weight [20, 156]

$$\Delta_n = \frac{c}{24}\left(n - \frac{1}{n}\right), \tag{1.4.11}$$

where c is the central charge of the initial CFT. If A consists of one single interval on the infinite line, the conformal invariance allows us to write

$$\mathrm{Tr}\rho_A^n = \langle \mathcal{T}_n(u)\bar{\mathcal{T}}_n(v)\rangle = c_n \left(\frac{|u-v|}{\epsilon}\right)^{-2\Delta_n}. \tag{1.4.12}$$

where c_n is the normalisation of the twist operators and ϵ is an ultraviolet cutoff. This expression for the moments of ρ_A leads to the famous scaling results ($|u-v| = \ell$) [20]

$$S_n^A = \frac{n+1}{n}\frac{c}{6}\log(\ell/\epsilon), \quad S_1^A = \frac{c}{3}\log(\ell/\epsilon). \tag{1.4.13}$$

Another framework in which the twist fields represent a powerful tool is the computation of the negativity. As shown in [152], if we take the partial transpose $\rho_A^{T_1}$ with respect to the degrees of freedom living on the interval $A_1 = [u_1, v_1]$, $\mathrm{Tr}(\rho_A^{T_1})^n$ can be written as a twist field correlator as in Eq. (1.4.9), the only difference being that the twist fields $\mathcal{T}_n$ and $\bar{\mathcal{T}}_n$ at the endpoints of A_1 are exchanged while the remaining ones stay untouched, i.e. [151, 152]

$$\mathrm{Tr}(\rho_A^{T_1})^n = \langle \bar{\mathcal{T}}_n(u_1)\mathcal{T}_n(v_1)\prod_{i=2}^{p}\mathcal{T}_n(u_i)\bar{\mathcal{T}}_n(v_i)\rangle. \tag{1.4.14}$$

This procedure can be generalised straightforwardly to the case where the partial transposition involves more than two intervals (the corresponding geometry for two intervals in the ground state is depicted in the right-hand-side of Fig. 1.3).

The situation in which $p = 2$ intervals are adjacent can be obtained from Eq. (1.4.14) by taking the limit $u_2 \to v_1$, giving $\mathrm{Tr}(\rho_A^{T_1})^n = \langle \bar{\mathcal{T}}_n(u_1)\mathcal{T}_n^2(u_2)\bar{\mathcal{T}}_n(v_2)\rangle$. As we already discussed for Eq. (1.4.9), in a generic CFT characterised by a central charge c, this last expectation value is evaluated by knowing the conformal dimensions of $\mathcal{T}_n, \bar{\mathcal{T}}_n$, $\mathcal{T}_n^2$ and $\bar{\mathcal{T}}_n^2$. The scaling dimensions of $\mathcal{T}_n^2$ and $\bar{\mathcal{T}}_n^2$ are equal, and depend on the parity of n as [151]

$$\Delta_n^{(2)} \equiv \begin{cases} \Delta_n & \text{odd } n \\ 2\Delta_{n/2} & \text{even } n \end{cases}, \tag{1.4.15}$$

where Δ_n are the scaling dimensions of $\mathcal{T}_n, \bar{\mathcal{T}}_n$ in Eq. (1.4.11).

1.4.2 Charged moments approach

In this subsection, we will find out how the replica trick can be also helpful for determing the SRREs up to slight modifications of what we have showed in the previous subsection.
The computation of the SREEs from the definitions of Eq. (1.3.3) requires the knowledge of the entanglement spectrum of ρ_A and its symmetry resolution. However, this is usually a very difficult

task, in particular if one is interested in analytical expressions. Alternatively, one can employ the *charged moments* of the RDM, which for ρ_A are defined as [84]

$$Z_n^A(\alpha) = \mathrm{Tr}[\rho_A^n e^{i\alpha Q_A}]. \tag{1.4.16}$$

Similar quantities were independently studied in holographic theories [158–161,163,164,631]. They can be interpreted as the partition function of the field theory on a Riemann surface, which is now coupled to an external magnetic flux. Partition functions with a background gauge field have been also introduced as non-local order parameters to detect symmetry-protected topological phases in interacting fermionic systems [165, 166].

In this specific case, the charged moments are not the main goal of our computations, but they represent a fundamental tool, because their Fourier transforms are the moments of the RDM restricted to the sector of fixed charge q

$$\mathcal{Z}_n^A(q) \equiv \mathrm{Tr}(\Pi_q \, \rho_A^n) = \int_{-\pi}^{\pi} \frac{d\alpha}{2\pi} e^{-i\alpha q} Z_n^A(\alpha), \quad p(q) \equiv \mathcal{Z}_1(q). \tag{1.4.17}$$

Here we rely on the Fourier representation of the projection operator, that can be also extended to the non-abelian case, as we will show in Chapter 3. Finally, the SREEs are given by

$$S_n^A(q) = \frac{1}{1-n} \log \left[\frac{\mathcal{Z}_n^A(q)}{\big(\mathcal{Z}_1^A(q)\big)^n} \right], \quad S_1^A(q) = \lim_{n\to 1} S_n^A(q). \tag{1.4.18}$$

The charged moments of ρ_A can be computed employing the framework of Sec. 1.4.1. As it is argued in Ref. [84], the operator $e^{i\alpha Q_A}$ can be interpreted as a magnetic flux between the sheets of the surface $\mathcal{R}_n$, such that a charged particle moving along a closed path that crosses all the sheets acquires a phase $e^{i\alpha}$. For this reason, we dub the modified surface $\mathcal{R}_{n,\alpha}$ (we stress that the geometry of the Riemann surface does not change, but the subscript α is helpful to keep in mind the presence of the flux). The phase can be implemented by a local $U(1)$ operator $\mathcal{V}_\alpha(x)$ that generates a phase shift $e^{i\alpha}$ along A (see also Fig. 1.4). If we are interested in one single interval on the infinite line, $A = [u, v]$, then the charged moments are equal to the two-point correlation function on the surface $\mathcal{R}_{n,\alpha}$

$$Z_n^A(\alpha) = Z_n^A(0) \langle \mathcal{V}_\alpha(u) \mathcal{V}_{-\alpha}(v) \rangle_{\mathcal{R}_{n,\alpha}}. \tag{1.4.19}$$

In the orbifold theory, the magnetic flux can be incorporated by considering the composite twist field $\mathcal{T}_{n,\alpha} \equiv \mathcal{T}_n \cdot \mathcal{V}_\alpha$. Thus, if we take a field $\mathcal{O}_k$ in the copy k of the orbifold, then the winding $(z-u) \mapsto e^{2\pi i}(z-u)$ around the point u where $\mathcal{T}_{n,\alpha}$ is inserted gives rise to a phase $e^{i\alpha/n}$,

$$\mathcal{T}_{n,\alpha}(u) \mathcal{O}_k(e^{2\pi i}(z-u)) = e^{i\alpha/n} \mathcal{O}_{k+1}(z-u) \mathcal{T}_{n,\alpha}(u). \tag{1.4.20}$$

Therefore, Eq. (1.4.19) can be reexpressed as the two-point function of the orbifold

$$Z_n^A(\alpha) = \langle \mathcal{T}_{n,\alpha}(u) \bar{\mathcal{T}}_{n,-\alpha}(v) \rangle. \tag{1.4.21}$$

In Ref. [84], it is shown that, if $\mathcal{V}_\alpha$ is a spinless primary operator with conformal weight $\Delta_\alpha^{\mathcal{V}}$, then so are the composite twist and antitwist fields, with conformal weights

$$\Delta_{n,\alpha} = \Delta_n + \frac{\Delta_\alpha^{\mathcal{V}}}{n}. \tag{1.4.22}$$

where Δ_n is given in Eq. (1.4.11).
The relation between the SREE and the charged moments can be further extended. For example,

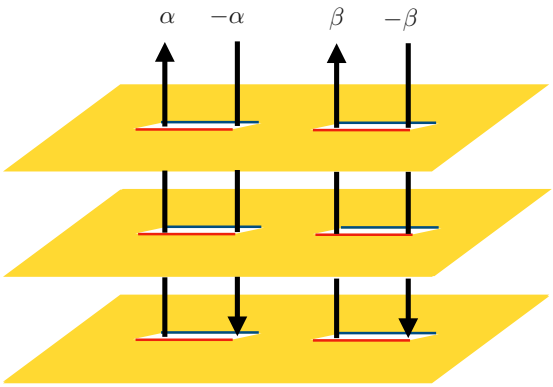

Figure 1.4: Representation of the n-sheeted Riemann surface $\mathcal{R}_{n,\alpha}$ for $n = 3$. The calculation of the multi-charged moments in Eq. (1.4.23) requires to insert different magnetic fluxes between the sheets, which we indicate by the arrows. The operator $e^{i\alpha Q_{A_1}}$ is implemented by the flux insertions α and $-\alpha$ along the left interval, while $e^{i\beta Q_{A_2}}$ corresponds to the fluxes β and $-\beta$ at the right interval.

to compute the symmetry resolved mutual information of Eq. (1.3.6), we need to determine $p(q_1, q-q_1)$, i.e. the probability that a measurement of Q_{A_1} and Q_{A_2} gives q_1 and $q-q_1$ respectively, with Q_A fixed to q. Thus, we can consider the generalisation of the charged moments in Eq. (1.4.16) introduced for the first time in Ref. [133],

$$Z_n^{A_1:A_2}(\alpha,\beta) = \mathrm{Tr}\left[\rho_A^n e^{i\alpha Q_{A_1}+i\beta Q_{A_2}}\right]. \tag{1.4.23}$$

We refer to them as *multi-charged moments* (see Fig. 1.4 and Chapter 4 for further details about this quantity). If we take the Fourier transform of Eq. (1.4.23),

$$\mathcal{Z}_n^{A_1:A_2}(q_1,q_2) = \int_{-\pi}^{\pi} \frac{d\alpha}{2\pi}\frac{d\beta}{2\pi} e^{-i\alpha q_1 - i\beta q_2} Z_n^{A_1:A_2}(\alpha,\beta), \tag{1.4.24}$$

then $\mathcal{Z}_1^{A_1:A_2}(q_1,q_2)$ can be interpreted as the probability of having q_1 and q_2 as outcomes of a measurement of Q_{A_1} and Q_{A_2} respectively, independently of the value of Q_A. Therefore, it satisfies the normalisation

$$\sum_{q_1,q_2} \mathcal{Z}_1^{A_1:A_2}(q_1,q_2) = 1, \tag{1.4.25}$$

and $p(q_1, q-q_1)$ can be calculated as the conditional probability

$$p(q_1,q-q_1) = \frac{\mathcal{Z}_1^{A_1:A_2}(q_1,q-q_1)}{p(q)}. \tag{1.4.26}$$

Let us conclude this section by explaining how the charged moments can be adapted for the computation of the charged moments of the RDM after the partial transpose operation, defined as

$$N_n^A(\alpha) = \mathrm{Tr}((\rho_A^{T_1})^n e^{iQ_{\mathrm{imb}}\alpha}). \tag{1.4.27}$$

We focus on two intervals $A = [u_1, v_1] \cup [u_2, v_2]$ on the infinite line. The phase factor $e^{i\alpha Q_{\mathrm{imb}}}$ can be implemented by two operators at u_1 and v_1, $\mathcal{V}_{-\alpha}$ and $\mathcal{V}_\alpha$ respectively, and two operators $\mathcal{V}_\alpha$ at

u_2 and $\mathcal{V}_{-\alpha}$ at v_2. In terms of the composite twist field $\mathcal{T}_{n,\alpha}$, in the limit $v_1 \to u_2$, the charged moments of the partial transpose read [116]

$$N_n^A(\alpha) = \langle \bar{\mathcal{T}}_{n,-\alpha}(u_1)\mathcal{T}^2_{n,2\alpha}(v_1)\bar{\mathcal{T}}_{n,-\alpha}(v_2)\rangle\,. \tag{1.4.28}$$

The conformal weight of $\mathcal{T}^2_{n,2\alpha}$ is

$$\Delta^{(2)}_{n,\alpha} = \Delta^{(2)}_n + \frac{\Delta^{\mathcal{V}}_{2\alpha}}{n}. \tag{1.4.29}$$

where $\Delta^{(2)}_n$ is given in Eq. (1.4.15). In order to correctly perform the replica limit, we have to distinguish the Fourier transforms to take as

$$\mathcal{Z}^A_n(q_{\rm imb}) = \int_{-\pi}^{\pi}\frac{d\alpha}{2\pi}e^{-i\alpha q_{\rm imb}}N^A_n(\alpha), \quad p(q_{\rm imb}) = \int_{-\pi}^{\pi}\frac{d\alpha}{2\pi}e^{-i\alpha q_{\rm imb}}N^A_1(\alpha), \tag{1.4.30}$$

from which the charge-imbalance resolved negativity reads

$$\mathcal{N}^A(q_{\rm imb}) = \frac{1}{2}\Big(\lim_{n_e\to 1}\frac{\mathcal{Z}^A_{n_e}(q_{\rm imb})}{p(q_{\rm imb})} - 1\Big). \tag{1.4.31}$$

1.4.3 Entanglement entropy from correlation matrix

Let us conclude this overview about the techniques to compute entanglement in extended quantum systems by exploring what can be done numerically in some priviledged contexts. It is clear that the computation of the REEs from the RDM ρ_A is a difficult task when the dimension of A is large enough. However, for the eigenstates of quadratic lattice Hamiltonians, we can bypass this problem expressing S^A_n in terms of the two-point correlation functions [167–169]. We are going to illustrate this computation of entanglement entropies in an exact and numerically efficient way focusing on fermionic systems, but similar techniques are available for free bosonic systems as well [170, 171].

Let us consider free fermions hopping on a N-site lattice with a general Hamiltonian

$$H = \sum_{n,m=1}^{N}\epsilon_{nm}c^\dagger_n c_m. \tag{1.4.32}$$

with $c^\dagger(c)$ denoting the creation (annihilation) fermionic operators. The ground-state $|\Psi\rangle$ is a Slater determinant and, therefore, it satisfies the Wick theorem: all even higher-order correlation functions can be written in terms of the two-point function, $C_{nm} = \langle\Psi|c^\dagger_n c_m|\Psi\rangle$, e.g.

$$\langle\Psi|c^\dagger_m c^\dagger_n c_k c_l|\Psi\rangle = C_{ml}C_{nk} - C_{mk}C_{nl}. \tag{1.4.33}$$

Taking a subsystem A with ℓ contiguous sites corresponds to restrict the correlation matrix to the subsystem, C^A_{nm}, with $n, m \in A$. By Wick theorem, it is possible to show that ρ_A can be written as a Gaussian operator [19, 167, 169, 172]

$$\rho_A = \frac{1}{Z}e^{-\mathcal{H}_A}, \quad H_A = \sum_{i,j=1}^{\ell}h_{i,j}c^\dagger_i c_j, \tag{1.4.34}$$

where Z is a normalisation constant and H_A is called entanglement Hamiltonian. In order to diagonalise it, it is necessary to introduce the fermionic operators d_k performing a linear transformation

$$c_j = \sum_{k=1}^{l}\phi_k(j)d_k, \tag{1.4.35}$$

where $\phi_m(j)$ are the eigenfunctions of $h_{i,j}$ with eigenvalues ε_k. In this case, H_A becomes

$$H_A = \sum_{k=1}^{l} \varepsilon_k d_k^\dagger d_k = \sum_{i,j=1}^{l} \sum_{k=1}^{l} \varepsilon_k \phi_k(i) \phi_k^*(j) c_i^\dagger c_j \to h_{ij} = \sum_{k=1}^{l} \varepsilon_k \phi_k(i) \phi_k^*(j). \tag{1.4.36}$$

The first thing to do is to relate the eigenvalues ε_k of H_A to those of the correlation matrix:

$$C_{ij}^A = \mathrm{Tr}(\rho_A c_i^\dagger c_j) = \sum_{k,k'=1}^{l} \phi_k(i) \phi_{k'}^*(j) \mathrm{Tr}_A(\rho_A d_k^\dagger d_{k'}). \tag{1.4.37}$$

By computing the correlator

$$\mathrm{Tr}_A(\rho_A d_k^\dagger d_{k'}) = \frac{1}{Z} \mathrm{Tr}_A[e^{-\sum_{k=1}^{l} \varepsilon_k d_k^\dagger d_k} d_k^\dagger d_{k'}] = \frac{\delta_{kk'}}{1+e^{\varepsilon_k}}, \tag{1.4.38}$$

we find

$$C_{ij}^A = \sum_{k=1}^{l} \frac{1}{1+e^{\varepsilon_k}} \phi_k(i) \phi_k^*(j). \tag{1.4.39}$$

Therefore, the eigenvalues of C^A are

$$\zeta_k = (1+e^{\varepsilon_k})^{-1} \tag{1.4.40}$$

or, in matrix form, we can write

$$h = \log[(1-C^A)/C^A]. \tag{1.4.41}$$

As a consequence, the diagonalisation of an $\ell \times \ell$ matrix C_A leads to the RDM ρ_A. Indeed, since the k-fermionic modes are uncorrelated, the RDM can be rewritten as

$$\rho_A = \bigotimes_{k=1}^{\ell} \frac{e^{-\varepsilon_k d_k^\dagger d_k}}{Z_k}, \tag{1.4.42}$$

where each single term in the Kronecker product can be interpreted as a single-particle RDM, and therefore Z_k has to be chosen to normalise it, i.e. $Z_k = 1 + e^{-\varepsilon_k}$. If the k-mode is occupied, the eigenvalues of ρ_A are given by $\dfrac{e^{-\varepsilon_k}}{1+e^{-\varepsilon_k}} = \zeta_k$, otherwise they are given by $\dfrac{1}{1+e^{-\varepsilon_k}} = 1-\zeta_k$.
One could also work with Majorana operators, $a_{2n-1} = (c_n + c_n^\dagger)$ and $a_{2n} = i(c_n - c_n^\dagger)$, and form the $2N \times 2N$ correlation matrix $\Gamma_{mn} = \langle a_m a_n \rangle - \delta_{mn}$. Both methods work for all states which satisfy Wick theorem and they can be also generalised to compute the REEs when $|\Psi\rangle$ is an excited state of Eq. (1.4.32).
The relation found between ρ_A and C_{nm}^A implies a drastic reduction of the computational complexity, from an exponential to a polynomial dependence on the size of the system. This simplification of the problem is valid provided that the density matrix satisfies the Wick decomposition (i.e. it describes a Gaussian state) and, therefore, all the information about the state is encoded in the two-point correlation functions.
At this point, the computation of entanglement entropies from the eigenvalues of C^A, ζ_k, is quite simple: the REEs read as

$$S_n^A = \frac{1}{1-n} \sum_{i=1}^{\ell} \log[\zeta_i^n + (1-\zeta_i)^n]. \tag{1.4.43}$$

whose limit $n \to 1$ gives

$$S_1^A = -\sum_{i=1}^{\ell} \left[\zeta_i \log \zeta_i + (1-\zeta_i)\log(1-\zeta_i)\right]. \tag{1.4.44}$$

If we are interested in the computation of the charged moments $Z_n(\alpha)$, we can write down the charge operator as

$$Q_A = \sum_{i\in A} c_i^\dagger c_i = \sum_{k=1}^{\ell} d_k^\dagger d_k, \tag{1.4.45}$$

such that

$$\rho_A e^{i\alpha Q_A} = \bigotimes_{k=1}^{\ell} \frac{e^{(-\varepsilon_k + i\alpha) d_k^\dagger d_k}}{Z_k}. \tag{1.4.46}$$

This allows us to express the charged moments in terms of the eigenvalues ζ_k as [84, 90]

$$Z_n^A(\alpha) = \sum_{i=1}^{\ell} \log[e^{i\alpha}\zeta_i^n + (1-\zeta_i)^n]. \tag{1.4.47}$$

The computation of the REE from the eigenvalues of the correlation matrix can be generalised to other entanglement measures. For example, the partial transpose of a bosonic Gaussian state is again a Gaussian operator and this simplifies the calculation of the negativity [173]. The analogous result for fermionic Gaussian states does not hold. This has motivated the introduction of another way of implementing a fermionic partial transpose [163], which has the merit that the partially transposed Gaussian state remains Gaussian and hence can be computed efficiently for free fermions. We will come back to this in the third part of this thesis.
We conclude this section by showing another powerful application of the algebra of Gaussian RDMs. When looking at the trace of products of RDMs in different eigenstates, they usually do not commute and so they cannot be simultaneously diagonalised in a common base. However, it is possible to use the composition properties of Gaussian density matrices [174]: let $\rho[\Gamma]$ denote a Gaussian density matrix characterised by its correlation function Γ written in terms of Majorana fermions as $\Gamma^{\Omega}_{ij} = \langle a_i a_j \rangle_\Omega - \delta_{ij}$, where Ω stands for the set of occupied single-particle levels. The composition of correlation matrices is indicated by $\Gamma \times \Gamma'$ and it is implicitly defined by

$$\rho[\Gamma]\rho[\Gamma'] = \mathrm{Tr}[\rho[\Gamma]\rho[\Gamma']]\rho[\Gamma \times \Gamma'], \tag{1.4.48}$$

leading to [174]

$$\Gamma \times \Gamma' = 1 - (1-\Gamma')\frac{1}{1+\Gamma\Gamma'}(1-\Gamma). \tag{1.4.49}$$

The trace of two fermionic operators can be computed as

$$\{\Gamma, \Gamma'\} \equiv \mathrm{Tr}(\rho_\Gamma \rho_{\Gamma'}) = \prod_{\mu \in \mathrm{Spectrum}[\Gamma\Gamma']/2} \frac{1+\mu}{2}, \tag{1.4.50}$$

namely it is the product of the eigenvalues of $(1+\Gamma\Gamma')/2$ with halved degeneracy.

1.5 Organisation of the thesis

The content of this thesis is provided by the research projects I have been doing during my PhD, thanks to several collaborations in and outside SISSA. After a general and broad introduction that has allowed me to define the main topics I will deal with throughout the thesis, it consists of three Parts, each one containing different Chapters. Let us look at their content in more details.

Part I The main problems we address in the first part concern the study of entanglement in (1+1)-dimensional QTFs, with particular care about the effect of symmetries on our systems.

- The first example of this thesis in which the symmetry resolution of entanglement is analysed is the content of Chapter 2: the systems under consideration are free quantum field theories, in particular Dirac and complex scalar fields in two dimensional dimensions, both in the massive and massless cases.
- In the realm of entanglement resolution, we tackle the non-abelian problem in Chapter 3. We consider systems having, in addition to conformal invariance, an internal Lie group symmetry. By using some group theory tools, we try to study the information one can get from the symmetry resolved entanglement about the underlying group structure.
- The analysis of the symmetry resolved mutual information in Chapter 4 allows us to study the multi-charged moments for two disjoint intervals in the ground state of two (1+1)-dimensional CFTs, i.e. the massless Dirac field theory and the compact boson.
- The replica trick and its implementation via the path-integral finds wide place in Chapter 5: for a free bosonic theory, the mode expansion of the fields allow us to develop an efficient strategy to compute the second generalised Rényi entropy for all the eigenstates of a (1+1)-dimensional CFT.
- The findings of the previous Chapter represent the starting point to develop a simulation scheme ideal to compute the entanglement in more generic (1+1)-dimensional QFTs. This is done in Chapter 6, by applying this technique to compute the entanglement after a quench in the sine-Gordon field theory.

Part II A typical framework in which entanglement is studied are lattice models, where different techniques can be exploited in order to derive exact results: in the second part of this thesis, these methods will be applied to study the symmetry resolution of entanglement.

- In Chapter 7, we study the symmetry resolved entanglement entropies in gapped integrable lattice models, finding exact results for a free system of complex bosons and the XXZ spin-chain. The connection between the symmetry resolved entanglement and the full counting statistics is also discussed. The key tool we adopt is the corner transfer matrix.
- We apply the dimensional reduction to study lattice models in any (spatial) dimension in Chapter 8: this strategy is based on the reduction of the initial d-dimensional problem into decoupled $d-1$-dimensional ones in a mixed space-momentum representation. We focus on the case $d=2$ and two lattice models possessing a $U(1)$ symmetry, i.e. free non-relativistic massless fermions and free complex (massive and massless) bosons.
- Chapter 9 is devoted to the investigation of the symmetry resolution of entanglement in the presence of long-range couplings. This feature of the system strongly affects entanglement, starting from the logarithmic behaviour with the size of the subsystem despite the mass gap.
- Inspired by the works by Page about entanglement in random pure states [30], we find some interesting analytical expressions about the symmetry resolved Page curves for Haar-random pure states and random fermionic Gaussian states in Chapter 10.
- Not only symmetries play a special role in this thesis, but also quantifying how much a symmetry is broken. This is the main topic of Chapter 11, where we introduce the notion of *entanglement asymmetry* as a subsystem measure of symmetry breaking.

Part III The third and last part of this thesis is focused on the study of entanglement in mixed-states, when the entanglement entropy does not properly describe the quantum correlations.

- Chapter 12 gives some standard definitions about the partial transpose operation and negativity, in particular for fermionic systems. Then, it also contains an operatorial characterisation of entanglemtent in mixed states, which we dub *negativity Hamiltonian*.
- In Chapter 13, we study the symmetry resolution of the entanglement negativity in free fermionic systems, which admits a decomposition in terms of the charge imbalance between the two subsystems.
- We compute the moments of the partial transpose RDM in Chapter 14. Given the relevance of these quantities which can be accessed experimentally in the context of the quantum simulation of many-body systems, we study their time evolution after a quench, providing a quasiparticle description for integrable models in the space-time scaling limit.
- In Chapter 15, we study the ground state of a (1+1)-dimensional CFT built with several species of massless free Dirac fermions coupled at one boundary point via a conformal junction. This system provides the playground to compute both the Rényi entropy for a given bipartition and the negativity between non-complementary parts.
- The last Chapter 16 contains the results of the first experimental measurement of the operator entanglement of a subsystem's RDM in a quantum many-body system. We also study the effect of the $U(1)$ symmetry, introducing the notion of symmetry resolved operator entanglement.

Every Chapter of this thesis contains an abstract, followed by a specific introduction, and the peculiar perspectives stemming from it. Still, this PhD work leaves room for many questions and open problems. The last Chapter contains some thoughts regarding promising directions for future research.

Part I

Entanglement and symmetries in quantum field theory

Chapter 2

Symmetry resolved entanglement entropies in quantum field theories

The main goal of this first Chapter is to investigate the field theoretical techniques for the computation of the charged moments in relativistic free two-dimensional quantum field theories (QFTs). Their Fourier transform provides the desired SRREs introduced in Eq. (1.3.3): we show that at the leading order, they satisfy entanglement equipartition and we identify the subleading terms that break it. This Chapter is based on Ref. [111].

2.1 Introduction

Let us present the first thorough analysis of the entanglement entropies related to different symmetry sectors of free QFTs with an internal $U(1)$ symmetry. We will mainly deal with a free fermionic field theory and with a complex scalar one, whose Euclidean actions are given, respectively, by

$$\begin{aligned} S_D =& \frac{1}{4\pi}\int dz d\bar{z}\,(\psi_R^*\partial_z\psi_R + \psi_L^*\partial_{\bar{z}}\psi_L + m(\psi_L^*\psi_R + \psi_R^*\psi_L)\,, \\ S_S =& \frac{1}{4\pi}\int dz d\bar{z}\,\left(\partial_z\varphi^*\partial_{\bar{z}}\varphi + \partial_{\bar{z}}\varphi^*\partial_z\varphi + m^2\varphi^*\varphi\right), \end{aligned} \tag{2.1.1}$$

where we employ complex coordinates $(z, \bar{z})$ for the two-dimensional spacetime. In S_D the fields $\psi_{R/L}$ are the chiral (right-moving R) and anti-chiral (left-moving L) components of the Dirac fermion. In S_S the field φ is a complex scalar. The actions in (2.1.1) exhibit a $U(1)$ symmetry, i.e. a symmetry under phase transformations of the fields given, respectively, by

$$\psi_{R/L} \to e^{i\alpha}\psi_{R/L}, \quad \psi^*_{R/L} \to e^{-i\alpha}\psi^*_{R/L}, \qquad \varphi \to e^{i\alpha}\varphi, \quad \varphi^* \to e^{-i\alpha}\varphi^*. \tag{2.1.2}$$

By Noether's theorem, this continuous symmetry transformation leads to a conserved quantity, which is the charge Q we introduced in Sec. 1.3.

The actions (2.1.1) played the role of the simplest massive quantum field theories to study the properties of the entanglement entropy. In the same spirit, they also represent the natural starting point for the field theoretical investigation of the charged moments and, as a consequence, of the SRREs. We provide explicit analytic computations for the charged moments of Dirac and complex scalar fields in two spacetime dimensions, both in the massive and massless cases, using two different approaches.

The first one is based on the replica trick, the computation of the partition function on Riemann surfaces with the insertion of a flux α, and the introduction of properly modified twist fields, whose

two-point function directly gives the scaling limit of the charged moments, as we have already learnt from Sec. 1.4.2. Being the theory free, a further simplification arises by the diagonalisation in the replica space: the n-sheeted problem can be mapped to an equivalent one in which one deals with n decoupled and multivalued free fields, generically referred as $\tilde{\phi}_k$. Thus, also the twist fields can be written as products of fields acting only on $\tilde{\phi}_k$, denoted as $\mathcal{T}_{n,k}$ and $\bar{\mathcal{T}}_{n,k}$. The total partition function is a product of n partition functions, ζ_k, each one given by (up to unimportant multiplicative constant)

$$\zeta_k \propto \langle \mathcal{T}_{n,k}(z_1)\bar{\mathcal{T}}_{n,k}(z_2)\rangle \,. \tag{2.1.3}$$

The second method also relies on mapping the problem from the determination of the partition function on $\mathcal{R}_n$, to the computation of n partition functions of a free field on a cut plane. However, the difference with respect to the previous approach is that each ζ_k is not computed as a two point-function of twist fields, but using the relation between the free energy and the Green's function of each sector k. Denoting by G_D the Green's function for the Dirac field and by G_S the one for the scalar (in each sector k of the n copies), they are related to the corresponding partition function ζ_k by, respectively,

$$\partial_m \log \zeta_k = \operatorname{tr} G_D, \qquad \partial_{m^2} \log \zeta_k = -\int dr^2\, G_S(\mathbf{r},\mathbf{r}'). \tag{2.1.4}$$

The strategy of Refs. [176, 177] was to exploit the rotational and translational symmetry of the Helmholtz equations satisfied by G_D and G_S and analyse their behaviour at the singular endpoints of the cut A so to determine the right hand sides of the above equations. The final expressions for ζ_k can be expressed in terms of the solution of second order non linear differential equations of the Painlevé V type. Here we only report the final results for the Rényi entropies of free fields in the limit $m\ell \to 0$ with $t = m\ell$ fixed [176, 177]

$$\begin{aligned} S_n^D =& \frac{n+1}{6n}\left(\log\frac{\ell}{\epsilon} - \frac{(m\ell)^2}{2}\log^2 m\ell\right) + O((m\ell)^2\log m\ell), \\ S_n^S =& \frac{n+1}{3n}\log\frac{\ell}{\epsilon} + \log\frac{\log m\ell}{\log m\epsilon} + O(m\ell). \end{aligned} \tag{2.1.5}$$

The Chapter is organised as follows. We report our main findings in Secs. 2.2, 2.3, and 2.4: in the first we employ the twist fields to compute the charged moments both in the massless and in the massive context (in the limit $m\ell \gg 1$). These results are extended in Secs. 2.3 and 2.4, where we write down the explicit form of the charged moments for arbitrary $m\ell$ and provide analytic asymptotic expansions valid for large and small $m\ell$. These outcomes are the starting point for the computation of the SRREs. Numerical checks for free fermions and bosons on the lattice are also provided as a benchmark of the analytical results. We draw our conclusions in Sec. 2.5 and we include a small appendix with some technicalities about the conformal dimensions of the twist fields.

2.2 Twist Field Approach

In this section we consider $1d$ critical and close to critical systems. We obtain a general exact result for the conformal invariant charged moments by exploiting the properties of the modified twist fields [158, 161]. This result includes and generalises the ones in Ref. [84]. The same approach also provides the leading asymptotic behaviour of the charged moments for (free) massive field theories.

2.2.1 Modified Twist Fields

As already mentioned in Sec. 1.4.2, rather than dealing with fields defined on a non trivial manifold $\mathcal{R}_{n,\alpha}$, it is more convenient to work on a single plane with a n-component field

$$\Phi = \begin{pmatrix} \phi_1 \\ \phi_2 \\ \vdots \\ \phi_n \end{pmatrix}, \tag{2.2.1}$$

where ϕ_j is the field on the j-th copy (here the field ϕ_j generically refers to either a scalar field φ_j or a chiral Dirac one ψ_j; the same applies to $\tilde{\phi}_k$ that we are going to introduce soon). Upon crossing the cut A, the vector field Φ transforms according to the transformation matrix T_α

$$T_\alpha = \begin{pmatrix} 0 & e^{i\alpha/n} & & \\ & 0 & e^{i\alpha/n} & \\ & & \ddots & \ddots \\ (-1)^{(n+1)f} e^{i\alpha/n} & & & 0 \end{pmatrix}, \tag{2.2.2}$$

where $f = 1$ for free Dirac fermions and $f = 0$ for free complex scalars. When $\alpha = 0$ we recover the usual transformations for the fields across the different replicas [178]. The matrix T_α has eigenvalues

$$\begin{aligned} f = 0: &\qquad \lambda_k = e^{i\frac{\alpha}{n}} e^{2\pi i \frac{k}{n}}, \quad k = 0, \dots, n-1, \\ f = 1: &\qquad \lambda_k = e^{i\frac{\alpha}{n}} e^{2\pi i \frac{k}{n}}, \quad k = -\frac{n-1}{2}, \dots, \frac{n-1}{2}. \end{aligned} \tag{2.2.3}$$

By diagonalising T_α with a unitary transformation, the problem is reduced to n decoupled fields $\tilde{\phi}_k$ in a $2d$ spacetime. Thus, the total partition function is a product of the partition functions for each k and the twist fields can be written as products of fields each acting on a different $\tilde{\phi}_k$, i.e.

$$\begin{aligned} f = 0: &\qquad \mathcal{T}_{n,\alpha} = \prod_{k=0}^{n-1} \mathcal{T}_{n,k,\alpha}, \qquad \tilde{\mathcal{T}}_{n,\alpha} = \prod_{k=0}^{n-1} \tilde{\mathcal{T}}_{n,k,\alpha}, \\ f = 1: &\qquad \mathcal{T}_{n,\alpha} = \prod_{k=-\frac{n-1}{2}}^{\frac{n-1}{2}} \mathcal{T}_{n,k,\alpha}, \qquad \bar{\mathcal{T}}_{n,\alpha} = \prod_{k=-\frac{n-1}{2}}^{\frac{n-1}{2}} \bar{\mathcal{T}}_{n,k,\alpha}, \end{aligned} \tag{2.2.4}$$

with $\mathcal{T}_{n,k,\alpha}\tilde{\phi}_{k'} = \delta_{k,k'} e^{i\alpha/n} e^{2\pi i k/n} \tilde{\phi}_k$ and $\tilde{\mathcal{T}}_{n,k,\alpha}\tilde{\phi}_{k'} = \delta_{k,k'} e^{-i\alpha/n} e^{-2\pi i k/n} \tilde{\phi}_k$. Since the partition function on $\mathcal{R}_{n,\alpha}$ can be written as the two-point function of the modified twist fields, from (2.2.4) we have

$$\begin{aligned} f = 0: &\qquad \log Z_n(\alpha) = \sum_{k=0}^{n-1} \log \langle \mathcal{T}_{n,k,\alpha} \bar{\mathcal{T}}_{n,k,\alpha} \rangle, \\ f = 1: &\qquad \log Z_n(\alpha) = \sum_{k=-(n-1)/2}^{(n-1)/2} \log \langle \mathcal{T}_{n,k,\alpha} \bar{\mathcal{T}}_{n,k,\alpha} \rangle. \end{aligned} \tag{2.2.5}$$

When dealing with a CFT (e.g. when $m = 0$ in (2.1.1)) $\mathcal{T}_{n,k,\alpha}$ and $\bar{\mathcal{T}}_{n,k,\alpha}$ are primary operators and their two-point function is fixed by conformal invariance to be

$$\langle \mathcal{T}_{n,k,\alpha} \bar{\mathcal{T}}_{n,k,\alpha} \rangle \propto \frac{1}{|u-v|^{4\Delta_k(\alpha)}}, \tag{2.2.6}$$

where (see the Appendix)

$$\begin{aligned} f=0: \qquad & \Delta_k(\alpha)=\frac{1}{2}\left(\frac{k}{n}+\frac{|\alpha|}{2\pi n}\right)\left(1-\frac{k}{n}-\frac{|\alpha|}{2\pi n}\right), \\ f=1: \qquad & \Delta_k(\alpha)=\frac{1}{2}\left(\frac{k}{n}+\frac{\alpha}{2\pi n}\right)^2. \end{aligned} \tag{2.2.7}$$

Let us stress that, in order to have operators with positive conformal dimension, the phase that bosons pick up going around one of the entangling points must be $0<\frac{k}{n}+\frac{\alpha}{2\pi n}<1$. This can be achieved, since $\alpha\in[-\pi,\pi]$, by trading α with $|\alpha|$ when we deal with scalar field theories.

Using Eqs. (2.2.5), (2.2.6) and (2.2.7) the logarithm of the partition function on $\mathcal{R}_{n,\alpha}$ reads

$$\begin{aligned} f=0: \quad & \log Z_n(\alpha)=-4\log\ell\sum_{k=0}^{n-1}\Delta_k(\alpha)=-\left[\frac{1}{3}\left(n-\frac{1}{n}\right)-\frac{\alpha^2}{2\pi^2 n}+\frac{|\alpha|}{\pi n}\right]\log\ell, \\ f=1: \quad & \log Z_n(\alpha)=-4\log\ell\sum_{k=-\frac{n-1}{2}}^{\frac{n-1}{2}}\Delta_k(\alpha)=-\left[\frac{1}{6}\left(n-\frac{1}{n}\right)+\frac{2}{n}\left(\frac{\alpha}{2\pi}\right)^2\right]\log\ell. \end{aligned} \tag{2.2.8}$$

The charged moments for the free massless Dirac field theory ($f=1$) have been already worked out in the literature with different techniques [84, 85, 158, 161]. Instead, the charged moments for a free massless complex scalar field ($f=0$) are consistent with the Appendix A of [158], where the heat kernel techniques have been exploited.

Let us stress that the presence of a flux in the Riemann surface changes some features of the twist fields in CFT: they remain primary operators (see Appendix for details), but they do depend on the theory and are not anymore identified only by the central charge (see also [84]).

2.2.2 Massive field theory and flux insertion

We now compute the charged moments $Z_n(\alpha)$ of a massive relativistic $2d$ QFT on the infinite line for a bipartition in two semi-infinite lines. Thus, we follow the same logic as in [20] (i.e. the continuum version of Baxter corner transfer matrix approach [179] for the reduced density matrix [20,180,182,353]), which in turn parallels the proof of the c-theorem by Zamolodchikov [183]. The results of this section are not limited to free theories but hold for *generic massive relativistic* QFT. Exploiting the rotational invariance about the origin of the Riemann surface $\mathcal{R}_{n,\alpha}$, the expectation values of the stress tensor of a massive euclidean QFT in complex coordinates, $T\equiv T_{zz}, \bar{T}\equiv T^*_{\bar{z}\bar{z}}$, and the trace, $\Theta\equiv 4T_{z\bar{z}}$, have the form

$$\begin{aligned} \langle T(z,\bar{z})\rangle &= F_{n,\alpha}(z\bar{z})/z^2, \\ \langle\Theta(z,\bar{z})\rangle-\langle\Theta\rangle_{1,\alpha=0} &= G_{n,\alpha}(z\bar{z})/z\bar{z}, \\ \langle\bar{T}(z,\bar{z})\rangle &= F_{n.\alpha}(z\bar{z})/\bar{z}^2, \end{aligned} \tag{2.2.9}$$

where $\langle\Theta\rangle_{1,\alpha=0}$ is a non-vanishing constant measuring the explicit breaking of scale invariance in the non-critical system, while $\langle T\rangle_{1,\alpha=0}$ and $\langle\bar{T}\rangle_{1,\alpha=0}$ both vanish. These quantities are related by the conservation equations of the stress-energy tensor ($4\partial_{\bar{z}}T+\partial_z\Theta=0$) as

$$(z\bar{z})\left(F'_{n,\alpha}+\frac{1}{4}G'_{n,\alpha}\right)=\frac{1}{4}G_{n,\alpha}. \tag{2.2.10}$$

The conservation equations as well as the rotational invariance are preserved in the presence of the flux α because the Riemann surface $\mathcal{R}_{n,\alpha}$ can be thought simply as a complex plane with

the insertion of two modified twist fields, as discussed in the previous subsection. Both $F_{n,\alpha}$ and $G_{n,\alpha}$ approach zero for $|z| \gg \xi$, while when $|z| \ll \xi$, they approach the CFT values given by the conformal dimension of the modified twist field, $\Delta_n(\alpha)$ [84]. Hence we have

$$\begin{aligned} F_{n,\alpha}^{CFT} &\to \frac{c}{24}\left(1-\frac{1}{n^2}\right)+\frac{\Delta_n(\alpha)}{n}, \\ G_{n,\alpha} &\to 0, \end{aligned} \tag{2.2.11}$$

and in particular for a massive Dirac field theory ($f=1$) and for a complex massive scalar theory ($f=0$), using the conformal weights (2.2.7), we have

$$\begin{aligned} F_{n,\alpha}^{f=1} &\to \frac{1}{24}\left(1-\frac{1}{n^2}\right)+\frac{1}{2n^2}\left(\frac{\alpha}{2\pi}\right)^2, \\ F_{n,\alpha}^{f=0} &\to \frac{1}{12}\left(1-\frac{1}{n^2}\right)+\frac{1}{2n^2}\left[\left(\frac{\alpha}{2\pi}\right)^2-\frac{|\alpha|}{2\pi}\right]. \end{aligned} \tag{2.2.12}$$

Changing variable to $R^2 = z\bar{z}$, we can rewrite the Eq. (2.2.10) as

$$R^2\frac{\partial}{\partial R^2}\left(F_{n,\alpha}(R^2)+\frac{1}{4}G_{n,\alpha}(R^2)\right)=\frac{1}{4}G_{n,\alpha}(R^2). \tag{2.2.13}$$

The corresponding integrated form using the boundary conditions in Eq. (2.2.11) is

$$\int_0^\infty \frac{G_{n,\alpha}(R^2)}{R^2}dR^2 = -\frac{c}{6}\left(1-\frac{1}{n^2}\right)-\frac{4\Delta_{n,\alpha}}{n}. \tag{2.2.14}$$

Taking into account the normalisation of the stress tensor, the definition of $G_{n,\alpha}$ in Eq. (2.2.9) and that $\int_{\mathcal{R}_n}\langle\Theta_{n,\alpha}\rangle\, dR^2$ corresponds to the variation of the free energy wrt a scale transformation (the mass m in this case) per each sheet of the whole n-sheeted surface, the left hand side of (2.2.14) is equal to

$$-\frac{2}{n}m\partial_m \log Z_n(\alpha). \tag{2.2.15}$$

We can therefore integrate this equation at fixed n and α to obtain $\log Z_n(\alpha)$. The additive non-universal integration constant can be absorbed in a UV cutoff $\epsilon_{n,\alpha}$ that consequently depends both on the Rényi index n and the parameter α (consistently with the lattice results in Ref. [90, 98] for massless theories). Finally we get

$$\log Z_n(\alpha) = \left[\frac{c}{12}\left(n-\frac{1}{n}\right)+2\Delta_n(\alpha)\right]\log(m\epsilon_{n,\alpha}), \tag{2.2.16}$$

or specialising to free Dirac ($f=1$) or complex Klein-Gordon ($f=0$) fields

$$f=1: \qquad \log Z_n(\alpha) = \left[\frac{1}{12}\left(n-\frac{1}{n}\right)+\frac{1}{n}\left(\frac{\alpha}{2\pi}\right)^2\right]\log(m\epsilon_{n,\alpha}), \tag{2.2.17}$$

$$f=0: \qquad \log Z_n(\alpha) = \left[\frac{1}{6}\left(n-\frac{1}{n}\right)-\frac{1}{n}\left(\frac{\alpha}{2\pi}\right)^2+\frac{|\alpha|}{2\pi n}\right]\log(m\epsilon_{n,\alpha}). \tag{2.2.18}$$

We anticipate that $\log Z_n(\alpha)$ for the Klein-Gordon field matches the continuum limit of a chain of complex oscillators obtained through the corner transfer matrix approach (see [98] and Chapter 7). We can specialise Eq. (2.2.16) to a Luttinger liquid with parameter K, whose underlying

field theory is a $c = 1$ CFT equivalent to a massless compact boson. In this case, one can use the results found in [84] for the conformal dimension of the modified twist field, obtaining

$$\log Z_n(\alpha) = \left[\frac{1}{12}\left(n - \frac{1}{n}\right) + \frac{K}{n}\left(\frac{\alpha}{2\pi}\right)^2\right] \log(m\epsilon_{n,\alpha}), \tag{2.2.19}$$

which for $K = 1$ gives the result found for fermions in Eq. (2.2.17), as it should.

2.2.3 From charged moments to symmetry resolved entropies

Performing the Fourier transforms of the charged moments above, one obtains symmetry resolved moments and entropies. For the Luttinger liquid, which includes Dirac Fermions at $K = 1$, the α dependence of the leading term is the same as in the massless cases. Hence the analysis is identical to the one of Refs. [84,90] and so we will just sketch the results here.The charged moments (ignoring for the time being the dependence on n and α of $\epsilon_{n,\alpha}$ in (2.2.19)), are

$$\mathcal{Z}_n(q) \simeq (m\epsilon)^{\frac{1}{12}\left(n-\frac{1}{n}\right)} \sqrt{\frac{n\pi}{K|\log m\epsilon|}} e^{-\frac{n\pi^2 q^2}{K|\log m\epsilon|}}, \tag{2.2.20}$$

and hence SRREs

$$S_n(q) = S_n - \frac{1}{2}\log\left(\frac{K}{\pi}|\log m\epsilon|\right) + O(1), \tag{2.2.21}$$

with S_n the total entropy. Exploiting the knowledge of $\mathcal{Z}_1(q)$ in (2.2.20) we also easily get the number or fluctuation entropy

$$S_{\rm num} = -\int_{-\infty}^{\infty} \mathcal{Z}_1(q) \log \mathcal{Z}_1(q) = \frac{1}{2}\log\left(\frac{K}{\pi}|\log m\epsilon|\right) + O(1)\,, \tag{2.2.22}$$

that in the sum for the total entropy cancels exactly the double logarithmic term in Eq. (2.2.21).

For the massive complex boson, we are interested in the Fourier transform of Eq. (2.2.18). In the saddle point approximation, we can neglect the term $\propto \alpha^2$ in Eq. (2.2.18) and the Fourier transform is

$$\mathcal{Z}_n(q) \simeq Z_n(0)\frac{2n|\log(m\epsilon)|}{4n^2\pi^2q^2 + \log^2(m\epsilon)} \simeq Z_n(0)\frac{2n}{|\log(m\epsilon)|}\left(1 - \frac{4n^2\pi^2q^2}{\log^2(m\epsilon)} + \dots\right), \tag{2.2.23}$$

and hence

$$S_n(q) = S_n - \log|\log m\epsilon| + O(1)\,, \tag{2.2.24}$$

with S_n the total entropy. Also in this case, one easily derives the number entropy from $\mathcal{Z}_1(q)$ obtaining again, at the leading order, the double logarithmic term in $S_n(q)$ in Eq. (2.2.24), i.e. $S_{\rm num} = \log(|\log m\epsilon|) + O(1)$.

2.3 The Green's function approach: The Dirac field

In this section we derive the charged moments for a massive Dirac field for arbitrary mass and then consider the limits of small and large mass. In Sec. 2.2.1 we showed that $Z_n(\alpha)$ can be written as product of partition functions ζ_a on the plane with proper boundary conditions along the cut A, explicitly given by

$$\tilde{\psi}_k(e^{2\pi i}z, e^{-2\pi i}\bar{z}) = e^{2\pi i a}\tilde{\psi}_k(z,\bar{z}), \qquad a = \frac{k}{n} + \frac{\alpha}{2\pi n}, \qquad k = -\frac{n-1}{2}, \cdots, \frac{n-1}{2}. \tag{2.3.1}$$

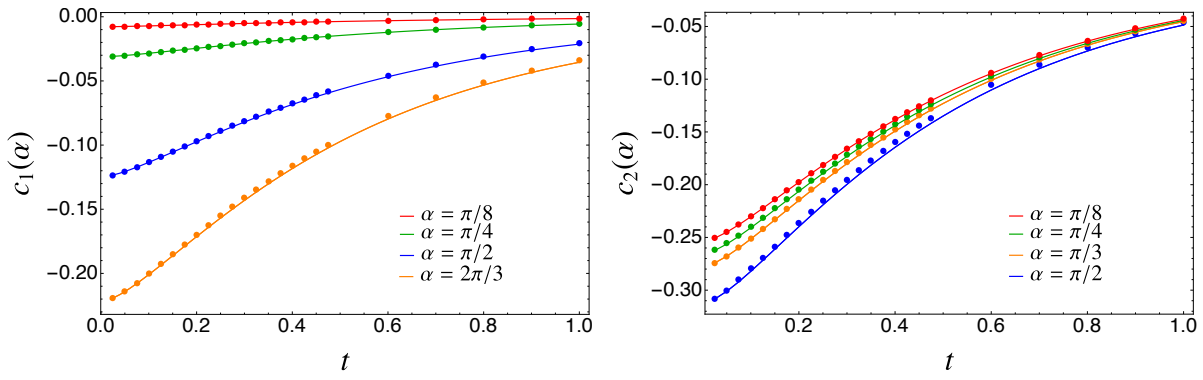

Figure 2.1: The universal constant $c_n(\alpha)$ extracted from the numerical solution of the Painlevé equation (2.3.6) for different values of α and n as a function of $t = m\ell$ (full lines). The numerical data are obtained varying ℓ between 200 and 400 lattice points and properly choosing m in such a way $t = m\ell \in (0, 1)$. For larger α and n, we need larger subsystem size to have a good match between field theory and lattice calculation because lattice corrections become stronger.

Hence we have

$$\log Z_n(\alpha) = \sum_{k=-\frac{n-1}{2}}^{\frac{n-1}{2}} \log \zeta_{\frac{k}{n}+\frac{\alpha}{2\pi n}}. \tag{2.3.2}$$

Let us introduce the auxiliary *universal* quantities

$$w_a \equiv \ell \partial_\ell \log \zeta_a, \qquad c_n(\alpha) \equiv \sum_k w_{\frac{k}{n}+\frac{\alpha}{2\pi n}}, \tag{2.3.3}$$

that, using (2.3.2), allow us to write the logarithmic derivative of the partition function in $\mathcal{R}_{n,\alpha}$ as

$$c_n(\alpha) = \ell \frac{\partial \log Z_n(\alpha)}{\partial \ell} \qquad \Rightarrow \qquad \log Z_n(\alpha) = \int_\epsilon^\ell \frac{c_n(\alpha)}{\ell'} d\ell'. \tag{2.3.4}$$

For $n = 1$, the function $c_n(\alpha)$ is the analogue of Zamolodchikov's c-function [183] in the presence of the flux α. The cutoff ϵ, in analogy to what discussed in Sec. 2.2.2 depends on both α and n, although we almost always omit such a dependence for conciseness.

As already discussed in Sec. 2.1, the key observation of this approach relies on the identity between the partition function ζ_a and the Green's function in the same geometry (see Eq. (2.1.4)). Through this relation, the function w_a has been already obtained for generic values of a for the massive Dirac fermion [176, 178].

The method that we just reviewed provides exact results for the charged moments of a free Dirac field. Indeed, in Ref. [176] it has been shown that the function w_a defined in (2.3.3) can be written as

$$w_a(t) = -\int_t^\infty y v_a^2(y) dy, \tag{2.3.5}$$

where $t = m\ell$ and v_a is the solution of the Painlevé V equation

$$v_a'' + \frac{v_a'}{t} = -\frac{v_a}{1 - v_a^2}(v_a')^2 + v_a(1 - v_a^2) + 4\frac{\left(a - \frac{1}{2}\right)^2}{t^2(1 - v_a^2)} v_a. \tag{2.3.6}$$

This equation can be straightforwardly solved numerically with any standard algorithm for ordinary differential equations, once we impose the boundary condition as $t \to 0$ [176]

$$v_a(t) = -2a(\log t + \kappa_D(a)) + O(t^2), \tag{2.3.7}$$

where

$$\kappa_D(a) = -\log 2 + 2\gamma_E + \frac{1}{2}(\psi(a) + \psi(-a)), \tag{2.3.8}$$

with $\psi(z) \equiv \Gamma'(z)/\Gamma(z)$ the digamma function and γ_E the Euler-Mascheroni constant. Plugging the numerical solution of the differential equation (2.3.6) into Eq. (2.3.3), we obtain the universal constant $c_n(\alpha)$. Then, with the further integration (2.3.4), the desired $\log Z_n(\alpha)$ is found to the price of introducing the non-universal cutoff ϵ. As examples we report in Fig. 2.1 the plots of the resulting $c_n(\alpha)$ for few values of α and n as functions of $t = m\ell$. In the figure we also compare our exact solution with the numerical results obtained from a lattice discretisation of the free Dirac theory. The agreement is excellent. We stress that in Fig. 2.1 there is no free parameter in matching analytical and numerical data for $c_n(\alpha)$ (as a difference compared to $Z_n(\alpha)$).

The method we just outlined provides exact results for the desired charged moments and, by Fourier transform, the SRREs. However, the procedure is completely numerical and we would appreciate an analytic handle on the subject. While in general this is not feasible, the limits of small and large t are analytically treatable, as we are going to show.

2.3.1 The expansion close to the conformal point $m\ell = 0$

Here we use the methods just introduced to derive an asymptotic expansion of the charged moments close to the conformal point, i.e. for $t = m\ell \to 0$. In this limit, the expansion of the function $w_a(t)$ has been worked out in Ref. [176], obtaining

$$w_a = -2a^2 + a^2(1 - 2\kappa_D + 2\kappa_D^2 + (4\kappa_D - 2)\log t + 2\log^2 t)t^2 - 2a^4 t^4 \log^4 t + O(t^4 \log^3 t), \tag{2.3.9}$$

where we omitted the dependence on a of κ_D. In order to compute $c_n(\alpha)$ through Eq. (2.3.3), we again set $a = \frac{k}{n} + \frac{\alpha}{2\pi n}$ and we compute the following sums

$$\sum_k a^2 = \frac{1}{12}\left(n - \frac{1}{n}\right) + \frac{\alpha^2}{4n\pi^2}, \tag{2.3.10a}$$

$$\Omega_n(\alpha) \equiv \sum_k a^2(\psi(a) + \psi(-a)) \equiv \Omega_n(0) + \frac{\alpha^2}{2\pi^2 n}\omega_n + \rho_n^{\omega}(\alpha), \tag{2.3.10b}$$

$$\Lambda_n(\alpha) \equiv \sum_k a^2(\psi(a) + \psi(-a))^2 \equiv \Lambda_n(0) + \frac{\alpha^2}{2\pi^2 n}\lambda_n + \rho_n^{\lambda}(\alpha), \tag{2.3.10c}$$

where $\omega_n = \pi^2 n \Omega_n''(\alpha)$ and $\lambda_n = \pi^2 n \Lambda_n''(\alpha)$ so that the remainder functions $\rho_n^{\omega/\lambda}(\alpha)$ are $O(\alpha^4)$. All the sums over k run from $-\frac{n-1}{2}$ to $\frac{n-1}{2}$. The quantities $\Omega(n,\alpha)$ and $\Lambda(n,\alpha)$ (and their derivatives) can be rewritten using the integral representation $\psi(x) = -\gamma_E + \int_0^1 dy \frac{1-y^{x-1}}{1-y}$ for the digamma function $\psi(x)$. This procedure allows for an analytic continuation in n, as explained with more details in [111].

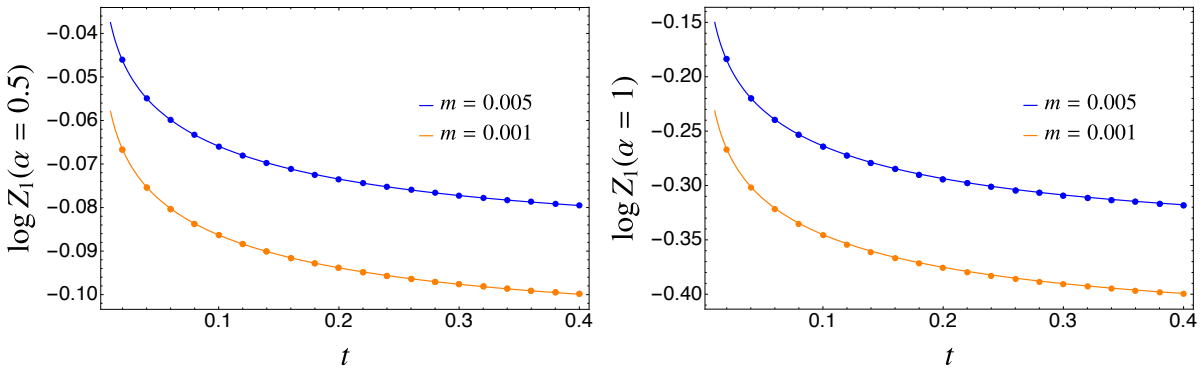

Figure 2.2: Leading scaling behaviour of the charged Rényi entropies with the insertion of a flux α. The numerical results (symbols) for two different values of α and masses m are reported as functions of $t = m\ell$ when $n = 1$. The data match well the prediction in Eq. (2.3.12) (solid lines) which includes lattice corrections as explained in the text.

From Eqs. (2.3.9)-(2.3.10) we obtain up to $O(t^2)$

$$\begin{aligned} c_n(\alpha) =& \frac{\partial \log Z_n(\alpha)}{\partial \log \ell} = \sum_{k=-(n-1)/2}^{(n-1)/2} w_{\frac{k}{n}+\frac{\alpha}{2\pi n}} = \left(\frac{1-n^2}{6n} - \frac{\alpha^2}{2\pi^2 n}\right)(1 - t^2 \log^2 t) + \\ &+ \left[\left(\frac{1-n^2}{6n} - \frac{\alpha^2}{2\pi^2 n}\right)(1 + 2\log 2 - 4\gamma_E) + 2\Omega_n(\alpha)\right] t^2 \log t + \\ &- \left[\left(\frac{1-n^2}{12n} - \frac{\alpha^2}{4\pi^2 n}\right)(1 + 2\log 2 - 4\gamma_E + 2(\log 2 - 2\gamma_E)^2) + \right. \\ &\left. + (1 - 4\gamma_E + 2\log 2)\Omega_n(\alpha) - \frac{\Lambda_n(\alpha)}{2}\right] t^2 + O(t^4 \log^3 t). \end{aligned} \tag{2.3.11}$$

Eq. (2.3.11) can be now integrated analytically, getting

$$\log Z_n(\alpha) = -\left(\frac{1}{6}\left(n - \frac{1}{n}\right) + \frac{\alpha^2}{2\pi^2 n}\right)\log\frac{\ell}{\epsilon} + y_n(t) - \frac{\alpha^2}{2\pi^2 n} z_n(t) + \rho_n^z(\alpha, t) + o(t^3), \tag{2.3.12}$$

where we defined

$$\begin{aligned} y_n(t) &= \frac{t^2}{6}\left(n - \frac{1}{n}\right)\left(\frac{1}{2}\log t^2 - \log t(1 - 2\gamma_E + \log 2) + \frac{3}{4} + 2\gamma_E^2 + \frac{\log^2 2}{2}\right. \\ &\left. -2\gamma_E(1 + \log 2) + \log 2\right) + (\log t - (\log 2 + 1 - 2\gamma_E))t^2\Omega_n(0) + \frac{t^2}{4}\Lambda_n(0), \end{aligned} \tag{2.3.13}$$

$$\begin{aligned} z_n(t) &= t^2\Big[-\frac{\log t^2}{2} + \log t(1 - 2\gamma_E + \log 2 - \omega_n) + \\ &-\frac{3}{4} - 2\gamma_E^2 - \frac{\log^2 2}{2} + 2\gamma_E(1 + \log 2) - \log 2 + (\log 2 + 1 - 2\gamma_E)\omega_n - \frac{\lambda_n}{4}\Big], \end{aligned} \tag{2.3.14}$$

$$\rho_n^z(\alpha, t) = t^2[(\log t - (\log 2 + 1 - 2\gamma_E))\rho_n^\omega(\alpha) + \rho_n^\lambda(\alpha)], \tag{2.3.15}$$

and $\rho_n^z(\alpha)$ is defined so that $\rho_n^z(\alpha) = O(\alpha^4)$. Notice, as we already stressed a few times, that in Eq. (2.3.12) the cutoff ϵ comes as an additive constant of integration and it generically depends on both n and α.

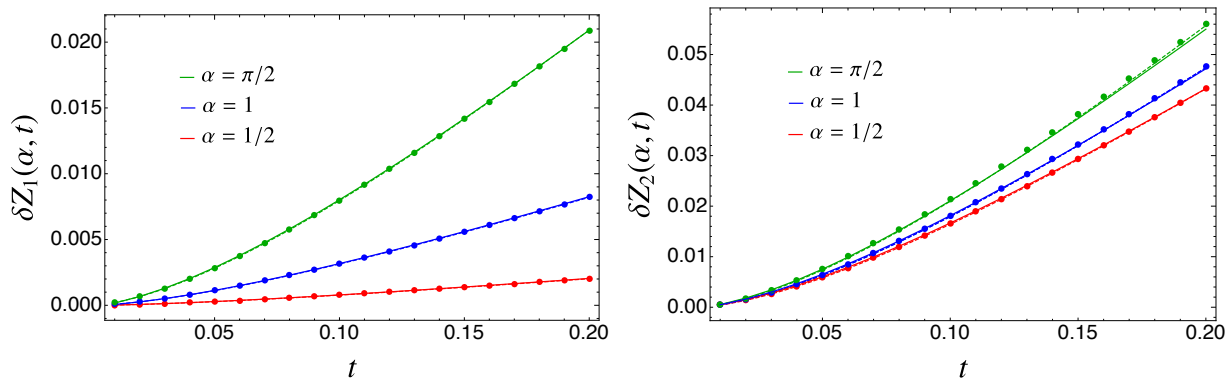

Figure 2.3: Subtracted universal charged entropy $\delta Z(\alpha, t)$ in Eq. (2.3.18). Left (right) panel is for $n = 1$ ($n = 2$). The dashed lines are the small t expansion in Eq. (2.3.12) for $n = 1$ while the solid lines are the Painlevé exact solution. The tiny discrepancies observed in some cases are finite ℓ corrections.

Eq. (2.3.12) represents our final field theoretical result for the charged entropies. We wish to test this prediction against exact lattice computations obtained with the methods of Sec. 1.4.3. However, in order to perform a direct comparison with lattice data, we have to take into account the additional non-universal contribution coming from the discretisation of the spatial coordinate, i.e. the explicit expression for the cutoff ϵ in Eq. (2.3.12) that, as already mentioned, does depend on α and cannot be simply read off from the result at $\alpha = 0$. We assume here (as Eq. (2.3.12) suggests at leading order) that the cutoff does not depend on the mass; consequently we can use the exact value for $m = 0$ [90] obtained with the use of Fisher-Hartwig techniques. The final result of Ref. [90] may be written as

$$\left(\frac{1}{6}\left(n-\frac{1}{n}\right)+\frac{\alpha^2}{2\pi^2 n}\right)\log(2\epsilon) = \Upsilon_n(\alpha) = ni\int_{-\infty}^{\infty} dw[\tanh(\pi w)-\tanh(\pi n w + i\alpha/2)]\log\frac{\Gamma(\frac{1}{2}+iw)}{\Gamma(\frac{1}{2}-iw)}\,, \quad (2.3.16)$$

and in particular we will use

$$\gamma(n) \equiv \frac{1}{2}\frac{\partial^2 \Upsilon_n(\alpha)}{\partial \alpha^2}\Big|_{\alpha=0} = \frac{ni}{4}\int_{-\infty}^{\infty} dw[\tanh^3(\pi n w)-\tanh(\pi n w)]\log\frac{\Gamma(\frac{1}{2}+iw)}{\Gamma(\frac{1}{2}-iw)}. \quad (2.3.17)$$

In Ref. [90] it has been shown that the cutoff in (2.3.16) is very well described by the quadratic expansion in α and higher corrections $O(\alpha^4)$ are negligible for most practical purposes.

In Fig. 2.2 we report the numerical data for the charged moments with the insertion of a flux α for two values of α and m with $n = 1$. The data are well described by the theoretical prediction (2.3.12) with the cutoff (2.3.16). Finally, in order to have a test of the prediction (2.3.12) that does not rely on an independent lattice calculation we can consider the difference between the charged entropy at finite t (i.e. finite mass) and the massless one. Specifically we consider

$$\delta Z(\alpha, t) = \log Z_n(\alpha, m) - \log Z_n(\alpha, m = 0), \quad (2.3.18)$$

in which both the cutoff and ℓ dependences cancel and it becomes a *universal* function solely of t (closely related to $c_n(\alpha)$). The results for $\delta Z(\alpha, t)$ are reported in Fig. 2.3. The agreement of the

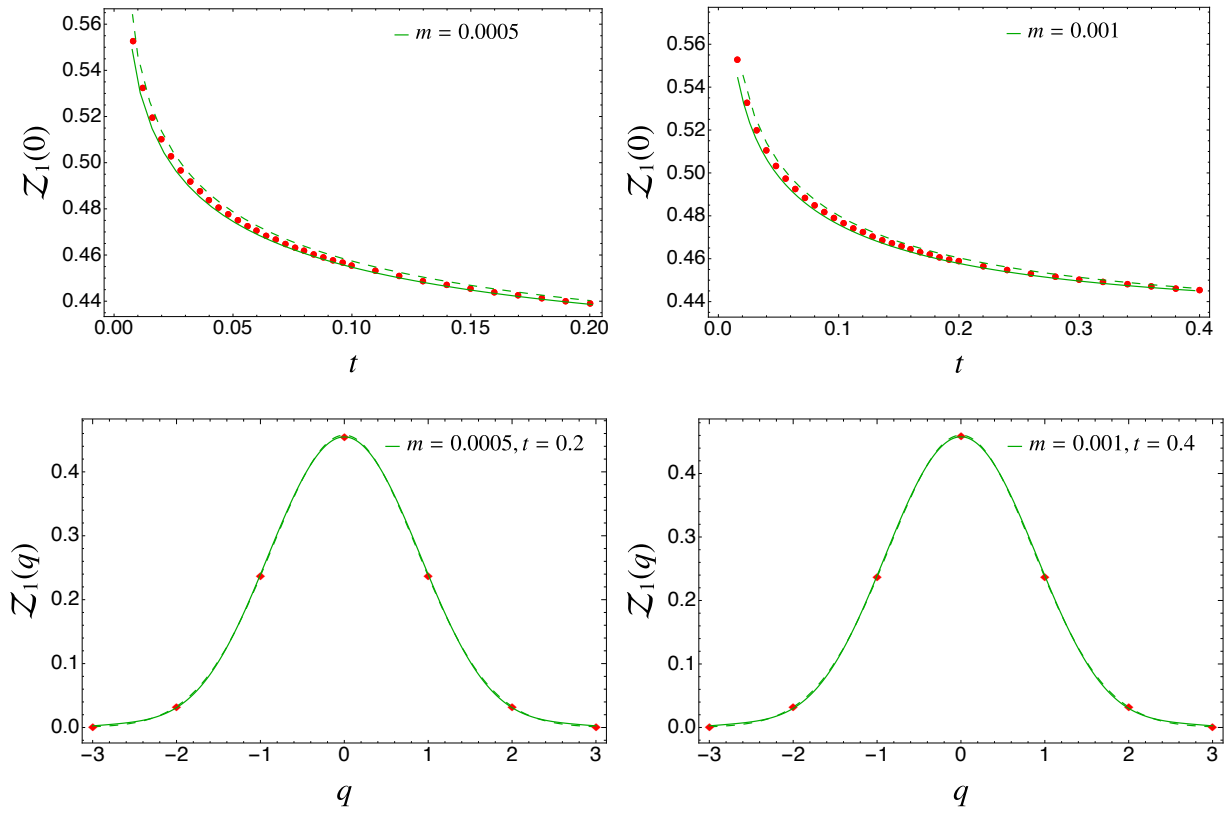

Figure 2.4: The probability $\mathcal{Z}_1(q)$. Top: As a function of $t = m\ell$ at fixed $q = 0$ for mass $m = 0.0005$ (left) and $m = 0.001$ (right). The dashed green line is $\mathcal{Z}_1(q)$ obtained by the saddle point approximation, i.e. Eq. (13.4.27). The solid green line is the exact Fourier transform without taking the quadratic approximation. For large ℓ (and t as a consequence) the saddle-point approximation converges to the exact value, as expected. Bottom: The same at fixed t as function of q.

numerics with the prediction (2.3.12) is perfect for small t. Furthermore, the differences emerging for larger t are correctly captured by the numerical exact solution of the Painlevé equation (2.3.6). The small discrepancies visible in the figure are just finite size effects that are stronger for larger values of n and α.

2.3.2 From the charged moments to symmetry resolution

We are now ready to study the true symmetry resolution by performing the Fourier transform of $Z_n(\alpha)$. In this Fourier transform we ultimately use a saddle-point approximation in which $Z_n(\alpha)$ is Gaussian and hence we truncate hereafter Eq. (2.3.12) at quadratic order in α. Consequently, the charged partition function can be well approximated as

$$Z_n(\alpha) = Z_n(0)e^{-b_n\alpha^2/2}, \tag{2.3.19}$$

where

$$b_n(\ell, t) = \frac{1}{\pi^2 n}(\log \ell + z_n(t)) - 2\gamma(n) + \frac{\log 2}{\pi^2 n} \equiv \frac{1}{\pi^2 n}\log \ell - h_n, \tag{2.3.20}$$

and we consistently approximated the cutoff at quadratic level and used the lattice cutoff with $\gamma(n)$ given in Eq. (2.3.17). A different cutoff just leads to a different additive constant in b_n (i.e.,

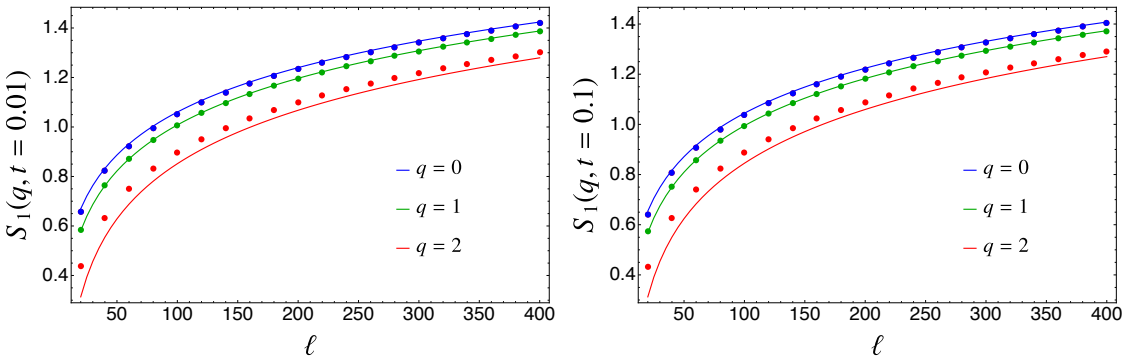

Figure 2.5: SRREs for a few different values of q as functions of ℓ. The field theory prediction is tested against exact lattice computations. The agreement with Eq. (2.3.24), that includes lattice effects, is remarkable. For large $|q|$, the approximation at the order q^2 is no longer sufficient and neglected corrections to the scaling become important, as well known for the massless case [90].

a different definition of h_n), but we will use its precise form only for the comparison with numerics and so all the following formulas are completely general.

Now we can compute the Fourier transform (1.4.17) that reads

$$\mathcal{Z}_n(q) = Z_n(0) \int_{-\pi}^{\pi} \frac{d\alpha}{2\pi} e^{-iq\alpha} e^{-\alpha^2 b_n(\ell,t)/2}. \tag{2.3.21}$$

When $\ell \to \infty$, we can perform the integral by saddle point approximation and the integration domain can be extended to the whole real line. We end up in a simple Gaussian integral, obtaining

$$\mathcal{Z}_n(q) = \frac{Z_n(0)}{\sqrt{2\pi b_n(\ell,t)}} e^{-\frac{q^2}{2b_n(\ell,t)}}. \tag{2.3.22}$$

We check Eq. (2.3.22) against numerical computations in Figure 2.4 focusing on $n = 1$ and the agreement is perfect. We test both the scaling with $t = m\ell$ for fixed q and at fixed t as a function of q.

Now we are ready to compute the SRREs. From the definition (1.4.18) we have

$$S_n(q) = S_n^D - \frac{1}{2}\log(2\pi) + \frac{1}{1-n}\log\frac{b_1(\ell,t)^{n/2}}{b_n(\ell,t)^{1/2}} - \frac{q^2}{2(1-n)}\left(\frac{1}{b_n(\ell,t)} - \frac{n}{b_1(\ell,t)}\right), \tag{2.3.23}$$

where S_n^D is the total n-th Rényi entropy for the Dirac fields (cf. Eq. (2.1.5) up to $O(t^2 \log^2 t)$). We can further expand the above equation for $\ell \to \infty$ since $b_n(\ell,t)$ diverges logarithmically, obtaining

$$S_n(q) = S_n^D - \frac{1}{2}\log\left(\frac{2}{\pi}\log\delta_n \ell\right) + \frac{\log n}{2(1-n)} - \frac{\pi^4 n(h_1 - nh_n)^2}{4(1-n)^2(\log\ell)^2} + \\ + q^2 n\pi^4 \frac{h_1 - nh_n}{2(1-n)(\log \ell\kappa_n)^2} + o(\log\ell^{-2}), \tag{2.3.24}$$

where

$$\log\delta_n = -\frac{\pi^2 n(h_n - h_1)}{1-n}, \tag{2.3.25}$$

and

$$\log\kappa_n = -\pi^2\frac{(h_1 + nh_n)}{2}. \tag{2.3.26}$$

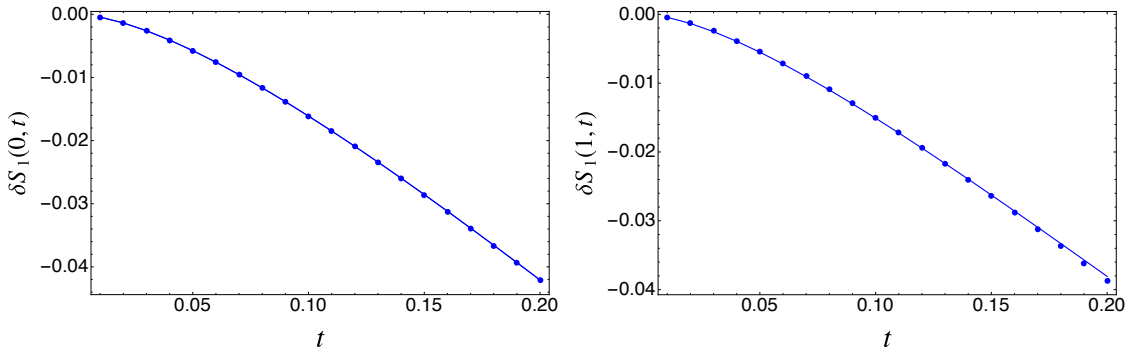

Figure 2.6: Subtracted SREE $\delta S_1(q,t) \equiv S_1(q,t) - S_1(q,t=0)$ for $q=0$ (left) and $q=1$ (right) as a function of t (fixing $\ell = 600$ and varying m). This subtracted quantity highlights the mass dependence of SRREs. The continuous lines are just the difference of the same subtracted entropies as obtained from the field theory expansion (2.3.24).

The above formula is valid also for the SREE taking properly the limits of the various pieces as $n \to 1$. By construction, the total entropy, S_n^D, coincides with the one obtained in [176] for the massive fermions in the conformal limit up to $O(t^2)$.

Let us critically discuss the result in Eq. (2.3.24). The leading terms for large ℓ (up to $O((\log \ell)^{-2})$ do not depend on q and they are given by the total entropies S_n^D in Eq. (2.1.5). We then conclude that at this order, the presence of the mass does not break entanglement equipartition found in conformal field theory [85]. The first term breaking equipartition is at order $O((\log \ell)^{-2})$ and its amplitude is governed by the constant h_n defined in Eq. (2.3.20). This constant gets contributions both from the non-universal cutoff and from the mass; the two contributions have the same analytic features. In Fig. 2.5 we test the accuracy of our total prediction against exact lattice numerical calculations. The agreement is remarkable for small values of $|q|$, but it worsens already at $q=2$; this does not come as a surprise since the same trend was already observed in the massless case [90]. Such discrepancies are entirely due to corrections of order $o(q^2)$ and are expected to reduce as ℓ gets larger. The drawback of the data reported in Fig. 2.5 is that universal field theory mass contributions and the lattice non-universal terms are mixed up and the latter are, by far, the largest one. It is then very difficult to observe the dependence on the mass in these plots. An effective and easy way to highlight the role of the mass is to subtract from the SRREs their value for the massless case, i.e. considering the numerical evaluation of the $\delta S_n(q,t) \equiv S_n(q,t) - S_n(q,0)$. Such subtracted entropies for $n=1$ and $q=0,1$ are reported in Fig. 2.6, showing that the entropy is a monotonous decreasing function of t (and hence of m at fixed ℓ).

2.3.3 The long distance expansion.

In this subsection we move to the analysis of the charged and SRREs in the limit of large t. The most effective way to proceed is, following Ref. [176], to employ in Eq. (2.3.6) a boundary condition for $t \to \infty$, that takes the form [176]

$$v_a(t) \sim \frac{2}{\pi} \sin(\pi a) K_{2a}(t), \tag{2.3.27}$$

where $K_{2a}(t)$ is the modified Bessel function of the second kind. This is the starting point for a systematic expansion for large t of the solution $v_a(t)$ of the differential equation (2.3.6). Plugging

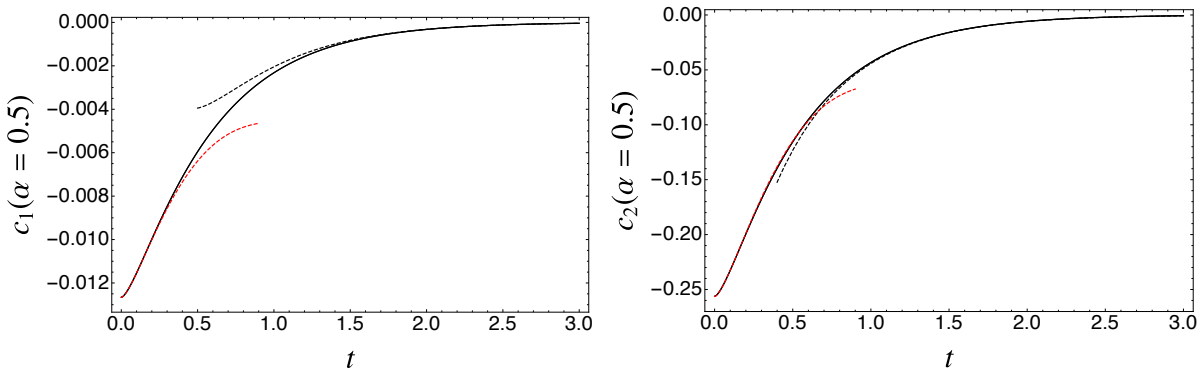

Figure 2.7: The solid lines are the functions $c_n(\alpha)$ obtained as exact numerical solutions of the differential equation (2.3.6). The dashed lines are the leading terms in the expansions for short (red) and long (black) distances, i.e. Eqs. (2.3.11) and (2.3.29), respectively.

the resulting expansion into the integral (2.3.5) for $w_a(t)$, we get

$$w_a(t) = -e^{-2t}\frac{\sin^2(a\pi)}{\pi}\left(1 + \frac{-1+16a^2}{4t} + O(t^{-2})\right). \tag{2.3.28}$$

Summing over $a = \frac{k}{n} + \frac{\alpha}{2\pi n}$, we obtain the long distance asymptotic expansion for the universal factor $c_n(\alpha)$

$$c_n(\alpha) = \frac{e^{-2t}}{2\pi}\left(-n + \frac{(4-n^2)\pi^2 - 12\alpha^2}{12nt\pi^2} - \frac{2\csc\frac{\pi}{n}(\pi\cot\frac{\pi}{n}\cos\frac{\alpha}{n} + \alpha\sin\frac{\alpha}{n})}{\pi nt} + O(t^{-2})\right), \tag{2.3.29}$$

and for $n = 1$

$$c_1(\alpha) = -\frac{e^{-2t}}{\pi}\sin^2\frac{\alpha}{2}\left(1 + \frac{\frac{4\alpha^2}{\pi^2} - 1}{4t} + O(t^{-2})\right). \tag{2.3.30}$$

This is consistent with the exact result $c_1(0) = 0$ coming from the normalisation of the reduced density matrix. For $\alpha = 0$, Eq. (2.3.29) reproduces the known results [176].

In Fig. 2.7 we report the numerical exact solution of the Painlevé equation (2.3.6) for $c_n(\alpha)$; we focus on $n = 1, 2$ and plot $c_n(\alpha)$ as a function of t. For large t, the solutions perfectly match the asymptotic expansions (2.3.29) and (2.3.30) (for completeness we also show the small t expansion in Eq. (2.3.11)). Let us emphasise the presence of a discontinuity in $c_n(\alpha)$ for $n \to 1$ as a function of n: it is due to the non-commutativity of the limits $n \to 1$ and $t \to \infty$, as well known and discussed at length in the literature for $\alpha = 0$ [175,176]. We show here that the presence of α does not cancel such a discontinuity, although for $\alpha \neq 0$ the leading term is of the same order e^{-2t}.

The charged entropy is simply given by the integral

$$\log Z_n(\alpha) = \int_{m\epsilon}^{m\ell} \frac{c_n(\alpha)}{t} dt. \tag{2.3.31}$$

At large t, the function $c_n(\alpha)$ goes to zero exponentially in t for any n; hence the charged entropies approach asymptotically a finite value for large ℓ. This saturation value is determined entirely by the infrared physics, i.e. by the value of $c_n(\alpha)$ at small t, indeed

$$\log Z_n(\alpha) \simeq \log Z_n^{(0)}(\alpha) \equiv \int_{m\epsilon}^{\infty} \frac{c_n(\alpha)}{t} dt \simeq \left(\frac{1}{6}\left(n - \frac{1}{n}\right) + \frac{\alpha^2}{2\pi^2 n}\right)\log m\epsilon. \tag{2.3.32}$$

This dependence on $\log(m\epsilon)$ coincides with the result in Sec. 2.2.2 (following the analysis of the properties of the energy momentum tensor on $\mathcal{R}_{n,\alpha}$), up to a factor 2 due to the number of the endpoints (cf. (2.2.17)).

The corrections in $m\ell$ to the ℓ-independent result (2.3.32) are obtained expanding the integral (2.3.31) in the ultraviolet. Keeping for conciseness only the leading order in t of Eqs. (2.3.29) and (2.3.30) and performing the integration, we get

$$\log Z_n(\alpha) = \log Z_n^{(0)}(\alpha) + \frac{ne^{-2t}}{4\pi t}, \qquad \log Z_1(\alpha) = \log Z_1^{(0)}(\alpha) + \frac{e^{-2t}}{2\pi t}\sin^2\frac{\alpha}{2}. \tag{2.3.33}$$

Once again, $Z_n(\alpha)$ are not continuous functions of n close to $n = 1$ (as it was already known for $\alpha = 0$, see [176]) and, above all, the correction of $\log Z_n(\alpha)$ does not depend on α for $n \neq 1$ at this order. Subleading corrections to (2.3.33) can be straightforwardly and systematically worked out, but they are not illuminating, although they do depend on α also for $n \neq 1$.

For $n \neq 1$, since the leading correction does not depend on α, the Fourier transform is not affected and the symmetry resolved moments with $n \neq 1$ just get a multiplicative correction to $\mathcal{Z}_n(q)$ in Eq. (2.2.20) (so additive for the logarithm), given by

$$\delta \log \mathcal{Z}_n(q) = \frac{ne^{-2t}}{4\pi t}\,. \tag{2.3.34}$$

For $n = 1$ the net effect of the $\sin^2(\alpha/2)$ term in Eq. (2.3.33) is to renormalise the variance with an exponential additive correction, i.e. the desired probability is

$$\mathcal{Z}_1(q) = e^{-\frac{2q^2\pi^2}{4|\log(m\epsilon)|+\pi e^{-2t}/t}}\sqrt{\frac{2\pi}{4|\log(m\epsilon)| + \pi e^{-2t}/t}} \tag{2.3.35}$$

The SRREs with $n \neq 1$ are straightforwardly obtained from Eq. (1.4.18). Indeed, plugging Eqs. (2.3.34) and (2.3.35) in (1.4.18), we get

$$S_n(q) = -\frac{n+1}{6n}\log(m\epsilon) - \frac{ne^{-2m\ell}}{4\pi m\ell(1-n)} + \frac{\log n}{2(1-n)} - \frac{1}{2}\log\left(\frac{2}{\pi}|\log m\epsilon| - \frac{ne^{-2m\ell}}{(1-n)2m\ell}\right) + \\ + O((\log m\epsilon)^{-1}, e^{-3m\ell}). \tag{2.3.36}$$

Such a result shows exact equipartition (at this order) which is a clear consequence of the simple form of (2.3.34). This is reminiscent of the exact results for integrable models studied in Ref. [98].

The limit $n \to 1$ for the von Neumann entropy should be handled with care. We start rewriting Eq. (1.4.18) as

$$S_1(q) = \log \mathcal{Z}_1(q) - \frac{1}{\mathcal{Z}_1(q)}\int_{-\pi}^{\pi}\frac{d\alpha}{2\pi}e^{-iq\alpha}Z_1(\alpha)\partial_n \log Z_n(\alpha)|_{n=1}. \tag{2.3.37}$$

We use this equation to obtain the entire correction in t due to the Bessel function and not only the leading exponential term (as done in Eq. (2.3.33)). The crucial computation is

$$\begin{aligned}\partial_n c_n(\alpha)|_{n=1} &= -\partial_n \int_t^\infty dy\, y \sum_{k=-(n-1)/2}^{(n-1)/2} v_a^2(y)\Big|_{n=1} = \\ &= -\left(\frac{2}{\pi}\right)^2 \partial_n \int_t^\infty dy\, y \sum_{k=-(n-1)/2}^{(n-1)/2} \sin^2(\pi a) K_{2a}^2(y)\Big|_{n=1},\end{aligned} \tag{2.3.38}$$

where $a = \frac{k}{n} + \frac{\alpha}{2\pi n}$. We can use the integral representation for the Bessel function

$$K_a(y) = \int_1^\infty du\, e^{-yu} \frac{(u+\sqrt{u^2-1})^a + (u+\sqrt{u^2-1})^{-a}}{2\sqrt{u^2-1}}, \tag{2.3.39}$$

to perform the sum over k in Eq. (2.3.38). Once we plug Eq. (2.3.39) into Eq. (2.3.38) , we get

$$\begin{aligned} c_n(\alpha) = &-\frac{2}{\pi^2}\int_t^\infty dy\, y \int_1^\infty du \int_1^\infty dv \frac{e^{-y(u+v)}}{\sqrt{u^2-1}\sqrt{v^2-1}} \times \\ &\times \left(F_{n,\alpha}((u+\sqrt{u^2-1})(v+\sqrt{v^2-1})) + F_{n,\alpha}\left(\frac{(u+\sqrt{u^2-1})}{(v+\sqrt{v^2-1})}\right)\right), \end{aligned} \tag{2.3.40}$$

where

$$F_{n,\alpha}(z) = \frac{z^{\frac{\pi-\alpha}{n\pi}}}{4}\left(z-\frac{1}{z}\right)\left(\frac{1+z^{\frac{2\alpha}{n\pi}}}{z^{\frac{2}{n}}-1} + \frac{(z^{\frac{2(\pi+\alpha)}{n\pi}}-1)\cos\frac{\pi-\alpha}{n} + (z^{\frac{2}{n}} - z^{\frac{2\alpha}{n\pi}})\cos\frac{\pi+\alpha}{n}}{1+z^{\frac{4}{n}}-2z^{\frac{2}{n}}\cos(\frac{2\pi}{n})}\right). \tag{2.3.41}$$

We now study the behaviour of $F_{n,\alpha}(z)$ when $n \to 1$. For $z = 1$, the limit $n \to 1$ is singular. We can isolate this singularity using the polar variables $(n-1, z-1) \to (\rho\cos\theta, \rho\sin\theta)$ and expanding in the radial coordinate ρ. The result of this procedure is

$$F_{n,\alpha}(z) = \frac{1}{2} - \frac{1}{2}\frac{(z-1)^2\cos\alpha}{\pi^2(n-1)^2 + (z-1)^2} + O(n-1, z-1), \tag{2.3.42}$$

whose derivative with respect to n is

$$\partial_n F_{n,\alpha}(z)\Big|_{n\to1} = \lim_{n\to1}\frac{F_{n,\alpha}(z) - F_{1,\alpha}(z)}{n-1} = \pi^2\left(\frac{1}{2} - \sin^2\frac{\alpha}{2}\right)\delta(z-1). \tag{2.3.43}$$

Plugging this result in Eq. (2.3.40) and taking the derivative wrt n, we get

$$\partial_n c_n(\alpha)\big|_{n\to1} = -\left(1-2\sin^2\frac{\alpha}{2}\right)\int_t^\infty dy y K_0(2y) = -\left(\frac{1}{2} - \sin^2\frac{\alpha}{2}\right) tK_1(2t), \tag{2.3.44}$$

which, once integrated in t according to Eq. (2.3.31), gives the full ultraviolet behaviour of $\partial_n \log Z_n(\alpha)\big|_{n\to1}$, i.e.

$$\partial_n \log Z_n(\alpha)\big|_{n\to1} = \left(\frac{1}{3} - \frac{\alpha^2}{2\pi^2}\right)\log(m\epsilon) + \left(\frac{1}{4} - \frac{1}{2}\sin^2\frac{\alpha}{2}\right)K_0(2t). \tag{2.3.45}$$

Plugging the above derivative into Eq. (2.3.37) finally yields

$$\begin{aligned} S_1(q) = &-\frac{1}{3}\log(m\epsilon) - \frac{1}{4}K_0(2m\ell) + \log\mathcal{Z}_1(q) + \frac{\log(m\epsilon)}{2\pi^2\mathcal{Z}_1(q)}\int_{-\pi}^{\pi}\frac{d\alpha}{2\pi}e^{-iq\alpha}Z_1(\alpha)\alpha^2 + \\ &+ \frac{K_0(2m\ell)}{2\mathcal{Z}_1(q)}\int_{-\pi}^{\pi}\frac{d\alpha}{2\pi}e^{-iq\alpha}Z_1(\alpha)\sin^2\frac{\alpha}{2} \\ \simeq &-\frac{1}{3}\log(m\epsilon) - \frac{1}{4}K_0(2m\ell) - \frac{1}{2}\log\left(\frac{2|\log(m\epsilon)|}{\pi}\right) - \frac{1}{2} + O((\log m\epsilon)^{-1}). \end{aligned} \tag{2.3.46}$$

The first two terms in (2.3.46) are respectively the leading and the subleading terms in the total entanglement entropy of a massive Dirac field, in agreement with the known results in Refs. [156, 175, 176]. The double logarithmic term appears only in the symmetry resolved result and, as already discussed in Eq. (2.2.21), it is related to the number entropy. The above derivation clearly highlight this correspondence. As for the Rényi entropy, at this order in $\log m\epsilon$, there is perfect entanglement equipartition that will be broken by higher order terms.

2.4 The Green's function approach: The complex scalar field

In this section we present a derivation of the charged moments for a complex massive scalar by generalising to $\alpha \neq 0$ the results obtained in [177,178]. In Sec. 2.2.1 we showed that $Z_n(\alpha)$ can be written as product of partition functions on the plane with boundary conditions along the cut A

$$\tilde{\varphi}_k(e^{2\pi i}z, e^{-2\pi i}\bar{z}) = e^{2\pi i a}\tilde{\varphi}_k(z,\bar{z}), \qquad a = \frac{k}{n} + \frac{\alpha}{2\pi n}, \qquad k = 0, \cdots n-1. \tag{2.4.1}$$

Denoting, as usual, by ζ_a these partition functions we have

$$\log Z_n(\alpha) = \sum_{k=0}^{n-1} \log \zeta_{\frac{k}{n}+\frac{\alpha}{2\pi n}}. \tag{2.4.2}$$

As for the analogous case of fermions, cf. Eq. (2.3.3), we define the auxiliary quantities

$$w_a \equiv \ell \partial_\ell \log \zeta_a, \qquad c_n(\alpha) \equiv \sum_{k=0}^{n-1} w_{\frac{k}{n}+\frac{\alpha}{2\pi n}}, \tag{2.4.3}$$

that, using (2.4.2), allow us to write the logarithmic derivative of the partition function in $\mathcal{R}_{n,\alpha}$ as

$$c_n(\alpha) = \ell \frac{\partial \log Z_n(\alpha)}{\partial \ell} \qquad \Rightarrow \qquad \log Z_n(\alpha) = \int_\epsilon^\ell \frac{c_n(\alpha)}{\ell'} d\ell'. \tag{2.4.4}$$

Even here, for $n = 1$, the function $c_n(\alpha)$ is the analogue of Zamolodchikov's c-function [183] in the presence of the flux α.

As already discussed in section 2.1, the key observation of this approach relies on the identity between the partition function ζ_a and the Green's function (see Eq. (2.1.4)). Through this relation, the function w_a has been obtained for generic values of a also for bosonic free massive field theories [178]. As already found in Sec. 2.2.1 using twist fields, also this approach requires that $0 < a < 1$ for the scalar theory (see [177] for details). Thus, in order to compute $Z_n(\alpha)$, we will use the results in [178] setting $a = \frac{k}{n} + \frac{|\alpha|}{2\pi n}$ for the complex Klein Gordon theory.

Here we consider the complex massive non-compact bosonic field theory with action given by (2.1.1) and mass m. The function w_a with $0 < a < 1$ defined in (2.4.3) can be written as [177]

$$w_a = -\int_t^\infty y u_a^2(y) dy, \tag{2.4.5}$$

where $t = m\ell$ and u_a is the solution of the Painlevé V equation

$$u_a'' + \frac{u_a'}{t} = \frac{u_a}{1+u_a^2}(u_a')^2 + u_a(1+u_a^2) + 4\frac{\left(a-\frac{1}{2}\right)^2}{t^2(1+u_a^2)}u_a. \tag{2.4.6}$$

The solution of Eq. (2.4.6) is showed in Fig. 2.8: the function w_a for a generic value of t can be obtained solving numerically Eq. (2.4.6) with the initial condition for $t \to 0$

$$u_a(t) = \frac{-1}{t\left(\log t + \kappa_S(a)\right)} - a(a-1)t(\log t + \kappa_S(a)) + O(t), \tag{2.4.7}$$

where [178]

$$\kappa_S(a) = 2\gamma_E + \frac{\psi(1-a)+\psi(a)}{2} - \log 2. \tag{2.4.8}$$

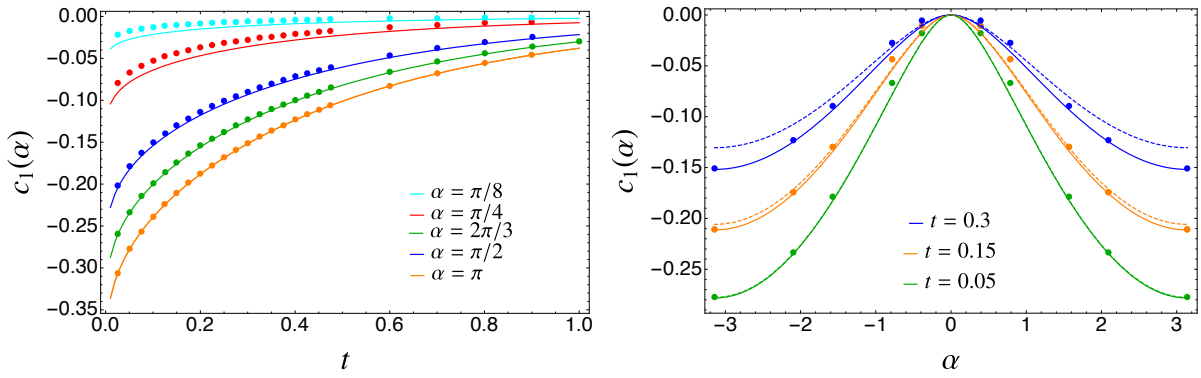

Figure 2.8: Left panel: Logarithmic derivative of the charged moments, $c_1(\alpha)$, as a function of $t = m\ell$ obtained by solving numerically the Painléve equation (2.4.6) (solid lines). The data (symbols) are obtained fixing (from top to bottom) $\ell = 720, 620, 420, 420, 320$ and varying properly m in such a way that $m\ell \in (0, 1)$. As discussed in the main text, the agreement with the numerical data worsens as α decreases. Right panel: the same quantity is plotted as a function of α from the numerical solution of the Painlevé equation (solid lines), showing also in this case that the agreement as $\alpha \to 0$ is not excellent. The dashed lines represent the small t expansion in Eq. (2.4.10): the smaller is t, the better the approximation works.

In the figure we compare the exact result from field theory with numerical data for a chain of complex oscillators, obtained exploiting the techniques we will present in Chapter 7. We have a fairly good agreement between lattice and field theory, although for small values of α the agreement gets worse and one needs a larger and larger subsystem length ℓ on the lattice to match the continuum limit. This is not surprising, already in Ref. [98] it was shown for the massless case that the lattice results approach the CFT ones in a non uniform way. In the following we will further discuss this issue in the limits when we have an analytic handle on the problem.

2.4.1 The expansion close to the conformal point

In the conformal limit $t \to 0$ we have that the solution of the Painlevé equation admits the expansion [177]

$$w_a = -2a(1-a) - \frac{1}{\log(t) + \kappa_S(a)} + O(t). \tag{2.4.9}$$

Using Eq. (2.4.3) we get

$$c_n(\alpha) = \sum_{k=0}^{n-1} w_{\frac{k}{n}+\frac{|\alpha|}{2\pi n}} = \frac{1-n^2}{3n} + \frac{\alpha^2}{2\pi^2 n} - \frac{|\alpha|}{\pi n} - \sum_{k=0}^{n-1} \frac{1}{\log t + \kappa_S(a(k))} + \dots . \tag{2.4.10}$$

Let us discuss first at the level of the universal function $c_n(\alpha)$ the origin of the non uniform behaviour in α. Eq. (2.4.10) is an exact asymptotic expansion valid for any $\alpha \neq 0$. For $\alpha \to 0$, there is a clear problem with the constant $\kappa_S(a(0))$ (i.e. of the mode with $k = 0$) which diverges as $\pi/|\alpha|$. Hence, since $\log t$ grows very slowly with t, the true asymptotic behaviour is attained only for $t \gtrsim e^{\pi/|\alpha|}$. For smaller values of t, the mode $k = 0$ looks almost constant ($\sim |\alpha|/\pi$) and similar to the leading term. Exactly for $\alpha = 0$, the mode $k = 0$ diverges, so its inverse is just zero and it does not affect the calculation. It is then clear that the approach to the asymptotic behaviour cannot be uniform in α, as already observed numerically in Fig. 2.8.

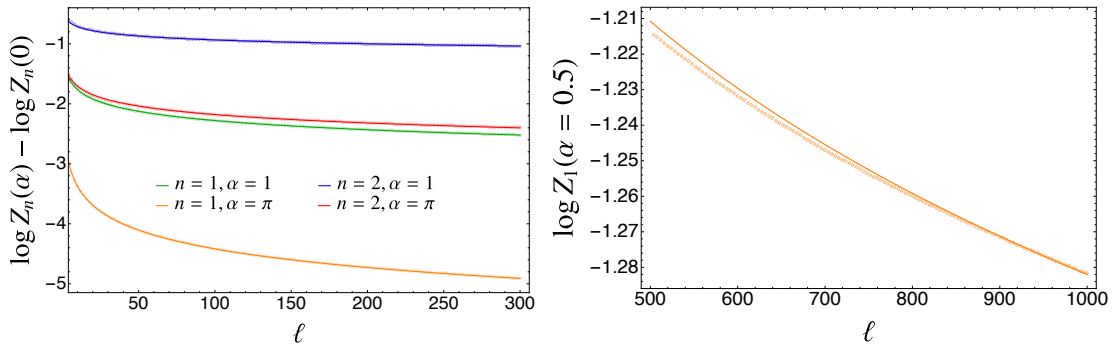

Figure 2.9: Charged moments for the free massive boson close to the critical regime. We benchmark the analytical prediction (2.4.11) (solid lines) with the numerical data (symbols) for different values of n and α at fixed $m = 10^{-10}$: the analytical formula matches well the data for large values of α (left), but for smaller α (right) much larger values of ℓ are necessary to observe a fair match, as explained in the text.

After having discussed this caveat with the small α behaviour, we are ready to integrate Eq. (2.4.10) to get the charged moments, according to Eq. (2.4.4), obtaining

$$\log Z_n(\alpha) = \left(\frac{1-n^2}{3n} + \frac{\alpha^2}{2\pi^2 n} - \frac{|\alpha|}{\pi n}\right) \log\left(\frac{\ell}{\epsilon}\right) + \sum_{k=0}^{n-1} \log\left|\frac{\log(m\epsilon) + \kappa_S(a(k))}{\log(m\ell) + \kappa_S(a(k))}\right|. \tag{2.4.11}$$

Let us remark that when $n = 1$, the last sum reduces to the term with $k = 0$. We recall that the cutoff ϵ depends both on n and α making the analysis even more troubling.

Even though we are in the conformal limit in which $m\ell \ll 1$, the additional constant $\kappa_S(a(0))$ cannot be neglected because of its divergent behaviour when $k = 0$ and $\alpha = 0$. The terms with $k > 0$ do not present any problem and $\kappa_S(a(k))$ can be safely neglected. The mode with $k = 0$ instead has three different regimes, depending on the value of $\kappa_S(k = 0)$ which is governed by α as follows:

- for very small α, i.e. such that $\alpha \lesssim n\pi/|\log(m\epsilon/2) + \gamma_E|$, $\kappa_S(k = 0)$ diverges faster than both $\log m\ell$ and $\log m\epsilon$. Hence, expanding the ratio in Eq. (2.4.11), this subleading term becomes of the same order of the leading one, i.e.

$$\log\left|\frac{\log(m\epsilon) + \kappa_S(a(0))}{\log(m\ell) + \kappa_S(a(0))}\right| \xrightarrow{\alpha\to 0} \frac{|\alpha|}{\pi n} \log\frac{\ell}{\epsilon} + \dots, \tag{2.4.12}$$

- for intermediate values of α, i.e. when $n\pi/|\log(m\epsilon/2) + \gamma_E| \lesssim \alpha \lesssim n\pi/|\log(m\ell/2) + \gamma_E|$, we have

$$\log\left|\frac{\log(m\epsilon) + \kappa_S(a(0))}{\log(m\ell) + \kappa_S(a(0))}\right| \sim \log\left|\frac{\log(m\epsilon)}{\kappa_S(a(0))}\right| + \dots, \tag{2.4.13}$$

  and hence this produces just an additive correction in ℓ, but depending on $m\epsilon$;

- for larger α, i.e. for $\alpha \gtrsim n\pi/|\log(m\ell/2) + \gamma_E|$, the term κ_S is a correction both for numerator and denominator and so

$$\log\left|\frac{\log(m\epsilon) + \kappa_S(a(0))}{\log(m\ell) + \kappa_S(a(0))}\right| \simeq \log\left|\frac{\log(m\epsilon)}{\log(m\ell)}\right| + \dots, \tag{2.4.14}$$

  as for the terms with $k \neq 0$. We stress that this third regime is the true asymptotic one for large ℓ at fixed α.

This competition among the three terms makes difficult the analytical treatment of the last sum in Eq. (2.4.11), and, at the same time, the non trivial dependence on the cutoff ϵ (that we recall also depends on α and n) complicates the comparison with the numerics. For this reason, we consider only the leading term in Eq. (2.4.11), which, strictly speaking, is valid in the massless case and in the third regime above. Such a leading term is the same provided as in the twist field approach (cf. Eq. (2.2.8)) and coincides with some equivalent ones in literature [98, 158]. The main advantage of Eq. (2.4.11) is that it clearly shows what are the problems one faces when considering only the leading term. The comparisons with the numerics are shown in Figure 2.9: we report the numerical data for different values of n and α; as expected from our previous discussion, the agreement with the predictions is very good for large α, but it worsens as α gets smaller and n gets larger. Smaller is α, larger is the value of ℓ on the lattice necessary to observe the true asymptotic behaviour.

Symmetry resolution

The symmetry resolved moments of the RDM can be computed through the Fourier transform of the leading term of the charged moments in Eq. (2.4.11)

$$\mathcal{Z}_n(q) = \int_{-\pi}^{\pi} \frac{d\alpha}{2\pi} e^{-iq\alpha} Z_n(\alpha) = Z_n(0) \int_{-\pi}^{\pi} \frac{d\alpha}{2\pi} e^{-iq\alpha} e^{\left(\frac{\alpha^2}{2\pi^2 n} - \frac{|\alpha|}{\pi n}\right) \log \frac{\ell}{\epsilon}} =$$
$$Z_n(0) \left(\frac{\ell}{\epsilon}\right)^{-\frac{1}{2n}} \sqrt{\frac{n\pi}{8\log(\ell/\epsilon)}} (-1)^q e^{\frac{n\pi^2 q^2}{2\log(\ell/\epsilon)}} \left[\mathrm{Erfi}\left(\frac{\log(\ell/\epsilon) - n\pi i q}{\sqrt{2n\log(\ell/\epsilon)}} \right) + \mathrm{Erfi}\left(\frac{\log(\ell/\epsilon) + n\pi i q}{\sqrt{2n\log(\ell/\epsilon)}} \right) \right], \tag{2.4.15}$$

where $\mathrm{Erfi}(x)$ is the imaginary error function (the overall result is real and positive for $q \in \mathbb{Z}$)

$$\mathrm{Erfi}(x) = \frac{-2i}{\sqrt{\pi}} \int_0^{ix} dt\, e^{-t^2} \xrightarrow{x\to\infty} \frac{e^{x^2}}{\sqrt{\pi} x}. \tag{2.4.16}$$

In the large ℓ limit, using the expansion in Eq. (2.4.16), the charged moments in Eq. (2.4.15) can be can be approximated as

$$\mathcal{Z}_n(q) = Z_n(0) \frac{n \log \ell/\epsilon}{n^2\pi^2 q^2 + \log^2 \ell/\epsilon}, \tag{2.4.17}$$

and hence the SRREs are given by

$$S_n(q) = \frac{1}{1-n} \log \frac{\mathcal{Z}_n(q)}{\mathcal{Z}_1(q)^n} \simeq S_n - \log\log \frac{\ell}{\epsilon} + \frac{\log n}{1-n}, \quad S_1(q) \simeq S_1 - \log\log \frac{\ell}{\epsilon} - 1. \tag{2.4.18}$$

The leading behaviour is described by the total Rényi entropies, with the usual correction $\log\log \ell$ that is independent on q, confirming the equipartition of the entanglement entropy for a complex massive scalar field theory, in agreement with the result for massive harmonic chains [98] (although the critical limit considered there is different from the one here). Let us mention that a further expansion of Eq. (2.4.15) leads to subleading corrections behaving as $q^2/(\log \ell)^2$ which explicitly depend on q, breaking the equipartition of the entanglement.

Let us now discuss the effect of the term that we disregarded in Eq. (2.4.11), namely the sum over k. The mode with $k \neq 0$ would provide double logarithimic corrections encountered also in other contexts, like non unitary CFTs [184, 185]. These in principle are calculable and partially under control. We mention that such terms have a non-trivial dependence on n in $\mathcal{Z}_n(q)$ and hence they are responsible of a further breaking of equipartition. Unfortunately, the determination of

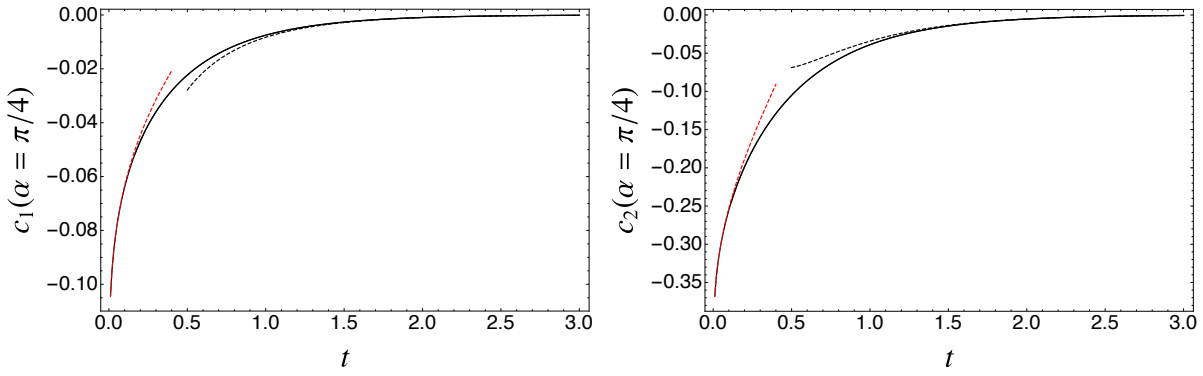

Figure 2.10: The solid lines are the functions $c_n(\alpha)$ as solutions of Eq. (2.4.6). The dashed lines are the short (red) and long (black) distance leading terms we evaluated analytically in Eq. (2.4.10) and Eq. (2.4.21), respectively.

this correction is not easy because it is influenced by the precise dependence on α and n of the non-universal cutoff ϵ (as it should be clear from Eq. (2.4.11)). Finally, as discussed for the charged moments, the effect of the mode $k = 0$ is even more dramatic and too difficult to keep under control.

2.4.2 The long distance expansion.

The boundary condition for Eq. (2.4.6) in the limit in which $t \to \infty$ is [177]

$$u_a(t) \sim \frac{2}{\pi} \sin(\pi a) K_{1-2a}(t). \tag{2.4.19}$$

The solution of Eq. (2.4.6) in the long distance regime together with Eq. (2.4.5) gives

$$w_a(t) = -e^{-2t} \frac{\sin^2(a\pi)}{\pi} \left(1 + \frac{3 - 16a + 16a^2}{4t}\right). \tag{2.4.20}$$

Summing over $a = \frac{k}{n} + \frac{|\alpha|}{2\pi n}$, we get

$$\begin{aligned} c_n(\alpha) &= \frac{e^{-2t}}{2\pi n t} \left(-n^2 t - \frac{8 + n^2}{12} + \frac{2|\alpha|}{\pi} - \frac{\alpha^2}{\pi^2} + 2\Big(\csc^2 \frac{\pi}{n} - \frac{|\alpha|}{\pi}\Big) \cos\frac{\alpha}{n} + \frac{2\alpha}{\pi} \cot\frac{\pi}{n} \sin\frac{\alpha}{n}\right), \\ c_1(\alpha) &= -\frac{e^{-2t}}{\pi} \sin^2\frac{\alpha}{2} \left(1 + \frac{3 + \frac{4\alpha^2}{\pi^2} - \frac{8|\alpha|}{\pi}}{4t}\right). \end{aligned} \tag{2.4.21}$$

The long distance leading term in Eq. (2.4.21) is showed in Fig. 2.10 for two different values of n: it approximates well the solution of the Painlevé equation (2.4.6) in the regime $t \gg 1$. The same feature was observed in Sec. 2.3.3 for the corresponding equations in fermionic systems as also the discontinuity for $n \to 1$, which can be ascribed to the non-commutativity of the limits $n \to 1$ and $t \to \infty$. Also for a complex scalar field, Eqs. (2.4.21) show that the functions $c_n(\alpha)$ vanish for large t and the charged moments stop growing. Hence,

$$\log Z_n(\alpha) \simeq \log Z_n^{(0)}(\alpha) \equiv \int_{m\epsilon}^{\infty} \frac{c_n(\alpha)}{t} dt \simeq -\Big(\frac{1 - n^2}{3n} + \frac{\alpha^2}{2\pi^2 n} - \frac{|\alpha|}{\pi n}\Big) \log m\epsilon. \tag{2.4.22}$$

As expected, the dependence on $\log(m)$ coincides with the one reported in Eq. (2.2.18), up to a factor 2 due to the number of endpoints.

Integrating $c_n(\alpha)$, we obtain up to order $O(e^{-2t}/t)$

$$\begin{aligned} \log Z_n(\alpha) &= \log Z_n^{(0)}(\alpha) - \frac{n e^{-2t}}{4\pi t}, \\ \log Z_1(\alpha) &= \log Z_1^{(0)}(\alpha) - \frac{e^{-2t}}{2\pi t} \sin^2 \frac{\alpha}{2}, \end{aligned} \tag{2.4.23}$$

which are the same expressions found for fermions in Sec. 2.3.3. The expression for $\delta\mathcal{Z}_n(q)$ is the same as in Eq. (2.3.34) for fermions, while $\mathcal{Z}_1(q)$ is given by

$$\mathcal{Z}_1(q) = \frac{|\log m\epsilon|}{\pi^2 q^2 + \log^2 m\epsilon} + O(1/(\log^2 m\epsilon)), \tag{2.4.24}$$

so that all contributions coming from the long-distance behaviour are negligible at order $O(1/(\log m\epsilon))$. The resolved entropies are the ones given in (2.2.24), where S_n also takes into account the term $\frac{ne^{-2t}}{4\pi t}$. The limit $n \to 1$ can be solved through a technique similar to the one used in Sec. 2.3.3.

2.5 Closing remarks

In this Chapter we characterised the SRREs for free massive fields in two dimensions, presenting the results for a Dirac field and a complex scalar theory. We showed that two well known techniques in the framework of the replica trick can be adapted –by modifying the n-sheeted Riemann surface and the corresponding partition function– to the calculation of charged moments. Both computations (via modified twist fields and the Green's function approach of Ref. [178]) mainly rely on the boundary conditions of the fields at the endpoints of the entangling region. In the first framework, the conformal dimensions of the twist fields get modified as in Eq. (2.2.8). In the second setting the change induced by the flux α lies in the precise form of the Painlevé V equations (2.3.6) and (2.4.6) providing the generalised partition function. These Painlevé equations are easily solved numerically for arbitrary values of the mass, but they can be also handled analytically in the limit of small masses, leading to the charged moments (2.3.12) for the Dirac field and (2.4.11) for the scalar theory. The opposite limit of mass much larger that the interval length can also be treated analytically. For the free complex scalar, we also obtain general results for the charged moments in arbitrary dimension when the entangling surface is an hyperplane.

From the Fourier transform of these charged moments, we extract the SRREs, stressing the relevant universal aspects. At leading order for small m, the SRREs for both theories satisfy equipartition of entanglement [85]. We also show that the entanglement equipartition is broken by the mass at order $(\log \ell)^{-2}$, which is the same one found in other circumstances [90, 98, 100, 117].

There is an interesting aspect that one can further study from this Chapter. It concerns the calculation of charged and SRREs in free scalars and fermions in arbitrary dimension and for entangling surfaces that are more complex than the simple hyperplane done in [111]. To this aim, we expect that some of the existing techniques in the literature, as e.g. in Refs. [186–189, 191–196, 219], should be readily adapted to our problem.

2.A Conformal dimensions of twist fields

The goal of this Appendix is to find the conformal dimension of the twist field $\mathcal{T}_{n,k,\alpha}$ defined in Eq. (2.2.4). We will call it generically $\mathcal{T}_a$, where $a = \frac{k}{n} + \frac{\alpha}{2\pi n}$, with $a \in [0, 1]$. As already discussed

in section 2.2.1, in the neighbourhood of a twist field the k-th component of ϕ undergoes a phase rotation

$$\tilde{\phi}_k(e^{2\pi i}z, e^{-2\pi i}\bar{z}) = e^{2\pi i a}\tilde{\phi}_k(z,\bar{z}). \tag{2.A.1}$$

Let us start from the case of the free complex scalar CFT with fields (φ_k, φ_k^*) and, following [155], consider the correlation function in the presence of four $\mathbb{Z}_n$ twist-fields

$$g(z,w;z_i) = \frac{\langle -\frac{1}{2}\partial_z\varphi_k\partial_w\varphi_k^*\mathcal{T}_a(z_1)\tilde{\mathcal{T}}_a(z_2)\mathcal{T}_a(z_3)\tilde{\mathcal{T}}_a(z_4)\rangle}{\langle \mathcal{T}_a(z_1)\tilde{\mathcal{T}}_a(z_2)\mathcal{T}_a(z_3)\tilde{\mathcal{T}}_a(z_4)\rangle}. \tag{2.A.2}$$

Imposing that for $z \to w$ we have $g(z,w;z_i) \sim (z-w)^{-2}$ and that for $z \to z_i$ we have $g(z,w;z_i) \sim (z-z_j)^{-a}$ for $j = 1,3$ and $g(z,w;z_i) \sim (z-z_j)^{-(1-a)}$ for $j = 2,4$, we can write (up to an additional constant independent of z and w, $A(z_j,\bar{z}_j)$)

$$\begin{aligned} g(z,w;z_i) =& \omega_a(z)\omega_{1-a}(w)\left[a\frac{(z-z_1)(z-z_3)(w-z_2)(w-z_4)}{(z-w)^2}\right. \\ &\left. +(1-a)\frac{(z-z_2)(z-z_4)(w-z_1)(w-z_3)}{(z-w)^2} + A(z_j,\bar{z}_j)\right], \end{aligned} \tag{2.A.3}$$

where

$$\omega_a(z) = [(z-z_1)(z-z_3)]^{-a}[(z-z_2)(z-z_4)]^{-(1-a)}. \tag{2.A.4}$$

In the limit $w \to z$

$$\lim_{w\to z}[g(z,w) - (z-w)^{-2}] = \frac{1}{2}a(1-a)\left(\frac{1}{z-z_1}+\frac{1}{z-z_2}+\frac{1}{z-z_3}+\frac{1}{z-z_4}\right)^2 + \cdots \tag{2.A.5}$$

This is exactly the expectation value of the insertion of the stress energy tensor of the field φ_k in the four-point correlation function. From the comparison with the conformal Ward identity, we can understand that $\mathcal{T}_a$ and $\tilde{\mathcal{T}}_a$ are primary fields with scaling dimensions

$$\Delta_a = \bar{\Delta}_a = \frac{1}{2}a(1-a) = \frac{1}{2}\left(\frac{k}{n}+\frac{|\alpha|}{2\pi n}\right)\left(1-\frac{k}{n}-\frac{|\alpha|}{2\pi n}\right). \tag{2.A.6}$$

In order to obtain the conformal dimensions of the twist fields of the free Dirac field theory, let us apply a similar procedure for the chiral or anti-chiral complex fermionic fields, (ψ_k, ψ_k^*). The scaling dimension of $\mathcal{T}_a$ can be extracted from the Green's function in presence of two $\mathbb{Z}_n$ twist fields

$$g(z,w;z_i) = \frac{\langle -\frac{1}{2}(\psi_k^*\partial_z\psi_k - \partial_w\psi_k^*\psi_k)\mathcal{T}_a(z_1)\tilde{\mathcal{T}}_a(z_2)\rangle}{\langle \mathcal{T}_a(z_1)\tilde{\mathcal{T}}_a(z_2)\rangle}. \tag{2.A.7}$$

Using the results in [201], the previous expression can be explicitly written as

$$\begin{aligned} g(z,w;z_i) = \omega_a(z)\omega_{-a}(w)\left[a\frac{(z_2-z_1)(w^2+z^2+2z_1z_2-(z_1+z_2)(w+z))}{2(z-w)}+\right. \\ \left.-\frac{(w-z_1)(w-z_2)(z-z_1)(z-z_2)}{(z-w)^2}\right], \end{aligned} \tag{2.A.8}$$

where

$$\omega_a(z) = [(z-z_1)]^{-a-1}[(z-z_2)]^{a-1}. \tag{2.A.9}$$

In the limit $w \to z$

$$\lim_{w\to z}[g(z,w) + (z-w)^{-2}] = \frac{1}{2}a^2\left(\frac{1}{z-z_1}-\frac{1}{z-z_2}\right)^2 + \cdots \tag{2.A.10}$$

This is the expectation value of the insertion of the stress energy tensor of the field ψ_k in the two-point correlation function and, as before, the comparison with the conformal Ward identity gives the dimensions of the primary twist fields $\mathcal{T}_a$ and $\tilde{\mathcal{T}}_a$ as

$$\Delta_a = \bar{\Delta}_a = \frac{1}{2}a^2 = \frac{1}{2}\left(\frac{k}{n} + \frac{\alpha}{2\pi n}\right)^2 . \tag{2.A.11}$$

Putting together the monodromy conditions (2.A.1) and the scaling dimension of the twist field in Eq. (2.A.11), we deduce that the twist field of a fermionic field admits a bosonisation formula. We can write the complex fermionic field as $\psi_k \sim e^{i\varphi_k}$ and the twist field as $\mathcal{T}_{n,k,\alpha}(z) = e^{i\left(\frac{k}{n}+\frac{\alpha}{2\pi n}\right)\varphi_k}$. By introducing the vertex operators $V_\beta(z) = e^{i\beta\varphi(z)}$, the twist fields take the form $\mathcal{T}_{n,k,\alpha}(z) = V_{\frac{k}{n}+\frac{\alpha}{2\pi n}}(z)$ and $\tilde{\mathcal{T}}_{n,k,\alpha}(z) = V_{-\frac{k}{n}-\frac{\alpha}{2\pi n}}(z)$ [158, 201]. Let us observe that at first sight this result could be misleading since the outcome for bosons in Eq. (2.A.6) does not appear to agree with that of fermions in Eq. (2.A.11) given that they are related by bosonisation in 1+1 dimensions [202–204]. However, via bosonisation of $U(1)$ complex fermions, the corresponding bosons transform by translation, and thus should instead satisfy the boundary condition $\varphi_k(e^{2\pi i}z) = \varphi_k(z) + a$. Therefore, our computation for charged bosons is not related to charged fermions by bosonisation.

Before concluding this appendix, let us emphasise that while CFTs are well understood objects, n-copies of a CFT after modding out the $\mathbb{Z}_N$ symmetry among the replicas form a more complicated object known as orbifold [155, 157]. The operator product expansions of the twist fields with other fields have been extensively explored (e.g., see [205–213]), but, unless a bosonisation procedure for free theories can be used, as for the compact boson, they remain elusive in general and require a case-by-case study.

Chapter 3

Symmetry resolved entanglement entropy in Wess-Zumino-Witten models

The present Chapter is devoted to the decomposition of the Rényi entanglement entropies in theories with a non-abelian symmetry by doing a thorough analysis of Wess-Zumino-Witten (WZW) models. We first consider $SU(2)_k$ as a case study and then generalise to an arbitrary non-abelian Lie group. We find that at leading order in the subsystem size ℓ the entanglement is equally distributed among the different sectors labelled by the irreducible representation of the associated algebra. We also identify the leading term that breaks this equipartition: it does not depend on ℓ but only on the dimension of the representation. Moreover, a $\log\log\ell$ contribution to the Rényi entropies exhibits a universal prefactor equal to half the dimension of the Lie group. This Chapter is based on Ref. [121].

3.1 Introduction

Two-dimensional conformal field theories are characterised by an infinite-dimensional algebra, known as a Virasoro algebra, that leads to their exact solution [202, 214, 269]. There exists a set of field theories that present, in addition to conformal invariance, an internal Lie group symmetry: the Wess-Zumino-Witten models, that possess interesting applications in a wide range of topics, such as the study of fundamental interactions, statistical mechanics, and condensed matter theory [215–218]. In the present Chapter, such theories will be the arena to study the decomposition of the entanglement into the charge sectors of the symmetry.

We specify the problem to address by generalising the concepts about the symmetry-resolution of Sec. 1.3 in the non-abelian case. We consider a 1+1d field theory on the infinite line $\mathbb{R}$, with the Hilbert space $\mathcal{H}$, and a symmetry group G that acts unitarily on $\mathcal{H}$. The spatial bipartition $\mathbb{R} = A \cup B$ with $A = [0, \ell]$ and $B = (-\infty, 0) \cup (\ell, +\infty)$ corresponds to a bipartition of the Hilbert space of the field theory, $\mathcal{H} = \mathcal{H}_A \otimes \mathcal{H}_B$, and we assume that the action of G is such that, for any element $g \in G$, the unitary matrix U_g acting on $\mathcal{H}$ can be decomposed as $U_g = U_g^A \otimes U_g^B$, where U_g^A (U_g^B) is a unitary operator acting on $\mathcal{H}_A$ ($\mathcal{H}_B$).

We focus on the SREE of the ground state of the quantum field theory. We assume that the ground state $|\psi_0\rangle$ is non-degenerate, so that it is invariant under the action of G: $U_g |\psi_0\rangle = |\psi_0\rangle$.

Consequently, the RDM ρ_A is also invariant (under the action of G restricted to $\mathcal{H}_A$):

$$\begin{aligned} U_g^A \rho_A U_g^{A\dagger} &= U_g^A \left(\mathrm{Tr}_B \left|\psi_0\right\rangle \left\langle\psi_0\right|\right) U_g^{A\dagger} = \mathrm{Tr}_B \left(U_g^A \left|\psi_0\right\rangle \left\langle\psi_0\right| U_g^{A\dagger}\right) \\ &= \mathrm{Tr}_B \left(U_{g^{-1}}^B U_g \left|\psi_0\right\rangle \left\langle\psi_0\right| U_g^\dagger U_{g^{-1}}^{B\dagger}\right) = \mathrm{Tr}_B \left(U_{g^{-1}}^B \left|\psi_0\right\rangle \left\langle\psi_0\right| U_{g^{-1}}^{B\dagger}\right) \\ &= \mathrm{Tr}_B \left|\psi_0\right\rangle \left\langle\psi_0\right| = \rho_A, \end{aligned} \tag{3.1.1}$$

where we have used the cyclicity of the trace and the unitarity of $U_{g^{-1}}^B$ to arrive at the last line. Thus, when decomposing the Hilbert space $\mathcal{H}_A$ into a direct sum of irreducible representations of G, the RDM ρ_A is block-diagonal in the corresponding basis:

$$\rho_A = \bigoplus_r p(r)\rho_A(r) = \left(\begin{array}{c|c|c} p(1)\rho_A(1) & & \\ \hline & p(2)\rho_A(2) & \\ \hline & & \ddots \end{array}\right). \tag{3.1.2}$$

Here r labels the irreducible representations of G.

In Eq. (3.1.2), the block $\rho_{A,r}$ is normalised such that $\mathrm{Tr}\rho_{A,r} = 1$, and $p_r \equiv \mathrm{Tr}(\Pi_r \rho_A)$ is a non-negative number such that $\sum_r p_r = \mathrm{Tr}\rho_A = 1$ (Π_r is the projector on the irrep r). As already showed for the abelian case in Sec. 1.3, the SREE measures the entanglement in the subsystem A for a fixed symmetry sector, i.e.

$$S_n(r) = \frac{1}{1-n} \log \mathrm{Tr}_A \rho_A(r)^n, \qquad S_1(r) = \lim_{n\to 1} S_n(r). \tag{3.1.3}$$

Similarly to Eq. (1.3.5), the total von Neumann entanglement entropy can be written as [10, 81]

$$S_1 = \sum_r p(r) S_1(r) - \sum_r p(r) \log p(r) \equiv S_{\mathrm{c}} + S_{\mathrm{num}}. \tag{3.1.4}$$

It is worth mentioning that the relation in Eq. (3.1.4) has also been exploited to study the entanglement structure for both abelian and non-abelian (lattice) gauge theories, e.g. in [219–224]. In the gauge theories, the symmetry resolved entropy $S_1(r)$ is further split into two contributions.

The goal of this Chapter is to study how the total entanglement splits into the contributions coming from symmetry sectors in CFTs with a non-abelian Lie group symmetry, i.e. the WZW models. They are described by a two-dimensional action which consists of a non-linear σ term plus the Wess-Zumino term, whose topological coupling factor k is constrained to be an integer number and it is referred to as the level of the model [215, 216]. Here we follow the conventions of Ref. [269]. For simplicity, we assume that the Lie group G is compact and simple.
These WZW models are the scaling limit of critical quantum spin chains with the same symmetry [217, 218, 225]. For instance, some possible discretisations of $SU(2)_k$ are the Heisenberg spin-1/2 chain or the Haldane-Shastry model for $k = 1$ [231–235]. They have been also studied in the context of topological anyons on 1D chains [236]. Spin chains associated with spin $j = k/2$, $k > 1$ correspond to $SU(2)_k$ WZW models, which can mark phase transitions between different gapped phases, as in the Babudjan-Takhtajan chains [237–239].

The Chapter is structured as follows. In Sec. 3.2, we review the example of a non-abelian resolution for a $SU(2)$ spin chain. In Sec. 3.3, we present the WZW-models, its symmetry algebra and we introduce the notion of character of a representation. Using the modular properties of unspecialised characters, we calculate the moments of the RDM in presence of a charge flux, that we call charged moments and we give an alternative derivation of the symmetry decomposition of entanglement for WZW-models with $SU(2)_k$ symmetry in Sec. 3.4. This strategy has the advantage of being generalisable for the computation of the SRREs for an arbitrary non-abelian symmetry, as showed in Sec. 3.5. We conclude in Sec. 3.6.

3.2 Overview of known results for $SU(2)$

In this section we review the known results about the symmetry resolution of a $SU(2)$ symmetry, following Ref. [84]. However, the method of Ref. [84] for the $SU(2)$ case is not generalisable to other groups G; nevertheless we review it here for completeness and as a comparison for our main derivation. The more general method is presented in details in Secs. 3.4 and 3.5.

3.2.1 $SU(2)$ symmetry resolved entanglement (after Ref. [84])

Let us recall that the charged moments for a single interval of length ℓ on the infinite line of a free massless compact boson (a generalisation of Eq. (2.2.8) for $K = 1$), which is the easiest CFT with $U(1)$ symmetry, behave as [84]

$$\frac{Z_n(\alpha)}{Z_1^n} = c_{n,\alpha}\ell^{-\frac{c}{6}(n-\frac{1}{n})-\frac{2K}{n}(\frac{\alpha}{2\pi})^2}, \tag{3.2.1}$$

where $c_{n,\alpha}$ is a non-universal constant which depends on the cutoff (i.e. the microscopic details of the model). To tackle the $SU(2)$ case, the authors of Ref. [84] rely on the following trick, which allows them to recycle the result for the $U(1)$ case. Decomposing the Hilbert space $\mathcal{H}_A$ into $SU(2)$ sectors with spin j and magnetisation j^z, they notice that, for an $SU(2)$-invariant RDM ρ_A,

$$\mathrm{Tr}_{J_A=j}\rho_A^n = (2j+1)(\mathrm{Tr}_{J_A^z=j}\rho_A^n - \mathrm{Tr}_{J_A^z=j+1}\rho_A^n). \tag{3.2.2}$$

Here the trace in the left-hand side is over all states in $\mathcal{H}_A$ with spin $J_A = j$, while the two traces in the right-hand side are over all states with fixed magnetisation J_A^z, without restriction on the total spin J_A. Eq. (3.2.2) is slightly different from the identity used in [84]:

$$\mathrm{Tr}_{J_A=j,J_A^z=j^z} = \mathrm{Tr}_{J_A^z=j}\rho_A^n - \mathrm{Tr}_{J_A^z=j+1}\rho_A^n, \tag{3.2.3}$$

i.e. the trace in the left-hand side is over all states with fixed spin $J_A = j$ and $J_A^z = j^z$, whose multiplet structure gives the contribution $(2j + 1)$ in our Eq. (3.2.2). A sketch of a derivation of that identity is given in [121]. First, let us explain how the $SU(2)$ SREE can be obtained from there. The point is that the operator J_A^z generates a $U(1)$ symmetry (an abelian subgroup of $SU(2)$) so it can be identified with the charge operator Q of the previous section (up to an unimportant constant). The two terms in the right-hand side of Eq. (3.2.2) can be computed using the same methods as for the $U(1)$ case. Indeed, the charged moments related to the $U(1)$ subgroup are just given by Eq. (3.2.1), with $K = k/2$, see Refs. [84, 85] and Sec. 3.4.2. The saddle point approximation of the Fourier transform gives

$$\begin{aligned}\mathcal{Z}_n(J_A^z = j) &= \frac{1}{Z_1^n}\int_{-\pi}^{\pi}\frac{d\alpha}{2\pi}e^{-i\alpha j}Z_n(\alpha) \\ &\simeq c_{n,0}\ell^{-\frac{c}{6}(n-\frac{1}{n})}e^{-\frac{nj^2\pi^2}{k\log(\ell/\epsilon)}}\left(\frac{(\pi n)^{1/2}}{k^{1/2}(\log\ell)^{1/2}}+\dots\right),\end{aligned} \tag{3.2.4}$$

where the dots stands for neglected subleading contributions, due e.g. to $c_{n,\alpha}$. From Eq. (3.2.2) we get

$$\mathcal{Z}_n(J_A = j) \simeq c_{n,0}e^{-\frac{nj^2\pi^2}{k\log(L/\epsilon)}}\ell^{-\frac{c}{6}(n-\frac{1}{n})}(2j+1)^2\frac{\pi^{5/2}n^{3/2}}{k^{3/2}(\log\ell)^{3/2}}, \tag{3.2.5}$$

where we keep the Gaussian factor in order to have a normalised probability $\mathcal{Z}_1^{J_A=j}(\ell)$. Eq. (3.2.5) leads to the desired SRREs for the spin-j representation:

$$S_n(j) = S_n - \frac{3}{2}\log(\log \ell) + 2\log(2j+1) - \log(2^{3/2}\pi^2) + \frac{3}{2}\left(-\log k + \frac{\log(n)}{1-n} + \log(2\pi^3)\right) + o(\ell^0). \quad (3.2.6)$$

This result is the first example of a non-abelian symmetry resolution in the literature, but it cannot be easily generalised to an arbitrary non-abelian symmetry because it strongly relies on the identity (3.2.2). However, an alternative derivation of the same result in Sec. 3.4 will allow us to perform such generalisation.

3.3 WZW models: currents and characters

In this section we introduce our conventions for WZW models and review some fundamental objects which will be useful later on. The interested readers can consult the comprehensive literature on the subject, for example in [202, 215, 240, 269].

3.3.1 WZW model on G and current algebra

We consider a compact simple Lie group G and the associated Lie algebra $\mathfrak{g} = \mathrm{Lie}(G)$. Let J^a ($a = 1, \ldots, \dim \mathfrak{g}$) be generators of $\mathfrak{g}$, with commutation relations

$$[J^a, J^b] = \sum_c i f^{ab}{}_c J^c, \quad (3.3.1)$$

with structure constants $f^{ab}{}_c$.
In the WZW model on the Lie group G, the symmetry is locally generated by the holomorphic and anti-holomorphic current $J^a(z)$ and $\overline{J}^a(\bar{z})$, where $(z, \bar{z})$ are complex coordinates for 2D Euclidean space. As usual in CFT, the holomorphic and anti-holomorphic components are independent and isomorphic. Focusing on the holomorphic components, the modes in their Laurent expansion

$$J^a(z) = \sum_{n=-\infty}^{\infty} \frac{J_n^a}{z^{n+1}} \quad (3.3.2)$$

obey the commutation relations of the Kac-Moody algebra at level k (the level k is a positive integer),

$$[J_n^a, J_m^b] = i\sum_c f^{ab}{}_c J_{m+n}^c + k\, m\, K(J^a, J^b)\, \delta_{m+n,0}. \quad (3.3.3)$$

Here,

$$K(X, Y) \equiv \frac{1}{2g}\mathrm{Tr}(\mathrm{ad}X \mathrm{ad}Y) \quad (3.3.4)$$

is the Killing form of $\mathfrak{g}$, which is positive definite because G is compact. We follow the normalisation convention of Ref. [269], with the inclusion of the factor $\frac{1}{2g}$ where g is the dual Coxeter number of $\mathfrak{g}$.
The currents can be multiplied to construct the energy-momentum tensor, whose mode expansion generates the Virasoro algebra. Mathematically, this means that the enveloping algebra of the Kac-Moody algebra contains a subalgebra that is the Virasoro algebra, a result which is known

as the Sugawara construction [269]. We can express the energy-momentum tensor in terms of the currents in the following way:

$$T(z) = \frac{1}{2(k+g)} \sum_a : J^a(z) J^a(z) :, \tag{3.3.5}$$

where :: denotes the normal ordering, which consists in the subtraction of the singular terms. The computation of the operator product expansion $T(z)T(w)$ determines the central charge c of the theory, which is

$$c = \frac{k \dim(G)}{k+g}, \tag{3.3.6}$$

where $\dim(G) = \dim \mathfrak{g}$ is the dimension of the Lie group G, or equivalently the dimension of $\mathfrak{g}$. As already mentioned, the stress-energy tensor can be expanded into mode operators, L_n, the Virasoro generators, that read

$$L_n = \frac{1}{2\pi i} \oint dz\, z^{n+1} T(z) = \frac{1}{2(k+g)} \sum_a \sum_m : J^a_m J^a_{n-m} :, \tag{3.3.7}$$

where the integration contour circles the origin and the normal ordering means that positive modes should appear to the right of negative ones.

3.3.2 The unspecialised characters and their asymptotic behaviour

Primary fields of WZW models are in one-to-one correspondence with highest weight representations of the Kac-Moody algebra (3.3.3), see e.g. Ref. [269]. Each primary field transforms as a representation r under conjugation by elements of G, so we can label them by irreps of G. The *unspecialised character* of the corresponding highest weight representation of the Kac-Moody algebra $\mathcal{M}_r$ is defined as

$$\chi_r(\mathbf{x}, \tau) = \mathrm{Tr}_{\mathcal{M}_r} e^{i \sum_a x_a J^a_0} e^{2\pi i \tau (L_0 - \frac{c}{24})}. \tag{3.3.8}$$

Here $\mathbf{x} = (x_1, \ldots, x_{\dim\, \mathfrak{g}})$ is the coordinate of elements in the Lie algebra, so $e^{i \sum_a x_a J^a}$ is viewed as an element of G via the exponential map. When $\mathbf{x} = 0$, Eq. (3.3.8) is referred to as the *specialised character*, $\chi_r(\tau) := \chi_r(0, \tau)$. We note that, in the literature (see e.g. [240]), unspecialised characters are sometimes defined alternatively as

$$\mathrm{Tr}_{\mathcal{M}_r} e^{i \sum_b \alpha_b H^b_0} e^{2\pi i \tau (L_0 - \frac{c}{24})}, \tag{3.3.9}$$

where H^b ($b = 1, \ldots, \mathrm{rank}\ \mathfrak{g}$) are Cartan generators (i.e. the generators of a maximal commuting subalgebra of $\mathfrak{g}$), so that $\sum_b \alpha_b H^b$ is an element of the Cartan subalgebra $\mathfrak{h} \subset \mathfrak{g}$, instead of an arbitrary element of $\mathfrak{g}$. We stress that this makes no difference, because any element of $\mathfrak{g}$ is conjugated to an element of $\mathfrak{h}$. In other words, for any element $\sum_a z_a J^a \in \mathfrak{g}$, there exists $g \in G$ such that $\sum_a z_a J^a = g^{-1} \sum_b \alpha_b H^b g$ for some $\sum_b \alpha_b H^b \in \mathfrak{h}$. Using the fact $[g, L_0] = 0$ and the cyclicity of the trace, one sees that the two definitions are equivalent.
In what follows, we will need the asymptotics of $\chi_r(\mathbf{x}, \tau)$ when $\tau \to i0^+$. This is obtained by using the modular properties of the characters. Under the modular transformation $\tau \to -1/\tau$, the unspecialised character (3.3.8) transforms as [240, 269]

$$\chi_r(\mathbf{x}, \tau) = e^{-i \frac{k}{4\pi\tau} K(\mathbf{x}\cdot\mathbf{J}, \mathbf{x}\cdot\mathbf{J})} \sum_{r'} S_{rr'}\ \chi_{r'}\left(\frac{\mathbf{x}}{\tau}, -\frac{1}{\tau}\right), \tag{3.3.10}$$

where S is the modular S-matrix, which is unitary and symmetric. In the argument of the exponential, we use the notation $\mathbf{x} \cdot \mathbf{J} = \sum_a x_a J^a$, and $K(.,.)$ is the positive definite Killing form,

normalised as in Eq. (3.3.4). As explained in the following sections, we are mainly interested in the behaviour of characters around the elements of the center of G, e.g. the unit element. Therefore, in the limit $\tau \to i0^+$, we can keep only the leading contribution of each character $\chi_{r'}\left(-\frac{1}{\tau}\right)$, i.e.

$$\chi_r(\mathbf{x},\tau) \underset{\tau\to i0^+}{\simeq} e^{-i\frac{k}{4\pi\tau}K(\mathbf{x}\cdot\mathbf{J},\mathbf{x}\cdot\mathbf{J})} \sum_{r'} S_{rr'} e^{-\frac{2\pi i}{\tau}(h_{r'}-\frac{c}{24})}, \tag{3.3.11}$$

where $h_{r'}$ is the conformal dimension of the primary field associated with the highest weight representation r'. The leading behaviour of Eq. (3.3.11) is given by the smallest dimension field. Since we are dealing with unitary theories, this is given by the identity with $h_0 = 0$, while the conformal dimensions of all other fields are strictly positive. As a consequence, we have [269]

$$\chi_r(\mathbf{x},\tau) \underset{\tau\to i0^+}{\simeq} S_{r,0}\; e^{\frac{\pi i c}{12\tau}}\; e^{-i\frac{k}{4\pi\tau}K(\mathbf{x}\cdot\mathbf{J},\mathbf{x}\cdot\mathbf{J})}. \tag{3.3.12}$$

This asymptotic behaviour plays a key role in our derivation of the SRREs below.

3.3.3 Haar measure on G from the Killing form, and orthonormality of group characters

Metric and Haar measure. Importantly, because G is compact and simple, the Killing form $K(.,.)$ is positive definite on $\mathfrak{g}$. The Killing form then gives rise to a Riemannian metric on G. In a local coordinate chart $\mathbf{x} \in \mathbb{R}^{\dim(G)} \mapsto g(\mathbf{x}) \in G$, this metric can be defined as follows:

$$K_{ab}(\mathbf{x}) \equiv K(i\; g^{-1}(\mathbf{x})\partial_a g(\mathbf{x}), i\; g^{-1}(\mathbf{x})\partial_b g(\mathbf{x})). \tag{3.3.13}$$

[The factors i come from the fact that we use the physics convention that the Lie algebra elements $X \in \mathfrak{g}$ are multiplied by i before being exponentiated to give a group element $e^{iX} \in G$. Then $g^{-1}(\mathbf{x})\partial_b g(\mathbf{x})$ needs to be multiplied by i to be in the Lie algebra.] This metric induces a volume form on G,

$$d\mu(g(\mathbf{x})) \equiv \sqrt{\det K(\mathbf{x})}\, d\mathbf{x}, \tag{3.3.14}$$

which turns out to be the Haar measure on G. We recall that the Haar measure is unique up to normalisation, and here the normalisation of the measure $d\mu$ is fixed by the normalisation of the Killing form. In particular, the volume of the group

$$\mathrm{Vol}(G) \equiv \int_G d\mu(g) \tag{3.3.15}$$

is fixed by this normalisation convention [241].

To see that the measure (3.3.14) is the Haar measure on G, one can check that it is invariant under left multiplication by a fixed group element $h \in G$,

$$d\mu(hg) = d\mu(g), \tag{3.3.16}$$

which is a consequence of the invariance of the Killing form under conjugation by elements of G,

$$K(h^{-1}Xh, h^{-1}Yh) \;=\; K(X,Y), \qquad \text{for all} \quad h \in G. \tag{3.3.17}$$

Moreover, for compact Lie groups, a left invariant measure must also be right invariant, i.e. $d\mu(gh) = d\mu(g)$, so it is the Haar measure on G.

Group characters. Finally, let us recall the definition of group characters. Given $g \in G$, a representation U_g is not unambiguous since any similarity transformation yields an equivalent form. In order to describe the invariant properties of the group, one could use the eigenvalues of a representation matrix which do not change under similarity transformations. This leads to the construction of the *Casimir operators*, the eigenvalues of which classify the representation. Since this is in general a very difficult problem, in many cases it is sufficient to use a simpler invariant, namely the group character of a representation r, which is defined in terms of the unitary matrix U_g as

$$\chi_r(g) = \mathrm{Tr} U_g, \tag{3.3.18}$$

and it is invariant under similarity transformations. Importantly, group characters of irredubile representations are orthonormal with respect to the Haar measure,

$$\frac{1}{\mathrm{Vol}(G)} \int_G d\mu(g) \chi_r(g) \chi^*_{r'}(g) = \delta_{rr'}. \tag{3.3.19}$$

3.4 Revisiting the $SU(2)_k$ case

In this section we provide a detailed derivation of the charged moments for $SU(2)_k$ and the corresponding entanglement decomposition. This alternative approach with respect to the one reviewed in Sec. 3.2.1 leads to a generalisation to an arbitrary non-abelian symmetry reported in the next section.

3.4.1 The entanglement Hamiltonian

We focus on a critical system described by the WZW-model $SU(2)_k$ at level k, and central charge $c = \frac{3k}{k+2}$, where we used Eq. (3.3.6) with $g = 2$. In CFT, the powers of the RDM, ρ_A^n, are expressed as [17, 242]

$$\rho_A^n = \frac{e^{-2\pi n K_A}}{Z_1^n}, \quad Z_1 = \mathrm{Tr}_A e^{-2\pi K_A}, \tag{3.4.1}$$

where $K_A = \int_A dx T_{00}(x)/f'(x)$ is the entanglement Hamiltonian and T_{00} is a component of the stress tensor (see also Chapter 12). The function $f(x)$ is the conformal map from the euclidean spacetime, with a cut along the interval A and two boundaries, into an annulus of width $2\log L/\epsilon$ and height 2π [242]. For the ground state of a CFT on the real line, K_A is proportional to the Virasoro generator L_0 up to an additive constant,

$$K_A = \frac{\pi}{2\log(L/\epsilon)} \left(L_0 - \frac{c}{24} \right), \tag{3.4.2}$$

therefore

$$Z_n = \mathrm{Tr}_A e^{-2\pi n K_A} = \mathrm{Tr}_A q^{L_0 - \frac{c}{24}}, \qquad q = e^{2\pi i \tau}, \tau = \frac{i\pi n}{2\log(\ell/\epsilon)} \tag{3.4.3}$$

with ϵ the UV cutoff. This is nothing but a consequence of the celebrated Bisognano-Wichmann theorem [243, 244] joined with conformal invariance [242, 245].

3.4.2 Charged moments and $SU(2)_k$ characters

We are interested in how Z_n can be resolved in the different j sectors of our theory, $\mathcal{Z}_n(j, \tau)$. The Hilbert space $\mathcal{H}_A$ is a linear combination of the modules, $\mathcal{M}_j$, corresponding to a given representation labelled by j, $\mathcal{H}_A = \oplus_j n_j \mathcal{M}_j$ with coefficients n_j. In order to achieve our goal, let

us focus on the charged moments for the conserved quantity J_0^z. In this section $Z_n(\alpha,\tau)$ stands for the charged moments (1.4.16) related to this $U(1)$ charge. They can be written as a linear combination of the unspecialised characters introduced in Eq. (3.3.8) [85], i.e.

$$Z_n(\alpha,\tau)=\sum_j n_j\chi_j(\alpha,\tau),\qquad \chi_j(\alpha,\tau)=\mathrm{Tr}_{\mathcal{M}_j}q^{L_0-\frac{c}{24}}e^{i\alpha J_0^z}. \tag{3.4.4}$$

Here the trace is over all states in the representation with highest weight j and level k, which belong to the module $\mathcal{M}_j$. The index $j=0,\frac{1}{2}\dots\frac{k}{2}$ labels all the unitary representations of the Kac-Moody algebra of $SU(2)_k$ [269]. At this point we are forced to make some physical assumptions on the allowed values of n_j, i.e. on the structure of the entanglement spectrum of the CFT. For example the approach reviewed in Sec. 3.2.1 comes from the continuum limit of an $SU(2)$ spin chain. In that case, the total spin of the subsystem A would be either integer or half-integer depending on the parity of the length ℓ of the subsystem. Consequently, $n_j=0$ for half-integer j when ℓ is even, while $n_j=0$ for integer j if ℓ is odd. From a CFT perspective, we conclude that the continuum limit of the spin chain induced boundary conditions at the two entangling point of the subsystem A that select only integer or half-integers values of j's (although this is difficult to prove directly, see e.g. [246] for a similar issue). We stress that, from the CFT side, other choices of n_j are also fully legitimate; anticipating the result, they all lead to the same double logarithmic factor in the SRREs, but to a different $O(1)$ term which is affected by a boundary factor $\log g$ (g is the Affleck-Ludwig non-integer ground state degeneracy [247]) resulting from the induced boundary CFT at the entangling points; in turn this is very similar to what is known for the total entanglement entropy [201, 246].

Going back to our main computation, the $SU(2)_k$ characters are known in the literature and in order to write them down in a compact form, we first define the level-k theta functions

$$\Theta_m^{(k)}(\alpha,\tau)\equiv\sum_{n\in\mathbb{Z}+\frac{m}{2k}}q^{kn^2}y^{kn},\qquad y=e^{i\alpha}. \tag{3.4.5}$$

Then the $SU(2)_k$ characters read [269]

$$\chi_j(\alpha,\tau)=\frac{\Theta_{2j+1}^{(k+2)}(\alpha,\tau)-\Theta_{-2j-1}^{(k+2)}(\alpha,\tau)}{\Theta_1^{(2)}(\alpha,\tau)-\Theta_{-1}^{(2)}(\alpha,\tau)}= \frac{\Theta_{2j+1}^{(k+2)}(\alpha,\tau)-\Theta_{-2j-1}^{(k+2)}(\alpha,\tau)}{q^{\frac{1}{8}}(y^{\frac{1}{2}}-y^{-\frac{1}{2}})\prod_{n=1}^{\infty}(1-q^n)(1-yq^n)(1-y^{-1}q^n)}. \tag{3.4.6}$$

In the limit $\ell\gg\epsilon$, one has $q\simeq 1$, so that a large number of terms contribute to Eq. (3.4.6). However, using the modular transformation $\tau\to-1/\tau$, we get

$$\chi_j(\alpha,\tau)=e^{-\frac{\pi ik(\alpha/(2\pi))^2}{2\tau}}\sum_{j'}S_{jj'}\chi_{j'}\left(\frac{\alpha}{\tau},-\frac{1}{\tau}\right),\qquad S_{jj'}=\sqrt{\frac{2}{k+2}}\sin\frac{\pi(2j+1)(2j'+1)}{k+2}. \tag{3.4.7}$$

In the limit $\ell\gg\epsilon$, only the term with $j'=0$ survives in the sum, so for α around 0 the final result is

$$Z_n(\alpha,\tau)=\sum_j n_j\chi_j(\alpha,\tau)\simeq c_{n,\alpha}\Big(\sum_j S_{j0}n_j\Big)e^{2\log(\ell/\epsilon)\left[\frac{c}{12}\left(\frac{1}{n}\right)-\frac{k}{2n}\frac{\alpha^2}{4\pi^2}\right]}, \tag{3.4.8}$$

as already obtained in [85]. Similar techniques have been employed for the entanglement entropies in Ref. [182]. Here $c_{n,\alpha}$ is a non-universal constant which depends on the cutoff (see also the discussion after Eq. (3.2.1) for the abelian case).

We already mentioned in Sec. 3.2 that we are ultimately interested in the saddle point evaluation of the integral which leads to the evaluation of the SRREs. As we explain in Sec. 3.4.3, in this case the saddle points are determined by the behaviour of the charged moments around $\alpha = 0$ and $\alpha = 2\pi$, which correspond to the two elements of the center of $SU(2)$, $Z = \{1, -1\}$ (see the parameterisation (3.4.13) of the elements of $SU(2)$). It is not sufficient to know the asymptotic behaviour (3.4.8) around $\alpha = 0$, we also need to know the one around $\alpha = 2\pi$. However, when we set $\alpha' \equiv 2\pi - \alpha$, we observe that

$$Z_n(\alpha, \tau) = \sum_j n_j \chi_j(2\pi - \alpha', \tau) = \sum_j n_j \mathrm{Tr}_{\mathcal{M}_j} (-1)^{2J_0^z} q^{L_0 - \frac{c}{24}} e^{i\alpha' J_0^z} = \sum_j n_j (-1)^{2j} \chi_j(\alpha', \tau). \tag{3.4.9}$$

Since either all j are integer or they are all half-integer, the factor $(-1)^{2j}$ simply reduces to an overall factor 1 or -1, respectively. Moreover, the previous asymptotic expansion yields, for α' around 0,

$$Z_n(2\pi - \alpha', \tau) \simeq c_{n,2\pi-\alpha'} \Big(\sum_j (-1)^{2j} S_{j0} n_j \Big) e^{2\log(\ell/\epsilon)\left[\frac{c}{12}\left(\frac{1}{n}\right) - \frac{k}{2n}\frac{\alpha'^2}{4\pi^2}\right]}. \tag{3.4.10}$$

To summarise, Eq. (3.4.8) gives the large ℓ behaviour when $\alpha \in [0, \pi]$, while Eq. (3.4.9) gives the leading contribution when $\alpha \in (\pi, 2\pi]$. We now turn to the analysis of the integral over all group elements parameterised by (3.4.13), where we use these asymptotic behaviours.

3.4.3 Projecting the charged moments on the spin j representation

The idea to project the charged moments on the spin j representation is to use the orthonormality of the group characters with respect to the Haar measure to isolate the contribution from all states of spin j in the trace (3.4.3), corresponding to the term proportional to the group character $\chi_j(\alpha)$. This is done by using the orthonormality of group characters with respect to the Haar measure, i.e. using the following relation between the matrix representation of the group element g in $\mathcal{H}_A$, U_g^A, and the projector Π_j on all states transforming in the represention j:

$$\Pi_j = \frac{(2j+1)}{\mathrm{Vol}(SU(2))} \int_G d\mu(g) \chi_j^*(g) U_g^A, \tag{3.4.11}$$

where the factor $(2j + 1)$ is the dimension of the representation. Let us observe that if we were interested in a symmetry decomposition of entanglement with respect to both j, j^z (as done in [84]), because of the multiplet structure of $SU(2)$, the factor $2j + 1$ in Eq. (3.4.11) should be removed. In other words, all the $2j + 1$ states belonging to the same irrep j give the same contribution to the entanglement. For $SU(2)$, the group characters are given by

$$\chi_j(\alpha) = \sum_{m=-j}^{j} y^m = \frac{y^{j+\frac{1}{2}} - y^{-j-\frac{1}{2}}}{y^{\frac{1}{2}} - y^{-\frac{1}{2}}} = \frac{\sin((j+\frac{1}{2})\alpha)}{\sin\frac{\alpha}{2}}, \tag{3.4.12}$$

whose behaviour around $\alpha = 0$ is $\chi_j(0) = 2j + 1$, while around $\alpha = 2\pi$ is $\chi_j(2\pi) = (-1)^{2j}(2j + 1)$.

As already discussed in Sec. 3.3.2, the simplest way to measure invariantly the volume of a group, $SU(2)$ in this case, is to start from the Killing metric in the Lie algebra. We can write down a generic element of $SU(2)$ in its exponential form as

$$g(x, y, z) = e^{i(x\sigma_x + y\sigma_y + z\sigma_z)/2} = \mathbb{1} \cos\frac{\alpha}{2} + i\frac{\sin(\alpha/2)}{\alpha}(x\sigma_x + y\sigma_y + z\sigma_z),$$
$$\alpha = \sqrt{x^2 + y^2 + z^2} \in [0, 2\pi] \tag{3.4.13}$$

where (x, y, z) are the coordinates of the Lie algebra $\mathfrak{su}(2)$ and σ_i the Pauli matrices. Let us observe that for $\alpha = 2\pi$, $g = -\mathbb{1}$, i.e. the behaviour of g around $\alpha = 0, 2\pi$ corresponds to the behaviour around the two elements of the center of $SU(2)$, $\mathbb{Z}_2$, i.e. respectively $+\mathbb{1}$ and $-\mathbb{1}$. The Killing form is given by

$$K(\sigma_i, \sigma_j) = \frac{1}{4}\mathrm{Tr}(\mathrm{ad}\frac{\sigma_i}{2}\,\mathrm{ad}\frac{\sigma_j}{2}) = \frac{1}{4}\mathrm{Tr}(\sigma_i\sigma_j) = \frac{\delta_{ij}}{2}, \qquad i, j \in \{x, y, z\} \tag{3.4.14}$$

where we used that $g = 2$ for $SU(2)$. Once we have found the Killing form, using Eq. (3.3.13), we can fix the metric $K_{ab}(x, y, z), a, b \in \{x, y, z\}$ and compute

$$\sqrt{\det K_{ab}(x, y, z)} = \sqrt{2}\Big(\frac{\sin(\alpha/2)}{\alpha}\Big)^2. \tag{3.4.15}$$

We can rewrite it in polar coordinates $(x, y, z) = (\alpha\cos\gamma\sin\beta, \alpha\sin\gamma\sin\beta, \alpha\cos\beta)$ such that

$$\begin{aligned}\mathrm{Vol}(SU(2)) =& \sqrt{2}\int_{\sqrt{x^2+y^2+z^2}\leq 2\pi} dx\,dy\,dz\,\Big(\frac{\sin(\alpha/2)}{\alpha}\Big)^2 = \\ =& \sqrt{2}\int_0^{2\pi}\int_0^{\pi}\int_0^{2\pi} d\alpha d\beta d\gamma \alpha^2\sin\beta\frac{\sin^2(\alpha/2)}{\alpha^2} = 2^{5/2}\pi^2.\end{aligned} \tag{3.4.16}$$

From the volume form in Eq. (3.4.15) we can explicitly write down the Haar measure for $SU(2)$ as

$$d\mu(\alpha, \beta, \gamma) = \sqrt{2}\sin^2\frac{\alpha}{2}\sin\beta\,d\alpha\,d\beta\,d\gamma \qquad 0 \leq \alpha \leq 2\pi, 0 \leq \beta \leq \pi, 0 \leq \gamma \leq 2\pi. \tag{3.4.17}$$

One can also explicitly check that using Eq. (3.4.17) and the $SU(2)$ characters in Eq. (3.4.12), the orthogonality relation in Eq. (3.3.19) is satisfied.

Using Eq. (3.4.8), we get

$$\begin{aligned}\mathcal{Z}_n(j) =& \frac{2j+1}{\mathrm{Vol}(SU(2))}\int d\mu(\alpha,\beta,\gamma)\frac{Z_n(\alpha,\tau)}{Z_1^n}\chi_j(\alpha) \\ \simeq& \frac{e^{-\frac{nj^2\pi^2}{k\log(\ell/\epsilon)}}}{2\mathrm{Vol}(SU(2))}(2j+1)^2\Big[\frac{Z_n(0,\ell)}{Z_1^n}\sqrt{\frac{2^5n^3\pi^9}{k^3\log^3(\ell/\epsilon)}} + \frac{Z_n(2\pi,\ell)}{Z_1^n}(-1)^{2j}\sqrt{\frac{2^5n^3\pi^9}{k^3\log^3(\ell/\epsilon)}}\Big] \\ \simeq& \frac{e^{-\frac{nj^2\pi^2}{k\log(\ell/\epsilon)}}}{\mathrm{Vol}(SU(2))}\frac{Z_n(0,\ell)}{Z_1^n}(2j+1)^2\sqrt{\frac{2^5n^3\pi^9}{k^3\log^3(\ell/\epsilon)}},\end{aligned} \tag{3.4.18}$$

where we approximate the first line by two integrals, one around $\alpha = 0$, the other around $\alpha = 2\pi$. Indeed, for $\alpha \in [0, 2\pi]$ there is a saddle point at $\alpha = 0$ and one at $\alpha = 2\pi$. The first one corresponds to study the charged moments around $g = \mathbb{1}$, while the second one around $g = -\mathbb{1}$, which are the two elements of the center of $SU(2)$. Let us stress again that since j is fixed to be integer or half-integer, the factors 1 or -1 overall simplify. Eq. (3.4.18) coincides with the result found in Eq. (3.2.5) once we use Eq. (3.4.16). Also here we have kept the Gaussian factor to get a normalised probability, i.e.,

$$\sum_j \mathcal{Z}_1(j) \simeq \sqrt{\frac{\pi^5}{k^3\log^3(\ell/\epsilon)}}\int_0^\infty dj e^{-\frac{j^2\pi^2}{k\log(\ell/\epsilon)}}(2j+1)^2 = 1, \tag{3.4.19}$$

where, in the large ℓ limit, we can approximate the sum over the irreducible representation as an integral.

As a byproduct of our results, from Eq. (3.4.18), we can compute the number entropy, i.e.

$$S_{\rm num} = -\sum_j \mathcal{Z}_1(j)\log\mathcal{Z}_1(j,\tau) \simeq -\int_0^\infty dj\,\mathcal{Z}_1(j)\log\mathcal{Z}_1(j)$$
$$\simeq \frac{1}{2}\log(k\log L) - 2 + \gamma_E - \frac{1}{2}\log\pi + \frac{3}{2}, \quad (3.4.20)$$

with γ_E the Euler constant. In full analogy with the $U(1)$ case, see e.g. [90], the leading term of the number entropy is a double logarithm in ℓ. The prefactor is $1/2$, exactly like for $U(1)$, but this will not be true in general, as shown in the next section. When computing the total entropy, this double log cancels with the same contributions coming from the configurational entanglement entropy, as we will show in the next paragraph.

3.4.4 Result for the symmetry resolved entanglement

At this point we can plug the result found in Eq. (3.4.18) into the definition of SRREs in Eq. (3.1.3), i.e.

$$S_n(j) = \frac{1}{1-n}\log\frac{\mathcal{Z}_n(j)}{\mathcal{Z}_1(j)^n} \propto \frac{1}{1-n}\log\left[\frac{Z_n(0,\ell)}{Z_1^n} n^{3/2}\left((2j+1)^2\frac{1}{2}\sqrt{\frac{\pi^5}{k^3\log^3(\ell/\epsilon)}}\right)^{1-n}\right]. \quad (3.4.21)$$

The first ratio in (3.4.21) just gives the total Rényi entropy of order n while the other term is

$$\log\left(\frac{1}{2}(2j+1)^2\sqrt{\frac{\pi^5}{k^3\log^3(\ell/\epsilon)}}\right) + \frac{3}{2(1-n)}\log(n) = \frac{3}{2}\log(\log\ell)$$
$$+\log\left(\frac{1}{2}(2j+1)^2\sqrt{\frac{\pi^5}{k^3}}\right) + \frac{3}{2(1-n)}\log(n) + o(\ell^0), \quad (3.4.22)$$

where we have neglected the (subleading) contributions due to the cutoff ϵ (see Ref. [90] for the $U(1)$ case in which the contribution $O(1/\log\ell)$ are taken into account, too). Putting everything together, the SRREs in the j sector are given by

$$S_n(j) = S_n(\ell) - \frac{3}{2}\log(\log\ell) - \frac{3}{2}\log(k) + 2\log(2j+1) + \frac{3}{2(1-n)}\log(n) +$$
$$\frac{5}{2}\log(\pi) + o(\ell^0). \quad (3.4.23)$$

Summing up the weighted symmetry resolved contributions (3.4.23) at $n = 1$, we get the configurational entanglement entropy

$$S_{\rm c} = \sum_j \mathcal{Z}_1^j(\tau)S_1^j(L) \simeq S_1 - \frac{1}{2}\log(k\log\ell) + 2 - \gamma_E - \frac{3}{2} + \frac{1}{2}\log(\pi). \quad (3.4.24)$$

Notice that the prefactor $1/2$ of the double logarithmic term comes from the combination of $3/2$ present already in Eq. (3.4.23) and another double log coming from the integral of the $\log(2j+1)$ term always in Eq. (3.4.23). As an important final sanity check, combining Eqs. (3.4.20) and (3.4.24), we straightforwardly verify that Eq. (3.1.4) is satisfied and the double logarithmic terms exactly cancel in order to recover the total vNEE, S_1.

Eq. (3.4.23) is equivalent to (3.2.6) and so it just represents a consistency check with some known results. However, this calculation is the starting point to study the entanglement resolution for a WZW-model with an arbitrary symmetry group and it would have been difficult to motivate many of some intermediate steps (e.g. the choice of n_j, the equivalent saddles from the elements of the center, etc.) without having in mind a concrete example.

3.5 Symmetry resolution for a general group G

This section contains the main results of the Chapter: after some explicit examples of symmetry decomposition for WZW-models, we find a general expression for the SRREs of these theories by emphasising its universal features.

3.5.1 Derivation of the main result

We generalise the method exploited for $SU(2)_k$, using the tools of Sec. 3.3.

Entanglement Hamiltonian and charged moments The entanglement Hamiltonian is still given by Eq. (3.4.2), i.e.

$$K_A = \frac{\pi}{2\log(\ell/\epsilon)}\left(L_0 - \frac{c}{24}\right), \tag{3.5.1}$$

therefore

$$Z_n = \mathrm{Tr}_A e^{-2\pi n K_A} = \mathrm{Tr}_A q^{L_0 - \frac{c}{24}}, \qquad q = e^{2\pi i \tau}, \tau = \frac{i\pi n}{2\log(\ell/\epsilon)} \tag{3.5.2}$$

with ϵ the UV cutoff. Given an element of the algebra $X \in \mathfrak{g}$, we define the charged moments as $Z_n(X,\tau) = Z_1^n \mathrm{Tr}[e^{iX}\rho_A^n]$. The total Hilbert space decomposes as

$$\mathcal{H}_A = \oplus_r n_r \mathcal{M}_r, \tag{3.5.3}$$

where n_r gives the multiplicity of the module $\mathcal{M}_r$ over the Kac-Moody algebra. Hence, the charged moments $Z_n(X,\tau)$ can be written as a linear combination of the unspecialised characters in Eq. (3.3.8)

$$Z_n(X,\tau) = \sum_r n_r \chi_r(X,\tau), \tag{3.5.4}$$

with the same coefficients n_r.

Asymptotics of the charged moments. In the limit $\ell \gg \epsilon$, we can use the expansion of the unspecialised characters reviewed in Sec. 3.3 to find the large-ℓ asymptotics of the charged moments

$$Z_n(X,\ell) \underset{\ell\to\infty}{\simeq} Z_n(0,\ell) e^{-\frac{k}{2\pi^2 n} K(X,X)\,\log(\ell/\epsilon)}, \qquad \text{for} \quad X \in \mathfrak{g}, \tag{3.5.5}$$

which is valid until $g = e^{iX}$ is in some small neighborhood of the unit element. However, as we have learnt from the $SU(2)$ case, when we project the charged moments onto the irreducible representations, we have to consider the contributions coming from all the saddle points. Apart from the unit element, the other obvious saddle points correspond to the elements $h \in Z(G)$ of the center of the Lie group. Indeed, as we explain below, the contribution around each element h is proportional to Eq. (3.5.5), up to a constant phase.

Furthermore, for simplicity we will assume that these are the only saddle points contributing to the integral. This seems like a reasonable assumption in view of the $SU(2)$ case, but we do not know how to prove that it holds for a general group G. It is under this assumption that we arrive at our main result. We stress that, even if other saddle points were present, the leading orders would remain unchanged; only the order $O(\ell^0)$ term would be affected.

If we consider group elements of the form $g = he^{iX}$, we have a slightly different asymptotic behaviour with respect to Eq. (3.5.5) when h is not simply the unit element. The unitary matrix U_g^A can be decomposed as $U_g^A = U_h^A U_{e^{iX}}$, where U_h^A is a representation of $Z(G)$, which is a finite abelian subgroup. Let $\Pi_m^{Z(G)}$, $m = 1, \cdots, |Z(G)|$, denote the projector onto states in $\mathcal{H}_A$ that

transform in the m-th irreducible (one-dimensional) representation of $Z(G)$. Irreps of $Z(G)$ are just phases times the identity in each block, i.e.

$$U_h = \sum_m e^{i\varphi_m(h)} \Pi_m^{Z(G)}. \tag{3.5.6}$$

This definition shows that the elements of the center of a group play the same role up to a constant (in ℓ) phase. We stress again that our intuition about these multiple saddle points has been suggested by the explicit computations done for the $SU(2)$ case in Sec. 3.4.3. In our case study $SU(2)$, the center is given by $\mathbb{Z}_2$, and we have already seen that around $g = \mathbb{1}$, $e^{i\varphi_j(1)} = 1$, while around $g = -\mathbb{1}$, $e^{i\varphi_j(-1)} = (-1)^{2j}$. However, these phases are fixed to be $+1$ or -1 by the boundary conditions at the entangling points of the subsystem through the coefficients n_r appearing in Eq. (3.5.4). In a similar way, for the general case we assume that all the non-zero n_r in Eq. (3.5.4) correspond to representations r that are in the same block in Eq. (3.5.6), i.e. there is a single term in the sum (3.5.6). As a consequence, U_h is fixed to be simply a phase, $U_h = e^{i\varphi(h)}$, and the asymptotic expression in the neighborhood of h reads

$$Z_n(X, L) \underset{L\to\infty}{\simeq} Z_n(0, L) e^{i\varphi(h)} e^{-\frac{k}{2\pi^2 n} K(X,X) \log(L/\epsilon)}, \qquad \text{for} \quad X \in \mathfrak{g},\, h \in Z(G). \tag{3.5.7}$$

Projecting the charged moment onto the representation r using the orthonormality of group characters. The main idea of our approach is to use the orthonormality of group characters to extract the contribution of the representation r from $\mathrm{Tr}[g\rho_A^n]$, i.e. recalling $\mathcal{Z}_n(r) = \mathrm{Tr}[\Pi_r \rho_A^n]$,

$$\mathcal{Z}_n(r) \;=\; \frac{\dim(r)}{\mathrm{Vol}(G)} \int d\mu(g) \mathrm{Tr}[g\rho_A^n] \chi_r^*(g). \tag{3.5.8}$$

Similarly to what has been discussed after Eq. (3.4.11), if we were interested in a symmetry resolution involving also the quantum numbers labelling the states within an irreducible representation r (e.g. j^z for the case study $SU(2)$), the prefactor $\dim(r)$ (the dimension of the representation) should be removed. The reason is that the entanglement Hamiltonian K_A is independent of them because it commutes with the corresponding charge generators, therefore each quantum number in a given irrep r gives the same contribution to $\mathrm{Tr}[g\rho_A^n]$, from which the prefactor $\dim(r)$ arises. Strictly speaking, $\mathrm{Tr}[g\rho_A^n]$ differs from the charged moments built with $\mathrm{Tr}[he^{iX}\rho_A^n]$ because the former is valid for arbitrary group elements $g \in G$, while the latter is valid only for elements in a neighbourhood of the element h in the center of the group. Nevertheless, the knowledge of only $\mathrm{Tr}[he^{iX}\rho_A^n]$ is enough for our aims because we are going to use a saddle point integral that is dominated by the elements of the group in some neighbourhood of $h \in Z(G)$.
Around h, it is convenient to use the local coordinate chart $\mathrm{x} \mapsto g(\mathrm{x}) = he^{i\sum_a x_a J^a}$. Replacing the integral over the whole group G by the integral over the neighbourhood of h parametrised by this chart, we have

$$\begin{aligned}
\mathcal{Z}_n(r) \;&=\; \sum_{h\in Z(G)} \frac{\dim(r)}{Z_1^n \mathrm{Vol}(G)} \int d\mu(he^{i\sum_a x_a J^a}) Z_n(\mathbf{x}, \ell) \chi_r^*(he^{i\sum_a x_a J^a}) \\
&=\; \sum_{h\in Z(G)} \frac{\dim(r)}{Z_1^n \mathrm{Vol}(G)} \int \sqrt{\det K(\mathbf{x})} d\mathbf{x} Z_n(\mathbf{x}, \ell) \chi_r^*(he^{i\sum_a x_a J^a}).
\end{aligned} \tag{3.5.9}$$

Now we use the asymptotics (3.5.7), and then we do a saddle point approximation around the elements of the center of the group,

$$\begin{aligned}
&\mathcal{Z}_n(r)\\
&\underset{L\to\infty}{\simeq} \sum_{h\in Z(G)} \frac{Z_n(0,\ell)}{Z_1^n}\frac{\dim(r)e^{i\varphi(h)}}{\mathrm{Vol}(G)}\int \sqrt{\det K(\mathbf{x})}e^{-\frac{k}{2\pi^2 n}\sum_{a,b}x_a x_b K(J^a,J^b)\,\log(\ell/\epsilon)}\chi_r^*(he^{i\sum_a x_a J^a})\,d\mathbf{x}\\
&\simeq \sum_{h\in Z(G)} \frac{Z_n(0,\ell)}{Z_1^n}\frac{\dim(r)e^{i\varphi(h)}}{\mathrm{Vol}(G)}\left(\frac{2\pi^3 n}{k\,\log(\ell/\epsilon)}\right)^{\dim(G)/2}\mathrm{Tr}\left[he^{-\frac{\pi^2 n}{2k\log(\ell/\epsilon)}\sum_{a,b}K^{-1}(J^a,J^b)J^aJ^b}\right],\\
&\simeq \frac{Z_n(0,\ell)}{Z_1^n}\frac{|Z(G)|}{\mathrm{Vol}(G)}\left(\frac{2\pi^3 n}{k\,\log(\ell/\epsilon)}\right)^{\dim(G)/2}\dim^2(r)e^{-\frac{\pi^2 n}{k\log(\ell/\epsilon)}C_r^{(2)}},
\end{aligned}\tag{3.5.10}$$

where in the last step we used that $(K(J^a,J^b)=\delta_{ab}/2)$,

$$\begin{aligned}
\mathrm{Tr}\,he^{-\frac{\pi^2 n}{2k\log(\ell/\epsilon)}\sum_{a,b}K^{-1}(J^a,J^b)J^aJ^b} &= e^{-i\varphi(h)}\mathrm{Tr}\,e^{-\frac{\pi^2 n}{k\log(\ell/\epsilon)}\sum_a J_aJ^a}\\
&= e^{-i\varphi(h)}e^{-\frac{\pi^2 n}{k\log(\ell/\epsilon)}C_r^{(2)}}\mathrm{Tr}\,\mathbb{1}_{\dim(r)\times\dim(r)} = e^{-i\varphi(h)}e^{-\frac{\pi^2 n}{k\log(\ell/\epsilon)}C_r^{(2)}}\dim(r),
\end{aligned}\tag{3.5.11}$$

and $C_r^{(2)}$ labels the eigenvalues of the quadratic Casimir operator of G. We also remark that the evaluation of the Gaussian integral holds for $J^a = O(\sqrt{\log\ell})$, such that the saddle-point approximation is valid.
From Eq. (3.5.10) for $n=1$, we also read that the probability introduced in Eq. (3.1.2) is in the large ℓ limit

$$p(r) \simeq \frac{|Z(G)|}{\mathrm{Vol}(G)}\left(\frac{2\pi^3}{k\,\log(\ell/\epsilon)}\right)^{\dim(G)/2}\dim^2(r)e^{-\frac{\pi^2}{k\log(\ell/\epsilon)}C_r^{(2)}}.\tag{3.5.12}$$

Interestingly, the normalisation of that probability distribution, $\sum_r p(r)=1$, in the large ℓ limit, leads us to the following asymptotic formula relating the quadratic Casimir operator and the dimension of irreducible representations of G,

$$\lim_{\eta\to 0^+}(2\pi\eta)^{\dim(G)/2}\sum_r \dim^2(r)e^{-\eta C_r^{(2)}} \;=\; \mathrm{Vol}(G).\tag{3.5.13}$$

Here the sum is over all irreps r of G. [This is the reason why the factor $|Z(G)|$ has dropped. It reenters if one restricts the sum to irreps r that transform identically under the action of the center $Z(G)$, see also the discussion in Sec. 2 of [121].] This formula may be viewed as an analog of the one for finite groups, that says that the square of dimensions of all irreps is equal to the order of the group, since one may regard $\mathrm{Vol}(G)/(2\pi\eta)^{\dim(G)/2}$ as the order of some finite approximation of the continuous Lie group G.

Unfortunately, we have not been able to find formula (3.5.13) in the mathematics literature. It is very likely that it comes from results on the Plancherel formula for Lie groups (see, e.g., Refs. [228, 229]), but we have not been able to find it in the explicit form (3.5.13) (also Ref. [230] is closely related to this subject). Nevertheless, in [121] we have checked its validity explicitly for the group $SU(N)$, for some values of N, using the actual form of the quadratic Casimir operator.

Final result. Finally, the SRREs is

$$S_n(r) \;=\; \frac{1}{1-n}\log\frac{\mathcal{Z}_n(r)}{(\mathcal{Z}_1(r))^n},$$

leading to our final result

$$S_n(r) = S_n - \frac{\dim(G)}{2}\log(\log\ell) + 2\log\dim(r) - \log\mathrm{Vol}(G) + \log|Z(G)| + \frac{\dim(G)}{2}\left(-\log k + \frac{\log n}{1-n} + \log(2\pi^3)\right). \quad (3.5.14)$$

This is the main result of this Chapter: at leading order, the SRRE satisfies equipartition, i.e. it is equally distributed in the different symmetry sectors. Interestingly, we find the term $2\log(\dim(r))$, at $O(\ell^0)$ which explicitly depends on the specific representation of the group G, breaking equipartition. This is different from what was found in the literature for the abelian case, where the first terms breaking equipartition usually occur at order $O((\log\ell)^{-2})$ (the two results are compatible since in the abelian case $\dim(r) = 1$ always). Also the prefactor of the double logarithmic correction has a universal behaviour which depends on the dimension of the group. Actually, the entire form (3.5.14) at order $O(\ell^0)$ is universal since the ultraviolet cutoff is fully encoded in the total entropy.

3.6 Closing remarks

In this Chapter, we considered the decomposition of the entanglement entropy into the various sector of a non-abelian symmetry. In particular, we studied the resolution of the entanglement entropy in WZW-models, which are associated to a group G and their symmetry algebra is a Kac-Moody algebra. Writing the charged moments as a linear combination of the unspecialised characters of these theories and using their modular properties, we have computed the resolved partition functions, i.e. the ones which take into account the preserved symmetry by including only states in a given representation of the group. We first characterised the general scaling behaviour of the charged moments; then we focused on the integration measure over the group manifold and the group characters around the elements of its center to extract the symmetry resolved moments and Rényi entropies. Our physically more relevant findings are: (i) SRRE satisfies equipartition at leading order; (ii) this equipartition is broken at $O(\ell^0)$ by a term depending only on the dimension of the irrep; (iii) the coefficient in front of the double logarithmic correction to the Rényi entropies is universal and it is equal to half of the dimension of the symmetry group of the model; (iv) the difference $S_n - S_n(r)$, between SRRE and total one, is universal up to order $O(\ell^0)$ and the cutoff enters only in higher order terms.

It is worth mentioning that while throughout all the Chapter we only wrote the results for the ground state of a single interval in the infinite line, it is easy to generalise our findings to different situations such as a finite interval in an infinite system at finite temperature, or finite interval in a finite system by using standard conformal transformations on the worldsheet.

Finally, our findings also lead to few very natural questions and generalisations. The most natural one is how other entanglement measures decompose in the sectors of a non-abelian symmetry and if there is some important difference with the abelian case [101, 116, 118, 119]. A second one is whether it is possible to generalise the form factor bootstrap program of Refs. [112–114] to the resolution of non-abelian symmetries. A last one is to identify the holographic dual of the SREE for theories with non-abelian symmetry and compare it with our results, as already done for the abelian case in [128].

Chapter 4

Multi-charged moments of two intervals in conformal field theory

The following Chapter is devoted to the study of the multi-charged moments for two disjoint intervals in the ground state of two $1+1$ dimensional CFTs with central charge $c=1$ and global $U(1)$ symmetry: the massless Dirac field theory and the compact boson (Luttinger liquid). For this purpose, we compute the partition function on the higher genus Riemann surface arising from the replica method in the presence of background magnetic fluxes between the sheets of the surface. We consider the general situation in which fluxes generate different twist boundary conditions at each branch point. The obtained multi-charged moments allow us to derive the symmetry resolution of the Rényi entanglement entropies and the mutual information for non complementary bipartitions. We check our findings against exact numerical results for the tight-binding model, which is a lattice realisation of the massless Dirac theory. This Chapter is based on Ref. [105].

4.1 Introduction

For bipartite systems in a pure state, the von Neumann and Rényi entropies can be used as measures of the entanglement shared between the two complementary parts. In the case considered in this Chapter in which A consists of two subsystems A_1 and A_2, i.e. $A = A_1 \cup A_2$, the ground-state entanglement entropy depends on the full operator content of the CFT, encoding all the conformal data of the model [206, 210, 248, 249]. It is important to remark that, in this situation, the entanglement entropies quantify the entanglement between A and B but not between the two parts of A, for which one must resort to other entanglement measures such as negativity [151, 152, 250–254]. Nevertheless, from the entanglement entropies, it is possible to construct the mutual information (1.1.10), which is a measure of the total correlations between A_1 and A_2. The computation of two-interval Rényi entanglement entropies is a difficult problem, even for minimal CFTs [253, 255], as it boils down in general to determine the partition function of the theory on a higher genus n-sheeted Riemann surface [206, 210]. In fact, exact analytic expressions are only available for the free theories or special limits [176, 206, 207, 210, 249, 256–263, 266, 267]. Moreover, the analytic continuation in n to obtain Eq. (1.1.6) is still a challenging open issue. As we already showed, the computation of entanglement itertwines with the presence of symmetries in a system. The symmetry resolution of entanglement in the two-interval case has not been much explored in CFT. Ref. [129] studies it at large central charge, in the context of holography, while, in Ref. [124], the charged Rényi negativity is analysed for the complex free boson. Here we take a different charge for each part of A, which leads to introduce the multi-charged moments of ρ_A (see Eq, (1.4.23)) that are the main subject of this Chapter. In CFT, they correspond to the partition function

on the n-sheeted Riemann surface, but with the insertion of a different magnetic flux across each subset of A. We will analyse the previous quantities in $1+1$-dimensional CFTs with a global $U(1)$ symmetry. We will assume that the entire system is in the ground state and that the spatial dimension is an infinite line which we will divide into two parts A and B, with A made up of two disjoint intervals, namely $A = A_1 \cup A_2 = [u_1, v_1] \cup [u_2, v_2]$. If we denote by ℓ_1 and ℓ_2 the lengths of the two intervals and d their separation, we have

$$\ell_1 = |v_1 - u_1|, \qquad \ell_2 = |v_2 - u_2|, \qquad d = |u_2 - v_1|, \qquad x = \frac{\ell_1 \ell_2}{(d+\ell_1)(d+\ell_2)}, \tag{4.1.1}$$

where we have also introduced the cross ratio x of the four end-points, which takes values between 0 and 1.

One can further consider other configurations for the magnetic fluxes between the sheets of the Riemann surface $\mathcal{R}_n$ (to enlighten the notation, we omit the pedix α's of $\mathcal{R}_{n,\alpha}$ here). In general, if we assume that a particle gets a different phase $e^{i\alpha_j}$ when it goes around each branch point, provided they satisfy the neutrality condition $\alpha_1 + \alpha_2 + \alpha_3 + \alpha_4 = 0$, then the partition function of this theory is given by

$$Z_n^{A_1:A_2}(\{\alpha_j\}) = Z_n^A(0) \langle \mathcal{V}_{\alpha_1}(u_1) \mathcal{V}_{\alpha_2}(v_1) \mathcal{V}_{\alpha_3}(u_2) \mathcal{V}_{\alpha_4}(v_2) \rangle_{\mathcal{R}_n}, \tag{4.1.2}$$

or, in terms of the composite twist fields, by

$$Z_n^{A_1:A_2}(\{\alpha_j\}) = \langle \mathcal{T}_{n,\alpha_1}(u_1) \tilde{\mathcal{T}}_{n,\alpha_2}(v_1) \mathcal{T}_{n,\alpha_3}(u_2) \tilde{\mathcal{T}}_{n,\alpha_4}(v_2) \rangle. \tag{4.1.3}$$

Then the multi-charged moments $Z_n^{A_1:A_2}(\alpha, \beta)$ can be treated as the particular case in which $\alpha_1 = -\alpha_2 = \alpha$ and, due to the neutrality condition, $\alpha_3 = -\alpha_4 = \beta$.

In Sec. 4.2, we will compute the charged moments $Z_n^{A_1:A_2}(\alpha, \beta)$, and more in general the partition functions $Z_n^{A_1:A_2}(\{\alpha_j\})$, for the massless Dirac fermion using the orbifold theory $\mathrm{CFT}^{\otimes n}/\mathbb{Z}_n$. On the other hand, in Sec. 4.3, we will adopt a geometric approach to obtain the multi-charged moments of the compact boson from the correlation function on the Riemann surface $\mathcal{R}_n$ of Eq. (4.1.2).

Finally, in Sec. 4.4, we apply the previous results to obtain the symmetry-resolution of the mutual information in these theories. When possible, we benchmark the analytic expressions with exact numerical calculations for lattice models in the same universality class. We draw our conclusions in Sec. 4.5 and we include one appendix, with more details about the numerical computations.

4.2 Free massless Dirac field theory

We have already learnt that the Dirac field theory described by the action (2.1.1) exhibits a global $U(1)$ symmetry. By Noether's theorem, this symmetry is related to the conservation of the charge $Q_{\mathrm{D}} = \int \mathrm{d}x_1 \psi^\dagger \psi$.

The ground state entanglement of a subsystem A made up of multiple disjoint intervals in the ground state of this theory was first investigated in Ref. [176]. For the case of two disjoint intervals, $A = A_1 \cup A_2$, it was found that the moments of ρ_A are

$$Z_n^A(0) = c_n \left[\ell_1 \ell_2 (1-x)\right]^{\frac{1-n^2}{6n}}, \tag{4.2.1}$$

where c_n is a non-universal constant.

In this section, we will compute the multi-charged moments of Eq. (1.4.23) in the ground state of the massless Dirac field theory. We will extend the approach introduced in Ref. [176] for the moments of Eq. (4.2.1), as already done in Chapter 2. We will benchmark our analytical results with exact numerical calculations in a lattice model.

4.2.1 Charged moments

In Sec. 1.4.2, we explained that the partition function $Z_n(\alpha)$ (and, as a consequence, also $Z_n^{A_1:A_2}(\{\alpha_j\})$) can be obtained either by considering the theory on a complicated Riemann surface or by replicating it n-times and working with the orbifold on the complex plane. For the massless Dirac field theory, the latter approach is more convenient. As done also in 2.2.1, let us take the n-component field

$$\Psi = \begin{pmatrix} \psi_1 \\ \psi_2 \\ \vdots \\ \psi_n \end{pmatrix}, \tag{4.2.2}$$

where ψ_j is the Dirac field on the j-th copy of the system. Eq. (1.4.20) describes the effect of the composite twist fields on the components of Ψ when going around the end-points of the subsystem $A = A_1 \cup A_2$. This transformation can be encoded in the matrix

$$T_a = \begin{pmatrix} 0 & e^{ia/n} & & \\ & 0 & e^{ia/n} & \\ & & \ddots & \ddots \\ (-1)^{n-1}e^{ia/n} & & 0 & \end{pmatrix}. \tag{4.2.3}$$

In the general case of Eq. (4.1.3), Ψ transforms according to $T_{\alpha_{2p-1}}$ when winding around the point u_p and to the transpose matrix $T^t_{\alpha_{2p}}$ when going around the points v_p, with $p = 1, 2$. The matrix T_a in Eq. (4.2.3), sometimes called *twist matrix*, was introduced for the case $a = 0$ in Refs. [156, 176] and for general a in Sec. 2.2.1. Its eigenvalues are of the form

$$t_k = e^{ia/n}e^{2\pi ik/n}, \qquad k = -\frac{n-1}{2}, \dots, \frac{n-1}{2}. \tag{4.2.4}$$

By simultaneously diagonalising all the T_{α_j} with a unitary transformation (which is independent of α_j), we can recast the replicated theory in n decoupled fields ψ_k on the plane, which are multi-valued,

$$\begin{aligned} \psi_k(e^{i2\pi}(z-u_p)) &= e^{i\alpha_{2p-1}/n}e^{2\pi ik/n}\psi_k(z-u_p), \\ \psi_k(e^{i2\pi}(z-v_p)) &= e^{i\alpha_{2p}/n}e^{-2\pi ik/n}\psi_k(z-v_p). \end{aligned} \tag{4.2.5}$$

For the free massless Dirac theory, this allows us to write the Lagrangian of the replicated theory as

$$\mathcal{L}_{\mathrm{D},n} = \sum_k \mathcal{L}_k, \qquad \mathcal{L}_k = \bar{\psi}_k \gamma^\mu \partial_\mu \psi_k. \tag{4.2.6}$$

Following this approach, the partition function of Eq. (4.1.3) factorises into

$$Z_n^{A_1:A_2}(\{\alpha_j\}) = \prod_{k=-\frac{n-1}{2}}^{k=\frac{n-1}{2}} Z_{k,n}^{A_1:A_2}(\{\alpha_j\}), \tag{4.2.7}$$

where $Z_{k,n}^{A_1:A_2}(\{\alpha_j\})$ is the partition function for a Dirac field ψ_k with the boundary conditions of Eq. (4.2.5).

The main difference between the partition functions $Z_{k,n}^{A_1:A_2}(\{\alpha_j\})$ and the standard computation of Ref. [176] for Rényi entropies is that the boundary conditions of the multi-valued fields

around the branch points now depend on the phases α_j. This multivaluedness can be removed, as done in [176] for $\alpha_j = 0$, by introducing an external $U(1)$ gauge field A_μ^k coupled to single-valued fields $\tilde{\psi}_k$. In fact, if we apply the singular gauge transformation

$$\psi_k(x) = e^{i\int_{x_0}^{x} dy^\mu A_\mu^k} \tilde{\psi}_k(x), \tag{4.2.8}$$

then the Lagrangian for the k-th mode can be rewritten as

$$\mathcal{L}_k = \bar{\tilde{\psi}}_k \gamma^\mu \left(\partial_\mu + i A_\mu^k\right) \tilde{\psi}_k, \tag{4.2.9}$$

with the advantage of absorbing the phase around the end-points of $A_1 \cup A_2$ into the gauge field. The only requirement that A_μ^k in Eq. (4.2.8) must satisfy is that, integrated along any closed curve $\mathcal{C}$ that encircles the end-points of A, the boundary conditions of Eq. (4.2.5) for ψ_k must be reproduced. For this purpose, we require

$$\oint_{\mathcal{C}_{u_p}} dy^\mu A_\mu^k = -\frac{2\pi k}{n} - \frac{\alpha_{2p-1}}{n}, \qquad \oint_{\mathcal{C}_{v_p}} dy^\mu A_\mu^k = \frac{2\pi k}{n} - \frac{\alpha_{2p}}{n}, \tag{4.2.10}$$

where $\mathcal{C}_{u_p}$ and $\mathcal{C}_{v_p}$ are closed contours around the end-points of the p-th interval. Moreover, we have to impose that, if $\mathcal{C}$ does not enclose any end-point, then $\oint_{\mathcal{C}} dy^\mu A_\mu^k = 0$. Applying the Stoke's theorem, the conditions of Eqs. (4.2.10) can be expressed in differential form,

$$\frac{1}{2\pi}\epsilon^{\mu\nu}\partial_\nu A_\mu^k(x) = \sum_{p=1}^{2}\left[\left(\frac{\alpha_{2p-1}}{2\pi n} + \frac{k}{n}\right)\delta(x-u_p) + \left(\frac{\alpha_{2p}}{2\pi n} - \frac{k}{n}\right)\delta(x-v_p)\right]. \tag{4.2.11}$$

Once the transformation of Eq. (4.2.8) is performed, the partition function $Z_{k,n}^{A_1:A_2}(\{\alpha_j\})$ of the k-th mode is equal to the vacuum expectation value

$$Z_{k,n}^{A_1:A_2}(\{\alpha_j\}) = \left\langle e^{i\int d^2x j_k^\mu A_\mu^k}\right\rangle, \tag{4.2.12}$$

where $j_k^\mu \equiv \bar{\tilde{\psi}}_k \gamma^\mu \tilde{\psi}_k$ is the conserved Dirac current for each mode. Eq. (4.2.12) can be easily computed via bosonisation [176], which allows us to write the current in terms of the dual scalar field ϕ_k such that $j_k^\mu = \epsilon^{\mu\nu}\partial_\nu\phi_k/\sqrt{\pi}$. If we use this result in Eq. (4.2.12), and we apply Eq. (4.2.11), then $Z_{k,n}^{A_1:A_2}(\{\alpha_j\})$ is equal to the following correlation function of vertex operators $V_a(y) = e^{-ia\phi_k(y)}$

$$Z_{k,n}^{A_1:A_2}(\{\alpha_j\}) = \langle V_{\frac{k}{n}+\frac{\alpha_1}{2\pi n}}(u_1) V_{-\frac{k}{n}+\frac{\alpha_2}{2\pi n}}(v_1) V_{\frac{k}{n}+\frac{\alpha_3}{2\pi n}}(u_2) V_{-\frac{k}{n}+\frac{\alpha_4}{2\pi n}}(v_2)\rangle. \tag{4.2.13}$$

Notice that the neutrality condition $\alpha_1+\alpha_2+\alpha_3+\alpha_4 = 0$ ensures that the latter correlator does not vanish. The correlation function of vertex operators in the complex plane is well-known (see, for instance, Ref. [269]) and, therefore, Eq. (4.2.13) can be easily calculated. Plugging the result into Eq. (4.2.7) and performing the product over k, we obtain

$$\begin{aligned} Z_n^{A_1:A_2}(\{\alpha_j\}) \propto \\ [\ell_1\ell_2(1-x)]^{\frac{1-n^2}{6n}} \left[d^{\alpha_2\alpha_3}\ell_1^{\alpha_1\alpha_2}\ell_2^{\alpha_3\alpha_4}(d+\ell_1)^{\alpha_1\alpha_3}(d+\ell_2)^{\alpha_2\alpha_4}(d+\ell_1+\ell_2)^{\alpha_1\alpha_4}\right]^{\frac{1}{2\pi^2 n}}, \end{aligned} \tag{4.2.14}$$

where x is the cross-ratio defined in Eq. (4.1.1). When we take $\alpha_1 = -\alpha_2 = \alpha$ and $\alpha_3 = -\alpha_4 = \beta$ in this expression, we get the multi-charged moments in Eq. (1.4.23) as

$$Z_n^{A_1:A_2}(\alpha,\beta) \;=\; c_{n;\alpha,\beta}\left[\ell_1\ell_2(1-x)\right]^{\frac{1-n^2}{6n}}\left[(1-x)^{-\alpha\beta}\,\ell_1^{-\alpha^2}\ell_2^{-\beta^2}\right]^{\frac{1}{2\pi^2 n}}. \tag{4.2.15}$$

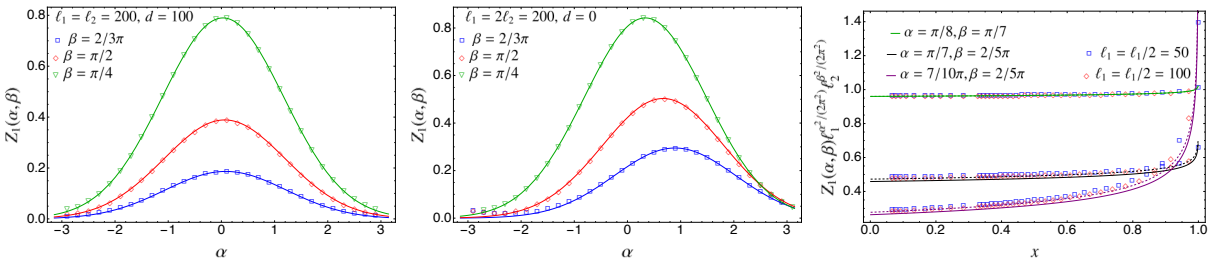

Figure 4.1: Analysis of $Z_1^{A_1:A_2}(\alpha,\beta)$ for the tight-binding model. In the left panel, we show $Z_1^{A_1:A_2}(\alpha,\beta)$ as a function of α at fixed β for different intervals of lengths ℓ_1, ℓ_2, separated by a distance $d > 0$. In this case, the solid lines are the theoretical predictions of Eq. (4.2.15), taking Eq. (4.2.19) for $c_{n;\alpha,\beta}$. In the middle panel, we repeat the analysis but considering adjacent intervals ($d = 0$) and the solid curves correspond to Eq. (4.2.17), with $\tilde{c}_{n;\alpha,\beta}$ conjectured in Eq. (4.2.21). In the right panel, we plot $Z_1^{A_1:A_2}(\alpha,\beta)$ as a function of the cross-ratio x. Here the solid lines correspond to Eq. (4.2.15) using the exact expression for $c_{n;\alpha,\beta}$ of Eq. (4.2.19), while for the dashed curves we have considered instead the quadratic approximation for this constant of Eq. (4.2.20). In all the cases, the points are the exact numerical values for $Z_1^{A_1:A_2}(\alpha,\beta)$ calculated as described in Appendix 4.A.

We assume that all the length scales in this formula have been regularised through a UV cutoff which is included in the multiplicative constant $c_{n;\alpha,\beta}$.

An interesting case to analyse is when the two intervals A_1 and A_2 become adjacent; that is, when $d \to 0$. In that limit, the cross-ratio x tends to one such that

$$1 - x = d\frac{\ell_1 + \ell_2}{\ell_1 \ell_2} + O(d^2), \tag{4.2.16}$$

and Eq. (4.2.15) vanishes. Nevertheless, in this regime, the distance d must be regarded as another UV cutoff, which can be absorbed in the multiplicative constant $c_{n;\alpha,\beta}$. Therefore, from Eqs. (4.2.16) and (4.2.15), one expects

$$Z_n^{A_1:A_2}(\alpha,\beta) = \tilde{c}_{n;\alpha,\beta}(\ell_1+\ell_2)^{\frac{1-n^2}{6n}} \left[\frac{\ell_1^{\alpha\beta-\alpha^2}\ell_2^{\alpha\beta-\beta^2}}{(\ell_1+\ell_2)^{\alpha\beta}}\right]^{\frac{1}{2\pi^2 n}}, \tag{4.2.17}$$

which agrees with the fact that the multi-charged moments $Z_n^{A_1:A_2}(\alpha,\beta)$ must tend to the three-point function of primaries $\langle \mathcal{T}_{n,\alpha}(u_1)\mathcal{V}_{-\alpha+\beta}(v_1)\tilde{\mathcal{T}}_{n,-\beta}(v_2)\rangle$, in the limit $d \to 0$.

In Fig. 4.1, we check the expressions obtained in Eqs. (4.2.15) and (4.2.17) for $Z_n^{A_1:A_2}(\alpha,\beta)$ with exact numerical calculations performed in the tight-binding model, which is a chain of non-relativistic free fermions whose scaling limit is described by the massless Dirac field theory. The details of the numerical techniques employed are given in Appendix 4.A. In order to compare Eqs. (4.2.15) and (4.2.17) with the numerical data, we need the concrete expression of the non-universal factors $c_{n;\alpha,\beta}$ and $\tilde{c}_{n;\alpha,\beta}$ for this particular model. When the two intervals A_1 and A_2 are far away, that is in the limit $d \to \infty$, the charged moments of $A_1 \cup A_2$ factorise into those of A_1 and A_2,

$$\lim_{d\to\infty} Z_n^{A_1:A_2}(\alpha,\beta) = Z_n^{A_1}(\alpha) Z_n^{A_2}(\beta). \tag{4.2.18}$$

Therefore, one expects $c_{n;\alpha,\beta}$ to be the product of the two non-universal constants associated to A_1 and A_2 as single intervals. The latter were obtained for the tight-binding model in Ref. [90]

by exploiting the asymptotic properties of Toeplitz determinants. We can also apply here those results, taking into account that each interval is associated to a different flux, either α or β. Then we have

$$c_{n;\alpha,\beta} = e^{\left[-\frac{1}{3}\left(n-\frac{1}{n}\right)-\frac{\alpha^2}{2\pi^2 n}-\frac{\beta^2}{2\pi^2 n}\right]\log 2+\Upsilon(n,\alpha)+\Upsilon(n,\beta)}, \tag{4.2.19}$$

where $\Upsilon(n,\alpha)$ is given by Eq. (2.3.16). Expanding $\Upsilon(n,\alpha)$ up to quadratic order in α, then Eq. (4.2.19) can be approximated as

$$c_{n;\alpha,\beta} \approx e^{-\frac{1}{3}\left(n-\frac{1}{n}\right)\log 2+2\Upsilon(n,0)-\frac{\zeta_n}{2\pi^2 n}(\alpha^2+\beta^2)}, \tag{4.2.20}$$

where $\zeta_n = \log 2 - 2\pi^2 n\gamma_2(n)$.

In the limit of adjacent intervals, given by Eq. (4.2.17), the multiplicative constant $\tilde{c}_{n;\alpha,\beta}$ cannot be determined using the known results for Toeplitz determinants. However, we can conjecture an analytical approximation for it at quadratic order in α and β. When $d \to 0$, we can associate to each end-point of the intervals u_1, $v_1 = u_2$ and v_2 the fluxes α, $\beta - \alpha$ and $-\beta$ respectively. From the results for one interval of Ref. [90], one can conjecture that each end-point with flux α contributes with a factor $e^{-\frac{\zeta_n}{4\pi^2 n}\alpha^2}$ to the constant $\tilde{c}_{n;\alpha,\beta}$, if we restrict to terms up to order α^2. Therefore, the combination of all the fluxes in our case should contribute with a total factor $e^{-\frac{\zeta_n}{4\pi^2 n}(\alpha^2+(\beta-\alpha)^2+\beta^2)}$. We then expect that $\tilde{c}_{n;\alpha,\beta}$ should be well be approximated by

$$\tilde{c}_{n;\alpha,\beta} = e^{-\frac{1}{6}\left(n-\frac{1}{n}\right)\log 2+\Upsilon(n,0)-\frac{\zeta_n}{2\pi^2 n}(\alpha^2+\beta^2-\alpha\beta)}. \tag{4.2.21}$$

When $\alpha = \beta = 0$, the expression above simplifies to the multiplicative constant for the moments of a single interval obtained in Ref. [268]. In spite of the heuristic reasoning of this result, in Fig. 4.1, we check its validity by comparing it against exact numerical data.

In Fig. 4.1, we study $Z_1^{A_1:A_2}(\alpha,\beta)$ as function of α, for various values of β, ℓ_1, ℓ_2 and d. The points correspond to the exact numerical values obtained as we described in Appendix 4.A while the solid curves are the analytic prediction of Eq. (4.2.15) ((4.2.17) for $d = 0$), taking as multiplicative constant $c_{n,\alpha,\beta}$ that in Eq. (4.2.19) (Eq. (4.2.21)). We find an excellent agreement. Finally, in the right panel, we plot $Z_1^{A_1:A_2}(\alpha,\beta)$ as function of the cross-ratio x, for various values of α, β, ℓ_1 and ℓ_2. The curves represent the prediction of Eq. (4.2.15). The continuous ones correspond to take as non-universal constant $c_{n;\alpha,\beta}$ the full expression of Eq. (4.2.19), while for the dashed ones we have used the quadratic approximation of Eq. (4.2.20). The agreement between the analytic prediction and the numerical data is extremely good, even considering the quadratic approximation for the non-universal constant. As expected, this agreement is better for small values of α and β, while, around $\pm\pi$, we need to take larger subsystem sizes ℓ_1, ℓ_2 in order to suppress the finite-size corrections which are well known and chracterised for the charged moments with a single flux insertion [90].

4.3 Free compact boson

The second theory we focus on in this Chapter is the free (real) compact boson, which is the CFT of the Luttinger liquid, and whose action reads

$$\mathcal{S}_{\rm b} = \frac{1}{8\pi}\int \mathrm{d}x_0\mathrm{d}x_1 \partial_\mu\varphi\partial^\mu\varphi. \tag{4.3.1}$$

The target space of the real field φ is compactified on a circle of radius R, i.e. $\varphi \sim \varphi + 2\pi m R$ with $m \in \mathbb{Z}$. The compactification radius R is related to the Luttinger parameter K as $R =$

$\sqrt{2/K}$. The action of Eq. (4.3.1) is invariant under the transformation $\varphi \mapsto \varphi + \alpha$ which, due to the compact nature of φ, realises a $U(1)$ global symmetry. The associated conserved charge is $Q_{\rm b} = \frac{1}{2\pi}\int {\rm d}x_1 \partial_{x_1}\varphi$.

The moments of the ground state reduced density matrix of this theory are well-known. An exact analytic expression for the two-interval case was obtained in Ref. [206], which was generalised to an arbitrary number of disjoint intervals in Ref. [260]. In particular, for two intervals, it reads [206]

$$Z_n^A(0) = c_n \left[\ell_1 \ell_2 (1-x)\right]^{\frac{1-n^2}{6n}} \mathcal{F}_n(x), \tag{4.3.2}$$

where c_n is a non-universal constant and

$$\mathcal{F}_n(x) = \frac{\Theta(\mathbf{0}|\Gamma(x)/K)\Theta(\mathbf{0}|\Gamma(x)K)}{\left[\Theta(\mathbf{0}|\Gamma(x))\right]^2}. \tag{4.3.3}$$

We denote by Θ the Riemann-Siegel Theta function

$$\Theta[{}^{\boldsymbol{\varepsilon}}_{\boldsymbol{\delta}}](\boldsymbol{u}|\Omega) \equiv \sum_{\boldsymbol{m}\in\mathbb{Z}^{n-1}} e^{i\pi(\boldsymbol{m}+\boldsymbol{\varepsilon})^t\cdot\Omega(\boldsymbol{m}+\boldsymbol{\varepsilon})+2\pi i(\boldsymbol{m}+\boldsymbol{\varepsilon})^t\cdot(\boldsymbol{u}+\boldsymbol{\delta})}, \tag{4.3.4}$$

with characteristics $\boldsymbol{\varepsilon},\boldsymbol{\delta} \in (\mathbb{Z}/2)^{n-1}$, $\boldsymbol{u} \in \mathbb{C}^{n-1}$ and Ω a complex $(n-1)\times(n-1)$ matrix. In Eq. (4.3.3), the characteristics are zero $\mathbf{0} = (0,\ldots,0)$ and, therefore, we have used the standard shorthand notation $\Theta(\boldsymbol{u}|\Omega) \equiv \Theta[{}^{\mathbf{0}}_{\mathbf{0}}](\boldsymbol{u}|\Omega)$. The matrix $\Gamma(x)$ in Eq. (4.3.3) has entries given by

$$\Gamma_{rs}(x) = \frac{2i}{n}\sum_{l=1}^{n-1} \cos\left[\frac{2\pi l(r-s)}{n}\right] \sin\left(\frac{\pi l}{n}\right) \beta_{l/n}(x), \quad r,s = 1,\ldots,n-1, \tag{4.3.5}$$

and

$$\beta_p(x) = \frac{I_p(1-x)}{I_p(x)}, \tag{4.3.6}$$

with $I_p(x) \equiv {}_2F_1(p,1-p,1,1-x)$. The function $\mathcal{F}_n(x)$ is invariant under $x \mapsto 1-x$ and it is normalised such that $\mathcal{F}_n(0) = \mathcal{F}_n(1) = 1$. Although the moments of ρ_A are known for all the integer n, its analytic continuation to complex n and, consequently, the von Neumann entropy of Eq. (1.1.6) is still not available for all the values of the Luttinger parameter.

A remarkable contact point between the theories described by the action of Eq. (2.1.1) (S_D) and (4.3.1) is the case $K = 1$. Notice that, when the Luttinger parameter takes this value, the function $\mathcal{F}_n(x)$ in Eq. (4.3.3) simplifies to $\mathcal{F}_n(x)$=1 and the moments of Eq. (4.3.2) for the massless compact boson present the same universal dependence on ℓ_1, ℓ_2 and x as the ones in Eq. (4.2.1) for the massless Dirac fermion. A detailed discussion on this identity can be found in Ref. [259], where it is explained the reason why, although these two theories are not related by a duality, their partition functions on the Riemann surfaces $\mathcal{R}_n$ arising in the two-interval replica method are actually equal. Here we find that this identity extends to the partition functions $Z_n^{A_1:A_2}(\{\alpha_j\})$ on the surface $\mathcal{R}_n$ with different twist boundary conditions at each branch point. In general, when A is made up of more than two intervals and the Rényi index n is larger than two, the moments of the reduced density matrix in these CFTs (and the corresponding Rényi entropies) are different [259].

4.3.1 Charged moments

We now generalise the result (4.3.2) to the multi-charged moments in Eq. (1.4.23). Starting from Eq. (1.4.19), we will compute them as the four-point function of the field $\mathcal{V}_\alpha$ on the Riemann

surface $\mathcal{R}_n$. Since the $U(1)$ conserved current is proportional to $\partial_{x_1}\varphi$, $\mathcal{V}_\alpha$ is identified in this case with the vertex operator [84]

$$\mathcal{V}_\alpha(z) = e^{i\frac{\alpha}{2\pi}\varphi(z)}, \tag{4.3.7}$$

which has conformal dimensions

$$h_\alpha^{\mathcal{V}} = \bar{h}_\alpha^{\mathcal{V}} = \left(\frac{\alpha}{2\pi}\right)^2 \frac{K}{2}. \tag{4.3.8}$$

In the following, it will be useful to introduce the *rescaled* Luttinger paratemeter $\eta = K/(2\pi^2)$ in order to lighten the expressions.

Without loss of generality, let us consider that the end-points of subsystem A are $u_1 = 0$, $v_1 = x$, $u_2 = 1$ and $v_2 = \infty$. Using Eq. (4.1.3), and given that the composite twist fields are primaries, we can eventually obtain the expression for an arbitrary set of end-points through a global conformal transformation. Therefore, according to Eq. (1.4.19), the multi-charged moments can be derived from the four-point correlation function of the vertex operators of Eq (4.3.7)

$$Z_n^{A_1:A_2}(\{\alpha_j\}) = Z_n^A(0)\langle \mathcal{V}_{\alpha_1}(0)\mathcal{V}_{\alpha_2}(x)\mathcal{V}_{\alpha_3}(1)\mathcal{V}_{\alpha_4}(\infty)\rangle_{\mathcal{R}_n(x)} \tag{4.3.9}$$

on the n-sheeted Riemann surface $\mathcal{R}_n(x)$ with branch points at 0, x, 1 and ∞. This surface of genus $n-1$ can be described by the complex curve

$$y^n = \frac{z(z-1)}{z-x}. \tag{4.3.10}$$

The correlator of vertex operators on a general Riemann surface of arbitrary genus was obtained in Ref. [271]. In order to give the explicit expression in our case, we need to introduce some notions about Riemann surfaces [270].

There are different parameterisations of the moduli space of genus $n-1$ Riemann surfaces. One possibility is through the matrix of periods, which we denote by Γ. This is a $(n-1)\times(n-1)$ symmetric matrix with positive definite imaginary part. Notice that, according to Eq. (4.3.10), the Riemann surface $\mathcal{R}_n(x)$ is parametrised by the cross-ratio x. Therefore, the corresponding matrix of periods only depends on x, i.e. $\Gamma = \Gamma(x)$. In order to define it, we need first to specify a particular homology basis for $\mathcal{R}_n(x)$, i.e. a basis of $2(n-1)$ oriented non-contractible curves on the surface, which we denote by a_r and b_r, with $r = 1, \ldots, n-1$. We also have to choose a basis of holomorphic differentials ν_r, $r = 1, \ldots, n-1$, normalised with respect to the a_r cycles. That is,

$$\oint_{a_r} \mathrm{d}z \nu_s(z) = \delta_{r,s}, \quad r, s = 1, \ldots, n-1. \tag{4.3.11}$$

Then the matrix of periods is defined as

$$\Gamma_{rs} = \oint_{b_r} \mathrm{d}z \nu_s(z). \tag{4.3.12}$$

For the surface $\mathcal{R}_n(x)$, the normalised holomorphic differentials read

$$\nu_r(z) = \frac{1}{\pi n} \sum_{l=1}^{n-1} \frac{e^{-\frac{i2\pi(r-1)l}{n}} \sin(\pi l/n)}{I_{l/n}(x)} (z(z-1))^{-l/n} (z-x)^{-1+l/n}. \tag{4.3.13}$$

Inserting it in Eq. (4.3.12), it is then easy to show that the entries of the matrix of periods $\Gamma(x)$ are precisely those of Eq. (4.3.5).

If we now consider four vertex operators inserted at generic points in the surface $\mathcal{R}_n(x)$ and with arbitrary dimensions satisfying the neutrality condition $\alpha_1+\alpha_2+\alpha_3+\alpha_4=0$, then its correlation function is of the form [271]

$$\langle \mathcal{V}_{\alpha_1}(z_1)\mathcal{V}_{\alpha_2}(z_2)\mathcal{V}_{\alpha_3}(z_3)\mathcal{V}_{\alpha_4}(z_4)\rangle_{\mathcal{R}_n(x)} = \prod_{1\leq j<j'\leq 4}\left|E(z_j,z_{j'})e^{-\pi \mathrm{Im}[\boldsymbol{w}(z_j)-\boldsymbol{w}(z_{j'})]^t\cdot \mathrm{Im}[\Gamma(x)^{-1}]\mathrm{Im}[\boldsymbol{w}(z_j)-\boldsymbol{w}(z_{j'})]}\right|^{\alpha_j\alpha_{j'}\eta}. \quad (4.3.14)$$

In this expression, we denote by $E(z,z')$ the prime form of the surface $\mathcal{R}_n(x)$, which we will define precisely later, and $\boldsymbol{w}(z)=(w_1(z),\ldots,w_{n-1}(z))$ is the Abel-Jacobi map, which relates a point z in the surface $\mathcal{R}_n(x)$ to a point $\boldsymbol{w}(z)$ in the genus $n-1$ complex torus $\mathbb{C}^{n-1}/\Lambda$, where $\Lambda=\mathbb{Z}^{n-1}+\Gamma\mathbb{Z}^{n-1}$. This map can be written in terms of the normalised holomorphic differentials of Eq. (4.3.13) as

$$w_r(z)=\int_0^z \nu_r \pmod{\Lambda}, \quad (4.3.15)$$

where we have taken as origin the branch point $z=0$. The images under the Abel-Jacobi map of the points $z=0$, x, 1, and ∞, where the vertex operators in Eq. (4.3.9) are inserted, can be easily computed using Eq. (4.3.13). Then we find

$$\begin{aligned} \boldsymbol{w}(0) &= \boldsymbol{0}, & (4.3.16)\\ \boldsymbol{w}(x) &= \boldsymbol{q}, & (4.3.17)\\ \boldsymbol{w}(1) &= \boldsymbol{q}+i\boldsymbol{p}(x), & (4.3.18)\\ \boldsymbol{w}(\infty) &= i\boldsymbol{p}(x), & (4.3.19)\end{aligned}$$

where $\boldsymbol{q}=(1/n,\ldots,1/n)$ and $\boldsymbol{p}(x)=(p_1(x),\ldots,p_{n-1}(x))$ with

$$p_r(x)=-\frac{1}{n}\sum_{l=1}^{n-1}\left[\cos\left[\frac{2\pi l(r-1)}{n}\right]\sin\left(\frac{\pi l}{n}\right)+\sin\left[\frac{2\pi l(r-1)}{n}\right]\cos\left(\frac{\pi l}{n}\right)\right]\beta_{l/n}(x). \quad (4.3.20)$$

Therefore, for the case $z_1=0$, $z_2=x$, $z_3=1$, $z_4=\infty$, Eq. (4.3.14) simplifies to

$$\langle \mathcal{V}_{\alpha_1}(0)\mathcal{V}_{\alpha_2}(x)\mathcal{V}_{\alpha_3}(1)\mathcal{V}_{\alpha_4}(\infty)\rangle_{\mathcal{R}_n(x)} = M_n(x)^{(\alpha_1+\alpha_2)(\alpha_3+\alpha_4)\eta}\prod_{1\leq j<j'\leq 4}\left|E(z_j,z_{j'})\right|^{\alpha_j\alpha_{j'}\eta}, \quad (4.3.21)$$

where

$$M_n(x)=e^{-\pi \boldsymbol{p}(x)^t\cdot[\mathrm{Im}\Gamma(x)]^{-1}\boldsymbol{p}(x)}. \quad (4.3.22)$$

Let us now focus on the prime form $E(z,z')$. It can be defined as [270]

$$E(z,z')=\frac{\Theta_{\frac{\boldsymbol{1}}{\boldsymbol{2}}}(\boldsymbol{w}(z)-\boldsymbol{w}(z')|\Gamma(x))}{\sqrt{g(z)}\sqrt{g(z')}}, \quad (4.3.23)$$

where $\Theta_{\frac{\boldsymbol{1}}{\boldsymbol{2}}}$ is a shorthand notation for the Theta function of Eq. (4.3.4) with both characteristics equal to $(1/2,0,\ldots,0)\in(\mathbb{Z}/2)^{n-1}$ and $g(z)$ is

$$g(z)=\sum_{r=1}^{n-1}\nu_r(z)\partial_{u_r}\,\Theta_{\frac{\boldsymbol{1}}{\boldsymbol{2}}}(\boldsymbol{u}|\Gamma(x))\Big|_{\boldsymbol{u}=\boldsymbol{0}}. \quad (4.3.24)$$

Notice that the holomorphic differentials $\nu_r(z)$ in Eq. (4.3.13) and, therefore, $g(z)$ are singular at the branch points of the curve that defines the surface $\mathcal{R}_n(x)$. This means that the correlation

function (4.3.14) is in principle not well-defined. In order to solve this issue, the vertex operators inserted at the branch points have to be regularised by redefining them as a proper limit from a non-singular point. We will first extract and remove from $g(z)$ the divergent terms at the branch points. Then, by considering the limit in which the distance between A_1 and A_2 tends to infinity, we will fix the correct definition of the regularised vertex operators at the branch points.

Close to the branch points $z = 0$, x, 1, and ∞, the holomorphic normalised differentials $\nu_r(z)$ of Eq. (4.3.13) behave as

$$\nu_r(z+\epsilon) = \epsilon^{\frac{1-n}{n}} \left[\nu_r^{(*)}(z) + O(\epsilon^{1/n})\right], \tag{4.3.25}$$

with $|\epsilon| \ll 1$,

$$\nu_r^{(*)}(z) = \begin{cases} -x^{-1/n} Q_{r,n}(x), & z = 0, \\ e^{-\frac{i\pi(4r-3)}{n}} (x(1-x))^{-1/n} Q_{r,n}(x), & z = x, \\ (1-x)^{-1/n} Q_{r,n}(x), & z = 1, \\ e^{-\frac{4\pi i(r-1)}{n}} Q_{r,n}(x), & z = \infty. \end{cases} \tag{4.3.26}$$

and

$$Q_{r,n}(x) = e^{\frac{2\pi i(r-1)}{n}} \frac{\sin(\pi/n)}{\pi n I_{1/n}(x)}. \tag{4.3.27}$$

Observe that, in the four singularities, the divergent term when $\epsilon \to 0$ is a global factor $\epsilon^{\frac{1-n}{n}}$ and, once we take it out, the subleading corrections in ϵ vanish. Therefore, these singularities can be removed in the correlation function of Eq (4.3.14) by defining the vertex operators at the branch points as the limit

$$\mathcal{V}_\alpha^{(*)}(z) = \lim_{\epsilon\to 0} \left(\kappa_n \epsilon^{\frac{n-1}{n}}\right)^{2h_\alpha^{\mathcal{V}}} \mathcal{V}_\alpha(z+\epsilon), \quad z = 0, x, 1, \infty. \tag{4.3.28}$$

In this definition, we have included a possible global rescaling factor κ_n, which may depend on the genus of the surface, and we will adjust by studying the limit of large separation between the two intervals. If we replace in Eq. (4.3.21) the vertex operators by the regularised ones introduced in Eq. (4.3.28), then the resulting correlation function can be written in the form

$$\begin{aligned} \langle \mathcal{V}_{\alpha_1}^{(*)}(0)\mathcal{V}_{\alpha_2}^{(*)}(x)\mathcal{V}_{\alpha_3}^{(*)}(1)\mathcal{V}_{\alpha_4}^{(*)}(\infty)\rangle_{\mathcal{R}_n(x)} = \\ = \kappa_n^{2h_T} M_n(x)^{(\alpha_1+\alpha_2)(\alpha_3+\alpha_4)\eta} \prod_{1\le j<j'\le 4} |E^{(*)}(z_j, z_{j'})|^{\alpha_j\alpha_{j'}\eta}, \end{aligned} \tag{4.3.29}$$

where $h_T = h_{\alpha_1} + h_{\alpha_2} + h_{\alpha_3} + h_{\alpha_4}$ and $E^{(*)}(z_j, z_j')$ stands for the regularised prime form

$$E^{(*)}(z_j, z_{j'}) = \frac{\Theta_{\frac{\mathbf{1}}{\mathbf{2}}}(\boldsymbol{w}(z_j) - \boldsymbol{w}(z_{j'})|\Gamma(x))}{\sqrt{g^{(*)}(z_j)}\sqrt{g^{(*)}(z_{j'})}} \tag{4.3.30}$$

with

$$g^{(*)}(z_j) = \sum_{r=1}^{n-1} \nu_r^{(*)}(z_j)\partial_{u_r}\, \Theta_{\frac{\mathbf{1}}{\mathbf{2}}}(\boldsymbol{u}|\Gamma(x))\Big|_{\boldsymbol{u}=\mathbf{0}}, \tag{4.3.31}$$

and the expressions of $\nu^{(*)}(z)$ at the branch points are those given in Eq. (4.3.26).

In [105], we conjecture and numerically check the following identities for the regularised prime forms that appear in Eq. (4.3.29),

$$|E^{(*)}(0,x)| = nx^{1/n}, \tag{4.3.32}$$

$$|E^{(*)}(x,1)| = \frac{n(1-x)^{1/n}}{M_n(x)}, \tag{4.3.33}$$

$$|E^{(*)}(1,\infty)| = n, \tag{4.3.34}$$

and

$$|E^{(*)}(0,1)| = |E^{(*)}(0,\infty)| = |E^{(*)}(x,\infty)| = \frac{n}{M_n(x)}. \tag{4.3.35}$$

Plugging them into Eq. (4.3.29), we finally find

$$\langle \mathcal{V}^{(*)}_{\alpha_1}(0)\mathcal{V}^{(*)}_{\alpha_2}(x)\mathcal{V}^{(*)}_{\alpha_3}(1)\mathcal{V}^{(*)}_{\alpha_4}(\infty)\rangle_{\Sigma_n(x)} = \left(\frac{\kappa_n}{n}\right)^{2h_T} x^{\frac{\alpha_1\alpha_2\eta}{n}}(1-x)^{\frac{\alpha_2\alpha_3\eta}{n}}. \tag{4.3.36}$$

In Eq. (4.3.9), once the vertex operators $\mathcal{V}_\alpha$ are replaced by the regularised ones $\mathcal{V}^{(*)}_\alpha$, we can exploit Eq. (4.3.36) to get

$$Z_n^{A_1:A_2}(\{\alpha_j\}) \propto \left(\frac{\kappa_n}{n}\right)^{2h_T} (x(1-x))^{\frac{1-n^2}{6n}} (x^{\alpha_1\alpha_2}(1-x)^{\alpha_2\alpha_3})^{\frac{\eta}{n}} \mathcal{F}_n(x). \tag{4.3.37}$$

In particular, when $\alpha_1 = -\alpha_2 = \alpha$ and $\alpha_3 = -\alpha_4 = \beta$, we get the multi-charged moments $Z_n^{A_1:A_2}(\alpha,\beta)$. After a global conformal transformation to a subsystem A with arbitrary end-points (u_1, v_1, u_2, v_2), we obtain the following result

$$Z_n^{A_1:A_2}(\alpha,\beta) = c_{n;\alpha,\beta}\left(\frac{\kappa_n}{n}\right)^{2h_T} (\ell_1\ell_2(1-x))^{\frac{1-n^2}{6n}} \left(\ell_1^{\alpha^2}\ell_2^{\beta^2}(1-x)^{\alpha\beta}\right)^{-\frac{\eta}{n}} \mathcal{F}_n(x). \tag{4.3.38}$$

Note that the rescaling factor κ_n, which was introduced in the definition of the regularised vertex operators at the branch points, is still undetermined. We can fix it by analysing the limit in which the two intervals A_1 and A_2 are far, i.e. $d \to \infty$, as done for the Dirac theory. In that case, the charged moments $Z_n^{A_1:A_2}(\alpha,\beta)$ must verify Eq. (4.2.18). Since $\mathcal{F}_n(0) = 1$ and the constant $c_{n;\alpha,\beta}$ factorises into those for the intervals A_1 and A_2, then Eq. (4.3.38) satisfies the limit $d \to \infty$ of Eq. (4.2.18) if $\kappa_n = n$.

In conclusion, for the massless compact boson, the partition function on the surface $\mathcal{R}_n$ with general twisted boundary conditions is of the form

$$\frac{Z_n^{A_1:A_2}(\{\alpha_j\})}{Z_n^A(0)} \propto [d^{\alpha_2\alpha_3}\ell_1^{\alpha_1\alpha_2}\ell_2^{\alpha_3\alpha_4}(d+\ell_1)^{\alpha_1\alpha_3}(d+\ell_2)^{\alpha_2\alpha_4}(d+\ell_1+\ell_2)^{\alpha_1\alpha_4}]^{\frac{K}{2\pi^2 n}}, \tag{4.3.39}$$

and the multi-charged moments are

$$Z_n^{A_1:A_2}(\alpha,\beta) = c_{n;\alpha,\beta}\,(\ell_1\ell_2(1-x))^{\frac{1-n^2}{6n}} \left(\ell_1^{\alpha^2}\ell_2^{\beta^2}(1-x)^{\alpha\beta}\right)^{-\frac{K}{2\pi^2 n}} \mathcal{F}_n(x). \tag{4.3.40}$$

When the Luttinger parameter is $K = 1$, then $\mathcal{F}_n(x) = 1$, and the partition function of Eq. (4.3.40) is equal to the one obtained in Eq. (4.2.14) for the massless Dirac field, as we anticipated at the beginning of this section. Interestingly, the factor in Eq. (4.3.40) due to the magnetic fluxes is the same, when $\alpha = \beta$, as the one derived in Ref. [129] for a large central charge CFT with the Luttinger parameter K replaced by the level of the Kac-Moody algebra of that theory.

4.4 Symmetry resolution

In this section, we apply the approach described in Sec. 1.4.2 in order to evaluate the symmetry resolution of the mutual information in the two CFTs analysed in Secs. 4.2 and 4.3 from the expressions obtained there for their multi-charged moments $Z_n^{A_1:A_2}(\alpha,\beta)$.

4.4.1 Fourier transforms

The first step is to determine the Fourier transform (1.4.24) of the multi-charged moments. We need to know how the non-universal constant $c_{n;\alpha,\beta}$ does depend on α and β. In Sec. 4.2, we have concluded that, for the tight-binding model, it can be well approximated if we only take into account the quadratic terms in α and β. In the following, we will assume that this is in general a good approximation [85]. Therefore, we will take

$$c_{n;\alpha,\beta} = c_{n;0,0}\lambda_n^{-\frac{(\alpha^2+\beta^2)K}{2\pi^2 n}}. \tag{4.4.1}$$

In the case of the tight-binding model ($K = 1$), we obtained in Eq. (4.2.20) that $\lambda_n = e^{\zeta_n}$.

Therefore, applying Eq. (4.4.1) in the result of Eq. (4.3.40), the multi-charged moments can be rewritten as

$$Z_n^{A_1:A_2}(\alpha,\beta) = Z_n^A(0)\left[(1-x)^{-\alpha\beta}\,\tilde{\ell}_1^{-\alpha^2}\tilde{\ell}_2^{-\beta^2}\right]^{\frac{K}{2\pi^2 n}}, \tag{4.4.2}$$

where $\tilde{\ell}_p = \lambda_n \ell_p$. The evaluation of Eq. (1.4.24) using the expression above yields the following multivariate Gaussian function for the Fourier modes of the multi-charged moments

$$\mathcal{Z}_n^{A_1:A_2}(q_1,q_2) = \frac{Z_n^A(0)\, n\pi e^{-2\pi^2 n \frac{q_1^2\log\tilde{\ell}_2 + q_2^2\log\tilde{\ell}_1 + q_1 q_2\log(1-x)}{K[4\log(\tilde{\ell}_1)\log(\tilde{\ell}_2) - \log^2(1-x)]}}}{K\sqrt{4\log(\tilde{\ell}_1)\log(\tilde{\ell}_2) - \log^2(1-x)}}. \tag{4.4.3}$$

Notice that the Luttinger parameter K enters in the Gaussian factor as an overall rescaling of its variance.

In the limit of large separation between the intervals, i.e. $d \to \infty$ ($x \to 0$), Eq. (4.4.3) tends to

$$\lim_{d\to\infty} \frac{\mathcal{Z}_n^{A_1:A_2}(q_1,q_2)}{Z_n^A(0)} = \frac{n\pi}{2K} \frac{e^{-\frac{n\pi^2 q_1^2}{2K\log\tilde{\ell}_1}}}{\sqrt{\log\tilde{\ell}_1}} \frac{e^{-\frac{n\pi^2 q_2^2}{2K\log\tilde{\ell}_2}}}{\sqrt{\log\tilde{\ell}_2}}, \tag{4.4.4}$$

namely $\mathcal{Z}_n^{A_1:A_2}(q_1,q_2)$ factorises into the contributions of A_1 and A_2. This is consistent with the probabilistic interpretation for the case $n = 1$: the outcomes of the charge measurements in the two intervals are independently distributed when the separation between A_1 and A_2 is large enough. On the other hand, in the limit of two adjacent intervals, i.e. $d \to 0$ ($x \to 1$), the multi-charged moments have the form (see also Eq. (4.2.17))

$$\lim_{d\to 0} \frac{Z_n^{A_1:A_2}(\alpha,\beta)}{Z_n^A(0)} = \left[\frac{\tilde{\ell}_1^{\alpha\beta-\alpha^2}\tilde{\ell}_2^{\alpha\beta-\beta^2}}{(\tilde{\ell}_1+\tilde{\ell}_2)^{\alpha\beta}}\right]^{\frac{K}{2\pi^2 n}}, \tag{4.4.5}$$

whose Fourier transform is

$$\lim_{d\to 0} \frac{\mathcal{Z}_n^{A_1:A_2}(q_1,q_2)}{Z_n^{A_1\cup A_2}(0)} = \frac{n\pi e^{-2\pi^2 n \frac{q_1^2\log\tilde{\ell}_2 + q_2^2\log\tilde{\ell}_1 + q_1 q_2[\log(\tilde{\ell}_1\tilde{\ell}_2) - \log(\tilde{\ell}_1+\tilde{\ell}_2))]}{4K\log(\tilde{\ell}_1)\log(\tilde{\ell}_2) - K[\log(\tilde{\ell}_1\tilde{\ell}_2) - \log(\tilde{\ell}_1+\tilde{\ell}_2))]^2}}}{K\sqrt{4\log(\tilde{\ell}_1)\log(\tilde{\ell}_2) - \left[\log(\tilde{\ell}_1\tilde{\ell}_2) - \log(\tilde{\ell}_1+\tilde{\ell}_2)\right]^2}}. \tag{4.4.6}$$

Setting $\alpha = \beta$ in Eq. (4.4.2), we obtain the charged moments (1.4.16) with a single flux

$$Z_n^A(\alpha) = Z_n^A(0)\left[(1-x)\tilde{\ell}_1\tilde{\ell}_2\right]^{-\frac{\alpha^2 K}{2\pi^2 n}}. \tag{4.4.7}$$

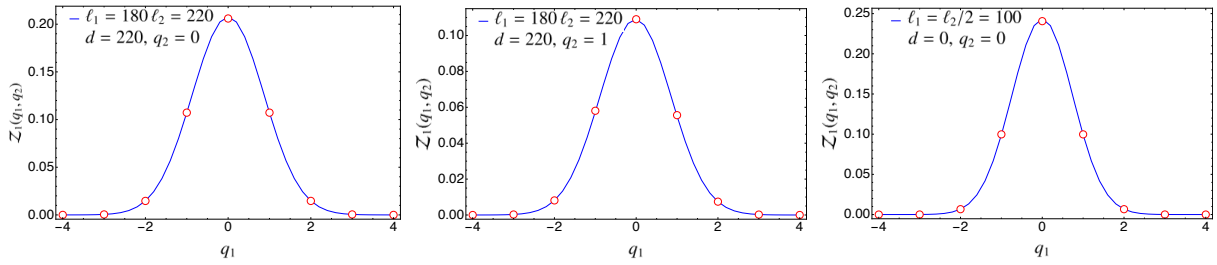

Figure 4.2: Probability $\mathcal{Z}_1(q_1, q_2)$ for the tight-binding model as a function of q_1 at fixed q_2 and for two disjoint intervals of lengths ℓ_1, ℓ_2, and separated a distance d. The points are the exact numerical values calculated using the methods of the Appendix 4.A. The solid line is the theoretical prediction in Eq. (4.4.3) taking for the non-universal constants the corresponding values for the tight-binding model indicated in the main text.

In this case, performing the Fourier transform of Eq. (1.4.17), we end up with

$$\mathcal{Z}_n^A(q) = \frac{Z_n^A(0)\sqrt{\pi n}}{\sqrt{2K \log\left[(1-x)\tilde{\ell}_1\tilde{\ell}_2\right]}} e^{-\frac{\pi^2 n q^2}{2K \log\left[(1-x)\tilde{\ell}_1\tilde{\ell}_2\right]}}. \tag{4.4.8}$$

Taking $n = 1$ in this expression, we obtain the probability $p(q)$ of having charge q in the subsystem A, namely $p(q) = \mathcal{Z}_1(q)$. Now we can plug it together with the result for $\mathcal{Z}_n(\alpha, \beta)$ found in Eq. (4.4.3) into Eq. (1.4.26) to obtain the conditional probability $p(q_1, q_2)$ of having charge q_1 and $q_2 = q - q_1$ in the intervals A_1 and A_2 if the total charge in A is q,

$$p(q_1, q_2) = \sqrt{\frac{2\pi \log\left[(1-x)\tilde{\ell}_1\tilde{\ell}_2\right]}{K[4\log(\tilde{\ell}_1)\log(\tilde{\ell}_2) - \log^2(1-x)]}} e^{-\frac{2\pi^2}{K}\left[\frac{q_1^2 \log\tilde{\ell}_2 + q_2^2 \log\tilde{\ell}_1 + q_1 q_2 \log(1-x)}{4\log(\tilde{\ell}_1)\log(\tilde{\ell}_2) - \log^2(1-x)} + \frac{(q_1+q_2)^2}{4\log\left[(1-x)\tilde{\ell}_1\tilde{\ell}_2\right]}\right]}. \tag{4.4.9}$$

In this expression, $\tilde{\ell}_p = \lambda_1 \ell_p$; in particular, for the tight-binding model $\lambda_1 = e^{\log 2 + 1 + \gamma_{\rm E}}$, with $\gamma_{\rm E}$ the Euler-Mascheroni constant. As a non-trivial consistency check, we have verified that the probability functions we have obtained satisfy the normalisation conditions

$$\int_{-\infty}^{\infty} \mathcal{Z}_1^{A_1:A_2}(q_1, q_2) dq_1 dq_2 = 1, \quad \int_{-\infty}^{q} p(q_1, q - q_1) dq_1 = 1, \tag{4.4.10}$$

in agreement with Eqs. (1.4.26) and (1.4.25).

In Fig. 4.2, we compare the expression for $\mathcal{Z}_1(q_1, q_2)$ found in Eq. (4.4.3) for the case of disjoint intervals with the exact numerical results obtained for the tight-binding model using the methods of the Appendix 4.A. The agreement is excellent. We remark that in Fig. 4.2 there is no free parameter when matching the analytical prediction with the numerical data since we know the expression of the non-universal constants for this particular system. We have also repeated the same analysis in the case of adjacent intervals ($d = 0$), checking the validity of Eq. (4.4.6).

4.4.2 Symmetry resolved mutual information

We compute now the symmetry resolved mutual information defined in Eq. (1.3.6). We need the probability $p(q_1, q - q_1)$ derived in Eq. (4.4.9) as well as the symmetry resolved entropies for A and its parts A_1 and A_2 separately. For the entropies of A_1 and A_2, we can use the results for a single

interval obtained in Ref. [90] while, for the full subsystem A, it can be derived from the Fourier transform of the charged moments determined in Eq. (4.4.8) by applying Eq. (1.4.18). The three symmetry resolved entropies can eventually be written in the form

$$S_1^X(q) = S_1^X - \frac{1}{2}\log\left(\frac{2K}{\pi}\log\delta^\sigma\Lambda\right) - \frac{1}{2} - \sigma\pi^4\frac{\xi^2}{(K\log(\lambda_1^\sigma\Lambda))^2} + \sigma q^2\pi^4\frac{\xi}{(K\log(\lambda_1^\sigma\Lambda))^2}. \quad (4.4.11)$$

where S_1^X is the total entanglement entropy of subsystem X. In this expression, when $X = A_p$, we have to take $\Lambda = \ell_p$ and $\sigma = 1$ while, if $X = A_1 \cup A_2$, then $\Lambda = \ell_1\ell_2(1-x)$ and $\sigma = 2$. The auxiliary quantities δ and ξ in Eq. (4.4.11) are defined in terms of λ_n as

$$\log\delta = \log\lambda_1 + 2\pi^2\xi, \qquad \xi = -\frac{1}{2\pi^2}\partial_n(\log\lambda_n)|_{n=1} \quad (4.4.12)$$

For the tight-binding model, we know the explicit value of these non-universal constants,

$$\log\delta = 2\pi^2\gamma_2'(1) + \log 2, \qquad \xi = \gamma_2(1) + \gamma_2'(1). \quad (4.4.13)$$

From Eqs. (4.4.9) and (4.4.11), we can now obtain an explicit expression for the symmetry resolved mutual information. Since the conditional probability $p(q_1, q-q_1)$ satisfies Eq. (4.4.10), we have

$$\begin{aligned} I^{A_1:A_2}(q) &= I^{A_1:A_2} - \frac{1}{2}\log\left[\frac{2K}{\pi}\frac{\log(\tilde\ell_1^\delta)\log(\tilde\ell_2^\delta)}{\log\left(\tilde\ell_1^\delta\tilde\ell_2^\delta(1-x)\right)}\right] - \frac{1}{2} - 2q^2\pi^4\frac{\xi}{K^2\log^2\left(\tilde\ell_1\tilde\ell_2(1-x)\right)} \\ &\quad -\pi^4\frac{\xi^2}{K^2}\left(\frac{1}{\log\tilde\ell_1} + \frac{1}{\log\tilde\ell_2} - \frac{1}{\log(\tilde\ell_1\tilde\ell_2(1-x))}\right) \\ &\quad +\frac{\pi^4}{K^2}\xi\int_{-\infty}^{\infty} p(q_1, q-q_1)\left[\frac{q_1^2}{\log^2\tilde\ell_1} + \frac{(q-q_1)^2}{\log^2\tilde\ell_2}\right]\mathrm{d}q_1, \end{aligned} \quad (4.4.14)$$

where $I^{A_1:A_2}$ is the total mutual information of Eq. (1.1.10) (when $n \to 1$) and we have introduced the rescaled subsystem length $\tilde\ell_p^\delta = \delta\ell_p$. As we anticipated, the symmetry resolved mutual information is not a good measure of total correlations between A_1 and A_2 in each symmetry sector since it can assume negative values. Finally, we can also derive the number mutual information defined in Eq. (1.3.8). Applying in that formula the result for $I^{A_1:A_2}(q)$ obtained in Eq. (4.4.14), we have

$$\begin{aligned} I_{\mathrm{num}}^{A_1:A_2} &= \frac{1}{2}\log\left[\frac{2K}{\pi}\frac{\log(\tilde\ell_1^\delta)\log(\tilde\ell_2^\delta)}{\log\left(\tilde\ell_1^\delta\tilde\ell_2^\delta(1-x)\right)}\right] + \frac{1}{2} + \frac{2\pi^2\xi}{K\log\left(\tilde\ell_1\tilde\ell_2(1-x)\right)} \\ &\quad -\pi^4\frac{\xi^2}{K^2}\left(\frac{1}{\log\tilde\ell_1} + \frac{1}{\log\tilde\ell_2} - \frac{1}{\log(\tilde\ell_1\tilde\ell_2(1-x))}\right) \\ &\quad -\pi^4\frac{\xi}{K^2}\int_{-\infty}^{\infty}\mathcal{Z}_1^{A_1:A_2}(q_1, q-q_1)\left[\frac{q_1^2}{\log^2\tilde\ell_1} + \frac{(q-q_1)^2}{\log^2\tilde\ell_2}\right]\mathrm{d}q_1\mathrm{d}q. \end{aligned} \quad (4.4.15)$$

Since $q = q_1 + q_2$ and

$$\int_{-\infty}^{\infty}\mathcal{Z}_1^{A_1:A_2}(q_1, q_2)q_p^2\mathrm{d}q_1\mathrm{d}q_2 = \frac{K\log\tilde\ell_p}{\pi^2}, \quad p = 1, 2, \quad (4.4.16)$$

then Eq. (4.4.15) becomes

$$I_{\rm num}^{A_1:A_2} = \frac{1}{2}\log\left[\frac{2K}{\pi}\frac{\log(\tilde{\ell}_1^{\delta})\log(\tilde{\ell}_2^{\delta})}{\log(\tilde{\ell}_1^{\delta}\tilde{\ell}_2^{\delta}(1-x))}\right] + \frac{1}{2} - \pi^4\frac{\xi^2}{K^2}\left(\frac{1}{\log\tilde{\ell}_1}+\frac{1}{\log\tilde{\ell}_2}-\frac{1}{\log(\tilde{\ell}_1\tilde{\ell}_2(1-x))}\right) - \pi^2\frac{\xi}{K}\left(\frac{1}{\log\tilde{\ell}_1}+\frac{1}{\log\tilde{\ell}_2}-\frac{2}{\log(\tilde{\ell}_1\tilde{\ell}_2(1-x))}\right). \quad (4.4.17)$$

In the limit $\ell_1, \ell_2, d \to \infty$, this expression behaves as

$$I_{\rm num}^{A_1:A_2} \sim \frac{1}{2}\log\left[\frac{2K}{\pi}\frac{\log\ell_1\log\ell_2}{\log\left(\ell_1\ell_2(1-x)\right)}\right] + \frac{1}{2}. \quad (4.4.18)$$

This result resembles the one for the number entropy of a single interval (see e.g. [90]), where a double logarithmic correction in the subsystem length also appears, even though, in our case, the dependence on the parameters ℓ_1, ℓ_2, d is more involved. On the other hand, it is a simple function of the Luttinger parameter K since, as we already pointed out, the only effect of K in the Gaussian factor of the Fourier transform of the multi-charged moments is renormalising its variance.

4.5 Closing remarks

In this Chapter, we have computed the multi-charged moments of two intervals in the ground state of the free massless Dirac field and the massless compact boson, with arbitrary compactification radius. Using the replica approach, the multi-charged moments are given by the partition function of the theory on a higher genus Riemann surface with a different magnetic flux inserted in each interval. We have carried out the analysis of such partition function for the two CFTs under investigation in full generality, allowing the background magnetic flux to generate a different twist boundary condition at each end-point of the intervals.

The multi-charged moments analysed here can be used to study the symmetry decomposition of the negativity in imbalance sectors [116]. A further generalisation is to identify the holographic dual of the multi-charged moments, which would be the starting point to compute the symmetry resolved mutual information in the AdS/CFT correspondence, as done for the entanglement entropy in Ref. [128]. Partition functions with twisted boundary conditions, as the ones considered here, have been also proposed as non-local order parameters to distinguish various topological phases of spin chains [165, 166]. We think that our analysis for the multi-charged moments can be useful to make progresses also in that direction. Finally, it would be interesting to obtain a rigorous proof of the identities for the prime forms that we have found and numerically checked here.

4.A Numerical Methods

For the numerical test of our field theory results, we consider the following lattice discretisation of the Dirac fermion, known as tight-binding model,

$$H = -\frac{1}{2}\sum_{j=-\infty}^{\infty}(c_{j+1}^{\dagger}c_j + \text{h.c.}), \quad (4.A.1)$$

where $c_j^\dagger$ and c_j are fermionic creation and annihilation operators that satisfy the anti-commutation relations $\{c_j, c_k^\dagger\} = \delta_{jk}$. In terms of them, the charge operator reads

$$Q = \sum_{j=-\infty}^{\infty} \left(c_j^\dagger c_j - \frac{1}{2} \right). \tag{4.A.2}$$

The two-point correlation functions in the ground state of Eq. (4.A.1) are of the form

$$\langle c_j^\dagger c_k \rangle = \frac{\sin(\pi(j-k))}{2\pi(j-k)}, \tag{4.A.3}$$

and, due to the particle number conservation, $\langle c_j c_k \rangle = 0$. As well-known [169, 171], the moments $\mathrm{Tr}[\rho_A^n]$ can be calculated from the restriction of the two-point correlation matrix to the subsystem A, that is $(C_A)_{j,k} = \langle c_j^\dagger c_k \rangle$, with $j, k \in A$. The charged moments $Z_n^{A=A_1 \cup A_2}(\alpha)$ can also be easily computed numerically in terms of the matrix C_A using the formula [84, 90]

$$Z_n^{A=A_1 \cup A_2}(\alpha) = \prod_{j=1}^{\ell_1+\ell_2} [(\varepsilon_j)^n e^{i\alpha/2} + (1-\varepsilon_j)^n e^{-i\alpha/2}], \tag{4.A.4}$$

where ε_j are the eigenvalues of C_A and ℓ_p is the number of sites in the interval A_p. In the case of the multi-charged moments $Z^{A_1:A_2}(\alpha, \beta)$ defined in Eq. (1.4.23), the method used to compute $Z_n^A(\alpha)$ can not be applied since ρ_A does not commute with the charges Q_{A_1} and Q_{A_2} of the two parts of A. Following Ref. [133] (which was based on [272]), we rewrite Eq. (1.4.23) as

$$Z_1^{A_1:A_2}(\alpha, \beta) = \tilde{Z}_A \mathrm{Tr}_A(\rho_A \tilde{\rho}_A), \tag{4.A.5}$$

where

$$\tilde{\rho}_A = \frac{1}{\tilde{Z}_A} e^{i\alpha Q_{A_1} + i\beta Q_{A_2}}, \quad \tilde{Z}_A = \mathrm{Tr}_A(e^{i\alpha Q_{A_1} + i\beta Q_{A_2}}). \tag{4.A.6}$$

Although $\tilde{\rho}_A$ is not a density matrix, it is a Gaussian operator with an associated two-point correlation matrix, $\tilde{C}_A$, given by

$$(\tilde{C}_A)_{kj} = \delta_{kj} \begin{cases} \frac{e^{i\alpha}}{1+e^{i\alpha}} & j \in A_1, \\ \frac{e^{i\beta}}{1+e^{i\beta}} & j \in A_2. \end{cases} \tag{4.A.7}$$

Applying the rules for the composition of Gaussian operators [174] and introducing $W = 2C_A - \mathbb{I}$, we get [133]

$$Z_1^{A_1:A_2}(\alpha, \beta) = (e^{-i\alpha/2} + e^{i\alpha/2})^{\ell_1} (e^{-i\beta/2} + e^{i\beta/2})^{\ell_2} \det\left(\frac{\mathbb{1}_{\ell_1+\ell_2} + W_{\alpha\beta}}{2} \right), \tag{4.A.8}$$

where

$$W_{\alpha\beta} = \begin{pmatrix} W_{11} & W_{12} \\ W_{21} & W_{22} \end{pmatrix} \begin{pmatrix} \frac{e^{i\alpha}-1}{e^{i\alpha}+1} \mathbb{1}_{\ell_1} & 0 \\ 0 & \frac{e^{i\beta}-1}{e^{i\beta}+1} \mathbb{1}_{\ell_2} \end{pmatrix}, \tag{4.A.9}$$

and the notation $W_{pp'}$, $p, p' = 1, 2$, refers to correlations between sites in A_p and $A_{p'}$. This result allows to exactly compute the multi-charged moments in the tight-binding model for different values of α and β, as showed in Fig. 4.1. The Fourier transform of $Z_1^{A_1:A_2}(\alpha, \beta)$ gives the quantities $\mathcal{Z}_1^{A_1:A_2}(q_1, q_2)$ analysed in Fig. 4.2.

Chapter 5

Generalised entanglement entropies in two-dimensional conformal field theory

In this Chapter we introduce and study the generalised Rényi entropies defined through the traces of products of $\mathrm{Tr}_B(|\Psi_i\rangle\langle\Psi_j|)$ where $|\Psi_i\rangle$ are eigenstates of a $2d$ CFT. When $|\Psi_i\rangle = |\Psi_j\rangle$ these objects reduce to the standard Rényi entropies of the eigenstates of the CFT. Exploiting the path integral formalism, we show that the second generalised Rényi entropies are equivalent to four point correlators. We then focus on a free bosonic theory for which the mode expansion of the fields allows us to develop an efficient strategy to compute the second generalised Rényi entropy for all eigenstates. As a byproduct, our approach also leads to new results for the standard Rényi and relative entropies involving arbitrary descendent states of the bosonic CFT. This Chapter is based on Ref. [275]

5.1 Introduction

An old and fundamental result that we reviewed in Chapter 1 is that the ground state entanglement entropy is universal [17, 20, 21]. The same is also true for all low-energy eigenstates [153, 276]. Indeed, denoting by ρ_Υ the RDM of the state associated to the field Υ by the operator-state correspondence (and hence $\rho_\mathbb{1}$ is the ground-state RDM), the ratio

$$F_{\Upsilon,n}(A) \equiv \frac{\mathrm{Tr}\rho_\Upsilon^n}{\mathrm{Tr}\rho_\mathbb{1}^n} = \exp[(1-n)(S^{(n)}_{A,\Upsilon} - S^{(n)}_{A,GS})], \tag{5.1.1}$$

is universal and calculable in CFT [153, 154]. The universal function $F_{\Upsilon,n}(A)$ measures the excess of entanglement of the excited state $|\Upsilon\rangle$ with respect to the ground state value. The simplest class of excited states in a CFT are those generated by the action of a primary field Υ. The von Neumann and Rényi entropies in excited states of CFT have then been the subject of intensive investigations [117, 153, 154, 277–290].

Another important quantum information quantity encoding the universal features of CFT low-lying excited states is the relative entanglement entropy [119, 291–304]. Given two RDMs, ρ_1 and ρ_0, the relative entropy is defined as [306, 307]

$$S_A(\rho_1\|\rho_0) = \mathrm{Tr}\left(\rho_1 \log \rho_1\right) - \mathrm{Tr}\left(\rho_1 \log \rho_0\right), \tag{5.1.2}$$

and can be interpreted as a measure of distinguishability of the two RDMs, providing a sort of distance between them in the Hilbert space (despite not being a proper metric because it is not

symmetric in ρ_1 and ρ_0). In a replica approach, $S_A(\rho_1\|\rho_0)$ can be obtained as the limit for $n \to 1$ of the logarithm of the universal ratio [291, 303]

$$G_{n,A}(\rho_1||\rho_0) \equiv \frac{\mathrm{Tr}(\rho_1\rho_0^{n-1})}{\mathrm{Tr}\rho_1^n}. \tag{5.1.3}$$

Similar quantities are also the starting point for the replica approach to the trace distance [308–310]. Both Eq. (5.1.1) and Eq. (5.1.3) have been studied intensively for the lowest-energy states corresponding to primary fields. Conversely, the study of descendant states (obtained from the primaries by the application of conformal generators) has been limited to a very few cases [283,285]. The drawback of the method of Refs. [283, 285] is that it becomes more and more cumbersome as the conformal level increases. Here we develop a strategy to obtain the Rényi entropies of excited states which is a more efficient way for theories with central charge $c = 1$ for which we can use the free boson representation.

As part of this, we introduce a novel quantity that we dub *generalised mixed state Rényi entropies* (GMSREs) defined as

$$R_{i_1,j_1;\ldots;i_n,j_n} = \mathrm{Tr}_A\left(\prod_{t=1}^{n}\mathrm{Tr}_B\left|\Psi_{i_t}\right\rangle\left\langle\Psi_{j_t}\right|\right), \tag{5.1.4}$$

where $|\Psi_{i_t}\rangle$ is the t-th copy ($1 \le t \le n$) of states $|\psi_i\rangle$ of the CFT. For brevity, we will often refer to them as generalised Rényi entropies. This object reduces to the usual Rényi entropies of excited states when $|\Psi_{i_t}\rangle\langle\Psi_{j_t}| = \delta_{i,j}|\Psi_i\rangle\langle\Psi_j|$ for each t-th copy. Let us stress that the states ψ_{i_l} in each copy can be different CFT eigenstates, i.e. $\psi_{i_1} \neq \psi_{i_2}$. Moreover, the CFT eigenstates are also known in literature as dilatation eigenstates, since they are the eigenstates of the CFT Hamiltonian given by the Virasoro generators $L_0 + \bar{L}_0$ (up to a constant), which is the dilatation operator. These objects also resemble the notion of pseudo-entropies recently introduced in [311,312], whose reduced density matrix is defined in terms of two different states. Apart from their intrinsic interest, these generalised non-diagonal entropies represent the building blocks for the calculation of the entanglement entropies in states that can be written as a linear combination of the elements of the CFT basis, as happens for example, in the truncated conformal space approach [305, 313–315].

The Chapter is organised as follows. In Sec. 5.2 we outline the path integral approach to the second generalised Rényi entropy and we show that it can be rewritten as a correlation function. In Sec. 5.3 we focus on the bosonic theory and we develop a CFT approach to compute the second generalised entropy for an arbitrary state of the CFT. We start from some simple examples and piece by piece, we lead the reader to the most general case in Sec. 5.4. Finally, we conclude and discuss some future perspectives in Sec. 5.5.

5.2 Path integral for the second generalised Rényi entropy

In this section, we focus on the second generalised Rényi entropy and we show that its calculation within the path integral formalism reduces to the computation of a four point correlator, by generalising the one for the ground state done in Sec. 1.4. Let L be the total length of a periodic 1D system, A a subsystem consisting of a segment of length ℓ, i.e $A = [u, v]$ with $v - u = \ell$, and B its complement. Because of the state-operator correspondence in CFT, each eigenstate $|\Psi_{i_t}\rangle$ is generated by an operator Ψ_{i_t}, acting on the vacuum and placed at the infinite past. Hence, the path integral representation of the off-diagonal density matrix $|\Psi_i\rangle\langle\Psi_j|$ is given, up to a normalisation

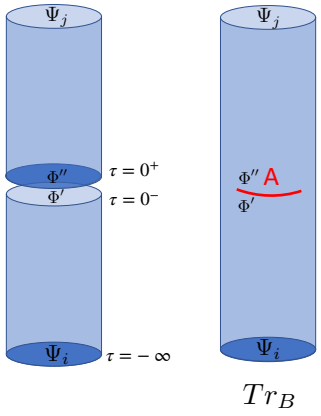

Figure 5.1: Left: Path integral representation of matrix elements of $|\Psi_i\rangle\langle\Psi_j|$, cf. Eq. (5.2.1). Right: Path integral representation of $\mathrm{Tr}_B(|\Psi_i\rangle\langle\Psi_j|)$, as in Eq. (5.2.2).

constant, by

$$\langle\Phi'|\Psi_i\rangle\langle\Psi_j|\Phi''\rangle \propto \int \mathcal{D}\varphi e^{-S(\varphi)} \prod_x (\delta(\varphi(x,\tau=0^-)-\Phi'(x)))\Psi_i(\tau=-\infty) \times \prod_x (\delta(\varphi(x,\tau=0^+)-\Phi''(x)))\Psi_j(\tau=\infty), \quad (5.2.1)$$

where the geometry of the integration surface is an infinite cylinder with a discontinuity of the field configurations at $\tau = 0$ and $S(\varphi)$ is the Euclidean action of the theory we are interested in (e.g. in the following we will focus on the bosonic CFT). We represent Eq. (5.2.1) graphically in the left panel of Fig. 5.1.

Let us now compute the off-diagonal reduced density matrix by tracing over the subsystem B (see the right panel of Fig. 5.1):

$$\langle\Phi'|\,\mathrm{Tr}_B(|\Psi_i\rangle\langle\Psi_j|)\,|\Phi''\rangle = C_{ij}\int \mathcal{D}\varphi e^{-S(\varphi)} \prod_{x\in A} (\delta(\varphi(x,\tau=0^-)-\Phi'(x)))\Psi_i(\tau=-\infty) \times \prod_{x\in A} (\delta(\varphi(x,\tau=0^+)-\Phi''(x)))\Psi_j(\tau=\infty), \quad (5.2.2)$$

where C_{ij} is a normalisation factor. By imposing the normalisation of the off-diagonal reduced density matrix to be $\mathrm{Tr}_A(\mathrm{Tr}_B(|\Psi_i\rangle\langle\Psi_j|)) = \delta_{ij}$, we can fix the constant C_{ij} as

$$\delta_{ij} = C_{ij} Z \langle\Psi_j(\tau=\infty)\Psi_i(\tau=-\infty)\rangle\,. \quad (5.2.3)$$

Here Z and $\langle\Psi_j(\tau=\infty)\Psi_i(\tau=-\infty)\rangle$ are, respectively, the partition function and the correlation function of the two fields.

As already mentioned, we are interested in the second generalised Rényi entropy. We thus make two copies of Eq. (5.2.2), and glue them together cyclically such that

$$\varphi_1(x,\tau=0^+) = \varphi_2(x,\tau=0^-), \quad \varphi_2(x,\tau=0^+) = \varphi_1(x,\tau=0^-), \quad \forall x\in A. \quad (5.2.4)$$

Starting from Eq. (5.2.2), we find the following expression for the elements of the off-diagonal

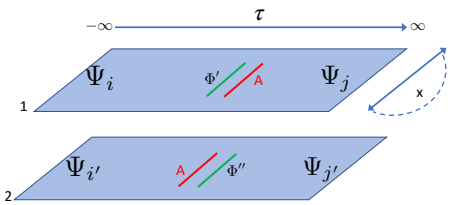

Figure 5.2: Representation of the spacetime geometry involving a 2-sheeted Riemann surface, $\mathcal{R}_2$, that appears in computing the second generalised entropy $R_{i,j;i',j'}$ in Eq. (5.2.6).

second Rényi entropy

$$\langle\Phi'|\,\mathrm{Tr}_B(|\Psi_i\rangle\langle\Psi_j|)\mathrm{Tr}_B(|\Psi_{i'}\rangle\langle\Psi_{j'}|)\,|\Phi''\rangle = C_{ij}C_{i'j'}\int\mathcal{D}\varphi_1\mathcal{D}\varphi_2 e^{-S(\varphi_1)-S(\varphi_2)} \times\prod_{x\in A}(\delta(\varphi_1(x,\tau=0^-)-\Phi'(x)))\prod_{x\in A}(\delta(\varphi_2(x,\tau=0^+)-\Phi''(x))) \times\Psi_i(\tau=-\infty)\Psi_j(\tau=\infty)\Psi_{i'}(\tau=-\infty)\Psi_{j'}(\tau=\infty), \quad (5.2.5)$$

where the path-integral is done over a 2-sheeted Riemann surface such that the first equality in Eq. (5.2.4) holds. Let us notice that the field φ_1 along A at $\tau=0^-$ is fixed at Φ', while φ_2 at $\tau=0^+$ is fixed at Φ''. Thus, by taking the trace over A, i.e. using also the second identification in Eq. (5.2.4), we obtain an expression for the second generalised Rényi entropy

$$R_{i,j;i',j'} = \mathrm{Tr}_A(\mathrm{Tr}_B(|\Psi_i\rangle\langle\Psi_j|)\mathrm{Tr}_B(|\Psi_{i'}\rangle\langle\Psi_{j'}|)) = C_{ij}C_{i'j'}\int\mathcal{D}\varphi_1\mathcal{D}\varphi_2 e^{-S(\varphi_1)-S(\varphi_2)} \times\prod_{x\in A}\delta(\varphi_1(x,\tau=0^-)-\Phi'(x))\delta(\varphi_2(x,\tau=0^+)-\Phi''(x))\Psi_i(\tau=-\infty)\Psi_j(\tau=\infty)\Psi_{i'}(\tau=-\infty) \times\Psi_{j'}(t=\infty) = C_{ij}C_{i'j'}Z_2(A)\,\langle\Psi_i(\tau=-\infty)\Psi_j(\tau=\infty)\Psi_{i'}(\tau=-\infty)\Psi_{j'}(\tau=\infty)\rangle_{\mathcal{R}_2}\,, \quad (5.2.6)$$

where $\mathcal{R}_2$ is the 2-sheeted Riemann surface that results from the sewing of the two copies of the original cylinder along the cuts associated with the interval A and $Z_2(A)$ is the partition function in the same geometry. This path integral is over a spacetime pictured in Fig. 5.2. The result in Eq. (5.2.6) shows that the second generalised entropy reduces to a 4-point correlation function.

Before embarking in the calculation of Eq. (5.2.6), we fix the normalisation constants, C_{ij}'s. As already discussed, the constants C_{ij}'s are independent of A. Thus if the segment A shrinks to zero, we decouple the two Riemann sheets and the 4-point function factorises into a product of 2-point ones:

$$C_{ij}C_{i'j'}Z^2\,\langle\Psi_i(\tau=-\infty)\Psi_j(\tau=\infty)\rangle_{\mathcal{R}_1}\,\langle\Psi_{i'}(\tau=-\infty)\Psi_{j'}(\tau=\infty)\rangle_{\mathcal{R}_1} = \delta_{ij}\delta_{i'j'}. \quad (5.2.7)$$

Now if we take the segment A to be the entire system (as the Tr_B operation is trivial), the two sheets of the Riemann surface are again no longer connected and

$$C_{ij}C_{i'j'}Z^2\,\langle\Psi_i(\tau=-\infty)\Psi_{j'}(\tau=\infty)\rangle_{\mathcal{R}_1}\,\langle\Psi_{i'}(\tau=-\infty)\Psi_j(\tau=\infty)\rangle_{\mathcal{R}_1} = \delta_{ij'}\delta_{i'j}, \quad (5.2.8)$$

i.e. the four-point function still factorises even though differently with respect to Eq. (5.2.7). Hence, the constant may be fixed as

$$C_{ij} = \frac{1}{Z\sqrt{\langle\Psi_i(\tau=-\infty)\Psi_i(\tau=\infty)\rangle_{\mathcal{R}_1}\,\langle\Psi_j(\tau=-\infty)\Psi_j(\tau=\infty)\rangle_{\mathcal{R}_1}}}, \quad (5.2.9)$$

and we can express ratios of the generalised entropies in terms of universal quantities:

$$\begin{aligned}\frac{R_{i,j;i',j'}}{R_{\mathbb{1},\mathbb{1};\mathbb{1},\mathbb{1}}} =& F_i F_j F_{i'} F_{j'} \langle \Psi_i(\tau=-\infty)\Psi_j(\tau=\infty)\Psi_{i'}(\tau=-\infty)\Psi_{j'}(\tau=\infty)\rangle_{\mathcal{R}_2}\,,\\ F_i =& \frac{1}{\sqrt{\langle \Psi_i(\tau=-\infty)\Psi_i(\tau=\infty)\rangle_{\mathcal{R}_1}}}.\end{aligned} \tag{5.2.10}$$

This expression can be easily extended to the n-th order generalised Rényi entropy introduced in Eq. (5.1.4) as

$$\begin{aligned}&\frac{R_{i_1,j_1;\ldots;i_n,j_n}}{R_{\mathbb{1},\mathbb{1};\ldots;\mathbb{1},\mathbb{1}}}\\ &\quad = F_{i_1}F_{j_1}\ldots F_{i_n}F_{j_n}\,\langle \Psi_{i_1}(\tau=-\infty)\Psi_{j_1}(\tau=\infty)\ldots\Psi_{i_n}(\tau=-\infty)\Psi_{j_n}(\tau=\infty)\rangle_{\mathcal{R}_n}\,.\end{aligned} \tag{5.2.11}$$

5.3 Bosonic theory: a CFT approach beyond primary fields

In the following sections, we compute the second generalised Rényi entropy for a massless free bosonic field theory whose Euclidean action is (we report it here for completeness, but it is the same action we already introduced in Eq. (4.3.1))

$$S(\varphi) = \int_0^L dx d\tau \left[\frac{1}{8\pi}\partial_\mu\varphi(x,\tau)\partial^\mu\varphi(x,\tau)\right]. \tag{5.3.1}$$

The mode expansion of the field $\varphi(x,\tau)$ is [269]

$$\varphi(x,\tau) = \varphi_0 - i\frac{4\pi}{L}\pi_0\tau + i\sum_{k\neq 0}\frac{1}{k}(a_k e^{\frac{2\pi k(ix-\tau)}{L}} - \bar{a}_{-k}e^{\frac{2\pi k(ix+\tau)}{L}}). \tag{5.3.2}$$

Here in Eq. (5.3.2) φ_0 is the bosonic zero mode and π_0 is its conjugate momenta. The modes $a_{-k}, \bar{a}_{-k}$ can be obtained as follows:

$$a_{-k} = -\frac{e^{-\frac{2\pi k\tau}{L}}}{2\pi}\int dx e^{\frac{2\pi ik}{L}x}\partial_\omega\varphi, \quad \omega = x+i\tau; \tag{5.3.3}$$

$$\bar{a}_{-k} = \frac{e^{-\frac{2\pi k\tau}{L}}}{2\pi}\int dx e^{-\frac{2\pi ik}{L}x}\partial_{\bar{\omega}}\varphi, \quad \bar{\omega} = x-i\tau. \tag{5.3.4}$$

Each mode $a_{-k}, \bar{a}_{-k}$ carries momentum $\pm 2\pi k/L$.

In Refs. [153,303], Eq. (5.1.1) and Eq. (5.1.3), respectively, have been computed for the excited states generated by primary fields of a free massless bosonic field described by Eq. (5.3.1). The primary fields of the theory consists just of the vertex operator, $V_{\alpha,\bar{\alpha}}$, and the derivative field $i\partial_\omega\varphi$ [269]. The general state can be written in terms of the modes as

$$|\Psi_i\rangle = a_{-k_1}\ldots a_{-k_i}\,|M_i\rangle\,, \quad |M_i\rangle =: e^{iM_i\beta\varphi(0)} : |0\rangle\,, \tag{5.3.5}$$

with $|M_i\rangle$ being the highest weight states and $: e^{iM_i\beta\varphi(0)} :$ is a vertex operator (:: denotes the normal ordering prescription in its mode expansion, i.e. positive modes should appear to the right of negative ones). Here β marks the compactification radius, β^{-1}, of the boson:

$$\varphi(x+L) \equiv \varphi(x) + 2\pi\beta^{-1}, \tag{5.3.6}$$

and M_i is an integer. In the following sections, we develop an efficient strategy to compute the generalised Rényi entropies involving descendant states.

5.3.1 A warmup: zero-momentum states with a pair of chiral and anti-chiral modes

As a first non-trivial example, let us evaluate the second generalised Rényi entropy for the following (normalised) states that involve a chiral and anti-chiral mode whose momentum sums to zero:

$$R_{k_1,k_2;k_3,k_4} = \mathrm{Tr}_A(\mathrm{Tr}_B(\frac{1}{k_1}a_{-k_1}\bar{a}_{-k_1}\left|0\right\rangle\left\langle 0\right|\frac{1}{k_2}a_{k_2}\bar{a}_{k_2})\mathrm{Tr}_B(\frac{1}{k_3}a_{-k_3}\bar{a}_{-k_3}\left|0\right\rangle\left\langle 0\right|\frac{1}{k_4}a_{k_4}\bar{a}_{k_4})). \quad (5.3.7)$$

We can write the state $\frac{1}{k}a_{-k}\bar{a}_{-k}\left|0\right\rangle$ as

$$\frac{1}{k}a_{-k}\bar{a}_{-k}\left|0\right\rangle = -\frac{1}{4\pi^2 k}e^{-\frac{4\pi k\tau_-}{L}}\int_0^L dx_1 dx_{1'}e^{\frac{2\pi ik}{L}(x_1-x_{1'})}\partial_{\omega_1}\varphi(\omega_1)\partial_{\bar{\omega}_{1'}}\varphi(\bar{\omega}_{1'})\left|0\right\rangle, \quad (5.3.8)$$

where $\omega_{1,1'} = x_{1,1'} + i\tau_-, \tau_\pm = \pm\infty$. Since these states are normalised, the F-factors of Eq. (5.2.10) are simply 1. With this representation, we can write $R_{k_1,k_2;k_3,k_4}$ as

$$\begin{aligned}
\frac{R_{k_1,k_2;k_3,k_4}}{R_{\mathbb{1},\mathbb{1};\mathbb{1},\mathbb{1}}} &= \frac{1}{256\pi^8\prod_{i=1}^4 k_i}e^{\frac{4\pi}{L}(k_2+k_4)\tau_+}e^{-\frac{4\pi}{L}(k_1+k_3)\tau_-}I_{1234}\bar{I}_{1'2'3'4'},\\
I_{1234} &= \int_0^L dx_1dx_2dx_3dx_4 e^{\frac{2\pi i}{L}(k_1x_1+k_3x_3-k_2x_2-k_4x_4)}\left\langle\partial\varphi(\omega_1)\partial\varphi(\omega_2)\partial\varphi(\omega_3)\partial\varphi(\omega_4)\right\rangle,\\
\bar{I}_{1'2'3'4'} &= \int_0^L dx_{1'}dx_{2'}dx_{3'}dx_{4'}e^{-\frac{2\pi i}{L}(k_1x_{1'}+k_3x_{3'}-k_2x_{2'}-k_4x_{4'})}\left\langle\partial\bar{\varphi}(\bar{\omega}_{1'})\partial\bar{\varphi}(\bar{\omega}_{2'})\partial\bar{\varphi}(\bar{\omega}_{3'})\partial\bar{\varphi}(\bar{\omega}_{4'})\right\rangle\\
&= I^*_{1234},
\end{aligned} \quad (5.3.9)$$

where $w_{1,1'} = x_{1,1'} + i\tau_-$ and $w_{2,2'} = x_{2,2'} + i\tau_+$ are coordinates on the first Riemann sheet while $w_{3,3'} = x_{3,3'} + i\tau_-$ and $w_{4,4'} = x_{4,4'} + i\tau_+$ are coordinates on the second Riemann sheet.

Let us next compute the correlators appearing in Eq. (5.3.9). The complex coordinate $\omega = x + i\tau$ parametrises an infinite cylinder of length L and the interval A is identified with the domain $u < \omega < v$. This cylinder can be mapped into the complex plane by the conformal transformation

$$\xi = \frac{\sin(\pi(\omega-u)/L)}{\sin(\pi(\omega-v)/L)}, \quad (5.3.10)$$

which maps the segment (u, v) into $(-\infty, 0)$. Then, the uniformizing map for $\mathcal{R}_2$, $z = \xi^{1/2}$ tranforms the double-sheeted surface into a single sheet. As a consequence, the coordinates become

$$\omega_{1,3} = x_{1,3} + i\tau_- \to \xi_- = e^{i\pi(v-u)/L} \equiv e^{i\pi r} \to z_1 = e^{i\pi r/2}, z_3 = -e^{i\pi r/2}, \quad (5.3.11)$$

$$\omega_{2,4} = x_{2,4} + i\tau_+ \to \xi_+ = e^{-i\pi(v-u)/L} \equiv e^{-i\pi r} \to z_2 = e^{-i\pi r/2}, z_4 = -e^{-i\pi r/2}, \quad (5.3.12)$$

each of the points ξ_- and ξ_+ gives rise to two points in the Riemann surface $\mathcal{R}_2$ with coordinates z_1, z_3 and z_2, z_4, respectively. Thus, we can write I_{1234} as ($z_{ij} \equiv z_i - z_j$)

$$\begin{aligned}
I_{1234} = &\int_0^L dx_1dx_2dx_3dx_4 e^{\frac{2\pi i}{L}(k_1x_1+k_3x_3-k_2x_2-k_4x_4)}\frac{dz}{d\omega}\Big|_{\omega=\omega_1}\frac{dz}{d\omega}\Big|_{\omega=\omega_2}\frac{dz}{d\omega}\Big|_{\omega=\omega_3}\frac{dz}{d\omega}\Big|_{\omega=\omega_4}\\
&\left(\frac{1}{z_{23}^2z_{14}^2}+\frac{1}{z_{12}^2z_{34}^2}+\frac{1}{z_{13}^2z_{24}^2}\right) =\\
&= \oint_{C_-^1}\oint_{C_+^2}\oint_{C_-^3}\oint_{C_+^4} dz_1dz_2dz_3dz_4 e^{\frac{2\pi i}{L}(k_1x_1+k_3x_3-k_2x_2-k_4x_4)}\left(\frac{1}{z_{23}^2z_{14}^2}+\frac{1}{z_{12}^2z_{34}^2}+\frac{1}{z_{13}^2z_{24}^2}\right),
\end{aligned} \quad (5.3.13)$$

where $C_-^{1,3}$ is a clockwise contour about $z_{1,3} = \pm e^{\pi i r/2}$ and $C_+^{2,4}$ is a counter clockwise contour about $z_{2,4} = \pm e^{-\pi i r/2}$. Using

$$\begin{aligned} e^{2\pi i x_{1,3}/L} &= e^{2\pi\tau_-/L} e^{2\pi i v/L} \frac{z_{1,3}^2 - e^{-i\pi r}}{z_{1,3}^2 - e^{i\pi r}}, \\ e^{2\pi i x_{2,4}/L} &= e^{-2\pi\tau_+/L} e^{-2\pi i v/L} \frac{z_{2,4}^2 - e^{i\pi r}}{z_{2,4}^2 - e^{-i\pi r}}, \end{aligned} \tag{5.3.14}$$

we can evaluate

$$\begin{aligned} I_{1234} &= e^{\frac{2\pi}{L}((k_1+k_3)\tau_- - (k_2+k_4)\tau_+)} \frac{16\pi^4}{\prod_{i=1}^4 \Gamma(k_i)} S(r,k_1,k_2,k_3,k_4), \\ S(r,k_1,k_2,k_3,k_4) &\equiv \partial_{z_1}^{k_1-1}\partial_{z_2}^{k_2-1}\partial_{z_3}^{k_3-1}\partial_{z_4}^{k_4-1} \left[\left(\frac{z_1^2 - e^{-i\pi r}}{z_1 + e^{i\pi r/2}} \right)^{k_1} \left(\frac{z_2^2 - e^{i\pi r}}{z_2 + e^{-i\pi r/2}} \right)^{k_2} \right. \\ &\left. \left(\frac{z_3^2 - e^{-i\pi r}}{z_3 - e^{i\pi r/2}} \right)^{k_3} \left(\frac{z_4^2 - e^{i\pi r}}{z_4 - e^{-i\pi r/2}} \right)^{k_4} \left(\frac{1}{z_{23}^2 z_{14}^2} + \frac{1}{z_{12}^2 z_{34}^2} + \frac{1}{z_{13}^2 z_{24}^2} \right) \right] \Bigg|_{\substack{z_{1,3}=\pm e^{i\pi r/2} \\ z_{2,4}=\pm e^{-i\pi r/2}}}, \end{aligned} \tag{5.3.15}$$

where Γ denotes the Gamma function. Therefore the second generalised entropy in Eq. (5.3.7) reads

$$\frac{R_{k_1,k_2;k_3,k_4}}{R_{\mathbb{1},\mathbb{1},\mathbb{1},\mathbb{1}}} = \frac{1}{\prod_{i=1}^4 k_i \Gamma(k_i)^2} |S(r,k_1,k_2,k_3,k_4)|^2. \tag{5.3.16}$$

For $k_i = 1, i = 1,\ldots,4$, it reduces to

$$\frac{R_{1,1;1,1}}{R_{\mathbb{1},\mathbb{1};\mathbb{1},\mathbb{1}}} = \frac{(7+\cos(2\pi r))^4}{64^2}. \tag{5.3.17}$$

This result reproduces what has been found in [153] for the (chiral) primary field $i\partial\varphi$. In a similar way, we can compute

$$\begin{aligned} \frac{R_{0,1;1,0}}{R_{\mathbb{1},\mathbb{1};\mathbb{1},\mathbb{1}}} &= \frac{R_{1,0;0,1}}{R_{\mathbb{1},\mathbb{1};\mathbb{1},\mathbb{1}}} = \frac{\sin^4 \pi r}{16\cos^4(\pi r/2)}, \\ \frac{R_{1,1;0,0}}{R_{\mathbb{1},\mathbb{1};\mathbb{1},\mathbb{1}}} &= \frac{R_{0,0;1,1}}{R_{\mathbb{1},\mathbb{1};\mathbb{1},\mathbb{1}}} = \frac{\sin^4 \pi r}{16\sin^4(\pi r/2)}, \\ \frac{R_{1,0;1,0}}{R_{\mathbb{1},\mathbb{1};\mathbb{1},\mathbb{1}}} &= \frac{\sin^4(\pi r)}{16}. \end{aligned} \tag{5.3.18}$$

The quantity $R_{0,0;1,1}/R_{\mathbb{1},\mathbb{1};\mathbb{1},\mathbb{1}}$ in Eq. (5.3.18) reproduces the results found for the relative entropy of the state described by the primary operator $i\partial\varphi$ with respect to the ground state, $G(\rho_{GS}||\rho_{i\partial\varphi})$, in Ref. [303].

5.3.2 An example involving vertex operators

As a second non-trivial example, we choose states involving both the derivative operator $i\partial\varphi$ and vertex operators. In particular, we consider one of the states to be

$$V_{\alpha,\bar\alpha}(\omega,\bar\omega)\,|0\rangle = \left(\frac{iL}{2\pi} e^{2\pi i/L\omega}\right)^{\alpha^2/2} \left(\frac{iL}{2\pi} e^{2\pi i/L\bar\omega}\right)^{\bar\alpha^2/2} : e^{i(\alpha\varphi(\omega)+\bar\alpha\bar\varphi(\bar\omega))} : |0\rangle\,, \quad \omega = i\tau_-. \tag{5.3.19}$$

Therefore the second generalised Rényi entropy we compute is

$$R_{k_1,k_2;V_{\alpha,\bar{\alpha}},V_{-\alpha,-\bar{\alpha}}} = \mathrm{Tr}_A(\mathrm{Tr}_B(\frac{1}{k_1}a_{-k_1}\bar{a}_{-k_1}\left|0\right\rangle\left\langle 0\right|\frac{1}{k_2}a_{k_2}\bar{a}_{k_2})\mathrm{Tr}_B(V_{\alpha,\bar{\alpha}}\left|0\right\rangle\left\langle 0\right|V_{-\alpha,-\bar{\alpha}})). \tag{5.3.20}$$

If we rename V_α and $V_{\bar{\alpha}}$ the holomorphic and antiholomorphic part of the vertex operator, respectively, Eq. (5.3.20) can be reformulated as

$$\begin{aligned}
&\frac{R_{k_1,k_2;V_{\alpha,\bar{\alpha}},V_{-\alpha,-\bar{\alpha}}}}{R_{\mathbb{1},\mathbb{1},\mathbb{1},\mathbb{1}}} = \frac{1}{16\pi^4k^2}e^{-\frac{4\pi}{L}(k_1\tau_- - k_2\tau_+)}I_{1234}\bar{I}_{1'2'3'4'};\\
&I_{1234} = \int_0^L dx_1dx_2e^{\frac{2\pi i}{L}(k_1x_1-k_2x_2)}\left\langle\partial\varphi(\omega_1)\partial\varphi(\omega_2)V_\alpha(\omega_3)V_{-\alpha}(\omega_4)\right\rangle;\\
&\bar{I}_{1'2'3'4'} = \int_0^L dx_{1'}dx_{2'}e^{-\frac{2\pi i}{L}(k_1x_{1'}-k_2x_{2'})}\left\langle\bar{\partial}\bar{\varphi}(\bar{\omega}_{1'})\bar{\partial}\bar{\varphi}(\bar{\omega}_{2'})V_{\bar{\alpha}}(\bar{\omega}_3)V_{-\bar{\alpha}}(\bar{\omega}_4)\right\rangle = I^*_{1234}.
\end{aligned} \tag{5.3.21}$$

Applying the conformal transformation of the primary fields, we obtain for the four point correlation function involving both derivative and vertex operators the following

$$\begin{aligned}
I_{1234} &= -\left(\frac{\sin(\pi r)}{2\sin(\pi r/2)}\right)^{\alpha^2}\int_0^L dx_1dx_2e^{\frac{2\pi i}{L}(k_1x_1-k_2x_2)}\frac{dz}{d\omega}\Big|_{\omega=\omega_1}\frac{dz}{d\omega}\Big|_{\omega=\omega_2}\left(\frac{1}{z_{12}^2}+\frac{\alpha^2z_{34}^2}{z_{13}z_{23}z_{14}z_{24}}\right)\\
&= -\left(\frac{\sin(\pi r)}{2\sin(\pi r/2)}\right)^{\alpha^2}\oint_{C_-}\oint_{C_+}dz_1dz_2e^{\frac{2\pi i}{L}(k_1x_1-k_2x_2)}\left(\frac{1}{z_{12}^2}+\frac{\alpha^2z_{34}^2}{z_{13}z_{23}z_{14}z_{24}}\right).
\end{aligned} \tag{5.3.22}$$

Let us notice that in evaluating the correlation function, any one of its term involves a single contraction of $\partial\varphi(z_i)$ with one other operator: when contracted with another $\partial\varphi(z_j)$, it gives a factor $-1/(z_i-z_j)^2$, while when contracted with a vertex operator $V_{\alpha_j}(z_j)$ gives $-i\alpha_j/(z_i-z_j)$. On the other hand, the terms of the correlation function can involve contractions of $V_{\alpha_i}(z_i)$ with multiple other operators. When contracted with another $V_{\alpha_j}(z_j)$ it gives a contribution $(z_i-z_j)^{\alpha_i\alpha_j}$. These rules will be useful for treating the most general case in Sec. 5.4.2.

Using Eqs. (5.3.14), we get

$$\begin{aligned}
&I_{1234} = e^{\frac{2\pi}{L}(k_1\tau_- - k_2\tau_+)}\frac{4\pi^2}{\Gamma(k_1)\Gamma(k_2)}S(r,\alpha,k_1,k_2),\\
&S(r,\alpha,k_1,k_2) \equiv \left(\frac{\sin(\pi r)}{2\sin(\pi r/2)}\right)^{\alpha^2}\\
&\times\partial_{z_1}^{k_1-1}\partial_{z_2}^{k_2-1}\left[\left(\frac{z_1^2-e^{-i\pi r}}{z_1+e^{i\pi r/2}}\right)^{k_1}\left(\frac{z_2^2-e^{i\pi r}}{z_2+e^{-i\pi r/2}}\right)^{k_2}\left(\frac{1}{z_{12}^2}+\frac{\alpha^2z_{34}^2}{z_{13}z_{23}z_{14}z_{24}}\right)\right]\Bigg|_{\substack{z_{1,3}=\pm e^{i\pi r/2}\\ z_{2,4}=\pm e^{-i\pi r/2}}},\\
&\frac{R_{k_1,k_2;V_{\alpha,\bar{\alpha}},V_{-\alpha,-\bar{\alpha}}}}{R_{\mathbb{1},\mathbb{1},\mathbb{1},\mathbb{1}}} = \frac{1}{\prod_{i=1}^2k_i\Gamma(k_i)^2}|S(r,\alpha,k_1,k_2)|^2.
\end{aligned} \tag{5.3.23}$$

5.3.3 A more complicated case: two chiral modes

The previous two examples have shown that we can focus only on the chiral states, since the contributions of the chiral and anti-chiral parts to the GMSREs factorise. Hence, let us consider an example in which there are states involving more than one chiral mode such as

$$R_{(1,1),(1,1);(1,1),(1,1)} = \mathrm{Tr}_A(\mathrm{Tr}_B(a_{-1}a_{-1}\left|0\right\rangle\left\langle 0\right|a_1a_1)\mathrm{Tr}_B(a_{-1}a_{-1}\left|0\right\rangle\left\langle 0\right|a_1a_1)). \tag{5.3.24}$$

The Fourier expansion of the field in Eq. (5.3.2) leads to

$$a_{-1}a_{-1}\left|0\right\rangle = \frac{e^{-\frac{2\pi(\tau_1+\tau_2)}{L}}}{4\pi^2}\int dx_1 dx_2 e^{\frac{2\pi i}{L}(x_1+x_2)}\partial_{\omega_1}\varphi(\omega_1)\partial_{\omega_2}\varphi(\omega_2)\left|0\right\rangle; \tag{5.3.25}$$

$$\left\langle 0\right| a_1 a_1 = \frac{e^{\frac{2\pi(\tau_3+\tau_4)}{L}}}{4\pi^2}\int dx_3 dx_4 e^{-\frac{2\pi i}{L}(x_3+x_4)}\left\langle 0\right|\partial_{\omega_3}\varphi(\omega_3)\partial_{\omega_4}\varphi(\omega_4). \tag{5.3.26}$$

Thus, the generalised entropy in Eq. (5.3.24) reads

$$\begin{aligned}\frac{R_{(1,1),(1,1);(1,1),(1,1)}}{R_{\mathbb{1},\mathbb{1},\mathbb{1},\mathbb{1}}} &= \frac{1}{\sqrt{2}^4}\frac{1}{(4\pi^2)^4}e^{-\frac{2\pi}{L}(\tau_1+\tau_2-\tau_3-\tau_4+\tau_5+\tau_6-\tau_7-\tau_8)}\\ &\times\int_0^L dx_1\dots dx_8 e^{\frac{2\pi i}{L}(x_1+x_2-x_3-x_4+x_5+x_6-x_7-x_8)}\left\langle\partial_{\omega_1}\varphi(\omega_1)\dots\partial_{\omega_8}\varphi(\omega_8)\right\rangle,\end{aligned} \tag{5.3.27}$$

where $\frac{1}{\sqrt{2}^4}$ normalises the states in Eq. (5.3.24). Once we perform the conformal mappings from the two-sheeted Riemann surface $\mathcal{R}_2$ to a single complex plane, the previous integral can be computed through the residue theorem. The points that the w_i's are mapped onto are given by

$$y_1 = e^{i\pi r/2},\quad y_2 = e^{-i\pi r/2},\quad y_3 = -e^{i\pi r/2},\quad y_4 = -e^{-i\pi r/2}. \tag{5.3.28}$$

The difference with respect to the computations involving one single mode is that now the poles seen by the spatial integrals can arise both from $z_i = y_j$ but also from $z_i = z_j$. For future convenience it is useful to write down the correlation function $\langle\partial_{z_1}\varphi(z_1)\dots\partial_{z_8}\varphi(z_8)\rangle$ so that all occurrences when there are contractions involving z_i's near the same point (one of the four y_i) are explicitly written, i.e.

$$\begin{aligned}\langle\partial_{z_1}\varphi(z_1)\dots\partial_{z_8}\varphi(z_8)\rangle &= \langle 12345678\rangle' + \frac{1}{z_{12}^2}\langle 345678\rangle' + \frac{1}{z_{34}^2}\langle 125678\rangle' + \frac{1}{z_{56}^2}\langle 123478\rangle'\\ &+ \frac{1}{z_{78}^2}\langle 123456\rangle' + \frac{1}{z_{12}^2 z_{34}^2}\langle 5678\rangle' + \frac{1}{z_{12}^2 z_{56}^2}\langle 3478\rangle' + \frac{1}{z_{12}^2 z_{78}^2}\langle 3456\rangle' + \frac{1}{z_{34}^2 z_{56}^2}\langle 1278\rangle'\\ &+ \frac{1}{z_{34}^2 z_{78}^2}\langle 1256\rangle' + \frac{1}{z_{56}^2 z_{78}^2}\langle 1234\rangle' + \frac{1}{z_{12}^2 z_{34}^2 z_{56}^2 z_{78}^2}.\end{aligned} \tag{5.3.29}$$

We use the prime, i.e. $\langle\dots\rangle'$, on the correlators to indicate that there are no contractions involving (1, 2) or (3, 4) or (5, 6) or (7, 8). Hence, we can evaluate the primed correlation functions as

$$\begin{aligned}\langle 12345678\rangle' =& \sum_{\substack{ijkl=1\\ ijkl\,\text{all distinct}}}\frac{1}{2}\frac{1}{(y_i-y_j)^4}\frac{1}{(y_k-y_l)^4} +\\ &2\frac{1}{(y_i-y_j)^2}\frac{1}{(y_i-y_k)^2}\frac{1}{(y_j-y_l)^2}\frac{1}{(y_k-y_l)^2};\\ \langle 1\cdots\widehat{2i-1}\widehat{2i}\cdots 8\rangle' =& 8\sum_{\substack{jkl\neq i\\ j<k<l}}\frac{1}{(y_j-y_k)^2}\frac{1}{(y_j-y_l)^2}\frac{1}{(y_k-y_l)^2},\ i=1,2,3,4;\\ \langle 1\cdots\widehat{2i-1}\widehat{2i}\cdots\widehat{2j-1}\widehat{2j}\cdots 8\rangle' =& 2\sum_{\substack{k<l\\ k,l\,\text{distinct from}\,i,j}}\frac{1}{(y_k-y_l)^4}, i<j, i,j=1,2,3,4.\end{aligned} \tag{5.3.30}$$

Let us now plug the results found in Eq. (5.3.30) in the integral in Eq. (5.3.27). We must evaluate integrals of the form:

$$\begin{aligned} I_{12} &= \int_0^L dx_1 dx_2 e^{\frac{2\pi}{L} i(x_1+x_2)} \frac{1}{z_{12}^2} \partial_{\omega_1} z_1 \partial_{\omega_2} z_2 \\ &= \oint_{C_-^1} dz_1 \oint_{C_-^2} dz_2 e^{\frac{2\pi}{L}(\tau_1+\tau_2)} e^{4\pi i v/R} \frac{1}{z_1-y_1} \frac{1}{z_2-y_1} \frac{1}{(z_1-z_2)^2} f(z_1,y_1) f(z_2,y_1), \\ I_{13} &= \int_0^L dx_1 dx_3 e^{\frac{2\pi}{L} i(x_1-x_3)} \frac{1}{z_{13}^2} \partial_{\omega_1} z_1 \partial_{\omega_3} z_3 \\ &= \oint_{C_-^1} dz_1 \oint_{C_+^3} dz_2 e^{\frac{2\pi}{L}(\tau_1-\tau_3)} \frac{1}{z_1-y_1} \frac{1}{z_3-y_2} \frac{1}{(z_1-z_3)^2} f(z_1,y_1) f(z_3,y_2), \end{aligned} \tag{5.3.31}$$

where

$$f(z_i, y_j) = \frac{z_i^2 - (y_j^*)^2}{z_i + y_j}. \tag{5.3.32}$$

In order to do the first integral, we will take $\tau_1 < \tau_2$ (without loss of generality), such that the contour C_-^1 is inside C_-^2, i.e. we can first perform the integral C_-^1 followed by C_-^2 (similarly for the integral along C_+^3), with the result

$$\begin{aligned} I_{12} =& -4\pi^2 e^{2\pi(\tau_1+\tau_2)/L} e^{4\pi i v/L} f(y_1,y_1) \frac{1}{2} \partial_z^2 f(z,y_1)|_{z=y_1} = -\frac{\pi^2}{y_1^2} e^{\frac{2\pi}{L}(\tau_1+\tau_2)} e^{4\pi i v/L} f(y_1,y_1)^2, \\ I_{13} =& 4\pi^2 \frac{1}{(y_1-y_2)^2} e^{\frac{2\pi}{L}(\tau_1-\tau_3)} f(y_1,y_1) f(y_2,y_2). \end{aligned} \tag{5.3.33}$$

The dependence on τ_i's cancel in Eq. (5.3.27), thus even though some w_i's are mapped onto the same point once $\tau_i \to \pm\infty$, if we keep them finite, we can do the integral and then take the limit, obtaining a finite result. We can then perform all the integrals along the lines discussed above and put everything together to get

$$\begin{aligned} \frac{R_{(1,1),(1,1);(1,1),(1,1)}}{R_{\mathbb{1},\mathbb{1},\mathbb{1},\mathbb{1}}} =& \frac{1}{4}\Big[\frac{(7+\cos(2\pi r))}{4096}(1606 + 335\cos(2\pi r) + 106\cos(4\pi r) + \cos(6\pi r)) \\ & - \frac{\sin^6(\pi r)}{2} + \frac{(7+\cos(2\pi r))^2 \sin^4(\pi r)}{1024} + \frac{\sin^8(\pi r)}{256}\Big] = \\ & \frac{88123 + 37256\cos(2\pi r) + 4604\cos(4\pi r) + 1080\cos(6\pi r) + 9\cos(8\pi x)}{131072}. \end{aligned} \tag{5.3.34}$$

We observe that this result coincides with the second Rényi entropy for the first descendant in the tower of a CFT with central charge $c = 1$, i.e., the state associated with the stress-energy tensor $T = L_{-2}\mathbb{1}$ ($\{L_p, p \in Z\}$ from the Virasoro algebra [269]).

5.4 GMSREs for arbitrary bosonic states

In this section we report the results for the generalised Rényi entropies involving arbitrary bosonic CFT states. To set the stage for the most general case, we first consider the case involving states with arbitrary mode content but no vertex operators.

5.4.1 Generalised mixed state Rényi entropies without vertex operators

Using what we have learnt from the previous simple examples, we now want to treat a much more general case, involving an arbitrary (even) number of modes but without vertex operators, i.e.

$$R_{k_1,\dots;\dots k_N} = A_1A_2A_3A_4 \\ \mathrm{Tr}_A(\mathrm{Tr}_B(\prod_{i=1}^{N_1} a_{-k_i}\,|0\rangle\,\langle 0|\prod_{i=1}^{N_2} a_{k_{N_1+i}})\mathrm{Tr}_B(\prod_{i=1}^{N_3} a_{-k_{N_1+N_2+i}}\,|0\rangle\,\langle 0|\prod_{i=1}^{N_4} a_{k_{N_1+N_2+N_3+i}})), \quad (5.4.1)$$

where $N = N_1 + N_2 + N_3 + N_4$ is the total number of the modes. Here $k_1, \dots k_N$ are all positive integers and the A_j's denote the normalisation of the states $a_{-k_1}^{n_{k_1}} \dots a_{-k_{M_j}}^{n_{k_{M_j}}}|0\rangle$ which are given by

$$A_j = 1/(\langle 0|\prod_{i=1}^{M_j} a_{k_i})\prod_{i=1}^{M_j} a_{-k_i}|0\rangle)^{1/2} = \frac{1}{\prod_{i=1}^{M_j}\sqrt{k_i^{n_{k_i}}(n_{k_i}!)}}. \quad (5.4.2)$$

Using the integral representation of modes, we have to compute the following correlation function:

$$\langle\prod_{i=1}^{N_1}\partial_{\omega_i}\varphi(\omega_i)\prod_{i=1}^{N_2}\partial_{\omega_{i+N_1}}\varphi(\omega_{i+N_1})\prod_{i=1}^{N_3}\partial_{\omega_{i+N_1+N_2}}\varphi(\omega_{i+N_1+N_2}) \\ \prod_{i=1}^{N_4}\partial_{\omega_{i+N_1+N_2+N_3}}\varphi(\omega_{i+N_1+N_2+N_3})\rangle = \prod_{i=1}^{N}\partial_{\omega_i}z_i \sum_{\substack{\sigma\in S_N \\ \sigma_{2i}<\sigma_{2i+1} \\ \sigma_1<\sigma_3<\dots\sigma_{2N-1}}} \prod_{i=1}^{N/2}\frac{1}{(z_{\sigma_{2i-1}}-z_{\sigma_{2i}})^2}, \quad (5.4.3)$$

where the second line comes from the conformal mapping from the two-sheeted Riemann surface to the plane. We can recognise that the last sum over $\sigma \in S_N$, with S_N the permutation group of the N indices, can be compactly rewritten as $\mathrm{Hf}\left(\frac{1}{(z_i-z_j)^2}\right)_{1\le i,j,\le N}$, where Hf denotes the Hafnian of a matrix B

$$\mathrm{Hf(B)} = \frac{1}{2^{N/2}N/2!}\sum_{\sigma\in S_N}\prod_{i=1}^{N/2} B_{\sigma(2i-1),\sigma(2i)}, \quad (5.4.4)$$

an object which contains $(N-1)!!$ terms. Let us now consider the needed integrations focusing on one of the term in the above sum, i.e.

$$\prod_{i=1}^{N/2}\frac{1}{(z_{\sigma_{2i-1}}-z_{\sigma_{2i}})^2}. \quad (5.4.5)$$

Its contribution to $R_{k_1,\dots;\dots k_N}/R_{\mathbb{1},\mathbb{1},\mathbb{1},\mathbb{1}}$ is

$$(-1)^{N_1+N_3}e^{2\pi i\frac{v}{L}(P_1+P_3-P_2-P_4)}\prod_{i=1}^{N/2} W(k_{\sigma_{2i-1}},k_{\sigma_{2i}},y_{\sigma_{2i-1}},y_{\sigma_{2i}}). \quad (5.4.6)$$

The factor $(-1)^{N_1+N_3}$ comes from the N contour integrals in total, N_1+N_3 that are clockwise and N_2+N_4 that are counterclockwise. Here P_i (the total momentum of the state) are given by

$$P_i = \sum_{j=1}^{N_i} k_{j+\sum_{\ell=1}^{i-1}N_\ell}, \quad i = 1\dots 4, \quad (5.4.7)$$

and the y_i's, $i = 1, \ldots, N$, are defined as

$$y_i = \begin{cases} e^{i\pi r/2}, & 1 \le i \le N_1; \\ e^{-i\pi r/2}, & N_1 + 1 \le i \le N_1 + N_2; \\ -e^{i\pi r/2}, & N_1 + N_2 + 1 \le i \le N_1 + N_2 + N_3; \\ -e^{-i\pi r/2}, & N_1 + N_2 + N_3 + 1 \le i \le N_1 + N_2 + N_3 + N_4. \end{cases} \tag{5.4.8}$$

The evaluation of $W(k_i, k_j, y_i, y_j)$ in Eq. (5.4.6) (for conciseness, we use the subscript (i, j) rather than $(\sigma_{2i-1}, \sigma_{2i})$) leads to

$$W(k_i, k_j, y_i, y_j) = \begin{cases} \frac{1}{\Gamma(k_i)} \sum_{l=0}^{k_i-1} \binom{k_i-1}{l} \frac{\Gamma(k_i-l+1)}{\Gamma(k_i+k_j-l+1)} (\partial_z^l f^{k_i})(z = y_i, y_i) & \\ \quad \times (\partial_z^{k_i+k_j-l} f^{k_j})(z = y_j, z = y_j), & y_i = y_j; \\ \frac{1}{\Gamma(k_i)\Gamma(k_j)} \partial_{z_i}^{k_i-1} \partial_{z_j}^{k_j-1} \left(\frac{f^{k_i}(z_i, y_i) f^{k_j}(z_j, y_j)}{(z_i - z_j)^2} \right) \Big|_{\substack{z_i = y_i \\ z_j = y_j}} & y_i \neq y_j; \end{cases} \tag{5.4.9}$$

This first case above ($y_i = y_j$) can be obtained by exploiting the product rule for higher-order partial derivatives, i.e.

$$\partial^\alpha (hg) = \sum_{\beta+\gamma=\alpha} \frac{\alpha!}{\beta!\gamma!} (\partial^\beta h)(\partial^\gamma g), \tag{5.4.10}$$

whose proof can be done by induction. Using this rule for $h = f(z_i, y_i)$ and $g = 1/(z_i - z_j)^2$, taking the derivative with respect to z_i, setting $z_i = y_i$, and then doing the integral in z_j, we obtain the first line of Eq. (5.4.9). This corresponds to the assumption $\tau_i < \tau_j$, but we can explicitly check that nothing changes for $z_i \leftrightarrow z_j$. We have applied this same logic in solving the integral I_{12} in Eq. (5.3.31). The second case of Eq. (5.4.9) is analogous to the solution of I_{13}: it can be obtained by simply applying the residue theorem since there are no contractions involving z_i's ($i = 1, \ldots N$) near the same point (one of four $\pm e^{\pm i\pi r/2}$). To summarise, we have

$$\frac{R_{k_1,\ldots;\ldots k_N}}{R_{\mathbb{1},\mathbb{1};\mathbb{1},\mathbb{1}}} = A_1 A_2 A_3 A_4 (-1)^{N_1+N_3} e^{2\pi i \frac{v}{L}(P_1+P_3-P_2-P_4)} \mathrm{Hf}\,(W)\,, \tag{5.4.11}$$

where W is the matrix which enters in Eq. (5.4.6). This result can be extended to generalised Rényi entropies with index n. The total number of modes is now given by $N = \sum_{i=1}^{2n} N_i$, the set of N points y_k is defined by

$$y_k = \begin{cases} e^{i\pi \frac{j}{n}(r+m)} & \sum_{j=1}^{N_m} N_j < k < \sum_{j=1}^{N_{m+1}} N_j - 1, \quad m \text{ even}; \\ e^{i\pi \frac{j}{n}(-r+m-1)} & \sum_{j=1}^{N_m} N_j < k < \sum_{j=1}^{N_{m+1}} N_j - 1, \quad m \text{ odd}, \end{cases} \tag{5.4.12}$$

while the formal expression for $W(k_i, k_j, y_i, y_j)$ is the one defined in Eq. (5.4.9) with the following definition for f's:

$$f(z_i, y_i) = \begin{cases} \dfrac{z_i^n - e^{i\pi r}}{\sum_{j=0}^{n-1} z_i^{n-j-1} e^{i\pi \frac{j}{n}(r+m)}}, & m \,\text{even}; \\ \dfrac{z_i^n - e^{-i\pi r}}{\sum_{j=0}^{n-1} z_i^{n-j-1} e^{i\pi \frac{j}{n}(-r+m-1)}}, & m \,\text{odd}. \end{cases} \tag{5.4.13}$$

Thus Eq. (6.3.17) becomes for generic n

$$\frac{R_{k_1,\ldots;\ldots k_N}}{R_{\mathbb{1},\ldots\mathbb{1};\mathbb{1},\ldots\mathbb{1}}} = A_1 \cdots A_{2n} (-1)^{\sum_{i\,\text{odd}} N_i} e^{2\pi i \frac{v}{L}(\sum_{i\,\text{odd}} P_i - \sum_{i\,\text{even}} P_i)} \mathrm{Hf}\,(W)\,. \tag{5.4.14}$$

5.4.2 Generalised mixed state Rényi entropies with vertex operators

The most general case involves states with arbitrary vertex operator content:

$$R^{\alpha_1,\alpha_2,\alpha_3,\alpha_4}_{k_1,\ldots,;\ldots k_N} = A_1^{\alpha_1}A_2^{\alpha_2}A_3^{\alpha_3}A_4^{\alpha_4} \\ \mathrm{Tr}_A(\mathrm{Tr}_B(\prod_{i=1}^{N_1} a_{-k_i}\left|\alpha_1\right\rangle\left\langle\alpha_2\right|\prod_{i=1}^{N_2} a_{k_{N_1+i}})\mathrm{Tr}_B(\prod_{i=1}^{N_3} a_{-k_{N_1+N_2+i}}\left|\alpha_3\right\rangle\left\langle\alpha_4\right|\prod_{i=1}^{N_4} a_{k_{N_1+N_2+N_3+i}})) \quad (5.4.15)$$

where the states $|\alpha_i\rangle$ are defined via

$$|\alpha_{1,3}\rangle \equiv (\frac{L}{2\pi i}e^{\frac{2\pi i}{L}\omega_{\alpha_{1,3}}})^{\alpha^2_{1,3}/2} : e^{i\alpha_{1,3}\varphi(\omega_{\alpha_{1,3}})} : |0\rangle \equiv c_{\alpha_{1,3}} : e^{i\alpha_{1,3}:\varphi(\omega_{\alpha_{1,3}})} : |0\rangle\,, \quad \omega_{\alpha_{1,3}} = -i\infty \\ \langle\alpha_{2,4}| \equiv \langle 0|\,(\frac{L}{2\pi i}e^{-\frac{2\pi i}{L}\omega_{\alpha_{2,4}}})^{\alpha^2_{2,4}/2} : e^{i\alpha_{2,4}\varphi(\omega_{\alpha_{2,4}})} :\equiv \langle 0|\, c_{\alpha_{2,4}} : e^{i\alpha_{2,4}\varphi(\omega_{\alpha_{2,4}})} :, \quad \omega_{\alpha_{2,4}} = i\infty \quad (5.4.16)$$

and the $A_j^{\alpha_j}$ are the normalisation of the states where now the vacuum is replaced by the state created by the vertex operator, i.e.

$$A_j^{\alpha_j} = 1/(\langle\alpha_j| \prod_{i=1+N_1+\cdots N_{j-1}}^{N_j} a_{k_i} \prod_{i=1+N_1+\cdots N_{j-1}}^{N_j} a_{-k_i}|\alpha_j\rangle)^{1/2}. \quad (5.4.17)$$

Eq. (5.4.15) can be rewritten as

$$\frac{R^{\alpha_1,\alpha_2,\alpha_3,\alpha_4}_{k_1,\ldots,k_N}}{R_{\mathbb{1},\mathbb{1},\mathbb{1},\mathbb{1}}} = \frac{(-1)^N}{(2\pi)^N}e^{-\frac{2\pi}{L}\sum_{i=1}^N \sigma_i k_i \tau_i}A_1^{\alpha_1}A_2^{\alpha_2}A_3^{\alpha_3}A_4^{\alpha_4} \\ \times \int_0^L dx_1 dx_2 \ldots dx_N e^{\frac{2\pi i}{L}\sigma_i k_i x_i} C(\omega_{\alpha_1},\omega_{\alpha_2},\omega_{\alpha_3},\omega_{\alpha_4},\omega_1,\ldots,\omega_N), \quad (5.4.18)$$

where $\sigma_i = \pm 1$ if the corresponding mode a is a creation/annihilation operator, the factor $(-1)^N$ comes from representing each a in terms of $\partial_\omega\varphi(\omega)$, and
$C(\omega_{\alpha_1},\omega_{\alpha_2},\omega_{\alpha_3},\omega_{\alpha_4},\omega_1,\ldots,\omega_N)$ is given by

$$C(\omega_{\alpha_1},\omega_{\alpha_2},\omega_{\alpha_3},\omega_{\alpha_4},\omega_1,\ldots,\omega_N) = c_{\alpha_1}c_{\alpha_2}c_{\alpha_3}c_{\alpha_4}\langle\prod_{i=1}^{N_1}\partial_{\omega_i}\varphi(\omega_i)e^{i\alpha_1\varphi(\omega_{\alpha_1})}e^{i\alpha_2\varphi(\omega_{\alpha_2})} \\ \times\prod_{i=1}^{N_2}\partial_{\omega_{i+N_1}}\varphi(\omega_{i+N_1})\prod_{i=1}^{N_3}\partial_{\omega_{i+N_1+N_2}}\varphi(\omega_{i+N_1+N_2})e^{i\alpha_3\varphi(\omega_{\alpha_3})}e^{i\alpha_4\varphi(\omega_{\alpha_4})} \\ \times\prod_{i=1}^{N_4}\partial_{\omega_{i+N_1+N_2+N_3}}\varphi(\omega_{i+N_1+N_2+N_3})\rangle. \quad (5.4.19)$$

This correlation function can be evaluated by considering all the possible contractions among operators: $e^{i\alpha_i\varphi(\xi_i)}$ must be contracted to all other operators, with a contribution $(\xi_i-\xi_j)^{\alpha_i\alpha_j}$ when contracted with another $e^{i\alpha_j\varphi(\xi_j)}$ and $-i\alpha_i/(\xi_i-z_j)$ when contracted with $\partial\varphi(z_j)$. The operators $\partial\varphi(z_i)$ must be contracted with one operator at a time, giving a factor $-1/(z_i-z_j)^2$ when contracted with another $\partial\varphi(z_j)$. These rules were the same already used to evaluate the correlation function in Eq. (5.3.21).

By summing up all these contributions, we get

$$\begin{aligned}C(\omega_{\alpha_1},\omega_{\alpha_2},\omega_{\alpha_3},\omega_{\alpha_4},\omega_1,\dots,\omega_N) &= M(\alpha_1,\alpha_2,\alpha_3,\alpha_4)\\ &\times\prod_{i=1}^{N}\partial_{\omega_i}z_i\Bigg[\langle\partial_{z_1}\varphi\dots\partial_{z_N}\varphi\rangle+i\sum_{i}^{4}\sum_{i'}^{N}\frac{\alpha_i\alpha_j}{(\xi_i-z_{i'})}\langle\prod_{l\neq i}^{N}\partial_{z_l}\varphi\rangle\\ &-\sum_{i,j}^{4}\sum_{i'<j'}^{N}\frac{\alpha_i\alpha_j}{(\xi_i-z_{i'})(\xi_j-z_{j'})}\langle\prod_{l\neq i,j}^{N}\partial_{z_l}\varphi\rangle\\ &+\sum_{i,j,k}^{4}\sum_{i'<j'<k'}^{N}\frac{\alpha_i\alpha_j\alpha_k}{(\xi_i-z_{i'})(\xi_j-z_{j'})(\xi_k-z_{k'})}\langle\prod_{l\neq i,j,k}^{N}\partial_{z_l}\varphi\rangle+\dots+i^N\sum_{i_1,i_2,\dots,i_N}^{4}\prod_{j=1}^{N}\frac{\alpha_{i_j}}{(\xi_{i_j}-z_j)}\Bigg].\end{aligned}\tag{5.4.20}$$

The prefactor $M(\alpha_1,\alpha_2,\alpha_3,\alpha_4)$ encodes all information about the purely vertex operator part of the correlation function:

$$\begin{aligned}M(\alpha_1,\alpha_2,\alpha_3,\alpha_4) &= c_{\alpha_1}c_{\alpha_2}c_{\alpha_3}c_{\alpha_4}\,\langle e^{i\alpha_1\varphi(\omega_{\alpha_1})}e^{i\alpha_2\varphi(\omega_{\alpha_2})}e^{i\alpha_3\varphi(\omega_{\alpha_3})}e^{i\alpha_4\varphi(\omega_{\alpha_4})}\rangle\prod_{i=1}^{4}(\partial_{\omega_{\alpha_i}}z_i)^{\alpha_i^2/2}|_{z_i=y_i}\\ &=\sin\Big(\frac{\pi r}{2}\Big)^{\alpha_1\alpha_2+\alpha_3\alpha_4}\cos\Big(\frac{\pi r}{2}\Big)^{\alpha_1\alpha_4+\alpha_2\alpha_3}\\ &\times 2^{-\bar\alpha\cdot\bar\alpha/2}\sin(\pi r)^{\bar\alpha\cdot\bar\alpha/2}(e^{-i\pi r}e^{2\pi iv/R})^{(\alpha_1^2+\alpha_3^2-\alpha_2^2-\alpha_4^2)/2},\end{aligned}\tag{5.4.21}$$

with $\bar\alpha=(\alpha_1,\alpha_2,\alpha_3,\alpha_4)$. When $\alpha_1=-\alpha_2=\alpha_3=-\alpha_4$, $M(\alpha_1,\alpha_2,\alpha_3,\alpha_4)=1$ as also found in Ref. [153].

Writing the correlation function in this way allows us to express $R^{\alpha_1,\alpha_2,\alpha_3,\alpha_4}_{k_1,\dots,k_N}$ in terms of Rényi entropies that do not involve the vertex operators, $R^{0,0,0,0}_{k_1,\dots,k_N}$, as follows:

$$\begin{aligned}\frac{R^{\alpha_1,\alpha_2,\alpha_3,\alpha_4}_{k_1,\dots,k_N}}{R_{\mathbb{1},\mathbb{1},\mathbb{1},\mathbb{1}}} &= M(\alpha_1,\alpha_2,\alpha_3,\alpha_4)\Big[\frac{R^{0,0,0,0}_{k_1,\dots,k_N}}{R_{\mathbb{1},\mathbb{1},\mathbb{1},\mathbb{1}}}+\sum_{i=1}^{N}\frac{R^{0,0,0,0}_{k_1,\dots,\widehat{k_i}\dots k_N}}{R_{\mathbb{1},\mathbb{1};\mathbb{1},\mathbb{1}}}N(k_i)L_{k_i}(\bar\alpha)\\ &+\sum_{i_1<i_2}^{N}\frac{R^{0,0,0,0}_{k_1,\dots,\widehat{k_{i_1}}\dots,\widehat{k_{i_2}},\dots k_N}}{R_{\mathbb{1},\mathbb{1};\mathbb{1},\mathbb{1}}}N(k_{i_1},k_{i_2})L_{k_{i_1}}(\bar\alpha)L_{k_{i_2}}(\bar\alpha)+\dots+\\ &\sum_{i_1<i_2,\dots<i_{N-2}}^{N}\frac{R^{0,0,0,0}_{k_1,\dots,\widehat{k_{i_1}}\dots,\widehat{k_{i_2}},\dots\widehat{k_{i_{N-2}}}\dots k_N}}{R_{\mathbb{1},\mathbb{1};\mathbb{1},\mathbb{1}}}N(k_{i_1},k_{i_2},\dots,k_{i_{N-2}})L_{k_{i_1}}(\bar\alpha)L_{k_{i_2}}(\bar\alpha)\dots L_{k_{i_{N-2}}}(\bar\alpha)\\ &+\prod_{i=1}^{N}L_{k_i}(\bar\alpha).\Big],\end{aligned}\tag{5.4.22}$$

where $\widehat{k_{i'}}$ indicates that the operator does not appear in the Rényi. Here the coefficients $N(k_i)$ arise as normalisations of the states after some of the creation/annihilation operators have been removed since we are dealing with Rényi entropies involving only properly normalised states. So for example $N(k_i)$ for $i<N_1$ reads

$$N(k_i)=\frac{(\langle\alpha_1|\prod_{j\neq i}^{N_1}a_{k_j}\prod_{j\neq i}^{N_1}a_{-k_j}|\alpha_1\rangle)^{1/2}}{(\langle\alpha_1|\prod_{j=1}^{N_1}a_{k_j}\prod_{j=1}^{N_1}a_{-k_j}|\alpha_1\rangle)^{1/2}}.\tag{5.4.23}$$

The functions L_i are defined as

$$\begin{aligned} L_{k_j}(\bar{\alpha}) =& \sum_{i=1}^{4} \alpha_i I_{ij} \\ I_{ij} =& \frac{e^{-\frac{2\pi}{L}\tau_j \sigma_j k_j}}{2\pi i} \int_0^L dx_j e^{\frac{2\pi}{L} i x_j \sigma_j k_j} \frac{1}{\xi_i - z_j} \partial_{\omega_j} z_j. \end{aligned} \tag{5.4.24}$$

The integral above gives

$$\begin{aligned} I_{ij} =& \sigma_j e^{\frac{2\pi}{L}\sigma_j i v} J_{ij}; \\ J_{ij} =& \begin{cases} \frac{1}{\Gamma(k_j+1)} \partial_{z_j}^{k_j} f^{k_j}(z_j, k_j) & i = j \\ \frac{1}{\Gamma(k_j)} \partial_{z_j}^{k_j - 1} \frac{f^{k_j}(z_j, k_j)}{z_j - y_i} & i \neq j. \end{cases} \end{aligned} \tag{5.4.25}$$

The terms like $e^{\frac{2\pi}{L}\sigma_j i v k_j}$ allow one to recover the factor $e^{\frac{2\pi}{L}(P_1 + P_3 - P_2 - P_4)}$ in Eq. (5.4.6). Eq. (5.4.22) is the main result of this Chapter. Despite its involved expression, it provides an efficient way to compute any generalised mixed state Rényi entropy of a bosonic CFT involving arbitrary excited states.

5.5 Closing remarks

In this Chapter we considered the generalised mixed state Rényi entropy defined in Eq. (5.1.4). We developed a strategy to compute the aforementioned quantities for a bosonic CFT using the representation of its Hilbert space in terms of massless modes and highest weight states created by vertex operators. This procedure allowed us to recover some known results about the entanglement of low-energy excitations represented by primary fields [153, 303] and of descendant states [283]. Exploiting the techniques of Sec. 1.4.3, one can aso numerically check our results for some simple excited states, as it is reported in [275].

Although we provided explicit results only for a bosonic theory, our approach can be extended to a generic state of a CFT written as a product of modes of primary fields (for example the Ising CFT). Our results represent the starting point to apply the truncated conformal space approach [305,313] to the evaluation of the Rényi entropies in both equilibrium and non-equilibrium situations. We use the results herein to describe the time evolution of the second Rényi entropy after a quench in the sine-Gordon model [315], as we are going to illustrate in the following Chapter.

A straightforward use of our results is the computation of entanglement measures involving two CFT states such as the relative entropy [292, 303] and the trace distance [308, 309]. Another relatively simple extension concerns the resolution of entanglement in systems endowed with an abelian symmetry [84]. A more challenging idea would be to derive similar non-diagonal objects for the negativity [151, 152].

Chapter 6

Post-Quantum Quench Growth of Rényi Entropies in Low Dimensional Continuum Bosonic Systems

The growth of Rényi entropies after the injection of energy into a correlated system provides a window upon the dynamics of its entanglement properties. In this Chapter, we develop a simulation scheme by which this growth can be determined in Luttinger liquids systems with arbitrary interactions, even those introducing gaps into the liquid. We apply this scheme to an experimentally relevant quench in the sine-Gordon field theory. While for short times we provide analytic expressions for the growth of the second and third Rényi entropy, to access longer times, we combine our scheme with truncated spectrum methods. This Chapter is based on Ref. [315]

6.1 Introduction

The time evolution of the Rényi entanglement entropy in out-of-equilibrium QFTs nowadays plays a crucial role in disparate situations ranging from quantum gravity and black hole physics [34, 35] to experiments in cold-atom and ion-trap setups [79, 88, 89, 316]. Very effective numerical techniques, based, e.g., on tensor networks allow us to compute their behaviour at not-too-long time scales in lattice systems [317–320]. Conversely, simulation algorithms performing well for generic interacting field theories are not available yet (although Continuous Matrix Product States [321–323] represent a promising framework). The main goal of this Chapter is to introduce and develop a new simulation scheme which in principle should work for a large class of $1d$ QFTs. The key idea is to use as computational basis the one of the Luttinger liquid and write a general exact expansion for the Rényi entropies. The coefficients entering in such an expansion can be effectively calculated by truncated spectrum methodologies (TSM) [305, 313, 314].

The root of the effectiveness of our algorithm is that Luttinger liquid is a cornerstone for the description of a wide variety of quasi-1D systems [204, 324, 325], spin-charge separation in 1D metals and nanotubes [326, 327], power-law correlations of the dynamic structure function in 1D cold atomic systems [328, 329], and the fractionalization of magnons into spinons in quasi-1D spin chains [330, 331]. Even when a Luttinger liquid is gapped out by an interaction, the underlying bosonic description of the unperturbed liquid provides an excellent starting point to understanding any underlying phenomena. Here our fundamental idea is to use the unperturbed liquid as the starting point for the description of a wide variety of non-equilibrium dynamics.

The main object of interest here is the Rényi entropy of a bosonic system with a time-dependent

reduced density matrix, $\rho(t)$. In this chapter, we will denote it as $S_n(t)$ to stress the time dependence.

While here we apply our machinery to the computation of time-dependent Rényi entropies, our framework also allows for the determination of time-dependent relative Rényi entropies [306, 307, 333, 334]. We start with a review of the non-equilibrium Luttinger liquids in Sec. 6.2, which provides the computational basis for the evaluation of the dynamical Rényi entropies. We analyse their early and longer time behaviour in Secs. 6.3 and 6.4 respectively. Finally, we discuss some possible outlooks in Sec. 6.5.

6.2 Model for Non-Equilibrium Luttinger Liquids

To explore the non-equilibrium Rényi entropies in non-equilibrium Luttinger liquids, we will consider a canonical Hamiltonian density describing their dynamics:

$$H(t) = \int dx \frac{v_F}{8\pi}(\partial_x\varphi^2 + \Pi^2) + 2J_1(t)\cos(\beta\varphi). \tag{6.2.1}$$

$\varphi(x,t)$ is a real compact Bose field which admits the following mode expansion [269] (see also Eq. (5.3.2) for $it = \tau$ and $m = 0$)

$$\varphi(x,t) \;=\; \varphi_0 + \frac{4\pi}{L}\Pi_0 t + \frac{2\pi m}{\beta L}x + i\sum_{l\neq 0}\frac{1}{l}\Big(a_l e^{\frac{2\pi i l}{L}(x-t)} - \bar{a}_{-l}e^{\frac{2\pi i l}{L}(x+t)}\Big). \tag{6.2.2}$$

The parameter β is related to the Luttinger parameter, K, of the theory via $\beta = (2K)^{-1/2}$. K determines the power law correlations in the model when $J_1 = 0$. This mode expansion assumes the boson has compactification radius $2\pi/\beta$, i.e. $\varphi(x+L,t) = \varphi(x,t) + \frac{2\pi}{\beta}m$, where m denotes the winding number, which is related to the $U(1)$ charge of the sector. The operator φ_0 is the 'center of mass' of the Bose field and Π_0 is its conjugate momentum, which has permitted values $n\beta$, with integer n. These obey the commutator $[\varphi_0, \Pi_0] = i$.
The bosonic Hilbert space emerges from an infinite set of highest weight states marked by the bosonic winding number and the value of conjugate momentum:

$$|n,m\rangle = e^{in\beta\varphi(0)+i\frac{m}{2\beta}\Theta(0)}|0\rangle. \tag{6.2.3}$$

These highest weight states $|n,m\rangle$ are defined by acting with vertex operators involving the boson and its dual on the vacuum $|0\rangle$. The dual boson, Θ, can be defined via the relation

$$\partial_x\Theta(x,t) = \partial_t\varphi(x,t). \tag{6.2.4}$$

The quantum number n gives the momentum of the bosonic zero mode for the state while the quantum number m gives the $U(1)$ charge of the state. The full Hilbert space is then constructed by the acting with the right and left moving modes (a_n and $\bar{a}_n$) of the field on the highest weight states:

$$|\Psi\rangle = \prod_{j=1}^{M} a_{k_j}\prod_{\bar{j}=1}^{\bar{M}}\bar{a}_{k_{\bar{j}}}|n,m\rangle. \tag{6.2.5}$$

The energy and momentum of such a state is

$$E_\Psi \;=\; \frac{2\pi}{L}\left(n^2\beta^2 + \frac{m^2}{4\beta^2} + \sum_{j=1}^{M}k_j + \sum_{\bar{j}=1}^{\bar{M}}k_{\bar{j}} - \frac{1}{12}\right),$$

$$P_\psi = \frac{2\pi}{L}\Big((n-m)+\sum_{j=1}^{M}k_j-\sum_{\bar{j}=1}^{\bar{M}}k_{\bar{j}}\Big). \tag{6.2.6}$$

The 1/12 term in E_Ψ reflects the fact that the vacuum energy in the conformal limit on the cylinder does not vanish if it is assumed to be zero on the plane. The $a_n/\bar{a}_n$ satisfy the following commutation relations:

$$[a_n,a_m]=n\delta_{n+m,0};\qquad [\bar{a}_n,\bar{a}_m]=n\delta_{n+m,0};\qquad [a_n,\bar{a}_m]=0. \tag{6.2.7}$$

These commutators, together with the relation for the commution of the modes with vertex operators

$$[a_n,e^{i\beta\varphi(0)}]=-\beta e^{i\beta\varphi(0)}, \tag{6.2.8}$$

allow one to compute generic matrix elements of the states with the vertex operators appearing in the sine-Gordon Hamiltonian.
After this generic introduction, we will now specify the computational basis we use to explain how time-dependent Rényi entropies, $S_n(t)$, can be computed in a non-equilibrium setting. Starting from Eq. (6.2.5), all states $|\Psi_i\rangle$ of the $J_1=0$ theory have the (unnormalised) form:

$$|\Psi_i\rangle=\prod_{k=1}^{N_i}a_{-n_k}\prod_{k=1}^{\bar{N}_i}\bar{a}_{-\bar{n}_k}|\nu_i\rangle,\quad |\nu_i\rangle\equiv e^{i\nu_i\varphi_0}|0\rangle. \tag{6.2.9}$$

Here the $|\nu_i\rangle=n_i\beta$, with n_i an integer, are plane waves states of the zero mode φ_0 of the boson and $N_i/\bar{N}_i$ is the number of chiral/anti-chiral modes in the state $|\Psi_i\rangle$.

We now want to imagine that we have done a quantum quench or that $J(t)$ has some non-trivial time dependence. We are going to suppose that we are tracking the time dependence of the state, $|\varphi(t)\rangle$, of the system via the following representation:

$$|\varphi(t)\rangle=\sum_i\alpha_i(t)|\Psi_i\rangle, \tag{6.2.10}$$

where $|\Psi_i\rangle$ are the states just discussed of the unperturbed bosonic theory. The corresponding density matrix of the system is

$$\rho(t)=\sum_{i,j}\alpha_i(t)\alpha_j^*(t)|\Psi_i\rangle\langle\Psi_j|. \tag{6.2.11}$$

It will be with the density matrix in this form that we attack the problem of computing $S_n(t)$.

6.2.1 Quenching from Luttinger Liquids to the sine-Gordon Model

Let us focus on the second Rényi entropy, $S_2(t)$, for simplicity. Imagine that we perform a partial trace of region B of the system ($=A\cup B$) from the density matrix in Eqn. 6.2.11. The second Rényi entropy will then take the form

$$\begin{aligned} S_2(t) &= -\log\big(\sum_{i,j,i',j'}\alpha_i(t)\alpha_j(t)^*\alpha_{i'}(t)\alpha_{j'}(t)^*R_{i,j;i',j'}\big),\\ R_{i,j;i',j'} &= \mathrm{Tr}_A(\mathrm{Tr}_B|\Psi_i\rangle\langle\Psi_j|\mathrm{Tr}_B|\Psi_{i'}\rangle\langle\Psi_{j'}|). \end{aligned} \tag{6.2.12}$$

Here we exploit the general closed form expressions for the GMSREs, $R_{i,j;i',j'}$ for bosonic field theories discussed in Chapter 5.

We now want to consider a specific quench, imagining preparing the system in the Luttinger liquid ground state (i.e., taking J_1=0 in Eqn. 6.2.1) and observe the dynamics of the system by turning on at $t = 0$ a finite J_1. For $J_1 > 0$ the dynamics of the system will be that of a far-from equilibrium sine-Gordon model. How far from equilibrium can be quantified. The energy of the ground state of the sine-Gordon model is

$$\begin{aligned} E_{gs} &= L\Delta_s^2 \tan(\pi\xi/2)/4, \quad \Delta_s = c(\beta^2) J_1^{(2-\beta^2)^{-1}}; \\ c(\beta) &= \frac{2\Gamma(\xi/2)}{\sqrt{\pi}\Gamma(1/2+\xi/2)} \Big(\frac{\pi\Gamma(1-\beta^2/2)}{2\Gamma(\beta^2/2)} \Big)^{1/(2-\beta^2)}, \end{aligned} \tag{6.2.13}$$

where $\xi = \beta^2/(2-\beta^2)$ and Δ_s is the gap of the sine-Gordon soliton excitation. $c(\beta^2)$ was first determined in [337]. On the other hand the energy of the pre-quench state $|\varphi(t=0)\rangle$ relative to the post-quench Hamiltonian is $-\pi/(6L)$ and so the quench pumps in a finite energy density of $\tan(\pi\xi/2)\Delta_s^2/4$ at large volumes into the system.

The sine-Gordon model is integrable and while integrability does not allow us to determine the non-equilibrium time evolution of the system, it does provide us with knowledge of the dynamically generated non-perturbative scales in the problem. This include the gap of the solitons, Δ_s, above in terms of J_1. It also includes the gaps of solitonic bound states, the breathers. In sine-Gordon's attractive regime, $\beta < 1$, the model has $\lfloor \xi^{-1} \rfloor$ breathers with gaps

$$\Delta_{b_n} = 2\Delta_s \sin(\pi n \xi/2), \quad n = 1, \cdots, \lfloor \xi^{-1} \rfloor . \tag{6.2.14}$$

For $\beta \ll 1$, the model has a large number of breathers much lighter than the soliton and it is these excitations that dominate the dynamics. In this Chapter we will be focusing on the attractive regime and will suppose that $\beta < 1$. With knowledge of these scales, it is possible to write down scaling behavior of various quantities post-quench. We will focus on both the time-dependent Rényi entropy density as well as the order parameter, $C(t) = \langle \cos(\beta\varphi) \rangle(t)$.

A quantity $O(t)$ with scaling dimension a is going to have a scaling form

$$O(t) = \Delta_{b_2}^a g_O(\Delta_{b_2} L, \Delta_{b_2} t) \tag{6.2.15}$$

where g_O is a dimensionless scaling function. For the order parameter C, $a = \beta^2$, while for the Rényi entropy densities, S_n/L, $a = 1$. We now will determine these scaling forms in the limit of early and late times focusing on the experimentally interesting limit of system sizes $L\Delta_{b_2} \gg 1$.

6.3 Early Time Analysis: UPT

At early times, we can use unitary perturbation theory (UPT) to determine the leading order term in J_1 to the scaling forms. At the heart of unitary perturbation theory is a similarity transformation that transforms the original unperturbed set of bosonic states to an energy-diagonal one where time evolution is easily evaluated. We adapt the unitary perturbation theory (UPT) of Ref. [338]. The main idea of this formalism is to bring the Hamiltonian into energy diagonal form. To do so we introduce a canonical anti-Hermitian transformation,

$$S = J_1 S_1 + \frac{J_1^2}{2} S_2 + O(J_1^3). \tag{6.3.1}$$

We will apply it to the Hamiltonian

$$\begin{aligned} H &= H_0 + H_1, \\ H_0 &= \frac{2\pi}{L}\left[\sum_k (a_{-k}a_k + \bar{a}_{-k}\bar{a}_k) + \pi_0^2 - \frac{1}{12}\right], \\ H_1 &= J_1 \left(\frac{2\pi}{L}\right)^{\beta^2} \int_0^L dx : \cos(\beta\varphi(x)) : . \end{aligned} \tag{6.3.2}$$

The action of S upon H in Eqn. (6.3.1) is given by

$$\begin{aligned} e^{-S}He^{-S} =& H_0 + J_1(H_1 + [S_1, H_0]) + J_1^2(\frac{1}{2}[S_2, H_0] + [S_1, H_1] + \frac{1}{2}[S_1, [S_1, H_0]]) + O(J_1^3), \\ \equiv& H_0 + J_1 H_{1,diag} + J_1^2 H_{2,diag} + O(J_1^3). \end{aligned} \tag{6.3.3}$$

We define S such that the matrix elements of $H_{n,diag}$ with respect to two eigenstates, $|n\rangle, |m\rangle$, of H_0 are only non-zero if $E_n = E_m$. Hence, we find that S satisfies at first order in J_1,

$$S_{1,nm} = \begin{cases} \frac{H_{1,nm}}{E_n - E_m} & E_n \neq E_m, \\ 0 & E_n = E_m, \end{cases} \tag{6.3.4}$$

and at second order,

$$S_{2,nm} = \begin{cases} \frac{[S_1, H_1 + H_{1,diag}]}{E_n - E_m} & E_n \neq E_m, \\ 0 & E_n = E_m. \end{cases} \tag{6.3.5}$$

The transformed Hamiltonian $H_{1/2,diag}$ reads to second order in J_1,

$$\begin{aligned} \langle n|H_{1,diag}|m\rangle =& \langle n|H_1|m\rangle; \quad E_n = E_m \\ \langle n|H_{2,diag}|m\rangle =& \sum_{k, E_k \neq E_n} \frac{H_{1,nk}H_{1,km}}{E_n - E_k}, \quad E_n = E_m. \end{aligned} \tag{6.3.6}$$

We can apply this formalism to find the time dependence of an observable A

$$\begin{aligned} \langle A(t)\rangle &= \langle 0|e^{iHt}Ae^{-iHt}|0\rangle \\ &= \langle 0|e^{-S}e^{iH_{diag}t}e^{S}Ae^{-S}e^{-iH_{diag}t}e^{S}|0\rangle \\ &\equiv \langle 0|e^{-S}e^{S(t)}A_{diag}(t)e^{-S(t)}ee^{S}|0\rangle \,, \end{aligned} \tag{6.3.7}$$

where $S(t) = e^{iH_{diag}t}Se^{-iH_{diag}t}$, $A_{diag}(t) = e^{iH_{diag}t}Ae^{-iH_{diag}t}$. We expand first the inner transformation as

$$e^{S(t)}A_{diag}(t)e^{-S(t)} = A_{diag}(t) + [S(t), A_{diag}(t)] + \frac{1}{2}[S(t), [S(t), A_{diag}(t)]] + O(J_1^3), \tag{6.3.8}$$

and then the outer back transformation

$$\begin{aligned} e^{-S}e^{S(t)}A_{diag}(t)e^{-S(t)}e^{S} =& A_{diag}(t) + [S(t) - S, A_{diag}(t)] \\ &+ \frac{1}{2}\left([S, [S - 2S(t), A_{diag}(t)]] + [S(t), [S(t), A_{diag}(t)]]\right) + O(J_1^3). \end{aligned} \tag{6.3.9}$$

Therefore we can write down $\langle A(t)\rangle$ in terms of its matrix elements as

$$\begin{aligned}\langle A(t)\rangle = A_{00} + \sum_j (\delta S_{0k}(t) A_{diag,k0}(t) - A_{diag,00}(t)\delta S_{k0}(t)) \\ + \frac{1}{2}\sum_{kl} (\delta S_{0k}(t)\delta S_{kl}(t) A_{diag,l0}(t) + A_{diag,0k}(t)\delta S_{kl}(t)\delta S_{l0}(t) \\ -2\delta S_{0k}(t) A_{diag,kl}(t)\delta S_{l0}(t)) + O(J_1^3), \quad (6.3.10)\end{aligned}$$

with $\delta S_{kl}(t) \equiv S_{kl}(t) - S_{kl}$.

We now use UPT to compute the time-dependence of the state of the system, $|\varphi(t)\rangle$. To do so, we write $|\varphi(t)\rangle$ in terms of the states of the unperturbed bosonic theory $|\Psi_a\rangle$ via:

$$|\varphi(t)\rangle = \sum_a \alpha_a(t)|\Psi_a\rangle. \quad (6.3.11)$$

By choosing the observable A as $\rho_{ab} = |\Psi_a\rangle\langle\Psi_b|$, we can use Eq. (6.3.10) to compute the time dependence of the density matrix elements

$$c_{ab}(t) \equiv \langle\varphi(t)|\rho_{ab}|\varphi(t)\rangle \quad (6.3.12)$$

to second order in J_1 as

$$c_{ab}(t) = \begin{cases} 1 + 2\sum_k S_{1,0k}S_{1,k0}(1-\cos((E_k-E_0)t)) & a=b=0 \\ e^{it(E_0-E_b)}S_{1,b0} - S_{1,b0} & \\ \quad +\frac{1}{2}\sum_k S_{1,bk}S_{1,k0}(1 - e^{i(E_0-E_k)t} - e^{i(E_k-E_b)t} + e^{i(E_0-E_b)t}) & a=0, b\neq 0 \\ -e^{it(E_a-E_0)}S_{1,0a} + S_{1,0a} + & \\ \quad \frac{1}{2}\sum_k S_{1,0k}S_{1,ka}(1 - e^{i(E_k-E_0)t} - e^{i(E_a-E_k)t} + e^{i(E_a-E_0)t}) & a\neq 0, b=0 \\ -(1 - e^{i(E_0-E_b)t} - e^{i(E_a-E_0)t} + e^{i(E_a-E_b)t})S_{1,0a}S_{1,b0} & a,b\neq 0 \end{cases} \quad (6.3.13)$$

This will allow us to back out the $\alpha_a(t)$'s.

At small β, the number of states we need to consider in the post-quench density matrix at leading order in the cosine coupling, J_1, and leading order in β include

$$\begin{aligned} &|0;0;0\rangle \equiv |0\rangle, \quad |0;0;m=\pm 1\rangle \equiv e^{im\beta\varphi(0)}|0\rangle, \quad |n;n;m=\pm 1\rangle \equiv \frac{1}{n}a_{-n}\bar{a}_{-n}e^{im\beta\varphi(0)}|0\rangle, \\ &|n,l;n,l;m=0,\pm 1\rangle \equiv \frac{1}{2^{\delta_{nl}}nl}a_{-n}a_{-l}\bar{a}_{-n}\bar{a}_{-l}e^{im\beta\varphi(0)}|0\rangle, \\ &|n,l;n+l;m=\pm 1\rangle \equiv \frac{1}{2^{\delta_{nl}/2}\sqrt{nl(n+l)}}a_{-n}a_{-l}\bar{a}_{-n-l}e^{im\beta\varphi(0)}|0\rangle, \\ &|n+l;n,l;m=\pm 1\rangle \equiv \frac{1}{2^{\delta_{nl}/2}\sqrt{nl(n+l)}}a_{-n-l}\bar{a}_{-n}\bar{a}_{-l}e^{im\beta\varphi(0)}|0\rangle. \end{aligned} \quad (6.3.14)$$

The energies of these states are given by

$$E_{(n_1,\cdots,n_r);(l_1,\cdots,l_s);m} = \frac{2\pi}{L}(\sum_{i=1}^{r} n_i + \sum_{i=1}^{s} l_i + m^2\beta^2). \quad (6.3.15)$$

We will further focus on the contribution of states involving chiral modes such that $\sum_{i=1}^{2} n_i \leq 2$ as these states provide the dominant contribution to $S_2(t)$. Thus we consider the contribution of

states: $|n;n;0,\pm1\rangle, n=0,1,2; |1,1;2;\pm1\rangle; |2;1,1;\pm1\rangle$, and $|1,1;1,1;0,\pm1\rangle$. Using Eq. (6.3.13), the coefficients, $\alpha_{n,m}(t)$, describing these states' time dependence post-quench are:

$$\begin{aligned}
\alpha_{n;n;\pm1}(t) &= \left(\frac{e^{it(E_{n;n;1}-E_{0;0;0})}-1}{E_{n;n;1}-E_{0;0;0}}\right) J_1\frac{\beta^2}{n}L\left(\frac{2\pi}{L}\right)^{\beta^2} \simeq iJ_1\frac{\beta^2}{n}L\left(\frac{2\pi}{L}\right)^{\beta^2} t;\\
\alpha_{0;0;\pm1}(t) &= \left(\frac{e^{it(E_{0;0;1}-E_{0;0;0})}-1}{E_{0;0;1}-E_{0;0;0}}\right) J_1 L\left(\frac{2\pi}{L}\right)^{\beta^2} \simeq iJ_1 L\left(\frac{2\pi}{L}\right)^{\beta^2} t;\\
\alpha_{0;0;0}(t) &= 1-2J_1^2L^2\left(\frac{2\pi}{L}\right)^{2\beta^2}\left[\frac{1-\cos(E_{0;0;\pm1}t)}{E_{0;0;\pm1}^2}+\sum_{k=1}^{2}\frac{\beta^4}{k^2}\frac{1-\cos(E_{k;k;\pm1}t)}{E_{k;k;\pm1}^2}\right]\\
&\simeq 1-J_1^2L^2t^2\left(\frac{2\pi}{L}\right)^{2\beta^2}\left[1+\sum_{k\neq0}\frac{\beta^4}{k^2}\right];\\
\alpha_{1,1;1,1;\pm1}(t) &= \frac{1}{2}\left(\frac{e^{it(E_{1,1;1,1;1}-E_{0;0;0})}-1}{E_{1,1;1,1;1}-E_{0;0}}\right) J_1\beta^4 L\left(\frac{2\pi}{L}\right)^{\beta^2} \simeq \frac{1}{2}iJ_1\beta^4 L\left(\frac{2\pi}{L}\right)^{\beta^2} t;\\
\alpha_{1,1;1,1;0}(t) &= \frac{1}{4}\sum_{E_k\neq0,E_{1,1;1,1;0}}\Big[\frac{H_{1,(1,1;1,1;0)k}H_{k0}}{(E_k-E_{0;0})(E_{1\,1;1,1;0}-E_k)}(1-e^{-i(E_k-E_{0;0})t}-e^{i(E_k-E_{1\,1;1,1;0})t}\\
&\quad+e^{-i(E_{1\,1;1,1;0}-E_{0;0})t})\Big] \simeq -3J_1^2L^2t^2\left(\frac{2\pi}{L}\right)^{2\beta^2}\beta^4;\\
\alpha_{1,1;2;1}(t) &= -\alpha_{2;1,1;-1}(t) \simeq \frac{1}{2\sqrt{2}}iJ_1\beta^3 R\left(\frac{2\pi}{R}\right)^{\beta^2} t.
\end{aligned} \tag{6.3.16}$$

With these coefficients in hand, we can plug them into our generalised Rényi entropy machinery to compute the time-dependence of the second Rényi entropy (see [315] for more details). Putting everything together, we find

$$\begin{aligned}
S_2(t)-S_{2,gs} &= L^2J_1^2\left(\frac{2\pi}{L}\right)^{2\beta^2}t^2\beta^4\Big(4\log^2(2)-\frac{447}{256}\Big)+O(t^3)\\
&= 0.17L^2J_1^2\left(\frac{2\pi}{L}\right)^{2\beta^2}t^2\beta^4+O(t^3).
\end{aligned} \tag{6.3.17}$$

We have kept only terms up to $O(\beta^4)$, and we neglected the contributions due to states $|1,1;2;\pm1\rangle$ because they are $O(\beta^6)$.

We see that $S_2(t)$ behaves as β^4t^2. The β^4 dependence of $S_2(t)$ means that we cannot ignore the contribution of states of the form $|n>0;l>0;m\rangle$, i.e. states with a non-trivial bosonic mode, $a_{-n},\bar{a}_{-n}$, content. Thus $S_2(t)$ probes at early times not just the zero mode dynamics of the field, $\varphi(t)$, but its field theoretic nature.

While we do not report here general formulae for the GMSREs needed to compute the third Rényi entropy, $S_3(t)$, (these are considerably more involved as they involve computing 6-point conformal correlation functions on a 3-sheeted Riemann surface), we can compute the handful of GMSREs needed to compute $S_3(t)$ at early times. Doing so for the sextuplets involving $|0,0\rangle, |n,\pm1\rangle, n=0,1$, we find

$$S_3(t)=L^2J_1^2(\frac{2\pi}{L})^{2\beta^2}t^2f_3(\beta), \tag{6.3.18}$$

where $f_3(\beta)$ for small β reads

$$f_3(\beta) \simeq \left(-\frac{31}{27} + 3\log\frac{27}{16}\log 3\right)\beta^4. \tag{6.3.19}$$

We again see the $\beta^4 t^2$ dependence and again find that we cannot ignore the contribution of states with non-trivial bosonic mode content.

Like with $S_2(t)$ and $S_3(t)$, we can use unitary perturbation theory to compute the time dependence of the order parameter, $C(t) = \langle\cos(\beta\varphi)\rangle(t)$. Here we find that the contribution of states involving only vertex operators, $|0;0;m=0,\pm1\rangle$, determine $C(t)$ at leading order in β and t to be:

$$C(t) = -(2\pi)^{1+2\beta^2} J_1 \beta^2 t^2 L^{-2\beta^2}. \tag{6.3.20}$$

We see that this contribution comes in at $\mathcal{O}(\beta^2)$. At early times $C(t)$ is then determined solely by the dynamics of the compact zero mode of the field, i.e. the problem is quantum mechanical not quantum field theoretic.
Using this framework, the scaling form, g_O, simplifies to

$$g_O(x,y) = x^{m(2-\beta^2)-a} h_O(y/x). \tag{6.3.21}$$

Here m is the order in J_1 that gives the leading order correction to g_0 in unitary perturbation theory. For the cosine order parameter, $m = 1$, while for the Rényi entropies $m = 2$ (see the Supplemental Material in [315] for further details).

6.4 Longer Time Analysis: TSM

While UPT can be used to compute the early time behavior of the growth of $C(t)$ and the Rényi entropies, for longer times we need to use a wholly numerical approach. The natural choice here is the truncated spectrum methodology (TSM) [305, 313, 314]. This method provides for a controlled computation of non-equilibrium quantities in a field theoretic setting. It employs as a computational basis the states of the unperturbed Luttinger liquid, i.e. the $|\Psi_i\rangle$'s, precisely the states for which we now know how to compute the generalised mixed state Rényi entropies. It gains its name from the need to introduce an energy cutoff, E_c, above which we exclude states in the Luttinger liquid basis. While we do not report here the technical details (see [315]), we discuss the results we obtain.

6.4.1 TSM results: Discussion

As a validation of the accuracy of our TSM results, we demonstrate scaling collapse. Fixing $L\Delta_{b2}$, we expect data collapse if we plot our post-quench data for $S_2/(\Delta_{b2}L)$ and $\cos(\beta\varphi)/\Delta_{b2}^{\beta^2}$ against $t\Delta_{b2}$ for different values of J_1 and L. This is what we find, as illustrated in Fig. 6.1. Here we present data that have been extrapolated in the TSM cutoff, $E_c \to \infty$ (for S_2 and $\langle\cos(\beta\varphi)\rangle$) and the GMSRE exclusion parameter, $W \to 0$ (see the Supplemental Material in [315]). If $|\bar{\alpha}_i\bar{\alpha}_j\bar{\alpha}_k\bar{\alpha}_l| < W$ ($\bar{\alpha}_i$ is the time-averaged counterpart of $\alpha_i(t)$), we exclude the contribution of $R_{i,j;i',j'}$ to $S_2(t)$ in Eq. (6.2.12). Because we work with computational bases of size $N_{cb} \sim 10^4$, computing all $R_{i,j;i',j'}$'s would require the computation of $\sim 10^{16}$ different quantities – something that is computationally prohibitive. Fortunately the contribution of the vast majority of GMSREs is negligible (because $|\alpha_i(t)\alpha_j(t)\alpha_k(t)\alpha_l(t)|$ is negligible) and we need to only compute a very small fraction of GMRSEs in order to compute $S_2(t)$.

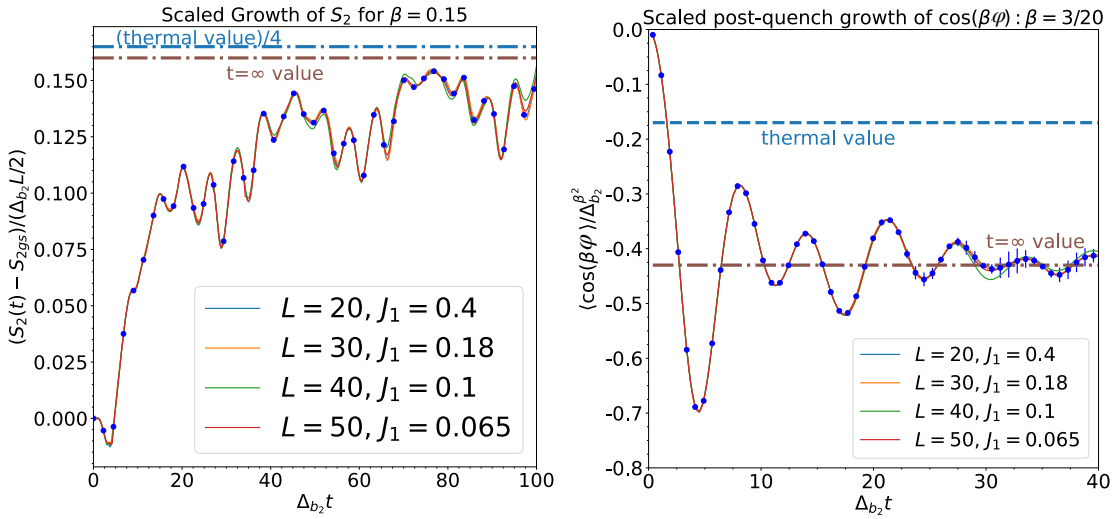

Figure 6.1: The growth of the second Renyi entropy (left panel) and of the order parameter (right panel) for an equal bipartition of the system as a function of time for different system sizes and postquench couplings J_1 chosen such that $\Delta_{b2} L$ is constant and thus scaling collapse is expected. Error bars (blue dots) arising from the extrapolation procedure are shown. We see the expected scaling collapse.

β	J_1	T_{eff}	$S_2(\infty) - S_{2gs}$	$R_2^{\text{therm.}}$	$\langle\cos(\beta\varphi)\rangle(\infty)$	$\langle\cos(\beta\varphi)\rangle^{\text{therm.}}$	S_2^{growth}	$\cos(\beta\varphi)^{\text{growth}}$
$3/20$	0.1	0.45	0.16	0.66	-0.43	-0.17	$0.009\Delta_{b2}$	$-0.003\Delta_{b2}$
$1/\sqrt{8}$	0.0375	0.29	0.058	0.19	-0.42	-0.31	$0.005\Delta_{b2}$	$-0.023\Delta_{b2}$
$1/\sqrt{2}$	0.0375	0.24	0.023	0.093	-0.41	-0.32	$0.01\Delta_{b2}$	$-0.14\Delta_{b2}$

Table 6.1: Here we report for three values of β the late time values of S_2 and $\cos(\beta\varphi)$, comparing them to their thermal values as determined by the effective temperature T_{eff}. The post-quench values of J_1 are chosen such that $\Delta_{b2}(\beta) L$ are constant. We also report these quantities' early time growth rates. All values of $S_2, \cos(\beta\varphi)$ are scaled by $\Delta_{b2} L/2, \Delta_{b2}^{\beta^2}$.

The $S_2(t)$ data at $\beta = 3/20$ presented in Fig. 6.1 show collapse for four different values of J_1 and L (chosen such that $\Delta_{b2} L$ is constant within a few percent) over a time window of $(0, 100/\Delta_{b2})$. We provide error bars associated with the extrapolation procedure. However for S_2 the extrapolation procedure is particularly robust and the error bars are small. For the collapsed $\langle\cos(\beta\varphi)\rangle(t)$ data in Fig. 6.1, we are restricted to a more narrow time window $(0, 40/\Delta_{b2})$.

At very early times, UPT predicts quadratic growth in time of $S_2(t)$ and $\langle\cos(\beta\varphi)\rangle(t)$. After UPT breaks down, both of these quantities experience a window in time where they grow linearly. We report this growth rate in Tab. 6.1 for three different values of β. We see that with increasing β, the growth rates increase in magnitude.

At late times both $S_2(t)$ and $\langle\cos(\beta\varphi)\rangle(t)$ saturate. We expect $S_2(t)$ to approach its late time value via a correction vanishing as $\log(t)/t^3$, valid for integrable quenches with coherent quasiparticles [339]. Using this as a fitting form, we report the value of $S_2(t = \infty)$ in Tab. 6.1. We see that asymptotic value of $S_2(t)$ is extremely sensitive to the value of β. The late time value of $\langle\cos(\beta\varphi)\rangle$ however is not. We see its final value is almost β independent. Because $\langle\cos(\beta\varphi)\rangle(t)$ approaches its asymptote by oscillating about it, its value can be determined most readily by

performing a time average over the data obtained after the initial linear growth.

One useful metric to which we can compare the $t = \infty$ values of S_2 and $\cos(\beta\varphi)$ are the values that would be obtained if the ensemble governing late time dynamics was thermal. Because we know the amount of energy injected by the quench, we can use the analytic expression for the energy of the sine-Gordon model arising from the thermodynamic Bethe ansatz (TBA) to compute both the effective temperature that governs the thermal ensemble with this same energy and then the $t = \infty$ values of S_2 and $\cos(\beta\varphi)$ [340,341]. We see the expected thermal values of $S_2(t = \infty)$ far exceed that of its post-quench extrapolated value. Because the sine-Gordon model is integrable, the generalised Gibbs ensemble that governs late time behaviour is going to involve contributions from the higher conserved quantities in the theory. The system is thus more tightly constrained and so the asymptotic value of the entropy S_2 will be smaller than would be expected in a thermal quench. We also see that the magnitude of $\cos(\beta\varphi)$ is in general larger than would be expected from the thermal value. As this expectation value is directly related to the interaction energy, we can see that the GGE arising from the quench favours interaction over kinetic energy uniformly for different values of β in comparison to the thermal ensemble.

6.4.2 Computation of Power Spectra of $S_2(t)$ and $C(t)$

As a final comparison between the behavior of $S_2(t)$ and $\cos(\beta\varphi)(t)$, we consider the power spectrum of the late time oscillations of these two quantities. This is, in effect, a spectroscopic probe of the post-quench Hamiltonian: the frequencies at which power appears here is at the differences of energies of the excitations [342, 343] of the post-quench sine-Gordon Hamiltonian. For $S_2(t)$ these differences involve four excitations while for $\cos(\beta\varphi)(t)$ the differences involve two excitations. In Fig. 6.2 we present the results of the power spectra. Because of the ability to compute accurately $S_2(t)$ out to longer times, our spectroscopic information for $S_2(t)$ is much resolved in energy than that for $\cos(\beta\varphi)(t)$.

Let us now explain how the power spectrum presented in Fig. 6.2 for the set of parameters $L = 20, \beta = 3/20, J_1 = 0.4$. In order to isolate the oscillating behaviour of $S_2(t)$, we do a

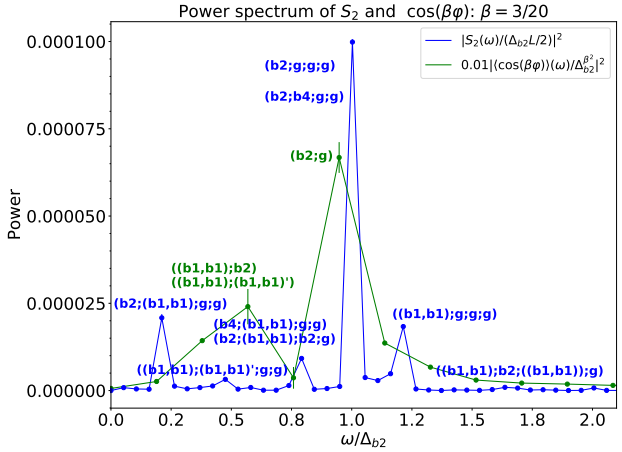

Figure 6.2: We analyse here $\beta = 0.15$ the oscillation frequencies of the late time behavior of S_2 and $\cos(\beta\varphi)$ via Fourier transform (FT). The notation (e_1, e_2) labeling peaks in the FT of $\langle\cos(\beta\varphi)\rangle(t)$ indicates a frequency $\omega = |E_{e_1} - E_{e_2}|$ where E_{e_i} is the energy of excitation e_i. The b_i's refer to states with single breathers, (b_i, b_j) refers to a state with two breathers, while g is the ground state. Similiarly the notation (e_1, e_2, e_3, e_4) indicates a frequency $\omega = |E_1 - E_2 + E_3 - E_4|$.

running time average using

$$\bar{S}_2(t) = \frac{1}{2\Delta_{t.avg}} \sum_{y=t-\Delta_{t.avg}}^{t+\Delta_{t.avg}} S_2(y), \tag{6.4.1}$$

for $\Delta_{t.avg} = 2\pi/\Delta_{b_2}$ over a time window $T \equiv |t_2 - t_1| = |132.8 - 6.8| = 126$. We then perform a discrete Fourier transform (DFT) on the time series $S_2(t) - \bar{S}_2(t) - \varepsilon$, for $t \in [t_1, t_2]$, where ε is chosen such that $S_2(t) - \bar{S}_2(t) = \varepsilon$ as $t \to \infty$:

$$S_2(\omega_n) = \frac{1}{T} \sum_{k=1}^{N} (S_2(t) - \bar{S}_2(t) - \varepsilon) e^{-i\omega_n k \Delta t}, \quad n = 1, \ldots, N. \tag{6.4.2}$$

The time averaging serves to suppress frequencies, $\omega_n \ll \omega_{b_2}$. Here the frequencies, ω_n, of the DFT are defined as $\omega_n = \frac{2\pi}{N\Delta t} n$ where $\Delta t = 0.4$ is the time step and $N = T/\Delta t$.

The time dependence of $S_2(t)$ can be understood in terms of the eigenstates, $\{|E_i\rangle\}$ of the post-quench Hamiltonian. A contribution to $S_2(t)$ of the form $|E_i\rangle\langle E_j|E_k\rangle\langle E_l|$ comes with a time dependence, $e^{it(E_i - E_j + E_k - E_l)}$ [315]. So the peaks in the Fourier transform will correspond to quadtuplets (E_i, E_j, E_k, E_l). In general, several possible combinations of the groundstate (g) and excited states are present. Looking at the low-lying energies of the states $|E_i\rangle$, we can identify the quadtuplets for each peak in the power spectrum. In the spectrum, the first excited state is the second breather (an excitation involving the first breather alone is forbidden by symmetry) and is denoted as b_2. The next two excited states are (b_1, b_1) and (b_1, b_1)' and are two-particle states of two first breathers. They are distinguished by the momentum carried by each constituent b_1 (although the total momentum of the state sums to zero). The fourth excited state is the fourth breather, b_4.

For the Fourier transform of the cosine operator, we do a DFT on the function $C(t) - C(t = \infty)$, i.e. we subtract the asymptotic value in order to obtain a power spectrum with $C(\omega = 0) = 0$. To perform the DFT, we use as a time window $T = |40 - 5| = 35$. In this case, the peaks in the Fourier transform correspond to pairs (E_i, E_j) rather than to quadruplets: in the computation, terms like $\langle E_j| \cos(\beta\varphi)|E_i\rangle$ appear and provide a $e^{it(E_i - E_j)}$ dependence to $C(t)$. Let us notice that the dominant peak in the DFT of $C(t)$ is due to the contribution of the first excited state, i.e. the second breather b_2, while the amplitude of the next largest peak is due to contributions from (b_1, b_1) and $(b_1, b_1)'$, the two low-lying energy states after b_2.

6.5 Closing Remarks

We close this Chapter by commenting on applications to quenches in cold atomic systems. The quench considered here (that of joining two Luttinger liquids) has been performed experimentally in Ref. [344] while the time evolution of $C(t)$ has been computed in Refs. [345, 346]. Our ability to compute $S_2(t)$ to relatively late times (in comparison to $C(t)$) gives us the time window needed to see equilibration in this system. At small β, the equilibriation time is 3 to 4 times longer than that needed by $C(t)$ to begin to oscillate about its $t = \infty$ value. In our spectroscopic analysis of the late time oscillations of $S_2(t)$ and $C(t)$, we can see the outsized role played by the breather excitations of the post-quench Hamiltonian. Importantly we see the post-quench dynamics cannot be described by the lowest breather alone. Finally our determination of a T_{eff} for the post-quench dynamics and corresponding thermal values of $S_2(t)$ and $C(t)$ allow us to quantify the importance of the higher conserved quantities in the GGE governing post-quench dynamics.

We mention that while the quasiparticle picture [46] provides the exact time evolution of the von Neumann entropy $(n = 1)$ for arbitrary integrable models [47, 48], the same is not true [347–

350] for the experimentally accessible Rényi entropies for which our approach is the only viable methodology for both integrable and chaotic post-quench dynamics. We remark that, although we present new and interesting results for the out-of-equilibrium Rényi entropies, the goal of this Chapter is not providing fundamental physical insights on the specific quench dynamics of the coupled Luttinger liquids per se, but rather using it as a playground for a simulation scheme ideal to compute the entanglement in more generic $1d$ QFTs.

Part II

Entanglement and symmetries: exact results

Chapter 7

Symmetry resolved entanglement in gapped integrable systems: a corner transfer matrix approach

Let us start the second part of this thesis with the study of SRREs in gapped integrable lattice models. We use the corner transfer matrix to investigate two prototypical gapped systems with a $U(1)$ symmetry: the complex harmonic chain and the XXZ spin-chain. While the former is a free bosonic system, the latter is genuinely interacting. We focus on a subsystem being half of an infinitely long chain. In both models, we obtain exact expressions for the charged moments and for the symmetry resolved entropies. While for the spin chain we found exact equipartition of entanglement (i.e. all the symmetry resolved entropies are the same), this is not the case for the harmonic system where equipartition is effectively recovered only in some limits. Exploiting the gaussianity of the harmonic chain, we also develop an exact correlation matrix approach to the symmetry resolved entanglement that allows us to test numerically our analytic results (as also done for the scalar field in Chapter 2). This Chapter is based on Refs. [98] and [99].

7.1 Introduction

For the ground state of critical one-dimensional systems with an underlying conformal field theory, the vNEE shows a remarkable universal scaling depending only on the central charge c (e.g., see Eq. (1.4.13)).

Such a universal behaviour is not strictly a prerogative of the gapless models, but it also occurs for gapped models in the vicinity of a quantum phase transition in the regime in which the correlation length ξ is large but finite [20]. Indeed, using ideas from the famous proof of the c-theorem by Zamolodchikov [183], already exploited in Sec. 2.2.2, it has been shown that for a bipartition of an infinite system into two semi-infinite halves, the leading behaviour of entanglement entropies is generically [20]

$$S_n \simeq \frac{c}{12}\left(1+\frac{1}{n}\right)\log\xi. \tag{7.1.1}$$

This result can be elegantly recovered for integrable lattice models through the Baxter corner transfer matrix (CTM) [179], as reported (and generalised) in many references [20, 182, 246, 351–357]. We will discuss explicitly this technique in the following sections. The CTM approach provided exact results not only close to the critical point, but gave generalisations also to the regime in which the correlation length, ξ, is small. When the subsystem A is a finite interval

of length ℓ, as long as $\ell \gg \xi$, the Rényi entropies are just twice the value in Eq. (7.1.1) as a consequence of cluster decomposition in the ground-state of these theories. However, as ℓ becomes of the order of ξ, a complicated crossover takes place that is not captured by CTM and requires more complicated techniques, see e.g. Refs. [156, 175, 199, 358].

In the spirit of exploring the relation between entanglement and symmetries and in particular how entanglement is shared between the various symmetry sectors of a theory [84, 86], in this Chapter we ask whether and when the *equipartition of entanglement* proven in conformal invariant systems [85] survives away from criticality. Thus, we study how the total entanglement splits into the contributions coming from disjoint symmetry sectors in gapped integrable models, using CTM techniques. We carry out this analysis for two non-critical quantum lattice models with a $U(1)$ symmetry, namely the double or complex harmonic chain (which is a free model) and the XXZ chain (which is genuinely interacting). To this aim, we first calculate the charged moments of the RDM, and then obtain the contributions of the sectors by Fourier transform.

In Sec. 7.2 we give an overview of how the RDM of an off-critical quantum chain is related to Baxter's CTM. For integrable models whose weights satisfy a Yang-Baxter relation, the eigenvalues of the RDM can be determined exactly. In Secs. 7.3 and 7.4 we exploit these exact results for the computation of the SRREs, for the complex harmonic chain and XXZ spin-chain respectively. We also benchmark the analytic results in Sec. 7.3 against exact numerical computations. In Sec. 7.5, we find analytic expressions for the full counting statistics in gapped XXZ spin-chain, pointing out its relation with the entanglement resolution. We conclude in Sec. 7.6 with some remarks and discussions. Some technical details about the complex harmonic chain can be found in the Appendix.

7.2 The corner transfer matrix and the entanglement entropy

In dealing with the geometric bipartition considered in this Chapter (i.e. two semi-infinite half lines) the corner transfer matrix provides an exact form for the reduced density matrix [180] and hence it is a formidable tool for the derivation of the charged moments and SRRE. In order to understand how the CTM works, we give a brief review of the construction of the RDM.

Generally, a direct computation of the density matrix of a system is tough. A trick to address this problem is to use the fact that the density matrix of the quantum chain is the partition function of a two-dimensional classical system on a strip [359–361]. The latter can be solved by means of the transfer matrix T and we can identify the eigenstate $|\Psi\rangle$ of T corresponding to its maximal eigenvalue. Given the Hamiltonian of the quantum chain H and its lattice spacing a, the transfer matrix is $T = e^{-aH}$ up to a prefactor; hence $|\Psi\rangle$ is the ground state of H. One then obtains the reduced density matrix of a subsystem A of the chain by tracing over all the coordinates belonging to the complement of A. Therefore ρ_A is the partition function of two half-infinite strips, one extending from $-\infty$ to 0 and the other from $+\infty$ to 0.

The CTM plays a crucial role: it connects a horizontal row to a vertical one. Choosing the lattice in a clever way [179], when the model is isotropic, the four possible corner transfer matrices [179] are all equivalent and the partition function is just $\mathrm{Tr}\hat{A}^4$, with $\hat{A}$ the CTM. Going back to our quantum problem, the reduced density matrix is [180]

$$\rho_A = \frac{\hat{A}^4}{\mathrm{Tr}\hat{A}^4}. \tag{7.2.1}$$

We will deal with integrable massive models satisfying the Yang-Baxter equations; in this case, it

is possible to show that Eq. (7.2.1) has an exponential form given by [180, 359]

$$\rho_A = \frac{e^{-H_{\rm CTM}}}{{\rm Tr}e^{-H_{\rm CTM}}}. \tag{7.2.2}$$

In the cases we are interested in, $H_{\rm CTM}$ (the entanglement or modular Hamiltonian) can be diagonalised as [180]

$$H_{\rm CTM} = \sum_{j=0}^{\infty} \epsilon_j n_j, \tag{7.2.3}$$

where n_j are number operators and ϵ_j are the single-particle levels of the entanglement Hamiltonian. The result (7.2.3) provides exact eigenvalues and degeneracies of the RDM (i.e. the entanglement spectrum of the system [335, 362]), from which one calculates straightforwardly the entanglement entropies [20]. We comment that this approach to the computation of the entanglement Hamiltonian provided exact results about lattice statistical mechanics and it goes parallel to alternative routes towards the study of this operator, like the one in axiomatic field theory provided by Bisognano and Wichmann that we already mentioned in Chapter 3. We will come back to this also in Chapter 12.

Eq. (7.2.3) contains no information about the distributions of the eigenvalues ϵ_j into the various symmetry sectors (indeed, it has exactly the same form for models with discrete and continuous symmetries). In order to use it to compute the SRREs in gapped integrable models, we should complement Eq. (7.2.3) with some other input providing the symmetry resolution, but this should be done on a case by case basis, as we are going to show.

7.3 The complex harmonic chain

In this section we use the CTM to derive the SRREs for a double or complex harmonic chain that is $U(1)$ symmetric and its continuum limit is a non-compact massive *complex* boson, i.e. a Klein-Gordon field theory. We will find an analytic expression for the charged moments as functions of α and we will discuss its limit close to the conformal invariant critical point, when the correlation length ξ is finite but large. Then we will use this result to compute the SRREs. All the analytical results will be compared against exact numerical computations based on correlation matrix techniques [169, 171, 366].

7.3.1 Brief recap of the free complex scalar field and its lattice discretisation

The meaning of the symmetry of a double harmonic chain is clearer in the field theory language and so we first consider a free complex scalar field $\varphi(x)$ described by the Hamiltonian

$$H = \int dx \left[\Pi^\dagger(x)\Pi(x) + \partial_x\varphi^\dagger(x)\partial_x\varphi(x) + m^2\varphi^\dagger(x)\varphi(x)\right], \tag{7.3.1}$$

with $\Pi(x)$ being the field conjugated to $\varphi(x)$. We use the dagger to denote the complex conjugation.

We can as well rewrite the model in terms of two scalar real fields $\varphi_x(x)$ and $\varphi_y(x)$

$$\varphi(x) = \frac{1}{\sqrt{2}}(\phi_x(x) + i\varphi_y(x)), \tag{7.3.2}$$

and the same for $\Pi(x)$. In these variables the $U(1)$ symmetry is an $O(2)$ rotation in the plane (φ_x, φ_y). The Hamiltonian (7.3.1) in terms of these variables is

$$H = \frac{1}{2}\int dx \left[\Pi_x^2(x) + (\partial_x\varphi_x(x))^2 + m^2\varphi_x^2(x)\right] + \frac{1}{2}\int dx \left[\Pi_y^2(x) + (\partial_x\varphi_y(x))^2 + m^2\varphi_y^2(x)\right]$$
$$= H_{\mathbb{R}}(\varphi_x) + H_{\mathbb{R}}(\varphi_y), \quad (7.3.3)$$

where in the second line we stressed that it is a sum of two identical Hamiltonians $H_{\mathbb{R}}$ for the real fields φ_x and φ_y. One introduces the modes $a_i^\dagger(p)$ and $a_i(p)$ for each field $i = x, y$ and momentum p. The Hamiltonian and the conserved charge are instead better written in terms of particles and antiparticles modes operators

$$a(p) = \frac{1}{\sqrt{2}}(a_x(p) + ia_y(p)), \qquad b(p) = \frac{1}{\sqrt{2}}(a_x^\dagger(p) + ia_y^\dagger(p)). \quad (7.3.4)$$

The Hamiltonian is

$$H = \int \frac{dp}{2\pi}\epsilon(p)(a^\dagger(p)a(p) + b^\dagger(p)b(p)), \quad (7.3.5)$$

(with $\epsilon^2(p) = m^2 + p^2$) while the conserved charge is

$$Q = \int \frac{dp}{2\pi}(a^\dagger(p)a(p) - b^\dagger(p)b(p)), \quad (7.3.6)$$

i.e. the total number of particles *minus* the number of antiparticles. The conserved charge can be as well written in real space and its value in a given subsystem A is the same integral restricted to A, i.e.

$$Q_A = \int_A dx(a^\dagger(x)a(x) - b^\dagger(x)b(x)). \quad (7.3.7)$$

For the construction of the RDM for the lattice version of the complex Klein-Gordon field theory, we start from discretising each of the two real Hamiltonians in Eq. (7.3.3). The lattice discretisation of each of them is the harmonic chain, i.e. a chain of L harmonic oscillators of mass $M = 1$ with equal frequency ω_0, coupled together by springs with elastic constant k (hereafter we set $\omega_0 = 1 - k$), i.e. the lattice discretisation of the Hamiltonian $H_{\mathbb{R}}$ is

$$H_{\rm HC}(q) = \sum_{i=1}^{L}\left(\frac{p_i^2}{2} + \frac{\omega_0^2 q_i^2}{2}\right) + \sum_{i=1}^{L-1}\frac{1}{2}k(q_{i+1} - q_i)^2, \quad (7.3.8)$$

where variables p_i and q_i satisfy standard bosonic commutation relations $[q_i, q_j] = [p_i, p_j] = 0$ and $[q_i, p_j] = i\delta_{ij}$. Hence, the lattice version of the complex field theory is the sum of two of the above harmonic chains in the variables q_x and q_y, i.e.

$$H_{CHC}(q_x + iq_y) = H_{\rm HC}(q_x) + H_{\rm HC}(q_y). \quad (7.3.9)$$

which we call complex or double harmonic chain.

The reduced density matrix, ρ_A, for half of the real harmonic chain was explicitly constructed by Peschel and Chung in [167] in the large L limit. The trick is to relate ρ_A to the partition function of a two-dimensional massive Gaussian model in the geometry of an infinite strip of width L with a cut perpendicular to it [363]. Due to the integrability of the Gaussian model, in the case where L is much larger than the correlation length, the $H_{\rm CTM}$ for the harmonic chain may be written in a diagonal form as in Eq. (7.2.3), where now we explicitly have

$$H_{\rm CTM} = \sum_{j=0}^{\infty}(2j+1)\epsilon\,\beta_j^\dagger\beta_j, \qquad \epsilon = \frac{\pi I(\sqrt{1-k^2})}{I(k)}. \quad (7.3.10)$$

Here $I(k)$ is the complete elliptic integral of the first kind, i.e.

$$I(k) = \int_0^{\pi/2} \frac{d\theta}{\sqrt{1 - k^2 \sin^2 \theta}}, \tag{7.3.11}$$

and $\beta_j, \beta_j^\dagger$ are bosonic annihilation and creation operators (satisfying $[\beta_i, \beta_j^\dagger] = \delta_{i,j}$). They are related to the ladder operators a_i of the original chain by a generalised Bogoliubov transformation [167] as

$$\beta_j = \sum_{i \in A} g_{ji} a_i + h_{ji} a_i^\dagger. \tag{7.3.12}$$

Notice that the transformation mixes a and $a^\dagger$ so it does not conserve the number operator.

The RDM for the double chain is clearly factorised in x and y part, i.e. the entanglement Hamiltonian is the sum of two H_{CTM} in Eq. (7.3.10) one with $\beta_{x,i}$ and one with $\beta_{y,i}$ ladder operators. Now we proceed as follows. First we rewrite these two entanglement Hamiltonians in terms of the local ladder operators $a_{x,i}$ and $a_{y,i}$ using the inverse of the Bogoliubov transformation (7.3.12). Then, using the lattice analogue of (7.3.4), i.e.

$$\begin{aligned} a_{x,i} &= \frac{1}{\sqrt{2}}(a_i + b_i), \qquad & a_{x,i}^\dagger &= \frac{1}{\sqrt{2}}(a_i^\dagger + b_i^\dagger), \\ a_{y,i} &= \frac{1}{\sqrt{2}i}(a_i - b_i), \qquad & a_{y,i}^\dagger &= \frac{1}{\sqrt{2}i}(b_i^\dagger - a_i^\dagger). \end{aligned} \tag{7.3.13}$$

we rewrite the entanglement hamiltonian in terms of local ladder operators for particles and antiparticles. This is clearly quadratic (it is the rewriting of a quadratic operator after two linear transformations and so it is quadratic) and commute with the charge operator. Hence, via another Bogoliubov transformation (see Appendix 7.A)

$$\alpha_i = \sum_{j \in A} g_{ij} a_j + h_{ij} b_j^\dagger, \qquad \gamma_i^\dagger = \sum_{j \in A} h_{ij}^* a_j^\dagger + g_{ij}^* b_j, \tag{7.3.14}$$

which conserves the charge, the entire entanglement Hamiltonian of half-chain is brought into the form

$$\mathcal{H}_A = \sum_{j=0}^{\infty} \epsilon(2j+1)(\alpha_j^\dagger \alpha_j + \gamma_j^\dagger \gamma_j), \tag{7.3.15}$$

The charge operator restricted to the semi-infinite line is just the discretisation of Eq. (7.3.7), i.e.

$$Q_A = \sum_{j \in A} a_j^\dagger a_j - b_j^\dagger b_j. \tag{7.3.16}$$

Once we apply the Bogoliubov transformation in Eq. (7.3.14), we have

$$Q_A = \sum_{j=0}^{\infty} \alpha_j^\dagger \alpha_j - \gamma_j^\dagger \gamma_j, \tag{7.3.17}$$

up to an unimportant additive constant that we neglect.

Since the α_i and γ_i operators in Eq. (7.3.15) commute, the RDM factorises as

$$\rho_A = \rho_A^\alpha \otimes \rho_A^\gamma, \tag{7.3.18}$$

where we denoted the RDM for α_i and γ_i with ρ_A^α and ρ_A^γ respectively. For the charged moments, we need to compute $\mathrm{Tr}\rho_A^n e^{iQ_A\alpha}$, but using also that Q_A is the difference of the number of α_i's and γ_i's, see Eq. (7.3.17), the trace factorises as

$$Z_n(\alpha) = \mathrm{Tr}\rho_A^n e^{iQ_A\alpha} = \mathrm{Tr}[(\rho_A^\alpha)^n e^{iN_A^\alpha\alpha}] \times [\mathrm{Tr}(\rho_A^\gamma)^n e^{-iN_A^\gamma\alpha}]. \tag{7.3.19}$$

where $N_A^\alpha = \sum_{j\in A}\alpha_j^\dagger\alpha_j$ and $N_A^\gamma = \sum_{j\in A}\gamma_j^\dagger\gamma_j$. The two factors are equal, except for the sign of α. It is very instructive to see how this factorisation happens for a chain of two oscillators as we report in Appendix.

If for a single harmonic chain, we introduce the quantity

$$F_n(\alpha) = \log[\mathrm{Tr}\rho_A^n e^{iN_A\alpha}], \tag{7.3.20}$$

then we have that the charged moments of the complex boson are given by

$$\log Z_n(\alpha) = F_n(\alpha) + F_n(-\alpha). \tag{7.3.21}$$

We stress that $F_n(\alpha)$ is not the log of a local charged moment because in the single harmonic chain there is no local $U(1)$ symmetry.

In the following we show how to compute $F_n(\alpha)$ by CTM methods for a single harmonic chain and after we use (7.3.21) to get the charged moments.

7.3.2 Charged moments from CTM

Here we first compute the quantity $F_n(\alpha)$ for a real harmonic chain and from this $Z_n(\alpha)$ is simply derived from Eq. (7.3.21). In the above subsection, N_A and ρ_A for the single chain have been already written in the same basis and the derivation of $F_n(\alpha)$ amounts to compute the trace

$$e^{F_n(\alpha)} = \frac{\mathrm{Tr}e^{-\sum_{j=0}^\infty(\epsilon_j n - i\alpha)n_j}}{\left(\mathrm{Tr}e^{-\sum_{j=0}^\infty\epsilon_j n_j}\right)^n} = \frac{\prod_{j=0}^\infty\sum_{k=0}^\infty e^{-((2j+1)\epsilon n - i\alpha)k}}{\left(\prod_{j=0}^\infty\sum_{k=0}^\infty e^{-(2j+1)\epsilon\, k}\right)^n} = \frac{\prod_{j=0}^\infty(1-e^{-(2j+1)\,\epsilon})^n}{\prod_{j=0}^\infty(1-e^{-(2j+1)\,\epsilon n+i\alpha})}, \tag{7.3.22}$$

whose logarithm is given by

$$F_n(\alpha) = \sum_{j=0}^\infty n\log[1-e^{-(2j+1)\epsilon}] - \sum_{j=0}^\infty\log[1-e^{-(2j+1)\epsilon n+i\alpha}]. \tag{7.3.23}$$

This formula is exact and can be easily computed numerically, since it converges very quickly. It is plotted in Figure 7.1 as a function of α for various values of ω_0 and n, but we will discuss its properties later.

The charged moments for the complex harmonic chain, cf. Eq. (7.3.21), are

$$Z_n(\alpha) = e^{F_n(\alpha)}e^{F_n^*(\alpha)} = \frac{\prod_{j=0}^\infty(1-e^{-(2j+1)\epsilon})^{2n}}{\prod_{j=0}^\infty(1-e^{-(2j+1)\epsilon n+i\alpha})\prod_{j=0}^\infty(1-e^{-(2j+1)\epsilon n-i\alpha})} =$$

$$= Z_n\frac{\theta_4(0|e^{-\epsilon n})}{\theta_4(\frac{\alpha}{2}|e^{-\epsilon n})}, \tag{7.3.24}$$

where in the last equality we factor out the total partition sum

$$Z_n \equiv Z_n(\alpha = 0) = \prod_{j=0}^{\infty} \frac{(1 - e^{-(2j+1)\epsilon})^{2n}}{(1 - e^{-(2j+1)\epsilon n})^2}, \tag{7.3.25}$$

and use the following definitions of the theta functions $\theta_r(z|u)$, $r = 2, 3, 4$ [368]

$$\begin{aligned} \theta_2(z|u) &= \sum_{k=-\infty}^{\infty} u^{\left(k+\frac{1}{2}\right)^2} e^{i(2k+1)z}, \\ \theta_3(z|u) &= \sum_{k=-\infty}^{\infty} u^{k^2} e^{2ikz}, \\ \theta_4(z|u) &= \sum_{k=-\infty}^{\infty} (-1)^k u^{k^2} e^{2ikz}. \end{aligned} \tag{7.3.26}$$

The shorthand $\theta_r(u)$ stands for $\theta_r(0|u)$, $r = 2, 3, 4$. Notice that the entire α dependence in Eq. (7.3.24) is encoded in the denominator of Eq. (7.3.24) and that $Z_1 = 1$, but $Z_1(\alpha) \neq 1$. Also the total Rényi entropies of the complex harmonic chains are

$$S_n = \frac{1}{1-n} \log Z_n = \frac{2}{1-n} \sum_{j=0}^{\infty} [n \log (1 - e^{-(2j+1)\epsilon}) - \log (1 - e^{-(2j+1)\epsilon n})], \tag{7.3.27}$$

i.e. the double of a real harmonic chain.

Poisson resummation and critical regime.

A drawback of the form (7.3.23) is that it does not directly allow a direct expansion in the critical regime, i. e. for small ϵ. Moreover, we cannot perform an Euler Mac-Laurin summation (as for $\alpha = 0$, see [20]) since the function $f(x) = \log(1 - e^{-2x})$ diverges for $x \to 0$. However, following Ref. [182], we can obtain the asymptotic expansion for small ϵ by using the (generalised) Poisson resummation formula:

$$\sum_{j=-\infty}^{\infty} f(|\epsilon(bj + a)|) = \frac{2}{\epsilon b} \sum_{k=-\infty}^{\infty} \hat{f}\left(\frac{2\pi k}{\epsilon b}\right) e^{2\pi i k a/b}, \tag{7.3.28}$$

where

$$\hat{f}(y) = \int_0^{\infty} f(x) \cos(yx) dx. \tag{7.3.29}$$

In order to use this resummation formula for Eq. (7.3.23), we must choose $a = 1/2$, $b = 1$ and

$$f_{n,\alpha}(x) = -\log(1 - e^{-2nx + i\alpha}), \tag{7.3.30}$$

which allows us to rewrite the sum (7.3.23) as

$$\begin{aligned} F_n(\alpha) &= \sum_{j=0}^{\infty} (n f_{1,\alpha=0}(\epsilon(j + 1/2)) - f_{n,\alpha}(\epsilon(j + 1/2))) \\ &= \frac{1}{2} \sum_{j=-\infty}^{\infty} (n f_{1,\alpha=0}|(\epsilon(j + 1/2)|) - f_{n,\alpha}(|\epsilon(j + 1/2))|). \end{aligned} \tag{7.3.31}$$

The cosine-Fourier transform of $f_{n,\alpha}(x)$ is

$$\hat{f}_{n,\alpha}(y) = \frac{ie^{i\alpha}}{2y}\left[\Phi(e^{i\alpha},1,1-\frac{iy}{2n}) - \Phi(e^{i\alpha},1,1+\frac{iy}{2n})\right], \tag{7.3.32}$$

where Φ is the Lerch transcendent function, defined as

$$\Phi(z,s,a) = \sum_{j=0}^{\infty} \frac{z^j}{(j+a)^s}. \tag{7.3.33}$$

If $\alpha = 0$ and $n = 1$, Eq. (7.3.32) simplifies to the known value [182]

$$\hat{f}_{1,0}(y) = \frac{1}{y^2} - \frac{\pi}{2y}\coth\left(\frac{\pi y}{2}\right). \tag{7.3.34}$$

Plugging Eq. (7.3.32) into the Poisson resummation formula, we rewrite $\log Z_n(\alpha)$ in such a way to isolate the contribution of the term $k = 0$ which gives the leading divergence in the limit $\epsilon \to 0$, i.e.

$$\begin{aligned} F_n(\alpha) =& \frac{\mathrm{Li}_2(e^{i\alpha})}{2\epsilon n} - \frac{n\pi^2}{12\epsilon} + \sum_{k=1}^{\infty}\left[(-1)^k\frac{n\epsilon}{2\pi^2k^2} + (-1)^{k+1}\frac{n}{2k}\coth\frac{\pi^2 k}{\epsilon}\right] + \\ & \frac{ie^{i\alpha}}{2\pi}\sum_{k=1}^{\infty}\frac{(-1)^k}{k}\left[\Phi(e^{i\alpha},1,1-\frac{i\pi k}{\epsilon n}) - \Phi(e^{i\alpha},1,1+\frac{i\pi k}{\epsilon n})\right]. \end{aligned} \tag{7.3.35}$$

Here we have introduced the polylogarithm of order 2, $\mathrm{Li}_2(z)$.

We are now interested in the critical region of the parameter space in which the correlation length ξ (inverse gap) is large but finite. In the critical regime $\xi \gg 1$ (or equivalently $\epsilon \ll 1$), the correlation length of the model behaves like

$$\log\xi \simeq \frac{\pi^2}{\epsilon} + \mathcal{O}(\epsilon^0). \tag{7.3.36}$$

Using the results of Ref. [367], the last sum over k in Eq. (7.3.35) in the limit $\epsilon \to 0$ behaves like

$$\frac{ie^{i\alpha}}{2\pi}\sum_{k=1}^{\infty}\frac{(-1)^k}{k}\left[\Phi(e^{i\alpha},1,1-\frac{i\pi k}{\epsilon n}) - \Phi(e^{i\alpha},1,1+\frac{i\pi k}{\epsilon n})\right] \to \frac{n\epsilon}{12}\frac{e^{i\alpha}}{1-e^{i\alpha}}. \tag{7.3.37}$$

and hence the only non-vanishing terms in the asymptotic expansion close to $\epsilon = 0$ are

$$F_n(\alpha) = \frac{\mathrm{Li}_2(e^{i\alpha})}{2\epsilon n} - \frac{n\pi^2}{12\epsilon} + \frac{n}{2}\log 2 + \mathcal{O}(\epsilon), \tag{7.3.38}$$

whose real part is

$$\mathrm{Re}[F_n(\alpha)] = \left[\frac{1}{2n}\left(\frac{\alpha}{2\pi}\right)^2 - \frac{|\alpha|}{4\pi n} + \frac{1}{12n} - \frac{n}{12}\right]\log\xi + \frac{n}{2}\log 2 + \mathcal{O}(\epsilon), \tag{7.3.39}$$

because

$$\frac{\mathrm{Re}[\mathrm{Li}_2(e^{i\alpha})]}{n} = \frac{1}{n}\left(\frac{\alpha}{2}\right)^2 - \frac{\pi|\alpha|}{2n} + \frac{\pi^2}{6n}. \tag{7.3.40}$$

The charged moments for the complex harmonic chain are now given by Eq. (7.3.21), i.e. $\log Z_n(\alpha) = F_n(\alpha) + F_n(-\alpha)$ and, in the limit $\epsilon \to 0$,

$$\log Z_n(\alpha) = \left[\frac{1}{n}\left(\frac{\alpha}{2\pi}\right)^2 - \frac{|\alpha|}{2\pi n} + \frac{1}{6n} - \frac{n}{6}\right]\log\xi + n\log 2 + \mathcal{O}(\epsilon). \tag{7.3.41}$$

Notice that while $F_n(\alpha)$ is generically complex, $\log Z_n(\alpha)$ for the complex chain is real and even in α. The expression (7.3.41) tells us that the leading term in the charged moments diverges logarithmically with ξ and matches the result found in (2.2.17) replacing ξ with the inverse of the mass of the continuum theory.

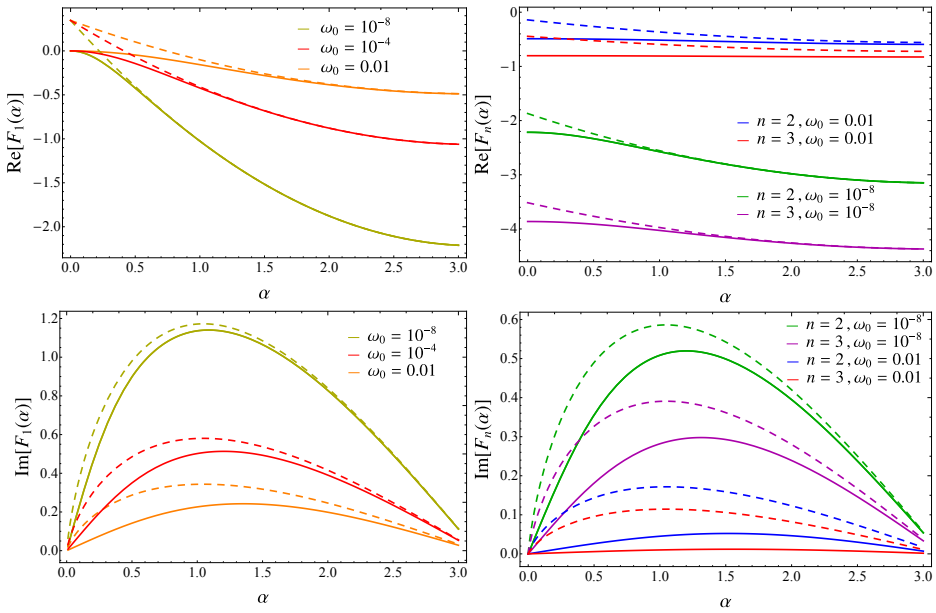

Figure 7.1: Charged moments for the harmonic chain: we report the real (top) and the imaginary (bottom) part of $F_n(\alpha)$, Eq. (7.3.23), as function of α for different values of ω_0. Everywhere, the dashed lines are the asymptotic expansions for $\epsilon \to 0$ and $\alpha \neq 0$ up to $\mathcal{O}(\epsilon)$, cf. Eq. (7.3.38). As discussed in the text, the convergence to the critical result is not uniform and it is slower for smaller $\alpha \neq 0$. The function $\log Z_n(\alpha)$ for the complex chain is twice the real part of $F_n(\alpha)$.

Discussions.

We concluded our exact computation of the charged moments and we are now ready to critically discuss our findings. Eq. (7.3.41) is very suggestive. It tells us that the leading term in the "charged entropies" diverges logarithmically with ξ but with a non-standard prefactor. Indeed, in the conformal field theory of the compactified boson, it has been found that when $\alpha \neq 0$, the additional term in the logarithm is proportional to α^2 [84] , while here we also have a linear contribution in α. Obviously the two results are not in contradiction, because the continuous limit of the harmonic chain is non-compact and the prefactor of α^2 in Ref. [84] diverges when the compactification radius is sent to infinity.

Another interesting fact is that the limit $\alpha \to 0$ and the expansion for ϵ around 0 do not commute, as a difference with other known cases (we believe that the origin of the non-commutativity is the non compact nature of the continuum limit). Indeed, if we consider first the limit $\alpha \to 0$ in Eq. (7.3.35), the last sum gives

$$\sum_{k=1}^{\infty} (-1)^k \left[-\frac{\epsilon n}{2k^2\pi^2} + \frac{1}{2k} \coth\left(\frac{k\pi^2}{\epsilon n}\right) \right], \tag{7.3.42}$$

leading to the known formula of the Rényi entropies of a real harmonic chain, that in the critical regime $\epsilon \to 0$ is [20, 182] (see Eq. (7.3.27))

$$S_n = \frac{\pi^2}{12\epsilon} \frac{1+n}{n} - \frac{\log 2}{2} + \mathcal{O}(\epsilon). \tag{7.3.43}$$

On the other hand, if we invert the order of these two operations, we obtain the divergent term in Eq. (7.3.37). Considering now the charged moments of the complex chain, $\log Z_n(\alpha) =$

$2\mathrm{Re}F_n(\alpha)$, the divergent term (7.3.37) cancels, but the finite part is not the total moment $\log Z_n$ in Eq. (7.3.25). This fact implies that the approach of $\log Z_n(\alpha)$ to the critical limit $\epsilon \to 0$ is non-uniform in α: exactly at $\alpha = 0$ the charged entropy approaches (7.3.27), but for any non-zero α the limit is (7.3.38) that as a consequence is reached for smaller and smaller ϵ (i.e. ω_0) as α gets closer to 0.

All these aspects are evident in Figure 7.1 where we show (for $\alpha \geq 0$ since $F_n(-\alpha) = F_n^*(\alpha)$) the exact result Eq. (7.3.35) (or equivalently (7.3.23)) together with its critical limit, Eq. (7.3.38). As we discussed above, the former converges to the latter as ω_0, therefore ϵ, decreases, but in a non-uniform way. Indeed, while for large α (i.e. close to π) the two curves are very close also when ω_0 is not so small, for smaller and non-zero values of α, we need much smaller ω_0 to approach the critical limit. For $\alpha = 0$ the limit is different. It is also clear that for higher values of n, the convergence is slower and starts at smaller values of ω_0. The last observation is a well known fact for $\alpha = 0$, cf. Ref. [182], and it is not surprising that the effect is amplified in the presence of a flux.

7.3.3 Symmetry resolved moments and entropies via Fourier trasform

The symmetry resolved moments $\mathcal{Z}_n(q)$ are obtained as Fourier transform of $Z_n(\alpha)$ in Eq. (7.3.24), i.e.

$$\mathcal{Z}_n(q) = \int_{-\pi}^{\pi} \frac{d\alpha}{2\pi} e^{-iq\alpha} Z_n(\alpha) = Z_n \theta_4(0|e^{-\epsilon n}) \int_{-\pi}^{\pi} \frac{d\alpha}{2\pi} e^{-iq\alpha} \frac{1}{\theta_4(\frac{\alpha}{2}|e^{-\epsilon n})}. \tag{7.3.44}$$

The integral in the rhs of the above equation can be found in Ref. [368] (exercise 14 at page 489), obtaining

$$\frac{\mathcal{Z}_n(q)}{Z_n} = \prod_{k=1}^{\infty} \left(\frac{1 - e^{-n\epsilon(2k-1)}}{1 - e^{-2n\epsilon k}} \right)^2 e^{-n\epsilon|q|} \sum_{k=0}^{\infty} (-1)^k e^{-n\epsilon k^2} e^{-n\epsilon(2|q|+1)k}, \tag{7.3.45}$$

which is our final result for the symmetry resolved moments. It is likely that the sum in Eq. (7.3.45) can be rewritten in terms of some special functions, but we did not find any particularly useful expression. We define the sum as

$$\Phi_q(u) = u^{|q|} \sum_{k=0}^{\infty} (-1)^k u^{k^2} u^{(2|q|+1)k}, \tag{7.3.46}$$

which can be written in few different equivalent ways that are useful for investigating diverse properties:

$$\Phi_q(u) = \sum_{k=0}^{\infty} (-1)^k u^{k^2+k+|q|(2k+1)} = u^{|q|-\frac{1}{4}} \sum_{k=0}^{\infty} (-1)^k u^{(k+\frac{1}{2})^2} u^{2|q|k}. \tag{7.3.47}$$

Clearly in terms of this function we have

$$\mathcal{Z}_n(q) = \prod_{k=1}^{\infty} \left(\frac{(1 - e^{-\epsilon(2k-1)})^n}{1 - e^{-2n\epsilon k}} \right)^2 \Phi_q(e^{-n\epsilon}), \tag{7.3.48}$$

where we used the explicit form of Z_n in Eq. (7.3.25).

The SRREs are now easily deduced from Eq. (1.4.18), obtaining

$$\begin{aligned} S_n(q) &= \frac{1}{1-n} \log \left[\frac{\mathcal{Z}_n(q)}{\mathcal{Z}_1(q)^n} \right] = \\ &= \frac{2}{1-n} \sum_{k=1}^{\infty} \Big[n \log(1 - e^{-2\epsilon k}) - \log(1 - e^{-2n\epsilon k}) \Big] + \frac{1}{1-n} \log \frac{\Phi_q(e^{-n\epsilon})}{(\Phi_q(e^{-\epsilon}))^n}. \end{aligned} \tag{7.3.49}$$

Taking the limit $n \to 1$, we get the von Neumann entropy

$$S_1(q) = -2\sum_{j=1}^{\infty}\left[\log(1-e^{-2\epsilon j}) - \frac{2\epsilon j e^{-2\epsilon j}}{1-e^{-2\epsilon j}}\right] + \log\Phi_q(e^{-n\epsilon}) + \epsilon e^{-\epsilon}\frac{\Phi_q'(e^{-n\epsilon})}{\Phi_q(e^{-n\epsilon})}. \tag{7.3.50}$$

The critical limit $\epsilon \to 0$ is easily understood if one focuses on the variation in q of moments and entropies, rather than on their absolute values. Indeed from Eq. (7.3.48), it is easy to see that

$$\frac{\mathcal{Z}_n(q)}{\mathcal{Z}_n(q=0)} = \frac{\Phi_q(e^{-n\epsilon})}{\Phi_0(e^{-n\epsilon})} \xrightarrow{\epsilon\to 0} e^{-n^2q^2\epsilon^2/2}\,, \tag{7.3.51}$$

where the last limit is performed by expanding to the second order in ϵ each term in the sum (7.3.46), making carefully the sum in terms of ζ functions, and finally re-exponentiating the result. We stress that this critical limit is *not* the Fourier transform of the critical limit for $Z_n(\alpha)$ in Eq. (7.3.41) because the two limiting procedures do not commute. The critical behaviour of the resolved entropies is then easily worked out as

$$S_n(q) = \frac{1}{1-n}\log\frac{\mathcal{Z}_n(q)}{\mathcal{Z}_1^n(q)} = S_n(q=0) + \frac{n\epsilon^2q^2}{2} + O(\epsilon^3), \tag{7.3.52}$$

which is valid also for $n = 1$ without any particular limit. Also in the critical limit, it is worth to mention the behaviour

$$S_n(q=0) = S_n - \log\frac{8\pi}{\epsilon} + \frac{\log n}{1-n} + o(1)\,, \tag{7.3.53}$$

which signals the presence of a subleading term proportional to $\log\epsilon \sim \log(\log\xi)$. Such a term has not a unique interpretation and origin for the (complex) harmonic chain. Indeed, we know that the total entropy of a massive free non-compact boson has such subleading terms in $\log(\log\xi)$ [177] in the small mass limit, but even that double logarithmic terms appear generically in the symmetry resolution, also for the critical compact boson [84, 90]. Let us now critically discuss our results. First of all, there is a very important difference compared to the conformal gapless case [84], i.e. the absence of equipartition of entanglement [85]: the Rényi entropies (7.3.49) depend explicitly on q. This dependence is reported in Figure 7.2 (a) where, in order to show its variation, we plot it as a continuous function of q, although only integer values are physical. The lack of exact equipartition is not surprising; also in critical models the leading terms for large ℓ show equipartition [85], while some subleading terms depend explicitly on q [84, 90]. In panel (b) of Figure 7.2 we focus on the critical limit of Rényi entropies (7.3.52) plotting $S_n(q) - S_n(q=0)$. As $\epsilon \to 0$, the result approaches the critical form (7.3.52), but clearly the convergence is not uniform: it is faster for smaller q and n. Indeed, since this dependence is all encoded in the function $\Phi_q(e^{-n\epsilon})$, the parameter that must be small is not ϵ, but $n\epsilon$. On the other hand, the higher order terms in ϵ, that have been neglected in (7.3.52), become important for large q. Another interesting feature of the SRREs for this complex harmonic chain is an *effective equipartition* in two limits. The first one is the limit of large q. Indeed, in Eq. (7.3.49) the entire q-dependence is encoded in the function $\Phi_q(e^{-n\epsilon})$. Looking at Eq. (7.3.47), it should be clear that all the terms with $qn\epsilon \gg 1$ are exponentially suppressed. Practically, the total sum is more or less the same for all q such that $n\epsilon q \gtrsim 1$ (from Eq. (7.3.36) this is equivalent to $nq\pi^2 \gtrsim \log\xi$ in the critical region). Hence, there is an *effective equipartition* among all $q \gtrsim 1/(n\epsilon)$. Actually, since the only physical values of q are the integers, this fact implies that there is an almost exact equipartition (with the exception of $S_n(0)$) of the entropy if $n\epsilon \gtrsim 1$, which corresponds to $\omega_0 \gtrsim 10^{-4}$ (for $n = 1$). In panel (c) we report the von Neumann entropies $S_1(q)$ for several values of ω_0, showing that, as q becomes large enough, the entropies $S_n(q)$ do not depend on q anymore. We also explicitly report the (approximate) crossover

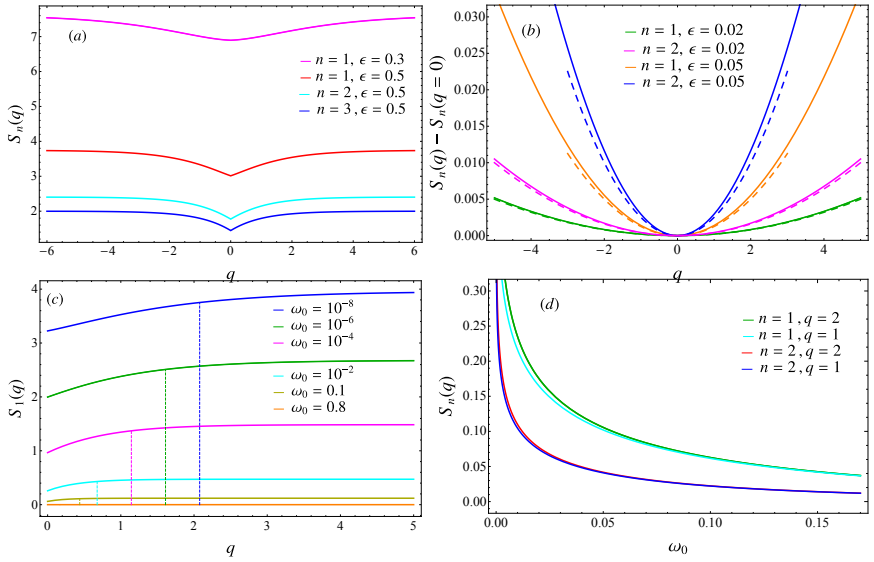

Figure 7.2: SRREs for the complex harmonic chain. Panel (a) shows $S_n(q)$ as functions of q for different values of ϵ and n. Panel (b) reports $S_n(q) - S_n(q=0)$ for small values of ϵ, showing the validity of the expansion in the critical regime (7.3.52). The critical limits in Eq. (7.3.52) are also reported as dashed lines showing its accuracy for small $n\epsilon$. The panel (c) shows the effective equipartition of entanglement for $q \gtrsim 1/\epsilon$ (these crossover values are reported as dashed vertical lines). The panel (d) shows $S_n(q)$ as function of ω_0 for different values of q and n.

values for $q \sim 1/\epsilon$ (as function of ω_0 is given by Eq. (7.3.10)), showing that it correctly captures the change of behaviour. Finally, we have effective equipartition also in the critical regime, but in this case also for small q. In fact, Eq. (7.3.52) shows that the q-dependent term is proportional to ϵ^2, while the leading term of $S_n(q)$ (say for $q = 0$) diverges as ϵ^{-1}. Thus the q-dependence is suppressed as ϵ^3 and there is an effective equipartition. Even if for large q, the expansion (7.3.52) breaks down, we do not expect that $S_n(q) - S_n(0)$ becomes of the order $S_n(0)$ and so there is an effective equipartition for all q: the numerical analysis of Eq. (7.3.49) seems to confirm this expectation. The functional form of the leading q-dependent term in Eq. (7.3.52) is reminiscent of the one found for free fermions [90].

7.3.4 Numerical checks

In this subsection we test the validity of the results in the previous ones against exact numerical computations. We work only with an infinite real harmonic chain (7.3.8) with finite ω_0. For the complex case, we just combine the results for two real chains. Let us consider a bipartition where the subsystem A is given by ℓ contiguous lattice sites. Let us call X_A and P_A the $\ell \times \ell$ matrices of the correlators restricted to the subsystem A, where $X_{ij} = \langle q_i q_j \rangle$ and $P_{ij} = \langle p_i p_j \rangle$. The explicit forms of these correlators in the ground state of the gapped harmonic chain have been already reported many times in the literature (see e.g. Refs. [15,366,369]) and we are not going to rewrite them here. Let us denote by σ_k, with $k = 1, \dots, \ell$, the eigenvalues of the matrix $\sqrt{X_A P_A}$. We introduce the vectors $|\boldsymbol{n}\rangle \equiv \bigotimes_{k=1}^{\ell} |n_k\rangle$, products of Fock states of the number operator in the subsystem A, namely N_A.

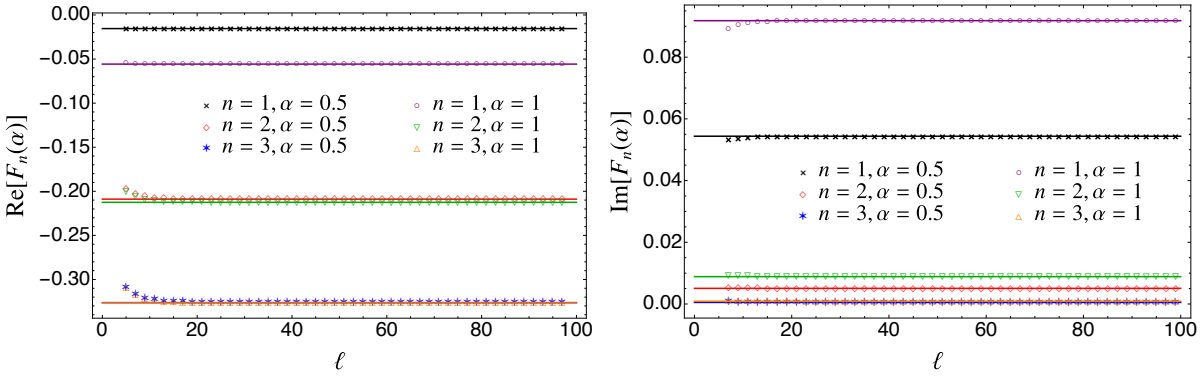

Figure 7.3: Numerical results for the charged moments for an interval of length ℓ embedded in the infinite harmonic chain. We report the real (left) and the imaginary (right) parts of $F_n(\alpha)$ as a function of the subsystem length ℓ, for different values of $n = 1, 2, 3$ and fixed $\omega_0 = 0.1$. The numerical data for an interval of length ℓ (divided by 2) are compared to the analytic CTM prediction (7.3.23): as ℓ is moderately large, the agreement is perfect. The charged moments are just $\log Z_n(\alpha) = 2\mathrm{Re}[F_n(\alpha)]$.

The reduced density matrix of A can be written as [370, 371]

$$\rho_A = \sum_{\boldsymbol{n}} \prod_{k=1}^{\ell} \frac{1}{\sigma_k + 1/2} \left(\frac{\sigma_k - 1/2}{\sigma_k + 1/2} \right)^{n_k} |\boldsymbol{n}\rangle\langle\boldsymbol{n}|, \tag{7.3.54}$$

where the non-negative integer n_k is the k-th element of the ℓ-dimensional vector $\boldsymbol{n}$. Since $N_A = \sum_{j\in A} n_j$ is the number operator in the orthonormal basis made of the states $|\boldsymbol{n}\rangle$, we can write

$$\mathrm{Tr}[\rho_A^n e^{iN_A\alpha}] = \sum_{\boldsymbol{n}} \prod_{k=1}^{\ell} \left[\frac{1}{\sigma_k + 1/2} \left(\frac{\sigma_k - 1/2}{\sigma_k + 1/2} \right)^{n_k} \right]^n e^{in_k\alpha}. \tag{7.3.55}$$

Summing over the possible occupation numbers n_k from 0 to ∞, we get

$$\mathrm{Tr}[\rho_A^n e^{iN_A\alpha}] = \prod_{k=1}^{\ell} \frac{1}{\left(\sigma_k + \frac{1}{2}\right)^n - e^{i\alpha}\left(\sigma_k - \frac{1}{2}\right)^n}. \tag{7.3.56}$$

This relation holds also in higher dimensions and for a generic shape of the subsystem A provided that ℓ is the number of sites in A. Notice the similarity of Eq. (7.3.56) with the analogous result for fermions (cf. Refs. [84, 90] and Eq. (1.4.47)): there are only some different signs, reflecting the different statistics. The formula (7.3.56) allows us to check numerically the results obtained via the CTM approach, and also the field theory predicitons for the scalar field in Chapter 2. Finally, the charged moments for an arbitrary subsystem A for a complex harmonic lattice model are

$$Z_n(\alpha) = \left|\mathrm{Tr}[\rho_A^n e^{iN_A\alpha}]\right|^2 = \prod_{k=1}^{\ell} \frac{1}{\left(\sigma_k + \frac{1}{2}\right)^n - e^{i\alpha}\left(\sigma_k - \frac{1}{2}\right)^n} \frac{1}{\left(\sigma_k + \frac{1}{2}\right)^n - e^{-i\alpha}\left(\sigma_k - \frac{1}{2}\right)^n}. \tag{7.3.57}$$

We comment that the machinery exploited here is also the tool to benchmark our analytical predictions for the free scalar theory in Sec. 2.4.

We now consider $F_n(\alpha) = \log \mathrm{Tr}[\rho_A^n e^{iN_A\alpha}]$ for a real harmonic chan. The numerical data for $F_n(\alpha)$ for an interval of length ℓ should converge to the double (because of the two end-points) of

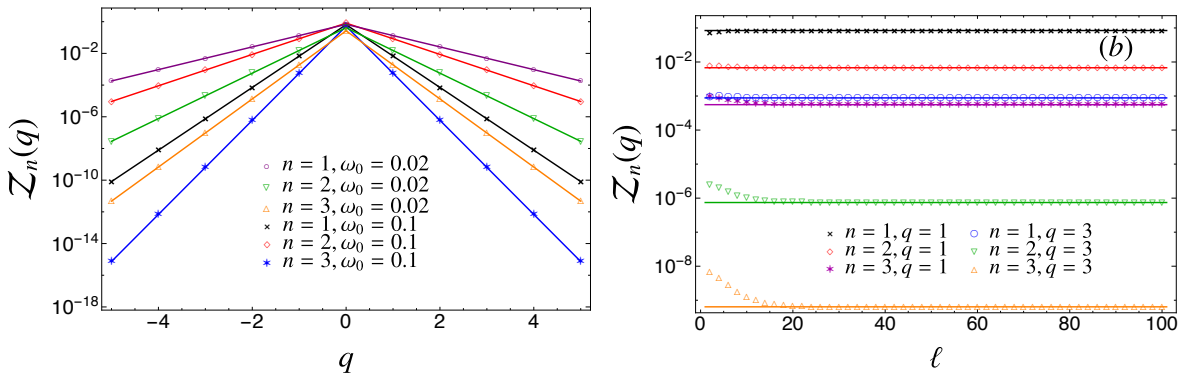

Figure 7.4: Numerical results for the symmetry resolved moments for the complex harmonic chain. (a): (Square root of the) symmetry resolved partition sums $\mathcal{Z}_n(q)$ as function of q. The numerical data for $n = 1, 2, 3$ are compared with the CTM prediction (7.3.45) for two values of ω_0. (b): The same quantity is plotted against the subsystem size ℓ for different values of $q = 20, 40$ and fixed $\omega_0 = 0.1$, showing the convergence towards the CTM prediction (7.3.45) for $n = 1, 2, 3$.

the CTM prediction for the semi-infinite line (with one-endpoint) as soon as ℓ becomes larger than the correlation length ξ. In Figure 7.3 we report the numerical data for (half of) the real and the imaginary parts of $F_n(\alpha)$ for different values of n and α. We have set $\omega_0 = 0.1$, so that after a short crossover in ℓ, the data saturate. The CTM prediction (7.3.23) is also reported for comparison, showing that the analytical result perfectly describes the saturation values. The charged moments for the complex harmonic chain are just $\log Z_n(\alpha) = 2\mathrm{Re}[F_n(\alpha)]$ both for numerics and analytics and so Figure 7.3 is a direct test also for them.

We now take the Fourier transform of the numerical data for $Z_n(\alpha)$ to test the validity and the accuracy of the CTM predictions for the symmetry resolved moments and entropies. In Figure 7.4 we report the (square roots of the) numerically calculated symmetry resolved partition sums $\mathcal{Z}_n(q)$. We compare the data for $n = 1, 2, 3$ with the CTM prediction (7.3.45). The latter perfectly captures the q-dependence, as shown in the panel (a), and gives the value at which the data saturate when studied as functions of ℓ, panel (b). Finally, in Figure 7.5 we report the SRREs for several values of q, n, ω_0. For large ℓ, the numerical data converge to (twice) the CTM predictions in Eqs. (7.3.49) and (7.3.50). Notice that for the larger values of ω_0 the saturation values do not depend on q because of the effective equipartition, but for smaller ω_0 they clearly do. As ω_0 becomes much smaller (such that $\epsilon \sim 0.1$), we expect again effective equipartition, although we do not report such data here because they require very large ℓ.

7.4 Gapped XXZ spin-chain

In this section we study the SRREs in the anisotropic Heisenberg model in the gapped antiferromagnetic regime using the CTM approach. The resolved moments are computed starting from the explicit expressions for the eigenvalues of the RDM and their degeneracies. Then the SRREs are deduced and their critical regime is investigated. The discrete Fourier transform of the resolved moments allows us to compute the charged moments and to discuss their behaviour in the critical regime.

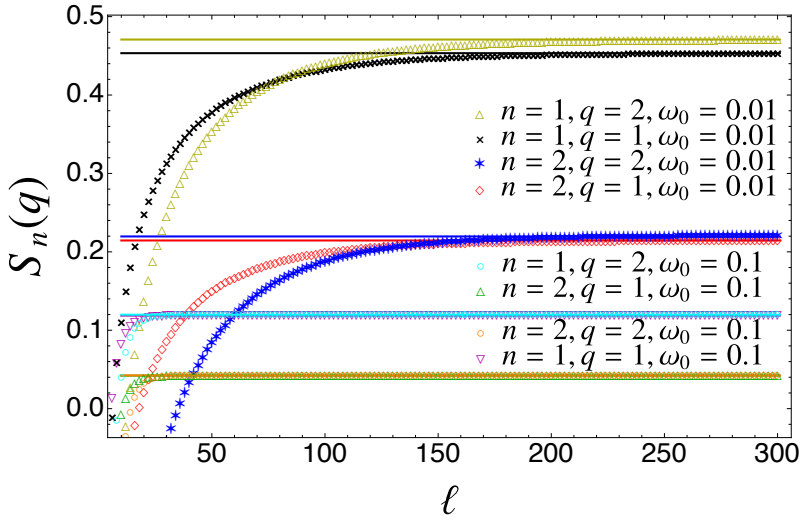

Figure 7.5: Numerical results for the SRREs for the complex harmonic chain. The numerical data for $q = 1, 2$, $n = 1, 2$ and $\omega_0 = 0.1$ and 0.01 are compared with the CTM predictions (7.3.49) and (7.3.50), to which they clearly approach. Notice that the convergence is slower for smaller ω_0. For $\omega_0 = 0.1$ we have an approximate equipartition, but this is not the case for $\omega_0 = 0.01$.

7.4.1 Symmetry resolved moments and entropies

The Hamiltonian of the anisotropic Heisenberg model (also known as XXZ chain) is

$$H_{\rm XXZ} = \sum_j \left[\sigma_j^x \sigma_{j+1}^x + \sigma_j^y \sigma_{j+1}^y + \Delta \sigma_j^z \sigma_{j+1}^z\right], \tag{7.4.1}$$

where σ^i, $i = x, y, z$ are the Pauli matrices. The model has a conformal quantum critical point for $\Delta = 1$, it is gapless when $|\Delta| \leq 1$ and gapped when $|\Delta| > 1$. We consider this model in the antiferromagnetic gapped regime with $\Delta > 1$.

The XXZ chain is solvable by Bethe Ansatz techniques; unfortunately this framework is not very effective to study the entanglement properties both in the coordinate [172] and in the algebraic [372, 373,375–380,645] approach. On the other hand, the CTM solution for the XXZ chain is a powerful tool to compute the entanglement entropies; in this approach, the reduced density matrix is related to the partition function of the six-vertex model on a strip with a cut. In Ref. [180] $H_{\rm CTM}$ has been found to be of the form (7.2.3) with

$$\epsilon_j = 2\epsilon j, \qquad \epsilon = \operatorname{arccosh}\Delta, \tag{7.4.2}$$

and n_j being some fermionic number operators. Since in the thermodynamic limit, the ground-state of the gapped XXZ spin-chain is doubly degenerate we should clarify which state we are going to deal with in this section. The entanglement Hamiltonian (7.2.3) together with (7.4.2) selects by construction the ground state that does not break the inversion symmetry, i.e. the one that in the limit of large Δ is $(|N_1\rangle + |N_2\rangle)/\sqrt{2}$ where $|N_i\rangle$ are the two possible Néel states. However, we prefer to work with the more physical symmetry breaking state $|N_i\rangle$. In CTM approach this can be constructed with an entanglement Hamiltonian of the form (7.2.3) where the sum over j starts from 1 rather than 0, i.e.

$$H_{\rm CTM} = \sum_{j=1}^{\infty} \epsilon_j n_j, \qquad \epsilon_j = 2\epsilon j, \qquad \epsilon = \operatorname{arccosh}\Delta. \tag{7.4.3}$$

In the remaining part of this section we always focus on the symmetry breaking ground state with the above $H_{\rm CTM}$. If one is interested into the other state, analogous results may easily be derived.

The entanglement spectrum is obtained by filling in all the possible ways the single particle levels in (7.4.3) (i.e. setting all n_j equal either to 0 or 1). The resulting levels are equally spaced with spacing 2ϵ and highly degenerate. The degeneracy of the level $2\epsilon s$, with $s = \sum_j j$ (see (7.4.2)) is $\mathcal{D}_{\rm h}(s)$, the number of partitions of s into smaller non-repeated integers (including zero). (Notice we use the non-standard symbol $\mathcal{D}_{\rm h}(s)$ instead of $q(s)$ to avoid confusion with q, the charge sector.)

We want to characterise how the entanglement of the semi-infinite line A with respect to its complement splits into the different sectors with fixed magnetisation $S_z \equiv \sum_j \sigma_j^z/2$. We indicate with q the possible values, in the subsystem A, of the *difference* of the magnetisation with respect to the antiferromagnetic Néel state chosen as a reference configuration. Such variable q is quantised in terms of integer numbers (each spin flip leads to a change of magnetisation of ± 1), i.e. $q \in \mathbb{Z}$. With a slight abuse of language, we will refer to q as the magnetisation, although it is a magnetisation difference. To derive the SRREs, we first write $\mathcal{Z}_n(q)$, defined in (1.4.17), as

$$\mathcal{Z}_n(q) = \sum_{s \in \mathcal{S}_q} \lambda_s^n \,, \tag{7.4.4}$$

where λ_s are the eigenvalues of the RDM and the sum is restricted to the levels with fixed value of q. Using Eq. (7.2.2) and the explicit expression of the entanglement spectrum from Eq. (7.4.3), we can write

$$\mathcal{Z}_n(q) = \frac{\sum_s \mathcal{F}_{\rm h}(q,s) e^{-2n\epsilon s}}{\Big(\sum_s \mathcal{D}_{\rm h}(s) e^{-2\epsilon s}\Big)^n} \,, \tag{7.4.5}$$

where $\mathcal{F}_{\rm h}(q,s)$ is the number of eigenvalues at level s with magnetisation q. The degeneracies $\mathcal{F}_{\rm h}(q,s)$ have been studied in Ref. [364] with a combination of perturbation theory and integrability arguments. The final result for the bipartition of our interest is $\mathcal{F}_{\rm h}(q,s) = \mathcal{P}_{\rm h}(\frac{s-m_{\rm h}(q)}{2})$ [364], with $\mathcal{P}_{\rm h}(n)$ the number of integer partitions of n and $m_{\rm h}(q) = q(2q-1)$. Using this result and changing variable in the sum of the numerator in Eq. (7.4.5) as $(s - m_{\rm h}(q))/2 \to s$, we obtain

$$\mathcal{Z}_n(q) = e^{-2n\epsilon q(2q-1)} \frac{\sum_s \mathcal{P}_{\rm h}(s) e^{-4n\epsilon s}}{\Big(\sum_s \mathcal{D}_{\rm h}(s) e^{-2\epsilon s}\Big)^n}, \tag{7.4.6}$$

where we have also exploited that $\mathcal{P}_{\rm h}(n)$ is non vanishing only if n is a positive integer.

The two sums in (7.4.6) can be conveniently rewritten in terms of generating functions

$$\sum_{s=0} \mathcal{P}_{\rm h}(s) x^s = \prod_{k=1}^{\infty} \frac{1}{1-x^k}, \qquad \sum_{s=0} \mathcal{D}_{\rm h}(s) y^s = \prod_{k=1}^{\infty} (1+y^k). \tag{7.4.7}$$

Setting $x = e^{-4n\epsilon}$ and $y = e^{-2\epsilon}$ in (7.4.7) and plugging them into (7.4.6) we obtain

$$\mathcal{Z}_n(q) = \frac{e^{-2n\epsilon q(2q-1)}}{\prod_{k=1}^{\infty} \Big(1 - e^{-4n\epsilon k}\Big) \prod_{k=1}^{\infty} \Big(1 + e^{-2\epsilon k}\Big)^n}. \tag{7.4.8}$$

We remark that $\mathcal{Z}_1(q)$ is normalised to one, i.e. $\sum_{q\in\mathbb{Z}}\mathcal{Z}_1(q)=1$, as it should be from the definition (7.4.4). This is consistent with the interpretation of $\mathcal{Z}_1(q)$ as a probability. The denominator of Eq. (7.4.8) can be expressed in terms of theta functions and then $\mathcal{Z}_n(q)$ reads

$$\mathcal{Z}_n(q)=\frac{2^{\frac{1+n}{3}}\left[\kappa(e^{-\epsilon})\right]^{\frac{n}{12}}e^{-4n\epsilon(q-\frac{1}{4})^2}}{\left[\kappa(e^{-2\epsilon n})\kappa'(e^{-2\epsilon n})\right]^{\frac{1}{6}}\left\{\left[\kappa'(e^{-\epsilon})\right]^{-\frac{2}{3}}-\left[\kappa'(e^{-\epsilon})\right]^{\frac{4}{3}}\right\}^{\frac{n}{8}}\theta_3\left(e^{-2\epsilon n}\right)}, \tag{7.4.9}$$

where κ and κ' are defined as

$$\kappa(u)\equiv\frac{\theta_2^2(u)}{\theta_3^2(u)},\qquad \kappa'(u)=\sqrt{1-\kappa(u)^2}=\frac{\theta_4^2(u)}{\theta_3^2(u)}. \tag{7.4.10}$$

Notice that $q=1/4$ is exactly the mean magnetisation of the subsystem in the critical limit $\epsilon\to 0$, as we can check by computing $\bar{q}=\int dqq\mathcal{Z}_1(q)$, since we are dealing with the symmetry breaking ground state. Notice that the dependence on q in Eq. (7.4.9) is entirely encoded in the Gaussian factor and it is symmetric for $q\to 1/2-q$. Moreover, exploiting the asymptotic behaviours [98], we have that in the critical regime $\mathcal{Z}_n(q)$ becomes

$$\mathcal{Z}_n(q)\simeq\sqrt{\frac{2^{1+n}\epsilon n}{\pi}}e^{-\frac{\pi^2}{24\epsilon}\left(n-\frac{1}{n}\right)}e^{-4n\epsilon(q-\frac{1}{4})^2}, \tag{7.4.11}$$

where we keep the Gaussian factor in order to have a meaningful result. Once the resolved moments $\mathcal{Z}_n(q)$ have been worked out, the SRREs follow straightforwardly

$$S_n(q)=\frac{1}{1-n}\sum_{k=1}^{\infty}\left[n\log\left(1-e^{-4\epsilon k}\right)-\log\left(1-e^{-4n\epsilon k}\right)\right], \tag{7.4.12}$$

and, taking the limit $n\to 1$,

$$S_1(q)=\sum_{k=1}^{\infty}\left[\frac{4\epsilon k}{e^{4\epsilon k}-1}-\log\left(1-e^{-4\epsilon k}\right)\right]. \tag{7.4.13}$$

Notice that as $\Delta\gg 1$, $S_n(q)\to 0$ (see also Figure 7.6), since in this limit the selected antiferromagnetic ground state is a product state. If we would have considered the non-symmetry breaking ground state $(|N_1\rangle+|N_2\rangle)/\sqrt{2}$, $\Delta\gg 1$ we would have found $S_n(q)\to\log 2$, as for the total entropy [20, 182, 246]. We stress that although there is entanglement equipartition, the functions $S_n(q)$ are not equal to the total entropies S_n because there is a non-vanishing fluctuation term like in Eq. (1.3.5) for $n=1$.

Remarkably, the expressions (7.4.12) and (7.4.13) for the SRREs and SREE do not depend on q for any value of n, i.e. they *exactly satisfy the equipartition of entanglement* for any value of Δ. In the critical case, only the leading terms satisfy such equipartition [85, 90].

The relation between the correlation length of the model and ϵ, in the critical regime $\xi\gg 1$, is [179]

$$\log\xi\simeq\frac{\pi^2}{2\epsilon}+O(\epsilon^0), \tag{7.4.14}$$

which combined with Eqs. (7.4.11) provides the expansions of the SRREs in the critical regime

$$\begin{aligned}S_n(q)&=\frac{1}{12}\left(1+\frac{1}{n}\right)\log\xi-\frac{1}{2}\log\left(\frac{\log\xi}{\pi}\right)+\frac{1}{2}\log 2+\frac{\log n}{2(1-n)},\\ S_1(q)&=\frac{1}{6}\log\xi-\frac{1}{2}\log\left(\frac{\log\xi}{\pi}\right)+\frac{\log 2-1}{2}.\end{aligned} \tag{7.4.15}$$

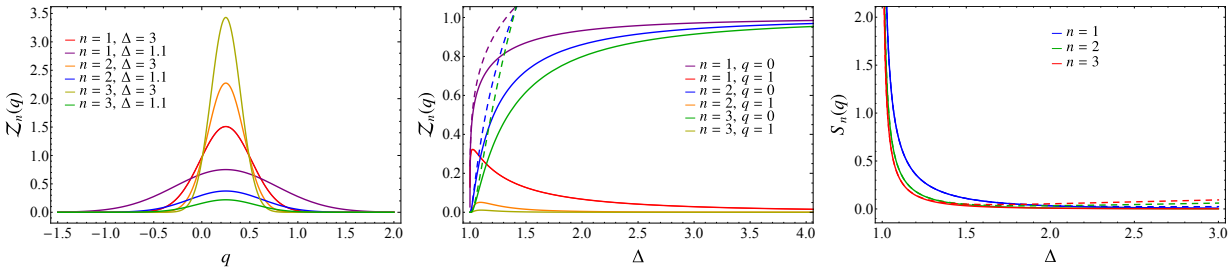

Figure 7.6: Magnetisation resolved moments and entropies for the XXZ spin-chain. The left panel shows the results for $\mathcal{Z}_n(q)$, Eq. (7.4.8), against q for different values of $n = 1, 2, 3$ and $\Delta = 1.1, 3$. In the middle panel, we report again $\mathcal{Z}_n(q)$ at fixed q and as function of Δ (full lines). As a comparison, we also report the asymptotic expansion (7.4.11) for Δ close to 1 (dashed lines). In the right panel, we report $S_n(q)$ and its critical limit, respectively Eq. (7.4.12) and Eq. (7.4.15), as function of Δ for $n = 1, 2, 3$. We recall that $S_n(q)$ does not depend on q because of entanglement equipartition.

We notice that the term $-\frac{1}{2} - \frac{1}{2}\log(\log \xi/\pi)$ appearing in $S_1(q)$ in Eq. (7.4.15) is canceled exactly by the fluctuation entanglement entropy once we consider the total von Neumann entanglement entropy. Indeed, using that the probability is $p_{\rm h}(q) = \mathcal{Z}_1(q)$, we write the fluctuation entropy as $-\int dq \mathcal{Z}_1(q) \log \mathcal{Z}_1(q)$. Using (7.4.9), computing the gaussian integral in q and then taking the critical limit, we find

$$-\int_{-\infty}^{\infty} dq \mathcal{Z}_1(q) \log \mathcal{Z}_1(q) = \frac{1}{2} + \frac{1}{2}\log(\log \xi/\pi), \tag{7.4.16}$$

which exactly cancels the contribution from the configurational entropy. This is in complete analogy with what has been found for critical systems for the $\log\log \ell$ term [90] (see also Chapter 2).

In Figure 7.6 we report symmetry resolved moments and entropies. The possible values of q are just integers, but since $\mathcal{Z}_n(q)$ becomes quickly small as q increases, we consider arbitrary real values. As anticipated, $\mathcal{Z}_n(q)$ has a peak at $q = 1/4$ and shows a clear Gaussian shape for all Δ. The exact result (7.4.8) is well approximated by its critical limit (7.4.11) for Δ close to 1, but the approach is not uniform and it is worse for larger q (as well as larger n). Clearly, the maximum of $\mathcal{Z}_n(q)$ is a decreasing function of n. In the last panel of Figure 7.6, we report the SRREs as functions of Δ (as we stressed because of equipartition, they do not depend on q). Notice that the window of Δ for which the critical limit of $S_n(q)$ in Eq. (7.4.15) is a good approximation of the exact expression (7.4.12) is wider for smaller values of q.

7.4.2 Charged moments via Fourier series

The charged moments are obtained from the resolved ones $\mathcal{Z}_n(q)$ by inverting the formula (1.4.17), i.e.

$$Z_n(\alpha) = \sum_{q=-\infty}^{\infty} \mathcal{Z}_n(q) e^{iq\alpha}. \tag{7.4.17}$$

Plugging in the above equation the result for $\mathcal{Z}_n(q)$ in Eq. (7.4.8) and using the definition of the theta function $\theta_3(z|u)$ (7.3.26), we obtain

$$Z_n(\alpha) = \frac{\theta_3(\frac{\alpha}{2} - in\epsilon | e^{-4\epsilon n})}{\prod_{k=1}^{\infty}\left(1 - e^{-4n\epsilon k}\right)\prod_{k=1}^{\infty}\left(1 + e^{-2\epsilon k}\right)^n}. \tag{7.4.18}$$

Setting $\alpha = 0$ and exploiting the infinite product representation of $\theta_3(z|u)$ [368], we get

$$Z_n(0) = \frac{\prod_{k=1}^{\infty} \left(1 + e^{-2\epsilon n k}\right)}{\prod_{k=1}^{\infty} \left(1 + e^{-2\epsilon k}\right)^n}, \tag{7.4.19}$$

as found in [20]. As for $\mathcal{Z}_n(q)$ in Section 7.4.1, we can express $Z_n(\alpha)$ in terms of theta functions obtaining

$$Z_n(\alpha) = \frac{2^{\frac{1+n}{3}} e^{-\frac{n}{4}\epsilon} \left[\kappa(e^{-\epsilon})\right]^{\frac{n}{12}}}{\left[\kappa(e^{-2\epsilon n})\kappa'(e^{-2\epsilon n})\right]^{\frac{1}{6}} \left\{\left[\kappa'(e^{-\epsilon})\right]^{-\frac{2}{3}} - \left[\kappa'(e^{-\epsilon})\right]^{\frac{4}{3}}\right\}^{\frac{n}{8}}} \frac{\theta_3(\frac{\alpha}{2} - in\epsilon \,|\, e^{-4\epsilon n})}{\theta_3\left(e^{-2\epsilon n}\right)}. \tag{7.4.20}$$

$Z_n(\alpha)$ in the critical regime is obtained using the asymptotic expansions of the theta functions [98], finding

$$Z_n(\alpha) \simeq 2^{-\frac{1-n}{2}} e^{-\frac{\pi^2}{24\epsilon}\left(n - \frac{1}{n}\right)} e^{-\frac{\alpha^2}{16 n \epsilon} + i\frac{\alpha}{4}}. \tag{7.4.21}$$

Taking the logarithm of $Z_n(\alpha)$ and using (7.4.14) we have

$$\log Z_n(\alpha) \simeq \left[\frac{1}{12}\left(\frac{1}{n} - n\right) - \frac{\alpha^2}{8\pi^2 n}\right] \log \xi + i\frac{\alpha}{4} - (1-n)\frac{\log 2}{2}. \tag{7.4.22}$$

Here, the linear term in α is just the mean magnetisation in A, $\bar{q} = 1/4$.

The leading term in Eq. (7.4.22) is very suggestive. Indeed, for the critical compact boson, in the case of A being an interval of length ℓ embedded in an infinite 1D system, $\log Z_n(\alpha)$ diverges logarithmically with ℓ as [84]

$$\log Z_n(\alpha) \simeq \left[\frac{1}{6}\left(\frac{1}{n} - n\right) - \frac{\alpha^2}{2\pi^2 n} K\right] \log \ell + \ldots, \tag{7.4.23}$$

as we have already remarked in Sec. 3.2.1. The prefactor of Eq. (7.4.22) is exactly half of the conformal result (7.4.23) for $K = \frac{1}{2}$, which is the Luttinger parameter at $\Delta = 1$. The multiplicative factor $1/2$ is simply understood because in our geometry there is a single endpoint instead of two as in the conformal case. It is natural to wonder under what hypotheses this can happen since we have seen that it is not true for the harmonic chain. Moreover, for the SRREs, the CFT result is $S_n(q) - S_n = -\frac{1}{2}\log((2K/\pi)\log\ell) + O(\ell^0)$ [84, 85], which is the same as in Eq. (7.4.15) with the replacement $\ell \to \xi$ and with $K = 1/2$.

7.5 Full counting statistics in the gapped XXZ spin chain

The process of measurement in quantum mechanics is intrinsically probabilistic: the measure of a given observable generically provides different outcomes in identically prepared systems. Hence, the probability distribution (PDF) of an observable is a natural quantity to consider in any quantum mechanical system and provides much more information than the average value of the same observable. In many-body systems, these PDFs, or equivalently their full counting statistics (FCS), have been the subject of intensive investigations since many years with a focus mainly on local observables (i.e. defined in a given point or lattice site) or global ones (i.e. extensive quantities involving the entire system). Only in recent time, the attention shifted to observables with support on a finite, but large, subsystem embedded in a thermodynamic one, partially motivated by some

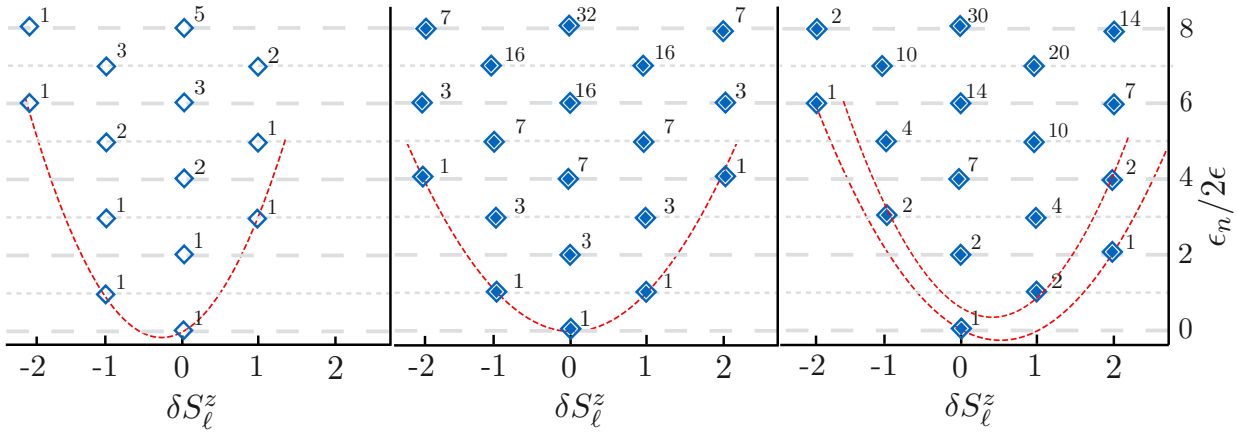

Figure 7.7: Entanglement spectra of the gapped XXZ spin chain in the three configurations we consider here. Left: Semi-infinite line. Center: A block of ℓ contiguous spins with ℓ even. Right: A block with ℓ odd. We report the logarithm of the eigenvalues of the reduced density matrix ϵ_n in units of 2ϵ, with $\epsilon = \text{arccosh}\Delta$, as function of δS^z_ℓ (cf. (7.5.1)). Each tilted square signals the presence of an eigenvalue with degeneracy given by the nearby number. The dashed-red parabolas are envelopes of the location of the largest eigenvalue of the RDM at fixed δS^z_ℓ. Notice that in the left and in the center, the towers of degeneracies are independent of δS^z_ℓ. Conversely, on the right, i.e. for odd blocks, there are two towers depending on the parity of δS^z_ℓ.

cold atomic experiments [383–388] and by the connection with the entanglement entropy of the same subsystem [66–68, 389, 390, 392–395, 650]. In spite of a large recent literature on the subject [272, 396–421], results based on integrability for one-dimensional exactly solvable *interacting* models are still scarse (see [409, 410]).

The FCS of a conserved charge within an extended subsystem is strictly related to the charged moments introduced in Eq. (1.4.16) in order to study the SRREs. Thus, it is natural to adapt the techinques developed for the entanglement resolution to the computation of the FCS. In this section, we provide an explicit exact calculation for the PDF and for the FCS of the total transverse magnetisation within an extended subsystem in an infinite XXZ spin chain. As also done in Sec. 7.4, we focus on the antiferromagnetic gapped regime with $\Delta > 1$ and, being the total transverse magnetisation ($\sum_j \sigma^z_j/2$) conserved, the FCS can be directly obtained from the entanglement spectrum of the subsystem. Indeed, the RDM ρ_ℓ of the subsystem is organised in blocks of fixed magnetisation (quantised in terms of integers or half-integers up to $\ell/2$ depending on the parity of ℓ). Following the discussion in Sec. 7.4.1, it is convenient to focus on the difference of the block magnetisation with the Néel state, i.e.

$$\delta S^z_\ell \equiv \sum_{j=1}^{\ell} \Big(\frac{\sigma^z_j}{2} - \frac{(-1)^j}{2} \Big) . \tag{7.5.1}$$

The probability of a measurement of the subsystem magnetisation with outcome $\delta S^z_\ell = q$ is just the trace of the block of ρ_ℓ in the sector with $\delta S^z = q$, i.e.

$$P(q) = \text{Tr}\rho_\ell \Pi_q = \sum_{s \in \mathcal{S}_q} \lambda_s \, , \tag{7.5.2}$$

where Π_q is the projector on the sector of magnetisation $\delta S^z = q$, λ_s are the eigenvalues of ρ_ℓ, and $\mathcal{S}_q$ stands for all the eigenvalues in that magnetisation sector (notice that $\sum_q P(q) = \text{Tr}\rho_\ell = 1$ by

construction). Similarly the FCS generating function is defined as (they can be also written as the $n = 1$ charged moments in Eq. (1.4.16))

$$G(\lambda) \equiv \mathrm{Tr}\rho_\ell e^{i\lambda\delta S^z_\ell} = \sum_q P(q)e^{iq\lambda}; \tag{7.5.3}$$

its derivatives in $\lambda = 0$ provide the moments of the observables δS^z_ℓ. Hence the exact knowledge of the entanglement spectrum also provides the FCS of the total transverse magnetisation (in general it provides the FCS of any conserved charge). As discussed in Sec. 7.4 for the ground state of the XXZ spin chain in the gapped regime, the entanglement spectrum has been obtained in Ref. [364]. We exploit its knowledge here to reconstruct the PDF and the FCS of the subsystem magnetisation.

7.5.1 Recap on the entanglement spectrum

As done in Sec. 7.4.1, in the following we consider an infinite XXZ chain in the symmetry broken ground state, i.e. the one that for large Δ converges to the Néel state. This state is doubly degenerate, so there are two equivalent states which are mapped into each other by the translation of one site. As already discussed in Sec. 7.4.1, when the subsystem is half of the chain, the result for the degeneracy of the eigenvalues of its RDM, ρ_ℓ, with $\delta S^z_\ell = q$ at level s is given by $\mathcal{F}_{\rm h}(q, s) = \mathcal{P}_{\rm h}(\frac{s-m_{\rm h}(q)}{2})$ [364], with $m_{\rm h}(q) = q(2q+1)$ (the other degenerate state –sometimes called Antineel for $\Delta \to \infty$– is obtained by sending $q \to -q$ with the net effect of having $m_{\rm h}(q) = q(2q-1)$). The first panel of Fig. 7.7 reports the structure of the entanglement spectrum of a semi-infinite subsystem based on this result. Exploting (7.4.9) with $n = 1$ and (1.4.17), we obtain $p(q)$ when the subsystem is half of the inifinite chain. It reads

$$p_{\rm h}(q) = \frac{e^{-2\epsilon q(2q+1)}}{\theta_3\left(i\epsilon|e^{-4\epsilon}\right)} \tag{7.5.4}$$

where ϵ is given by (7.4.2). The subscript h has been introduced just to stress that the result (7.5.4) holds for the case of semi-infinite subsystem, in contrast with the results reported in the following subsections for finite blocks.

Now, still following the approach of Ref. [364], we explain how to use these results to obtain the entanglement spectrum of a finite large interval. As long as ℓ is larger than the correlation length, the reduced density matrix ρ_ℓ of a single interval with two boundaries factorises into $\rho_L \otimes \rho_R$, where $\rho_{L/R}$ are the reduced density matrices for the semi-infinite lines having the left/right end-point of the interval. The combination of these two spectra into a single one is graphically reported in Fig. 7.7. We show both cases for even and odd subsystems (center and right respectively). For an even subsystem we should combine two different spectra $m_L(x) = m_{\rm h}(x) = x(2x+1)$ and $m_R(x) = m_{\rm a}(x) = x(2x-1)$ from left and right. Conversely, for odd blocks, the left and the right spectra to combine are equal, e.g. $m_L(x) = m_R(x) = x(2x+1)$. The final results for the degeneracies are reported in the figure. In the even case, we have that the degeneracy at fixed q at level s can be written as $\mathcal{F}_{\rm e}(q, s) = \mathcal{P}_{\rm e}(\frac{s-m_{\rm e}(q)}{2})$ with $m_{\rm e}(q) = q^2$ and $p_{\rm e}$ generated by

$$\sum_{s=0} \mathcal{P}_{\rm e}(s)x^s = \prod_{k\geq 1} \frac{(1+x^k)^2}{1-x^k}\,, \tag{7.5.5}$$

leading to the generating function for the total degeneracy $D_{\rm e}(s)$ of level s

$$\sum_{s=0} D_{\rm e}(s)x^s = \prod_{k\geq 1}(1+x^k)^2. \tag{7.5.6}$$

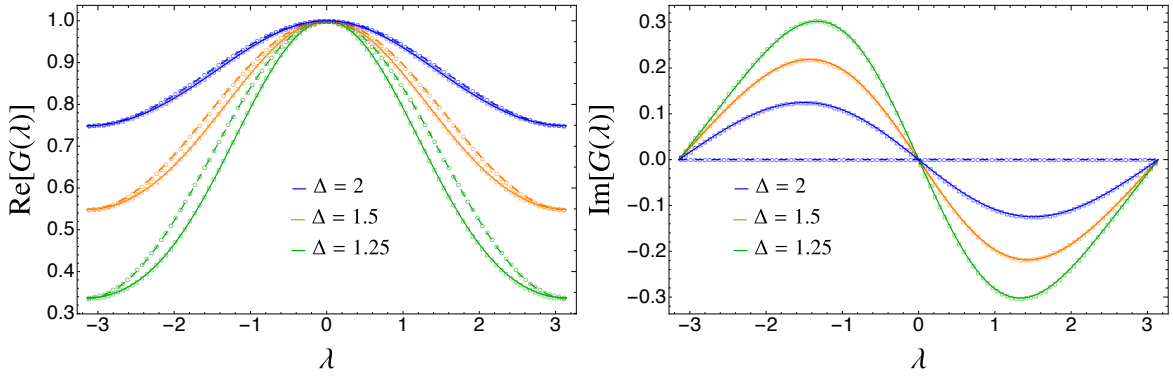

Figure 7.8: Full counting statistics generating functions $G(\lambda)$ for the gapped XXZ spin chain for three values of Δ. The left (right) panel is the real (imaginary) part of $G(\lambda)$. The symbols are the iTEBD data that perfectly match the superimposed analytic predictions (full lines for odd ℓ and dashed for even ℓ). The data are for infinite chains and subsystems equal to $\ell = 200$ (circles) or 201 (squares). Notice that the real parts for even and odd q are qualitatively similar, but quantitatively different.

Notice that while the generating function for $D_{\rm e}(s)$ is the square of the one for $D_{\rm h}(s)$, the same is not true for $\mathcal{P}_{\rm e}$. Again we employ the convention $\mathcal{P}_{\rm e}(x) = 0$ for negative numbers and for half-integers.

For odd blocks, it is more complicated to combine the two spectra for even and odd q. The degeneracies of both sectors have the generating function

$$\sum_{s=0} \mathcal{P}^{\rm b}_{\rm o}(s) x^s = \prod_{k\geq 1} \frac{(1-x^{2k})^3}{(1-x^k)^2(1-x^{4k})^2}, \tag{7.5.7}$$

where even (odd) powers of x correspond to even (odd) values of q. However, a single generating function for different q is not a too useful tool to write symmetry resolved quantities. Exploiting some identities of theta functions $\theta_{2,3}$, we can extract the even and the odd part of (7.5.7) we are interested in. After some algebra we get (for $x > 0$)

$$\sum_{s=0} \mathcal{P}_{\rm o}(s,q) x^s = \frac{(\theta_2(x^4))^{\frac{1-(-1)^q}{2}} (\theta_3(x^4))^{\frac{1+(-1)^q}{2}}}{\prod_{k\geq 1}(1+x^{2k})(1-(-x)^k)(1-x^k)}, \tag{7.5.8}$$

which does depend on the parity of q. Hence the degeneracy of the level s with fixed q is

$$\mathcal{F}_{\rm o}(q,s) = \mathcal{P}_{\rm o}(s - m_{\rm o}(q)), \tag{7.5.9}$$

with $m_{\rm o}(q) = q^2 - q$. Indeed $m_{\rm o}(q)$ and $m_{\rm o}(q)+1$ are the two parabolas in Fig. 7.7, envelopes of the largest eigenvalues of the RDM for even and odd q respectively. The generating function for the total degeneracy $D_{\rm o}(s)$ of level s is the same as $D_{\rm e/h}(s)$ in Eq. (7.5.6).

7.5.2 Full counting statistics: even number of sites

The easiest way to get the PDF $p_{\rm e}(q)$ for the interval is to combine the PDFs at the right and left boundary as

$$p_{\rm e}(q) = \sum_{q_1=-\infty}^{\infty} p_L(q_1) p_R(q-q_1) = \sum_{q_1=-\infty}^{\infty} p_{\rm h}(q_1) p_{\rm h}(q_1 - q), \tag{7.5.10}$$

where we used that the PDF at the two boundaries are $p_L(q) = p_{\rm h}(q_1)$ and $p_R(q) = p_{\rm h}(-q)$. The sum is easily rewritten as

$$p_{\rm e}(q) = \mathcal{N}^2 e^{-2\epsilon(q^2-1/4)} \sum_{q_1=-\infty}^{\infty} e^{-2\epsilon(2q_1+q+1/2)^2}. \tag{7.5.11}$$

The remaining sum over q_1 does not depend on q, for integer q. Hence the PDF is Gaussian

$$p_{\rm e}(q) = \mathcal{N}_{\rm e} e^{-2q^2\epsilon}, \tag{7.5.12}$$

and the normalisation factor is $\mathcal{N}_{\rm e}^{-1} = \sum_q e^{-2q^2\epsilon} = \theta_3(e^{-2\epsilon})$. The FCS is the Fourier series (7.5.3) which immediately leads to

$$G_{\rm e}(\lambda) = \frac{\theta_3\left(\frac{\lambda}{2}, e^{-2\epsilon}\right)}{\theta_3(e^{-2\epsilon})}. \tag{7.5.13}$$

Notice that this is real and even in λ. As a cross check, the same result is re-obtained by directly summing over the eigenvalues of the RDM with the degeneracies reported in Fig. 7.7 (to perform the sum, one exploits (7.5.5) the product representation of the θ_3 function [368]).

The FCS generating function is directly measured in iTEBD simulations [422], as explained in details, e.g., in Refs. [406, 416]. The results in the thermodynamic limit for three values of $\Delta > 1$ and for $\ell = 200$ are shown in Figure 7.8. The agreement is always excellent (data and predictions are superimposed) for all considered values of Δ. We mention that as Δ gets close to 1, one should consider much larger values of ℓ to reach such good agreement due to the diverging correlation length at the isotropic point.

7.5.3 Full counting statistics: odd number of sites

Also for this case, the PDF can be obtained combining two single-boundary ones as

$$p_{\rm o} = \sum_{q_1=-\infty}^{\infty} p_L(q_1) p_R(q-q_1) = \sum_{q_1=-\infty}^{\infty} p_{\rm h}(q_1) p_{\rm h}(q-q_1), \tag{7.5.14}$$

where we used that the PDF at the two boundaries are the same. Again, the sum is easily rewritten as

$$p_{\rm o}(q) = \mathcal{N}^2 e^{-2\epsilon(q^2-q)} \sum_{q_1=-\infty}^{\infty} e^{-2\epsilon(2q_1-q)^2}. \tag{7.5.15}$$

However, this time the remaining sum *does* depend on the parity of q. Performing this sum, the PDF is

$$p_{\rm o}(q) = \mathcal{N}_{\rm o} e^{-2\epsilon(q^2-q)} \times \begin{cases} \theta_3(e^{-8\epsilon}), & q \text{ even}, \\ \theta_2(e^{-8\epsilon}), & q \text{ odd}, \end{cases} \tag{7.5.16}$$

with $\mathcal{N}_0$ easily obtained from the normalisation.

The FCS is the Fourier series (7.5.3) which, after some manipulations using the properties of theta functions, leads to

$$G_{\rm o}(\lambda) = \left(\frac{\theta_3\left(i\epsilon - \frac{\lambda}{2}, e^{-4\epsilon}\right)}{\theta_3(i\epsilon, e^{-4\epsilon})} \right)^2. \tag{7.5.17}$$

Notice that this FCS has a non-vanishing and non-trivial imaginary part, but satisfy $G_{\rm o}(\lambda)^* = G_{\rm o}(-\lambda)$. Again, as a cross check, this result is re-obtained by directly summing over the eigenvalues of the RDM with the degeneracies reported in Fig. 7.7.

Also for odd ℓ, the analytical prediction (7.5.17) is tested against iTEBD simulations in Figure 7.8. In these simulations, we measure the FCS of the operator S^z_ℓ and not δS^z_ℓ; hence the numerical data have been divided by $e^{i\lambda/2}$. After this normalisation, the agreement between data and prediction is extremely good in all considered cases.

7.5.4 Byproduct: symmetry resolved entropies

In order to further highlight the relation between the FCS and the SRREs, in this subsection we compute the SRREs for subsystems made by a finite number of sites. The symmetry resolution of the entanglement spectrum reported in Figure 7.7 allows us to access the symmetry resolved moments (1.4.17) as

$$\mathcal{Z}_n(q) \equiv \sum_{s\in\mathcal{S}_q} \lambda_s^n = \frac{\sum_j \mathcal{F}_\alpha(q,s)e^{-2n\epsilon s}}{\big(\sum_j D_\alpha(s)e^{-2\epsilon s}\big)^n}\,, \tag{7.5.18}$$

where $\alpha \in \{\mathrm{h},\mathrm{e},\mathrm{o}\}$ and $\mathcal{F}_\alpha(q,s)$ and $D_\alpha(s)$ are respectively the degeneracies of the s-th eigenvalue for fixed q and total for the three cases of interest. In the definition of the SRREs given by (1.4.18) only the ratio $\mathcal{Z}_n(q)/\mathcal{Z}_1^n(q)$ matters and therefore the dependence on $D_\alpha(s)$ cancels leading to

$$\frac{\mathcal{Z}_n(q)}{\mathcal{Z}_1^n(q)} = \frac{\sum_s \mathcal{F}_\alpha(q,s)e^{-2n\epsilon s}}{\Big(\sum_s \mathcal{F}_\alpha(q,s)e^{-2\epsilon s}\Big)^n} = \frac{\sum_s \mathcal{P}_\alpha(s)e^{-2an\epsilon s}}{\Big(\sum_s \mathcal{P}_\alpha(s)e^{-2a\epsilon s}\Big)^n}, \tag{7.5.19}$$

where $\alpha \in \{\mathrm{h},\mathrm{e},\mathrm{o}\}$ and in the last equality we used $\mathcal{F}_\alpha(q,s) = \mathcal{P}_\alpha(\frac{s-m_\alpha(q)}{a})$ (with $a=2$ for semi-infinite and even ℓ, while $a=1$ for odd ℓ) and shifted the sum as $(s-m_\alpha(q))/a \to s$ (notice that the actual value of $m_\alpha(q)$ is unessential).

Combining (7.5.19) with $\alpha = \mathrm{h}$ and (7.4.7), we recover the SRREs for the semi-infinite line given by (7.4.12).

Now we derive the entropies for a finite interval of both even and odd length. For even ℓ, the two sums in (7.5.19) with $\alpha = \mathrm{e}$ can be rewritten in terms of generating functions (7.5.5) (with $x = e^{-4n\epsilon}$), obtaining

$$S^{\mathrm{e}}_n(q) = \frac{\displaystyle\sum_{k=1}^{\infty}\Big[\log\frac{(1+e^{-4n\epsilon k})^2}{1-e^{-4n\epsilon k}} - n\log\frac{(1+e^{-4\epsilon k})^2}{1-e^{-4\epsilon k}}\Big]}{1-n}. \tag{7.5.20}$$

Very importantly, the SRREs are *not the double* of the single resolved entropies (7.4.12) for the half line as it is the case for the total one (mathematically this is a consequence of the relation between the generating function for $D_{\mathrm{e}}(s)$ and $D_{\mathrm{h}}(s)$, but not for $\mathcal{P}_{\mathrm{e}}$ and $\mathcal{P}_{\mathrm{h}}$). Also, these SRREs are independent of q and hence satisfy the equipartition of entanglement [85] exactly.

In the very same fashion, we can repeat the calculation for odd ℓ, setting $\alpha = \mathrm{o}$ in (7.5.19) and obtaining the more cumbersome expression

$$\begin{aligned} S^{\mathrm{o}}_n(q) = \frac{1}{1-n}\Bigg[\sum_{k=1}^{\infty}\Bigg(& n\log(1+e^{-4\epsilon k})(1-e^{-2\epsilon k})(1-(-)^k e^{-2\epsilon k}) \\ & - \log(1+e^{-4\epsilon nk})(1-e^{-2\epsilon nk})(1-(-)^k e^{-2\epsilon nk})\Bigg) \\ & + \frac{1+(-)^q}{2}(\log\theta_3(e^{-8\epsilon n}) - n\log\theta_3(e^{-8\epsilon}) + \frac{1-(-)^q}{2}(\log\theta_2(e^{-8\epsilon n}) - n\log\theta_2(e^{-8\epsilon})\Bigg]. \end{aligned} \tag{7.5.21}$$

Hence, for odd ℓ, the SRREs do depend on the parity of q and the equipartition of entanglement is explicitly broken.

We finally mention, as a highly non-trivial crosscheck, that it is possible, but cumbersome, to sum over the various sectors q in order to recover the total entanglement through (1.3.5), both for even and odd ℓ.

7.6 Closing remarks

In this Chapter we found exact results for the SRREs of half line in infinite integrable systems in the gapped regime. We considered two models for which the RDM (and therefore the entanglement spectrum) of the subsystem can be obtained through the Baxter CTM. We applied this tool to investigare the symmetry resolution of entanglement in the massive regime of the complex harmonic chain and for the XXZ chain in the antiferromagnetic gapped regime. Finally, we computed the FCS of the transverse magnetisation in gapped XXZ chains within a spin block of length ℓ, for ℓ larger than the correlation length.

Let us mention some possible directions for future investigations motivated by the results we have presented in this Chapter. A first and natural question is to understand what happens when integrability is absent: while a general treatment seems impossible, the results for the entanglement spectrum in Refs. [364,381] suggests that in some non-trivial regimes general results may be derived. Finally, one expects that the symmetry resolved entanglement should help in reconstructing the entanglement (or modular) Hamiltonian, but it is still unclear how. This issue is very timely given the large current effort devoted to understand the structure of the entanglement Hamiltonians both in field theories and lattice models, as we will explain in Chapter 12.

7.A Details for the complex harmonic chain

7.A.1 A two-site chain with complex oscillators

For a single harmonic chain with two sites, the RDM has been worked out e.g. in [167]. The entanglement Hamiltonian of one site is

$$\mathcal{H}_A = \varepsilon \beta^\dagger \beta. \tag{7.A.1}$$

For this site, the β's are related to the a's as

$$\beta = a \cosh\theta + a^\dagger \sinh\theta\,, \tag{7.A.2}$$

which is the specialisation of Eq. (7.3.12) to the case of A being one site. Here $e^\theta = (1+\omega_0^2/4)^{1/4}$, but its explicit value is unimportant. Hence, in terms of the ladder operators $a, a^\dagger$, $\mathcal{H}_A$ can be rewritten as

$$\mathcal{H}_A = \varepsilon \left(\frac{1}{2}(a^{\dagger 2} + a^2) \sinh 2\theta + a^\dagger a \cosh^2\theta + a a^\dagger \sinh^2\theta \right). \tag{7.A.3}$$

Rather then one real harmonic oscillator, we consider a complex one, which is the same as two real harmonic oscillators described by the ladder operators $a_i^\dagger, a_i$, $i = x, y$ such that the only non-vanishing commutators are $[a_i, a_i^\dagger] = 1$, $i = x, y$. Therefore, the entanglement Hamiltonian of these two real harmonic oscillators is simply the sum of two single ones:

$$\mathcal{H}_A = \sum_{i=x,y} \varepsilon \left(\frac{1}{2}(a_i^{\dagger 2} + a_i^2) \sinh 2\theta + a_i^\dagger a_i \cosh^2\theta + a_i a_i^\dagger \sinh^2\theta \right). \tag{7.A.4}$$

Let us rewrite Eq. (7.A.4) in terms of the particle and antiparticle ladder operators a and b in Eq. (7.3.13), i.e.

$$\begin{aligned} a_x &= \frac{1}{\sqrt{2}}(a+b) \qquad a_x^\dagger = \frac{1}{\sqrt{2}}(a^\dagger + b^\dagger) \\ a_y &= \frac{1}{\sqrt{2}i}(a-b) \qquad a_y^\dagger = \frac{1}{\sqrt{2}i}(b^\dagger - a^\dagger). \end{aligned} \tag{7.A.5}$$

One can check that $[a, a^\dagger] = [b, b^\dagger] = 1$, while all other commutators vanish. Plugging Eqs. (7.A.5) into Eq. (7.A.4), we obtain

$$\mathcal{H}_A = \varepsilon \left((a^\dagger b^\dagger + ab) \sinh 2\theta + (a^\dagger a + b^\dagger b) \cosh^2\theta + (aa^\dagger + bb^\dagger) \sinh^2\theta \right), \tag{7.A.6}$$

or, equivalently (up to an additive constant we can absorb in the normalisation factor of the RDM)

$$\mathcal{H}_A = \varepsilon \left((a^\dagger b^\dagger + ab) \sinh 2\theta + (a^\dagger a + bb^\dagger) \cosh 2\theta \right). \tag{7.A.7}$$

One can bring Eq. (7.A.7) into a diagonal form through Bogoliubov transformations, i.e.

$$\begin{aligned} \alpha &= \cosh\theta\, a + \sinh\theta\, b^\dagger, \qquad \alpha^\dagger = \cosh\theta\, a^\dagger + \sinh\theta\, b, \\ \gamma &= \sinh\theta\, a + \cosh\theta\, b^\dagger, \qquad \gamma^\dagger = \sinh\theta\, a^\dagger + \cosh\theta\, b, \end{aligned} \tag{7.A.8}$$

where $[\alpha, \alpha^\dagger] = [\gamma, \gamma^\dagger] = 1$, while $[\alpha, \gamma] = 0$. As a result, one finds that the RDM for one single complex harmonic oscillator ρ_1 has the form

$$\rho_1 = K e^{-\mathcal{H}_A}, \qquad \mathcal{H}_A = \varepsilon \left(\alpha^\dagger \alpha + \gamma^\dagger \gamma \right). \tag{7.A.9}$$

Since the operators γ and α commute, we can rewrite Eq. (7.A.9)

$$\rho_1 = K e^{-\mathcal{H}_A^{(\alpha)}} \otimes e^{-\mathcal{H}_A^{(\gamma)}}. \tag{7.A.10}$$

7.A.2 The Bogoliubov transformation for a chain of arbitrary length

For a real harmonic chain of arbitrary length $2L$, the entanglement Hamiltonian for half system is [167]

$$\mathcal{H}_A = \sum_{j=0}^{L-1} \varepsilon_j \beta_j^\dagger \beta_j, \tag{7.A.11}$$

where the eigenvalues ε_j depend on L and in the thermodynamic limit are given by Eq. (7.3.10) while for $L = 1$ by Eq. (7.A.1).

The ladder operator β_j as function of the local ladder operators are given by Eq. (7.3.12), i.e.

$$\beta_j = \sum_{i \in A} g_{ji} a_i + h_{ji} a_i^\dagger. \tag{7.A.12}$$

Hence, the entanglement Hamiltonian in terms of local operators is

$$\mathcal{H}_A = \sum_j \varepsilon_j \sum_{i_1, i_2} \left(g_{i_1 j}^* g_{j i_2} a_{i_1}^\dagger a_{i_2} + g_{i_1 j}^* h_{j i_2} a_{i_1}^\dagger a_{i_2}^\dagger + h_{i_1 j}^* g_{j i_2} a_{i_1} a_{i_2} + h_{i_1 j}^* h_{j i_2} a_{i_1} a_{i_2}^\dagger \right). \tag{7.A.13}$$

Therefore, the entanglement Hamiltonian of a complex chain is just the sum of two real ones with local ladder operators $a_{a,j}$ with $a = x, y$ as in the case of two oscillators in the previous subsection. Such $\mathcal{H}_A$ can be rewritten in terms of the particle and antiparticle ladder operators in Eq. (7.3.13), obtaining (up to constants)

$$\mathcal{H}_A = \sum_j \varepsilon_j \sum_{i_1,i_2} \left((g^*_{i_1 j} g_{j i_2} + h^*_{i_1 j} h_{j i_2})(a^\dagger_{i_1} a_{i_2} + b^\dagger_{i_1} b_{i_2}) + g^*_{i_1 j} h_{j i_2} a^\dagger_{i_1} b^\dagger_{i_2} + h^*_{i_1 j} g_{j i_2} a_{i_1} b_{i_2} \right), \quad (7.A.14)$$

which we can put in the diagonal form

$$\mathcal{H}_A = \sum_{j=0}^{\infty} \varepsilon_j (\alpha^\dagger_j \alpha_j + \gamma^\dagger_j \gamma_j), \quad (7.A.15)$$

by the transformation (7.3.14).

Chapter 8

Symmetry resolved entanglement in 2d systems via dimensional reduction

We continue with the study of entanglement resolution in $2d$ many-body systems of free bosons and fermions by *dimensional reduction*. When the subsystem is translational invariant in a transverse direction, this strategy allows us to reduce the initial two-dimensional problem into decoupled one-dimensional ones in a mixed space-momentum representation. While the idea straightforwardly applies to any dimension d, here we focus on the case $d = 2$ and derive explicit expressions for two lattice models possessing a $U(1)$ symmetry, i.e., free non-relativistic massless fermions and free complex (massive and massless) bosons. Our derivation gives a transparent understanding of the well known different behaviours between massless bosons and fermions in $d \geq 2$: massless fermions presents logarithmic violation of the area which instead strictly hold for bosons, even massless. This is true both for the total and the symmetry resolved entropies. Interestingly, we find that the equipartition of entanglement into different symmetry sectors holds also in two dimensions at leading order in subsystem size; we identify for both systems the first term breaking it. All our findings are quantitatively tested against exact numerical calculations in lattice models for both bosons and fermions. This Chapter is based on Ref. [100].

8.1 Introduction

One of the most fascinating aspects of the entanglement entropy in the ground states of extended quantum systems is that it scales with the area of a subsystem rather than its volume, as it happens, instead, for generic eigenstates in the middle of the spectrum. We have already mentioned in the introduction that this feature is known as *area law* [15]. In higher dimensions, massless systems behave rather differently depending on the fine details of the model. It is impossible to mention all aspects of the problem, but the most striking feature is that while free massless non-relativistic fermions show logarithmic violations of the area law [97, 423–430, 650], in free massless bosons it strictly holds [170, 194, 423, 431–433]. Despite in general it is not known how the entanglement scales in interacting massless bosons and fermions, there are indications that the structure found for free systems should be robust also against interactions, see e.g. Refs. [188, 434–444].

A natural and transparent way to see this fundamental difference between free bosons and fermions is *dimensional reduction*, a strategy for the computation of the entanglement entropy first suggested in [170] and since then exploited in many different circumstances. The idea is very simple: if the subsystem of a free $2d$ model is translational invariant in one compact direction (that we call transverse, say along the y-axis), we can perform Fourier transform in this direction and reduce the problem to the sum of $1d$ ones, for which exact results are known. Two examples

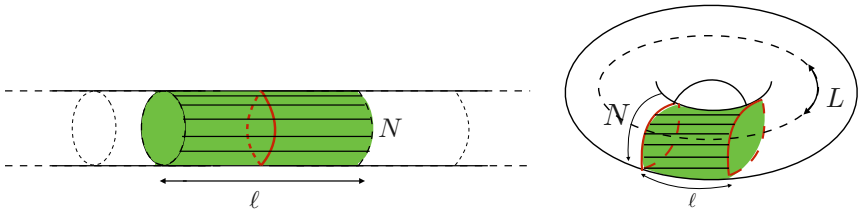

Figure 8.1: The geometries of the $2d$ systems we study in this Chapter: along the longitudinal x-direction the system is either infinite (left) or finite with length L (right). In both cases, periodic boundary conditions are imposed along the transverse y-direction of size N. The geometry is then either an infinite cylinder (left) or a torus (right). The entangling region is always a periodic strip of length ℓ along the x-axis, as highlighted in green.

of geometries for which the dimensional reduction works are shown in Figure 11.1 and they are the only ones we will consider in this Chapter. Actually, this technique can be straightforwardly applied in generic dimensions d (with $d-1$ compact ones), but we focus here in $2d$ for clarity of the presentation (the only difference in the final result is just the sum over many transverse components).

The organisation of the Chapter is the following. In Sec. 8.2 we will do a brief recap of the needed $1d$ results for bosons [98] and fermions [90,91]. Secs. 8.3 and 8.4 are the core of the Chapter, where we derive our results for total and symmetry resolved entropies for fermions and bosons, respectively, by applying the dimensional reduction. Step by step, we benchmark our analytic results against exact numerical computations. We draw our conclusions in Sec. 8.5.

8.2 One-dimensional recap

In this section, we provide an overview of the the results about one-dimensional models that we will need for the dimensional reduction in the following sections.

We start by considering the one-dimensional tight binding model, i.e., the free spinless fermions described by the Hamiltonian

$$H_{FF} = -\frac{1}{2}\sum_i \left(c^\dagger_{i+1}c_i + c^\dagger_i c_{i+1}\right) + \sum_i \mu c^\dagger_i c_i, \tag{8.2.1}$$

where μ is the chemical potential. We only focus on the ground state here. When $|\mu| < 1$ the theory is gapless. The Jordan Wigner transformation maps the model to the spin-1/2 XX chain in a magnetic field. We consider the subsystem A to be an interval made of ℓ consecutive sites. For large ℓ, the asymptotic scaling of the entanglement entropies is given by [268, 445]

$$S_n = \frac{1+n^{-1}}{6}\log\left(2\ell\sin k_F\right) + \frac{\Upsilon_n(0)}{1-n}, \tag{8.2.2}$$

where $k_F = \arccos(\mu/2)$ is the Fermi momentum. The leading logarithmic term in Eq. (8.2.2) is universal and follows from conformal field theory [17, 20, 21, 62]; in contrast, the non-universal constant $\Upsilon_n(0)$ has been derived using the Fisher-Hartwig conjecture [268]. For a finite system of length L with PBC's, the same form also holds replacing ℓ with $\frac{L}{\pi}\sin\frac{\pi\ell}{L}$ [20]. In the one-dimensional tight-binding model, the generalised Fisher-Hartwig conjecture has been also used to obtain the asymptotic behaviour of the SRREs at leading and subleading orders [90, 91]. The

charged moments are

$$\log Z_n(\alpha) = \frac{ik_F\ell}{\pi}\alpha - \left[\frac{1}{6}\left(n-\frac{1}{n}\right) + \frac{2}{n}\left(\frac{\alpha}{2\pi}\right)^2\right]\log 2\ell\sin k_F + \Upsilon_n(\alpha) + o(1), \tag{8.2.3}$$

where $\Upsilon_n(\alpha)$ has been defined in Eq. (2.3.16). Taking the Fourier transforms and expanding for large ℓ, one gets for the SRREs at the leading orders [90]

$$S_n(q) = S_n - \frac{1}{2}\log\left(\frac{2}{\pi}\log(2\ell\sin k_F)\right) + \frac{\log n}{2(1-n)} + o(1). \tag{8.2.4}$$

The first term breaking equipartition appears at order $O(1/(\log\ell)^2)$ [90].

Exact results are available also for free bosonic systems on the lattice, i.e., for the harmonic chain. In this case, one exploits the Baxter corner transfer matrix (CTM) approach [179], as we reviewed in Chapter 7. In the following, we will mainly be interested in systems with a $U(1)$ internal symmetry. We then consider a complex bosonic theory which on the lattice is a chain of complex oscillators (we dub complex or double harmonic chain). The entanglement resolution has been also investigated for off-critical quantum bosonic chains through the Baxter's CTM for the bipartition in two semi-infinite systems, as we described in Chapter 7.

8.3 Two-dimensional Free Fermions

In this section we compute the REEs and the SRREs in the ground state of a two-dimensional free fermionic system. For the total entropies, our results confirm the known logarithmic violation of the area law [424–428], which generalises also to the symmetry resolved analogue.

8.3.1 The model and the bipartition

Let us consider a quadratic fermionic system on a two-dimensional square lattice with isotropic hopping between nearest-neighbour sites. It is described by the following Hamiltonian

$$H_{FF} = -\frac{1}{2}\sum_{\langle\mathbf{i},\mathbf{j}\rangle}(c^\dagger_{\mathbf{i}}c_{\mathbf{j}} + c^\dagger_{\mathbf{j}}c_{\mathbf{i}}) + \mu\sum_{\mathbf{i}} c^\dagger_{\mathbf{i}}c_{\mathbf{i}}, \tag{8.3.1}$$

where μ is the chemical potential for the spinless fermions $c_{\mathbf{i}}$, with $\mathbf{i} = (i_1, i_2)$ a vector identifying a given lattice site, and $\langle\mathbf{i},\mathbf{j}\rangle$ stands for nearest neighbours. Specifically, we consider a set of N coupled identical parallel chains, hence N is the finite length along one direction (say the y-axis). In the other direction, say the x-axis, the system is either infinite or finite with length L. PBC's are imposed along the y-axis. The subsystem A is a (periodic) strip of length ℓ along the x-axis, (see Figure 11.1). Given the special geometry we consider, we can take the Fourier transform along the transverse y direction. The partial Fourier transforms $\tilde{c}_{j_1,r}$ and its inverse are

$$\tilde{c}_{j_1,r} = \frac{1}{\sqrt{N}}\sum_{j=0}^{N-1} c_{j_1,j}e^{-2\pi ijr/N}, \qquad c_{j_1,j_2} = \frac{1}{\sqrt{N}}\sum_{r=0}^{N-1}\tilde{c}_{j_1,r}e^{2\pi ij_2r/N}, \tag{8.3.2}$$

leading to the Hamiltonian in mixed space-momentum representation

$$H_{FF} = \sum_{r=0}^{N-1} H_{k_y^{(r)}}. \tag{8.3.3}$$

The operator $H_{k_y^{(r)}}$ is the Hamiltonian in the $k_y^{(r)} = \frac{2\pi r}{N}$ transverse momentum sector:

$$H_{k_y^{(r)}} = -\frac{1}{2}\sum_{i=1}^{L}\left(\tilde{c}^\dagger_{i,r}\tilde{c}_{i+1,r} + \text{h.c.}\right) + \sum_i \mu_r \tilde{c}^\dagger_{i,r}\tilde{c}_{i,r}, \tag{8.3.4}$$

where

$$\mu_r = \mu - \cos k_y^{(r)}, \tag{8.3.5}$$

and L is the length of the chain along the x-axis. In this way, the Hamiltonian is mapped to a sum of N independent one-dimensional chains with chemical potential μ_r depending on the transverse momentum $k_y^{(r)}$.

We focus on the critical regime of the whole $2d$ system, which is in attained for $0 < \mu < 2$. In terms of the one dimensional systems, this constraint on μ means that all transverse modes with $|\mu_r| < 1$ are critical, while the others are not. This inequality is satisfied for

$$r \in \Omega_\mu = \left[0, \frac{\arccos(\mu-1)N}{2\pi}\right[\cup \left]N\left(1 - \frac{\arccos(\mu-1)}{2\pi}\right), N-1\right]. \tag{8.3.6}$$

The inner extremes of the intervals are not part of Ω_μ. The case $\mu = 0$ deserves particular attention: when dealing with a finite number of chains, also the mode $r = 0$ has to be removed from Ω_μ. This difference is irrelevant in the limit $N \to \infty$ when the fraction of critical chains is simply given by $\frac{\arccos(\mu-1)}{\pi}$.

Since the Hamiltonian is a sum of different sectors, the ground state density matrix factorises and so does the RDM

$$\rho_A = \bigotimes_{r=1}^{N} \rho^A_{k_y^{(r)}} = \bigotimes_{r\in\Omega_\mu} \rho^A_{k_y^{(r)}}. \tag{8.3.7}$$

In the last equality, we stress that the only relevant modes are the ones corresponding to critical 1d chains. The blocks corresponding to non-critical chains are projectors on the 1d vacuum state, i.e. without fermions. As a consequence, hereafter, we only take into account the gapless modes, which belong to Ω_μ. The RDM $\rho^A_{k_y^{(r)}}$ of the 1d subsystem associated to the r-th mode can be written as [169, 171, 366]

$$\rho^A_{k_y^{(r)}} = \det C_{k_y^{(r)}} \exp\left(\sum_{i,j}[\log(C^{-1}_{k_y^{(r)}} - 1)]_{i,j}\tilde{c}^\dagger_{i,r}\tilde{c}_{j,r}\right), \tag{8.3.8}$$

where the matrix $C_{k_y^{(r)}} \equiv \langle \tilde{c}^\dagger_{i,r}\tilde{c}_{j,r}\rangle$ is the correlation matrix restricted to the r-th subsystem A. The entanglement entropy is easily expressed in terms of the eigenvalues of such correlation matrix.

We start by considering the model in the thermodynamic limit in the longitudinal (x) direction, i.e., $L \to \infty$ (Figure 11.1, left panel). For the ground-state of N infinite chains the correlation matrix $\mathbf{C}$ of the whole (two-dimensional) subsystem can be written as

$$\mathbf{C} = \oplus_r C_{k_y^{(r)}}, \tag{8.3.9}$$

where $C_{k_y^{(r)}}$ reads

$$C_{k_y^{(r)}}(i,j) = \frac{\sin k_r^F (i-j)}{\pi(i-j)}, \qquad k_r^F = \arccos\mu_r, \tag{8.3.10}$$

as a function of the Fermi momentum k_r^F of each r-th chain (μ_r is given in Eq. (8.3.5)). This is due to the factorisation of the Hilbert space into the different modes, which corresponds to a block diagonal structure of the correlation matrix: each block is associated to a transverse mode and, as a consequence, to a given 1d ground state.

8.3.2 Rényi and Entanglement Entropies

From the structure of the Hamiltonian in Eq. (8.3.3), the Rényi entropies can be computed by invoking the one-dimensional results [268]: the entanglement entropy is additive on tensor products and therefore decomposes as

$$S_n^{2d}\left(\bigotimes_{r\in\Omega_\mu}\rho^A_{k_y^{(r)}}\right)=\sum_{r\in\Omega_\mu}S^{1d}_{n,r},\qquad S^{1d}_{n,r}=\frac{1}{6}\Big(1+\frac{1}{n}\Big)\log(2\ell\sin k_r^F)+\Upsilon_n+o(1),\tag{8.3.11}$$

where Υ_n is $\Upsilon_n(\alpha=0)/(1-n)$ in Eq. (2.3.16).

Note that in our setting, the Fermi momentum of each transverse mode-chain can be explicitly written down as

$$\sin k_r^F=\sqrt{1-\left(\mu-\cos\left(\frac{2\pi r}{N}\right)\right)^2}.\tag{8.3.12}$$

Plugging this relation into Eq. (8.3.11) we get

$$S_n^{2d}=\frac{f_N(\mu)N}{6}\Big(1+\frac{1}{n}\Big)\log(2\ell)+f_N(\mu)N\Upsilon_n+\frac{1}{12}\Big(1+\frac{1}{n}\Big)\sum_{r\in\Omega_\mu}\log\left[1-\left(\mu-\cos\left(\frac{2\pi r}{N}\right)\right)^2\right],\tag{8.3.13}$$

where $f_N(\mu)$ denotes the fraction of critical modes (i.e., the number of modes belonging to Ω_μ divided by N). It is useful to define also the quantity

$$A_N(\mu)=\frac{1}{2N}\sum_{r\in\Omega_\mu}\log\left[1-\left(\mu-\cos\left(\frac{2\pi r}{N}\right)\right)^2\right],\tag{8.3.14}$$

so that we have

$$S_n^{2d}=\frac{1}{6}\Big(1+\frac{1}{n}\Big)\Big(f_N(\mu)\log\,2\ell+A_N(\mu)\Big)N+Nf_N(\mu)\Upsilon_n,\tag{8.3.15}$$

As aforementioned, when $N\to\infty$ the prefactor of the logarithmic term simply becomes

$$Nf_\infty(\mu)=N\frac{\arccos(\mu-1)}{\pi}.\tag{8.3.16}$$

In the left panel of Figure 8.2 we report $f_N(\mu)$ as function of N for a few values of μ, showing the approach to $N\to\infty$.

In the right panel of Figure 8.2 we report a similar plot for $A_N(\mu)$, as function of N for four different values of μ. As N increases, it approaches an asymptotic value that can be explicitly calculated. In fact, in the limit of large N, the sum in Eq. (8.3.13) turns into

$$\begin{aligned}&\frac{1}{2}\sum_{r\in\Omega_\mu}\log\left|1-\left(\mu-\cos\left(\frac{2\pi r}{N}\right)\right)^2\right|\to\\&\frac{N}{2\pi}\int_0^{\arccos(\mu-1)}dx\,\log\Big(1-(\mu-\cos(x))^2\Big)-\frac{1-\log(2\pi\sqrt{\mu(2-\mu)})+\log N}{2},\end{aligned}\tag{8.3.17}$$

where we have subtracted the (divergent) contribution from the upper extreme of integration, corresponding to the modes $r=\{f_\infty(\mu)N,(1-f_\infty(\mu))N\}$, which are excluded from the sum in

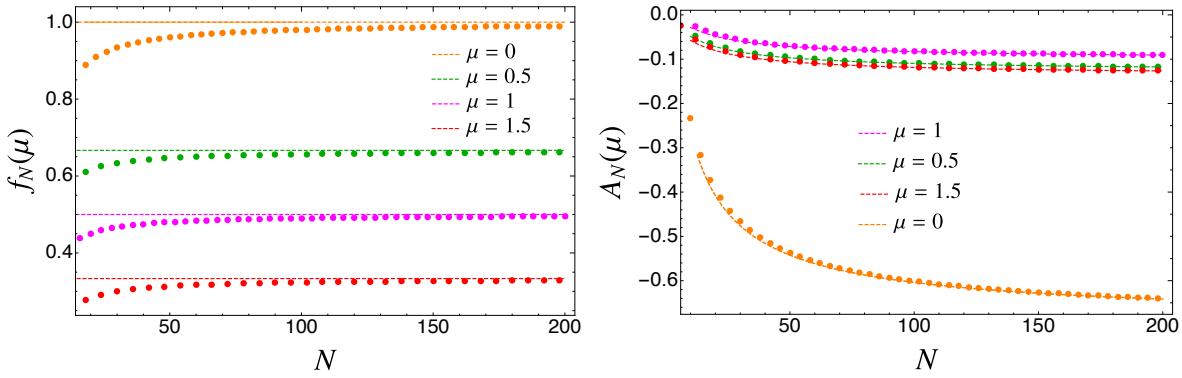

Figure 8.2: Left panel: The fraction of critical modes, $f_N(\mu)$, is plotted as a function of length N of the transverse direction for four different values of chemical potential μ. The curves approach the constant value reported in Eq. (8.3.16) and plotted as dashed lines. Right panel: The function $A_N(\mu)$ in Eq. (8.3.14) as a function of N for four different values of chemical potential μ. For all μ, the curves approach $A_\infty(\mu)$ reported as dashed lines including the correction up to $O(1/N)$, which are clearly important to have a good match even for N as large as 200.

the left hand side (see Eq. (8.3.6)). The explicit computation of the integral gives

$$\frac{N}{2\pi}\int_0^{\arccos(\mu-1)} dx\, \log\Big(1-(\mu-\cos(x))^2\Big) = \\ -\frac{N}{2\pi}\Big[\pi\log(1+4\mu+2\mu^2-2(1+\mu)\sqrt{\mu^2+2\mu})+\arccos(\mu-1)\log(4(1+\mu+\sqrt{\mu^2+2\mu}))+ \\ +\mathrm{Im}(\mathrm{Li}_2(e^{2i\arccos(\mu-1)})+2\mathrm{Li}_2(e^{i\arccos(\mu-1)}(1+\mu+\sqrt{\mu^2+2\mu})))\Big], \quad (8.3.18)$$

where Li_2 is the dilogarithmic function $\mathrm{Li}_2 \equiv \sum_{k=1}^{\infty}\frac{z^k}{k^2}$. Once again, the case $\mu = 0$ deserves particular attention because also the divergence coming from the lower extreme of integration in (8.3.17) has to be subtracted (i.e., the limits $\mu \to 0$ and $N \to \infty$ do not commute). Thus, one has to carefully perform a Taylor expansion of the integrand around both extremes of integration. The final result is

$$A_N(0) \to A_\infty(0) = -\log 2 - \frac{2-2\log\pi+2\log N}{N}. \quad (8.3.19)$$

The logarithmic correction for small values of N is evident in Figure 8.2 for all values of μ, but it is more pronounced for $\mu = 0$, as clear from the analytic expressions. Hence the total entropy for large N is

$$S_n^{2d} = \frac{f_\infty(\mu)N}{6}\Big(1+\frac{1}{n}\Big)\log 2\ell + \frac{N}{6}\Big(1+\frac{1}{n}\Big)A_\infty(\mu) + f_\infty(\mu)N\Upsilon_n, \quad (8.3.20)$$

which we recall is valid at order $o(\ell^0)$ and $O(N^0)$. We will see that to have a good agreement with numerical data at finite but large ℓ, it is needed to keep the $\log N$ contribution in $A_N(\mu)$.

When both ℓ and N are large, it is useful to look at the special case of the subsystem A being a square strip with $N = \ell$, when Eq. (8.3.20) is rewritten as

$$S_n^{2d} = \frac{f_\infty(\mu)}{6}\Big(1+\frac{1}{n}\Big)\ell\log 2\ell + \ell\frac{1}{6}\Big(1+\frac{1}{n}\Big)A_\infty(\mu) + f_\infty(\mu)\ell\Upsilon_n + O(\ell^0). \quad (8.3.21)$$

(Actually, any choice of N and ℓ proportional to each other, $N = a\ell$, would be equivalent, with just an overall factor a, but for simplicity let us just think to $a = 1$.) Let us briefly comment

Eq. (8.3.21). It shows the expected logarithmic correction to the area law and our derivation gives a clearer understanding of such behaviour: it is a simple consequence of the fact that we are dealing with an extensive a number of critical chains, i.e. proportional to $N = \ell$, whose entropy obeys a logarithmic scaling so that each of them contributes proportionally to $\log \ell$ to the total entropy. Moreover, it also agrees with the result obtained by the application of Widom conjecture (see, e.g., [424–426]) that provides an explicit formula for the prefactor of the leading term of the entanglement entropy of free fermions in any dimension, i.e., $S_1 = C\ell^{d-1} \log \ell + O(\ell^{d-1})$, with C given by

$$C = \frac{1}{12(2\pi)} \int_{\partial\Lambda} \int_{\partial\Gamma(\mu)} |n_x \cdot n_p| dS_x dS_p, \tag{8.3.22}$$

where Λ is the considered subsystem with volume normalised to one, $\Gamma(\mu)$ is the volume in momentum space enclosed by the Fermi surface, n_p, n_x are the unit normals to the boundaries of these volumes and the integration is carried over the surface of both domains. In the case of interest for this Chapter, given the compactification along the y direction, the Fermi surface is defined by the solutions of $S_p = 0$ (with $S_p = \mu - \cos k_x - \cos k_y$). By performing the line integrals, Eq. (8.3.22) becomes

$$C = \frac{\arccos(\mu - 1)}{3\pi}, \tag{8.3.23}$$

in agreement with Eq. (8.3.21). We stress that while the leading terms in the two approaches are identical, the dimensional reduction provides an explicit prediction also for the subleading term proportional to ℓ, as in Eq. (8.3.21), which cannot be derived by Widom conjecture.

Some generalisations.

The same approach is straightforwardly adapted to the computation of the entanglement entropies in the case of Dirichlet (open) boundary conditions (DBC's) along the transverse direction (y-axis), i.e., imposing $c_{j_1,0} = c_{j_1,N} = 0$. Although these boundary conditions break the translational invariance in the transverse direction, one can use the Fourier sine transform (rather than the standard one). The only final difference is that the set of modes Ω_μ in (8.3.6) corresponding to critical chains will now start from $r = 1$ (instead of $r = 0$). The same strategy applies when the total system is a finite block of L sites along the x-direction, with PBC's (see the right panel in Figure (11.1)). In this case, the only difference is that the scaling of the one-dimensional Rényi entropies for a system with PBC's reads

$$S^{1d}_{n,j} = \frac{1+n}{6n} \log\left(\frac{2L}{\pi} \sin\left(\frac{\pi\ell}{L}\right) \sin k^F_j\right) + \Upsilon_n. \tag{8.3.24}$$

Therefore, we have for any finite N

$$S^{2d}_n = \frac{n+1}{6n} \left[f_N(\mu) \log\left(\frac{L}{2\pi} \sin\left(\frac{\pi\ell}{L}\right)\right) + A_N(\mu) \right] N + f_N(\mu) N \Upsilon_n, \tag{8.3.25}$$

and similarly for large N with $f_N(\mu) \to f_\infty(\mu)$ and $A_N(\mu) \to A_\infty(\mu)$.

Numerical checks.

We now benchmark the results for the total entropies against exact numerical calculations obtained by the free-fermion techniques reported in Sec. 1.4.3. In Figure 8.3 we report the numerical data of the Rényi entropies for different values of the index n and chemical potential μ, both for infinite (panel (a)) and finite (panel (b)) system size. We fix the transverse direction N to be equal to the

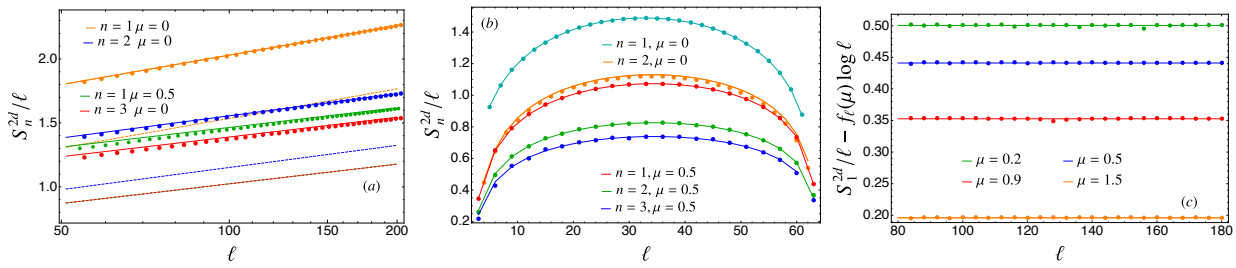

Figure 8.3: Leading scaling behaviour of the Rényi entropies S_n^{2d} of $2d$ free fermions both for infinite (a) and finite system size L (b) in the longitudinal direction. In the transverse direction, we fix the periodic size N to equal ℓ, the subsystem length in the longitudinal direction. The numerical results (symbols) for different values of μ and n are reported as function of ℓ. They match well the theoretical prediction of Eqs. (8.3.21) and (8.3.25); the dashed lines in (a) are the leading behaviour $\propto \ell \log \ell$ which is clearly not enough accurate. The non-universal coefficient proportional to the area, 2ℓ, in Eq. (10.3.26) is well captured by the numerics, as highlighted in (c).

longitudinal subsystem length ℓ, so that the subsystem A is a square with PBC in the transverse direction. We also properly choose the values of μ and ℓ such that $\ell f_\ell(\mu)$ is an integer number to eliminate effects due to partial fillings of modes. The theoretical predictions for the leading scaling in Eqs. (8.3.21) and (8.3.25) are also reported for comparison. These include both the leading term and the subleading one proportional to the area (2ℓ) between the subsystem A and the rest of the system.

It is evident that the analytical results correctly describe the data. We also report (as dashed lines) the sole leading universal behaviour $\propto \ell \log \ell$: this universal term alone does not match the data for these values of ℓ, highlighting the importance of the subleading terms $\propto \ell$ that we calculated analytically here. In the panel (c) of the same figure, we plot the data for the von Neumann entropy where we subtracted the leading term $f_\ell(\mu)\ell \log \ell$ to show the non-universal subleading terms found in Eq. (8.3.21) alone.

8.3.3 Symmetry Resolved Entanglement Entropies

The same dimensional reduction technique can further be used to compute the SRREs. Indeed, from Eq. (8.3.1) the particle number $Q = \sum_{\mathbf{i}} c_{\mathbf{i}}^\dagger c_{\mathbf{i}}$ is a conserved $U(1)$ charge of the model in arbitrary dimension. The strategy is exactly as before: we consider a finite system in the transverse direction with PBC and so reduce to a one-dimensional problem for the charged moments and then, via Fourier transform, we get the SRREs.

Charged moments.

Because of the factorisation of the RDM (8.3.7) and of the additivity of the conserved charge, we can rewrite

$$\rho_A^n e^{iQ_A\alpha} = \bigotimes_{r\in\Omega_\mu} \rho^n_{A,k_y^{(r)}} e^{iQ_A^{(r)}\alpha}\,, \tag{8.3.26}$$

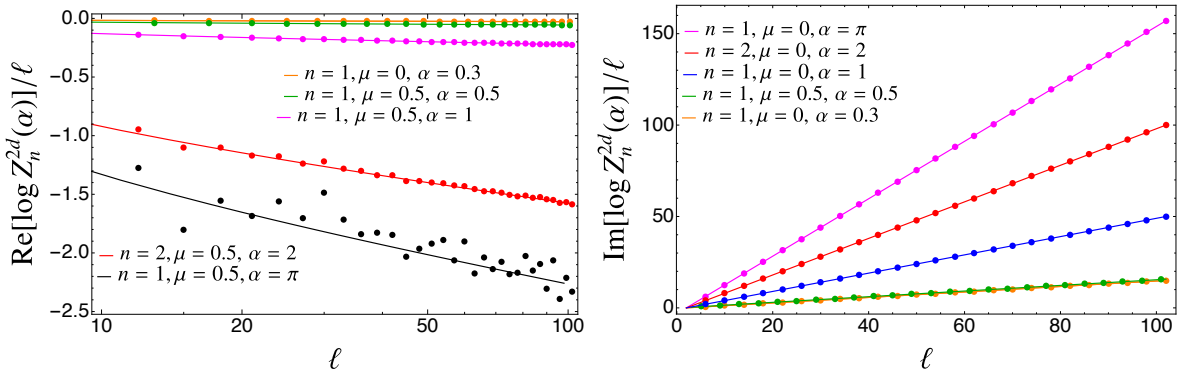

Figure 8.4: Leading scaling behaviour of the real and imaginary part of the charged moments $\log Z_n^{2d}(\alpha)$ in $2d$ free fermionic model for an infinite cylinder with transverse length $N = \ell$, equal to the subsystem length in the longitudinal direction. The numerical results (symbols) for several values of α and n are reported as function of ℓ for different μ's. Different colours represent different choices of the parameters n, α, μ. The corresponding analytic predictions (continuous lines), Eqs. (8.3.28) and (8.3.34), are also reported.

where $Q_A^{(r)}$ is the charge operator restricted to the r-th transverse mode. This factorisation allows us to rewrite in terms of the one-dimensional results for the charged moment

$$\log Z_n^{2d}(\alpha) = \sum_{r \in \Omega_\mu} \log Z_{n,r}^{1d}(\alpha), \tag{8.3.27}$$

and, using the explicit 1d result Eq. (8.2.3), the sum is performed as

$$\log Z_n^{2d}(\alpha) \;\simeq\; i\bar{q}\alpha \;-\; \left[\frac{1}{6}\left(n - \frac{1}{n}\right) + \frac{2}{n}\left(\frac{\alpha}{2\pi}\right)^2\right] \left(f_N(\mu) \log 2\ell + A_N(\mu)\right) N \;+\; N f_N(\mu) \Upsilon_n(\alpha). \tag{8.3.28}$$

The first term in Eq. (8.3.28) is purely imaginary and it is the average number of particle within A, for large N explicitly given by

$$\bar{q} = \frac{N\ell}{\pi^2} \int_0^{\arccos(\mu-1)} dx \arccos(\mu - \cos x). \tag{8.3.29}$$

It is extensive in the subsystem volume ($N\ell$), as it should, and at half-filling, $\mu = 0$, it reproduces the simple result $\bar{q} = N\ell/2$.

In Eq. (8.3.28), it is useful to write $\Upsilon_n(\alpha)$ as

$$\Upsilon_n(\alpha) = \Upsilon(n) + \gamma(n)\alpha^2 + \epsilon(n, \alpha), \qquad \epsilon(n, \alpha) = O(\alpha^4), \tag{8.3.30}$$

where

$$\gamma(n) = \frac{ni}{4} \int_{-\infty}^{\infty} dw [\tanh^3(\pi n w) - \tanh(\pi n w)] \log \frac{\Gamma(\frac{1}{2} + iw)}{\Gamma(\frac{1}{2} - iw)}. \tag{8.3.31}$$

In Ref. [90] it has been shown that the quadratic approximation of Eq. (8.3.30) is appropriate for many of applications since $\epsilon(n, \alpha) \ll \gamma(n)\alpha^2$. In particular, this approximation allows for an

explicit analytic computation of the symmetry resolved moments $\mathcal{Z}_n(q)$. Therefore, hereafter we will keep only the terms up to $O(\alpha^2)$ and we rewrite (8.3.28) in the compact form as:

$$\log Z_n^{2d}(\alpha) \simeq \log Z_n^{2d}(0) + i\bar{q}\alpha - \alpha^2(\mathcal{B}_n f_N(\mu)\log 2\ell + \mathcal{C}_n)N, \tag{8.3.32}$$

with

$$\begin{aligned} \mathcal{B}_n &= \frac{1}{2\pi^2 n}, \\ \mathcal{C}_n &= \frac{A_N(\mu)}{2\pi^2 n} - f_N(\mu)\gamma(n). \end{aligned} \tag{8.3.33}$$

In Figure 8.4 we report the numerical data both for the real and the imaginary part of $\log Z_n^{2d}(\alpha)$ for different values of n and α. Here the system is an infinite cylinder of circumference ℓ and the subsystem A is again a periodic square strip with longitudinal length equal to ℓ. Here and throughout this section, the values of μ and ℓ are chosen such that $\ell f_\ell(\mu)$ is an integer number. Moreover, when $\mu = 0$, we focus on the case ℓ even. The theoretical prediction in Eq. (8.3.28) is also reported for comparison, showing that the analytical result correctly describes the data as long as $|\alpha| < \pi$ (as well known already in 1d, see e.g. [90, 91]). The oscillating corrections to the scaling become relevant when α moves close to $\pm\pi$. The reason is that some terms in the generalised Fisher-Hartwig approach become larger and Eq. (8.2.3) is not a good approximation at the considered intermediate values of ℓ [90,91]. In the figure it is evident that these oscillations arise also for $n = 1$, contrarily to what happens for $\alpha = 0$.

A simple but interesting generalisation of the calculation we just presented concerns the geometry of a torus as depicted in the right of Figure 11.1. The longitudinal size of the system is L. The charged moments are again obtained by summing up the contribution of the different transverse modes as critical $1d$ chains, using the finite size form with the chord length. Summing up the contributions of the the transverse modes we get

$$\begin{aligned} &\log Z_n^{2d}(\alpha) \simeq \\ &\quad \simeq i\alpha\bar{q} - \left[\frac{1}{6}\Big(n - \frac{1}{n}\Big) + \frac{2}{n}\left(\frac{\alpha}{2\pi}\right)^2\right] N\left[f_N(\mu)\log\left[\frac{2L}{\pi}\sin\left(\frac{\pi\ell}{L}\right)\right] + A_N(\mu)\right] + N f_N(\mu)\Upsilon_n(\alpha). \end{aligned} \tag{8.3.34}$$

Symmetry resolution.

We now can compute the Fourier transform $\mathcal{Z}_n^{2d}(q)$ of the charged moments using the leading order terms of $Z_n^{2d}(\alpha)$ taking into account the effect of the non-universal pieces. This Fourier transform is

$$\mathcal{Z}_n^{2d}(q) = \int_{-\pi}^{\pi}\frac{d\alpha}{2\pi}e^{-iq\alpha}Z_n^{2d}(\alpha) \simeq Z_n^{2d}(0)\int_{-\pi}^{\pi}\frac{d\alpha}{2\pi}e^{-i(q-\bar{q})\alpha-\alpha^2 b_n}, \tag{8.3.35}$$

where the coefficient of the quadratic term is

$$b_n = N\mathcal{B}_n f_N(\mu)\log 2\ell + \mathcal{C}_n N. \tag{8.3.36}$$

For large subsystem size ℓ and/or N, we can treat the integral by means of the saddle point approximation and use as domain of integration $[-\infty, +\infty]$, getting

$$\mathcal{Z}_n^{2d}(q) \simeq Z_n^{2d}(0)e^{-\frac{(q-\bar{q})^2}{4N(\mathcal{B}_n f_N(\mu)\log 2\ell + \mathcal{C}_n)}}\sqrt{\frac{1}{4\pi N(\mathcal{B}_n f_N(\mu)\log 2\ell + \mathcal{C}_n)}}, \tag{8.3.37}$$

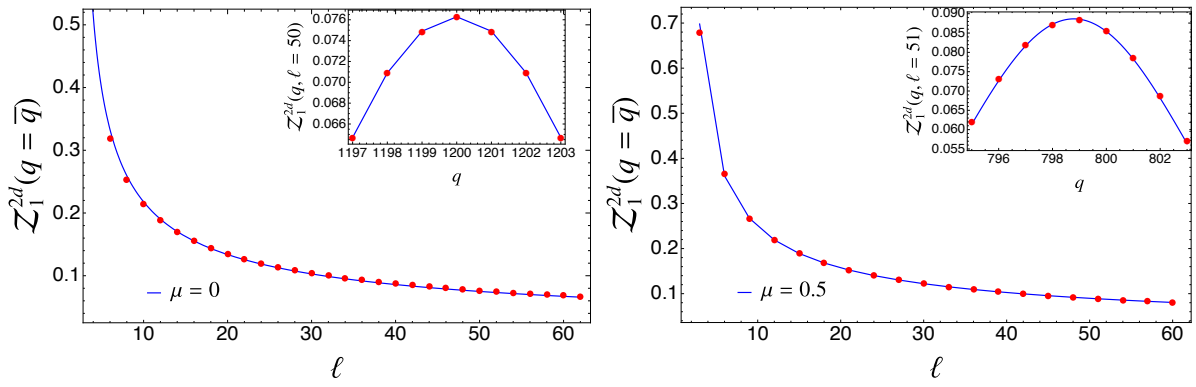

Figure 8.5: The probability $\mathcal{Z}_1^{2d}(q)$ for $2d$ free fermions with chemical potential $\mu = 0$ (left) and $\mu = 0.5$ (right). The red symbols are the numerical values and blue lines are the analytical prediction (8.3.37). In the main frame $\mathcal{Z}_1^{2d}(q = \bar{q})$ is shown as a function of ℓ, whereas in the inset we fix ℓ and $\mathcal{Z}_1^{2d}(q)$ is plotted as a function of q.

where $Z_n^{2d}(\alpha)$ is given in Eq. (8.3.28) and we report it again for completeness in a coincise form for $\alpha = 0$

$$Z_n^{2d}(0) = \left((2\ell)^{f_N(\mu)} e^{A_N(\mu)}\right)^{-\frac{1}{6}(n-\frac{1}{n})N} e^{\Upsilon(n) N f_N(\mu)}. \tag{8.3.38}$$

In full analogy to the $1d$ case, the probability distribution functions given by these moments are still Gaussian with mean $\bar{q}$ and variance that for large ℓ and N grows as $\sqrt{N \log \ell}$. An equivalent result was already obtained in Refs. [91, 94] for Fermi gases in arbitrary dimension using the Widom's conjecture. The novelty of this formula is an exact prediction for the coefficient $\mathcal{C}_n$ that renormalises the variance at order $O(\ell)$ and, as we will see, will play a crucial role for an accurate computation of the SRREs.

Let us briefly discuss the terms that have been neglected in the derivation of Eq. (8.3.37) which are the same as in $1d$ [90]. The main approximation is to ignore $\epsilon(n, \alpha)$ in Eq. (8.3.31) which induces a correction going like $1/(N \log \ell)$. Finally the corrections coming from having replaced the extremes of integration $\pm\pi$ with $\pm\infty$ are really small: they decay as $e^{-\pi^2 b_n}/b_n$, i.e., exponentially in N.

The accuracy of Eq. (8.3.37) is checked for different values of μ in Figure 8.5 where we report the numerically calculated Fourier transforms and the analytical prediction. It is evident from the data in the main frames and in the insets that both the ℓ and the q dependence of $\mathcal{Z}_n(q)$ is perfectly captured by our approximation.

With these ingredients at our disposal, we are ready to compute the asymptotic behaviour of the SRRE, given by

$$S_n^{2d}(q) = \frac{1}{1-n} \log \left[\frac{\mathcal{Z}_n^{2d}(q)}{\mathcal{Z}_1^{2d}(q)^n} \right] \simeq \frac{1}{1-n} \log \frac{Z_n^{2d}(0)}{(Z_1^{2d}(0))^n} \frac{e^{-\frac{(q-\bar{q})^2}{4b_n}}}{e^{-\frac{n(q-\bar{q})^2}{4b_1}}} \frac{(4\pi b_n)^{-1/2}}{(4\pi b_1)^{-n/2}}. \tag{8.3.39}$$

After some simple algebra, we can write

$$S_n^{2d}(q) = S_n^{2d} - \frac{1}{2} \log \left(\frac{2N}{\pi} \left(f_\infty(\mu) \log(2\ell) + f_\infty(\mu)\delta_n + A_\infty(\mu) \right) \right) + \frac{\log n}{2(1-n)} + (q-\bar{q})^2 \pi^4 \frac{n}{1-n} \frac{(\gamma(1) - n\gamma(n))}{N[f_{\infty(\mu)} \log(2\ell) + f_\infty(\mu)\kappa_n + A_\infty(\mu)]^2} + \cdots, \tag{8.3.40}$$

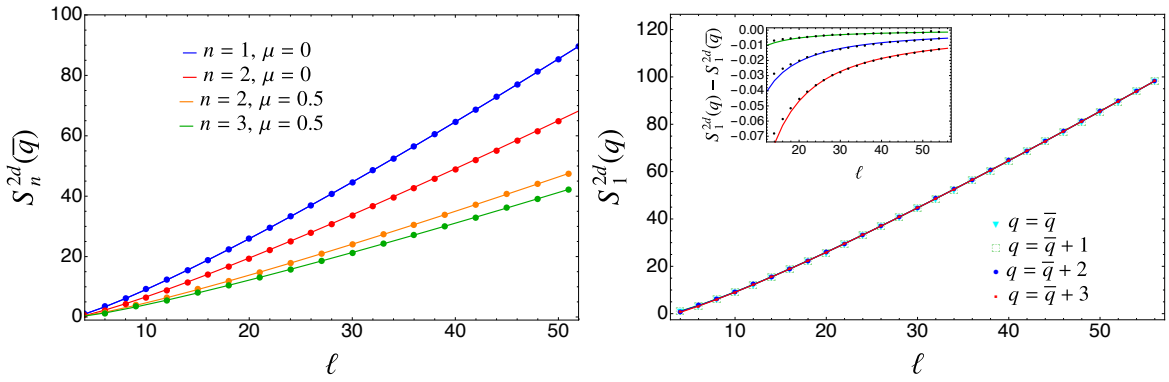

Figure 8.6: SRREs $S_n^{2d}(q)$ of $2d$ free fermions for $n = 1, 2, 3$ and different values of μ. We fix the transverse direction $N = \ell$, equal to the length of the subsystem in the longitudinal direction. In the left panel the numerical data (symbols) of $2d$ free fermions for $q = \bar{q}$ are compared with the theoretical predictions of Eqs. (8.3.40) and (8.3.43). In the right panel we show four values of q (namely $q - \bar{q} = 0, 1, 2, 3$). The data are almost coinciding on this scale, so in the inset we report their difference which is perfectly captured by the theoretical prediction.

where S_n^{2d} is the total Rényi entropy,

$$\delta_n = -\frac{2\pi^2 n(\gamma(n) - \gamma(1))}{1 - n}, \tag{8.3.41}$$

and

$$\kappa_n = -\pi^2(\gamma(1) + n\gamma(n)). \tag{8.3.42}$$

Eq. (8.3.40) provides the leading behaviour for large ℓ and N as well as the non-universal additive constants, and a q-dependent subleading correction which scales as $N^{-1}(\log \ell)^{-2}$. Such correction provides the first term in the expansion for large ℓ and N which depends on the symmetry sector. As in the corresponding $1d$ calculation [90], it can be calculated from the subleading terms of the variance of $\mathcal{Z}_n^{2d}(q)$, in particular the additive non-universal constant $\mathcal{C}_n$ in Eq. (8.3.33). So while few leading terms satisfy the equipartition of entanglement, we can precisely identify the first term that breaks it. Taking now the limit for $n \to 1$ of (8.3.40), we get the von Neumann entropy

$$S_1^{2d}(q) = S_1^{2d} - \frac{1}{2}\log\left(\frac{2N}{\pi}\left(f_\infty(\mu)\log(2\ell) + f_\infty(\mu)\delta_1 + A_\infty(\mu)\right)\right) - \frac{1}{2} + \\ + (q - \bar{q})^2\pi^4 \frac{(\gamma(1) + \gamma'(1))}{N[f_\infty(\mu)\log(2\ell) + f_\infty(\mu)\kappa_1 + A_\infty(\mu)]^2} + \cdots \tag{8.3.43}$$

These predictions for the SRREs are compared with the numerical data in Figure 8.6. In the left panel we consider the scaling with ℓ of $S_n(\bar{q})$ and it is evident that the numerical data perfectly match with the theoretical prediction in Eqs. (8.3.40) and (8.3.43). The corrections in $(q - \bar{q})$ are suppressed as $1/(N(\log \ell)^2)$ and the curves in the right panel seem to be on top of each other on the scale of the plot. In order to appreciate their distance, in the inset we report the differences with $S_n(\bar{q})$ (focusing on $n = 1$) and we show that they are well described by our prediction. The agreement is excellent even for relatively small values of ℓ and N of the order of 20.

We quickly discuss now what happens in the case of the torus geometry: we only report the final results, since the calculations are only a slight modification of the previous ones. The Fourier

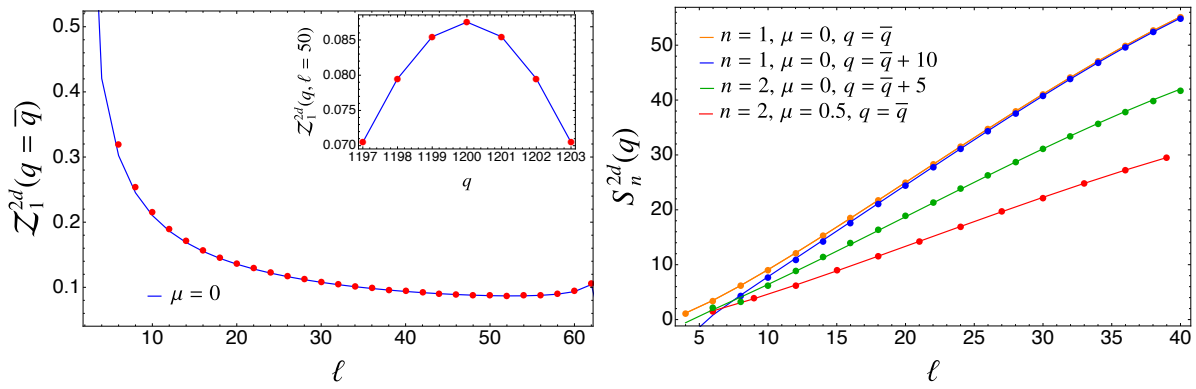

Figure 8.7: Left panel: $\mathcal{Z}_1^{2d}(q = \bar{q})$ of $2d$ free fermions for different values of μ and finite torus of longitudinal length $L = 64$. We fix the transverse size N equal to the subsystem length ℓ. Red symbols correspond to numerical data. The blue lines show the analytical prediction (8.3.44). The inset shows $\mathcal{Z}_1^{2d}(q)$ for $\ell = 10$ as a function of q. Right panel: SRREs $S_n^{2d}(q)$ of $2d$ free fermions for $n = 1, 2$ and different μ's and q: the numerical data (symbols) are compared with the theoretical prediction (continuous lines) of Eq. (8.3.46). As $(q - \bar{q})$ increases, the neglected terms become more relevant, therefore the agreement between numerics and analytical predictions worsens.

transform of Eq. (8.3.34) is

$$\mathcal{Z}_n(q) \simeq Z_n^{2d}(0) \frac{e^{-\frac{(q-\bar{q})^2}{4N\left[\frac{1}{2\pi^2 n}\left(f_N(\mu)\log\left(\frac{2L}{\pi}\sin\left(\frac{\pi\ell}{L}\right)\right)+A_N(\mu)\right)-f_N(\mu)\gamma(n)\right]}}}{\sqrt{4N\pi\left[\frac{1}{2\pi^2 n}\left(f_N(\mu)\log\left(\frac{2L}{\pi}\sin\left(\frac{\pi\ell}{L}\right)\right)+A_N(\mu)\right)-f_N(\mu)\gamma(n)\right]}} \tag{8.3.44}$$

where

$$Z_n^{2d}(0) = e^{\Upsilon(n)N f_N(\mu)}\left(e^{A_N(\mu)}\left(\frac{2L}{\pi}\sin(\frac{\pi\ell}{L})\right)^{f_N(\mu)}\right)^{-\frac{1}{6}(n-\frac{1}{n})N}. \tag{8.3.45}$$

The SRREs are then easily worked out as

$$S_n^{2d}(q) = S_n^{2d} - \frac{1}{2}\log\left[\frac{2N}{\pi}\left(f_\infty(\mu)\log\left(\frac{2L}{\pi}\sin(\frac{\pi\ell}{L})\right)+f_\infty(\mu)\delta_n+A_\infty(\mu)\right)\right]+\frac{\log n}{2(1-n)}+$$
$$(q-\bar{q})^2\pi^4\frac{n}{1-n}\frac{(\gamma(1)-n\gamma(n))}{N[f_\infty(\mu)\log\left(\frac{2L}{\pi}\sin(\frac{\pi\ell}{L})\right)+f_\infty(\mu)\kappa_n+A_\infty(\mu)]^2}+\cdots. \tag{8.3.46}$$

These results are tested with numerics in Figure (8.7).

8.4 Two-dimensional Free Bosons

In this section we consider the entanglement entropy and its partition into the different charge sectors for a lattice discretisation of the complex Klein–Gordon theory, namely coupled complex harmonic oscillators on a two-dimensional square lattice. Here we will apply the same strategy of the previous section to recast, once again, our problem into the sum of uncoupled one-dimensional chains.

8.4.1 Rényi and Entanglement Entropies

Let us examine a two-dimensional system of $L \times N$ real coupled oscillators, where L and N are the lengths along the x– (longitudinal) and y–direction (transverse), respectively (see Figure 11.1). The $2d$ Hamiltonian describing a real $2d$ square lattice of harmonic oscillators is

$$H_B = \frac{1}{2}\sum_{x=1}^{L}\sum_{y=1}^{N}\left[p_{x,y}^2 + \omega_0^2 q_{x,y}^2 + \kappa_x(q_{x+1,y} - q_{x,y})^2 + \kappa_y(q_{x,y+1} - q_{x,y})^2\right], \tag{8.4.1}$$

where $q_{x,y}, p_{x,y}$ and ω_0 are coordinate, momentum and self-frequency of the oscillator at site (x, y) while κ_x and κ_y are the nearest-neighbour couplings. As in the one-dimensional case, the $2d$ lattice of complex oscillators is

$$H_{CB}(p^{(1)} + ip^{(2)}, q^{(1)} + iq^{(2)}) = H_B(p^{(1)}, q^{(1)}) + H_B(p^{(2)}, q^{(2)}). \tag{8.4.2}$$

If we define $\mathbf{p} = \frac{p^{(1)}+ip^{(2)}}{\sqrt{2}}$ and $\mathbf{q} = \frac{q^{(1)}+iq^{(2)}}{\sqrt{2}}$, Eq. (8.4.2) becomes

$$\begin{aligned} H_{CB} = &\sum_{x=1}^{L}\sum_{y=1}^{N}\Big[\mathbf{p}_{x,y}^\dagger \mathbf{p}_{x,y} + \omega_0^2 \mathbf{q}_{x,y}^\dagger \mathbf{q}_{x,y} + \\ &+\kappa_x(\mathbf{q}_{x+1,y} - \mathbf{q}_{x,y})^\dagger(\mathbf{q}_{x+1,y} - \mathbf{q}_{x,y}) + \kappa_y(\mathbf{q}_{x,y+1} - \mathbf{q}_{x,y})^\dagger(\mathbf{q}_{x,y+1} - \mathbf{q}_{x,y})\Big]. \end{aligned} \tag{8.4.3}$$

Imposing PBC's along the y-direction, we can exploit the translational invariance and use Fourier transform in the transverse direction, to get the mixed space-momentum representation

$$\mathbf{q}_{x,y} = \frac{1}{\sqrt{N}}\sum_{r=0}^{N-1}\tilde{q}_{x,r}e^{2\pi i r y/N}, \tag{8.4.4}$$

and similarly for $\mathbf{p}_{x,y}$. We set $\kappa_y = \kappa_x = 1$ to shorten the notation (indeed they can be absorbed by a canonical transformation). The Hamiltonian (8.4.2) then becomes

$$H_{CB} = \sum_{x=1}^{L}\sum_{r=0}^{N-1}\tilde{p}_{x,r}^\dagger\tilde{p}_{x,r} + \omega_r^2\tilde{q}_{x,r}^\dagger\tilde{q}_{x,r} + (\tilde{q}_{x+1,r} - \tilde{q}_{x,r})^\dagger(\tilde{q}_{x+1,r} - \tilde{q}_{x,r}). \tag{8.4.5}$$

where

$$\omega_r^2 = \omega_0^2 + 4\sin^2\frac{\pi r}{N}. \tag{8.4.6}$$

Because of the additivity of the independent transverse chain modes in Eq. (8.4.5), the entanglement entropy can be computed by using the $1d$ results, as we did for free fermions.

As already discussed in Chap. (7), the ground-state reduced density matrices of each $1d$ chain is obtained by means of corner transfer matrices, for the bipartition of the infinite chain in two halves. Therefore, the entanglement spectrum associated to the r-mode/chain along the y direction is given by Eq. (7.3.10), specialised to the frequency ω_r, i.e., the eigenvalues of the entanglement Hamiltonian are now given by

$$\epsilon_j^{(r)} = \epsilon_r(2j+1), \tag{8.4.7}$$

where the energy levels are

$$\epsilon_r = \frac{\pi I(\sqrt{1-\kappa_r^2})}{I(\kappa_r)}, \qquad \kappa_r = \frac{1}{2}(2 + \omega_r^2 - \omega_r\sqrt{4+\omega_r^2}). \tag{8.4.8}$$

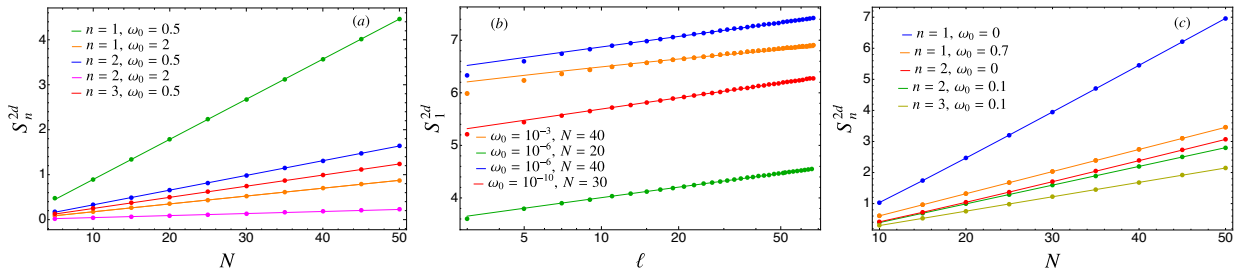

Figure 8.8: Entanglement entropies in the $2d$ lattice of complex oscillators. (a): S_n^{2d} in the non-critical regime, against the length of the transverse direction N, for different ω_0 and n at fixed subsystem size $\ell = 50$. Periodic BC are imposed along y. The symbols correspond to numerical data, while continuous lines are the analytic predictions (8.4.10). Different colours denote different choices of the parameters n and ω_0. (b): Entanglement entropy S_1^{2d} in the critical regime $\omega_0 \to 0$. Solid lines are the prediction (8.4.12) for different ω_0 and N. The smaller ω_0, the better Eq. (8.4.12) works. The additive constant c_1^{1d} is numerically extrapolated through a fitting procedure for a chain. (c): Same as in (a), but with DBC's along the transverse direction. The theoretical prediction is Eq. (8.4.14).

The parameter κ_r is obtained by solving the equation $\omega_r^2 = (1-\kappa_r)^2/\kappa_r$.

In our semi infinite strip, each mode gives a contribution to the entanglement entropy which can be computed through the CTM approach. Since they are independent, such contributions simply add up leading to

$$S_n^{2d} = \frac{2}{1-n} \sum_{r=0}^{N-1} \sum_{j=0}^{\infty} \Big(n \log[1 - e^{-(2j+1)\epsilon_r}] - \log[1 - e^{-(2j+1)n\epsilon_r}] \Big) . \tag{8.4.9}$$

This result is valid for arbitrary integer N. We can now take the limit of large transverse direction. The sum becomes an integral in $\zeta = r/N$, we can write ($\epsilon_r \to \epsilon(\zeta)$)

$$S_n^{2d} = \frac{2N}{1-n} \int_0^1 d\zeta \sum_{j=0}^{\infty} \Big(n \log[1 - e^{-(2j+1)\epsilon(\zeta)}] - \log[1 - e^{-(2j+1)n\epsilon(\zeta)}] \Big) , \tag{8.4.10}$$

and in the limit $n \to 1$

$$S_1^{2d} = 2N \int_0^1 d\zeta \sum_{j=0}^{\infty} \left(\frac{(2j+1)\epsilon(\zeta)}{e^{(2j+1)\epsilon(\zeta)} - 1} - \log[1 - e^{-(2j+1)\epsilon(\zeta)}] \right) . \tag{8.4.11}$$

These results for the entanglement entropies are numerically tested in panel (a) of Figure 8.8 using the free-boson techniques reported in Sec. 7.3.4 (from the numerical expression of the charged moments in Eq. (7.3.56), one easily finds $\mathrm{Tr}\rho_A^n$ setting $\alpha = 0$ and, eventually, the replica limit by taking the derivative with respect to n and $n \to 1$). The considered subsystem is a strip, periodic in the transverse direction (hence of length N) and of longitudinal size equal to ℓ, but such that ℓ is much larger than the correlation length of the system (of order ω_0^{-1}) and so the entanglement is just the double of the one for a semi-infinite subsystem. We have fixed $\ell = 50$ which is large enough for the considered values of ω_0. Eqs. (8.4.10) and (8.4.11) perfectly predict the prefactor of the area-law term, in all cases when the thermodynamic limit along the transverse direction is a good approximation.

We now discuss the critical regime $\omega_0 \to 0$. Here we do not set $\omega_0 = 0$ from the beginning, but we take a very small ω_0 and then take the large ℓ limit. The two limits are known to not commute in $1d$ [177]. Although the technique to obtain the $2d$ results from $1d$ one is the same for bosons and fermions, the physics is very different. Indeed, while for fermions the N chains in the Hamiltonian (8.3.3) are all critical, just with renormalised chemical potentials (8.3.5), for free bosons only the zero-mode chain is critical and all the other have a gap given by Eq. (8.4.6) that does not close as $\omega_0 \to 0$. This different behaviour is the origin of the logarithmic multiplicative correction to the area law for massless fermions, while massless bosons follow a strict area law, with additive logarithmic corrections. While these physical results are well known in the literature (see, e.g., [423]) we find their explanation with dimensional reduction particularly clear.

We can now sum the contributions of the various transverse modes to get the total entanglement entropy. For the zero-mode with $r = 0$ we take the result from the massive Klein-Gordon theory [177]. Summing up the various contributions, we have for the two-dimensional lattice complex oscillators

$$S_n^{2d} = \frac{n+1}{3n} \log \ell + n \log(-\log(\omega_0 \ell)) + c_n^{1d} + \\ + \frac{2}{1-n} \sum_{r=1}^{N-1} \sum_{j=0}^{\infty} \Big(n \log[1 - e^{-(2j+1)\epsilon_r}] - \log[1 - e^{-(2j+1)n\epsilon_r}] \Big) . \quad (8.4.12)$$

Here the first line is the zero gapless transverse mode and the second is the sum over all massive ones. The additive constant c_n^{1d} is non-universal and is not predicted by field theory; we will fix it numerically with a standard fit of the $1d$ system. All the chains with $r > 0$ give a $O(1)$ contribution in ℓ since, for large enough ℓ, it holds $\ell \gg \omega_r^{-1}$; hence they give rise to an area-law scaling (i.e., $\propto N$). The panel (b) of Figure 8.8 confirms the accuracy of the prediction (8.4.12) for the critical regime as a function of N.

Some generalisations.

As in the fermionic case, let us mention that this technique can also be applied when imposing DBC's along the transverse direction, i.e., $q_{i,0} = q_{i,N} = p_{i,0} = p_{i,N} = 0$. Because of the breaking of translational invariance, we can simply use the Fourier sine transform for $\tilde{q}_{x,y}$ and $\tilde{p}_{x,y}$. The key difference with respect to the periodic case is that the frequencies of the transverse modes are

$$\omega_r^2 = \omega_0^2 + 4 \sin^2 \frac{\pi r}{2N}, \quad r = 1, \cdots, N-1. \quad (8.4.13)$$

Thus, within these BC, the frequencies are *all* different from zero, even for $\omega_0 = 0$. The Rényi entanglement is

$$S_n^{2d} = \frac{2}{1-n} \sum_{r=1}^{N-1} \sum_{j=0}^{\infty} \Big(n \log[1 - e^{-(2j+1)\epsilon_r}] - \log[1 - e^{-(2j+1)n\epsilon_r}] \Big) . \quad (8.4.14)$$

We can now take the limit of large N, similarly to what done in Eq. (8.4.10) for $\omega_0 > 0$, to get

$$S_n^{2d} = \frac{2N}{1-n} \int_0^1 d\zeta \sum_{j=0}^{\infty} \Big(n \log[1 - e^{-(2j+1)\epsilon(\zeta)}] - \log[1 - e^{-(2j+1)n\epsilon(\zeta)}] \Big) \\ - \frac{2}{1-n} \sum_{j=0}^{\infty} \Big(n \log[1 - e^{-(2j+1)\epsilon_0}] - \log[1 - e^{-(2j+1)n\epsilon_0}] \Big) , \quad (8.4.15)$$

where we need to subtract the contribution from the zero mode, since in Eq. (8.4.14) the sum starts from $r = 1$ rather than 0. The accuracy of Eq. (8.4.14) is checked by numerics in the panel (c) of Figure 8.8 in which the agreement is perfect.

8.4.2 Symmetry Resolved Entanglement Entropies

Here we compute the contributions to the entanglement entropy coming from the different $U(1)$ symmetry sectors for the $2d$ lattice of oscillators. The conserved charge reduced to the subsystem is just the $2d$ generalisation of Q_A in Eq. (7.3.17).

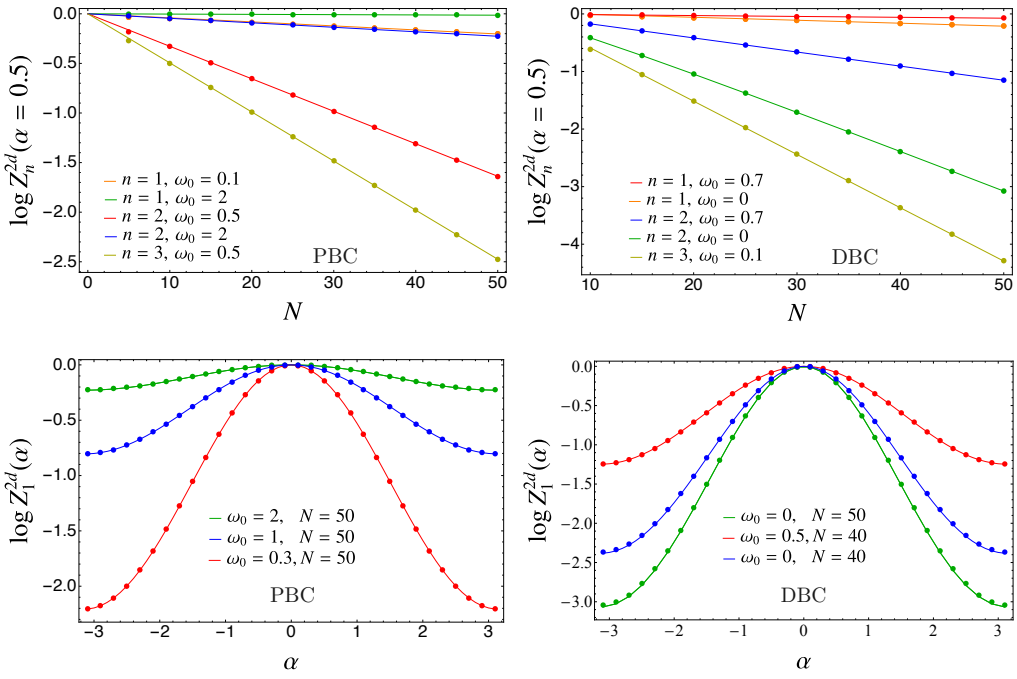

Figure 8.9: Logarithm of the charged moments $\log Z_n(\alpha)$ for the $2d$ lattice of oscillators in the off-critical regime. Top panels: Plots as a function of N, for different n and ω_0, imposing PBC's (left) and DBC's (right) along the transverse direction. Bottom panel: Plots against α for different ω_0 and N (again with PBC's (left) and DBC's (right)). In the right panels, numerical data (symbols) are compared with the analytic predictions (solid lines) of Eq. (8.4.17). In the left panels, data are compared with the analytic prediction for DBC's, which is the same as Eq. (8.4.16), but the sum starts from $r = 1$ rather than $r = 0$.

Charged moments.

For the $2d$ lattice and for a subsystem being a periodic strip, the charged moments are obtained as a sum of the N independent chains as

$$\log Z_n^{2d}(\alpha) = \sum_{r=0}^{N-1} \sum_{j=0}^{\infty} \left[2n \log[1 - e^{-(2j+1)\epsilon_r}] - \log[1 - e^{-(2j+1)n\epsilon_r + i\alpha}] - \log[1 - e^{-(2j+1)n\epsilon_r - i\alpha}] \right], \tag{8.4.16}$$

and, taking the limit of large N

$$\log Z_n^{2d}(\alpha) = N \int_0^1 d\zeta \sum_{j=0}^{\infty} \big[2n \log[1 - e^{-(2j+1)\epsilon(\zeta)}] - \log[1 - e^{-(2j+1)n\epsilon(\zeta)+i\alpha}] + \\ - \log[1 - e^{-(2j+1)n\epsilon(\zeta)-i\alpha}]\big]. \quad (8.4.17)$$

Notice that $\log Z_n^{2d}(\alpha)$ is real and even in α. We plot $\log Z_n^{2d}(\alpha)$ as a function of α and N in Figure 8.9 (left panels) together with the corresponding numerical data (for the numerical details see the Sec. 7.3.4). The agreement is perfect for all considered values of n, α, N, and ω_0. We find that for all α, $\log Z_1^{2d}(\alpha)$ is a monotonously increasing function of the self frequency of the oscillators, ω_0. As a function of α, they have a single maximum at $\alpha = 0$. The plots as a function of N show that the integral in Eq. (8.4.17) well predicts the prefactor of the area-law term of $Z_n(\alpha)$ in the massive case, $N \gg \omega_0^{-1}$. To obtain the data in the figure we fix $\ell = 50$ which is much larger than the correlation length at all considered ω_0; hence, by cluster decomposition, they approach the double of the prediction (8.4.17). We also analyse the scaling of the charged moments for DBC's along the transverse direction. The corresponding results are also displayed in the right panels of Figure 8.9. The computation through the dimensional reduction perfectly works for every ω_0.

In the critical regime, $\omega_0 \to 0$, the subsystem is a finite strip of longitudinal length ℓ and the resulting pattern is similar to the case encountered when $\alpha = 0$. Using Eq. (7.3.41) and assuming that $\ell \gg \xi$, we obtain

$$\log \frac{Z_n^{2d}(\alpha)}{Z_n^{2d}(0)} \simeq \frac{2}{n} \left[\Big(\frac{\alpha}{2\pi}\Big)^2 - \frac{|\alpha|}{2\pi} \right] \log \ell + \\ - \sum_{r=1}^{N-1} \sum_{j=0}^{\infty} \big[\log[1 - e^{-(2j+1)n\epsilon_r + i\alpha}] + \log[1 - e^{-(2j+1)n\epsilon_r - i\alpha}] \big], \quad (8.4.18)$$

where the second line is an additive (ℓ-independent) term that represents the contribution of the chains with $r > 0$.

Symmetry resolution.

In order to get the symmetry resolution it is convenient to first rewrite $\log Z_n^{2d}(\alpha)$ in the limit $N \to \infty$ as

$$\log Z_n^{2d}(\alpha) = N \int_0^1 d\zeta \log \left[\frac{\theta_4(0|e^{-n\epsilon(\zeta)})}{\theta_4(\frac{\alpha}{2}|e^{-n\epsilon(\zeta)})} \prod_{j=1}^{\infty} \frac{(1 - e^{-(2j-1)\epsilon(\zeta)})^{2n}}{(1 - e^{-(2j-1)n\epsilon(\zeta)})^2} \right] \equiv N f_n(\alpha). \quad (8.4.19)$$

where θ_4 is defined in Eq. (7.3.26). Then, the Fourier transform $\mathcal{Z}_n^{2d}(q)$ is

$$\mathcal{Z}_n^{2d}(q) = \int_{-\pi}^{\pi} \frac{d\alpha}{2\pi} e^{-iq\alpha} \prod_{r=0}^{N-1} Z_{n,r}^{1d}(\alpha), \quad (8.4.20)$$

i.e., it is the convolution of the Fourier transforms $\mathcal{Z}_{n,r}^{1d}(q)$ of $Z_{n,r}^{1d}(\alpha)$. This formula can be easily evaluated for any finite N, even very large. In order to test its accuracy we take the Fourier transform of the numerical data for $Z_n^{2d}(\alpha)$ in the previous section and compare it with Eq. (8.4.20). The results are shown in Figure 8.10 where the symmetry resolved moments are plotted both

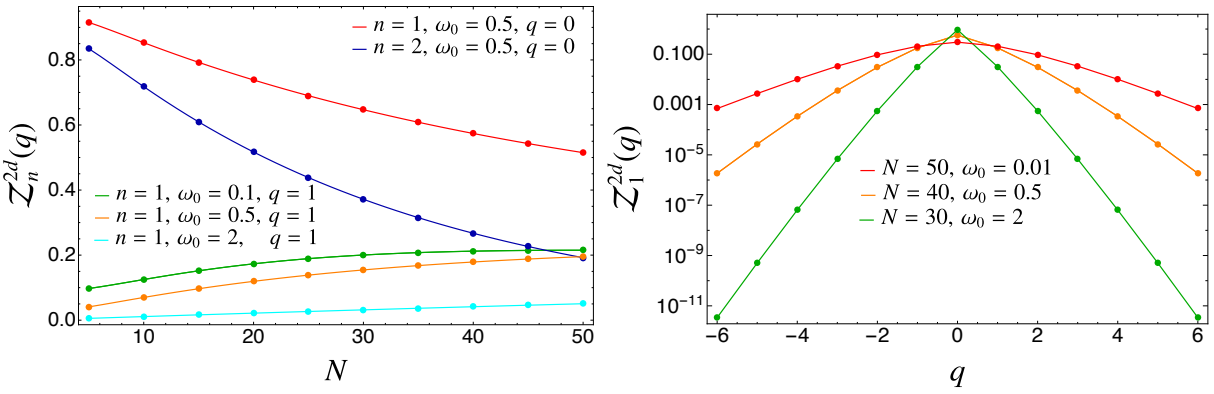

Figure 8.10: $\mathcal{Z}_n^{2d}(q)$ in the $2d$ harmonic lattice for different values of ω_0, q, and n, as a function of N (left panel) and q (right panel). Data (symbols) are compared with the analytic prediction (solid lines) of Eq. (8.4.20). $\mathcal{Z}_1^{2d}(q)$ is peaked at $q = 0$, which is the average charge in the subsystem. Here we do not test the large N result (11.3.13).

against N and q for different values of ω_0. The agreement is excellent. Note that $\mathcal{Z}_n(q)$ is peaked at $q = 0$, which is the average charge in the subsystem.

For large N, we can use Eq. (8.4.19) so that Eq. (8.4.20) can be rewritten as

$$\mathcal{Z}_n^{2d}(q) \simeq \int_{-\pi}^{\pi} \frac{d\alpha}{2\pi} e^{-iq\alpha} e^{N f_n(\alpha)}. \tag{8.4.21}$$

Given that we are interested in the large N limit, the integral may be performed by saddle point method, with the only maximum of $f_n(\alpha)$ in $\alpha = 0$, as we can see in Fig. 8.9. Therefore, the integral becomes

$$\mathcal{Z}_n^{2d}(q) \simeq e^{N f_n(0)} \int_{-\infty}^{\infty} \frac{d\alpha}{2\pi} e^{-iq\alpha} e^{-\frac{N\alpha^2}{2} \int_0^1 d\zeta \frac{\theta_4''(0|e^{-n\epsilon(\zeta)})}{4\theta_4(0|e^{-n\epsilon(\zeta)})}} = Z_n^{2d}(0) \frac{e^{-\frac{q^2}{2g(n)N}}}{\sqrt{2\pi N g(n)}}, \tag{8.4.22}$$

where we defined

$$g(n) \equiv \int_0^1 d\zeta \frac{\theta_4''(0|e^{-n\epsilon(\zeta)})}{4\theta_4(0|e^{-n\epsilon(\zeta)})}. \tag{8.4.23}$$

The probability distributions given by these moments are Gaussian with mean $\bar{q} = 0$ and variance that grows as $\sqrt{N}$. Unfortunately it is difficult to test Eq. (11.3.13) against numerical calculations because we would need rather large values of N. We instead checked that indeed Eq. (8.4.20) converges for large N to (11.3.13). Anyhow, we will show the corresponding plot only for the SRREs below.

The last step now is to use Eq. (8.4.20) to calculate the SRREs

$$S_n^{2d}(q) = \frac{1}{1-n} \log \left[\frac{\mathcal{Z}_n^{2d}(q)}{\mathcal{Z}_1^{2d}(q)^n} \right], \tag{8.4.24}$$

whose limit $n \to 1$ is the SREE

$$S_1^{2d}(q) \simeq -\frac{\partial_n \mathcal{Z}_n^{2d}(q)|_{n=1}}{\mathcal{Z}_1^{2d}(q)} + \log \mathcal{Z}_1^{2d}(q). \tag{8.4.25}$$

Using the previously obtained $\mathcal{Z}_n^{2d}(q)$, we have analytic predictions valid for any N. In Figure 8.11 we test the accuracy of this prediction for the entropy in each symmetry sector for N as large as

200. The figure clearly shows that *for these relatively small values of* N, the equipartition of the entanglement does not hold, even though for $n = 1$ data start becoming parallel to each other, suggesting a possible onset of equipartition.

In order to understand if and how equipartition is attained at larger values of N, we work out the large N limit. In the limit $N \to \infty$ plugging Eq. (11.3.13) into Eq. (8.4.24), we obtain

$$S_n^{2d}(q) = \frac{1}{1-n} \log \frac{Z_n^{2d}(0)}{(Z_1^{2d}(0))^n} e^{-\frac{q^2}{2N}\left(\frac{1}{g(n)} - \frac{n}{g(1)}\right)} \frac{(2\pi N g(1))^{n/2}}{(2\pi N g(n))^{1/2}}. \tag{8.4.26}$$

The first ratio in Eq. (8.4.26) just gives the total Rényi entropy of order n, while the non-trivial dependence on n of $g(n)$ is responsible for the breaking of the equipartition of the entanglement. After some algebra, we obtain

$$S_n^{2d}(q) = S_n^{2d} - \frac{1}{2}\log(2\pi N) - \frac{1}{2(1-n)} \log \frac{g(n)}{g(1)^n} - \frac{q^2}{2(1-n)N}\left(\frac{1}{g(n)} - \frac{n}{g(1)}\right), \tag{8.4.27}$$

whose limit $n \to 1$ is

$$S_1^{2d}(q) = S_1^{2d} - \frac{1}{2}\log(2\pi N) - \frac{q^2}{2N}\frac{g'(1)+g(1)}{g(1)^2} + \frac{1}{2}\left(\frac{g'(1)}{g(1)} - \log g(1)\right). \tag{8.4.28}$$

Hence, we have shown that the leading terms in the expansion for large N satisfy the equipartition of entanglement. The first term breaking it is at order $1/N$ and has an amplitude proportional to q^2. Unfortunately, as already mentioned, it is difficult to test numerically the validity of Eq. (8.4.27) because it requires too large value of N. A posteriori, the reason of this peculiar behaviour is easily understood from Eqs. (8.4.27) and (8.4.28): the prefactor of the equipartition breaking term multiplying q^2/N is $-103.485\ldots$ for $n = 1$ and $-1793.66\ldots$ for $n = 2$, very large in both cases. Hence, we should get to values of N of order of thousands in order to see equipartition and this is not simply done numerically. What instead we can easily do is to test that for large N the analytic prediction (8.4.24) tends indeed to the predicted asymptotic behaviour (8.4.27). This is shown in the left of Figure 8.11 where we see that very large values of N are required to recover the asymptotic behaviour, especially for large values of q and n. Hence equipartition is attained for larger and larger values of N as q and n grow, as very clear from the figure.

8.5 Closing remarks

In this Chapter we exploited *dimensional reduction* for the computation of Rényi and symmetry resolved entropies of two-dimensional systems of free fermions and bosons with a translational invariant geometry in the transverse direction.

The different structure of the entanglement equipartition in 2d bosonic and fermionic systems clearly shows how such intriguing phenomenon is related to the gaussianity of the probability distribution of the conserved $U(1)$ charge, which generically follows from the central limit theorem emerging from the large number of elementary constituents. Yet, there are important counterexamples, like the $1d$ free boson we discussed in Chapter 7, which affect also the physics of some $2d$ systems we considered here. Understanding the fine details of entanglement equipartition, such as the precise conditions for its validity and the form of the first subleading term breaking it, remains an important open issue.

Having understood how dimensional reduction works for the symmetry resolved entanglement in 2d free theories is also the starting point for studying interacting ones, e.g. along the lines of Refs. [284, 436, 444] for the total entanglement, but a lot of challenging work is still necessary to get results in this direction.

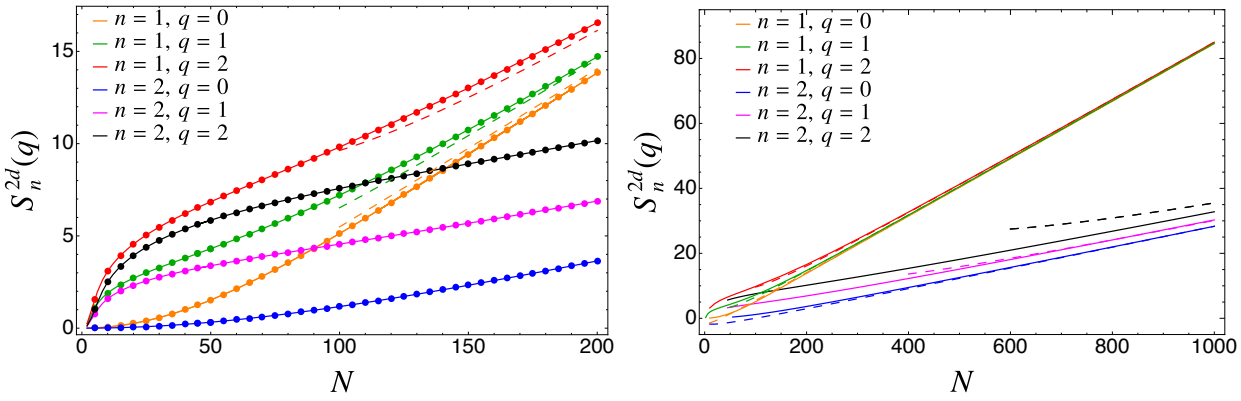

Figure 8.11: Left: Numerical results for the SRREs $S_n^{2d}(q)$ of the $2d$ lattice of complex oscillators. The numerical data for $q = 0, 1, 2$, $n = 1, 2$ and $\omega_0 = 0.5$ are compared with the predictions (8.4.24) and (8.4.25) finding perfect agreement. For these relatively small values of N, equipartition of entanglement does not hold, even though for $n = 1$ data start approaching the asymptotic behaviour described by Eq. (8.4.28) and plotted through the dashed lines. Right: We plot the analytic prediction for the SRREs (8.4.24) (full lines) valid at any N together with its asymptotic expansion (8.4.27) (dashed lines), showing that for large N equipartition of entanglement is recovered. Notice that, as n and q grow, equipartition occurs at much larger values of N.

Chapter 9

Symmetry resolved entanglement in a long-range system

In this Chapter, we investigate the symmetry resolution of entanglement in the presence of long-range couplings. To this end, we study the SREE in the ground state of a fermionic chain that has dimerised long-range hoppings with power-like decaying amplitude, a long-range generalisation of the Su-Schrieffer-Heeger model. This is a system that preserves the number of particles. The entropy of each symmetry sector is calculated via the charged moments of the reduced density matrix. We exploit some recent results on block Toeplitz determinants generated by a discontinuous symbol to obtain analytically the asymptotic behaviour of the charged moments and of the symmetry resolved entropies for a large subsystem. At leading order we find entanglement equipartition, but comparing with the short-range counterpart its breaking occurs at a different order and it does depend on the hopping amplitudes. This Chapter is based on Ref. [102].

9.1 Introduction

One of the most fundamental properties of entanglement is its behaviour with the size of the subsystem considered. So far, we have considered cases in which the mass gap is zero, the correlation length diverges, and the area law is corrected by a logarithmic term proportional to the central charge of the CFT that describes the low-energy spectrum of the model [17, 19–21, 172, 446]. Nevertheless, this scenario changes and becomes more involved for systems with long-range couplings. For instance, in that case, the ground state entanglement entropy may display a logarithmic growth even if the mass gap is not zero, as occurs in the long-range Kitaev chain [447–450]. In general, other more exotic behaviours may arise, depending on the specific form of the couplings [451]. The theoretical study of long-range systems has also been stimulated by the development of experimental techniques that allow to simulate them in a laboratory [452–455]. In fact, Rényi entanglement entropies and generalisations have been experimentally measured in these ion-trap setups, especially out of equilibrium [80, 89, 456].

Given the relevance of this subject, we intestigate the symmetry resolution of entanglement in the presence of long-range couplings. Natural questions are if the SRRE, as the total one, presents different behaviours with the size of the subsystem, whether it satisfies equipartition, and if yes what are the subleading terms breaking it. The goal of this Chapter is to address these questions and to study how the total ground state entanglement splits into the contributions coming from the symmetry sectors of a gapped model with long-range couplings.

More specifically, the physical system that we will examine is the Su-Schrieffer-Heeger (SSH) model with long-range hoppings. The short-range version, a dimerised tight-binding fermionic

chain, was initially introduced to analyse solitons in conducting polymers such as polyacetylene [457, 458]. In recent years, it has attracted a lot of interest because it supports two topologically distinct phases [459–461]: a topologically non-trivial phase, which presents zero energy states exponentially localised at the edges of the open chain, and a trivial phase, which is just an insulator without boundary modes. The relation between the entanglement properties and these two topological phases has been also investigated (see e.g. [462–465]). Here we extend the SSH chain by including long-range dimerised hoppings whose amplitude decays with a power law — this is a gapped $U(1)$ symmetric theory that preserves the number of particles. Other long-range generalisations of the SSH chain have been considered in the arena of topological insulators [466–470].

The organisation of the Chapter is the following. In Sec. 9.2, we introduce the SSH chain with long-range hoppings and we calculate the ground state two-point correlation function. In the first part of Sec. 9.3, we use the latter to obtain the charged moments in the thermodynamic limit. In particular, we derive their asymptotic behaviour for a large interval by applying some recent results on block Toeplitz determinants with discontinuous symbols. In the second part of Sec. 9.3, we employ these results to analyse the SREE and finally find an asymptotic expression for it. We also benchmark the analytic results against exact numerical computations. We conclude in Sec. 9.4 with some remarks and discussions.

9.2 Su-Schrieffer-Heeger model with long-range hoppings

We would like to analyse the SRREs in a system with long-range couplings. We will in particular consider the following fermionic chain with dimerised long-range hoppings

$$H = -\sum_{n=1}^{N}\sum_{l=1}^{N/2} J_l \frac{1+(-1)^n\delta}{2} c_n^\dagger c_{n+l} + h.c. \tag{9.2.1}$$

and periodic boundary conditions $c_{n+N} = c_n$. This Hamiltonian commutes with the particle number operator $Q = \sum_i c_i^\dagger c_i$. We are going to consider the case where the hopping amplitude decays with the distance between sites as a power law, i.e.

$$J_l = \begin{cases} (l+1)^{-\nu}, & l \text{ odd} \\ 0, & l \text{ even.} \end{cases} . \tag{9.2.2}$$

The parameter $\nu \geq 0$ characterises the dumping of the hopping with the distance. For simplicity, we only allow hoppings between even and odd sites. In order to enrich the later discussion on the SRREs, we have taken dimerised hoppings and, therefore, the hopping amplitudes between even-odd and odd-even sites differ when $\delta \neq 0$. Thus the Hamiltonian is invariant under two-site translations. If $\delta = \pm 1$, the chain is fully dimerised and there is not hopping between even-odd (odd-even) sites. In the case $\delta = 0$, the chain is homogeneous and corresponds to the long-range analogue of the tight-binding model. This Hamiltonian can be easily diagonalised by performing a Fourier plus a Bogoliubov transformation. In the diagonal basis, it reads

$$H = \sum_{k=0}^{N-1} \omega(\theta_k)\left(d_k^\dagger d_k - \frac{1}{2}\right), \tag{9.2.3}$$

where $\theta_k = 2\pi k/N$ and $\omega(\theta)$ is the dispersion relation. In the thermodynamic limit $N \to \infty$, we replace θ_k by a continuous variable $\theta \in [-\pi, \pi]$ and the dispersion relation can be written in the form

$$\omega(\theta) = \sqrt{F(\theta)^2 - G(\theta)^2}, \tag{9.2.4}$$

with

$$F(\theta) = \frac{1}{2^{\nu+1}} \left[e^{-i\theta} \mathrm{Li}_\nu(e^{i2\theta}) + e^{i\theta} \mathrm{Li}_\nu(e^{-i2\theta}) \right], \tag{9.2.5}$$

and

$$G(\theta) = -\frac{\delta}{2^{\nu+1}} \left[e^{-i\theta} \mathrm{Li}_\nu(e^{i2\theta}) - e^{i\theta} \mathrm{Li}_\nu(e^{-i2\theta}) \right]. \tag{9.2.6}$$

Here $\mathrm{Li}_\nu(z)$ denotes the polylogarithm function of order ν [473]. The appearance of this function is due to the infinite-range hoppings with power-law decaying amplitude. The properties of the polylogarithm with the dumping exponent ν originate the features of the long-range SSH model that differ from the short-range systems. In particular, $\mathrm{Li}_\nu(z)$ diverges at $z = 1$ when $0 \leq \nu < 1$, while it has a finite value for $\nu > 1$. This will be fundamental in the later analysis of the entanglement resolution. In the dispersion relation, such behaviour of the polylogarithm causes it to diverge at $\theta = 0, \pm\pi$ when $0 \leq \nu < 1$, while it is always finite for $\nu > 1$. For $\delta > 0$ and $\nu \geq 0$, the dispersion relation is always strictly positive, $\omega(\theta) > 0$, and therefore the mass gap is not zero. The gap closes when $\delta = 0$, the non-dimerised chain, as $\omega(\theta)$ vanishes at $\theta = \pm\pi/2$. In any case, since the dispersion relation is non-negative, the ground state of H is the Bogoliubov vacuum, $|0\rangle$, defined by the property $d_k |0\rangle = 0$, for all k.

As the Hamiltonian is quadratic, the ground state two-point correlation functions are the only ingredient that we will need to calculate exactly the (symmetry resolved) entanglement entropy in such state [167]. Since the particle number is conserved, we have $\langle 0| c_n^\dagger c_m^\dagger |0\rangle = \langle 0| c_n c_m |0\rangle = 0$, while it will be useful to arrange the correlations of the form $\langle 0| c_n^\dagger c_m |0\rangle$ in a $N \times N$ matrix V with entries

$$V_{l,l'} = 2 \left\langle 0 \left| \begin{pmatrix} c_{2l}^\dagger \\ c_{2l+1}^\dagger \end{pmatrix} (c_{2l'}, c_{2l'+1}) \right| 0 \right\rangle - \delta_{l,l'}, \quad l, l' = 1, \ldots, N/2. \tag{9.2.7}$$

In the thermodynamic limit $N \to \infty$, V is a block Toeplitz matrix,

$$V_{l,l'} = \frac{1}{2\pi} \int_0^{2\pi} \mathcal{G}(\theta) e^{i\theta(l-l')} d\theta, \tag{9.2.8}$$

generated by the 2×2 symbol

$$\mathcal{G}(\theta) = \begin{pmatrix} 0 & e^{i\left(\frac{\theta}{2} - 2\xi(\theta)\right)} \\ e^{-i\left(\frac{\theta}{2} - 2\xi(\theta)\right)} & 0 \end{pmatrix}, \tag{9.2.9}$$

where

$$\cos(2\xi(\theta)) = \frac{F(\theta/2)}{\sqrt{F(\theta/2)^2 - G(\theta/2)^2}}, \quad \sin(2\xi(\theta)) = \frac{iG(\theta/2)}{\sqrt{F(\theta/2)^2 - G(\theta/2)^2}}, \tag{9.2.10}$$

and the functions $F(\theta)$ and $G(\theta)$ are defined in Eqs. (9.2.5) and (9.2.6). Note that the 2×2 block structure of the matrix V is a consequence of the two-site translational invariance of the chain.

9.3 Symmetry resolved entanglement entropy

In this section, we focus on the calculation of the SRREs in the ground state $|0\rangle$ of the long-range SSH model. We start by computing exactly the charged moments for this model and then, from their Fourier transforms, we evaluate the SRREs.

9.3.1 Charged moments

Since the long-range SSH model is a system described by a quadratic fermionic Hamiltonian, the reduced density matrix $\rho_A = \mathrm{Tr}_{\mathcal{H}_B} |0\rangle \langle 0|$ satisfies the Wick theorem and its charged moments, defined in Eq. (1.4.16), can be computed from the two-point correlation matrix V introduced in Eq. (9.2.7). More specifically, see Refs. [84, 90, 167],

$$Z_n(\alpha) = \det \left[\left(\frac{I + V_A}{2} \right)^n e^{i\alpha} + \left(\frac{I - V_A}{2} \right)^n \right], \tag{9.3.1}$$

where V_A denotes the restriction of V to subsystem A. We will employ this expression to compute numerically the charged moments and the SRREs by diagonalizing the correlation matrix V.

If we take into account that the eigenvalues of V_A lie on the real interval $[-1, 1]$ and we use the residue theorem, then the previous expression can be rewritten as the contour integral [90, 268]

$$\log Z_n(\alpha) = \frac{1}{2\pi i} \lim_{\varepsilon \to 1^+} \oint_{\mathcal{C}} f_n(\lambda/\varepsilon, \alpha) \frac{d}{d\lambda} \log D_A(\lambda) d\lambda, \tag{9.3.2}$$

where the integration contour $\mathcal{C}$ encloses the interval $[-1, 1]$,

$$f_n(\lambda, \alpha) = \left(\frac{1 + \lambda}{2} \right)^n e^{i\alpha} + \left(\frac{1 - \lambda}{2} \right)^n, \tag{9.3.3}$$

and $D_A(\lambda)$ denotes the characteristic polynomial of V_A, i.e. $D_A(\lambda) = \det(\lambda I - V_A)$.

The previous discussion is valid for any subsystem A. Here we will focus on one consisting of a single interval of ℓ contiguous sites. In this case, the restriction V_A is a $\ell \times \ell$ block Toeplitz matrix with symbol the 2×2 matrix $\mathcal{G}(\theta)$ of Eq. (9.2.9). To deduce the large ℓ behaviour of $D_A(\lambda)$ and, therefore, of the charged moments $Z_n(\alpha)$, we will apply the results on the asymptotic behaviour of block Toeplitz determinants obtained in Ref. [450]. In particular, if the symbol $\mathcal{G}_\lambda(\theta) = \lambda I - \mathcal{G}(\theta)$ satisfies $\det \mathcal{G}_\lambda(\theta) \neq 0$ and is a piecewise continuous function in θ with jump discontinuities at $\theta = \theta_1, \ldots, \theta_R$, then

$$\log D_A(\lambda) = \frac{\ell}{4\pi} \int_0^{2\pi} \log \det \mathcal{G}_\lambda(\theta) d\theta + \frac{\log \ell}{4\pi^2} \sum_{r=1}^{R} \mathrm{Tr}[\log \mathcal{G}^-_{\lambda,r} (\mathcal{G}^+_{\lambda,r})^{-1}]^2 + O(1), \tag{9.3.4}$$

where $\mathcal{G}^\pm_{\lambda,r}$ are the lateral limits of $\mathcal{G}_\lambda(\theta)$ in the jump discontinuity at $\theta = \theta_r$,

$$\mathcal{G}^\pm_{\lambda,r} = \lim_{\theta \to \theta_r^\pm} \mathcal{G}_\lambda(\theta). \tag{9.3.5}$$

Eq. (9.3.4) is a generalisation of the Fisher-Hartwig conjecture for block Toeplitz determinants [474, 475]. If the symbol $\mathcal{G}_\lambda(\theta)$ has continuous entries in θ, then there is no logarithmic term in the asymptotic expansion of $\log D_A(\lambda)$, and Eq. (9.3.4) simplifies to

$$\log D_A(\lambda) = \frac{\ell}{4\pi} \int_0^{2\pi} \log \det \mathcal{G}_\lambda(\theta) d\theta + O(1). \tag{9.3.6}$$

This is the Szegő-Widom theorem [476].

Let us first consider the case $\delta = 0$ when the chain is not dimerised and the mass gap is zero. In this situation, the symbol $\mathcal{G}_\lambda(\theta)$ presents a jump discontinuity at $\theta = \pi$ due to the zeros of the dispersion relation $\omega(\theta)$. The lateral limits at this point are

$$\mathcal{G}^\pm_{\lambda,\pi} = \lambda I \pm \sigma_y, \tag{9.3.7}$$

where σ_y is the Pauli matrix. Thus, by applying the result of Eq. (9.3.4), we conclude that there is a logarithmic term in $\log D_A(\lambda)$,

$$\log D_A(\lambda) = \log(\lambda^2-1)\ell + \frac{\log \ell}{2\pi^2}\left(\log\frac{\lambda-1}{\lambda+1}\right)^2 + O(1). \tag{9.3.8}$$

If we plug this result into the contour integral of Eq. (9.3.2), we obtain that the charged moments for $\delta = 0$ are of the form

$$\log Z_n(\alpha) = i\frac{\alpha\ell}{2} + B_n(\nu,0,\alpha)\log\ell + O(1), \tag{9.3.9}$$

where

$$B_n(\nu,0,\alpha) = \frac{1}{\pi^3 i}\lim_{\varepsilon\to 1^+}\oint_{\mathcal{C}}\frac{f_n(\lambda/\varepsilon,\alpha)}{1-\lambda^2}\log\left(\frac{1+\lambda}{1-\lambda}\right)d\lambda. \tag{9.3.10}$$

This integral has already appeared in Ref. [90], where it is explicitly worked out. The final result is

$$B_n(\nu,0,\alpha) = -\left[\frac{1}{6}\left(n-\frac{1}{n}\right)+\frac{\alpha^2}{2\pi^2 n}\right]. \tag{9.3.11}$$

$B_n(\nu,0,\alpha)$ is equal to the coefficient of the logarithmic term of the charged moments for the ground state of the tight-binding model, see Eq. (8.2.3). This is a consequence of the fact that for $\delta = 0$ the ground state is always a Fermi sea, independently of the values of ν. Therefore, when the long-range chain of Eq. (9.2.1) is not dimerised, i.e. $\delta = 0$, the discussion on the SRREs follows similar lines as for the short-range chain of Ref. [90, 91].

In order to get a behaviour different from the short-range case, we need to dimerise the chain, that is, to take $\delta \neq 0$. Now the source of discontinuities in the symbol $\mathcal{G}_\lambda(\theta)$ is the polylogarithm function $\mathrm{Li}_\nu(z)$ that encodes the long-range hoppings. In the interval $0 \leq \nu < 1$, $\mathrm{Li}_\nu(z)$ diverges at the point $z = 1$. This divergence produces a jump discontinuity in $\mathcal{G}_\lambda(\theta)$ at $\theta = 0$ for $0 \leq \nu < 1$ and $\delta \neq 0$ with lateral limits

$$\mathcal{G}^{\pm}_{\lambda,0} = \lambda I + \cos\xi_0\sigma_z \pm \sin\xi_0\sigma_y, \tag{9.3.12}$$

where σ_y and σ_z are the Pauli matrices and

$$\cos\xi_0 = \frac{\sin(\pi\nu/2)}{\sqrt{\delta^2\cos^2(\pi\nu/2)+\sin^2(\pi\nu/2)}}, \tag{9.3.13}$$

and

$$\sin\xi_0 = \frac{\delta\cos(\pi\nu/2)}{\sqrt{\delta^2\cos^2(\pi\nu/2)+\sin^2(\pi\nu/2)}}. \tag{9.3.14}$$

According to Eq. (9.3.4), this discontinuity gives rise to a logarithmic term in $\log D_A(\lambda)$. If we plug Eq. (9.3.12) into Eq. (9.3.4), we find that

$$\log D_A(\lambda) = \log(\lambda^2-1)\ell + b_0(\lambda)\log\ell + O(1), \tag{9.3.15}$$

for $0 \leq \nu < 1$ and $\delta \neq 0$, with

$$b_0(\lambda) = \frac{2}{\pi^2}\left(\log\frac{\sqrt{\lambda^2-\cos^2\xi_0}+\sin\xi_0}{\sqrt{\lambda^2-1}}\right)^2. \tag{9.3.16}$$

For $\nu > 1$, the polylogarithm $\mathrm{Li}_\nu(z)$ converges in all the unit circle $z = e^{i\theta}$. This implies that the symbol $\mathcal{G}_\lambda(\theta)$ has continuous entries in θ when $\nu \geq 1$ and $\delta \neq 0$. In this case, there is no logarithmic term in $\log D_A(\lambda)$, and

$$\log D_A(\lambda) = \log(\lambda^2-1)\ell + O(1). \tag{9.3.17}$$

In what follows, we will focus on the range $0 \leq \nu < 1$ and $\delta \neq 0$. If we insert Eq. (9.3.15) in Eq. (9.3.2), we obtain the following asymptotic behaviour for the charged moments of ρ_A

$$\log Z_n(\alpha) = i\frac{\alpha\ell}{2} + B_n(\nu,\delta,\alpha)\log\ell + O(1), \tag{9.3.18}$$

when $0 \leq \nu < 1$ and $\delta \neq 0$. The coefficient $B_n(\nu,\delta,\alpha)$ is given by the contour integral

$$B_n(\nu,\delta,\alpha) = \frac{1}{2\pi i}\lim_{\varepsilon\to 1^+}\oint_{\mathcal{C}} f_n(\lambda/\varepsilon,\alpha)\frac{db_0(\lambda)}{d\lambda}d\lambda, \tag{9.3.19}$$

which, following similar steps as in Ref. [450], can be reduced to the real integral

$$B_n(\nu,\delta,\alpha) = \frac{4}{\pi^2}\int_{\cos\xi_0}^{1} g_n(\lambda,\alpha)\log\left(\frac{\sqrt{1-\lambda^2}}{\sqrt{\lambda^2-\cos^2\xi_0}+\sin\xi_0}\right)d\lambda, \tag{9.3.20}$$

where

$$g_n(\lambda,\alpha) = n\frac{(1+\lambda)^{2n-1}+\cos\alpha\left[(1+\lambda)^{n-1}(1-\lambda)^n-(1+\lambda)^n(1-\lambda)^{n-1}\right]-(1-\lambda)^{2n-1}}{(1+\lambda)^{2n}+2[(1+\lambda)(1-\lambda)]^n\cos\alpha+(1-\lambda)^{2n}}. \tag{9.3.21}$$

In Fig. 9.1, we check numerically the asymptotic behaviour for the charged moments $Z_n(\alpha)$ predicted in Eq. (9.3.18). We obtain an excellent agreement once the subleading corrections are taken into account. Unfortunately, to our knowledge, there are no results in the theory of block Toeplitz determinants that allow us to extract analytically these corrections, as a difference with the short-range case [182,445]. Nevertheless, from the analysis of the numerical data, we conjecture that the first subleading terms in Eq. (9.3.18) are of the form $C_n(\nu,\delta,\alpha) + D_n(\nu,\delta,\alpha)\ell^{-D'_n(\nu,\delta,\alpha)}$. The value of the coefficients $C_n(\nu,\delta,\alpha)$, $D_n(\nu,\delta,\alpha)$ and $D'_n(\nu,\delta,\alpha)$ for different sets of parameters can be estimated by a fit with the numerical data, as we explain in detail in the caption of Fig. 9.1.

Compared with the short-range systems, the most striking feature of the charged moments in the ground state of the long-range SSH model is the appearance of a $\log\ell$ term in $\log Z_n(\alpha)$ when the dumping exponent is $0 \leq \nu < 1$, even though the mass gap is not zero. On the contrary, in systems with short-range couplings, such term arises when the mass gap vanishes, as it is evident from Eq. (3.2.1). In the gapped short-range systems studied so far, such as for example the complex harmonic chain [98] and the XXZ spin chain [99], there is no logarithmic term in $\log Z_n(\alpha)$ and its real part saturates to a constant in the limit $\ell \to \infty$, as occurs in our case when $\nu \geq 1$. The presence of this logarithmic term for gapped systems is a genuine feature of the long-range hoppings.

Here the coefficient $B_n(\nu,\delta,\alpha)$ of the logarithmic term in $\log Z_n(\alpha)$ is not universal. It vanishes when $\nu \geq 1$ and it smoothly tends to zero in the limit $\nu \to 1^-$. An interesting case is $\nu = 0$: starting from Eq. (9.3.12), then Eq. (9.3.19) simplifies for any $\delta \neq 0$ to the same integral of Eq. (9.3.10), obtained when $\delta = 0$, and therefore

$$B_n(0,\delta,\alpha) = -\left[\frac{1}{6}\left(n-\frac{1}{n}\right)+\frac{\alpha^2}{2\pi^2 n}\right]. \tag{9.3.22}$$

Notice that this is equal to the coefficient of the logarithmic term of $\log Z_n(\alpha)$ in the gapless tight-binding model reported in Eq. (3.2.1). Nevertheless, it is important to recall that in our case the system is gapped if $\delta \neq 0$ and, moreover, when $\nu = 0$ the hopping couplings, which extend over the whole chain, do not decay with the distance between sites.

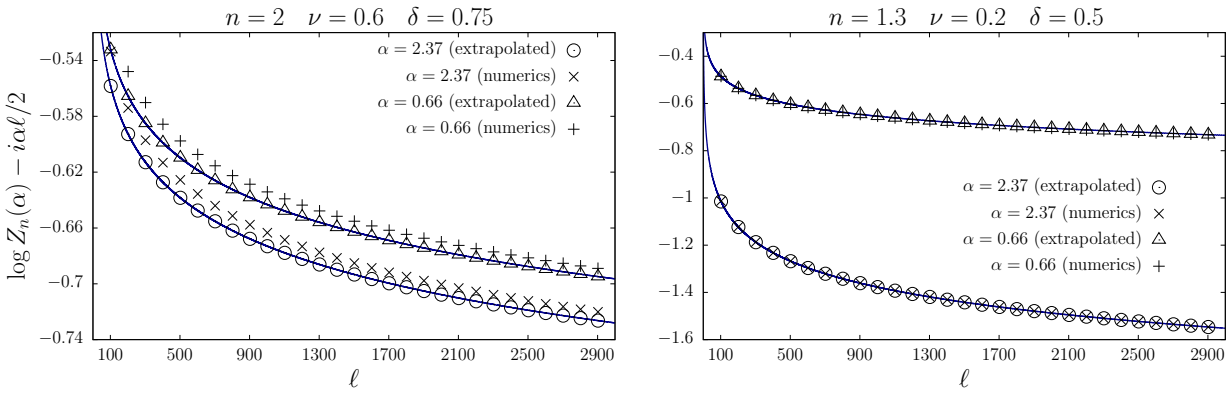

Figure 9.1: Numerical check of the asymptotic behaviour derived in Eq. (9.3.18) for the charged moments of ρ_A for two different sets of couplings ν and δ. The points indicated as *numerics* have been directly obtained from Eq. (9.3.1) by exact diagonalisation of the correlation matrix V_A. Using these points we have estimated the first $O(1)$ corrections in Eq. (9.3.18): we have subtracted from them the leading contribution $B_n(\nu,\delta,\alpha)\log\ell$ and then, with the resulting points, we have fitted the function $C_n(\nu,\delta,\alpha) + D_n(\nu,\delta,\alpha)\ell^{-D'_n(\nu,\delta,\alpha)}$. The *extrapolated* points have been obtained from the *numerics* ones by subtracting the term $D_n(\nu,\delta,\alpha)\ell^{-D'_n(\nu,\delta,\alpha)}$ with the values for $D_n(\nu,\delta,\alpha)$ and $D'_n(\nu,\delta,\alpha)$ found in the fit. The continuous line represents $B_n(\nu,\delta,\alpha)\log\ell + C_n(\nu,\delta,\alpha)$, taking for $C_n(\nu,\delta,\alpha)$ the value given by the fit.

The coefficient $B_n(\nu,\delta,\alpha)$ presents remarkable properties also as a function of the parameters α and n. It will be useful to consider the difference

$$\Delta_n(\nu,\delta,\alpha) = B_n(\nu,\delta,\alpha) - B_n(\nu,\delta,0). \tag{9.3.23}$$

In general, $\Delta_n(\nu,\delta,\alpha)$ has the following power series expansion in α around $\alpha = 0$,

$$\Delta_n(\nu,\delta,\alpha) = \sum_{j=1}^{\infty} \Delta_n^{(2j)}(\nu,\delta)\alpha^{2j}, \tag{9.3.24}$$

with $\Delta_n^{(2)} < 0$. This is in contrast to the tight-binding chain [90, 91], for which $\Delta_n = -1/(2\pi^2 n)$ (equal to the cases $\delta = 0$ and $\nu = 0$ analysed in Eqs. (9.3.10) and (9.3.22) respectively), i.e. it is a quadratic function in α, as also happens in the critical limit of the complex Harmonic chain [98] and in all cases present in the literature. Moreover, in these short-range models, Δ_n is proportional to $1/n$, something that, in general, does not hold in our case.This fact will have important consequences in the SRRE of the long-range SSH.

9.3.2 Symmetry resolution via Fourier transform

Now we can derive from Eq. (9.3.15) the asymptotic behaviour of the Fourier tranforms of the charged moments $Z_n(\alpha)$ for $0 \le \nu < 1$, defined in Eq. (1.4.17). In our case, using the results of the previous subsection, they can be rewritten in the form

$$\mathcal{Z}_n(q) = \frac{Z_n(0)}{2\pi} \int_{-\pi}^{\pi} e^{-i\alpha(q-\ell/2)} e^{\Delta_n(\nu,\delta,\alpha)\log\ell + O(1)} d\alpha. \tag{9.3.25}$$

In this expression we have factorised the $\alpha = 0$ contribution, which behaves for large ℓ as

$$Z_n(0) = e^{B_n(\nu,\delta,0)\log\ell + O(1)}, \tag{9.3.26}$$

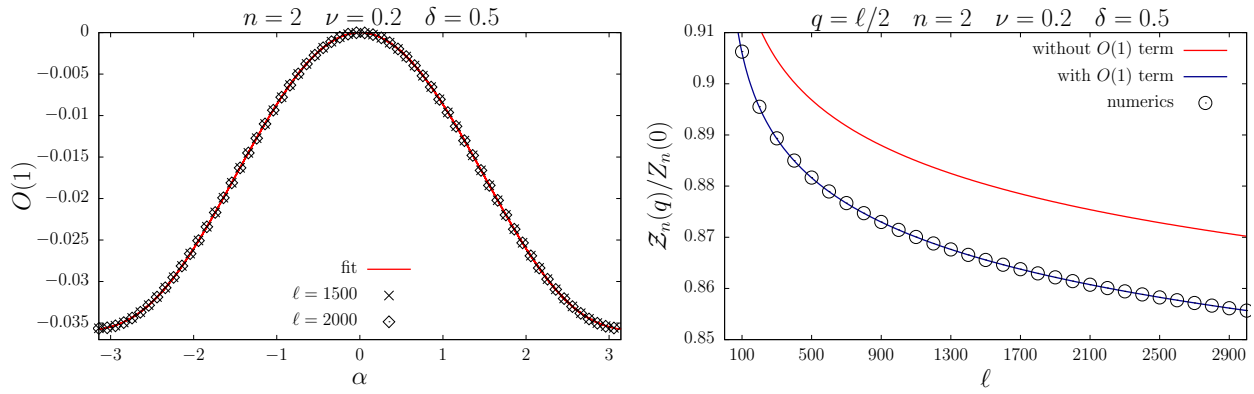

Figure 9.2: In the left panel, we represent the $O(1)$ term of the exponent of the integrand of Eq. (9.3.25), obtained numerically using Eq. (9.3.1) for two different interval lengths. We have fitted a function of the form $\sum_{j=1}^{8} b_{2j}\alpha^{2j}$ to the points of the case $\ell = 1500$. The continuous line represents this function using the coefficients arising from the fit. In the right panel, we analyse the $q = \ell/2$ Fourier coefficient $\mathcal{Z}_n(q)$ of the charged moments. The points have been obtained from the diagonalisation of the correlation matrix V_A through Eq. (9.3.1). The red line corresponds to performing the numerical integration of Eq. (9.3.25) without including the $O(1)$ terms while in the blue curve we have added the $O(1)$ term estimated in the fit with the $\ell = 1500$ points of the left plot of the present Figure.

and eventually yields the total Rényi entanglement entropy,

$$S_n = \frac{1}{1-n}\log Z_n(0) = \frac{B_n(\nu,\delta,0)}{1-n}\log\ell + O(1). \tag{9.3.27}$$

As we already pointed out for the charged moments, despite the mass gap of the system does not vanish, we find a logarithmic growth of the entanglement rather than the usual saturation to a constant value [20, 50, 182].

The coefficient $\Delta_n(\nu,\delta,\alpha)$ in the integrand of Eq. (9.3.25) is the difference defined in Eq. (9.3.23). As we have already mentioned, we do not have analytical methods to obtain the subleading terms in ℓ that appear in the exponent of this integrand. In Fig. 9.2, we have studied numerically the $O(1)$ term for a particular set of couplings. In general, this term is an even function in α and, therefore, can be expressed as a power series of the form $\sum_{j=1}^{\infty} b_{2j}\alpha^{2j}$. In the left panel of Fig. 9.2, we have fitted this function, truncated at order eight, to the numerical points. In the right panel of Fig. 9.2, we have calculated $\mathcal{Z}_n(q)$ for $q = \ell/2$ as a function of ℓ both diagonalising exactly the correlation matrix and using Eq. (9.3.1) (dots) as well as integrating numerically the expression in Eq. (9.3.25) (continuous lines). In the latter case, we have performed the integration both neglecting the $O(1)$ term (red line) and including it by taking the function fitted in the left panel of this figure (blue line). From this plot it is clear that Eq. (9.3.25) matches with the exact numerical points if we take into account the $O(1)$ term.

From the large ℓ expansion of $\mathcal{Z}_n(q)$ in Eq. (9.3.25), we conclude that at leading order $\mathcal{Z}_n(q)$ are Gaussian functions of q

$$\mathcal{Z}_n(q) \sim Z_n(0)\frac{e^{-\frac{(q-\ell/2)^2}{4\left|\Delta_n^{(2)}(\nu,\delta)\right|\log L}}}{2\sqrt{\pi\left|\Delta_n^{(2)}(\nu,\delta)\right|\log\ell}}, \tag{9.3.28}$$

centred at $q = \ell/2$ and with variance $2\Delta_n^{(2)}(\nu,\delta)\log\ell$. Recall that $\Delta_n^{(2)}$ is the coefficient of the α^2 term of the quantity $\Delta_n(\nu,\delta,\alpha)$ that we introduced in Eq. (9.3.24). Plugging this result into Eq. (1.4.18), we find that the SRRE in the ground state of the long-range SSH model behaves for large ℓ as

$$S_n(q) = S_n - \frac{1}{2}\log\log\ell + \Upsilon_n(\nu,\delta)\frac{(q-\ell/2)^2}{\log\ell} + \Upsilon'_n(\nu,\delta) + o(1/\log\ell), \tag{9.3.29}$$

in the interval $0 \leq \nu < 1$, with

$$\Upsilon_n(\nu,\delta) = \frac{1}{4(n-1)}\left[\frac{1}{\left|\Delta_n^{(2)}(\nu,\delta)\right|} - \frac{n}{\left|\Delta_1^{(2)}(\nu,\delta)\right|}\right], \tag{9.3.30}$$

and

$$\Upsilon'_n(\nu,\delta) = \frac{1}{1-n}\log\left[(2\sqrt{\pi})^{n-1}\frac{\left|\Delta_1^{(2)}(\nu,\delta)\right|^{n/2}}{\left|\Delta_n^{(2)}(\nu,\delta)\right|^{1/2}}\right]. \tag{9.3.31}$$

Let us discuss the result in Eq. (9.3.29). The leading terms for large ℓ (up to $O(1)$) do not depend on the charge q; at first order in ℓ, they are given by the total Rényi entanglement entropy S_n in Eq. (9.3.27). Moreover, note that the coefficient of the double logarithmic correction is $1/2$, as in the short-range case. In Ref. [121], it was proven that, for CFTs with an internal Lie group symmetry, the coefficient of such term is equal to half of the dimension of the group, which here is $U(1)$. Thus, somehow, the long-range hoppings do not spoil this result. The first term that breaks equipartition is at order $O((\log\ell)^{-1})$ and its amplitude is governed by the coefficient $\Upsilon_n(\nu,\delta)$ defined in Eq. (9.3.30). The presence of such term is a novelty with respect to what happens in the critical short-range systems, where the first term breaking the equipartition occurs at order $O((\log\ell)^{-2})$. In the case of the tight-binding model, the modes $\mathcal{Z}_n(q)$ are also Gaussian in the large ℓ limit, but the variance is proportional to $1/n$, cf. Eq. (8.2.3). The latter implies that the term of order $O((\log\ell)^{-1})$ in the SRRE vanishes. On the contrary, in our case, the variance, which is given by the coefficient $\Delta_n^{(2)}(\nu,\delta)$, has a complicated dependence on n. For this reason, the $O((\log\ell)^{-1})$ term does not cancel in the long-range case, as it would occur if $\Delta_n^{(2)}(\nu,\delta) \propto 1/n$. This is precisely the situation at $\nu = 0$, for which $\Delta_n^{(2)}(0,\delta) = -1/(2\pi^2 n)$, and therefore $\Upsilon_n(\nu=0,\delta) = 0$, i.e. the correction at $O((\log\ell)^{-1})$ disappears. In this case, the additive term $\Upsilon'_n(\nu,\delta)$ in Eq. (9.3.29) reads

$$\Upsilon'_n(\nu=0,\delta) = \frac{1}{2}\frac{\log n}{1-n} + \frac{1}{2}\log\frac{\pi}{2}, \tag{9.3.32}$$

and it is the same as that of the tight-binding model [90].

The asymptotic expression found in Eq. (9.3.29) properly describes the SRREs for values of ℓ that are not accessible numerically by diagonalising the correlation matrix. In Fig. 9.3, we check that the SRREs obtained by integrating numerically Eq. (9.3.25) match the exact values computed from the diagonalization of the correlations. Nevertheless, for the range of ℓ considered in the right panel of this figure, the SRREs are still far from behaving as Eq. (9.3.29) predicts in the large ℓ limit. In fact, from that plot is clear that the difference $S_n(q) - S_n$ is not in general a monotonic decreasing function on ℓ, as Eq. (9.3.29) actually is. In Fig. 9.4, we take larger values of ℓ and we show that the SRREs computed through the numerical integration of Eq. (9.3.25) tend to the asymptotic expression of Eq. (9.3.29) when $\ell > 10^{200}$, an unreasonably large number. Such a gigantic scale is not a consequence of any peculiar feature of the long-range SSH model, but just a very unfortunate coincidence. In general, one does not expect such enormous scale to observe the predicted asympotic behaviour. For example, in the tight-binding model, the SRRE tends to the asymptotic behaviour when the length of the interval is $\ell > 10^2$, see Ref. [90].

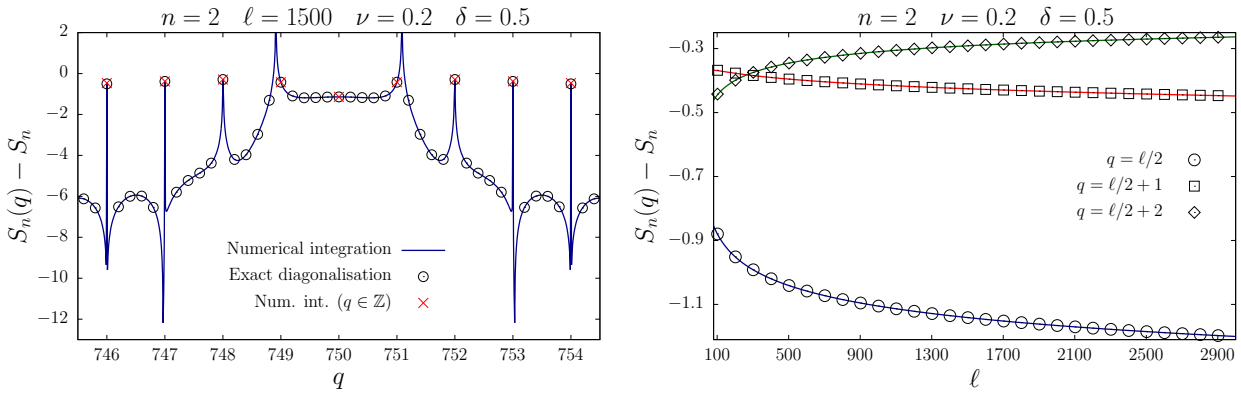

Figure 9.3: In the left panel, we study the SRRE $n = 2$ as a function of the charge q for an interval of fixed length $\ell = 1500$. Note that we subtract the entanglement entropy S_n. The points $\circ$ have been obtained by computing numerically the charged moments through Eq. (9.3.1). The continuous line corresponds to integrating numerically Eq. (9.3.25), taking as $O(1)$ term the function fitted in the left plot of Fig. 9.2, $\sum_{j=1}^{8} b_{2j}\alpha^{2j}$. We indicate by $\times$ the values that this curve takes when q is an integer. In the right panel, we analyse the SRRE $n = 2$ by varying the length of the interval ℓ for different fixed values of the charge. As in the left plot, the points have been obtained by calculating numerically the charged moments applying Eq. (9.3.1) while the lines correspond to integrating numerically Eq. (9.3.25) with the same $O(1)$ term as before.

9.4 Closing remarks

In this Chapter, we have derived exact results for the SRREs of an interval of size ℓ in an infinite quadratic fermionic chain with dimerised long-range couplings, decaying as a power law with the distance. A general feature of systems with this kind of couplings is that they effectively behave as a short-range model above a certain value of the dumping exponent ν of the coupling, while below such value they genuinely display a long-range character [452]. Here we have seen that this also occurs when we study the symmetry resolution of the ground state entanglement.

Let us indicate some possible directions for future investigations. Here we have taken as subsystem a single interval of contiguous sites. Our analysis can be straightforwardly extended to disjoint intervals by applying the results on minors of (block) Toeplitz matrices derived in Ref. [477] for the study of the entanglement entropy of disjoint intervals in quadratic, homogeneous fermionic chains. This multipartite geometry also opens the way to examine the entanglement negativity, which is a quantifier of the entanglement in mixed states both total [151, 152, 163, 478, 479, 559] and symmetry resolved [88, 101, 116, 118]. Finally, it would be interesting to explore the effect of the long-range couplings also in interacting systems, e.g. the XXZ spin chain [452]: one may wonder whether the universal prefactor of the logarithmic term of the charged moments [84] keeps its universal behaviour or is affected by the long-range couplings, as happens in the (dimerised) free case. A final intriguing related calculation concerns the study of the symmetry resolution of long-range hierarchical models, generalising known results for the total entanglement [480, 481].

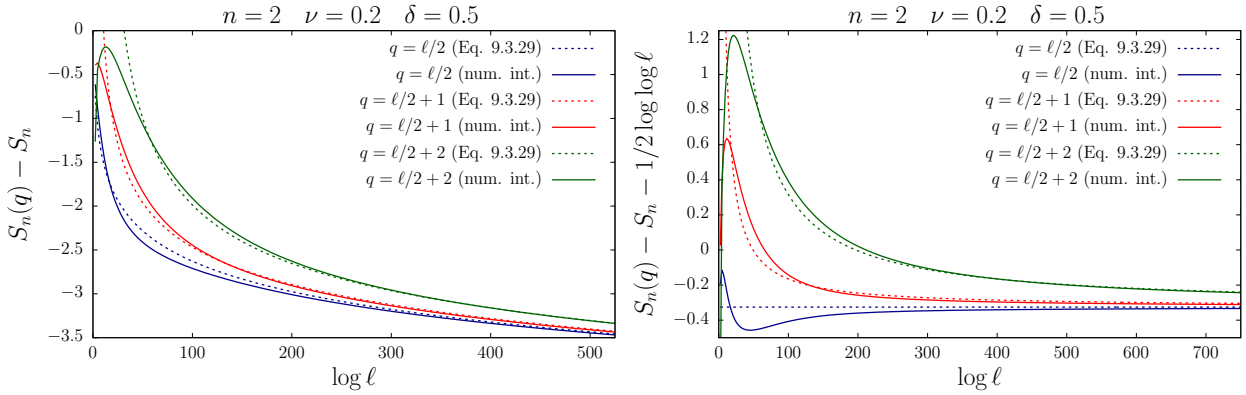

Figure 9.4: Analysis of the SRRE $n = 2$ as a function of the length of the interval ℓ for different charges q. The continuous curves represent the result obtained by integrating numerically Eq. (9.3.25), using the function fitted in the left panel of Fig. 9.2 as $O(1)$ term, while the dashed ones correspond to the asympotic prediction of Eq. (9.3.29). Note that, comparing with Fig. 9.3, here we have considered larger intervals, up to $\ell = 10^{500}$. In the plot on the left, we have removed the contribution from the Rényi entanglement entropy while in the right one we have also subtracted the term $-1/2 \log \log \ell$.

Chapter 10

Symmetry resolved Page curves

Given a statistical ensemble of quantum states, the corresponding *Page curve* quantifies the average entanglement entropy associated with each possible spatial bipartition of the system. In this Chapter, we study a natural extension in the presence of a conservation law and introduce the *symmetry resolved Page curves*, characterising average bipartite symmetry resolved entanglement entropies. We derive explicit analytic formulae for two important statistical ensembles with a $U(1)$-symmetry: Haar-random pure states and random fermionic Gaussian states. In the former case, the symmetry resolved Page curves can be obtained in an elementary way from the knowledge of the standard one. This is not true for random fermionic Gaussian states. In this case, we derive an analytic result in the thermodynamic limit based on a combination of techniques from random-matrix and large-deviation theories. We test our predictions against numerical calculations and discuss the sub-leading finite-size corrections. This Chapter is based on Ref. [106].

10.1 Introduction

Consider an isolated quantum system S in a random pure state $|\psi\rangle$. Taking a bipartition $S = A \cup B$, one may ask what is the corresponding entanglement entropy [10]. The answer is encoded in an elegant formula conjectured by Page [30], now a classical result in quantum mechanics. Page's contribution is one of the first steps towards a systematic characterisation of entanglement in random quantum states, with important applications in different fields, ranging from the black-hole information paradox [31–35] to foundations in statistical mechanics [36,37]. From the point of view of many-body physics, Page's formula provides qualitative insight into generic systems, as random states are expected to capture the behavior of either eigenstates of typical Hamiltonians [482,484–487,523], or of states generated by a sufficiently chaotic dynamics [488,489]. In addition, it shows the power of random ensembles to characterise entanglement-related quantities. This is particularly interesting, given the established difficulty to study them in many-body systems [13,15,21].

In his work, Page considered pure states distributed according to the Haar measure and focused on the averaged von Neumann entanglement entropy S_1, describing what is now known as the *Page curve*. Although it is non-trivial, its form becomes elementary in the limit of large Hilbert-space dimensions: given the Hilbert space $\mathcal{H} = \mathcal{H}_A \otimes \mathcal{H}_B$ associated with the system bipartition $S = A \cup B$, Page's formula gives

$$S_1 = \min(\log d_A, \log d_B) + O(1), \tag{10.1.1}$$

where d_A, d_B are the dimensions of $\mathcal{H}_A$, $\mathcal{H}_B$. That is, up to subleading corrections, the average entanglement entropy of a subsystem is the maximal one, meaning that typical states display almost maximal bipartite entanglement.

Page's formula, which built upon earlier results [490, 491], was later proven in Refs. [492–495], and inspired generalisations in a series of works characterising higher entanglement moments [496–500], large deviations [500–509], entanglement spectrum [510–512], mixed-state purity [513] and negativity [514–520]. Recently, some of these results were also extended to ensembles of *random Gaussian states*, capturing the typical behavior of *non-interacting* systems. In particular, motivated by studies of entanglement in random spin chains [521, 522, 524–526], the Page curve for fermionic Gaussian states was computed for finite systems in Ref. [527], while further results were obtained in the thermodynamic limit [528–530], see Ref. [487] for a review.

In this context, an important problem is the characterisation of entanglement in random ensembles displaying a conserved quantity, a setting which resembles more closely typical many-body systems. While a number of previous studies have focused on the standard entanglement entropy [487, 500, 508, 514, 530], a very natural question pertains to its symmetry resolved (SR) version [84–86] (see also [531]).

In this Chapter, we investigate the SREE in the two statistical ensembles discussed above: Haar-random and fermionic Gaussian random states, with an additional $U(1)$ symmetry. We derive explicit analytic formulae for the corresponding *symmetry resolved Page curves*. First, following Ref. [500], we show that the latter can be derived in an elementary way for Haar-random states. This is not true for random fermionic Gaussian states. In this case, we show that an analytic result can be obtained in the thermodynamic limit, based on a combination of techniques from random-matrix (RM) and large-deviation theories. We test our predictions against numerical calculations and discuss the sub-leading finite-size contributions.

The rest of this Chapter is organised as follows. In Sec. 10.2 we study the ensemble of Haar-random pure states, and show that the SR Page curve can be related in an elementary way to the standard one. The ensemble of random fermionic Gaussian states is discussed in Sec. 10.3. Using a combination of different techniques, we derive an explicit analytic formula valid in the thermodynamic limit, and provide exact numerical results at finite system sizes. Our conclusions are consigned to Sec. 10.4.

10.2 Haar-random pure states

We start by studying an ensemble of Haar-random pure states with a $U(1)$ charge. This can be realised, for instance, as the ensemble of states constructed by following up to late times a stochastic unitary dynamics with a $U(1)$ charge [532–534]. We focus on a lattice of L two-level quantum systems, associated with the Hilbert space $\mathcal{H} = \bigotimes_{j=1}^{L} \mathcal{H}_j$, where $\mathcal{H}_j \simeq \mathbb{C}^2$, and introduce the explicit symmetry operator

$$\hat{Q} = \frac{1}{2}\sum_{j=1}^{L}(\sigma_j^z + 1) \tag{10.2.1}$$

where σ_j^z are Pauli matrices (we use the notation $\hat{Q}$ or $\hat{Q}_A$ to distinguish the charge operators from the eigenvalues Q). We can decompose the Hilbert space as $\mathcal{H} = \bigoplus_{M=0}^{L} \mathcal{H}(M)$, where $\mathcal{H}(M) \subset \mathcal{H}$ is the charge eigenspace associated with the eigenvalue M. Finally, we introduce the ensemble of random states $|\psi\rangle$ drawn out of the uniform Haar distribution over the set of all states in $\mathcal{H}(M)$.

We will consider a bipartition $S = A \cup B$, where A and B contain ℓ and $L-\ell$ sites, respectively. Differently from the case studied in [30], the Hilbert space $\mathcal{H}(M)$ does not factorise into a tensor product, but we have the decomposition

$$\mathcal{H}(M) = \bigoplus_{Q=0}^{M} \mathcal{H}_A(Q) \otimes \mathcal{H}_B(M-Q)\,. \tag{10.2.2}$$

Here $\mathcal{H}_A(Q)$ is the eigenspace of Q_A associated with eigenvalue Q, and similarly for $\mathcal{H}_B(M-Q)$.

Ensembles of Haar-random states over spaces admitting a decomposition of the form (10.2.2) were studied recently in Ref. [500], where analytic formulae for the Page curve and its variance were derived. In fact, the results presented in Ref. [500] also allow one to directly obtain the SREE, as we now explain.

Given $|\psi\rangle \in \mathcal{H}(M)$, we can exploit the structure of $\mathcal{H}(M)$ in Eq. (10.2.2) to write

$$|\psi\rangle = \sum_{Q=0}^{M} \sqrt{p_Q}\, |\phi_Q\rangle \tag{10.2.3}$$

where $|\phi_Q\rangle \in \mathcal{H}_A(Q) \otimes \mathcal{H}_B(M-Q)$ is a normalised state, while $p_Q \geq 0$, with $\sum_Q p_Q = 1$. The reduced density matrix over A then reads

$$\rho_A = \sum_{Q=0}^{M} p_Q \rho_A(Q)\,, \tag{10.2.4}$$

where

$$\rho_A(Q) = \mathrm{tr}_B(|\phi_Q\rangle\langle\phi_Q|)\,. \tag{10.2.5}$$

Here we used

$$\mathrm{tr}_B(|\phi_Q\rangle\langle\phi_{Q'}|) = \delta_{Q,Q'}\rho_A(Q)\,, \tag{10.2.6}$$

which follows from the definition of $|\phi_Q\rangle$. Our goal is to compute the average entropy of the density matrix $\rho_A(Q)$ in (10.2.5).

It was shown in Ref. [500] that the uniform measure over $\mathcal{H}(M)$ factorises as

$$\mathrm{d}\mu_M(\psi) = \mathrm{d}\nu\,(p_0,\ldots,p_M) \prod_{Q=0}^{M} \mathrm{d}\mu\,(\phi_Q)\,, \tag{10.2.7}$$

where $\mathrm{d}\mu\,(\phi_Q)$ is the uniform measure over pure states in each sector $\mathcal{H}_A(Q)\otimes\mathcal{H}_B(M-Q)$, while $\mathrm{d}\nu\,(p_0,\ldots,p_M)$ is the multivariate beta distribution [500]

$$\mathrm{d}\nu\,(p_0,\ldots,p_M) = \frac{1}{\mathcal{Z}}\delta(\sum_Q p(Q)-1)\prod_Q p(Q)^{d_A(Q)d_B(Q)}\mathrm{d}p(Q). \tag{10.2.8}$$

The constant $\mathcal{Z}$ is introduced to normalise the measure to unity. Eq. (10.2.7) immediately yields the SR Page curve. Indeed, using (10.2.5), we can write the averaged bipartite Rényi entropies as

$$S_n(Q) = \frac{1}{1-n}\int \mathrm{d}\mu\,(\phi_Q)\log \mathrm{Tr}\rho_A^n(Q). \tag{10.2.9}$$

Eq. (10.2.7) implies that $|\phi_Q\rangle$ is distributed according to the invariant measure over $\mathcal{H}_A(Q)\otimes\mathcal{H}_B(M-Q)$. Therefore, we are left with the problem of computing the average entanglement entropy of a random state in a factorised Hilbert space, which is the problem studied by Page [30, 487]. For the case of the von Neumann entanglement entropy, $n=1$, we can thus apply directly Page's formula, and, for $d_A(Q)\leq d_B(Q)$, the final result reads

$$S_1(Q) = \Psi\left(d_A(Q)d_B(Q)+1\right) - \Psi\left(d_B(Q)+1\right) - \frac{d_A(Q)-1}{2d_B(Q)}\,, \tag{10.2.10}$$

where $\Psi(x) = \Gamma'(x)/\Gamma(x)$ is the digamma function (here, $\Gamma(x)$ is the Gamma function), while $d_A(Q)$ and $d_B(Q)$ are the dimensions of $\mathcal{H}_A(Q)$ and $\mathcal{H}_B(M-Q)$, namely

$$d_A(Q) = \binom{\ell}{Q}, \; d_B(Q) = \binom{L-\ell}{M-Q}. \tag{10.2.11}$$

For $d_A(Q) > d_B(Q)$, we can simply exploit the symmetry under exchange $A \leftrightarrow B$: the final result is obtained from Eq. (10.2.10) by exchanging $d_A(Q) \leftrightarrow d_B(Q)$.

We now consider the thermodynamic limit of Eq. (10.2.10). This is performed by taking $L \to \infty$, and keeping the ratios

$$\xi = \frac{\ell}{L}, \quad m = \frac{M}{L}, \quad q = \frac{Q}{L}, \tag{10.2.12}$$

constant. In this limit, the SREE behaves like $S_1(Q) \simeq \log d_A(Q)$, and a simple computation yields

$$\frac{S_1(Q)}{L} = \xi \log \xi - q \log q - (\xi - q)\log(\xi - q) - 1/(2L) \log\, L + o(1/L)\,. \tag{10.2.13}$$

Importantly, we see that this formula does explicitly depend on the charge sector Q, breaking the equipartition at leading order $O(L)$. This is similar to what has been predicted for the SREE in thermodynamic states of integrable systems [109]. However, it is different than what has been observed so far in the study of the zero-temperature entanglement resolution, see, e.g. Ref. [85]. Our result is related to the specific order of limits we are taking, i.e. $L \to \infty$ with q fixed. Conversely, we see that the next-to-leading term is independent of Q. Eq. (10.2.13) holds for $d_A(Q) \leq d_B(Q)$, i.e.

$$\xi \log \xi - q \log q - (\xi - q)\log(\xi - q) < (1-\xi)\log(1-\xi) - (m-q)\log(m-q) - (1-\xi-m+q)\log(1-\xi-m+q)\,. \tag{10.2.14}$$

When this inequality is not satisfied, the SREE is obtained from Eq. (10.2.13) replacing $\xi \leftrightarrow 1-\xi$, $q \leftrightarrow m - q$. Interestingly, we see that, in the thermodynamic limit, the SR Page curve does not depend explicitly on m when (10.2.14) holds. Moreover, up to subleading corrections, Eq. (10.2.13) gives us the maximal value of the entropy for the bipartition $\mathcal{H}_A(Q) \otimes H_B(M-Q)$, i.e. $\log d_A(Q)$.

The number entropy The number entropy defined in Eq. (1.3.5) is obtained as an integral over the probability distribution (10.2.8). The calculation is technically rather cumbersome, but fortunately can be found in disguise in Ref. [500] (see appendix B there), where it is calculated via the replica trick. Here, we only report the final result, which reads

$$S_{\text{num}} = \Psi(d_M + 1) - \sum_Q \frac{d_A(Q) d_B(Q)}{d_M} \Psi(d_A(Q) d_B(Q) + 1), \tag{10.2.15}$$

where $d_M = \sum_Q d_A(Q) d_B(Q)$ is the dimension of the Hilbert space $\mathcal{H}(M)$.

We can also easily extract the thermodynamic limit from the finite-size result in Eq. (10.2.15). In order to simplify the derivation, we note that, in this limit, the averaged number entropy equals the number entropy of the averaged probability, as $\mathbb{E}[p(Q)]$ becomes peaked around $q = m\xi$. The latter is given by $\mathbb{E}[p(Q)] = d_A(Q) d_B(Q)/d_M$, as one can obtain by integrating $p(Q)$ over the distribution (10.2.8) [500]. By taking the thermodynamic limit of $d_A(Q), d_B(Q)$, we find

$$\begin{aligned} S_{\text{num}} &= -\, L \int_0^\xi dq\, \mathbb{E}[p(Q)] \log \mathbb{E}[p(Q)] = 0 + o(L), \\ S_{\text{c}} &= L \int_0^\xi dq\, \mathbb{E}[p(Q)] S_1(Q) = L((m-1)\log(1-m) - m \log m) + o(L). \end{aligned} \tag{10.2.16}$$

The configurational entropy S_c coincides with the total entanglement entropy $S_1(\rho_A)$, satisfying the sum rule in Eq. (1.3.5). In order to compute the first sub-leading contribution to the number entropy, we can expand $\mathbb{E}[p(Q)]$ quadratically around $q = m\xi$, yielding

$$S_{\text{num}} = -\mathcal{N}^{-1} L \int_0^{\xi} dq\, e^{-\frac{(q-m\xi)^2}{2\sigma}} \log(\mathcal{N}^{-1} e^{-\frac{(q-m\xi)^2}{2\sigma}}), \tag{10.2.17}$$

where

$$\sigma = (1-m)m\xi(1-\xi)/L, \quad \mathcal{N} = L \int_0^{\xi} dq\, e^{-\frac{(q-m\xi)^2}{2\sigma}}. \tag{10.2.18}$$

By performing the integral in Eq. (10.2.17), we get

$$S_{\text{num}} = \frac{1}{2} \log(2\pi m(1-m)\xi(1-\xi)L) + \frac{1}{2}. \tag{10.2.19}$$

To summarise, we have found that the number entropy is sub-leading with respect to the total entropy and it scales as the logarithm of the variance of $p(Q)$, with a prefactor which does not depend on m, ξ but it is equal to $1/2$. This can be connected to the result for conformal field theories with an internal Lie group symmetry [121], where the authors showed that the coefficient of such term is equal to half of the dimension of the group, which here is $U(1)$. Thus, despite we are not at criticality, this result is not spoiled and it seems to be even more general.

10.3 Random fermionic Gaussian states

We now move on to study the ensemble of fermionic random Gaussian states with a $U(1)$ symmetry [487]. We take a model of L fermionic modes associated with the creation and annihilation operators c_j, $c_j^\dagger$ with $\{c_j^\dagger, c_k\} = \delta_{j,k}$. The charge is the particle number

$$\hat{Q} = \sum_{j=1}^{L} c_j^\dagger c_j \,. \tag{10.3.1}$$

We recall that Gaussian states can be defined as the states satisfying Wick's theorem [537] and that, in the case where the particle number is fixed, they are completely specified by the covariance matrix

$$C_{i,j} = \langle \psi | c_i^\dagger c_j | \psi \rangle \,. \tag{10.3.2}$$

The ensemble of random Gaussian states with fixed particle number M can be defined by the ensemble of covariance matrices $C = V^\dagger C_0(M) V$, where V is drawn out of the uniform Haar distribution over the unitary group $U(L)$ and

$$C_0(M) = \text{diag}(\underbrace{1, \dots, 1}_{M}, \underbrace{0, \dots, 0}_{L-M}) \,. \tag{10.3.3}$$

This distribution can be achieved as the late-time limit of stochastic Gaussian dynamics.

In this case, it is not possible to apply directly the logic of the previous section. While, given a random Gaussian state $|\psi\rangle$, we can still write the decomposition (10.2.3), the projected states $|\phi_Q\rangle$ are in general not Gaussian. Therefore, one cannot compute the corresponding bipartite entanglement entropy in terms of random Gaussian ensembles. Nevertheless, in the next subsection we show that the SR Page curve can be computed analytically in the thermodynamic limit (10.2.12), where we have the scaling

$$S_1(Q) \sim L s_1(q) + o(L) \,. \tag{10.3.4}$$

In the next subsections we will compute $s_1(q)$ as a function of ξ, defining the SR Page curve. Our approach is based on a combination of the Gärtner-Ellis theorem [538], detailed in Sec. 10.3.1, and the Coulomb-gas (CG) method of RM theory [539, 540], explained in Sec. 10.3.2.

10.3.1 SR entanglement from the Gärtner-Ellis theorem

In principle, the SREE could be computed using the strategy outlined in Sec. 1.4.2. However, the Fourier transform in (1.4.17) introduces some technical complications from the analytic point of view. In this section, we provide an alternative approach valid in the thermodynamic limit, which is based on an application of the Gärtner-Ellis theorem from large deviation theory [538]. This method has been recently introduced in Ref. [109] to compute the SREE of thermodynamic states in quantum integrable models.

Let us denote by ρ the density matrix of the subsystem A. First, using

$$[\rho, \Pi_Q] = 0\,, \tag{10.3.5}$$

and the fact that $\Pi_Q^n = \Pi_Q$ for any power n, we can write

$$\mathrm{tr}[\rho^n(Q)] = p_n(Q)\frac{\mathrm{tr}[\rho^n]}{(p_1(Q))^n}\,, \tag{10.3.6}$$

where we have introduced

$$p_n(Q) = \frac{\mathrm{tr}[\Pi_Q \rho^n]}{\mathrm{tr}[\rho^n]}\,. \tag{10.3.7}$$

Therefore, the averaged SRRE is

$$\mathbb{E}[S_n(Q)] = \frac{1}{1-n}\left(\mathbb{E}\left[\log p_n(Q)\right] - n\mathbb{E}\left[\log p_1(Q)\right]\right) + \mathbb{E}\left[S_n\right]\,, \tag{10.3.8}$$

where S_n is the standard (non-resolved) Rényi entropy, while $\mathbb{E}[\cdot]$ now denotes the average over the ensemble of random Gaussian states.

In order to proceed, we make the assumption that

$$\mathbb{E}\left[\log p_n(Q)\right] = \log \mathbb{E}\left[p_n(Q)\right] + o(L)\,, \tag{10.3.9}$$

namely that, up to sub-leading-order corrections, we can bring the average "inside the logarithm". We have tested numerically the validity of this assumption, cf. 10.3.4, which can be justified invoking the concentration of measure for fermionic random Gaussian states [527, 530]. Now, it is immediate to see that $\mathbb{E}\left[p_n(Q)\right] \geq 0$ and $\sum_Q \mathbb{E}\left[p_n(Q)\right] = 1$. Therefore, $\mathbb{E}\left[p_n(Q)\right]$ can be interpreted as a probability distribution. Setting $q = Q/L$, we expect on physical grounds that $\mathbb{E}\left[p_n(Q)\right]$ follows a large deviation principle in the large-L limit, that is,

$$\mathbb{E}\left[p_n(Q)\right] \sim e^{-I_n(q)L}\,, \tag{10.3.10}$$

where $I_n(q)$ is referred to as the *rate function* [538]. To compute it, we define the generating function

$$G_n(w) = \mathbb{E}\left[\frac{\mathrm{tr}\left[\rho^n e^{w\hat{Q}}\right]}{\mathrm{tr}[\rho^n]}\right]\,, \qquad w \in \mathbb{R}\,, \tag{10.3.11}$$

and

$$f_n(w) = \lim_{L\to\infty}\frac{1}{L}\log G_n(w)\,. \tag{10.3.12}$$

The Gärtner–Ellis theorem [538] states that we can compute $I_n(q)$ as the Legendre transform of $f_n(w)$, namely

$$I_n(q) = w_{n,q} q - f_n\left(w_{n,q}\right) , \tag{10.3.13}$$

where $w_{n,q}$ is determined by the condition

$$\frac{d}{dw}(f_n(w) - wq)\Big|_{w=w_{n,q}} = 0 . \tag{10.3.14}$$

Finally, introducing the density of SRRE

$$s_n(q) = \lim_{L\to\infty} \frac{S_n(qL)}{L} , \tag{10.3.15}$$

and using (10.3.8), we obtain

$$s_n(q) = s_n + \frac{1}{1-n}\left[-I_n(q) + nI_1(q)\right] , \tag{10.3.16}$$

where

$$s_n = \lim_{L\to\infty} \frac{\mathbb{E}\left[S_n\right]}{L} , \tag{10.3.17}$$

is the density of the standard (non-resolved) Rényi entropy. The SREE is obtained taking the limit $n \to 1$

$$s_1(q) = s_1 + I_1(q) + \frac{\mathrm{d}I_n(q)}{\mathrm{d}n}\Big|_{n=1} . \tag{10.3.18}$$

10.3.2 The Coulomb-gas approach

In order to obtain the SRRE, we need to compute the function $f_n(w)$ in Eq. (10.3.12). To this end, we make use of the CG approach [539, 540]. In the context of fermionic random Gaussian states, this method has been recently applied in Refs. [528–530] to compute average bipartite entanglement entropies and their large deviations. Here, we briefly review the aspects of these works directly relevant for our purposes.

As mentioned, the covariance matrix (10.3.2) contains full information about the corresponding Gaussian state, encoding also its bipartite entanglement entropy [169]. In particular, given a region A containing ℓ sites, and denoting by C^A the $\ell \times \ell$ matrix with $C^A_{i,j} = C_{i,j}$ for $i, j \in A$, the corresponding Rényi entropy reads

$$S_n = \frac{1}{1-n}\sum_{j=1}^{\ell} \log\left[\lambda_j^n + (1-\lambda_j)^n\right] . \tag{10.3.19}$$

Here $\{\lambda_j\}_{j=1}^{\ell}$ are the eigenvalues of C^A, satisfying $0 \le \lambda_j \le 1$. When C is sampled according to the invariant measure discussed above, the eigenvalues λ_j are random variables. Their probability distribution, $P[\{\lambda_j\}]$, is known [539], and takes the form

$$P[\{\lambda_i\}] = \frac{1}{\mathcal{N}} \prod_{j<k} |\lambda_j - \lambda_k|^2 \prod_{i=1}^{\ell} \lambda_i^{M-\ell}(1-\lambda_i)^{L-\ell-M} , \tag{10.3.20}$$

where $\mathcal{N}$ is a normalisation constant. This distribution defines the β-Jacobi ensemble (with $\beta = 2$), see Refs. [541–543] for applications in different physical contexts .

In principle, Eq. (10.3.20) allows one to compute the expectation value of arbitrary functions of the eigenvalues. However, for finite ℓ this is often complicated, as averages involve integrals in ℓ-dimensional spaces. When $\ell \to \infty$, the problem can be simplified using a standard method of RM theory, consisting in a mapping between the eigenvalues λ_j and a Coulomb gas of repulsive point charges [539]. In order to see how it works, we consider a function $g(\{\lambda_k\})$ and write its expectation value as

$$\mathbb{E}[g(\{\lambda_k\})] = \frac{1}{\mathcal{N}} \int_0^1 \prod_{j=1}^{\ell} \mathrm{d}\lambda_j \, e^{-\ell^2 E[\{\lambda_j\}]} g(\{\lambda_k\}) \,, \tag{10.3.21}$$

with

$$E[\{\lambda_i\}] = -\frac{2}{\ell^2} \sum_{i<j} \log|\lambda_i - \lambda_j| - \frac{(M-\ell)}{\ell^2} \sum_i \log \lambda_i - \frac{(L-M-\ell)}{\ell^2} \sum_i \log(1-\lambda_i) \ .$$

Within the CG formalism, $E[\{\lambda_i\}]$ is interpreted as the energy of a gas of charged particles with coordinates $\lambda_j \in [0,1]$ and subject to an external potential. The integral (10.3.21) is the thermal partition function for the CG. In the large-ℓ limit, the configuration of the particles may be described in terms of the normalised density $\rho(\lambda) = \ell^{-1} \sum_j \delta(\lambda - \lambda_i)$, and the multiple integral in Eq. (10.3.21) can be cast into a functional integral over all possible densities $\rho(\lambda)$, i.e.

$$\mathbb{E}[g] = \int \mathcal{D}\rho \, e^{-\ell^2 E[\rho]} g[\rho] \,. \tag{10.3.22}$$

To the leading order in ℓ, $E[\rho]$ reads

$$E[\rho] = -\int_0^1 \mathrm{d}\lambda \int_0^1 \mathrm{d}\mu \, \rho(\lambda)\rho(\mu) \log|\lambda - \mu| + \int_0^1 \mathrm{d}\lambda \rho(\lambda) V(\lambda) + u \left\{ \int_0^1 \mathrm{d}\lambda \, \rho(\lambda) - 1 \right\} \,, \tag{10.3.23}$$

where we introduced the Lagrange multiplier u enforcing normalisation, and the effective potential

$$V(\lambda) = -\left(\frac{m}{\xi} - 1\right) \log \lambda - \left(\frac{1-m}{\xi} - 1\right) \log(1-\lambda) \ , \tag{10.3.24}$$

where m, ξ are the density of fermions and the rescaled interval length introduced in Eq. (10.2.12).

The functional integral (10.3.22) can be computed via the saddle-point method, and the average is dominated by the typical distribution function $\rho^*(\lambda)$ satisfying $\delta E[\rho]/\delta\rho|_{\rho=\rho^*} = 0$. The solution is known [544, 545] and reads

$$\rho^*(\lambda) = \frac{1}{2\pi\xi} \frac{\sqrt{(\nu_+ - \lambda)(\lambda - \nu_-)}}{\lambda(1-\lambda)} \,, \tag{10.3.25}$$

with $\lambda \in [\nu_-, \nu_+]$ and $\nu_\pm = [\sqrt{m(1-\xi)} \pm \sqrt{\xi(1-m)}]^2$. Eq. (10.3.25) allows us to compute directly, in the thermodynamic limit, averages of extensive quantities which can be written as sums over the eigenvalues, by replacing them with integrals over $\lambda \in [\nu_-, \nu_+]$. For example, the averaged Rényi entropy (10.3.19) can be computed as

$$\mathbb{E}[S_n] = \ell \int_{\nu_-}^{\nu_+} \mathrm{d}\lambda \rho^*(\lambda) \sigma_n(\lambda) \,, \tag{10.3.26}$$

where $\sigma_n(\lambda) = \frac{1}{1-n} \log[\lambda^n + (1-\lambda)^n]$, see Ref. [529] for an explicit expression of this integral.

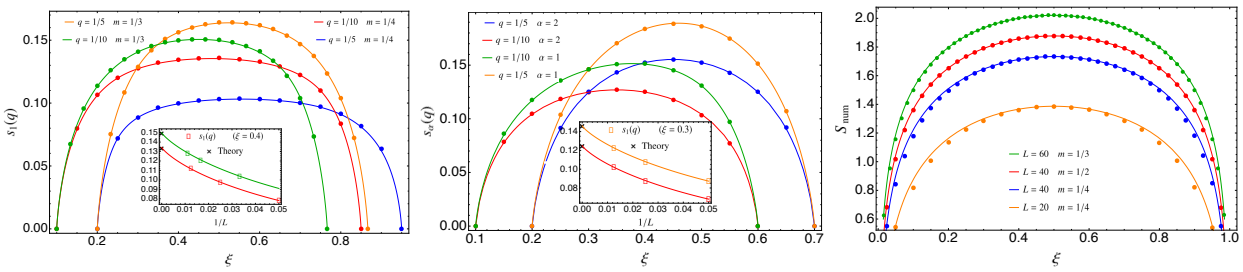

Figure 10.1: Left/middle panel: Comparison between the asymptotic results derived in subsection 10.3.3 and the exact values of the average entanglement entropy $s_n(q)$ computed numerically for $L \to \infty$ (symbols). They have been obtained by using the extrapolation form $s_1(q) = a - 1/(2L)\log L + b/L$. Insets show data for different values of L. The solid line for $n = 1$ corresponds to Eq. (10.3.35) and its extension to $\xi > m$ according to Eq. (10.3.36). Right panel: The average number entropy in Eq. (10.3.42) for different values of m, ξ, L.

10.3.3 Exact SR Page curves

We finally combine the techniques outlined in the previous subsections, and obtain an analytic result for the SREE. Our starting point is the computation of $f_n(w)$ defined in Eq. (10.3.12). Once again, we can use a typicality argument and exchange the order of the expectation value and the logarithm in Eqs. (10.3.8), (10.3.12). We are left with the task of computing

$$f_n(w) = \mathbb{E}[\log \mathrm{tr}(\rho^n e^{w\hat{Q}})] - \mathbb{E}[\log \mathrm{tr}(\rho^n)]\,. \tag{10.3.27}$$

Following the previous subsection, we write the rhs in terms of the eigenvalues λ_j of the reduced covariance matrix C^A. In particular, we have

$$\log \mathrm{tr}(\rho^n e^{w\hat{Q}}) = \sum_{j=1}^{\ell} \log\left[e^w \lambda_j^n + (1-\lambda_j)^n\right]\,. \tag{10.3.28}$$

In the thermodynamic limit $\ell \to \infty$, we can apply the CG approach and obtain

$$\lim_{L\to\infty} \frac{\mathbb{E}[\log \mathrm{tr}(\rho^n e^{w\hat{Q}})]}{L} = \xi \int_{\nu_-}^{\nu_+} d\lambda \rho^*(\lambda) \log(e^w \lambda^n + (1-\lambda)^n). \tag{10.3.29}$$

Consequently, $I_n(q)$ in Eq. (10.3.13) reads

$$I_n(q) \;=\; w_{n,q} q - \xi \int_{\nu_-}^{\nu_+} d\lambda \rho^*(\lambda) \log(e^{w_{n,q}} \lambda^n + (1-\lambda)^n) + \xi \int_{\nu_-}^{\nu_+} d\lambda \rho^*(\lambda) \log(\lambda^n + (1-\lambda)^n)]. \tag{10.3.30}$$

The value of $w_{n,q}$ is fixed by Eq. (10.3.14), which can be rewritten as

$$q = \xi \int_{\nu_-}^{\nu_+} d\lambda \rho^*(\lambda) \frac{e^{w_{n,q}} \lambda^n}{e^{w_{n,q}} \lambda^n + (1-\lambda)^n}\,. \tag{10.3.31}$$

Plugging $w_{n,q}$ into the expression for $I_n(q)$ in Eq. (10.3.30), we get the density of SRRE $s_n(q)$ in Eq. (10.3.16). From Eq. (10.3.31), we see that $w_{n,q}$ can be obtained by inverting the equation numerically, after evaluating simple integrals. We followed this procedure to generate plots of the

function $s_n(q)$ for $n > 1$, as reported in Fig. 10.1. For generic n, we were not able to find an analytical expression of $w_{n,q}$. However, Eq. (10.3.31) can be computed explicitly and inverted in the limit $n \to 1$ (see [106] for the details). In this case, we find

$$w_{1,q} = \log\left[\frac{q(-1+m-q+\xi)}{(m-q)(q-\xi)}\right], \tag{10.3.32}$$

and, according to Eq. (10.3.18), we are left with

$$\begin{aligned} s_1(q) =& -(w_{1,q} - w'_{1,q})q + \xi \int_{\nu_-}^{\nu_+} d\lambda \rho^*(\lambda) \log(e^{w_{1,q}}\lambda + (1-\lambda)) \\ &- \xi \int_{\nu_-}^{\nu_+} d\lambda \rho^*(\lambda) \frac{(1-\lambda)\log(1-\lambda) + e^{w_{1,q}}\lambda(\log\lambda)}{(e^{w_{1,q}}-1)\lambda + 1} - \int_{\nu_-}^{\nu_+} \frac{d\lambda}{2\pi} \frac{\sqrt{(\lambda-\nu_-)(\nu_+-\lambda)}}{(1-\lambda)} \frac{e^{w_{1,q}} w'_{1,q}}{(e^{w_{1,q}}-1)\lambda+1}. \end{aligned} \tag{10.3.33}$$

In order to simplify our computation, we observe that, from Eq. (10.3.31),

$$\int_{\nu_-}^{\nu_+} \frac{d\lambda}{2\pi} \frac{\sqrt{(\lambda-\nu_-)(\nu_+-\lambda)}}{(1-\lambda)} \frac{e^{w_{1,q}}}{(e^{w_{1,q}}-1)\lambda+1} = q, \tag{10.3.34}$$

which can be straightforwardly substituted in the last term of Eq. (10.3.33) giving $-w'_{1,q}q$. This implies that we do not need the compute $w'_{1,q}$, as it cancels out in Eq. (10.3.33). The remaining integrals can be solved following the techniques used in Ref. [529]. Putting all together, we arrive at the final result (for $q \le \xi \le m$)

$$\begin{aligned} s_1(q) =& \frac{(-1+m)q(-1+\xi)\log(1-m)}{q-m\xi} + \frac{m(q-\xi)(1-\xi)\log m}{q-m\xi} + \frac{m(q-\xi)(-1+\xi)\log(m-q)}{q-m\xi} \\ &- q\log q - \frac{(1-m)q(1-\xi)\log(1-m+q-\xi)}{q-m\xi} + \xi\log\xi + (q-\xi)\log(\xi-q)\,. \end{aligned} \tag{10.3.35}$$

We remark that the equipartition of the entanglement entropy is explicitly broken also in this case. For $\xi > m$, we can obtain the SREE using the symmetries of the problem [487]. In particular, it is not difficult to show that the following relations hold (making explicit the dependence on ξ and m)

$$s_1(m;q;\xi) = s_1(\xi;q;m), \quad m < \xi \le 0.5 \tag{10.3.36}$$

$$s_1(m;q;\xi) = s_1(1-\xi;m-q;m), \ 0.5 < \xi \le 1-m \tag{10.3.37}$$

$$s_1(m;q;\xi) = s_1(m;m-q;1-\xi), \ 1-m < \xi \le 1-m+q. \tag{10.3.38}$$

Eq. (10.3.35) is our main result, which will be further discussed in the next subsection.

Finally, let us compute the averaged number entropy. To this end, we assume again that, in the thermodynamic limit, it equals the number entropy of the averaged probability. Using $\mathbb{E}[p(Q)] = e^{-LI_1(q)}\mathcal{N}$ [where $\mathcal{N}$ is a normalisation constant], we have that $\mathbb{E}[p(Q)]$ is peaked around $q = m\xi$, and to the leading order in L we have

$$\begin{aligned} S_{\rm num} =& -L\int_0^\xi dq\, \mathbb{E}[p(Q)]\log\mathbb{E}[p(Q)] = 0 + o(L), \\ S_{\rm c} =& L^2 \int_0^\xi dq\, \mathbb{E}[p(Q)] s_1(q) = L\left\{(\xi-1)\log(1-\xi) + \xi[(m-1)\log(1-m) - m\log m - 1]\right\} + o(L). \end{aligned} \tag{10.3.39}$$

This implies that the sum rule in Eq. (1.3.5) is satisfied and the number entropy is sub-leading with respect to the total entropy. In order to find the first sub-leading term, we can expand $\mathbb{E}[p(Q)]$ quadratically around $q = m\xi$, and we obtain

$$S_{\rm num} = -\mathcal{N}^{-1}\, L \int_0^\xi dq\, e^{-\frac{(q-m\xi)^2}{2\sigma}} \log(\mathcal{N}^{-1}\, e^{-\frac{(q-m\xi)^2}{2\sigma}}), \tag{10.3.40}$$

where

$$\sigma = (1-m)m\xi(1-\xi)/L, \quad \mathcal{N} = L\int_0^\xi dq\, e^{-\frac{(q-m\xi)^2}{2\sigma}}. \tag{10.3.41}$$

By comparing this result with Eq. (10.2.18), this computation shows that the expressions for $\mathbb{E}[p(Q)]$ for Haar-random and random Gaussian states are the same in the thermodynamic limit. Therefore, remarkably, we get the same result for the first sub-leading correction to the number entropy

$$S_{\rm num} = \frac{1}{2}\log(2\pi m(1-m)\xi(1-\xi)L) + \frac{1}{2}. \tag{10.3.42}$$

10.3.4 Numerical results

We have tested Eq. (10.3.35) against numerical computations. We have sampled the ensemble of random Gaussian states at finite system sizes by generating covariance matrices $V^\dagger C_0(M)V$, where $C_0(M)$ is defined in Eq. (10.3.3) and V is drawn from the uniform distribution over $U(L)$. For each Gaussian state, we have computed the SREEs following the method outlined in Sec. 1.4.2, using that the charged moments can be expressed in terms of the eigenvalues of the correlation matrix C^A, i.e.

$$Z_n(\alpha) = \prod_{j=1}^{\ell} [\lambda_j^n e^{i\alpha} + (1-\lambda_j)^n]\,. \tag{10.3.43}$$

For fixed m, ξ, we have considered 10^3 random samples. The SRREs are obtained by taking the mean value over them. We have repeated this procedure for different system sizes, L, and we have extrapolated the data at finite L in order to recover the thermodynamic limit $L \to \infty$. This allows us to compare the numerical data against the analytical predictions found in the previous subsection.

In Fig. 10.1, we show the comparison between the extrapolated data in the thermodynamic limit and the density of the SR entropies for different values of q, m, ξ, n. In all cases, the error associated with the finite-number of samples and the fitting procedure is not visible in the scales of the plot, and is therefore omitted. As in the case of Haar-random pure states, we see that the SR Page curves are not symmetric with respect to $\xi = 0.5$, and are vanishing for $\xi < q$ and $\xi > 1 - m + q$. The numerical results are found to be in excellent agreement with our analytic predictions.

It is interesting to discuss the finite-size corrections and our fitting procedure. Interestingly, our numerical results convincingly show that the sub-leading corrections to $s_n(q)$ are proportional to $(1/2)\log L/L$, independent of q, m and ξ, cf. the inset of Fig. 10.1. Accordingly, we have performed a fit of our data against the function

$$s_1(q) = a - 1/(2L)\log L + b/L\,. \tag{10.3.44}$$

We note that the sub-leading behavior is exactly the same as that for Haar random pure states, cf. Eq. (10.2.13). We note also that the sub-leading behavior $-(1/2)\log L$ to the SREEs $S_n(q)$ have

been observed in other contexts when the total entropies are extensive, see for instance Ref. [132, 136]

Finally, we have tested the first sub-leading correction to the number entropy described in Eq. (10.3.42) in the right panel of Fig. 10.1. We find that the agreement improves as the system size L increases, being excellent for $L = 60$.

10.4 Closing remarks

In this Chapter, we have considered the computation of the SR Page curves for two important statistical ensembles with a $U(1)$-symmetry: Haar-random pure states and random fermionic Gaussian states. In the former case, we have shown how an exact result can be obtained in an elementary way for finite systems and in the thermodynamic limit. This is not true for fermionic Gaussian states. Still, we were able to compute the corresponding SR Page curve in the thermodynamic limit. Our main technical tools have been the Coulomb gas method and the Gärtner-Ellis theorem. We expect that our approach could allow for the computation of SRREs in other situations where the latter are extensive.

One could wonder whether similar calculations can be extended to ensembles of random bosonic Gaussian states. As pointed out in Ref. [487], however, the only bosonic Gaussian state with a fixed particle number is the vacuum state. In addition, while one could choose an ensemble of bosonic Gaussian states with a fixed average number of particles, the very definition of SREE requires an exact conservation law. Obviously, one could also consider complex bosons and in that case the $U(1)$ symmetry is easily implemented and the SREE is always well defined, as in the field theory case [111]. We are not aware of any work in this direction.

Our results are expected to be relevant in a number of cases. They could be used as a comparison in more general situations, for instance to evaluate non-Gaussian effects in the SREE of thermodynamic states in interacting integrable systems [109]. Finally our results might be relevant for the information paradox in charged black holes in analogy to the role played by the original the Page curve for the neutral case. In particular, the results for replica wormholes [34, 35] should have a counterpart also for charged black holes.

Chapter 11

Entanglement asymmetry as a probe of symmetry breaking

Not only symmetry, but also symmetry breaking is a pillar of modern quantum physics. Still, quantifying how much a symmetry is broken is an issue that has received little attention. In extended quantum systems, this problem is intrinsically bound to the subsystem of interest. Hence, in this Chapter, we borrow methods from the theory of entanglement we have learnt so far to introduce a subsystem measure of symmetry breaking that we dub *entanglement asymmetry*. As a prototypical illustration, we study the entanglement asymmetry in a quantum quench of a spin chain in which an initially broken global $U(1)$ symmetry is restored dynamically. We adapt the quasiparticle picture for entanglement evolution to the analytic determination of the entanglement asymmetry. We find, expectedly, that larger is the subsystem, slower is the restoration, but also the counterintuitive result that more the symmetry is initially broken, faster it is restored, a sort of quantum Mpemba effect. This Chapter is based on Ref. [549].

11.1 Introduction

Since the introduction of this thesis, we have dealt with symmetries and the special place they hold in every branch of physics, from relativity to quantum mechanics, passing through gauge/gravity duality and numerical algorithms. However, sometimes it happens that, when a parameter reaches a critical value, the lowest energy configuration respecting the symmetry of the theory becomes unstable and new asymmetric lowest energy solutions can be found. This phenomenon does not require an input, whence the name spontaneous symmetry breaking. Other times a symmetry can be explicitly broken, in the sense that the Hamiltonian describing the system contains terms that manifestly break it. The present Chapter fits in this framework: our main goal is to find a tool that measures quantitatively how much a symmetry is broken.

To be more specific, the setup we are interested in is an extended quantum system in a pure state $|\Psi\rangle$, which we divide into two spatial regions A and B. The state of A is described by the reduced density matrix $\rho_A = \mathrm{Tr}_B(|\Psi\rangle\langle\Psi|)$. We consider a charge operator Q that generates a global $U(1)$ symmetry group, hence satisfying $Q = Q_A + Q_B$. If $|\Psi\rangle$ is an eigenstate of Q, then $[\rho_A, Q_A] = 0$ and ρ_A displays a block-diagonal structure, which has allowed us to compute the SREE (see Sec. 1.3). Here we consider the opposite situation: a state $|\Psi\rangle$ that breaks the global $U(1)$ symmetry. Therefore, $[\rho_A, Q_A] \neq 0$ and ρ_A is not block-diagonal in the eigenbasis of Q_A. The goal of this Chapter is to introduce a quantifier of the symmetry breaking at the level of the

subsystem A, which is the *entanglement asymmetry* defined as

$$\Delta S_A = S(\rho_{A,Q}) - S(\rho_A). \tag{11.1.1}$$

Here $\rho_{A,Q} = \sum_{q\in\mathbb{Z}} \Pi_q \rho_A \Pi_q$, where Π_q is the projector onto the eigenspace of Q_A with charge $q \in \mathbb{Z}$. Thus $\rho_{A,Q}$ is block-diagonal in the eigenbasis of Q_A. In Fig. 11.1, we pictorially show how $\rho_{A,Q}$ is obtained from ρ_A. A similar quantity, but for the full system, was introduced in Ref. [107] to study the inseparability of mixed states.

The entanglement asymmetry (11.1.1) satisfies two natural properties to quantify symmetry breaking: (i) $\Delta S_A \geq 0$, because by definition it is equal to the relative entropy between ρ_A and $\rho_{A,Q}$, $\Delta S_A = \mathrm{Tr}[\rho_A(\log \rho_A - \log \rho_{A,Q})]$, which is actually non-negative [10]; (ii) $\Delta S_A = 0$ if and only if the state is symmetric since, in this case, ρ_A is block diagonal in the eigenbasis of Q_A and $\rho_{A,Q} = \rho_A$.

A replica construction — The entanglement asymmetry can be computed from the moments of the density matrices ρ_A and $\rho_{A,Q}$ by exploiting the replica trick [17, 20]. Indeed, simply defining the Rényi entanglement asymmetry as

$$\Delta S_n^A = \frac{1}{1-n}\left[\log \mathrm{Tr}(\rho_{A,Q}^n) - \log \mathrm{Tr}(\rho_A^n)\right], \tag{11.1.2}$$

one has that $\lim_{n\to 1} \Delta S_n^A = \Delta S_A$. As usual, the advantage of this construction is that for integer n, ΔS_n^A can be accessed from (charged) partition functions. Indeed, using the Fourier representation of the projector Π_q, the post-measurement density matrix $\rho_{A,Q}$ can be alternatively written in the form

$$\rho_{A,Q} = \int_{-\pi}^{\pi} \frac{\mathrm{d}\alpha}{2\pi} e^{-i\alpha Q_A} \rho_A e^{i\alpha Q_A}, \tag{11.1.3}$$

and its moments as

$$\mathrm{Tr}(\rho_{A,Q}^n) = \int_{-\pi}^{\pi} \frac{\mathrm{d}\alpha_1 \dots \mathrm{d}\alpha_n}{(2\pi)^n} Z_n(\boldsymbol{\alpha}), \tag{11.1.4}$$

where $\boldsymbol{\alpha} = \{\alpha_1, \dots, \alpha_n\}$ and

$$Z_n(\boldsymbol{\alpha}) = \mathrm{Tr}\left[\prod_{j=1}^{n} \rho_A e^{i\alpha_{j,j+1} Q_A}\right], \tag{11.1.5}$$

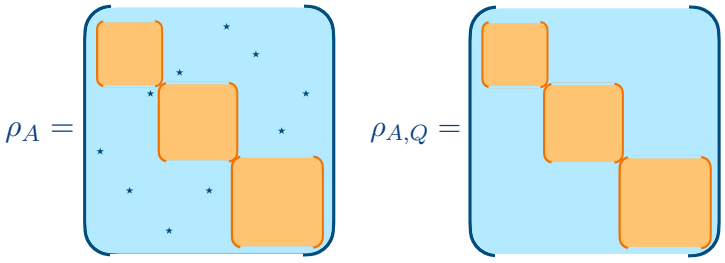

Figure 11.1: The density matrices ρ_A and $\rho_{A,Q}$ entering in the definitions (11.1.1) and (11.1.2) of the entanglement asymmetries. In the eigenbasis of the subsystem charge Q_A, ρ_A generically displays off-diagonal elements. Under a projective measurement of Q_A, we get $\rho_{A,Q}$, where the off-diagonal blocks are annihilated. The difference ΔS_n^A between the entanglement entropies of these matrices is our probe of symmetry breaking.

with $\alpha_{ij} \equiv \alpha_i - \alpha_j$ and $\alpha_{n+1} = \alpha_1$. Notice that, if $[\rho_A, Q_A] = 0$, then $Z_n(\boldsymbol{\alpha}) = Z_n(\mathbf{0})$, which implies $\mathrm{Tr}(\rho_{A,Q}^n) = \mathrm{Tr}(\rho_A^n)$ and $\Delta S_n^A = 0$. Furthermore the order of terms in Eq. (11.1.5) matters because $[\rho_A, Q_A] \neq 0$. We will refer to $Z_n(\boldsymbol{\alpha})$ as *charged moments* because they are a modification of Eq. (1.4.16). With these definitions in mind, the plan of the following part is to test their effectiveness both in and out-of equilibrium in Secs. 11.2 and 11.3, respectively. We conclude in Sec. 11.4.

11.2 Tilted Ferromagnet

As warm up, we consider an infinite spin chain prepared in the tilted ferromagnetic state

$$|\theta; \nearrow\nearrow\cdots\rangle = e^{i\frac{\theta}{2}\sum_j \sigma_j^x} |\uparrow\uparrow\cdots\rangle. \tag{11.2.1}$$

For $\theta \neq \pi m$, $m \in \mathbb{Z}$, this state breaks the $U(1)$ symmetry associated to the conservation of the total transverse magnetisation $Q = \frac{1}{2}\sum_j \sigma_j^z$. When $\theta = \pi m$, it corresponds to a fully polarised state in the z-direction, for which the transverse magnetisation is preserved. The angle θ controls how much the state breaks this symmetry and, therefore, the state (11.2.1) is an ideal testbed for the entanglement asymmetry, although it is a trivial product state. Let the subsystem A consist of ℓ contiguous sites of the chain; then $\Delta S_A = 0$ for $\theta = \pi m$ and $\Delta S_A > 0$ otherwise. Since the state is separable, $\mathrm{Tr}(\rho_A^n) = 1$, and $Z_n(\boldsymbol{\alpha})$ is straightforwardly obtained as

$$Z_n(\boldsymbol{\alpha}) = \prod_{j=1}^{n} f(\cos(\theta), \alpha_{j,j+1})^\ell \quad \text{where} \quad f(\lambda, \alpha) = i\lambda \sin\left(\frac{\alpha}{2}\right) + \cos\left(\frac{\alpha}{2}\right). \tag{11.2.2}$$

Plugging Eq. (11.2.2) into the Fourier transform (11.1.4), we obtain

$$\Delta S_n^A = \frac{1}{1-n} \log\left[\cos^{2n\ell}\left(\frac{\theta}{2}\right) \sum_{p=0}^{\ell} \binom{\ell}{p}^n \tan^{2np}\left(\frac{\theta}{2}\right)\right]. \tag{11.2.3}$$

In Fig. 11.2, we plot this entanglement asymmetry as a function of $\theta \in [0, \pi]$. As expected, it vanishes for $\theta = 0, \pi$ while it takes the maximum value at $\theta = \pi/2$, when all the spins point in the x direction and the symmetry is maximally broken. Between these extremal points, ΔS_A is a monotonic function of θ (but this is not true for all n). For a large interval, it behaves as

$$\Delta S_n^A = \frac{1}{2}\log \ell + \frac{1}{2}\log \frac{\pi n^{\frac{1}{n-1}} \sin^2\theta}{2} + O(\ell^{-1}). \tag{11.2.4}$$

The limit $\theta \to 0$ is not well defined in Eq. (11.2.4). Indeed, the limits $\ell \to \infty$ and $\theta \to 0$ do not commute: to recover the symmetry, one should take first $\theta \to 0$ in Eq. (11.2.2) and then consider the large interval regime.

11.3 Quench to the XX spin chain

We now analyse the time evolution of the entanglement asymmetry after a quantum quench. We prepare the infinite spin chain in the state

$$|\Psi(0)\rangle = \frac{|\theta; \nearrow\nearrow\cdots\rangle - |-\theta; \nearrow\nearrow\cdots\rangle}{\sqrt{2}}, \tag{11.3.1}$$

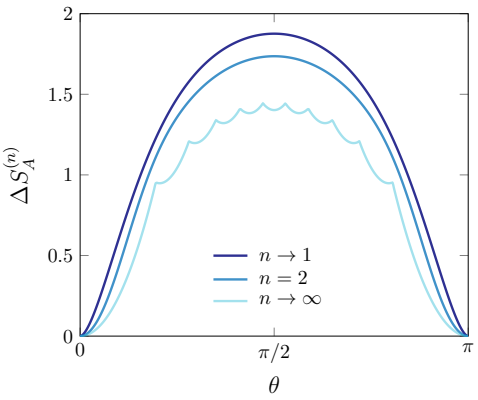

Figure 11.2: The Rényi entanglement asymmetry ΔS_n^A in Eq. (11.2.4) for the tilted ferromagnetic state as a function of the tilting angle θ for different values of the replica index n.

which is the *cat* version of the symmetry-breaking state in Eq. (11.2.1). We then let it evolve

$$|\Psi(t)\rangle = e^{-itH}|\Psi(0)\rangle, \tag{11.3.2}$$

with the symmetric XX Hamiltonian ($[H, Q] = 0$)

$$H = -\frac{1}{4}\sum_{j=-\infty}^{\infty}\left[\sigma_j^x\sigma_{j+1}^x + \sigma_j^y\sigma_{j+1}^y\right]. \tag{11.3.3}$$

This Hamiltonian is diagonalised via the Jordan-Wigner transformation to fermionic operators $\boldsymbol{c}_j = (c_j^\dagger, c_j)$ followed by a Fourier transform to momentum space [550]. The one-particle dispersion relation is $\epsilon(k) = -\cos(k)$.

11.3.1 The analytic computation

We now embark in the exact computation of the time evolution of the charged moments (11.1.5). The reader uninterested in these details can skip directly to the next paragraph in which we discuss the results for the entanglement asymmetry.

We choose as initial state the linear combination of Eq. (11.3.1), instead of Eq. (11.2.1), because the corresponding reduced density matrix is a Gaussian operator in terms of $\boldsymbol{c}_j$. We can then use Wick theorem to express $\rho_A(t)$ in terms of the two-point correlation matrix

$$\Gamma_{jj'}(t) = 2\mathrm{Tr}\left[\rho_A(t)\boldsymbol{c}_j^\dagger\boldsymbol{c}_{j'}\right] - \delta_{jj'}, \tag{11.3.4}$$

with $j, j' \in A$ [169]. If A is a subsystem of length ℓ, then $\Gamma(t)$ has dimension $2\ell\times 2\ell$ and entries [339]

$$\Gamma_{jj'}(t) = \int_0^{2\pi}\frac{\mathrm{d}k}{2\pi}\mathcal{G}(k,t)e^{-ik(j-j')}, \tag{11.3.5}$$

with

$$\mathcal{G}(k,t) = \begin{pmatrix} \cos\Delta_k & -ie^{-2it\epsilon(k)}\sin\Delta_k \\ ie^{2it\epsilon(k)}\sin\Delta_k & -\cos\Delta_k \end{pmatrix},$$

$$\cos\Delta_k = \frac{2\cos(\theta) - (1+\cos^2\theta)\cos(k)}{1+\cos^2\theta - 2\cos(\theta)\cos(k)}. \tag{11.3.6}$$

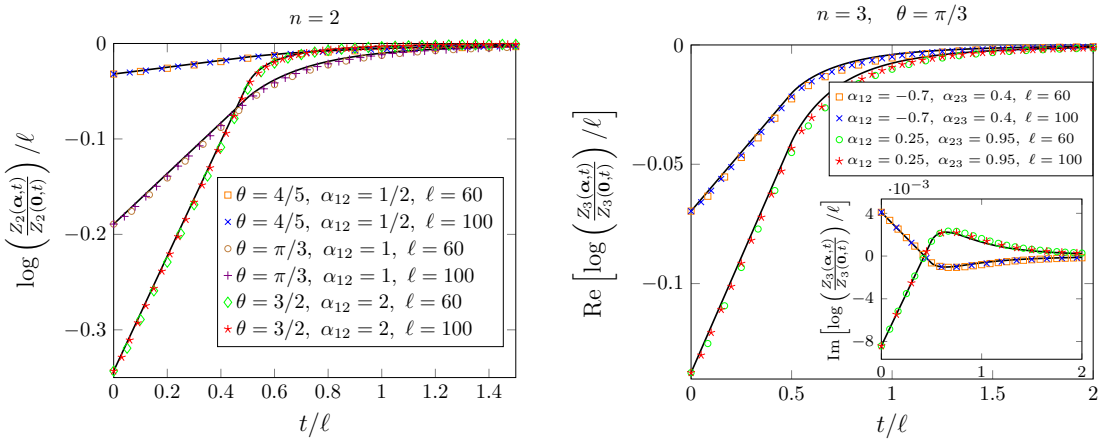

Figure 11.3: Time evolution of $Z_n(\boldsymbol{\alpha}, t)$ after the quench (11.3.2) for $n = 2$ (upper panel) and $n = 3$ (lower panel). We plot it as a function of t/ℓ for several values of θ, ℓ and $\alpha_{j,j+1}$. The symbols were obtained numerically using Eq. (11.3.7) and the continuous lines correspond to the analytic prediction (11.3.9).

Under the Jordan-Wigner transformation, the transverse magnetisation is mapped to the fermion number operator and $e^{i\alpha Q_A}$ turns out to be Gaussian, too. Therefore, $Z_n(\boldsymbol{\alpha})$ in Eq. (11.1.5) is the trace of the product of Gaussian fermionic operators, ρ_A and $e^{i\alpha_{j,j+1}Q_A}$. Employing their composition properties [174,551] (see also Sec. 1.4.3), we express $Z_n(\boldsymbol{\alpha})$ as a determinant involving the corresponding correlation matrices, finding

$$Z_n(\boldsymbol{\alpha}, t) = \sqrt{\det\left[\left(\frac{I - \Gamma(t)}{2}\right)^n \left(I + \prod_{j=1}^{n} W_j(t)\right)\right]}, \tag{11.3.7}$$

with $W_j(t) = (I + \Gamma(t))(I - \Gamma(t))^{-1} e^{i\alpha_{j,j+1} n_A}$ and n_A is a diagonal matrix with $(n_A)_{2j,2j} = 1$, $(n_A)_{2j-1,2j-1} = -1$, $j = 1, \cdots, \ell$. We use Eq. (11.3.7) to numerically compute the time evolution of the Rényi entanglement asymmetry $\Delta S_n^A(t)$ and test the analytical predictions presented in what follows.

At time $t = 0$, for large ℓ, $Z_n(\boldsymbol{\alpha}, 0) \sim e^{A(\boldsymbol{\alpha})\ell}/2^{n-1}$ with

$$A(\boldsymbol{\alpha}) = \log \prod_{j=1}^{n} e^{i\sigma_j/2} f(\cos(\theta), \alpha_{j,j+1} - \sigma_j), \tag{11.3.8}$$

where $\sigma_j = 0$ if $|\alpha_{j,j+1}| \leq \pi/2$ and $\sigma_j = \pi$ otherwise ($f(\lambda, \alpha)$ is defined in Eq. (11.2.2)). Therefore, $\Delta S_n^A(t = 0)$ behaves asymptotically as Eq. (11.2.4). After the quench, the natural ballistic regime is the scaling limit $t, \ell \to \infty$ with $\zeta = t/\ell$ fixed [339, 629] in which we expect

$$Z_n(\boldsymbol{\alpha}, t) = Z_n(\mathbf{0}, t) e^{\ell(A(\boldsymbol{\alpha}) + B(\boldsymbol{\alpha}, \zeta))}. \tag{11.3.9}$$

For the function $B(\boldsymbol{\alpha}, \zeta)$ we conjecture

$$B(\boldsymbol{\alpha}, \zeta) = -\int_0^{2\pi} \frac{\mathrm{d}k}{2\pi} \min(2\zeta|\epsilon'(k)|, 1) \log \prod_{j=1}^{n} f(e^{i\Delta_k}, \alpha_{j,j+1}), \tag{11.3.10}$$

and $\epsilon'(k) = \mathrm{d}\epsilon(k)/\mathrm{d}k$ (likely this expression can be rigorously derived by properly adapting the calculations for the symmetry resolved entanglement [132, 133, 135], but this is far beyond the scope of this Chapter). This cumbersome expression does not come out of a magician hat, but from the *quasiparticle picture* [44, 47, 589]: the time evolution of the entanglement is given by the pairs of entangled excitations shared by A and B that are created after the quench and propagate ballistically with momentum $\pm k$. Let us explain how to apply this idea to deduce Eq. (11.3.10). According to Refs. [552, 553, 607], in the quench protocol analised here, the $U(1)$ symmetry is restored in the large time limit, i.e. $\Delta S_n^A(t) \to 0$. Therefore, $Z_n(\boldsymbol{\alpha}, t)$ has to tend to $Z_n(\mathbf{0}, t)$, which implies $B(\boldsymbol{\alpha}, \zeta) \to -A(\boldsymbol{\alpha})$ as $\zeta \to \infty$. Considering Eq. (11.3.8), we notice that, at $t = 0$ and large ℓ, $Z_n(\boldsymbol{\alpha}, 0)$ factorises into

$$Z_n(\boldsymbol{\alpha}, 0) \sim 2 \prod_{j=1}^{n} \frac{e^{i\sigma_j/2}}{2} \mathrm{Tr}(\rho_A(0) e^{i(\alpha_{j,j+1} - \sigma_j) Q_A}). \tag{11.3.11}$$

The expectation value $\mathrm{Tr}(\rho_A(0) e^{i\alpha Q_A})$ is the full counting statistics of the transverse magnetisation in the subsystem A. We can now take advantage of the fact that $|\Psi(0)\rangle$ is also the ground state of a XY spin chain [1] to exploit the knowledge of the FCS in that system [272, 396, 400, 421, 554]. In particular, employing the results of Ref. [421], we can rewrite $A(\boldsymbol{\alpha})$ in Eq. (11.3.8) as an integral in momentum space

$$A(\boldsymbol{\alpha}) = -B(\boldsymbol{\alpha}, \zeta \to \infty) = \int_0^{2\pi} \frac{\mathrm{d}k}{2\pi} \log \prod_{j=1}^{n} f(e^{i\Delta_k}, \alpha_{j,j+1}). \tag{11.3.12}$$

Now, using the quasiparticle picture, the integrand in Eq. (11.3.12) can be interpreted as the contribution to $B(\boldsymbol{\alpha}, \zeta)$ from each entangled excitation of momentum k created after the quench. Since they propagate with velocity $|\epsilon'(k)|$, the number of these pairs shared between A and its complement at time t is determined by $\min(2t|\epsilon'(k)|, \ell)$. Combining these two ingredients, we get Eq. (11.3.9). This approach makes also clear the crucial role that entanglement plays in the restoration of the symmetry. In Fig. 11.3, we check Eq. (11.3.9) against exact numerical computations performed using Eq. (11.3.7) for different values of n, θ, and $\boldsymbol{\alpha}$, finding a remarkable agreement: note that Eq. (11.3.9) is exact for $\ell \to \infty$ and the points are closer to the curves for larger ℓ.

11.3.2 The entanglement asymmetry after the quench

The entanglement asymmetry $\Delta S_n^A(t)$ for any $\zeta = t/\ell$ in the scaling limit $t, \ell \to \infty$ is obtained by plugging the charged moments (11.3.9) into Eq. (11.1.4). The resulting curves are plotted in Fig. 11.4 as a function of ζ for several values of θ, finding a remarkable agreement with the exact numerical values (symbols). We can also write a very effective closed-form approximation of $\Delta S_n^A(t)$. Indeed when in Eq. (11.3.9) $A(\boldsymbol{\alpha}) + B(\boldsymbol{\alpha}, \zeta)$ is close to zero, the Fourier transform can be done analytically as

$$\Delta S_n^A(t) \simeq \frac{\pi^2 b(\zeta) \ell}{24}, \quad b(\zeta) = \frac{\sin^2\theta}{2} - \int_0^{2\pi} \frac{\mathrm{d}k}{2\pi} \min(2\zeta|\epsilon'(k)|, 1) \sin^2 \Delta_k, \tag{11.3.13}$$

which is independent of the replica index n. This approximation becomes *exact* in the limit of large ζ and its effectiveness also for not too large ζ is proven by the inset of Fig. 11.4.

[1] The corresponding parameters h, γ of the XY chain (see Eq. (12.5.1)) are given by $\gamma^2 + h^2 = 1$ and $\cos^2\theta = (1-\gamma)/(1+\gamma)$.

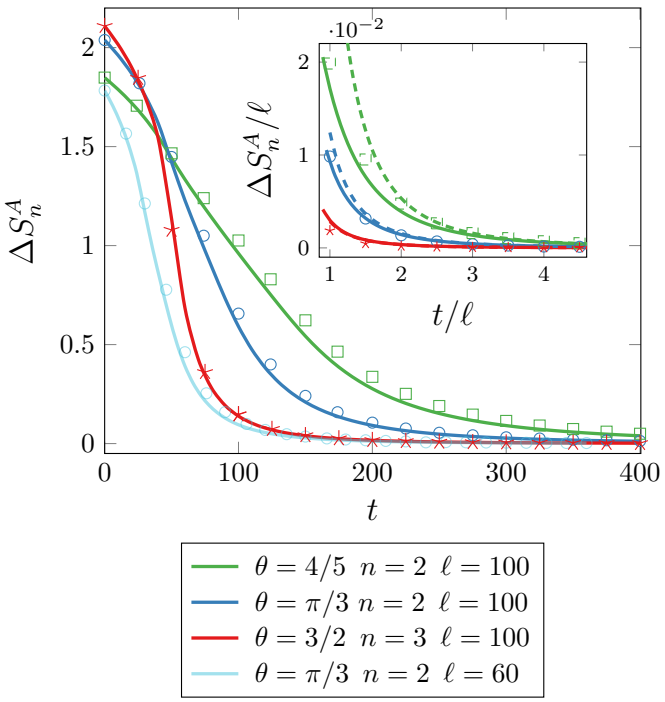

Figure 11.4: Time evolution of the Rényi entanglement asymmetry $\Delta S_n^A(t)$ after the quench (11.3.2). The symbols are the exact numerical results for various values of ℓ, n, and θ. The continuous lines are our prediction obtained by plugging Eq. (11.3.9) into (11.1.4) and (11.1.2). In the inset, we check the asymptotic behavior (11.3.13) (full lines) and (11.3.14) (dashed) of $\Delta S_n^A(t)$ for large t/ℓ.

We now discuss some relevant features of the entanglement asymmetry and show that it encodes a lot of new physics. First, as expected, $\Delta S_n^A t)$ tends to zero for large ζ (i.e. large t) and the $U(1)$ symmetry, broken by the initial state, is restored. This is analytically shown by Eq. (11.3.13) that indeed at leading order in large ζ is

$$\Delta S_n^A(t) = \frac{\pi}{1152}\Big(1 + 8\frac{\cos^2\theta}{\sin^4\theta}\Big)\frac{\ell}{\zeta^3}\,, \tag{11.3.14}$$

i.e. it vanishes for large times as t^{-3} for any value of θ. Another characteristic, following from having a space-time scaling, is that larger subsystems require more time to recover the symmetry, as it is clear from Fig. 11.4 and Eq. (11.3.13): this justifies the significance of the definition of ΔS_n^A in terms of ρ_A rather than the full state $|\Psi\rangle$. Finally, a very odd and intriguing feature is that the more the symmetry is initially broken, i.e. the larger θ, the smaller the time to restore it. This is a quantum Mpemba effect: more the system is out of equilibrium, the faster it relaxes. At a qualitative level this is a consequence of the fact that for larger symmetry breaking there is a sharper drop of the (entanglement) asymmetry at short time, see Fig. 11.4, before the truly asymptotic behavior takes place. Furthermore, we can *quantitatively* understand the quantum Mpemba effect: from Eq. (11.3.14) the prefactor of the t^{-3} decay is a monotonously decreasing function of θ in $[0, \pi/2]$. Thus the quantum Mpemba effect is not as controversial as its classical version [555]. To the best of our knowledge this awkward effect was not known in the literature, showing the power of the entanglement asymmetry to identify new physics.

11.4 Closing remarks

In this Chapter, we introduced the entanglement asymmetry, a probe to study how much a symmetry is broken at the level of subsystems of many-body systems. As an application to show its potential, we have studied its dynamics after a quench from an initial state breaking a $U(1)$ symmetry and evolving with a Hamiltonian preserving it. We showed that the entanglement asymmetry detects neatly all the physical relevant features of the dynamics and in particular the restoration of the symmetry at late times. It also identifies the appearance of an unexpected Mpemba effect, a phenomenon that very likely happens in many settings that can be studied through the entanglement asymmetry. It is then very important to study other quench protocols (e.g. different initial state, interacting Hamiltonians, etc.) and understand how to modify the quasiparticle description, following e.g. Ref. [556], to describe these more general situations.

We can easily imagine many other applications of the entanglement asymmetry. The first one is in equilibrium situations that have been left out here. In this respect, it would be useful to recast the charged moments (11.1.5) in terms of twist fields [20, 156] within the path-integral approach: this would allow us to explore more complicated situations, e.g. the symmetry breaking from $SU(2)$ to $U(1)$, which are also relevant in high-energy physics. Similarly, our setup can be extended to non-Abelian symmetries [121] to explore, e.g., how the asymptotic behavior of ΔS_A with the subsystem size of Eq. (11.2.4) depends on the symmetry group.

Finally, $\Delta S_A(t)$ can be experimentally accessible by developing a protocol based on the random measurement toolbox [557, 558]. This would require the post-selection of data from an experiment like the one in [80], but with an initial state breaking the $U(1)$ symmetry.

Part III

Quantum correlations in mixed states

Chapter 12

The Negativity Hamiltonian: An operator characterization of mixed-state entanglement

In the context of ground states of quantum many-body systems, the locality of entanglement between connected regions of space is directly tied to the locality of the corresponding entanglement Hamiltonian (EH): the latter is dominated by local, few-body terms. In this Chapter, we introduce the negativity Hamiltonian as the (non hermitian) effective Hamiltonian operator describing the logarithm of the partial transpose of a many-body system. This allows us to address the connection between entanglement and operator locality beyond the paradigm of bipartite pure systems. As a first step in this direction, we study the structure of the negativity Hamiltonian for fermionic conformal field theories and a free fermion chain: in both cases, we show that the negativity Hamiltonian assumes a quasi-local functional form, that is captured by simple functional relations. This Chapter is based on Ref. [559].

12.1 Introduction

The EH fully characterises the "local" properties of entanglement in a many-body system - that is, it allows to understand whether the RDM can be interpreted as the exponential of a local operator composed solely of few-body local terms. In the context of quantum field theory, this principle of locality is an established pillar - the Bisognano-Wichmann theorem [244, 301]. Such locality is at the heart of several physical phenomena - from topological order, to the nature of area laws in gapped systems-, and is the key element at the basis of theory and experiments aimed at large-scale reconstructions of the RDM [560–562]. However, it is presently unknown whether it is possible to associate locality and entanglement in a similar way for the case of mixed-state entanglement, that encompasses a variety of scenarios of key experimental and theoretical relevance - from mixed states, to correlations between partitions in pure states.

In this Chapter, we introduce and investigate the negativity Hamiltonian - an operator that allows us to cast the relation between locality and entanglement (in particular, that related to Peres-Horodecki criterion) for general mixed states.

For the case of a subpartition of $A = A_1 \cup A_2$, we define the *negativity Hamiltonian* $\mathcal{N}_A$ as

$$\rho_A^{T_1} = Z_A^{-1} e^{-\mathcal{N}_A}. \tag{12.1.1}$$

Clearly $\mathcal{N}_A$ is non-hermitian because negative eigenvalues of $\rho_A^{T_1}$ are the signature of mixed-state

entanglement. Nevertheless, it is still natural to wonder about the locality properties of $\mathcal{N}_A$ and about the location of its eigenvalues in the complex plane.

After discussing the definition of $\mathcal{N}_A$ for both bosonic (spin) and fermionic systems in Sec. 12.2, we unveil the operator structure of $\mathcal{N}_A$ for two relevant cases: (1+1)-d fermionic conformal field theory (Secs. 12.3 and 12.4) and a tight-binding model of spinless fermions on a chain (Sec. 12.5). Both cases show a characteristic quasi-local (in a sense to be specified below) structure - a first demonstration of the relation between entanglement and locality at the operator level beyond the case of complementary partitions. On top of its conceptual relevance, and similarly to what has been discussed in the context of pure states for the case of local EHs, this fact enables some immediate consequences: i) interpreting the negativity spectrum, i.e. the analog of the pure-state entanglement spectrum for mixed states [515,563], ii) simulating this object in nowadays available quantum platforms [80] iii) applying well-established statistical mechanics tools such as tensor networks [42,317] and quantum Monte Carlo [564] to access the entire partial transpose $\rho_A^{T_1}$.

12.2 The partial transpose operation

The partial transposition introduced in Sec. 1.1 has also an interpretation in terms of a time-reversal transformation or mirror reflection in phase space [60]. Namely, considering the one-to-one correspondence between density matrices and Wigner distribution functions $W(q,p)$ then $\rho_A \to \rho_A^T \iff W(q,p) \to W(q,-p)$. This can be conveniently observed starting from a bosonic density matrix written in a coherent state basis, since time-reversal transformation ($\mathcal{T}$) can be identified with the complex conjugation [163]. Taking $|\alpha\rangle$, a bosonic coherent state, one has

$$(|\alpha\rangle\langle\alpha^*|) \xrightarrow{\mathcal{T}} |\alpha^*\rangle\langle\alpha| = (|\alpha\rangle\langle\alpha^*|)^T. \tag{12.2.1}$$

In the case of fermionic systems, the equivalence above does not hold and the definition of partial transposition differs when looking at the density matrix or at the Wigner distribution function. In a coherent state basis the RDM reads [163,165,173,565]

$$\rho_A = \frac{1}{Z}\int \mathrm{d}[\xi]\ \mathrm{d}[\bar{\xi}] e^{-\sum_j \bar{\xi}_j \xi_j} \langle\{\xi_j\}|\rho_A|\{\bar{\xi}_j\}\rangle |\{\xi_j\}\rangle\langle\{\bar{\xi}_j\}|. \tag{12.2.2}$$

Here $\xi, \bar{\xi}$ are Grassman variables and $|\xi\rangle = e^{-\xi c^\dagger}|0\rangle$,$\langle\bar{\xi}| = \langle 0|\, \epsilon^{-c\bar{\xi}}$ are the related fermionic coherent states. The partial time reversal, analog of Eq. (12.2.1), is [163]

$$|\xi\rangle\langle\bar{\xi}| \xrightarrow{\mathcal{T}} |i\bar{\xi}\rangle\langle i\xi|. \tag{12.2.3}$$

The partial time reversal $\rho_A^{R_1}$, obtained by acting with (12.2.3) in (12.2.2) only in A_1, provides the fermionic negativity considering the trace norm of $\rho_A^{R_1}$, although its spectrum is not real in general [164].

In the following section we discuss in details the partial transpose operation of fermionic Gaussian states, both using the bosonic and the fermionic definition. Then, we show how for Gaussian states the correlation matrices suffice to compute all the properties of the systems [163,164,173].

12.2.1 From bosonic to fermionic negativity

For a bosonic system, the partial transpose of the reduced density matrix $\rho^{T_{A_1}}$ with respect to A_1 is defined by performing a standard transposition in the Hilbert space associated to A_1, $\mathcal{H}_{A_1}$, according to the definition (1.1.12). However, the same is not true for fermions because of the anticommutation relations.

To construct the partial transpose for fermionic systems, let us start by writing the density matrix in terms of Majorana operators a_j, which are defined in terms of the fermionic operators c_j obeying $\{c_k^\dagger, c_j\} = \delta_{kj}$ as

$$\begin{cases} a_{2j-1} = c_j + c_j^\dagger, \\ a_{2j} = i(c_j - c_j^\dagger). \end{cases} \tag{12.2.4}$$

We consider a system $\mathcal{S} = A_1 \cup A_2$ and denote with the subscripts $\{m_1, \ldots, m_{\ell_1}\}$ the operators in the subset A_1 and with $\{n_1, \ldots, n_{\ell_2}\}$ the ones in the subset A_2; here $\ell_1(\ell_2)$ corresponds to the number of sites in subsystem $A_1(A_2)$. One can write [173]:

$$\rho_A = \sum_{\boldsymbol{\kappa},\boldsymbol{\tau}} w_{\boldsymbol{\kappa},\boldsymbol{\tau}} a_{m_1}^{\kappa_1} \ldots a_{m_{2\ell_1}}^{\kappa_{2\ell_1}} a_{n_1}^{\tau_1} \ldots a_{n_{2\ell_2}}^{\tau_{2\ell_2}} \tag{12.2.5}$$

where we defined $\boldsymbol{\kappa} = (\kappa_1, \ldots, \kappa_{2\ell_1})$ and $\boldsymbol{\tau} = (\tau_1, \ldots, \tau_{2\ell_2})$ with $\kappa_j, \tau_j = 0, 1$. We define the moduli $|\kappa| = \sum_{j=1}^{2\ell_1} \kappa_j$ and $|\boldsymbol{\tau}| = \sum_{j=1}^{2\ell_2} \tau_j$. Since the physical fermionic states must commute with the parity operator one has that the sum of the moduli of $\boldsymbol{\kappa}$ and $\boldsymbol{\tau}$ must be even. The partial transpose (1.1.12) leaves unaltered the state in A_2 and exchanges the states in A_1 as

$$\rho_A^{T_1} = \sum_{\boldsymbol{\kappa},\boldsymbol{\tau}} (-1)^{f(\boldsymbol{\kappa})} w_{\boldsymbol{\kappa},\boldsymbol{\tau}} a_{m_1}^{\kappa_1} \ldots a_{m_{2\ell_1}}^{\kappa_{2\ell_1}} a_{n_1}^{\tau_1} \ldots a_{n_{2\ell_2}}^{\tau_{2\ell_2}} \tag{12.2.6}$$

where

$$(-1)^{f(\boldsymbol{\kappa})} = \begin{cases} 0 & |\boldsymbol{\kappa}| \bmod 4 \in \{0, 3\} \\ 1 & |\boldsymbol{\kappa}| \bmod 4 \in \{1, 2\} \end{cases} . \tag{12.2.7}$$

The easiest way to see this is to perform the partial transpose in the occupation number basis and then write the density matrix in terms of Majorana operators.

Having understood how the standard partial transpose acts on the fermionic degrees of freedom written in terms of Majorana operator, we move on to consider Gaussian states. They can be written in the form

$$\rho_A = \frac{1}{Z} \mathrm{e}^{\frac{1}{4} \sum_{kl} W_{kl} a_k a_l}, \tag{12.2.8}$$

where W is a $2\ell \times 2\ell$ matrix (ℓ size of the system described by ρ_A), with eigenvalues $\in \mathbb{R}$. The latter is related to the correlation matrix Γ (i.e. the matrix with elements $\Gamma_{i,j} = \frac{1}{2}\langle [a_i, a_j] \rangle$, see also Sec. 1.4.3) by the relation

$$\Gamma = \tanh \frac{W}{2}. \tag{12.2.9}$$

Here Γ has eigenvalues between $[-1, 1]$. It is convenient to introduce the block structure of Γ as

$$\Gamma = \begin{pmatrix} \Gamma_{A_1 A_1} & \Gamma_{A_1 A_2} \\ \Gamma_{A_2 A_1} & \Gamma_{A_2 A_2} \end{pmatrix}. \tag{12.2.10}$$

Using Eq. (12.2.6) it can be shown that [173]

$$\rho_A^{T_1} = \frac{1 - i}{2} O_+ + \frac{1 + i}{2} O_- \tag{12.2.11}$$

where $O_\pm = \sum_{\boldsymbol{\kappa},\boldsymbol{\tau}} o_{\boldsymbol{\kappa},\boldsymbol{\tau}}^\pm a_{m_1}^{\kappa_1} \ldots a_{m_{2l_1}}^{\kappa_{2\ell_1}} a_{n_1}^{\tau_1} \ldots a_{n_{2l_2}}^{\tau_{2\ell_2}}$ with

$$o_{\boldsymbol{\kappa},\boldsymbol{\tau}}^\pm = \begin{cases} \pm i (-1)^{\frac{|\boldsymbol{\kappa}|-1}{2}} w_{\boldsymbol{\kappa},\boldsymbol{\tau}} & |\boldsymbol{\kappa}| \text{ odd} \\ i (-1)^{\frac{|\boldsymbol{\kappa}|}{2}} w_{\boldsymbol{\kappa},\boldsymbol{\tau}} & |\boldsymbol{\kappa}| \text{ even.} \end{cases} \tag{12.2.12}$$

The operators $O_\pm$ are Gaussian and can be written as

$$O_+ = O_-^\dagger = \frac{1}{Z} \mathrm{e}^{\frac{1}{4}\sum_{kl}(N_A)_{kl} a_k a_l} \tag{12.2.13}$$

where N_A is related (as in Eq. (12.2.9)) to the correlation matrix Γ_+ defined according to the following equation:

$$\Gamma_+ = \begin{pmatrix} -\Gamma_{A_1 A_1} & i\Gamma_{A_1 A_2} \\ i\Gamma_{A_2 A_1} & \Gamma_{A_2 A_2} \end{pmatrix}. \tag{12.2.14}$$

It is clear that the partially transposed reduced density matrix (12.2.11) is not a Gaussian operator, but rather the sum of two of them. Even more troubling, it does not satisfy additivity nor subadditivity and fails to capture, for this reason, some topological features of fermionic Majorana systems such as the entanglement due to zero-energy modes in Kitaev's chain [163].

For all the above reasons, a different partial transpose has been introduced for fermionic systems starting from the analogy with the time-reversal transformation [163–165]: we have already understood that the action of the fermionic partial transpose (R) is not just exchanging bra and ket but also multiply them by i (see Eq. (12.2.3)). This definition can be readily generalised to multi-particle states. Considering a system $\mathcal{S} = A_1 \cup A_2$ one has

$$\left(|\{\xi_j\}_{j\in A_1}\{\xi_j\}_{j\in A_2}\rangle \langle\{\bar{\chi}_j\}_{j\in A_1}\{\bar{\chi}_j\}_{j\in A_2}|\right)^{R_1} = |\{i\bar{\chi}_j\}_{j\in A_1}\{\xi_j\}_{j\in A_2}\rangle \langle\{i\xi_j\}_{j\in A_1}\{\bar{\chi}_j\}_{j\in A_2}|\,, \tag{12.2.15}$$

with obvious meaning of all the actors in the formula. In the occupation number basis, the above equation reads [163]

$$\left(|\{n_j\}_{j\in A_1}\{n_j\}_{j\in A_2}\rangle \langle\{\bar{n}_j\}_{j\in A_1}\{\bar{n}_j\}_{j\in A_2}|\right)^{R_1} = (-1)^{\phi(\{n_j,\bar{n}_j\})} \times |\{\bar{n}_j\}_{j\in A_1}\{n_j\}_{j\in A_2}\rangle \langle\{n_j\}_{j\in A_1}\{\bar{n}_j\}_{j\in A_2}|\,. \tag{12.2.16}$$

Here the term $\phi(\{n_j, \bar{n}_j\})$ is a phase factor depending on the occupation number

$$\phi(\{n_j,\bar{n}_j\}) = \frac{\tau_{A_1}(\tau_{A_1}+2)}{2} + \frac{\bar{\tau}_{A_1}(\bar{\tau}_{A_1}+2)}{2} + \tau_{A_2}\bar{\tau}_{A_2} + \tau_{A_1}\tau_{A_2} + \bar{\tau}_{A_1}\bar{\tau}_{A_2} + (\bar{\tau}_{A_1}+\bar{\tau}_{A_2})(\tau_{A_1}+\tau_{A_2}), \tag{12.2.17}$$

with $\tau_{A_1} = \sum_{j\in A_1} n_j$ ($\tau_{A_2} = \sum_{j\in A_2} n_j$) and $\bar{\tau}_{A_1} = \sum_{j\in A_1} \bar{n}_j$ ($\bar{\tau}_{A_2} = \sum_{j\in A_2} \bar{n}_j$). Hence the definition in Eq. (12.2.16) is equivalent to a standard partial transposition up to phase factor depending on the parity of the two subsystems, as in Eq. (12.2.17). In terms of Majorana operators, the transformation in Eq. (12.2.16) can be rewritten as

$$\rho_A^{R_1} = \sum_{|\boldsymbol{\kappa}|+|\boldsymbol{\tau}|even} w_{\boldsymbol{\kappa},\boldsymbol{\tau}} i^{|\boldsymbol{\kappa}|} a_{m_1}^{\kappa_{m_1}} \cdots a_{m_{2l_1}}^{\kappa_{m_{2l_1}}} a_{n_1}^{\tau_{n_1}} \cdots a_{n_{2l_2}}^{\tau_{n_{2l_2}}} \tag{12.2.18}$$

where we used the notation $a_x^0 = \mathbb{1}$, $a_x^1 = a_x$. The matrix $\rho_A^{R_1}$ satisfies three necessary properties for a partial transposition:

1. $(\rho_A^{R_1})^{R_2} = \rho_A^R$,
2. $(\rho_A^{R_1})^{R_1} = \rho_A$,
3. $(\rho_1 \otimes \rho_2 \cdots \rho_n)^{R_1} = \left(\rho_1^{R_1} \otimes \rho_2^{R_1} \otimes \cdots \otimes \rho_n^{R_1}\right)$.

Notice that $\rho_A^{R_{A_1}}$ is nothing but O_+ in Eq. (12.2.11). This density operator is not Hermitian and, in general, has complex eigenvalues. Nevertheless, one can still define a fermionic logarithmic negativity as [163]

$$\mathcal{E} = \log \mathrm{Tr}\sqrt{(\rho_A^{R_1})^\dagger \rho_A^{R_1}} \tag{12.2.19}$$

where the object $(\rho_A^{R_1})^\dagger \rho_A^{R_1}$ is Hermitian and its spectrum is positive. This expression can be slightly generalised defining the fermionic Rényi negativities as [163]

$$\mathcal{E}_n = \begin{cases} \log[\mathrm{Tr}(\rho_A^{R_1})^\dagger \rho_A^{R_1}) \dots \rho_A^{R_1})^\dagger \rho_A^{R_1})], & n \quad \text{even}, \\ \log[\mathrm{Tr}(\rho_A^{R_1})^\dagger \rho_A^{R_1}) \dots \rho_A^{R_1})^\dagger)], & n \quad \text{odd}, \end{cases} \tag{12.2.20}$$

from which $\mathcal{E} = \lim_{n_e \to 1} \mathcal{E}_{n_e}$.

In spite of the name, the fermionic negativity has nothing to do with the negativeness of the spectrum of $(\rho_A^{R_1})$. It can be however proved that is a proper entanglement monotone [478] and it has been shown that can detect entanglement when the standard negativity fails [163].

12.3 The Bisognano-Wichmann theorem

The Bisognano-Wichmann (BW) theorem gives a general structure for the entanglement Hamiltonian of the ground state of a relativistic invariant quantum field theory with Hamiltonian density $H(\mathbf{x})$, when considering a bipartition between two half spaces of an infinite system. In formulas, considering a d-dimensional system, $\mathbf{x} = \{x_1, \dots, x_d\}$, and a partition $A = \{\mathbf{x} | x_1 > 0\}$, the EH of the ground state is $H_A = 2\pi \int_{\mathbf{x} \in A} \mathrm{d}\mathbf{x}\, x_1 H(\mathbf{x}) + c$, where c is a normalization constant. This result does not depend on the dimensionality of the system or on any apriori knowledge of the ground state and can be applied to a large variety of systems and quantum phases. For conformal invariant theories, the BW theorem is easily generalised to some different geometries by conformal mappings [189, 242, 566, 567]. Nevertheless, in general it is not an easy task to get analytic expressions, even in CFTs. One of these examples is the modular Hamiltonian for the ground state of the free $1+1$ dimensional massless Dirac fermion for several disjoint intervals on the infinite line [256, 568, 569]. We report here the result by slightly adapting it to the massless $1+1$ dimensional real (Majorana) field $\Psi(t, x)$. It is a doublet made by the two real fields

$$\Psi(t, x) = \begin{pmatrix} \psi_1(t, x) \\ \psi_2(t, x) \end{pmatrix}. \tag{12.3.1}$$

The normal ordered component of the energy-momentum tensor of the Majorana field corresponding to the energy density reads

$$T_{tt}(t, x) \equiv \frac{i}{2} : [((\partial_x \psi_1)\psi_1 - \psi_1 \partial_x \psi_1)(x + t) - ((\partial_x \psi_2)\psi_2 - \psi_2 \partial_x \psi_2)(x - t)] : . \tag{12.3.2}$$

The modular Hamiltonian for two disjoint intervals $A \equiv [a_1, b_1] \cup [a_2, b_2]$ on the line can be written as the sum $H_A = H_{\mathrm{loc}} + H_{\mathrm{q-loc}}$, where the local term H_{loc} and the quasi-local term $H_{\mathrm{q-loc}}$ are defined respectively as

$$\begin{aligned} H_{\mathrm{loc}} &= 2\pi \int_A \beta_{\mathrm{loc}}(x) T_{tt}(0, x) dx, \\ H_{\mathrm{q-loc}} &= 2\pi \int_A \beta_{\mathrm{q-loc}}(x) T_{\mathrm{q-loc}}(0, x, \bar{x}) dx, \end{aligned} \tag{12.3.3}$$

with $T_{tt}(0, x)$ the energy density in Eq. (12.3.2), while $T_{\mathrm{q-loc}}(0, x, y)$ is given by

$$T_{\mathrm{q-loc}}(t, x, y) \equiv i : [\psi_1(x + t)\psi_1(y + t) - \psi_2(x - t)\psi_2(y - t)] : . \tag{12.3.4}$$

The other functions in Eq. (12.3.3) can be written as

$$\beta_{\mathrm{q-loc}}(x) = \frac{1}{w'(x)} \qquad \beta_{\mathrm{q-loc}}(x) = \frac{\beta_{\mathrm{loc}}(\bar{x}(x))}{x - \bar{x}(x)}, \tag{12.3.5}$$

with

$$
\begin{aligned}
w(x) &= \log\left[-\frac{(x-a_1)(x-a_2)}{(x-b_1)(x-b_2)}\right], \\
\bar{x}(x) &= \frac{(b_1b_2-a_1a_2)x+(b_1+b_2)a_1a_2-(a_1+a_2)b_1b_2}{(b_1-a_1+b_2-a_2)x+a_1a_2-b_1b_2}.
\end{aligned}
\tag{12.3.6}
$$

Here x and $\bar{x}(x)$ belong to different intervals in A (if $x \in A_1$ then $\bar{x} \in A_2$ and viceversa). In the limit $b_1 \to a_2$ we get back a single interval and so the quasi-local part vanishes.

We will make explicit use of this example in the following.

12.4 The Negativity Hamiltonian and its quasi-local structure

To build the negativity Hamiltonian, we should first recall the path integral construction of the (bosonic) partial transpose [151, 152]. The partial transposition corresponds to the exchange of row and column indices in A_1 which naturally leads to a space inversion within A_1. On a fundamental level, this fact can be deduced from CPT theorem. Indeed, the partial transposition is equivalent to a partial time reversal that, by CPT, is the same as a parity operation in the world-sheet combined with a charge conjugation. This second construction holds true also for $\rho_A^{R_1}$ in fermionic systems.

Therefore, starting from the entanglement hamiltonian for two disjoint intervals and doing a spatial inversion of the interval $A_1 = [a_1, b_1]$, one obtains the partial time reversal of the density matrix. Although this procedure is fully general, the entanglement hamiltonians of disjoint intervals are known only in few cases [256,568–574]. In particular, the result for Majorana fermions can be obtained from the previous section without any further effort. We mention that one can easily derive also the result for the Dirac field, which can be written in terms of two Majorana spinors. In this case, the negativity (entanglement) hamiltonian is the sum of the two negativity (entanglement) hamiltonians for each real component of the complex field [256]. Only the definition of $T_{tt}(0,x)$ and $T_{\mathrm{q-loc}}(t,x,y)$ in terms of a real or complex fermionic field change.

Starting from the EH H_A for the massless Majorana fermion $\Psi(t,x)$ reported in Eq. (12.3.3), and performing this inversion, we get after simple algebra

$$
\begin{aligned}
\mathcal{N}_A &= \mathcal{N}_{A,\mathrm{loc}} + i\mathcal{N}_{A,\mathrm{q-loc}}, \\
\mathcal{N}_{A,\mathrm{loc}} &= 2\pi \int_A \beta^R_{\mathrm{loc}}(x) T_{tt}(0,x)dx, \\
\mathcal{N}_{A,\mathrm{q-loc}} &= 2\pi \int_A \beta^R_{\mathrm{q-loc}}(x) T_{\mathrm{q-loc}}(0,x,\bar{x}^R(x))dx,
\end{aligned}
\tag{12.4.1}
$$

where

$$
\beta^R_{\mathrm{loc}}(x) = \frac{1}{w^R(x)'}, \qquad \beta^R_{\mathrm{q-loc}}(x) = \frac{\beta^R_{\mathrm{loc}}(\bar{x}^R(x))}{x-\bar{x}^R(x)},
\tag{12.4.2}
$$

with

$$
\begin{aligned}
w^R(x) &= \log\left[-\frac{(x-b_1)(x-a_2)}{(x-a_1)(x-b_2)}\right], \\
\bar{x}^R(x) &= \frac{(a_1b_2-b_1a_2)x+(a_1+b_2)b_1a_2-(b_1+a_2)a_1b_2}{(a_1-b_1+b_2-a_2)x+b_1a_2-a_1b_2}.
\end{aligned}
\tag{12.4.3}
$$

Here $T_{tt}(0,x)$ is the one in Eq. (12.3.2) while $T_{\mathrm{q-loc}}(0,x,\bar{x})$ in defined in Eq. (12.3.4).

The structure of Eq. (12.4.1) is very suggestive: it consists of a local term proportional to the energy density and an additional non local part given by a quadratic expression in the fermionic

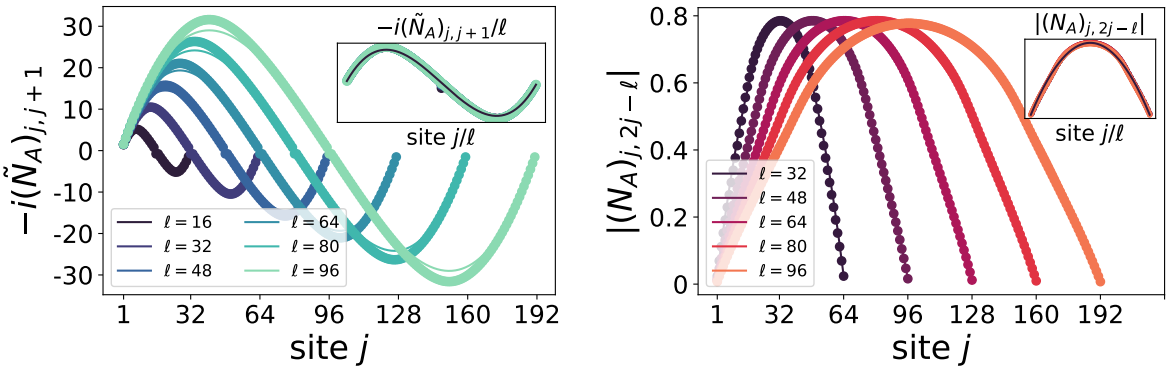

Figure 12.1: Negativity Hamiltonian corresponding to $\rho_A^{R_1}$ for real fermions on two adjacent intervals of equal length ℓ on the infinite line. The symbols correspond to numerical data, while the solid lines correspond to the discretised form of Eq. (12.4.1). The right panel is $N_{A,\mathrm{loc}}$, while the left one is $|N_{A,\mathrm{q-loc}}|$. Here we have $a_1 = 0$, $b_1 = \ell = a_2$, $b_2 = 2\ell$.

field. The latter, however, has a mild non-locality: each point $x \in A_1$ is coupled to only a specific $y = \bar{x}^R \in A_2$ (that is a consequence of the mirror symmetry for equal intervals). Thus, following [256], we refer to $\mathcal{N}_{A,\mathrm{q-loc}}$ as a quasi-local operator. Its existence is the reason of the imaginary components in the spectrum of $\mathcal{N}_A$, which is one characteristic treat of $\rho_A^{R_1}$. The shape of $|\mathcal{N}_{A,\mathrm{q-loc}}|$ (see also Fig. 12.1) is compatible with the results of the negativity contour [581] suggesting that the largest contribution to the negativity comes from the boundary region between A_1 and A_2.

12.5 Lattice Negativity Hamiltonian and numerical checks

In this section we review the numerical procedure that we used to benchmark our analytical results. We consider lattice systems described by the quadratic Hamiltonian

$$H(\lambda,\gamma) = \frac{i}{2}\sum_{l=-\infty}^{\infty}\Big(\frac{1+\gamma}{2}a_{2l}a_{2l+1} - \frac{1-\gamma}{2}a_{2l-1}a_{2l+2} + \lambda a_{2l-1}a_{2l}\Big). \tag{12.5.1}$$

The one-particle energy levels are

$$\Lambda_k = \sqrt{(\lambda-\cos k)^2 + \gamma^2\sin^2 k} \tag{12.5.2}$$

where $k \in [-\pi,\pi]$ is the physical momentum. For $(\lambda,\gamma) = (1,1)$ the system is critical and Lorentz invariant at low energy, so its critical behavior is described by the conformal field theory of a free massless real fermion with central charge equal to $1/2$. Thus, the Hamiltonian (12.5.1), $H(1,1)$, is the ideal setting to compute the lattice negativity Hamiltonian $\mathcal{N}_A$ and benchmark the analytical expression in Eq. (12.4.1).

The elements of the covariance matrix of the ground state of the Hamiltonian (12.5.1) are

$$\Gamma_{2j_1-1,2j_2} = -\Gamma_{2j_2,2j_1-1} = g_{j_2-j_1}, \tag{12.5.3}$$

where

$$g_j = -\frac{i}{\pi}\frac{1}{j+\frac{1}{2}}. \tag{12.5.4}$$

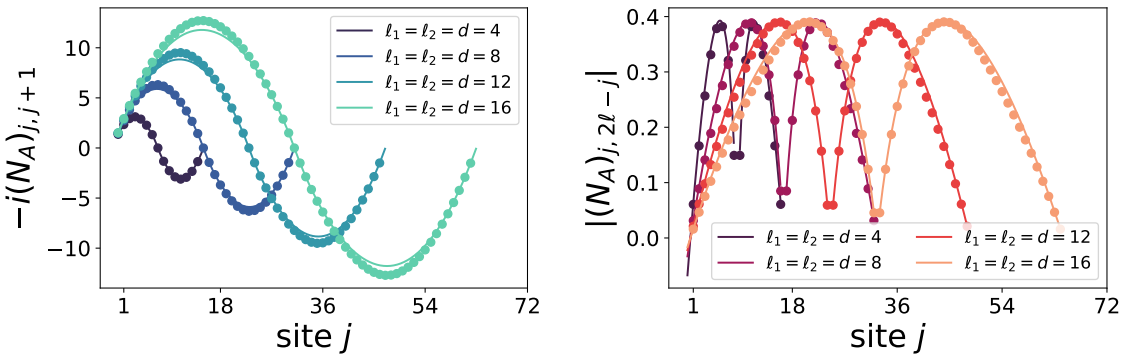

Figure 12.2: Negativity Hamiltonian for a real free fermion and for the geometry of two disjoint intervals at distance d of equal length ℓ on the infinite line. The symbols correspond to numerical data, while the solid lines correspond to the discretised form of N_A (12.4.1), both the local part (left panel) and the quasi-local one (right panel).

If now we focus on two intervals $A = A_1 \cup A_2$, adjacent or disjoint and of arbitrary lengths, the correlation matrix Γ_A is obtained from the Γ above simply restricting to the subsystem of interest and leading to the block structure of Eq. (12.2.10). If the total length of A is $\ell_1+\ell_2$, the covariance matrix has dimension $2(\ell_1 + \ell_2) \times 2(\ell_1 + \ell_2)$. From this, the covariance matrix Γ_+ corresponding to the fermionic partial transpose is obtained by building Eq. (12.2.14).

Intervals of equal length $\ell_1 = \ell_2$: Because of the gaussianity of $\rho_A^{R_1}$ [163], the numerical evaluation of the negativity Hamiltonian amounts to compute the single particle operator N_A defined as $\mathcal{N}_\mathcal{A} = \sum_{ij}(N_A)_{i,j}\psi_j\psi_i$, related to the covariance matrix as $N_A = \log \frac{1+\Gamma_+}{1-\Gamma_+}$ [169, 171]. We focus on two equal adjacent intervals $A = A_1 \cup A_2$ made up of ℓ sites labelled by $1 \leq j \leq 2\ell$. In this case, the point $\bar{x}^R$ in Eq. (12.4.3) is just $\bar{x}^R = 2\ell - x$ and so the quasi-local term lies entirely on the antidiagonal. As a consequence, in Fig. 12.1 we show only the subdiagonal $(N_A)_{j,j+1}$ (a similar behaviour can be found for $(N_A)_{j+1,j}$) and the antidiagonal $(N_A)_{j,2\ell-j}$ which correspond, respectively, to the local and to the quasi-local parts of N_A. The agreement between lattice exact and field-theoretical discretised N_A is remarkable over the all parameter regime, and even for modest system sizes. Small discrepancies up to a few percent are present far from the boundaries: those have very little effects on the negativity, as they affect only very small (in absolute value) eigenvalues of the partial transpose. We verified that the other matrix elements of N_A are negligible, in the sense that they are subleading as $\ell \to \infty$ (in the same sense as subleading terms in the EH are negligible, see Refs. [167, 464, 575–580]).

We now move to another geometry. In Fig. 12.2 we report the case of two equal disjoint intervals at distance d and we benchmark once again our analytical result found in Eq. (12.4.1). The curves again show a good agreement with the numerical computation, since the discrepancy is at most $\sim 6\%$.

Intervals of different length $\ell_1 \neq \ell_2$: Finally, we analyse in Fig. 12.3 the case of two disjoint intervals of different length, $\ell_1 \neq \ell_2$ for a real fermion. In this case, the reflected point $\bar{x}^R$ (12.4.3) is not on the antidiagonal and does not correspond to an integer number. Consequently its contributions "spread" to the neighbouring integer. Such an effect is well shown in the right panel of 12.3 in which it is clear that the largest terms of the quasi-local parts of the negativity Hamiltonian are centered around $\bar{x}^R$. A more quantitative analysis of the quasilocal terms would require a

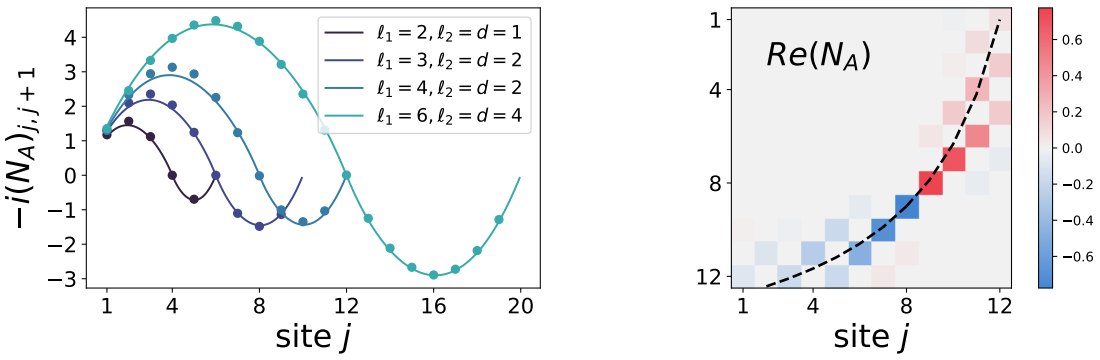

Figure 12.3: Negativity Hamiltonian for a real free fermion and for two disjoint intervals of different length $\ell_1 \neq \ell_2$. In this case, the discretised form of N_A correctly reproduces the local behavior of the negativity Hamiltonian (left panel). However, the reflected point $\bar{x}^R$ is not an integer living on the antidiagonal, as in the case of two intervals of equal length. Therefore, we only plot the location of $\bar{x}^R$, Eq. (12.4.3), in order to show that its shape is compatible with the structure of the quasi-local part of N_A. Here we fix $\ell_1 = 2\ell_2 = 2d = 4$ (right panel).

weighted sum of the nearby elements to get the correct continuum limit, a procedure similar to the one exploited for the entanglement Hamiltonian in Refs. [301, 464, 580, 582, 583] (steps in this direction can be already found in [585]). Such analysis is beyond the scope of this thesis and for this reason we focus on the local term which instead is easily discretised. This is shown in the left panel of Fig. 12.3. Also in this case, the field theory prediction correctly matches the numerics, with small deviations that are at most $\sim 6\%$ for the system sizes considered.

12.6 Closing remarks

In this Chapter we initiated the study of the negativity Hamiltonian in many-body quantum systems. Although our field theoretical construction in terms of the EH of disjoint intervals is very general, its applicability relies crucially on the exact knowledge of the latter, that is not always available. We hope that this will spark further studies on disjoint intervals's EH and, at the same time, the search for alternative constructions of N_A. Furthermore, we stress that the knowledge of this operator encodes the entire information content about the entanglement in the mixed states. This is remarkable with respect to the scalar quantities used to compute the entanglement (e.g. the negativity), which do not allow to reconstruct the whole partial transpose reduced density matrix. We expect that the quasi-local structure of the negativity Hamiltonian can be generalised to other contexts, at least for free fermions, such as a single interval in an infinite system at finite temperature [242], or two disjoint intervals in the presence of a point-like defect [571]. At present, it is unclear whether this quasi-local structure survives to finite interaction strengths and in higher dimensions. Having established an explicit approximate functional form for the negativity Hamiltonian paves the way for a direct reconstruction of partial transposes in experiments, utilizing, e.g., Hamiltonian reconstruction methods that have already been combined with the BW theorem [561]. These applications would allow a direct measurement of the negativity spectrum, something that is presently unachievable by any method other than full state tomography. Moreover, it may be possible to design efficient classical or hybrid classical-quantum algorithms for the *ab initio* determination of N_A, similarly to what has been done for the EH following a BW inspired ansatz [560, 562, 584].

Chapter 13

Symmetry decomposition of negativity of massless free fermions

We consider the problem of symmetry decomposition of the entanglement negativity in free fermionic systems. The negativity admits a resolution in terms of the charge imbalance between the two subsystems. We introduce a normalised version of the imbalance resolved negativity which has the advantage to be an entanglement proxy for each symmetry sector, but may diverge in the limit of pure states for some sectors. Our main focus is then the resolution of the negativity for a free Dirac field at finite temperature and size. We consider a tripartite geometry and exploit conformal field theory to derive universal results for the charge imbalance resolved negativity. To this end, we use a geometrical construction in terms of an Aharonov-Bohm-like flux inserted in the Riemann surface defining the entanglement. We interestingly find that the entanglement negativity is always equally distributed among the different imbalance sectors at leading order. Our analytical findings are tested against exact numerical calculations for free fermions on a lattice. This Chapter is based on Ref. [101].

13.1 Introduction

In this Chapter, we consider a many-body system with an internal global symmetry and address the question of how mixed state entanglement splits into contributions arising from distinct symmetry sectors. For mixed states, the pioneering work is Ref. [116], where it was proven that whenever there is a conserved extensive charge, the negativity admits a resolution in terms of the charge imbalance between the two subsystems, as already explained in Sec 1.3. Here, we first point out that by properly normalising the imbalance sectors (as also done in Ref. [89]) one obtains a clearer resolution of the entanglement in the imbalance; then we show that the imbalance-decomposition of negativity also holds using the partial transpose definition for free fermions we reviewed in Chapter 12. We then use such decomposition to study the symmetry resolution of the entanglement of free fermions at finite temperature and size, exploiting the same field theory methods used for the total negativity [151, 479]. Thus, the spacetime geometry we are interested in is a torus defined by two periods which, in our units, are 1 and $\tau = i\beta/L$, where $\beta = 1/T$ is the inverse temperature. The partition functions depend on the boundary conditions along the two cycles, which specify the spin structure of the fermion on the torus. Let z be a holomorphic coordinate on the torus: it has the periodicities $z = z + 1$ and $z = z + \tau$. The holomorphic component of the fermion on the torus satisfies four possible boundary conditions

$$\tilde{\psi}_k(z+1) = e^{2\pi i \nu_1}\tilde{\psi}_k(z), \qquad \tilde{\psi}_k(z+\tau) = e^{2\pi i \nu_2}\tilde{\psi}_k(z), \tag{13.1.1}$$

where ν_1 and ν_2 take the values 0 or $\frac{1}{2}$. The anti-holomorphic component is a function of $\bar{z}$ and satisfies the same boundary conditions as the holomorphic part. We denote the $\nu = (\nu_1, \nu_2)$ sector where $\nu = 1, 2, 3, 4$ corresponds to $(0,0), (0,1/2), (1/2,1/2), (1/2,0)$, respectively (for standard fermions, the physical boundary conditions are anti-periodic along both cycles and so $\nu = 3$, but the other spin structures have important applications too). The Chapter is organised as follows. In Sec. 13.2, after a brief summary of the results found in [116], we motivate our work by simple examples for a tripartite geometry, using both the standard and the fermionic partial transpose operation to explore the block-diagonal structure of the reduced density matrix. In Sec. 13.3, we apply the method based on the replica trick and described in detail in Sec. 4.2 to provide results for charged and imbalance resolved negativity for a tripartite setting. Numerical checks for free fermions on the lattice are also presented as a benchmark of the analytical results. We draw our conclusions in Sec. 13.5. One appendix is also included to give details about the numerical computations.

13.2 Charge imbalance resolved negativity

In this section, we present the symmetry resolution of the standard and fermionic partial transpose of the density matrix. Simple examples will lead to a general definition of the imbalance resolution of entanglement negativity, both fermionic and bosonic (see Sec. 1.3 for the latter). We closely follow Ref. [116], but we normalise differently the partial transpose in each symmetry sector, so that the symmetry resolved negativity is a genuine indicator of entanglement in the sector.

13.2.1 Imbalance entanglement via bosonic partial transpose

In the presence of symmetries, the RDM has a block diagonal structure which allows to identify contributions to the entanglement entropy from individual charge sectors. In order to understand how symmetry is reflected in a block structure of the density matrix after partial transpose, we start with a simple example, taken from Ref. [116]. Consider a particle in one out of three boxes, A_1, A_2, B, described by a pure state $|\Psi\rangle = \alpha\,|100\rangle + \beta\,|010\rangle + \gamma\,|001\rangle$. The RDM of $A = A_1 \cup A_2$ is $\rho_A = \mathrm{Tr}_B|\psi\rangle\langle\psi| = |\gamma|^2\,|00\rangle\langle 00| + (\alpha\,|10\rangle + \beta\,|01\rangle)(\alpha^*\langle 10| + \beta^*\langle 01|)$, i.e.

$$\rho_A = \begin{pmatrix} |\gamma|^2 & 0 & 0 & 0 \\ 0 & |\beta|^2 & \alpha^*\beta & 0 \\ 0 & \beta^*\alpha & |\alpha|^2 & 0 \\ 0 & 0 & 0 & 0 \end{pmatrix}, \tag{13.2.1}$$

in the basis $\{|00\rangle, |01\rangle, |10\rangle, |11\rangle\}$. This matrix is clearly block diagonal with respect to the total occupation number $N_A = N_1 + N_2$, where N_1 and N_2 respectively denote the particle number of the subsystem A_1 and A_2. According to Eq. (1.1.12), the partial transpose of ρ_A is

$$\rho_A^{T_1} = \begin{pmatrix} |\gamma|^2 & 0 & 0 & \alpha\beta^* \\ 0 & |\beta|^2 & 0 & 0 \\ 0 & 0 & |\alpha|^2 & 0 \\ \beta\alpha^* & 0 & 0 & 0 \end{pmatrix}. \tag{13.2.2}$$

The total negativity is $\mathcal{N} = \left|\frac{1}{2}|\gamma|^2 - \sqrt{\frac{1}{4}|\gamma|^4 + |\alpha\beta|^2}\right|$. Once we reshuffle the elements of rows and columns in the basis of $\{|10\rangle, |00\rangle, |11\rangle, |01\rangle\}$, we get

$$\rho_A^{T_1} = \begin{pmatrix} |\alpha|^2 & 0 & 0 & 0 \\ 0 & |\gamma|^2 & \alpha\beta^* & 0 \\ 0 & \beta\alpha^* & 0 & 0 \\ 0 & 0 & 0 & |\beta|^2 \end{pmatrix}, \tag{13.2.3}$$

which has a block structure where each block is labelled by the occupation imbalance $q = N_2 - N_1$ (we call it q rather than $q_{\rm imb}$ as in Sec. 1.3 to simplify the notation):

$$\rho_A^{T_1} \cong \left(|\alpha|^2\right)_{q=-1} \oplus \begin{pmatrix} |\gamma|^2 & \alpha\beta^* \\ \beta\alpha^* & 0 \end{pmatrix}_{q=0} \oplus \left(|\beta|^2\right)_{q=1}. \tag{13.2.4}$$

The structure of the above example is easily generalised to a many-body ρ_A, leading to the definition of the *charge-imbalance resolved negativity* defined in Eq. (1.3.12).

We now discuss the important "pathological" case when $p(q) = 0$ for some values of the imbalance q, but $\rho_A^{T_1}(q)$ is non-zero and so the negativity of the sectors diverges, although the total one is finite. For example, this happens setting $\gamma = 0$ in Eq. (13.2.1); in this case ρ_A corresponds to a pure state. Actually, it is obvious that every time that ρ_A is a pure state there will be some $p(q) = 0$ because $N_1 + N_2$ is fixed and hence also the parity of $N_1 - N_2$ is (so all the $p(q)$'s where q has a different parity vanish). In such case, the origin of the problem can be traced back to the fact that the (pure-state) entanglement (entropy) is better resolved in terms of N_1 or N_2 rather than in the imbalance, i.e. the symmetries of ρ_A and $\rho_A^{T_1}$ are larger than in the standard mixed case. However, mixed states with some zero $p(q)$ can be also easily built, although they are difficult to encounter as mixed states in physical settings (and they all correspond to states in which there is more symmetry than the imbalance). To understand the situation better, let us recall that $p(q)$ is always the sum of some diagonal elements of both $\rho_A^{T_1}(q)$ and ρ_A. For the latter, the diagonal elements are the populations of states in the Fock basis. Hence, we need at least a few zero populations to have a vanishing $p(q)$ (and, e.g., this will never happen in a Gibbs state at finite temperature). In the matrix ρ_A, if the populations in a given sector of the total charge are zero, the entire block is zero (and hence the entanglement entropy of the sector is zero). However, when taking the partial transpose, the off-diagonal elements are reshuffled in the matrix and, after being re-organised in terms of the imbalance, we can end up with some blocks with all zeros on the diagonal (and so $p(q) = 0$) but with non-zero off-diagonal elements. In these instances, we cannot normalise with $p(q)$. (Have always in mind the example of Eq. (13.2.1) with $\gamma = 0$: there are two sectors in ρ_A with zero populations, $N_1 + N_2 = 0, 2$; after the partial transposition, they both end up in imbalance $q = 0$, see Eq. (16.3.8) which has non-zero off-diagonal terms). Anyhow, it makes sense that the imbalance negativity diverges in these cases. We are indeed facing sectors that have exactly zero populations, but still have some quantum correlations. In practice, as we shall see in the next section, these vanishing $p(q)$ are encountered only in the limit of a pure state (e.g. for $T \to 0$) and so diverging imbalance negativity signals that the state is getting pure and that a better resolution of the entanglement is in N_1 or N_2 rather than in the imbalance.

The example of tripartite CFT.

As a first simple example to show the importance of the normalisation $p(q)$ in the definition of imbalance resolved negativity, we reanalyse a simple known result [116] for the ground state of a Luttinger liquid (with parameter K) in a tripartite geometry. Thus, the results in this subsection

describe gapless interacting $1d$ fermions. We focus on two adjacent intervals of length ℓ_1 and ℓ_2 respectively embedded in an infinite line.

Following [116], we start with the computation of the charged moments of the partial transpose

$$N_n^{T_1}(\alpha) \equiv \mathrm{Tr}((\rho_A^{T_1})^n e^{i\hat{Q}\alpha}) = \langle \mathcal{T}_n \mathcal{V}_\alpha(u_1) \mathcal{T}_{-n}^2 \mathcal{V}_{-2\alpha}(v_1) \mathcal{T}_n \mathcal{V}_\alpha(v_2) \rangle \,, \tag{13.2.5}$$

where, in the right hand side, we use the correspondence with the 3-point correlation function of fluxed twist field $\mathcal{T}_n \mathcal{V}_\alpha$ with scaling dimension

$$\Delta_n(\alpha) = \frac{1}{24}\Big(n - \frac{1}{n}\Big) + \frac{K}{2n}\left(\frac{\alpha}{2\pi}\right)^2, \qquad \Delta_{\mathcal{T}_{n_o}^2} = \Delta_{n_o} \qquad \Delta_{\mathcal{T}_{n_e}^2} = 2\Delta_{n_e/2}. \tag{13.2.6}$$

Using these scaling dimensions, one finds

$$\log N_n^{T_1}(\alpha) = \log R_n - \frac{K}{2n}\left(\frac{\alpha}{\pi}\right)^2 \log\Big[\frac{\ell_1^2 \ell_2^2}{(\ell_1+\ell_2)\epsilon^3}\Big], \tag{13.2.7}$$

where R_n are neutral Rényi negativities and ϵ is an ultraviolet cutoff. Notice in Eq. (13.2.7) only R_n does depend on the parity of n [151], while the α dependence is the same for even and odd n.

Upon performing a Fourier transform of Eq. (13.2.7), we obtain, through the saddle-point approximation, the (normalised) charge imbalance RN

$$R_n(q) = R_n \frac{\int_{-\pi}^{\pi} \frac{d\alpha}{2\pi} e^{-i(q-\bar{q})\alpha} e^{-\alpha^2 b_n/2}}{\big[\int_{-\pi}^{\pi} \frac{d\alpha}{2\pi} e^{-i(q-\bar{q})\alpha} e^{-\alpha^2 b_1/2}\big]^n} \simeq R_n \sqrt{\frac{(2\pi b_1)^n}{2\pi b_n}} e^{-\frac{(q-\bar{q})^2}{2}\left(\frac{1}{b_n} - \frac{n}{b_1}\right)}, \tag{13.2.8}$$

where $\bar{q}$ is the expectation value of the charge operator $\hat{Q}$ and

$$b_n = \frac{1}{\pi^2 n} \log\Big[\frac{\ell_1^2 \ell_2^2}{(\ell_1+\ell_2)\epsilon^3}\Big]. \tag{13.2.9}$$

The saddle-point approximation holds for two intervals of length $\ell_1, \ell_2 \to \infty$ embedded in an infinite line at zero temperature. The replica limit $n_e \to 1$ is easily taken since there is no parity dependence in the imbalance part. For large $\ell_1, \ell_2 \to \infty$ (hence $b_n \to \infty$), we get

$$\mathcal{N}(q) = \mathcal{N} + o(1), \tag{13.2.10}$$

i.e. we found the equipartition of negativity in the different imbalance sectors at leading order for large subsystems. This behaviour is reminiscent of the equipartition of entanglement entropy in a pure quantum system that possesses an internal symmetry [85]. It is clear that *negativity equipartition* can be shown only by properly normalising the partial transpose in each sector as done here. As an important difference compared to the entanglement entropies, we do not have additional $\log\log\ell$ [90] corrections to the symmetry resolved quantities.

13.2.2 Imbalance entanglement of fermions via partial TR

Now we are ready to understand the block structure of the fermionic partially transposed density matrix and how the fermionic negativity splits according to the symmetry. We first revisit the simple example of the previous section in Eq. (13.2.1) for fermions. According to Eq. (12.2.16), the partial transpose of ρ_A in Eq. (13.2.1) is

$$\rho_A^{R_1} = \begin{pmatrix} |\gamma|^2 & 0 & 0 & i\alpha\beta^* \\ 0 & |\beta|^2 & 0 & 0 \\ 0 & 0 & |\alpha|^2 & 0 \\ i\beta\alpha^* & 0 & 0 & 0 \end{pmatrix}, \tag{13.2.11}$$

i.e. the partial transpose transformation does not spoil the block matrix structure according to the occupation imbalance $q = N_2 - N_1$:

$$\rho_A^{R_1} \cong \big(|\alpha|^2\big)_{q=-1} \oplus \begin{pmatrix} |\gamma|^2 & i\alpha\beta^* \\ i\beta\alpha^* & 0 \end{pmatrix}_{q=0} \oplus \big(|\beta|^2\big)_{q=1}\,. \tag{13.2.12}$$

The (total) fermionic negativity is

$$\mathcal{N} = \frac{|\gamma|^2}{2}\left(-1 + \sqrt{\frac{1}{2} + \frac{|\alpha\beta|^2}{|\gamma|^4} + \sqrt{\frac{1}{4} + \frac{|\alpha\beta|^2}{|\gamma|^4}}} + \sqrt{\frac{1}{2} + \frac{|\alpha\beta|^2}{|\gamma|^4} - \sqrt{\frac{1}{4} + \frac{|\alpha\beta|^2}{|\gamma|^4}}}\right). \tag{13.2.13}$$

For a many-body state, the analogue of the commutation relation in Eq. (1.3.9) now reads

$$[\rho_A^{R_1}, \hat{N}_2 - \hat{N}_1^{R_1}] = 0, \tag{13.2.14}$$

while the (normalised) charge imbalance resolved negativity is given by

$$\mathcal{N}(q) = \frac{\mathrm{Tr}|(\rho_A^{R_1}(q))| - 1}{2}, \qquad \rho_A^{R_1}(q) = \frac{\mathcal{P}_q \rho_A^{R_1} \Pi_q}{\mathrm{Tr}(\Pi_q \rho_A^{R_1})}. \tag{13.2.15}$$

We also define the *charge imbalance resolved RN*

$$R_n(q) = \begin{cases} \mathrm{Tr}(\rho_A^{R_1}(q)\rho_A^{R_1}(q)^\dagger \dots \rho_A^{R_1}(q)\rho_A^{R_1}(q)^\dagger), & n \quad \text{even}, \\ \mathrm{Tr}(\rho_A^{R_1}(q)\rho_A^{R_1}(q)^\dagger \dots \rho_A^{R_1}(q)), & n \quad \text{odd}, \end{cases} \tag{13.2.16}$$

from which $\mathcal{N}(q) = \frac{1}{2}\Big(\lim\limits_{n_e \to 1} R_{n_e}(q) - 1\Big)$. It is important to stress that the diagonal elements of $\rho_A^{R_1}$ are the same as $\rho_A^{T_1}$ (the TR operation does not touch the diagonal elements) and so the probabilities $p(q)$ are identical for both the standard and the fermionic partial transpose. Thus, all the considerations for the vanishing of $p(q)$ in the previous subsection apply also here. For the example of Eq. (13.2.12), the imbalance negativities are $\mathcal{N}(\pm 1) = 0$ and $\mathcal{N}(0) = \frac{1}{2}\left(-1 + \sqrt{\frac{1}{2} + \frac{|\alpha\beta|^2}{|\gamma|^4} + \sqrt{\frac{1}{4} + \frac{|\alpha\beta|^2}{|\gamma|^4}}} + \sqrt{\frac{1}{2} + \frac{|\alpha\beta|^2}{|\gamma|^4} - \sqrt{\frac{1}{4} + \frac{|\alpha\beta|^2}{|\gamma|^4}}}\right)$ with $p(0) = |\gamma|^2$. As a further check, $\sum_q p(q)\mathcal{N}(q)$ gives back the total negativity in Eq. (13.2.13).

13.3 Charged moments of the partial transpose

In this section, we adapt the replica approach to the charged entropies of Sec. 4.2 to the charged of the fermionic partial transpose defined as

$$N_n(\alpha) = \begin{cases} \mathrm{Tr}(\rho_A^{R_1}(\rho_A^{R_1})^\dagger \dots \rho_A^{R_1}(\rho_A^{R_1})^\dagger e^{i\hat{Q}_A\alpha}), & n \quad \text{even}, \\ \mathrm{Tr}(\rho_A^{R_1}(\rho_A^{R_1})^\dagger \dots \rho_A^{R_1} e^{i\hat{Q}_A\alpha}), & n \quad \text{odd}. \end{cases} \tag{13.3.1}$$

Hence, in order to compute the imbalance resolved negativity, we need to study the composite operator $\rho_A^{R_1}(\rho_A^{R_1})^\dagger$. The charged moments in Eq. (13.3.1) are defined for two subsystems A_1 and A_2 with different twist matrices respectively denoted by $T_\alpha^{R_1}$ and T_α. We will focus on the case $n = n_e$, which is the relavant case for the computation of negativity. The new twist matrix $T_\alpha^{R_1}$ for the transposed subsystem is given by

$$T_\alpha^{R_1,n} = -T_\alpha^{-1}. \tag{13.3.2}$$

The two matrices, T_α and $T_\alpha^{R_1}$, are simultaneously diagonalisable. Consequently, we can decompose our problem into n decoupled copies in which the fields have different twist phases along the two subsystems. As a result, $N_n(\alpha)$ is decomposed as

$$N_n(\alpha) = \prod_{k=-(n-1)/2}^{(n-1)/2} Z_{R_1,k}(\alpha), \tag{13.3.3}$$

where $Z_{R_1,k}(\alpha)$ is the partition function for fields with twist phases equal to $e^{2\pi i(\frac{k}{n}+\frac{\alpha}{2\pi n})}$ and $-e^{-2\pi i(\frac{k}{n}+\frac{\alpha}{2\pi n})}$, respectively along A_2 and A_1. The probability $p(q)$ is the Fourier transform of $N_1(\alpha) = \mathrm{Tr}[\rho^{R_1} e^{i\hat{Q}\alpha}]$, that, with a minor abuse of terminology, we dub *charged probability*. In this case, the twist matrices along the two intervals are just phases given by $T_\alpha = e^{i\alpha}$ and $T_\alpha^{R_1} = T_\alpha^{-1} = e^{-i\alpha}$.

A Fourier transform leads us to the imbalance resolved negativities (13.2.16)

$$\mathcal{Z}_{R_1,n}(q) = \int_{-\pi}^{\pi} \frac{d\alpha}{2\pi} e^{-i\alpha q} N_n(\alpha), \quad p(q) = \int_{-\pi}^{\pi} \frac{d\alpha}{2\pi} e^{-i\alpha q} N_1(\alpha), \tag{13.3.4}$$

from which

$$R_n(q) = \frac{\mathcal{Z}_{R_1,n}(q)}{p^n(q)}, \qquad \mathcal{N}(q) = \frac{1}{2}\Big(\lim_{n_e\to 1} R_{n_e}(q) - 1\Big). \tag{13.3.5}$$

Let us stress the replica limit for $R_n(q)$ is $\lim_{n_e\to 1} \dfrac{\mathcal{Z}_{R_1,n_e}(q)}{p(q)}$, i.e. while it is sufficient to set $n = 1$ in the denominator, the numerator requires an analytic continuation from the even sequence at $n_e \to 1$. These relations are the same appearing in Sec. 1.4.2, with the only difference that now we employ the fermionic definition for the partial transpose. In the following section, we compute the imbalance resolved entanglement negativity for a tripartite geometry.

13.4 Symmetry resolved negativities in a tripartite geometry

Let us study the negativity of two subsystems consisting of two adjacent intervals A_1, A_2, of lengths ℓ_1, ℓ_2 out of a system of length L. We place the branch points at $u_1 = -\ell_1/L = -r_1, v_1 = u_2 = 0$, and $v_2 = \ell_2/L = r_2$ and the multivalued fields ψ_k take up a phase $-e^{-2\pi i(\frac{k}{n}+\frac{\alpha}{2\pi n})}$ at u_1, $-e^{2\pi i(\frac{k}{n}+\frac{\alpha}{2\pi n})} e^{2\pi i(\frac{k}{n}+\frac{\alpha}{2\pi n})}$ at v_1 and $e^{-2\pi i(\frac{k}{n}+\frac{\alpha}{2\pi n})}$ at v_2. By introducing a gauge field A_μ^k, as explained in Sec. 4.2, we have to impose proper monodromy conditions such that the field is almost pure gauge except at the branch points, where delta function singularities are necessary to recover the correct phases of the multivalued fields. Hence, the flux of the gauge fields is given by

$$\begin{aligned}&\frac{1}{2\pi}\epsilon^{\mu\nu}\partial_\nu A_\mu^k(x)\\ &= -\left(\frac{k}{n}+\frac{\alpha}{2\pi n}-\frac{1}{2}\right)\delta(x-u_1) + \left(\frac{2k}{n}+\frac{\alpha}{\pi n}-\frac{1}{2}\right)\delta(x-v_1) - \left(\frac{k}{n}+\frac{\alpha}{2\pi n}\right)\delta(x-v_2).\end{aligned} \tag{13.4.1}$$

Through bosonisation, $Z_{R_1,k}^{(\nu)}(\alpha)$ can be written as a correlation function of vertex operators $V_a(x) = e^{-ia\phi_k(x)}$ as

$$\begin{aligned}Z_{R_1,k}^{(\nu)}(\alpha) &= \big\langle V_{\frac{k}{n}+\frac{\alpha}{2\pi n}-\frac{1}{2}}(u_1) V_{-\frac{k}{n}-\frac{\alpha}{2\pi n}+\frac{1}{2}}(v_1) V_{-\frac{k}{n}-\frac{\alpha}{2\pi n}}(v_1) V_{\frac{k}{n}+\frac{\alpha}{2\pi n}}(v_2)\big\rangle\\ &= \big\langle V_{\frac{k}{n}+\frac{\alpha}{2\pi n}-\frac{1}{2}}(u_1) V_{-\frac{2k}{n}-\frac{\alpha}{\pi n}+\frac{1}{2}}(v_1) V_{\frac{k}{n}+\frac{\alpha}{2\pi n}}(v_2)\big\rangle.\end{aligned} \tag{13.4.2}$$

Using the correlation function of vertex operators on a torus reported in [269], the final result is [1]

$$Z^{(\nu)}_{R_1,k}(\alpha) = |\theta_1(r_1|\tau)|^{-2(\frac{k}{n}+\frac{\alpha}{2\pi n}-\frac{1}{2})(\frac{2k}{n}+\frac{\alpha}{\pi n}-\frac{1}{2})}|\theta_1(r_2|\tau)|^{-2(\frac{k}{n}+\frac{\alpha}{2\pi n})(\frac{2k}{n}+\frac{\alpha}{\pi n}-\frac{1}{2})}$$
$$|\theta_1(r_1+r_2|\tau)|^{2(\frac{k}{n}+\frac{\alpha}{2\pi n})(\frac{k}{n}+\frac{\alpha}{2\pi n}-\frac{1}{2})} \times \Big|\frac{\epsilon}{L}\partial_z\theta_1(0|\tau)\Big|^{-\Delta_k(\alpha)}\Big|\frac{\theta_\nu((\frac{k}{n}+\frac{\alpha}{2\pi n})(r_2-r_1)+\frac{1}{2}r_1|\tau)}{\theta_\nu(0|\tau)}\Big|^2, \tag{13.4.3}$$

where

$$\Delta_k(\alpha) = -6\frac{k^2}{n^2} - 6\frac{k\alpha}{n^2\pi} - 3\frac{\alpha^2}{2n^2\pi^2} + 3k\frac{1}{n} + 3\frac{\alpha}{2n\pi} - \frac{1}{2} - 2\theta(-k)(\frac{3k}{n}+\frac{3\alpha}{2n\pi}), \tag{13.4.4}$$

and $\theta(x)$ is the step function. It is important to note that for $k<0$, we have to modify the flux at u_1 and v_1, π, by inserting an additional 2π and -2π fluxes. Essentially, we need to find the dominant term with the lowest scaling dimension in the mode expansion, as discussed in more details in [101]. Putting together the various pieces and using Eq. (13.3.3), the logarithm of the charged moments of $\rho_A^{R_1}$ are given by

$$\log N^{(\nu)}_n(\alpha) = \log N_{n,0}(\alpha) + \log N^{(\nu)}_{n,1}(\alpha), \tag{13.4.5}$$

where the spin-independent part is

$$\begin{aligned}\log N_{n,0}(\alpha) =& \log R_n - \frac{\alpha^2}{2\pi^2 n}\log\Big|\theta_1(r_1|\tau)^2\theta_1(r_2|\tau)^2\theta(r_1+r_2|\tau)^{-1}\Big(\frac{\epsilon}{L}\partial_z\theta_1(0|\tau)\Big)^{-3}\Big|,\\ \log R_n =& -\Big(\frac{n^2-4}{12n}\Big)\log\Big|\theta_1(r_1|\tau)\theta_1(r_2|\tau)\Big(\frac{\epsilon}{L}\partial_z\theta_1(0|\tau)\Big)^{-2}\Big|\\ &-\Big(\frac{n^2+2}{12n}\Big)\log\Big|\theta(r_1+r_2|\tau)\Big(\frac{\epsilon}{L}\partial_z\theta_1(0|\tau)\Big)^{-1}\Big|.\end{aligned} \tag{13.4.6}$$

The spin structure dependent term is

$$\log N^{(\nu)}_{n,1}(\alpha) = 2\sum_{k=-(n-1)/2}^{(n-1)/2}\log\Big|\frac{\theta_\nu((\frac{k}{n}+\frac{\alpha}{2\pi n})(r_2-r_1)+\frac{r_1}{2}|\tau)}{\theta_\nu(0|\tau)}\Big|. \tag{13.4.7}$$

Although our main focus is the state with $\nu=3$, we notice that $N^{(1)}_{n,1}(\alpha)$ above is strictly infinite because $\theta_1(0|\tau)=0$. This is related to the fermion zero mode in this sector and is not a prerogative of the charged quantities.

In the case of intervals of equal lengths $\ell_1=\ell_2=\ell$ the charged logarithmic negativity (i.e., $\mathcal{E}^\nu(\alpha)\equiv\lim_{n_e\to1}\log N^{(\nu)}_{n_e}(\alpha)$) simplifies as

$$\begin{aligned}\mathcal{E}^\nu(\alpha) =& \mathcal{E}^{(\nu)} - \frac{\alpha^2}{2\pi^2}\log\Big|\theta_1(r|\tau)^4\theta(2r_1|\tau)^{-1}\Big(\frac{\epsilon}{L}\partial_z\theta_1(0|\tau)\Big)^{-3}\Big|,\\ &\text{with}\qquad \mathcal{E}^{(\nu)} = \frac{1}{4}\log\Big|\theta_1(r|\tau)^2\theta(2r|\tau)^{-1}\Big(\frac{\epsilon}{L}\partial_z\theta_1(0|\tau)\Big)^{-1}\Big| + 2\log\Big|\frac{\theta_\nu(\frac{r}{2}|\tau)}{\theta_\nu(0|\tau)}\Big|,\end{aligned} \tag{13.4.8}$$

where $r=\ell/L$.

[1] Differently from Eq. (41) in [479] or Eq. (80) in [163], rather then using the absolute values we explicitly change the phase $\pi\to-\pi$ for $k<0$.

Eq. (13.4.8) represents our final field theoretical result for the charged logarithmic negativities in a tripartite geometry with two equal intervals. We now test this prediction against exact lattice computations obtained with the techniques reported in Appendix 13.A. However, for a direct comparison without fitting parameters, we have to take into account the non-universal contribution coming from the discretisation of the spatial coordinate, i.e. the explicit expression for the cutoff ϵ in (13.4.8) that does depend also on α, but not on the size and temperature. We can exploit the latter property to deduce its exact value from the knowledge of the lattice negativities at $T = 0$ in the thermodynamic limit that can be determined via Fisher-Hartwig techniques. The numerical results for the charged negativities are shown in Fig. 13.1, where four panels highlight the dependence on ℓ, T, α, and ℓ/L, respectively. The agreement with the parameter-free asymptotic results (13.4.8) is always excellent. Let us critically discuss these results. First, it is known for $\alpha = 0$, the logarithmic negativity saturates at finite temperature once $\ell T \gg 1$ [479], i.e., obeys an area law; conversely the top-left panel of Fig. 13.1 shows that $\mathcal{E}(\alpha)$ follows a volume law. This scaling can be also inferred analytically from the high-temperature limit reported in the following subsection. In the top-right panel of the same figure, we observe that $\mathcal{E}(\alpha)$ has a plateau at low temperatures, i.e when $T \ll 1/L$ so that the temperature is smaller than the energy finite-size gap (of order $1/L$); consequently the system behaves as if it is at zero temperature with exponentially small corrections in TL. For larger T a linear decrease sets up for low enough T, before an exponential high temperature behaviour takes place (this is not shown in the picture, but see next subsection). In the bottom-left panel, we show that the difference $\mathcal{E}(\alpha, T) - \mathcal{E}(\alpha, 0)$ is a universal function of β/L and ℓ/L: we verify this behaviour by looking at various system sizes, L, and showing that they all collapse on the same curve. The agreement also slightly improves as L increases, as it should.

Let us conclude this subsection reporting the result for the charged probability $N_1(\alpha) = \mathrm{Tr}[\rho^{R_1} e^{i\hat{Q}\alpha}]$ that requires to specialise the above discussion to the case $n = 1$. Hence, $N_1^{(\nu)}(\alpha)$ reduces to one mode, $k = 0$, and Eq. (13.4.1) becomes

$$\frac{1}{2\pi}\epsilon^{\mu\nu}\partial_\nu A^0_\mu(x) = \left(\frac{\alpha}{2\pi}\right)\delta(x-u_1) - \left(\frac{\alpha}{\pi}\right)\delta(x-v_1) + \left(\frac{\alpha}{2\pi}\right)\delta(x-v_2). \tag{13.4.9}$$

As detailed in [101], we need to find the dominant term, i.e. with the lowest scaling dimension, in the mode expansion. In particular, it turns out that for $|\alpha/\pi| > 2/3$ an additional -2π flux has to be inserted at v_1 while an additional 2π has to be added at u_1 or, equivalently, at v_2. This is the only difference with respect to $n_o \neq 1$, when the 2π flux has to be inserted only in u_1. Hence, the final expression is given by

$$N_1^{(\nu)}(\alpha) = \begin{cases} \dfrac{|\theta_1(r_1|\tau)|^{-\frac{\alpha^2}{\pi^2}}|\theta_1(r_2|\tau)|^{-\frac{\alpha^2}{\pi^2}}|\theta_1(r_1+r_2|\tau)|^{\frac{\alpha^2}{2\pi^2}}}{|\epsilon_N/L\partial_z\theta_1(0|\tau)|^{-\frac{3\alpha^2}{2\pi^2}}}\left|\dfrac{\theta_\nu(|\frac{\alpha}{2\pi}|(r_2-r_1)|\tau)}{\theta_\nu(0|\tau)}\right|^2 & |\alpha| \leq \frac{2\pi}{3} \\ f(r_1,r_2;|\alpha|)\dfrac{\theta_1(r_1+r_2|\tau)|^{|\frac{\alpha}{\pi}|(|\frac{\alpha}{2\pi}|-1)}}{|\epsilon_N/L\partial_z\theta_1(0|\tau)|^{-\frac{3|\alpha|(-|\alpha|+2\pi)}{2\pi^2}-2}}\left|\dfrac{\theta_\nu(|\frac{\alpha}{2\pi}|(r_2-r_1)+r_1|\tau)}{\theta_\nu(0|\tau)}\right|^2 & |\alpha| > \frac{2\pi}{3} \end{cases} \tag{13.4.10}$$

where $f(x,y;q) = \frac{1}{2}[x^{2(q-1)(-2q+1)}y^{2q(-2q+1)} + x \leftrightarrow y]$. The cutoff related to the charged probability is denoted as ϵ_N. Its explicit expression, for a lattice regularisation of the Dirac field, is given in [101]. This introduction of a new symbol ϵ_N is necessary in order to avoid confusion with the cutoff ϵ obtained in the replica limit as $n_e \to 1$. The analytical prediction in Eq. (13.4.10) is compared with the exact lattice computations at different β in the bottom-right panel of Fig. 13.1.

13.4.1 Low and high temperature limits.

In this section we report the low and high temperature limits of the charged Rényi negativity. Actually, the results that we are going to derive in the following for the tripartite geometry can

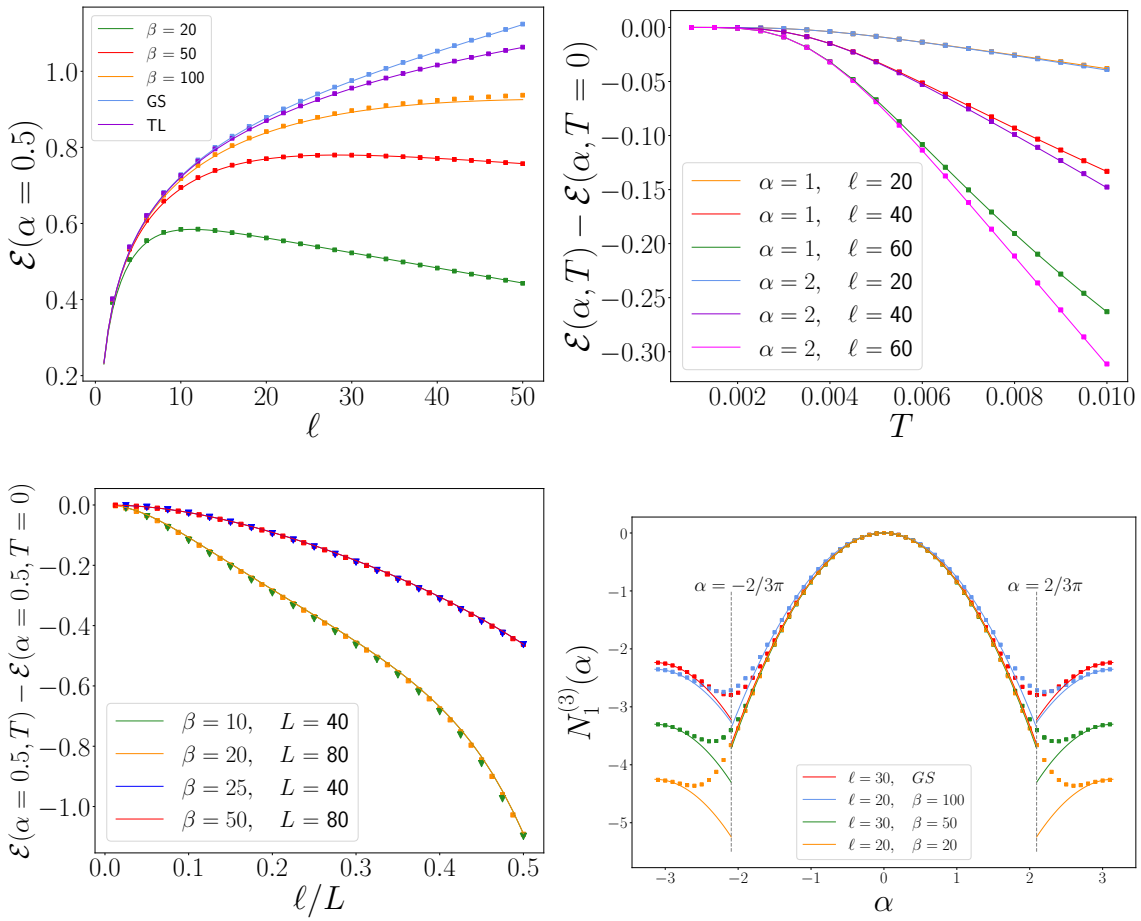

Figure 13.1: Charged negativity $\mathcal{E}(\alpha)$ in a tripartite torus with subsystem length $\ell_1 = \ell_2 = \ell$. CFT results (13.4.8), lines, against numerics on the lattice, symbols. Top-left: $\mathcal{E}(\alpha)$ as a function of ℓ for $\alpha = 0.5$. We consider different values of $\beta = 1/T$: in particular, GS stands for ground state, i.e. $T = 0$ while TL refers to the thermodynamic limit $T = 0, L \to \infty$. System size is fixed to $L = 200$ sites, except for the TL curve. Top-right: $\mathcal{E}(\alpha)$ as a function of the temperature T for different values of α and ℓ, with $L = 200$. The subtraction of the value $\mathcal{E}(\alpha, T = 0)$ cancels the dependence on the cutoff and the resulting curves are universal. Bottom-left: Scaling collapse of the charged negativity as a function of β/L and ℓ/L. We fix $\alpha = 0.5$. Bottom-right: The charged probability $N_1^{(3)}(\alpha)$ for tripartite geometry as a function of α. We set $L = 100$. Analytical prediction in Eq. (13.4.10) are compared with the exact lattice computations at different β. Notice the discontinuities at $\alpha = \pm 2/3\pi$.

be much more easily deduced by mapping the results in the complex plane (13.2.7) (i.e. both $L, \beta \to \infty$) to a cylinder periodic in either space or time (obtaining the forthcoming Eqs. (13.4.15) and (13.4.22), respectively). It is however a highly non trivial check for the correctness of our formulas that these results are re-obtained in the proper limits.

In the low temperature limit where $\tau = i\beta/L \to i\infty$, we can take advantage of the relation

$$\lim_{\beta\to\infty} \theta_1(z|i\beta/L) = 2e^{-\pi\beta/(4L)} \sin \pi z + O(e^{-2\pi\beta/L}). \tag{13.4.11}$$

In this way we obtain for the spin-independent part

$$\log N_{n,0}(\alpha) = \log R_n - \frac{\alpha^2}{2\pi^2 n} \log \left| \left(\frac{L}{\pi\epsilon}\right)^3 \frac{\sin^2\left(\frac{\pi\ell_1}{L}\right)\sin^2\left(\frac{\pi\ell_2}{L}\right)}{\sin\left(\frac{\pi(\ell_1+\ell_2)}{L}\right)} \right| + O(e^{-2\pi/(LT)}), \tag{13.4.12}$$

while using the product representation of the theta function [368], the spin structure dependent term (13.4.7) can be rewritten as

$$\begin{aligned} &\log N^{(3)}_{n,1}(\alpha) = \\ &\quad = 2\sum_{j=1}^{\infty} \frac{(-1)^{j+1}}{j} \frac{1}{\sinh(\pi j\beta/L)} \left(\cos(j(r_1-r_2)\alpha/n) \frac{\sin(\pi j r_2) - \sin(\pi j r_1)}{\sin(\pi j(r_2-r_1)/n)} - n \right). \end{aligned} \tag{13.4.13}$$

Thus, at the leading order, Eq. (13.4.12) is the whole story at zero temperature, since in the replica limit the above expression contributes to the charged negativity as

$$\mathcal{E}^{(3)}_1(\alpha) = \lim_{n_e\to 1} \log N^{(3)}_{n_e,1}(\alpha) = 4e^{-\pi/(LT)} \left(\cos((r_1-r_2)\alpha) \frac{\cos(\pi(r_2+r_1)/2))}{\cos(\pi(r_2-r_1)/2)} - 1 \right). \tag{13.4.14}$$

Putting everything together, in the low temperature limit the logarithmic charged negativity of two adjacent intervals for spatially antiperiodic fermions is given by

$$\mathcal{E}(\alpha, LT \ll 1) = \mathcal{E} - \frac{\alpha^2}{2\pi^2 n} \log \left| \left(\frac{L}{\pi\epsilon}\right)^3 \frac{\sin^2\left(\frac{\pi\ell_1}{L}\right)\sin^2\left(\frac{\pi\ell_2}{L}\right)}{\sin\left(\frac{\pi(\ell_1+\ell_2)}{L}\right)} \right| + O(e^{-2\pi/(LT)}), \tag{13.4.15}$$

where $\mathcal{E}(LT \ll 1) = \frac{1}{4}\log\left|(\frac{L}{\pi\epsilon})\frac{\sin(\frac{\pi\ell_1}{L})\sin(\frac{\pi\ell_2}{L})}{\sin(\frac{\pi(\ell_1+\ell_2)}{L})}\right|$. We can also study the low-temperature behaviour of Eq. (13.4.10), which reads

$$\begin{aligned} &N_1(\alpha, LT \ll 1) \simeq \\ &\begin{cases} -\frac{\alpha^2}{2\pi^2}\log|\frac{L^3}{\pi^3\epsilon_N^3}\frac{\sin^2(\frac{\pi\ell_1}{L})\sin^2(\frac{\pi\ell_2}{L})}{\sin(\frac{\pi(\ell_1+\ell_2)}{L})}|, & |\alpha| \le \frac{2\pi}{3} \\ \frac{(2\pi-|\alpha|)|\alpha|}{2\pi^2}\log|\frac{L^3}{\pi^3\epsilon_N^3}\frac{\sin^2(\frac{\pi\ell_1}{L})\sin^2(\frac{\pi\ell_2}{L})}{\sin(\frac{\pi(\ell_1+\ell_2)}{L})}| - \log|\frac{L^2}{\pi^2\epsilon_N^2}\sin(\frac{\pi\ell_1}{L})\sin(\frac{\pi\ell_2}{L})|. & |\alpha| > \frac{2\pi}{3}. \end{cases} \end{aligned} \tag{13.4.16}$$

To investigate the high temperature behaviour, $\tau = i\beta/L \to 0$, we can use the modular transformation rules for the theta functions:

$$\begin{aligned} \theta_1(z|\tau) &= -(-i\tau)^{-1/2} e^{-i\pi z^2/\tau} \theta_1(z/\tau|-1/\tau), \\ \theta_3(z|\tau) &= (-i\tau)^{-1/2} e^{-i\pi z^2/\tau} \theta_3(z/\tau|-1/\tau), \end{aligned} \tag{13.4.17}$$

and the asymptotic form of the θ_1 function in the small β limit

$$\theta_1(z/\tau|-1/\tau) = -2ie^{-\frac{\pi L}{4\beta}}\sinh(\frac{\pi z L}{\beta}) + O(e^{\frac{3\pi L}{\beta}(z-3/4)}), \quad 0 \leq z \leq 1/2. \tag{13.4.18}$$

Therefore, the leading terms of the spin-independent part of the charged negativities can be written as

$$\log N_{n,0}(\alpha) = \log R_n + \frac{(\ell_1-\ell_2)^2\alpha^2}{2\pi n\beta L} - \frac{\alpha^2}{2\pi^2 n}\log\left|\left(\frac{\beta}{\pi\epsilon}\right)^3 \frac{\sinh^2\left(\frac{\pi\ell_1}{\beta}\right)\sinh^2\left(\frac{\pi\ell_2}{\beta}\right)}{\sinh\left(\frac{\pi(\ell_1+\ell_2)}{\beta}\right)}\right| + O(e^{-\pi LT}), \tag{13.4.19}$$

while for the spin structure dependent term (13.4.7) we find

$$\log N^{(3)}_{n,1}(\alpha) = -\frac{\pi}{2\beta L}\left[\left(\frac{n^2-1}{3n}\right)(\ell_2-\ell_1)^2 + n\ell_1(\ell_2-\ell_1) + n\ell_1^2\right] - \frac{(\ell_2-\ell_1)^2\alpha^2}{2\pi L\beta n} + \\ - 2\sum_{j=1}^{\infty}\frac{(-1)^j}{j}\frac{1}{\sinh(\frac{\pi jL}{\beta})}\left(\cosh\left(\frac{j(\ell_1-\ell_2)\alpha}{\beta n}\right)\frac{\sinh(\pi\ell_2 j/\beta)-\sinh(\pi\ell_1 j/\beta)}{\sinh\left(\frac{\pi(\ell_2-\ell_1)j}{n\beta}\right)} - n\right). \tag{13.4.20}$$

For fixed $\ell_{1,2}/\beta$ and $\tau = i\beta/L \to 0$ we get

$$\mathcal{E}^{(3)}_1(\alpha) = -\frac{\pi\ell_1\ell_2}{2\beta L} - \frac{(\ell_2-\ell_1)^2\alpha^2}{2\pi L\beta}, \tag{13.4.21}$$

and therefore,

$$\mathcal{E}(\alpha, LT \gg 1) = \mathcal{E} - \frac{\alpha^2}{2\pi^2 n}\log\left|\left(\frac{\beta}{\pi\epsilon}\right)^3 \frac{\sinh^2\left(\frac{\pi\ell_1}{\beta}\right)\sinh^2\left(\frac{\pi\ell_2}{\beta}\right)}{\sinh\left(\frac{\pi(\ell_1+\ell_2)}{\beta}\right)}\right| + O(e^{-\pi LT}), \tag{13.4.22}$$

where $\mathcal{E}(LT \gg 1) = \frac{1}{4}\log\left|(\frac{\beta}{\pi\epsilon})\frac{\sinh(\frac{\pi\ell_1}{\beta})\sinh(\frac{\pi\ell_2}{\beta})}{\sinh(\frac{\pi(\ell_1+\ell_2)}{\beta})}\right|$. This limit confirms analytically the volume law behaviour observed in Fig. 13.1.

The high-temperature limit of the charged probability $N_1(\alpha)$ in Eq. (13.4.10) is

$$N_1(\alpha, LT \gg 1) \simeq \\ \begin{cases} -\frac{\alpha^2}{2\pi^2}\log|\frac{\beta^3}{\pi^3\epsilon_N^3}\frac{\sinh^2(\frac{\pi\ell_1}{L})\sinh^2(\frac{\pi\ell_2}{L})}{\sinh(\frac{\pi(\ell_1+\ell_2)}{L})}| & |\alpha| \leq \frac{2\pi}{3}, \\ \frac{(2\pi-|\alpha|)|\alpha|}{2\pi^2}\log|\frac{\beta^3}{\pi^3\epsilon_N^3}\frac{\sinh^2(\frac{\pi\ell_1}{L})\sinh^2(\frac{\pi\ell_2}{L})}{\sinh(\frac{\pi(\ell_1+\ell_2)}{L})}| - \log|\frac{\beta^2}{\pi^2\epsilon_N^2}\sinh(\frac{\pi\ell_1}{L})\sinh(\frac{\pi\ell_2}{L})|. & |\alpha| > \frac{2\pi}{3} \end{cases} \tag{13.4.23}$$

Let us conclude the subsection comparing these new results with those for the standard (bosonic) charged negativity reported in Eq. (13.2.7). At zero temperature and in the thermodynamic limit $\ell_i \ll L$, Eq. (13.4.12) matches exactly the bosonic negativity (13.2.7) (at $K = 1$ to describe free fermions) obtained in the same limit. As discussed deeply in Ref. [479] for the Rényi negativity (at $\alpha = 0$), this shows that the choice of charged moments of the fermionic partial transpose we made in Eq. (13.3.1) provides a partition function evaluated on the same worldsheet $\mathcal{R}_n$ as the one for the moments of the standard charged partial transpose in [116].

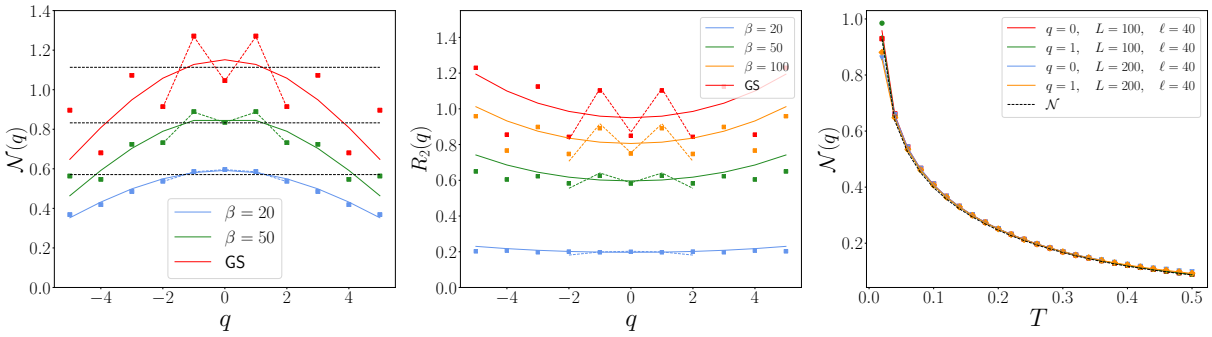

Figure 13.2: Imbalance resolved negativities for a few different values of q, $L = 200$, $\ell_1 = \ell_2 = \ell = 30$, with $n_e \to 1$ (left-panel) and $n = 2$ (middle-panel). The dashed black lines are the truly asymptotic result (13.4.31) showing equipartition, while the solid lines include the first correction due to the cutoffs as in Eq. (13.4.30). The dashed coloured lines are the ratio between the Fourier transforms without exploiting the saddle point approximation. For small q, the field theory prediction (in which the lattice cutoffs are included) well describes the numerical data. In the right-panel, $\ell = 40$ is fixed, we report two system sizes and two values of q and plot $\mathcal{N}(q)$ as a function of T. The coloured lines are Eq. (13.4.30) while the dashed one represents Eq. (13.4.31). The plot confirms the equipartition of negativity. Moreover, for large T, $\mathcal{N}(q)$ becomes a universal function of $\pi\ell T$.

13.4.2 Symmetry resolution

Again for conciseness of the various formulas, in this subsection we focus on the case $\ell_1 = \ell_2 = \ell$ (when also a closed-form expression for the spin-dependent part is easier to write), but more general formulas are similarly derived. Since we are ultimately using a saddle point approximation to make the Fourier transform (13.3.4), the charged moments (13.3.1) can be truncated at Gaussian level in α as

$$N_n^{(\nu)}(\alpha) = R_n^{(\nu)} e^{-b_n \alpha^2/2}, \tag{13.4.24}$$

where

$$b_n = \frac{1}{\pi^2 n} \log \left| \theta_1(r_1|\tau)^4 \theta(2r_1|\tau)^{-1} \Big(\frac{\epsilon}{L} \partial_z \theta_1(0|\tau) \Big)^{-3} \right|. \tag{13.4.25}$$

The Fourier transform reads

$$\mathcal{Z}^{(\nu)}_{R_1,n}(q) = R_n^{(\nu)} \int_{-\pi}^{\pi} \frac{d\alpha}{2\pi} e^{-iq\alpha} e^{-\alpha^2 b_n/2}, \tag{13.4.26}$$

where we used that the expectation value of the charge imbalance operator Q_A for a free Dirac field is $\bar{q} = 0$ at any temperature. In the saddle point approximation the integration domain is extended to the whole real line and we end up in a simple Gaussian integral, obtaining

$$\mathcal{Z}^{(\nu)}_{R_1,n}(q) \simeq \frac{R_n^{(\nu)}}{\sqrt{2\pi b_n}} e^{-\frac{q^2}{2b_n}}. \tag{13.4.27}$$

Through a similar analysis, we compute

$$p^{(\nu)}(q) = \int_{-\pi}^{\pi} \frac{d\alpha}{2\pi} e^{-iq\alpha} N_1^{(\nu)}(\alpha), \tag{13.4.28}$$

which through the saddle-point approximation reads

$$p(q) \simeq \frac{e^{-\frac{q^2}{2b_N}}}{\sqrt{2\pi b_N}} \quad b_N = \frac{1}{\pi^2}\log\Big|\theta_1(r_1|\tau)^4\theta(2r_1|\tau)^{-1}\Big(\frac{\epsilon_N}{L}\partial_z\theta_1(0|\tau)\Big)^{-3}\Big|. \tag{13.4.29}$$

Let us note that for $\alpha \in [-\pi,\pi]$, the quantity $N_1^\nu(\alpha)$ has a global maximum for $\alpha = 0$ and two local maxima for $\alpha = \pm\pi$, see Fig. 13.1 (bottom-right). However, since $N_1^\nu(\pm\pi) < N_1^\nu(0)$, we can neglect the contributions to the integral coming from the regions close to the extrema at $\alpha = \pm\pi$. Once again, let us stress the difference between the cutoff ϵ_N and the cutoff ϵ obtained in the replica limit $b = \lim_{n_e\to 1} b_{n_e}$, whose lattice expression are reported in [101] Putting everything together, we obtain

$$R_n^{(\nu)}(q) = R_n^{(\nu)}\sqrt{\frac{(2\pi b_N)^n}{2\pi b_n}}e^{-\frac{q^2}{2}(\frac{1}{b_n}-\frac{n}{b_N})}, \qquad \mathcal{N}^{(\nu)}(q) = \frac{1}{2}\Big(e^{\mathcal{E}^{(\nu)}}\sqrt{\frac{b_N}{b}}e^{-\frac{q^2}{2}(\frac{1}{b}-\frac{1}{b_N})} - 1\Big). \tag{13.4.30}$$

When the $O(1)$ terms are negligible with respect to the leading order ones in the variance, $b_N \simeq b$, hence

$$\mathcal{N}^{(\nu)}(q) \simeq \mathcal{N}^{(\nu)}, \tag{13.4.31}$$

i.e. exact equipartition of negativity in the different imbalance sectors at leading order, as shown for the bosonic negativity in Sec. (13.2.1). A similar result holds even if $\ell_1 \neq \ell_2$ in the low/high temperature limits, it would be sufficient to modify the expression of the variances in Eqs. (13.4.25) and (13.4.29).

It is instructive to explicitly write down the first term breaking the equipartition. For large L, we can expand the exponential in Eq. (13.4.30) as

$$e^{-\frac{q^2}{2}(\frac{1}{b}-\frac{1}{b_N})} \simeq 1 - \frac{q^2\log(|\epsilon/\epsilon_N|)\pi^2}{6(\log L)^2} \equiv 1 - \frac{\gamma}{(\log L)^2}q^2, \tag{13.4.32}$$

and

$$\sqrt{\frac{b_N}{b}} \simeq 1 + \frac{\gamma'}{\log L}, \tag{13.4.33}$$

where γ and γ' are implicitly defined, also in terms of the cutoffs ϵ and ϵ_N. To sum up, we get

$$\mathcal{N}^{(\nu)}(q) \simeq \mathcal{N}^{(\nu)}\Big(1 + \frac{\gamma'}{\log L} - \frac{\gamma}{(\log L)^2}q^2 + \dots\Big), \tag{13.4.34}$$

where we have derived the leading q-dependent contributions and shown that the equipartition is broken at order $1/(\log L)^2$.

In Fig. 13.2 we test the accuracy of our predictions against exact lattice numerical calculations. It is evident that equipartition is broken for all the values of ℓ, T, L we considered and the effect is more pronounced as $|q|$ is increased. However, the main smooth part of corrections to the scaling is captured by Eq. (13.4.30), see the full line in the plots, and does not come as a surprise. Also the presence of further subleading oscillating (in q) corrections have been observed for the resolved entropies [90] and were expected. In our case, such corrections are enhanced by the presence of the maxima at $\alpha = \pm\pi$ in $N_1(\alpha)$, see Fig. 13.2, that provide large corrections to the scaling in $p(q)$. Indeed, taking the Fourier transforms without making the saddle-point approximation, the agreement between numerics and field theory is perfect. As $\ell \gg 1/T$, all these corrections become smaller and imbalance resolved negativity flattens in q, mainly as a consequence of the lowering of the maxima at $\alpha = \pm\pi$ in $N_1(\alpha)$, see Fig. 13.2.

13.5 Closing remarks

We studied the entanglement negativity in systems with a conserved local charge and we found it to be decomposable into symmetry sectors. The fermionic partial transpose operation does not spoil the result found for the standard partial transposition operation [116]: the resulting operator that commutes with the partial transpose density matrix is not the total charge, but rather an imbalance operator, which is essentially the difference operator between the charge in the two regions. We introduced a normalised version of the charge imbalance resolved negativity (both fermionic and bosonic) which has the great advantage to be an entanglement proxy also for the symmetry sectors, e.g. it vanishes if the standard partial transpose has only positive eigenvalues in the sector. The price to pay is that the normalised symmetry resolved negativity diverges (for some sectors) in the limit of pure states, as a consequence of the fact that the imbalance is no longer the best quantity to resolve the entanglement. Another interesting property of this normalisation for the sector partial transpose is the *negativity equipartition*, i.e. the entanglement is the same in all imbalance sectors, in full analogy to entropy equipartition for pure states [85].

There are different aspects left open for further study. One may use the corner transfer matrix to investigate the symmetry decomposition of negativity in gapped one-dimensional models by combining former studies of the total negativity [357] with those for symmetry resolution [98] (and Chapter 7). Eventually, the generalisation of one-dimensional results to higher dimensions can be done using the dimensional reduction approach, as already done for the total negativity in [479]. Decoupling the initial d-dimensional problem into one-dimensional ones in a mixed space-momentum representation [100] would allow to generalise the above results to higher dimensional Fermi surfaces.

13.A Numerical methods

In this appendix, we report how to numerically calculate the charged negativity associated with the partial TR (12.2.18) for free fermions on a lattice described by the hopping Hamiltonian on a chain

$$H_{FF} = -\sum_{j=0}^{L-2} f_{j+1}^\dagger f_j + f_0^\dagger f_{L-1} + \text{H.c.}, \tag{13.A.1}$$

with anti-periodic condition (corresponding to the $\nu = 3$ sector discussed in the main text). The technique is a straightforward generalisation to $\alpha \neq 0$ of the one presented in [479]. This method is used throughout the main text to obtain all lattice numerical results.

Even though we use the computational basis of the Majorana modes, for particle-number conserving systems such as the lattice model in Eq. (13.A.1), the covariance matrix is simplified into the form $\sigma_2 \otimes \Gamma$, with $\Gamma = \mathbb{I} - 2C$, $C_{ij} = \text{Tr}(\rho f_i^\dagger f_j)$ is the correlation matrix and σ_2 is the second Pauli matrix (see Ref. [303] for a more detailed discussion). For a thermal state, the single-particle correlator reads

$$C_{ij} = \sum_k \frac{u_k^*(i) u_k(j)}{e^{\beta\omega_k} + 1}, \tag{13.A.2}$$

where ω_k and $u_k(i)$ are the single-particle eigenvalues and eigenvectors of the Hamiltonian (13.A.1). For a bipartite Hilbert space $\mathcal{H}_A \otimes \mathcal{H}_B$ where $A = A_1 \cup A_2$, the covariance matrix takes a block form

$$\Gamma = \begin{pmatrix} \Gamma_{11} & \Gamma_{12} \\ \Gamma_{21} & \Gamma_{22} \end{pmatrix}, \tag{13.A.3}$$

where Γ_{11} and Γ_{22} are the reduced covariance matrices of the two subsystems A_1 and A_2, respectively, while Γ_{12} and $\Gamma_{21}^\dagger$ contain the cross correlations between them. By simple Gaussian states' manipulations, the correlation matrices associated with $\rho_A^{R_1}$, $(\rho_A^{R_1})^\dagger$ can be written as ([479] and Eq. (12.2.14))

$$\Gamma_\pm = \begin{pmatrix} -\Gamma_{11} & \pm i\Gamma_{12} \\ \pm i\Gamma_{21} & \Gamma_{22} \end{pmatrix}. \tag{13.A.4}$$

The objects we are interested in are $N_{n_e} = \mathrm{Tr}[(\rho^{R_1}(\rho^{R_1})^\dagger)^{n_e/2} e^{i\hat{Q}\alpha}]$ and $N_1(\alpha) = \mathrm{Tr}[\rho^{R_1} e^{i\hat{Q}\alpha}]$. The imbalance of the relativistic Dirac field corresponds to the discretised operator $\hat{Q} = \hat{N}_{A_1\cup A_2} - 1/2(\ell_1+\ell_2)$. Notice that in this basis, $\hat{Q}$ is not the difference, but the sum of the number operators. Furthermore, it presents a shift compared to the number operator of the non-relativistic fermions. The single particle correlation matrix associated to the normalised composite density operator $\rho_{\mathrm{x}} = \rho^{R_1}(\rho^{R_1})^\dagger/Z_{\mathrm{x}}$ is [174, 479]

$$\Gamma_{\mathrm{x}} = (\mathbb{1} + \Gamma_+\Gamma_-)^{-1}(\Gamma_+ + \Gamma_-), \tag{13.A.5}$$

where the normalisation factor is $Z_{\mathrm{x}} = \mathrm{Tr}(\Gamma_{\mathrm{x}}) = \mathrm{Tr}(\rho_A^2)$. In terms of eigenvalues of correlation matrices, we can write [479]

$$\begin{aligned} \log N_n(\alpha) = &- i\alpha\frac{\ell_1+\ell_2}{2} + \sum_{j=1}^{N} \log\left[\left(\frac{1-\nu_j^{\mathrm{x}}}{2}\right)^{n/2} + e^{i\alpha}\left(\frac{1+\nu_j^{\mathrm{x}}}{2}\right)^{n/2}\right] + \\ &+ \frac{n}{2}\sum_{j=1}^{N} \log\left[\zeta_j^2 + (1-\zeta_j)^2\right], \end{aligned} \tag{13.A.6}$$

where ν_j^{x} and ζ_j are eigenvalues of the matrices Γ_{x} (13.A.5) and C (13.A.2), respectively. In terms of the eigenvalues ν's of Γ_+ (13.A.4), the charged normalisation $N_1(\alpha)$ is

$$\log N_1(\alpha) = -i\alpha\frac{\ell_1+\ell_2}{2} + \sum_{j=1}^{N} \log\left[\left(\frac{1-\nu_j}{2}\right) + e^{i\alpha}\left(\frac{1+\nu_j}{2}\right)\right]. \tag{13.A.7}$$

Taking the Fourier transform of the numerical data for $N_{n_e}(\alpha)$ and $N_1(\alpha)$, we finally obtain the imbalance resolved negativities.

Chapter 14

Quench dynamics of Rényi negativities and the quasiparticle picture

The study of the moments of the partially transposed density matrix provides a new and effective way of detecting bipartite entanglement in a many-body mixed state. In this Chapter, we study the time evolution after a quantum quench of the moments of the partial transpose, and several related quantities, such as the Rényi negativities. By combining CFT results with integrability, we show that, in the space-time scaling limit of long times and large subsystems, a quasiparticle description allows for a complete understanding of the Rényi negativities. We test our analytical predictions against exact numerical results for free-fermion and free-boson lattice models, even though our framework applies to generic interacting integrable systems. This Chapter is based on Ref. [586].

14.1 Introduction

As already remarked in the introduction of this thesis, during the last decades, the study of entanglement became a powerful tool to explore the out of equilibrium dynamics of quantum systems. For closed bipartite systems, the von Neumann and the Rényi entropies of reduced density matrices can be used as *bona fide* measures of the entanglement shared between the two complementary parts. However, for mixed states, the entanglement can be studied via the *partial transpose* of the RDM.

Unfortunately, computing the negativity or measuring it experimentally in quantum many-body systems is a daunting task. This fact sparked a lot of activity aiming at finding alternative entanglement witnesses for mixed states always starting from the partially transposed RDM. To this aim, several protocols to measure the moments $\mathrm{Tr}(\rho_A^{T_1})^n$ of the partial transpose have been proposed [88,456,587,588] culminating with the actual experimental measure in an ion-trap setting using shadow tomography [88, 456]. However, these moments are not direct indicators of the sign of the eigenvalues of $\rho_A^{T_1}$ and hence of entanglement. Nevertheless, some linear combinations of them are sufficient conditions (known as p_n-PPT conditions, see below) for the presence of negative eigenvalues in the spectrum [88, 456] and so are witnesses of entanglement in mixed states. However, in contrast with the logarithmic negativity, for which a quasiparticle picture was derived in Ref. [589], results for the dynamics of the moments of the partial transpose are available only for CFTs [581, 590, 591].

Here, by combining CFT and integrability, we derive the quasiparticle picture describing the dynamics of the moments of the partial transpose, and several related quantities, after a quantum quench in integrable systems. Specifically, we consider the Rényi negativities $\mathcal{E}_n = \log(\mathrm{Tr}(\rho_A^{T_1})^n)$. Note that $\mathcal{E}_n$ are not proper entanglement measures, although the limit $\lim_{n_e \to 1} \mathcal{E}_{n_e}$, with n_e an even integer, defines the logarithmic negativity. In the following, we denote $\mathcal{E}_n^{(b)}$ the standard negativity defined according to Eq. (1.1.12) (that is an entanglement monotone for both bosonic and fermionic systems) and $\mathcal{E}_n^{(f)}$ the fermionic one (that exist only for fermionic models), in according to Eq. (12.2.20).

We also consider the ratios R_n as

$$R_n = \frac{\mathrm{Tr}(\rho_A^{T_1})^n}{\mathrm{Tr}\rho_A^n}. \tag{14.1.1}$$

The ratios R_n are studied in CFT [151,152,250,251,592], due to their universality. Recently, they were studied at finite-temperature critical points [593], and to probe thermalization [594,595] (note that in Chapter 13 we refer to the ratios R_n as Rényi negativities, unlike here). Here we derive the quasiparticle picture for both $\mathcal{E}_n$ and R_n, focusing on the situation in which the subsystem A is made of two equal-length intervals at distance d. The formulas that we derive hold in the space-time scaling limit of $t, \ell, d \to \infty$, with the ratios $t/\ell, d/\ell$ fixed. Furthermore, these results allow us to obtain predictions for all the p_n-PPT conditions introduced in Refs. [88, 456]. Interestingly, we argue that the ratios R_n in the space time scaling limit become proportional to the Rényi mutual information. Finally, we provide numerical benchmarks of our results for both free-fermion and free-boson models, although they are expected to hold for generic integrable systems.

After the introuction of the p_n-PPT conditions in Sec. 14.2, in Sec. 14.3 we review the CFT predictions for the out-of-equilibrium behavior of the Rényi negativities. Specifically, in Sec. 14.3.1 we derive the out-of-equilibrium behavior of the Rényi negativities and the ratios R_n in CFTs. In Sec. 14.4 we introduce the quasiparticle picture (in section 14.4.1) for the spreading of entanglement and negativity, generalizing it to the moments of the partial transpose in section 14.4.2. In section 14.5 we present numerical benchmarks for free bosonic (in section 14.5.1) and fermionic theories (in Sec. 14.5.2). In section 14.5.3 we discuss the quasiparticle predictions for the p_n-PPT conditions. Finally, in Sec. 14.6 we draw our conclusions and we discuss some possible extensions of this Chapter.

14.2 Entanglement detection through partial transpose moments

Despite several sufficient conditions for entanglement in mixed states have been developed in the literature, many of them cannot be straightforwardly implemented experimentally since they require the knowledge of the full density matrix [13]. This is for instance the case of the PPT condition. To overcome this difficulty, it was shown in [456] that the first few moments of the partial transpose can be used to define some simple yet powerful tests for bipartite entanglement. Given $\rho_A^{T_1}$, we denote its k-th order moment as

$$p_k \equiv \mathrm{Tr}(\rho_A^{T_1})^k, \tag{14.2.1}$$

with $p_1 = \mathrm{Tr}(\rho_A^{T_1}) = 1$ and p_2 equal to the purity $p_2 = \mathrm{Tr}\rho_A^2$. The p_3-PPT condition states that any positive semi-definite partial transpose satisfies [456]

$$p_3 p_1 > p_2^2, \tag{14.2.2}$$

or, in other words, if $p_3 < p_2^2$, then ρ_A violates the PPT condition and must therefore be entangled. The condition in Eq. (14.2.2) belongs to a more general set of conditions, dubbed Stieltjes$_n$, involving inequalities among the moments p_k of order up to n. They were introduced in [88] together with a set of experimentally accessible conditions for detecting entanglement in mixed states. The condition Stieltjes$_3$ is equivalent to p_3-PPT, and so we rename here the Stieltjes$_n$-conditions as p_n-PPT. As examples, p_5-PPT and p_7-PTT read, respectively [88]

$$D_5 \equiv \det \begin{pmatrix} p_1 & p_2 & p_3 \\ p_2 & p_3 & p_4 \\ p_3 & p_4 & p_5 \end{pmatrix} \geq 0, \quad D_7 \equiv \det \begin{pmatrix} p_1 & p_2 & p_3 & p_4 \\ p_2 & p_3 & p_4 & p_5 \\ p_3 & p_4 & p_5 & p_6 \\ p_4 & p_5 & p_6 & p_7 \end{pmatrix} \geq 0, \tag{14.2.3}$$

from which one deduces easily the rationale for higher order condition.

14.3 Quench dynamics of Rényi negativities in CFT

In this section we review the CFT calculation of the temporal evolution of the Rényi negativities between two intervals after a global quench in CFT as derived in Ref. [590]. We consider $A = A_1 \cup A_2$, where the intervals A_1 and A_2 can be either adjacent or disjoint (see Fig. 1.1).

14.3.1 Out-of-equilibrium dynamics of the Rényi negativities

Before discussing the out-of-equilibrium dynamics after a quantum quench of the Rényi negativities in CFTs, it is useful to recall the imaginary time formalism for the description of quantum quenches [44–46]. The family of initial states that are easy to work with in CFT have the form $e^{-\tau_0 H}|\psi_0\rangle$, with $|\psi_0\rangle$ being a boundary state. The expectation value of a local operator O is then

$$\langle O(t,x)\rangle = Z^{-1} \langle\psi_0| e^{iHt-\tau_0 H} O(x) e^{-iHt-\tau_0 H} |\psi_0\rangle , \tag{14.3.1}$$

where the damping factors $e^{-\tau_0 H}$ have been introduced to make the path integral absolutely convergent (see below), and $Z = \langle\psi_0|e^{-2\tau_0 H}|\psi_0\rangle$ is the normalisation factor. The correlator in Eq. (14.3.1) may be represented by a path integral in imaginary time τ as [45]

$$\langle O(t,x)\rangle = Z^{-1} \int [d\varphi(x,\tau)] O(x, \tau = \tau_0 + it) e^{-\int_{\tau_1}^{\tau_2} L d\tau} \langle\psi_0|\phi(x,\tau_2)\rangle\langle\phi(x,\tau_1)|\psi_0\rangle , \tag{14.3.2}$$

where L is the (euclidean) Lagrangian corresponding to the dynamics induced by H, τ_1 can be identified with 0 and τ_2 with $2\tau_0$. As shown in [44, 46], the computation of the path integral in Eq. (14.3.2) can be done considering τ real and only at the end analytically continuing it to the complex value $\tau = \tau_0 + it$.

In this way, the problem of the dynamics is mapped to the thermodynamics of a field theory in a strip geometry of width $2\tau_0$ and boundary condition $|\psi_0\rangle$ at the two edges of the strip in the imaginary time direction. At this point we have all the ingredients to derive the dynamics of the Rényi negativities after a global quench in CFT. To calculate the time-dependent $\mathrm{Tr}(\rho_A^{T_1})^n$ one has to compute the correlator

$$\mathrm{Tr}(\rho_A^{T_1})^n = \langle \tilde{\mathcal{T}}_n(\omega_1)\mathcal{T}_n(\omega_2)\mathcal{T}_n(\omega_3)\tilde{\mathcal{T}}_n(\omega_4)\rangle , \tag{14.3.3}$$

where the expectation value has to be calculated in the field theory confined in a strip, and where we denoted by $\omega_i = u_i + i\tau$ the complex coordinate on the strip ($u_i \in \mathbb{R}$ and $0 < \tau < 2\tau_0$). It is convenient to employ the conformal transformation $z = ie^{\pi\omega/(2\tau_0)}$, which maps the strip onto

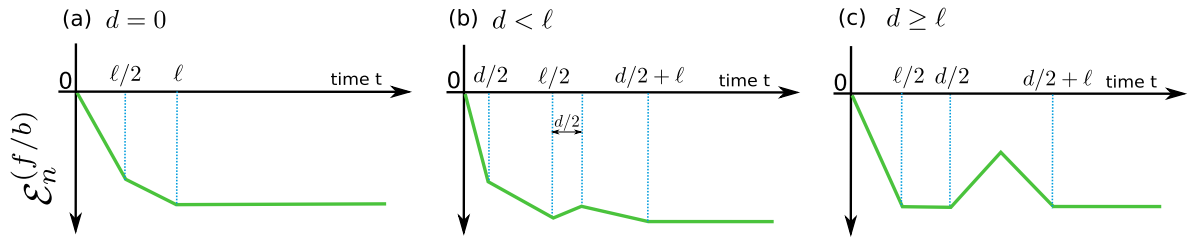

Figure 14.1: Time dependence of the Rényi negativities for quasiparticles with linear dispersion. We consider two disjoint subsystems with equal length ℓ at distance $d = 0$ (a), $d < \ell$ (b), $d \geq \ell$ (c). The piece-wise linear behavior is described by Eq. (14.3.4).

the half plane, where the four point correlation functions of the twist fields can be computed by knowing that they behave as primary fields with scaling dimenions Δ_n (cf. (1.4.15)). After the analytic continuation to real time, in the space-time scaling limit $t, |u_i - u_j| \gg \tau_0$, from Eq. (14.3.3), the Rényi negativities $\mathcal{E}_n$ (cf. Eq. (1.4.14)) read [590]

$$\mathcal{E}_n = -\frac{\pi}{\tau_0}\Big[2\Delta_n t + \Delta_n\left(\frac{\ell_1+\ell_2}{2} - \max(t,\ell_1/2) - \max(t,\ell_2/2)\right) + (\Delta_n^{(2)}/2 - \Delta_n)$$
$$\times\,(\max(t,(\ell_1+\ell_2+d)/2) + \max(t,d/2)) - \max(t,(\ell_1+d)/2) - \max(t,(\ell_2+d)/2)\Big], \quad (14.3.4)$$

where $\Delta_n^{(2)}$ is in Eq. (1.4.15), and we defined $\ell_1 = |u_1 - u_2|$, $\ell_2 = |u_3 - u_4|$, and $d = |u_3 - u_2|$ (see Fig. 1.1). In deriving Eq. (14.3.4) we neglected an additive time-independent constant that originates from the correlation function of the twist fields, and that depends on the details of the CFT under consideration. This is justified because Eq. (14.3.4) holds in the scaling limit $\ell_1, \ell_2, d, t \to \infty$ with their ratios fixed, and it describes only the leading behavior of the Rényi negativities $\mathcal{E}_n$ in that limit, otherwise the computation of the four-point correlation function (14.3.3) would be non-trivial. Crucially, Eq. (14.3.4) depends on both Δ_n and $\Delta_n^{(2)}$. Notice that even for finite d, $\mathcal{E}_n$ exhibits a linear behavior at short times, due to the first term in Eq. (14.3.4). This signals that $\mathcal{E}_n$ are not good measures of the entanglement or the correlation between A_1 and A_2. The reason is that for $t \ll d$ no correlation can be shared between A_1 and A_2 because the maximum velocity in the system is finite (see Fig. 14.1). We stress that Eq. (14.3.4) is not directly applicable to microscopic integrable models: Eq. (14.3.4) is only valid for CFT, in which there is a perfect linear dispersion, i.e., only one velocity. This is not the case in integrable lattice models, where the excitations have a nonlinear dispersion. In the next sections, we will show how to adapt Eq. (14.3.4) to describe the dynamics of the Rényi negativities after a quantum quench in microscopic integrable systems.

Finally, the dynamics of the ratio R_n in Eq. (14.1.1) can be derived combining Eq. (14.3.4) with the results for $\mathrm{Tr}\rho_A^n$ in [46]. The final result reads [590]

$$\log R_n = \frac{\pi\Delta_n^{(2)}}{\tau_0}$$
$$\times\,(-\max(t,(\ell_1+\ell_2+d)/2) - \max(t,d/2)) + \max(t,(\ell_1+d)/2) + \max(t,(\ell_2+d)/2). \quad (14.3.5)$$

In contrast with Eq. (14.3.4), Eq. (14.3.5) does not depend explicitly on Δ_n, but only on $\Delta_n^{(2)}$.

Before concluding, it is useful to discuss the qualitative behavior of $\mathcal{E}_n^{(f/b)}$ and $-\log(R_n^{(f/b)})$. The typical behavior of the Rényi negativities, as obtained from Eq. (14.3.4), is reported in Fig. 14.1 for three typical values of the distance d between the two intervals of equal length ℓ. $\mathcal{E}_n$ is

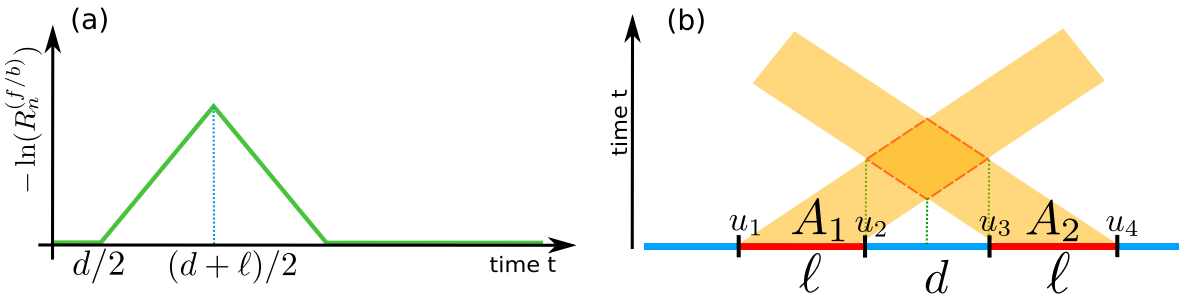

Figure 14.2: Illustration of the dynamics of $-\log R_n^{(f/b)}$ for two disjoint subsystems with equal length ℓ at distance d. On the left we report the shape of $-\log R_n^{(f/b)}$ with a single velocity of quasiparticles. On the right, there is a graphical representation for the quasi-particle spreading of entanglement (for the case with all quasi-particles having the same velocity $v = 1$ as in a CFT). Horizontal slices of the dark orange region count the quasiparticles shared between the two disjoint sets at a given time.

always a piecewise linear function and it is negative at any time. For $d = 0$ one has a two-slope linear behavior followed by a saturation to a volume-law scaling at long times. At intermediate distance $0 < d < \ell$ the behavior is more complicated with a change in the sign of the slope. For $d > \ell$, $\mathcal{E}_n^{(f/b)}$ exhibits an initial linear decrease followed by a saturation, and a dip-like feature at $d/2 \leq t \leq d/2 + \ell$.

The dynamics of $-\log(R_n^{(f/b)})$ (cf. Eq. (14.3.5)) is shown in Fig. 14.2 for two equal-length intervals. For $t < d/2$, it vanishes; for $d/2 \leq t \leq (d + \ell)/2$ it linearly increases, then it linearly decreases with the same (in absolute value) slope until $t \leq (d + 2\ell)/2$, when it vanishes and stays zero for all larger times. Therefore, at a given time t, it is proportional to the width of the intersection between the two shaded areas starting from $A_1 \cup A_2$ and showed in Fig. 14.2 (b). In other words, it is proportional to the total number of entangled pairs shared between A_1 and A_2. This property suggests that in the scaling limit, R_n becomes an indicator of the mutual entanglement between the intervals, although in general it is not an entanglement monotone.

Let us remark that Eq. (14.3.5) is identical to the evolution of the Rényi mutual information in Eq. (1.1.10) apart from the prefactor. We will come back to the connection between these two quantities in the following sections.

14.4 Quasiparticle picture for the Rényi negativities in integrable systems

The goal of this section is to adapt Eq. (14.3.4) and Eq. (14.3.5) to describe the dynamics of the Rényi negativities and the ratios R_n after a quantum quench in integrable systems. The main observation is that Eq. (14.3.4) and Eq. (14.3.5) admit an interpretation in terms of a simple hydrodynamic picture, a.k.a. the quasiparticle picture.

14.4.1 Quasiparticle picture

The quasiparticle picture for the entanglement dynamics after a global quantum quench has been proposed in Ref. [46]. The underlying idea is that the pre-quench initial state has very high energy with respect to the ground state of the Hamiltonian governing the dynamics; hence it can be seen as a source of quasiparticle excitations at $t = 0$. We assume that quasiparticles are uniformly

created in uncorrelated pairs with quasimomenta $(k, -k)$ and traveling with opposite velocities $v(k) = -v(-k)$ (for free models the uncorrelated pair assumption can be released, see [596–599]; for interacting integrable models it has been argued that the pair structure is what makes the quench integrable [600]). Quasiparticles produced at the same point in space are entangled, whereas quasiparticles created far apart are incoherent. The quasiparticles travel through the system as free-like excitations. At a generic time t, the von Neumann entropy and the Rényi entropies between a subsystem A and the rest is proportional to the total number of quasiparticles that were created at the same point at $t = 0$ and are shared between A and its complement at time t (see Fig. 14.1 (a)). Let us focus on the quasiparticle picture for the Rényi entropies in free models (the quasiparticle picture has been derived rigorously for free-fermion models in Ref. [339]). In formulas it reads as

$$S_A^{(n)}(t) = \int \frac{dk}{2\pi} s_{GGE}^{(n)}(k) \min(2|v(k)|t, \ell). \tag{14.4.1}$$

Here ℓ is the length of subsystem A, and $v(k)$ is the group velocity of the fermionic excitations. Importantly, in Eq. (14.4.1) $s_{GGE}^{(n)}(k)$ is the density (in momentum space) of the Rényi entropies of the GGE thermodynamic state [601–603] that describes the steady state after the quench. Eq. (14.4.1) predicts a linear growth for $t \leq \ell/(2v_{\max})$, with $v_{\max} \equiv \max_k(v(k))$ the maximum velocity in the system, and then saturates to an extensive value at $t \to \infty$.

For $n = 1$, i.e., for the von Neumann entropy the validity of Eq. (14.4.1) for a generic interacting integrable model has been conjectured in Ref. [47, 48]. Eq. (14.4.1) remains essentially the same. Precisely, the contribution of the quasiparticles to the von Neumann entropy $s_{GGE}^{(1)}$ is the density of GGE thermodynamic entropy. The group velocities of the quasiparticles are obtained as particle-hole excitations over the GGE thermodynamic macrostate [48, 604]. This conjecture has been explicitly worked out in several cases [47, 48, 605, 606] and tested against numerics in several interacting integrable models. [47,48,607,608] Eq. (14.4.1) has been generalised to describe the steady-state value of the Rényi entropies [347–349]. On the other hand, the full-time dynamics of the Rényi entropies is still an open problem, with the exception of one model [609, 610]. Eq. (14.4.1) can be straightforwardly generalised to describe the dynamics of the mutual information between two intervals. This allows to reveal how quantum information is scrambled in integrable systems [611, 612]. Remarkably, the quasiparticle picture for the logarithmic negativity has been derived in Ref. [246]. By combining the quasiparticle picture with the framework of the Generalized Hydrodynamics [613, 614] it is possible to describe the entanglement dynamics after quenches from inhomogeneous initial states [615–620]. The quasiparticle picture for the entanglement dynamics has been also tested in the rule 54 chain, which is believed to be a representative "toy model" for generic interacting integrable systems [609, 610]. Very recently, the quasiparticle picture has been generalised to take into account dissipative effects, at least in free-fermion and free-boson models [621–624], to describe the evolution of the symmetry-resolved entanglement entropies [132, 133], and for the characterization of the prethermalization dynamics [625].

To proceed it is useful to compare Eq. (14.4.1) with the CFT prediction for the dynamics of the Rényi entropies [46]

$$S_A^{(n)} = -\frac{1}{1-n} \frac{\pi \Delta_n}{2\tau_0} \min(2t, \ell). \tag{14.4.2}$$

A crucial observation is that Eq. (14.4.1) can be formally obtained from the CFT result in Eq. (16.4.11) by replacing $t \to |v(k)|t$, integrating over the quasiparticles with quasimomentum k, and replacing $-\pi\Delta_n/(2\tau_0) \to s_{GGE}^{(n)}$.

14.4.2 The quasiparticle description for Rényi negativities

The quasiparticle picture described above can be adapted to describe the Rényi negativities $\mathcal{E}_n^{(f/b)}$ and the ratios $\log(R_n^{(f/b)})$, in integrable systems after a global quench.

Indeed, similarly to the Rényi entropies, from Eqs. (14.3.4) and (14.3.5), by using Eq. (1.4.15), after replacing $-\pi\Delta_n/(2\tau_0) \to \varepsilon_n$, $-\pi\Delta_n^{(2)}/(2\tau_0) \to \varepsilon_n^{(2)}$, and by integrating over k, one obtains that

$$\mathcal{E}_n^{(f/b)} = \int \frac{dk}{2\pi}\Big[4\varepsilon_n|v|t + 2\varepsilon_n\left(\frac{\ell_1+\ell_2}{2} - \max(|v|t,\ell_1/2) - \max(|v|t,\ell_2/2)\right) - (2\varepsilon_n - \varepsilon_n^{(2)})\big(\max(|v|t,(\ell_1+\ell_2+d)/2) + \max(|v|t,d/2) - \max(|v|t,(\ell_1+d)/2) - \max(|v|t,(d+\ell_2)/2)\big)\Big], \quad (14.4.3)$$

while the ratios $R_n^{(f/b)}$ read

$$\log(R_n^{(f/b)}) = \int \frac{dk}{2\pi}\varepsilon_n^{(2)}\big(\max(|v|t,d/2) - \max(|v|t,(\ell_1+d)/2) - \max(|v|t,(\ell_2+d)/2) + \max(|v|t,(\ell_1+\ell_2+d)/2)\big). \quad (14.4.4)$$

We defined

$$\varepsilon_n^{(2)}(k) \equiv \begin{cases} \varepsilon_n(k) & \text{odd } n \\ 2\varepsilon_{n/2}(k) & \text{even } n \end{cases}, \quad \varepsilon_n(k) = s_{GGE}^{(n)}(k). \quad (14.4.5)$$

Clearly, Eq. (14.4.5) mirrors the structure of Eq. (1.4.15).

It is interesting to remark that by comparing Eq. (14.4.4) with the quasiparticle picture for the Rényi mutual informations [48] $I_{A_1:A_2}^{(n)}$, one obtains

$$\log(R_n^{(f/b)}) = \begin{cases} (1-n/2)I_{A_1:A_2}^{(n/2)} & n \text{ even} \\ \\ (1-n)\frac{I_{A_1:A_2}^{(n)}}{2}, & n \text{ odd.} \end{cases} \quad (14.4.6)$$

Moreover, by taking the replica limit $n_e \to 1$ in $\mathcal{E}_{n_e}^{(f/b)}$, we recover the quasiparticle prediction for the negativity [589]

$$\mathcal{E}^{(f/b)} = \int \frac{dk}{2\pi}\varepsilon_{1/2}(k)\big(\max(2|v|t,d) - \max(2|v|t,\ell_1+d) - \max(2|v|t,\ell_2+d) + \max(2|v|t,\ell_1+\ell_2+d)\big). \quad (14.4.7)$$

It was pointed out in [589] that Eq. (14.4.7) is the same as for the Rényi mutual information (of any index) by replacing $\varepsilon_{1/2}$ with the density of Rényi entropy. We stress that the same prediction is valid for both standard (bosonic) partial transpose and for the fermionic one.

Finally, it is useful to observe that Eq. (14.4.6) can be derived by using that if $A_1 \cup A_2$ is in a pure state then $\mathrm{Tr}((\rho_A^{T_1})^n)$ can be expressed in terms of $\mathrm{Tr}(\rho_{A_1}^n)$. More precisely, one can prove that [152]

$$\mathrm{Tr}(\rho_A^{T_1})^n = \begin{cases} \mathrm{Tr}\rho_{A_1}^n & n \text{ odd} \\ (\mathrm{Tr}\rho_{A_1}^{n/2})^2 & n \text{ even} \end{cases} \quad (14.4.8)$$

where $\rho_{A_1} = \mathrm{Tr}_{A_2}\rho_A$. Now, one can recover Eq. (14.4.6) by using Eq. (14.4.8), and the definition in Eq. (1.1.10), and that if $A_1 \cup A_2$ is in a pure state, $S_{A_1}^{(n)} = S_{A_2}^{(n)}$. The fact that the result of the

quasiparticle picture (14.3.4) is not sensitive to $A_1 \cup A_2$ not being in a pure state reflects that the initial state has low entanglement and that during the dynamics the entanglement is transported ballistically.

Finally, for Eq. (14.4.3) and Eq. (14.4.4) to be predictive one has to fix the function $s_{GGE}(k)$ (cf. Eq. (14.4.5)). Here we focus on out-of-equilibrium protocols for free-fermion and free-boson models. In this situation, $s_{GGE}(k)$ is determined from the population of the modes $\rho(k)$ of the postquench Hamiltonian in the stationary state (see Refs. [49, 626] for a pedagogical review). Actually, since $\rho(k)$ are conserved they can be equivalently computed in the initial state, without solving the dynamics. Specifically, one has that

$$s_{\rm GGE}^{(n,f/b)}(k) = \pm \log(\pm\rho(k)^n + (1 \mp \rho(k))^n), \tag{14.4.9}$$

where the upper and lower signs are for fermionic and bosonic systems, respectively (and not to fermionic and bosonic negativity). We remark that, although the quasiparticle prediction in Eqs. (14.4.3) and (14.4.4) is expected to be valid also for interacting integrable models, the full quasiparticle picture for the Rényi entropies is not known.

14.5 Time evolution of Rényi negativities in free models: Numerical results

In this section we provide numerical benchmarks for the results of Sec. 14.4.2. As an example of free-bosonic system, we consider the harmonic chain. Our results for free-fermion systems are tested against exact numerical data for a fermionic chain.

14.5.1 Mass quench in the harmonic chain

Let us start discussing the dynamics of the Rényi negativities after a mass quench in the harmonic chain. The harmonic chain is described by the Hamiltonian

$$H = \frac{1}{2}\sum_{n=0}^{L-1} p_n^2 + m^2 q_n^2 + (q_{n+1} - q_n)^2, \quad q_0 = q_L,\, p_0 = p_L, \tag{14.5.1}$$

where L is the number of lattice sites, q_n and p_n are canonically conjugated variables, with $[q_n, p_m] = i\delta_{nm}$, and m is a mass parameter. The harmonic chain can be diagonalised in Fourier space and is equivalent to a system of free bosons. The dispersion relation of the bosons is given by [49]

$$e(k) = [m^2 + 2(1 - \cos(k))]^{1/2}. \tag{14.5.2}$$

The group velocities are obtained from the single particle energies $e(k)$ as

$$v(k) = \frac{de(k)}{dk} = \sin(k)[m^2 + 2(1 - \cos(k))]^{-1/2}, \tag{14.5.3}$$

and the maximum one is $v_{\max} = \max_k v(k)$. In the mass quench protocol, the system is prepared in the ground state $|\psi_0\rangle$ of the Hamiltonian (14.5.1) with $m = m_0$. At $t = 0$ the mass parameter is quenched from m_0 to a different value m and the system unitarily evolves under the new Hamiltonian $H(m)$, namely $|\psi(t)\rangle = e^{-iHt}|\psi_0\rangle$. The density $\rho(k)$ (cf. Eq. (14.4.9)) of the bosons is written in terms of the pre- and post-quench dispersions $e_0(k)$ and $e(k)$ as [45, 46, 49]

$$\rho(k) = \frac{1}{4}\left(\frac{e(k)}{e_0(k)} + \frac{e_0(k)}{e(k)}\right) - \frac{1}{2}. \tag{14.5.4}$$

For free bosonic systems the Rényi negativities can be constructed from the two-point correlation functions $\langle q_i q_j \rangle$, $\langle p_i p_j \rangle$ and $\langle q_i p_j \rangle$. Indeed, given a subsystem A containing $\tilde{\ell}$ sites, which could be either all in one interval or in disjoint intervals, the reduced density matrix for A can be studied [171,590] by constructing the $\tilde{\ell} \times \tilde{\ell}$ matrices $Q^A_{ij} = \langle q_i q_j \rangle$, $P^A_{ij} = \langle p_i p_j \rangle$ and $R^A_{ij} = \mathrm{Re}\, \langle q_i p_j \rangle$, where the superscript A means that the indices i, j are restricted to subsystem A. Crucially, a similar strategy can be used to construct the Rényi negativities (for the details we refer to Ref. [590]). The main idea is that the net effect of the partial transposition with respect to a subinterval A_1 is the inversion of the signs of the momenta corresponding to the sites belonging to A_1.

For the following, we restrict ourselves to the physical situation with A made of two disjoint parts, i.e., $A = A_1 \cup A_2$, with A_1, A_2 two equal-length intervals of length ℓ. We denote as d the distance between A_1 and A_2 (see Fig. 1.1). We only discuss the ratios $-\log(R^{(b)}_n)$ (cf. Eq. (14.1.1)). The results are shown in Fig. 14.3. Panels (a) and (b) show the quantities $-\log(R^{(b)}_n)/\ell$ for adjacent intervals, i.e., $d = 0$. The data are for several values of the intervals' length ℓ up to $\ell \leq 80$. Since we are interested in the scaling limit, we plot $-\log(R^{(b)}_n)/\ell$ versus the rescaled time t/ℓ. For two adjacent intervals, the ratio exhibits a linear growth for $t/\ell \sim 1.25$, which reflects the maximum velocity being $v_{\max} \sim 0.4$. For larger times we observe a slow decrease toward zero for $t/\ell \to \infty$. This slow decay is due to the slower quasiparticles with $v < v_{\max}$. The solid line is the theoretical prediction in Eq. (14.4.4). At finite ℓ and t the data exhibit some small corrections from Eq. (14.4.4), which is recovered in the scaling limit $t, \ell \to \infty$ with their ratio fixed.

It is also useful to investigate directly the validity of Eq. (14.4.6), which establishes a relationship between $R^{(f/b)}_n$ and the mutual information. To this aim, we introduce the difference $d^{(f/b)}_n$ as

$$d^{(f/b)}_n = \begin{cases} \log(R^{(f/b)}_n) - (1 - n/2) I^{(n/2)}_{A_1:A_2} & n \text{ even} \\ \log(R^{(f/b)}_n) - (1 - n) \frac{I^{(n)}_{A_1:A_2}}{2}, & n \text{ odd} \end{cases} \tag{14.5.5}$$

As it is clear from the insets in Fig. 14.3, $d^{(b)}_n$ is very small in the region of linear growth, i.e., for $2v_{\max} t/\ell \leq 1$ (an obvious fact, since in the scaling limit it is just $0 - 0$). At fixed ℓ, in the non-trivial region, i.e. for larger values of the scaling variable $2v_{\max} t/\ell$, $d^{(b)}_n$ is larger. However, at fixed t/ℓ, the deviations $d^{(b)}_n$ decrease with increasing ℓ, and in the scaling limit $\ell \to \infty$ one recovers Eq. (14.4.6). Precisely, the data suggest a behavior $d^{(b)}_n \propto 1/\ell$.

14.5.2 Quench in a free fermion chain

We now discuss numerical results for free-fermion systems described by the Hamiltonian

$$H = \sum_{j=1}^{L} \left(\frac{1}{2} [c^\dagger_j c^\dagger_{j+1} + c_{j+1} c_j + c^\dagger_j c_{j+1} + c^\dagger_{j+1} c_j] - h c^\dagger_j c_j \right), \tag{14.5.6}$$

where $\{c_i, c^\dagger_j\} = \delta_{ij}$ are anti-commuting fermionic operators, h is a coupling parameter, e.g. a magnetic field, and we neglect boundary terms (we are interested in the thermodynamic limit $L \to \infty$). A Jordan-Wigner transformation maps the Hamiltonian to the well-known transverse field Ising chain. However, the spin RDM is not simply mapped to the fermion RDM for two disjoint intervals [174, 627]. Instead, for the case of adjacent intervals they are mapped into each other and so the following results for fermions apply also to the spin variables.

In terms of the momentum space Bogoliubov fermions the Hamiltonian is diagonal and the single-particle energies are

$$e(k) = [h^2 - 2h \cos(k) + 1]^{1/2}. \tag{14.5.7}$$

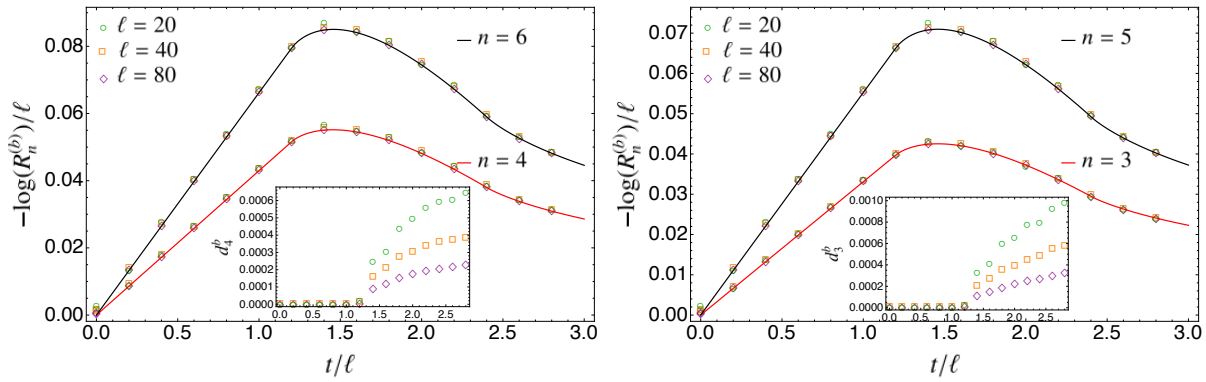

Figure 14.3: Logarithms of the moments of the (bosonic) partial transpose after the mass quench from $m_0 = 1$ to $m = 2$ in the harmonic chain. The quantity $-\log(R_n^b)/\ell$ is plotted versus rescaled time t/ℓ, with ℓ the intervals' length. The analytical predictions represented by continuous lines correspond to Eq. (14.4.4). The insets represent Eq. (14.5.5) and they prove the validity of Eq. (14.4.6), i.e. the connection between the ratio R_n and the Rényi mutual information.

We consider the non-equilibrium unitary dynamics that follows from a quench of the field h at $t = 0$ from h_0 to $h \neq h_0$. In order to parametrise the quench it is useful to introduce the angle $\Delta(k)$ as [45]

$$\cos(\Delta(k)) = \frac{1 + hh_0 - (h + h_0)\cos(k)}{e(k)e_0(k)}. \tag{14.5.8}$$

As for free-bosons, the central object to obtain the quasiparticle prediction is the density $\rho(k)$ of the Bogoliubov fermions. This is given by [628, 629]

$$\rho(k) = \frac{1}{2}(1 - \cos(\Delta(k))). \tag{14.5.9}$$

The reduced density matrix can be completely characterised [171] by the two-point correlation functions restricted to the subsystem A. From the covariance matrix associated to ρ_A, one can build the covariance matrix corresponding to the partial time reversal $\rho_A^{R_1}$ (see Ref. [163–165, 478, 479, 630]). The fermionic Rényi negativities $\mathcal{E}_n^{(f)}$ introduced in Eq. (12.2.20) can be efficiently computed in terms of the eigenvalues of the covariance matrix.

We discuss the numerical results for $R_n^{(f)}$ for two adjacent intervals in Fig. 14.4, for the quench with $h_0 = 10$ and $h = 2$. The data for $-\log(R_n^{(f)})$ exhibit a linear behavior up to $t/\ell \sim 0.5$, reflecting that $v_{\max} \sim 1$. Similar to the bosonic case, finite-size corrections are present, although the analytical prediction in Eq. (14.3.5) is recovered in the scaling limit. In the inset, we also investigate these scaling corrections. The symbols are the data at fixed $t/\ell = 0.5$ while the x-axis shows $1/\ell$. The crosses are the theoretical results in the scaling limit. The solid lines are fits to the behavior $1/\ell$, and are clearly consistent with the data.

14.5.3 Quasiparticle predition for the p_n-PPT conditions

Using the quasiparticle predictions obtained in the previous sections for the Rényi negativity, one can write down the quasiparticle formulas for the p_n-PPT conditions introduced in Sec. 14.2, see Eq. (14.2.3). For instance, the p_3-PPT condition quantifies the violation of Eq. (14.2.2). Specifically, the condition $D_3 \equiv p_3 - p_2^2 < 0$ signals the presence of quantum entanglement. As

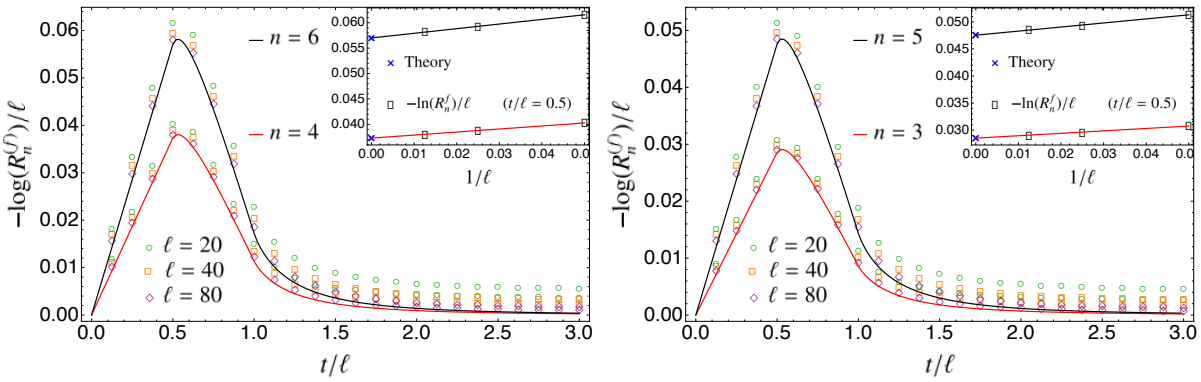

Figure 14.4: Logarithms of the moments of the (fermionic) partial transpose after a quench in the fermionic chain (with $h_0 = 10$ and $h = 2$) for two adjacent intervals. Both $-\log(R_n^{(f)})/\ell$ and $\mathcal{E}_n^{(f)}/\ell$ are plotted versus rescaled time t/ℓ, with ℓ the intervals' length. The analytical predictions represented by continuous lines correspond to Eq. (14.4.3) (top panels) and (14.4.4) (bottom panels). The insets investigate the finite-size scaling corrections: the symbols are for the fermionic negativity at fixed $t/\ell = 0.5$; the crosses are the theoretical results in the thermodynamic limit; the solid lines are linear fits.

explained in Sec. 14.2, other conditions $D_n \geq 0$ can be obtained by considering higher moments of the partial transpose.

We numerically investigate the p_n-PPT conditions in Fig. 14.5 for $n = 3, 5, 7$, and for quenches in both the fermionic and harmonic chains. We focus on the situation with two adjacent intervals and we are interested in understanding how the p_n-PPT conditions are violated as a function of time. The results in Fig. 14.5 are obtained by using the quasiparticle picture prediction. As it is clear from the figure, all p_n-PPT conditions are violated at short times in both models. At infinite times all the p_n-PPT conditions give zero. These results are consistent with the behavior of the logarithmic negativity [589].

Also the fine structure of these p_n-PPT conditions is very interesting. In the short-time region with a lot of entanglement (compare with the previous figures for R_n) all the conditions are violated. As the time increase and the entanglement becomes much less, the first condition to be satisfied is p_3 (i.e. $D_3 > 0$) and only after the other one (the panel on the left is particularly clear in this respect) This implies that higher and higher p_n-PPT conditions are necessary to detect the very little amount of entanglement present at large time. This fact is not surprising, but it is remarkable that it is captured so neatly by the quasiparticle picture.

14.6 Closing remarks

We derived the quasiparticle picture for the dynamics of the moments of the partially transposed reduced density matrix after a quantum quench in integrable systems, and several related quantities such as the Rényi negativities $\mathcal{E}_n$ and the ratios R_n. An interesting result is that the ratio R_n is proportional to the Rényi mutual information. Furthermore, this ratio is qualitatively similar to the negativity and so it is then an indicator of the entanglement barrier for the quench dynamics at intermediate time [589, 631–633]. Moreover, our results allow us to derive the behavior of the p_n-PPT conditions, which in contrast with standard entanglement measures for mixed states, such as the logarithmic negativity, are easily computable and experimentally measurable for quantum

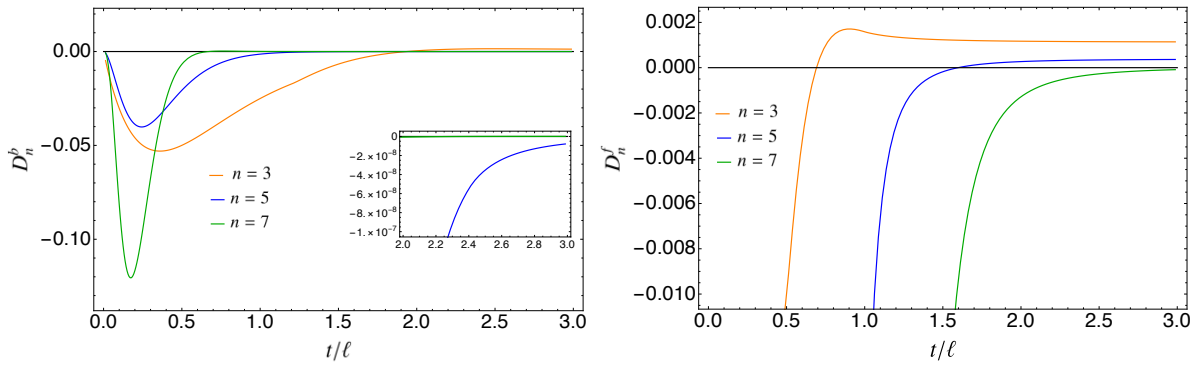

Figure 14.5: The p_n-PPT conditions for $n = 3, 5, 7$ for the quasiparticle predictions of the moments of the partial transpose introduced in Eq. (14.2.1). The quench parameters are $h_0 = 10, h = 2$ for the fermionic chain and $m = 2, m_0 = 0.1$ for the harmonic chain. We plot the quantity D_n in Eq. (14.2.3). The p_n-PPT condition is $D_n \geq 0$. To compare data for different n we multiply the D_5 by 10 and D_7 by 10^6 for bosons ($\ell = 30$). For fermions the D_5 is multiplied by 10^7 and D_7 by 10^{19} ($\ell = 50$). The violation of these conditions for at least one value of n reveals the presence of entanglement between A_1 and A_2.

many-body systems [88, 456]. We tested our predictions against exact numerical results for both free-fermion and free-boson systems.

A natural followup of the results presented here is to test numerically the equality between Rényi mutual informations and the ratios R_n for interacting integrable models. Another important research direction is to investigate the Rényi negativities and the ratios R_n in the presence of dissipation [623].

Chapter 15

Rényi entropies and negativity for massless Dirac fermions at conformal interfaces and junctions

We investigate the ground state of a (1+1)-dimensional conformal field theory built with M species of massless free Dirac fermions coupled at one boundary point via a conformal junction/interface. Each CFT represents a wire of finite length L. We develop a systematic strategy to compute the Rényi entropies for a generic bipartition between the wires and the entanglement negativity between two non-complementary sets of wires. Both these entanglement measures turn out to grow logarithmically with L with an exactly calculated universal prefactor depending on the details of the junction and of the bipartition. These analytic predictions are tested numerically for junctions of free Fermi gases, finding perfect agreement. This Chapter is based on Ref. [634].

15.1 Introduction

The remarkable scaling behaviour of the REEs in Eq. (1.4.13) is altered at leading order by the presence of a boundary [20]. For conformally invariant boundary conditions (bc's), the entanglement entropy can be studied via boundary CFT [635–637], a framework that already found a large number of applications in condensed matter and particle physics, such as quantum impurity problems [638], the multi-channel Kondo problem [639], D-brane physics [640] etc. For a finite size CFT of length $2L$ with conformal invariant bc's at the two edges, the Rényi entanglement entropy between the half-chain $A = [0, L]$ and the other half is [20, 21]

$$S_n(A) = \frac{c}{12}\Big(1 + \frac{1}{n}\Big) \log \frac{L}{\varepsilon} + \dots , \tag{15.1.1}$$

up to finite terms that depend on the bc's. At leading order in $L/\varepsilon \to \infty$, Eqs. (1.4.13) and (15.1.1) differ by a factor 2. This is heuristically understood because the two geometries differ by the number of entangling points and, in general, one expects the entanglement entropy to be proportional to the size of the boundary of the subsystem. In both geometries mentioned above the origin of the entanglement relies on the presence of *completely transmissive entangling points*, resulting in some degree of quantum coherence among the subsystem and its complement. Conversely, when the entangling points are completely reflective because of some additional boundary conditions, the subsystems decouple, and the entanglement entropy between them vanishes.

A natural generalisation of the above scenarios regards the intermediate setting in which the entangling points are partially transmitting and reflecting [641]. In the literature, such special

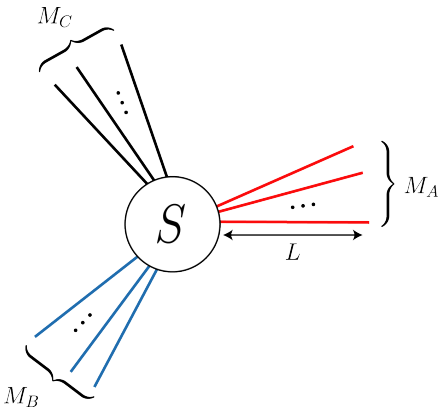

Figure 15.1: The conformal junction: M wires are joined together at $x = 0$ by a conformally invariant scattering matrix S. We consider a tripartition in three sets A, B, C with M_A, M_B, M_C wires each. The entanglement between A and B is given by the negativity (1.1.14). A bipartite configuration is simply obtained by letting $M_C = 0$.

situations are known as permeable interfaces, defects, or impurities (and indeed we will refer to them using all these equivalent names). A crucial result is that for free massless theories the defect is marginal [642] and so can alter the leading behaviour of the entanglement entropy. Conversely, interactions make the defect either relevant or irrelevant [642] ending up asymptotically in a completely reflective or transmitting situation, respectively, as shown also by the scaling of the entanglement entropy itself [643, 644]. For free theories in the presence of a conformal interface (i.e., scale invariant) Sakai and Satoh exploited boundary CFT to show that the scaling of the entanglement entropy, (15.1.1) for $n = 1$, is modified as [645]

$$S(A) = \frac{c_{\text{eff}}(\sqrt{\mathcal{T}})}{6} \log \frac{L}{\varepsilon} + \dots, \tag{15.1.2}$$

where $\mathcal{T}$ is a parameter which represents the transmission probability and $c_{\text{eff}}(\sqrt{\mathcal{T}})$, dubbed as *effective central charge*, is a monotonic function of its argument satisfying

$$c_{\text{eff}}(0) = 0, \quad c_{\text{eff}}(1) = c. \tag{15.1.3}$$

Ref. [645] focuses on the free massless boson, but Eq. (15.1.2) with a different $c_{\text{eff}}(\sqrt{\mathcal{T}})$ has been subsequently derived also for free massless fermions both by means of CFT [571, 646, 647], and explicitly solving microscopic models [648–652] in the same universality class. While the scaling in Eq. (15.1.2) is expected to be a generic feature of conformal invariant (1+1)-dimensional systems, the explicit functional form of the effective central charge depends both on the theory and the details of the interface, eventually encoded in a interface operator (or, equivalently, in a boundary state as explained in [646]). We mention that a class of completely transmissive interfaces, dubbed topological interfaces, has been also considered in the literature [653–659]. While their effective central charge is always c, and they could be erroneously considered trivial, the $O(1)$ terms shrugged off in Eq. (15.1.2) still contains important information about the boundary conditions, strictly related to the boundary entropy of Affleck-Ludwig [247].

The permeable interface between two CFTs can be generalised to a junction of M wires. The resulting geometry is depicted in Fig. 15.1 in which the junction is fully characterised by a scattering matrix S between the wires. Imposing that this matrix S preserves conformal invariance, one finds consistency conditions that have been studied and solved for a large number of physical

configurations [660–668]. The bipartite entanglement in these conformal (or star) junctions has been studied in Refs. [650,669–671] but focusing on the entanglement between a single wire and the remaining $M-1$ ones. A unifying framework to compute the entanglement of a generic bipartition among the wires of the junctions is still missing.

The conformal junction is also a very obvious setup for the study of multipartite entanglement because it is made of several wires and it is very natural to wonder about the entanglement between a subset of them, not only two complementary subsystems. In this respect, the first configuration that comes to mind is the tripartition in A, B, C with M_A, M_B, M_C wires each, as depicted in Fig. 15.1. To study the entanglement of this tripartition, one can integrate out the M_C wires in C, to get the reduced density matrix $\rho_{A\cup B}$. Then the entanglement between A and B with the mixed density matrix $\rho_{A\cup B}$ is measured by the negativity. In the presence of a defect, it has been computed for a bipartite geometry with $M = 2$ [672], exploiting its relation with the 1/2-Rényi entropy for the bipartition of a pure state, but for a genuinely tripartite geometry at a junction there are no results yet.

The main goal of this Chapter is to provide a general framework to deal with the entanglement through permeable junctions of M $(1 + 1)$-dimensional free-fermion CFT. Following Refs. [641, 645], the strategy is to constrain the form of the general boundary state in a folded theory. Then, being the theory free, we can reduce the problem to the computation of a charged partition function in the presence of this boundary state. This approach also allows us to compute the negativity in a tripartite geometry by properly implementing a partial transpose operation for free fermions.

The Chapter is organised as follows. In Sec. 15.2 we review the folding trick which turns the problem of constructing conformal interfaces into the one of building boundary states. We review the construction of fermionic boundary states and we compute the partition functions in the junction geometry. Using this result and the replica trick, we obtain the entanglement entropy analytically for a generic bipartition between wires. In Sec. 15.3, we combine the previous formalism with the replica trick for the fermionic negativity. This allows us to obtain an analytic prediction that we benchmark against numerical computations in Sec. 15.4. In the same section, we also describe an alternative technique for the computation of the entanglement of a fermion gas on a star graph modelling the junction of interest. We draw our conclusions in Sec. 15.5.

15.2 CFT approach: Rényi entropies

In this section we present the CFT approach for the evaluation of the entanglement in permeable junctions of (1+1)-dimensional free-fermion CFTs, following closely Refs. [641,645,646]. As a first application, we employ this method to compute the Rényi entropies between an arbitrary number of wires at the junction.

Let us consider M wires of length L, each of them described by a CFT denoted by

$$\mathrm{CFT}_j, \quad j = 1, \dots, M. \tag{15.2.1}$$

In Euclidean space-time, the junction looks like a booklet (with each page corresponding to one CFT) bound along the imaginary axis at $x = 0$, see the left panel of Fig. 15.2. As custom in this kind of systems, we are going to work in the folded picture in which the system is represented as a single CFT

$$\text{M-CFT} = \mathrm{CFT}_1 \otimes \cdots \otimes \mathrm{CFT}_M, \tag{15.2.2}$$

i.e. the world-sheet is a single infinite strip of width L (we are dealing with a finite size quantum system at zero temperature, so the space-time coordinate w satisfies $\mathrm{Re}(w) \in [0, L]$) where M

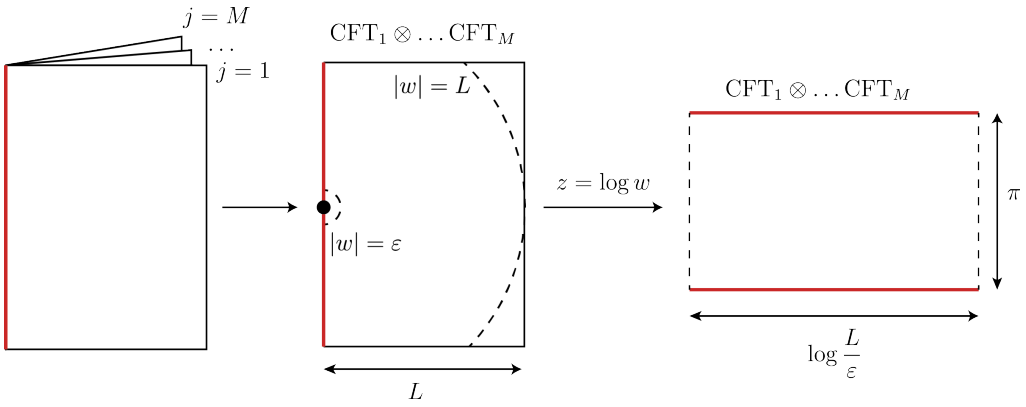

Figure 15.2: The folding procedure. The junction in Euclidean spacetime is the booklet with the CFTs bound in $x = 0$ (left panel). The folding consists in merging together the M CFTs in a worldsheet being a single infinite strip with an appropriate boundary state $|S\rangle$ at $x = 0$ (middle panel). To compute the entanglement, we cut the system for $|w| < \varepsilon$ and $w > |L|$ (dashed lines) and map the M-CFT onto a rectangle of size $\log \frac{L}{\varepsilon} \times \pi$ (right) with $\mathrm{Re}(z) \in [\log \varepsilon, \log L]$ and $\mathrm{Im}(z) \in [-\pi/2, \pi/2]$.

copies of the CFT live. See the middle panel of Fig. 15.2 for a pictorial representation. The joining between the distinct wires is specified by the boundary conditions along the lines

$$\mathrm{Re}(w) = 0, \quad \mathrm{Re}(w) = L. \tag{15.2.3}$$

We require that the boundary condition at $\mathrm{Re}(w) = L$ decouples the replicas, and can be thus described by a boundary state $|B\rangle$ factorised as

$$|B\rangle = |B_1\rangle \otimes \dots |B_M\rangle\,, \tag{15.2.4}$$

with $|B_j\rangle$ being a boundary state of CFT_j. Instead, we assume that the boundary conditions at $\mathrm{Re}(w) = 0$ (describing the defect/junction), in general couple explicitly distinct wires. We denote by $|S\rangle$ the associated boundary state in M-CFT. In the remainder of the Chapter, the precise details of the boundary state $|B\rangle$ appearing at $\mathrm{Re}(w) = L$ would not matter and so we do not specify more about it. The physical motivation is that, as long as it decouples the wires, we do not expect that its features affect (at least at leading order) the correlation properties among distinct wires. In contrast, this is not the case for the boundary state $|S\rangle$, and for this reason we have to be very careful about its characterisation.

In order to have under control ultraviolet and infrared divergences in the entanglement entropy, a standard trick [17, 18, 242, 246, 673] consists in cutting the theory for $|w| < \varepsilon$ and $|w| > L$ (see Fig. 15.2, middle panel). The cut strip can then be mapped into a rectangle by the conformal transformation

$$z = \log w. \tag{15.2.5}$$

The semicircles $|w| = \varepsilon$ and $|w| = L$ are mapped respectively onto the segments

$$z \in \log \varepsilon + i[-\pi/2, \pi/2], \quad z \in \log L + i[-\pi/2, \pi/2]. \tag{15.2.6}$$

The defect line at $\mathrm{Re}(w) = 0$ is split into the two lines $\mathrm{Im}(z) = \pm\pi/2$. This mapping is shown in the right panel of Fig. 15.2.

The partition function in this geometry can be written as

$$\mathcal{Z} = \langle S| \exp(-\pi H) |S\rangle\,, \tag{15.2.7}$$

where π is the height of the rectangle (see Fig. 15.2), while the hamiltonian is

$$H = \frac{2\pi}{\log \frac{L}{\varepsilon}} \left(L_0 + \bar{L}_0 \right), \tag{15.2.8}$$

with $L_0, \bar{L}_0$ being generators of the Virasoro algebra of $\mathrm{CFT}_1 \otimes \ldots \mathrm{CFT}_M$.

So far, everything is general and no assumption on the bulk theory or the boundary state $|S\rangle$ has been made yet. However, the knowledge of $|S\rangle$ is required to evaluate the partition function (and, by replicas, the entanglement). From now on, we thus restrict the analysis to massless free fermions for which we can provide a precise characterisation for the boundary state $|S\rangle$.

15.2.1 Boundary states for free-fermions

In this section, we first review the construction of boundary states for a theory of many species of massless Majorana fermions [641, 671]. Then we discuss the straightforward generalisation to Dirac fermions, obtained through a doubling of the degrees of freedom [269].

We consider M species of Majorana fermions. This CFT has central charge $c = M/2$ and it is described in terms of the left/right chiral fermionic fields

$$\psi^j, \quad \bar{\psi}^j, \quad j = 1, \ldots, M. \tag{15.2.9}$$

In radial quantisation [269], restricting the analysis to the Neveu-Schwarz (NS) sector, one can decompose the fermionic fields in their Laurent modes

$$\psi^j(z) = \sum_{k \in \mathbb{Z}+1/2} \frac{\psi^j_k}{z^{k+1/2}}, \quad \bar{\psi}^j(\bar{z}) = \sum_{k \in \mathbb{Z}+1/2} \frac{\bar{\psi}^j_k}{\bar{z}^{k+1/2}}. \tag{15.2.10}$$

(In the Ramond sector, k would be integer and the discussion would be slightly more involved due to the presence of a zero mode for $k = 0$.) Within this convention, the creation/annihilation operators of a fermion of the j-th species in the mode k ($k > 0$) are $\psi^j_{\mp k}$. The number k is (proportional to) the momentum of the particle. More precisely, one can show that the commutation relations between the fermionic fields and the Virasoro operators $L_0, \bar{L}_0$ are

$$[L_0, \psi^j_{-k}] = k\psi^j_{-k}, \quad [\bar{L}_0, \bar{\psi}^j_{-k}] = k\bar{\psi}^j_{-k}. \tag{15.2.11}$$

The effect of the scattering matrix S at the junction (as in in Fig. 15.1) is nothing but a consistency condition for the boundary state $|S\rangle$ reading

$$\left(\psi^j_k + iS_{jj'} \bar{\psi}^{j'}_{-k} \right) |S\rangle = 0, \tag{15.2.12}$$

where, hereafter, repeated indices are summed over. It has been shown [647, 674], that in order to preserve conformal invariance at the boundary, S must be orthogonal

$$S \in O(M). \tag{15.2.13}$$

In particular the possible k-dependence of the scattering matrix is ruled out by scale invariance. The solution for $|S\rangle$ of Eq. (15.2.12) is simply

$$|S\rangle = \prod_{k \in \mathbb{N}-1/2} \exp\left(iS_{jj'} \psi^j_{-k} \bar{\psi}^{j'}_{-k} \right) |0\rangle, \tag{15.2.14}$$

with $|0\rangle$ being the vacuum of the theory. Notice that the different values of k are decoupled, a fact that will simplify the forthcoming computations. Nevertheless, in general, different species of particles are coupled, due to the possible occurrence of non-diagonal terms in the matrix S. Those terms represent physically the amplitudes of transmission between different wires and cause the entanglement among them.

We now consider a theory of M free Dirac fermions (having central charge $c = M$), for which the associated fields are

$$\Psi^j, \quad \Psi^{\dagger j}, \quad \overline{\Psi}^j, \quad \overline{\Psi}^{\dagger j}, \quad j = 1, \dots, M, \tag{15.2.15}$$

where Ψ and $\Psi^\dagger$ represent the particles/antiparticles respectively. This theory is equivalent to a theory with $2M$ Majorana fermions, and so the previous derivation is valid also in this case. The number of degrees of freedom is doubled and one should take an orthogonal real $2M \times 2M$ scattering matrix $S \in O(2M)$. However, if we further impose that the global $U(1)$ symmetry

$$\Psi \to e^{i\theta}\Psi, \quad \Psi^\dagger \to e^{-i\theta}\Psi^\dagger \tag{15.2.16}$$

is preserved by the boundary conditions, there are additional constraints on the scattering matrix. This requirement corresponds to the property that a left/right particle can be produced from the vacuum (through the boundary state) together with its right/left antiparticle only. Requiring that this symmetry is preserved by the boundary conditions, we end up into a complex unitary scattering matrix

$$S \in U(M), \tag{15.2.17}$$

that constrains the boundary state $|S\rangle$ as

$$\left(\Psi^{\dagger j}_k + iS_{jj'}\overline{\Psi}^{j'}_{-k}\right)|S\rangle = 0, \quad \left(\Psi^j_k + i\overline{S}_{jj'}\overline{\Psi}^{\dagger j'}_{-k}\right)|S\rangle = 0, \tag{15.2.18}$$

with $\bar{S}$ being the matrix complex conjugated to S. The solution of such constraint is

$$|S\rangle = \prod_{k\in\mathbb{N}-1/2} \exp\left(iS_{jj'}\Psi^{\dagger j}_{-k}\overline{\Psi}^{j'}_{-k} + (\Psi \leftrightarrow \Psi^\dagger)\right)|0\rangle\,. \tag{15.2.19}$$

A property of the state $|S\rangle$ in Eq. (15.2.19) is that it contains two decoupled contributions, depending on the right and left moving particles. We will use this property to simplify the computations in the following sections.

15.2.2 Rényi entropies for a generic bipartition between wires

We describe how to compute the n-th Rényi entropies of a subset made up of $M_A \leq M$ wires via the replica trick. Given a subsystem A of a generic QFT, the Rényi entropies (1.1.5) of integer order n can be obtained in a replicated theory with n copies of the QFT, i.e. in $\text{QFT}^{\otimes n}$, which are cyclically joined along A by a branch-cut connecting the i-th and the $(i+1)$-th replica [20]. The moments of the reduced density matrices can be then written in terms of a ratio of partition functions as [20, 21]

$$\text{Tr}\,(\rho_A^n) = \frac{\mathcal{Z}_n}{\mathcal{Z}_1^n}, \tag{15.2.20}$$

where $\mathcal{Z}_n$ is the partition function of the replicated theory while $\mathcal{Z}_1^n$ is just the partition function of a single replica raised to the n-th power.

In the case of the bulk free Dirac fermion, the partition function $\mathcal{Z}_n$ can be further factorised using the replica diagonalisation as, e.g., shown in [176] and exploited in Chapters 2, 4, 13. Within this method, the replicated partition function $\mathcal{Z}_n$ can be rewritten as

$$\mathcal{Z}_n = \prod_{p=-\frac{n-1}{2}}^{\frac{n-1}{2}} \mathcal{Z}_1\left(\alpha_p = \frac{2\pi p}{n}\right). \tag{15.2.21}$$

Plugging Eq. (15.2.21) for $\mathcal{Z}_n$ into Eq. (15.2.20) one has $\mathrm{Tr}\,(\rho_A^n) = \prod_p (\mathcal{Z}_1(\alpha_p)/\mathcal{Z}_1)$ in which the ratio $\mathcal{Z}_1(\alpha_p)/\mathcal{Z}_1$ can be expressed as the vacuum expectation value of the operator associated to the action of the $U(1)$ symmetry restricted to A, namely

$$\mathcal{Z}_1(\alpha) = \langle 0|e^{i\alpha Q_A}|0\rangle. \tag{15.2.22}$$

Here Q_A is the charge operator which counts the difference between particles and antiparticles in the subsystem A, while $|0\rangle$ is the vacuum of the theory. Notice that these charged partition sums are the same appearing in the calculation of the SREEs 1.4.2.

While Ref. [176] and most of the subsequent literature focus on the ground state of the system in the absence of boundaries, the same considerations apply more generically and in particular to the case of interest here. The reason is that the boundary state of interest (15.2.19) is Gaussian (it is an exponential of a bilinear of fermions) and thus the functional measure is Gaussian too: in other words, the theory is free both in the bulk and at the boundary. Hence, in our specific case, we start from the theory M-CFT $= \mathrm{CFT}_1 \otimes \ldots \mathrm{CFT}_M$ and we replicate it n times, ending up with M-CFT$^{\otimes n}$. Then, to compute $\mathcal{Z}_n$ we perform a diagonalisation in replica space and end up with the product of n charged partition functions which are given by Eq. (15.2.7) with the insertion of the appropriate flux, i.e. (with our normalisation $\mathcal{Z}_1 = 1$)

$$\mathcal{Z}_1(\alpha) = \langle S|\, e^{i\alpha Q_A} q^{L_0+\bar{L}_0}\, |S\rangle\,. \tag{15.2.23}$$

Here the modular parameter

$$q = \exp\left(-\frac{2\pi^2}{\log\left(L/\varepsilon\right)}\right), \tag{15.2.24}$$

has been introduced for later convenience. Our goal then becomes the computation of

$$\mathcal{Z}_1(\alpha) = \prod_{k\in\mathbb{N}-1/2} \langle 0|\exp\left(-i(S^\dagger)_{jj'}\overline{\Psi}^j_k \Psi^{\dagger j'}_k + (\Psi \leftrightarrow \Psi^\dagger)\right) q^{L_0+\bar{L}_0} e^{i\alpha Q_A} \times \\ \exp\left(iS_{jj'}\Psi^{\dagger j}_{-k}\overline{\Psi}^{j'}_{-k} + (\Psi \leftrightarrow \Psi^\dagger)\right)|0\rangle\,, \tag{15.2.25}$$

in the limit $q \to 1$, corresponding to $\frac{L}{\varepsilon} \to \infty$. For this purpose, we firstly decompose S, which is a unitary $M \times M$ matrix, in a block diagonal form

$$S = \begin{pmatrix} S_{AA} & S_{AB} \\ S_{BA} & S_{BB} \end{pmatrix}. \tag{15.2.26}$$

Here A stands for the M_A species belonging to the subsystem A, while B refers to the remaining $M_B = M - M_A$ species. Further, we split the set of indices $j = 1, \ldots, M_A + M_B$, associated to all the species, in the following two sets

$$a = 1, \ldots, M_A, \quad b = 1, \ldots, M_B \tag{15.2.27}$$

to shorthand the species of A and B respectively. In this way, the charge operator Q_A is

$$Q_A = \sum_{k\in\mathbb{N}-1/2} \Psi^a_{-k}\Psi^a_k + \bar{\Psi}^a_{-k}\bar{\Psi}^a_k - (\Psi \to \Psi^\dagger), \tag{15.2.28}$$

where the summation over the index a is understood.

We consider the contribution to the partition function (15.2.25) coming from the single Laurent mode k, which requires the evaluation of

$$\langle 0| \exp\left(-i(S^\dagger)_{jj'}\overline{\Psi}^j_k\Psi^{\dagger j'}_k\right) q^{L_0+\bar{L}_0} e^{i\alpha Q_A} \exp\left(iS_{jj'}\Psi^{\dagger j}_{-k}\overline{\Psi}^{j'}_{-k}\right)|0\rangle\,. \tag{15.2.29}$$

The details of this computation can be found in [634], where we have found the analytic expression of the $U(1)$ charged partition function in Eq. (15.2.25), which reads

$$\mathcal{Z}_1(\alpha) \propto \prod_{k\in\mathbb{N}-1/2} \det\left(1 + 2(S^\dagger_{AA}S_{AA} + (1 - S^\dagger_{AA}S_{AA})\cos\alpha)q^{2k} + q^{4k}\right)^2. \tag{15.2.30}$$

According to Eq. (15.2.21), the n-sheeted partition function $\mathcal{Z}_n$ can be written finally as

$$\begin{aligned}\mathcal{Z}_n = &\prod_{p=-\frac{n-1}{2}}^{\frac{n-1}{2}} \mathcal{Z}_1(\alpha = 2\pi p/n) \propto \\ &\prod_{p=-\frac{n-1}{2}}^{\frac{n-1}{2}} \prod_{k\in\mathbb{N}-1/2} \det\left(1 + 2(S^\dagger_{AA}S_{AA} + (1 - S^\dagger_{AA}S_{AA})\cos(2\pi p/n))q^{2k} + q^{4k}\right)^2,\end{aligned} \tag{15.2.31}$$

which is the main result of this section, although not yet written in a very transparent form.

From Eq. (15.2.31) it is clear that in the presence of several wires belonging to A, $M_A \geq 1$, there are M_A factorised contributions depending on the eigenvalues of $1 - S^\dagger_{AA}S_{AA}$ and coming from the presence of the determinant of a $M_A \times M_A$ matrix. In other words, if we define

$$\mathcal{Z}_{n,\mathcal{T}_a} = \prod_{p=-\frac{n-1}{2}}^{\frac{n-1}{2}} \prod_{k\in\mathbb{N}-1/2} \left(1 + 2((1 - \mathcal{T}_a) + \mathcal{T}_a\cos(2\pi p/n))q^{2k} + q^{4k}\right)^2, \tag{15.2.32}$$

as the contribution coming from the generic eigenvalue $\mathcal{T}_a \in \mathrm{Spec}(1 - S^\dagger_{AA}S_{AA})$, one has

$$\mathcal{Z}_n = \prod_{a=1}^{M_A} \mathcal{Z}_{n,\mathcal{T}_a}, \tag{15.2.33}$$

where $\mathcal{T}_a$ can be interpreted as generalised effective transmission probabilities. Plugging this relation in the definition of the Rényi entropies in Eq. (1.1.5), one gets

$$S_n(A) = \sum_{a=1}^{M_A} S_{n,\mathcal{T}_a}, \tag{15.2.34}$$

with

$$S_{n,\mathcal{T}_a} = \frac{1}{1-n}\log\frac{\mathcal{Z}_{n,\mathcal{T}_a}}{\mathcal{Z}^n_{1,\mathcal{T}_a}} \tag{15.2.35}$$

being the Rényi entropies associated to each $\mathcal{T}_a$.

For the sake of completeness, we provide the explicit result for the partition functions and for the entanglement entropies in the relevant limit $\frac{L}{\varepsilon} \to \infty$. Since the total entropy is just given by the sum of M_A independent contributions with effective transmission $\mathcal{T}_a$ it is sufficient to write only one term. For convenience, we also define a parameter α', being a function of α and the effective transmission $\mathcal{T}_a$, satisfying

$$2\cos\alpha' = 2(1 - \mathcal{T}_a + \mathcal{T}_a \cos\alpha). \tag{15.2.36}$$

The infinite product appearing in Eq. (15.2.30) which gives the $U(1)$ partition function is explicitly evaluated in [634], obtaining

$$\frac{\mathcal{Z}_1(\alpha)}{\mathcal{Z}_1(0)} = \left(\frac{\theta_3\left(\frac{\alpha'}{2\pi}, q\right)}{\theta_3(0,q)}\right)^2. \tag{15.2.37}$$

In the limit $q \to 1$, the leading term of the partition function gives

$$\log\frac{\mathcal{Z}_1(\alpha)}{\mathcal{Z}_1(0)} \simeq \frac{1}{\log q}\left(\mathrm{Li}_2(-e^{i\alpha'}) + \mathrm{Li}_2(-e^{-i\alpha'}) - 2\mathrm{Li}_2(-1)\right) = -\left(\frac{\alpha'}{2\pi}\right)^2 \log\frac{L}{\varepsilon}, \tag{15.2.38}$$

with α' given by (15.2.36). Summing over the n values of the flux α, one gets straightforwardly the n-th Rényi entropies plugging Eq. (15.2.38) into Eq. (15.2.21). After some long but simple algebra, the final result is

$$S_{n,\mathcal{T}_a} = \left(\frac{2}{\pi^2(n-1)}\sum_{p=1}^{\lfloor n/2\rfloor} \arcsin^2\left(\sqrt{\mathcal{T}_a}\cos\frac{(2p-1)\pi}{2n}\right)\right)\log\frac{L}{\varepsilon}, \tag{15.2.39}$$

which matches the one in Ref. [650] where also the analytic analytical continuation to $n \to 1$ can be found and it is not repeated here. We stress that the major advance in this section compared to the existing literature [650, 671] has been to understand how the elements of S_{AA} combine (via the eigenvalues of $(1 - S_{AA}^\dagger S_{AA})$) to give the entanglement entropy of more than one wire, while previous studies focused on a single one. This result is also preparatory to the calculation of the negativity reported in the following section.

15.3 CFT approach: Fermionic Negativity

In this section we apply the CFT formalism to the calculation of the (fermionic) negativity between two subsets of wires of a conformal junction. We will proceed via the evaluation of the Rényi negativity for even $n = n_e$ and then we will study the replica limit $n_e \to 1$.

15.3.1 Rényi negativities

We consider the conformal junction of Fig. 15.1 with the subsystems A, B, and C formed by three sets of wires. We are interested in the (fermionic) negativity between A and B. We denote by $\hat{\mathcal{Z}}_n$ the partition function in the n-sheeted Riemann surface built in such a way to implement the partial transpose in the subsystem B (see Refs. [151, 152, 163, 164], Sec. 12.2 for more details on the partial transpose also for the fermionic case). $\hat{\mathcal{Z}}_n$ can be further factorised using the replica diagonalisation, such that it becomes the product of n single-replica $U(1)$ charged partition functions, similarly to what has been done for $\mathcal{Z}_n$ in the previous section, but with some differences. Let us focus on even $n = n_e$, which is the only necessary object to compute the negativity. The

needed charged partition $\hat{\mathcal{Z}}_1(\alpha)$ has twisting phases equal to $e^{i\alpha}$ in A and $e^{i(\pi-\alpha)}$ in B, i.e. it reads [163, 479]

$$\hat{\mathcal{Z}}_1(\alpha) = \langle 0|e^{i\alpha Q_A} e^{-i(\alpha-\pi)Q_B}|0\rangle\,. \tag{15.3.1}$$

The operator $e^{i\alpha Q_A}$ implements the $U(1)$ symmetry restricted to A, while $e^{-i(\alpha-\pi)Q_B}$ inverts the flux ($\alpha \to -\alpha$) and it introduces an additional phases -1 along B, which is the combined net effect of the partial transpose operation on fermionic systems. The final result of this approach is that the n_e-th Rényi negativity can be computed as

$$\mathcal{E}_{n_e} \equiv \log \mathrm{Tr}\left(|\rho_{AB}^{R_B}|^{n_e}\right) = \log \mathrm{Tr}\left((\rho_{AB}^{R_B})^{n_e}\right) = \sum_{p=-\frac{n_e-1}{2}}^{\frac{n_e-1}{2}} \log \frac{\hat{\mathcal{Z}}_1(\alpha = 2\pi p/n_e)}{\hat{\mathcal{Z}}_1(0)}. \tag{15.3.2}$$

In the presence of boundaries, the $U(1)$ charged partition function straightforwardly becomes

$$\begin{aligned}\hat{\mathcal{Z}}_1(\alpha) = \langle S|\, q^{L_0+\bar{L}_0} e^{i\alpha Q_A - i(\alpha-\pi)Q_B}\,|S\rangle = \\ \prod_{k\in\mathbb{N}-1/2} \langle 0|\exp\left(-i(S^\dagger)_{jj'}\overline{\Psi}^j_k \Psi^{\dagger j'}_k + (\Psi \leftrightarrow \Psi^\dagger)\right) q^{L_0+\bar{L}_0} \times \\ e^{i\alpha Q_A - i(\alpha-\pi)Q_B} \exp\left(iS_{jj'}\Psi^{\dagger j}_{-k}\overline{\Psi}^{j'}_{-k} + (\Psi \leftrightarrow \Psi^\dagger)\right)|0\rangle\,,\end{aligned} \tag{15.3.3}$$

Eq. (15.3.2) with (15.3.3) holds for a generic tripartite fermionic system with no assumption. To proceed for the calculation of the wire junction we restrict to the following specific situation:

- $M_A, M_B, M_C = 1$, so that the total number of wires is $M = 3$.
- S is not only unitary but also Hermitian, which means that $S^2 = 1$ and its eigenvalues can be just ± 1. For some physical systems (including the Schrodinger junction in the next section), the hermiticity of the S matrix is a necessary condition for physical consistency. Hence this is not at all a very restrictive assumption.

With these working assumptions it is possible to obtain nice analytic results in a rather compact form. More general expressions (e.g. for more wires) can also be obtained, but at the price of more cumbersome computations and less intelligible final results without any major physical insight.

It is clear from Eq. (15.3.3) that for $M = 3$ the key object to be evaluated is

$$\begin{aligned}\langle 0|\exp\left(-iS_{jj'}\overline{\Psi}^j_k\Psi^{\dagger j'}_k\right) q^{L_0+\bar{L}_0} e^{i\alpha Q_A - i(\alpha-\pi)Q_B} \exp\left(iS_{jj'}\Psi^{\dagger j}_{-k}\overline{\Psi}^{j'}_{-k}\right)|0\rangle = \\ \det\left(1 + q^{2k} S \begin{pmatrix} S_{AA} & -e^{-i2\alpha}S_{AB} & e^{-i\alpha}S_{AC} \\ -e^{i2\alpha}S_{BA} & S_{BB} & -e^{i\alpha}S_{BC} \\ e^{i\alpha}S_{CA} & -e^{-i\alpha}S_{CB} & S_{CC}\end{pmatrix}\right),\end{aligned} \tag{15.3.4}$$

where we used the commutation relations between $q^{L_0+\bar{L}_0}e^{i\alpha Q_A - i(\alpha-\pi)Q_B}$ and the fields and the formula for the vacuum expectation value [634]. The determinant of the 3×3 matrix appearing in (15.3.4) can be evaluated directly, but it is useful to discuss first the constraints due to the unitarity of S. We define the matrix $\mathcal{O}$ as

$$\mathcal{O} = S \begin{pmatrix} S_{AA} & -e^{-i2\alpha}S_{AB} & e^{-i\alpha}S_{AC} \\ -e^{i2\alpha}S_{BA} & S_{BB} & -e^{i\alpha}S_{BC} \\ e^{i\alpha}S_{CA} & -e^{-i\alpha}S_{CB} & S_{CC}\end{pmatrix}, \tag{15.3.5}$$

and we verify the following properties:

- $\mathcal{O}$ is unitary ($\mathcal{O}\mathcal{O}^\dagger = 1$) and its eigenvalues are phases;
- $\det(\mathcal{O}) = 1$ and the product of the eigenvalues is 1;
- $\mathcal{O} = S\mathcal{O}^\dagger S$ and the spectrum of $\mathcal{O}$ is thus invariant under complex conjugation, a feature that relies on our hermiticity assumption $S = S^\dagger$.

These properties imply that the spectrum of $\mathcal{O}$ has to take this form

$$\mathrm{Spec}\,(\mathcal{O}) = \{1, e^{i\hat{\alpha}'}, e^{-i\hat{\alpha}'}\}, \tag{15.3.6}$$

with $\hat{\alpha}'$ a real parameter depending on S and α, defined by the following property

$$2\cos\hat{\alpha}' + 1 = \mathrm{Tr}(\mathcal{O}), \tag{15.3.7}$$

which is a consequence of Eq. (15.3.6). The determinant $\det(1 + q^{2k}\mathcal{O})$ can be thus computed taking the product over the eigenvalues of $\mathcal{O}$ as follows

$$\det\Big(1 + q^{2k}\mathcal{O}\Big) = (1+q^{2k})(1+q^{2k}e^{i\hat{\alpha}'})(1+q^{2k}e^{-i\hat{\alpha}'}) = (1+q^{2k})(1+q^{2k}(\mathrm{Tr}(\mathcal{O})-1)+q^{4k}). \tag{15.3.8}$$

Evaluating $\mathrm{Tr}(\mathcal{O})$ and using again the unitarity of S, we can rewrite Eq. (15.3.8) as

$$\det\Big(1 + q^{2k}\mathcal{O}\Big) = (1 + q^{2k})(1 + 2\cos\hat{\alpha}'q^{2k} + q^{4k}), \tag{15.3.9}$$

and the explicit expression of $\hat{\alpha}'$ as a function of the S matrix is

$$2\cos\hat{\alpha}' = -1+S_{AA}^2+S_{BB}^2+S_{CC}^2+(-1-S_{CC}^2+S_{BB}^2+S_{AA}^2)\cos(2\alpha)+2(S_{BB}^2-S_{AA}^2)\cos\alpha. \tag{15.3.10}$$

Notice that $\hat{\alpha}'$ does only depend on the diagonal entries of the matrix S and on the flux α. Putting all the pieces together, we express the partition function $\hat{\mathcal{Z}}_1(\alpha)$ as

$$\hat{\mathcal{Z}}_1(\alpha) = \prod_{k\in\mathbb{N}-1/2} (1 + q^{2k})^2(1 + 2\cos\hat{\alpha}'q^{2k} + q^{4k})^2. \tag{15.3.11}$$

We find the same formal structure of the partition function which appeared for the Rényi entropies in Eq. (15.2.30), up to the replacement $\alpha' \to \hat{\alpha}'$. Analogously to Eq. (15.2.38), for $L/\epsilon \gg 1$, we have

$$\log\frac{\hat{\mathcal{Z}}_1(\alpha)}{\hat{\mathcal{Z}}_1(0)} \simeq -\left(\frac{\hat{\alpha}'}{2\pi}\right)^2 \log\frac{L}{\varepsilon}, \tag{15.3.12}$$

with $\hat{\alpha}'$ given by Eq. (15.3.10), which is the main result of this section. Indeed, by plugging this result into Eq. (15.3.2), we obtain the Rényi negativities

$$\mathcal{E}_{n_e} = -\Big(\frac{1}{4\pi^2}\sum_{p=-(n_e-1)/2}^{(n_e-1)/2} \arccos^2\left(S_{CC}^2 + (-1 - S_{CC}^2 + S_{BB}^2 + S_{AA}^2)\cos(2\pi p/n_e)^2 + \right.$$
$$\left. + (S_{BB}^2 - S_{AA}^2)\cos(2\pi p/n_e)\right)\Big)\log\frac{L}{\varepsilon}\,. \tag{15.3.13}$$

15.3.2 Analytic continuation

The representation of $\mathcal{E}_{n_e}$ as a sum, appearing in Eq. (15.3.13), gives an expression valid only when n_e is an even natural number. To proceed to the calculation of the negativity, we should provide its analytic continuation for n_e being a generic number in the complex plane. To this goal, the strategy we device is the following:

- The $U(1)$ partition function $\hat{\mathcal{Z}}_1(\alpha)$ in Eq. (15.3.12) can be expressed through an integral representation in the limit $q \to 1$

$$\log \frac{\hat{\mathcal{Z}}_1(\alpha)}{\hat{\mathcal{Z}}_1(0)} = \sum_{k \in \mathbb{N}-1/2} 2 \log[(1+q^{2k})^{-2}(1+2\cos\alpha' q^{2k}+q^{4k})] \\ \simeq -\frac{1}{\log q}\int_0^\infty \frac{dt}{t}[\log(1+2\cos\alpha' t+t^2)-2\log(1+t^2)]; \quad (15.3.14)$$

- The sum over the value of fluxes (15.3.13) can now be performed inside the integral. Through some simple trigonometric identities, this leads to an analytic continuation of the integrand.
- The final result is an integral, which represents our analytic continuation.

Let us report here the final result of this computation:

$$\mathcal{E} = \frac{\log(L/\varepsilon)}{\pi^2}\int_0^1 \frac{dt}{t} \\ \log \frac{((x_1-\sqrt{-c^2+x_1^2})^{1/2}+(x_1+\sqrt{-c^2+x_1^2})^{1/2})((x_2-\sqrt{-1+x_2^2})^{1/2}+(x_2+\sqrt{-1+x_2^2})^{1/2})}{2(1+t)}. \quad (15.3.15)$$

15.4 Schroedinger junction

In this section, we describe a fermion gas on a star graph modelling a junction made up of M wires of length L, joined together through a single defect. We introduce a slightly different framework (compared to the existing ones in the literature) which allows us to efficiently perform exact numerical computations also for the negativity. The CFT predictions of the previous sections are checked against these exact numerical results.

15.4.1 Correlation functions

Let us consider a star graph like the one in Fig. 15.1 where now on each wire there is a gas made of N spinless fermions. The M wires are decoupled everywhere but in the vertex of the graph and their mixing is described by a non-trivial scattering matrix. We consider the ground state of such system with N particles. The same system has been studied in Ref. [650] by the overlap matrix approach [669, 676] which is the starting point of our analysis. Each point of the junction is parametrised by a pair

$$(x, j), \quad x \in [0, L], \quad j = 1, \dots, M, \quad (15.4.1)$$

where j is the index identifying the wire and $x > 0$ the spatial coordinate along the wire. The bulk hamiltonian of the system is

$$H = \sum_{j=1}^{M} \int_0^L dx \frac{1}{2}\left(\partial_x \Psi_j^\dagger(x)\right)\left(\partial_x \Psi_j(x)\right), \quad (15.4.2)$$

with $\Psi_j, \Psi_j^\dagger$ being the fermionic fields associated to the j-th wire (also called Schroedinger field, from which the name Schroedinger junction). We consider a scattering matrix

$$S_{ij}, \quad i,j = 1,\dots,M, \tag{15.4.3}$$

describing the defect at $x = 0$, which has to be hermitian and unitary [650, 663]

$$S = S^\dagger, \quad SS^\dagger = 1. \tag{15.4.4}$$

The most general boundary condition along the junction is

$$\lambda(1-S)\Psi(0) - i(1+S)\partial_x\Psi(0) = 0, \tag{15.4.5}$$

where $\Psi = \{\Psi_j\}_{j=1,\dots,M}$, λ is an arbitrary real parameter with the dimension of mass. To fully specify the problem, we also need to impose boundary conditions at the external edges of each wire that generically take the form

$$(\partial_x\Psi_i)(L) = \mu_i\Psi_i(L), \tag{15.4.6}$$

where μ_i are again real parameters with the dimension of mass. In order to simplify the treatment, it is possible to diagonalise S via a unitary transformation $\mathcal{U}$ and its eigenvalues are just ± 1. It is custom [663, 664] to introduce a set of unphysical fields $\{\varphi_j(x)\}$

$$\Psi_i(x) = \sum_{j=1}^{M} \mathcal{U}_{ij}\varphi_j(x), \tag{15.4.7}$$

so that in terms of these $\varphi_j(x)$, the boundary conditions decouple as

$$\begin{aligned} \partial_x\varphi_i(0) &= \eta_i\varphi_i(0), \\ \partial_x\varphi_i(L) &= \mu_i'\varphi_i(L), \end{aligned} \tag{15.4.8}$$

where the μ_i''s are linear function of the μ_i's whose form is irrelevant. For the junction to be scale-invariant, we require each of the dimensionful parameters η_i and μ_i to be either 0 or ∞. The choice corresponds to either Neumann ($\partial_x\varphi_i = 0$) or Dirichlet ($\varphi_i = 0$) boundary conditions at $x = 0$ and $x = L$. We impose Dirichlet boundary conditions ($\mu_i = \infty$) at $x = L$ for all wires. Conversely, the values of η_i being 0 or ∞ depends on the diagonalisation of the S matrix, see [650, 663, 664]. Hence, the unphysical fields $\varphi_j(x)$ have Dirichlet bc's at $x = L$ and either (Neumann or Dirichlet) at $x = 0$, so that it is natural to use the short-hand notation

$$ND \quad \text{Neumann-Dirichlet}, \quad DD \quad \text{Dirichlet-Dirichlet}, \tag{15.4.9}$$

to refer to the two possibbilities. For these two possible boundary conditions, the single-particle wavefunctions are

$$\begin{aligned} \phi^{DD}(n,x) &= \sqrt{\frac{2}{L}}\sin\frac{n\pi x}{L}, \quad n = 1,\dots \\ \phi^{ND}(n,x) &= \sqrt{\frac{2}{L}}\cos\frac{(n-1/2)\,\pi x}{L}, \quad n = 1,\dots. \end{aligned} \tag{15.4.10}$$

We work in the ground state with fixed particle number N for each wire, so that the correlation function is

$$\langle\varphi_i(x)\varphi_j(y)\rangle = \delta_{ij} \times \begin{cases} C_{DD}(x,y), & DD \text{ bc's} \\ C_{ND}(x,y), & ND \text{ bc's}, \end{cases} \tag{15.4.11}$$

with

$$\begin{aligned} C_{DD}(x,y) &= \sum_{n=1}^{N} \phi^{DD}(n,x)\overline{\phi^{DD}(n,y)} = \frac{\sin\frac{N+1/2}{L}\pi(x-y)}{2L\sin\frac{\pi(x-y)}{2L}} - (y\to -y) \\ C_{ND}(x,y) &= \sum_{n=1}^{N} \phi^{ND}(n,x)\overline{\phi^{ND}(n,y)} = \frac{\sin\frac{N}{L}\pi(x-y)}{2L\sin\frac{\pi(x-y)}{2L}} + (y\to -y). \end{aligned} \tag{15.4.12}$$

Going back to the physical fields $\{\Psi_j\}_j$, linear algebra straightforwardly gives

$$C_{ij}(x,y) \equiv \langle \Psi_j^\dagger(x)\Psi_i(y)\rangle = \left(\frac{1+S}{2}\right)_{ij} C_{ND}(x,y) + \left(\frac{1-S}{2}\right)_{ij} C_{DD}(x,y). \tag{15.4.13}$$

The matrices $\frac{1\pm S}{2}$ are the projectors over the eigenspaces of S with eigenvalues ± 1 respectively.

The correlation functions (15.4.13) are continuous kernel of the spatial variables. While it is possible to work directly with such kernels (as done, e.g., in Refs. [394,677]), it is more convenient to work with a finite-dimensional representation of such correlation. In [634], a representation which is particularly useful for numerical applications has been derived and it is equivalent to the overlap matrix approach [669]. The main result reads

$$C = \frac{1-S}{2}\otimes\begin{pmatrix} 1 & Q \\ 0 & 0 \end{pmatrix} + \frac{1+S}{2}\otimes\begin{pmatrix} 0 & 0 \\ Q^\dagger & 1 \end{pmatrix}, \tag{15.4.14}$$

with Q being a $N\times N$ matrix defined by

$$Q_{n,n'} = 2\int_0^1 dx \sin(n\pi x)\cos\left(\left(n'-\frac{1}{2}\right)\pi x\right) = \frac{2n}{\pi\left(n^2-(n'-1/2)^2\right)}. \tag{15.4.15}$$

15.4.2 The Rényi entropies between two arbitrary sets of wires

A useful auxiliary quantity for the computation of the entanglement entropy and negativity is the matrix $\Gamma = 1-2C$ (sometimes referred to as covariance matrix). Using Eq. (15.4.13) and the finite-dimensional representation of the correlation matrix in the previous section, we can express it as

$$1-\Gamma^2 = 4C(1-C) = (1-S^2)\otimes(C_{ND}-C_{DD})^2. \tag{15.4.16}$$

When Γ refers to the entire system, given that $S^2=1$, it is zero in the "wire space". However, Eq. (15.4.16) has a very convenient form for the restriction of Γ to a subsystem A made of M_A wires because of the tensor product structure in internal and spatial coordinates. It is in fact enough to replace $S\to S_{AA}$, i.e. the projected S-matrix to obtain Γ_{AA}, the covariance matrix restricted to the subsystem of interest:

$$1-\Gamma_{AA}^2 = (1-S_{AA}^2)\otimes(C_{ND}-C_{DD})^2, \tag{15.4.17}$$

with S_{AA} being a $M_A\times M_A$ matrix. In general $1-S_{AA}^2\geq 0$, and so $1-\Gamma_{AA}^2$ is positive semidefinite. We recall that the matrix representation for $(C_{ND}-C_{DD})^2$ is

$$(C_{ND}-C_{DD})^2 = \begin{pmatrix} 1-QQ^\dagger & 0 \\ 0 & 1-Q^\dagger Q \end{pmatrix}. \tag{15.4.18}$$

Since $1-QQ^\dagger$ and $1-Q^\dagger Q$ have the same spectrum, the spectrum of $(C_{ND}-C_{DD})^2$ is obtained by two copies of the spectrum of $1-QQ^\dagger$.

To start, let us recover the results [650] for the case when A is a single wire. First, taking $M = 2$ and the completely transmissive S-matrix

$$S = \begin{pmatrix} 0 & 1 \\ 1 & 0 \end{pmatrix}, \tag{15.4.19}$$

the correlation function of a single wire A satisfies

$$1 - \Gamma_{AA}^2 = (C_{ND} - C_{DD})^2. \tag{15.4.20}$$

The spectral properties of $1 - \Gamma_{AA}^2$ are then the one of a gas on the line $[-L, L]$ bipartite as $A = [0, L]$ and $B = [-L, 0]$. For a generic S-matrix of two wires [641, 663]

$$S = \begin{pmatrix} \sqrt{1-|s|^2} & se^{i\phi} \\ \bar{s}e^{-i\phi} & -\sqrt{1-|s|^2} \end{pmatrix}, \tag{15.4.21}$$

Γ_{AA} is

$$1 - \Gamma_{AA}^2 = |s|^2 (C_{ND} - C_{DD})^2, \tag{15.4.22}$$

and so the eigenvalues of $1 - \Gamma_{AA}^2$ are just rescaled by a factor $|s|^2$, in agreement with what known [650] from the overlap matrix. In the case of A being one of the M wires in a junction, in the above equation is enough to replace s with the transmission coefficient of A.

Once the covariance matrix Γ_{AA} is known, the entanglement Rényi entropies are [171]

$$S_n(A) = \frac{1}{1-n} \mathrm{Tr} \log \left(\left(\frac{1+\Gamma_{AA}}{2} \right)^n + \left(\frac{1-\Gamma_{AA}}{2} \right)^n \right) = \sum_{\mathcal{T}_a} S_{n,\mathcal{T}_a}, \tag{15.4.23}$$

Using the basic property about the spectrum of a tensor product

$$\mathrm{Spec}(X \otimes Y) = \{x_i y_j\}_{ij}, \quad x_i \in \mathrm{Spec}(X), \qquad y_j \in \mathrm{Spec}(Y), \tag{15.4.24}$$

we get that the Rényi entropies between A and the complementary wires B are

$$S_n(A) = \sum_{\mathcal{T}_a} S_{n,\mathcal{T}_a}, \tag{15.4.25}$$

where the $\mathcal{T}_a$'s are the eigenvalues of $1 - S_{AA}^2$, which play the role of a transmission probability, and $S_{n,\mathcal{T}_a}$ is the Rényi entropies of a single wire with transmission probability $\mathcal{T}_a$. This analytic results for the microscopic model perfectly match Eq. (15.2.39) in CFT. We also notice that the relation $S_n(A) = S_n(B)$ comes from the fact that $1 - S_{AA}^2$ and $1 - S_{BB}^2$ have the same non-zero spectrum (i.e., the same eigenvalues up to the vanishing ones).

To conclude this subsection, we present a numerical test for the validity of the CFT result for the logarithmic scaling of the Rényi entropies. Since the case of A consisting of a single wire has been discussed and tested in Ref. [650], we focus here on a four-wire junction and the subsystem A consisting of two wires. The S matrix is chosen of the form

$$S = U \begin{pmatrix} -\sqrt{1-s^2} & -s & 0 & 0 \\ -s & \sqrt{1-s^2} & 0 & 0 \\ 0 & 0 & -1 & 0 \\ 0 & 0 & 0 & 1 \end{pmatrix} U^{-1}, \quad U = \begin{pmatrix} 1 & 0 & 0 & 0 \\ 0 & -\cos\theta & -\cos\theta \sin\theta & \sin^2\theta \\ 0 & \sin\theta & -\cos^2\theta & \cos\theta\sin\theta \\ 0 & 0 & \sin\theta & \cos\theta \end{pmatrix}. \tag{15.4.26}$$

The numerical results are reported in Fig. 15.3 finding a perfect agreement with CFT.

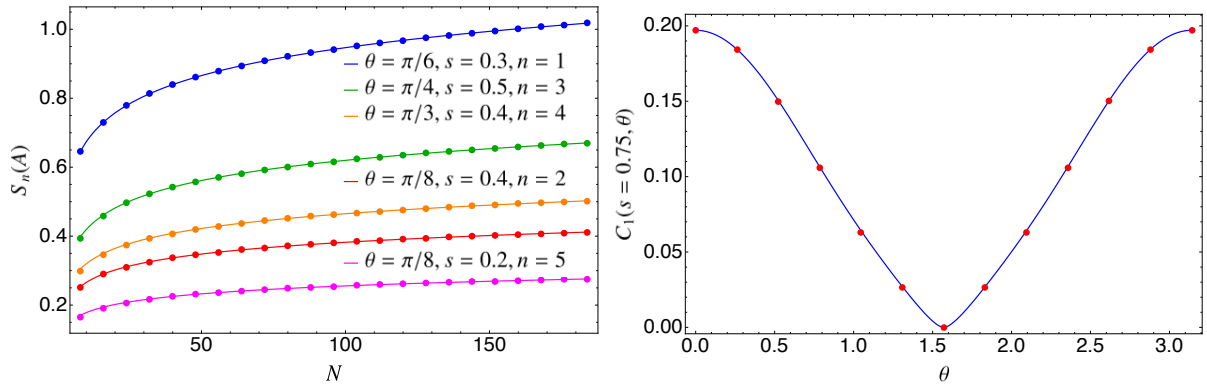

Figure 15.3: Left panel: The Rényi entropies $S_n(A)$ in a four-wire junction where A is made up of two wires. We choose different values of s, θ, n and we plot it as a function of the number of particles N. The lines show the curve $C_n(s,\theta)\log N + b_0 + b_1 N^{-1/n}$ where the coefficients b_i are fitted using the data for $N \geq 80$. The coefficients $C_n(s,\theta)$ are obtained by summing over the single-wire results, as explained in Eq. (15.2.39). Right panel: The coefficient of the logarithmic term of the negativity between two wires (A and B) as a function of θ, with fixed $s = 0.75$. The solid line corresponds to Eq. (15.3.15) while the points have been obtained through a fit of the numerics with the form $a\log N + b_0 + b_1 N^{-1}$.

15.4.3 Entanglement negativity

We now consider a tripartition $A \cup B \cup C$, where A (B) contains M_A (M_B) wires, and we study the entanglement negativity between A and B. This amounts to project the scattering-matrix S over a subset of rows/columns belonging to $A \cup B$. In particular, we denote

$$(C_{A\cup B})_{ij}(x,y) \equiv \langle \Psi_j^\dagger(x)\Psi_i(y)\rangle, \quad i,j = 1,\dots,M_A+M_B, \tag{15.4.27}$$

as the correlation function of $A \cup B$, and

$$(S_{A\cup B})_{ij} \equiv S_{ij}, \quad i,j = 1,\dots,M_A+M_B, \tag{15.4.28}$$

as the restriction of the scattering matrix; $S_{A\cup B}$ is not unitary in general, and it satisfies the following relations

$$(S_{A\cup B})^\dagger = (S_{A\cup B}), \quad 0 \leq (S_{A\cup B})^2 \leq 1. \tag{15.4.29}$$

Using the matrix representation of the correlation function C in Eq. (15.4.14) and restricting it to $A \cup B$, we obtain a $(2N(M_A+M_B), 2N(M_A+M_B))$ matrix $C_{A\cup B}$. The covariance matrix $\Gamma_{A\cup B}$ has the natural block form

$$\Gamma_{A\cup B} = \begin{pmatrix} \Gamma_{AA} & \Gamma_{AB} \\ \Gamma_{BA} & \Gamma_{BB} \end{pmatrix}, \tag{15.4.30}$$

from which we construct the matrix [163, 173]

$$\Gamma^{\times}_{A\cup B} \equiv \frac{2}{1+\Gamma^2_{A\cup B}} \begin{pmatrix} -\Gamma_{AA} & 0 \\ 0 & \Gamma_{BB} \end{pmatrix}. \tag{15.4.31}$$

The latter matrix $\Gamma^{\times}_{A\cup B}$ is the crucial object to write the Rényi negativities $\mathcal{E}_{n_e}$ which indeed are [163]

$$\mathcal{E}_{n_e} \equiv \log \mathrm{Tr}\left(|\rho_{A\cup B}|^{n_e}\right) = \mathrm{Tr}\log\left(\left(\frac{1+\Gamma^{\times}_{A\cup B}}{2}\right)^{n_e/2} + \left(\frac{1-\Gamma^{\times}_{A\cup B}}{2}\right)^{n_e/2}\right) + \frac{n_e}{2}\mathrm{Tr}\log\left(\left(\frac{1+\Gamma_{A\cup B}}{2}\right)^{2} + \left(\frac{1-\Gamma_{A\cup B}}{2}\right)^{2}\right), \quad (15.4.32)$$

The above equation is valid for arbitrary real n_e (i.e. also for a non-even integer) and so the negativity $\mathcal{E}$ is obtained just by taking $n_e = 1$.

Eq. (15.4.32) gives the Rényi negativities in terms of the correlation matrices that, once numerically evaluated, provides a test of the CFT results for the coefficient of the logarithm obtained in Sec. 15.3. For the numerical evaluation, we focus on a three-wire junction and on the two-parameter family of scattering matrices given by

$$S = U \begin{pmatrix} -\sqrt{1-s^2} & -s & 0 \\ -s & \sqrt{1-s^2} & 0 \\ 0 & 0 & -1 \end{pmatrix} U^{-1}, \quad U = \begin{pmatrix} 1 & 0 & 0 \\ 0 & -\cos\theta & \sin\theta \\ 0 & \sin\theta & \cos\theta \end{pmatrix}. \quad (15.4.33)$$

We select as subsystems A and B the first two wires and compute numerically the Rényi negativity for several values of s, θ, and N. In Fig. 15.3 we reported the coefficient of the logarithm obtained as follows. We fixed $s = 0.75$ and we selected some values of θ; for each value of (s, θ), we calculated numerically the negativity, for several values of N up to 200. We fitted the obtained numerical results with $a \log N + b_0 + b_1 N^{-1}$. Fig. 15.3 finally reports the best fit of a as a function of theta and compares it to the corresponding analytic result in Eq. (15.3.15), finding perfect agreement.

15.5 Closing remarks

In this Chapter we investigated the entanglement entropy and negativity for the ground state of M species of free massless Dirac fermions coupled at one boundary point via a conformal interface/junction.

We stress that our results apply to some different physical situations, too. For example, our predictions are expected to hold also for lattice models of free fermions, in particular for M tight binding chains of length L joined at a single common vertex (as, e.g., done in [651] for $M = 2$). Furthermore, the logarithmic prefactors we obtained for entropy and negativity should appear also in the study of a star junction of M infinite CFT, but when the subsystems consist of segments of length ℓ starting from the interface.

We conclude the Chapter discussing few outlooks. The main focus of this work has been the free-fermion CFT, but our formalism can be easily adapted to free complex boson too, to study, e.g., the entanglement entropy and negativity across junctions of harmonic chains. The same formalism can be further applied to the study of some out-of-equilibrium protocols for free CFTs in the presence of defects (see, e.g., [644, 652, 672, 678]). Another interesting open problem is the generalisation to other CFTs such as the compact boson, WZW models (see [656] for the interfaces of WZW), or minimal models. In all those cases we do not expect any kind of replica diagonalisation, due to the lack of Gaussian measures, but still one could employ the replica construction to investigate the negativity, as well as other entanglement measures.

Chapter 16

Entanglement barrier and its symmetry resolution: theory and experiment

The operator entanglement (OE) is a key quantifier of the complexity of the RDM, and in out-of-equilibrium situations —e.g. after a quantum quench from a product state—, it is expected to exhibit an *entanglement barrier*. The OE of the RDM initially grows linearly as entanglement builds up between the local degrees of freedom, it then reaches a maximum, and it ultimately decays to a small finite value as the reduced matrix converges to a simple stationary state through standard thermalization mechanisms. Here, we report the results of the first experimental measurement of the OE of a subsystem's RDM in a quantum many-body system performing a new data analysis of the published experimental results of Ref. [80]. The OE thus obtained displays the expected *barrier* as long as the experimental system is large enough. For smaller systems it is absent. As $U(1)$ symmetry plays a key role in our analysis, we introduce the notion of symmetry resolved operator entanglement (SROE), in addition to the total OE. To gain further insights into the SROE, we provide a thorough theory analysis of this new quantity in chains of non-interacting fermions, which, in spite of their simplicity, capture most of the main features of OE and SROE. In particular, we uncover three main physical effects: the presence of a barrier in any charge sector, a time delay for the onset of the growth of SROE, and an effective equipartition between charge sectors.

16.1 Introduction

As we discussed in the previous chapters, the investigation of the dynamics of isolated quantum many-body systems is still one of the main challenges of quantum mechanics. Recent developments in quantum simulation, opening the possibility of generating and probing complex quantum states, have stimulated the investigation of out-of-equilibrium phenomena such as quantum chaos, thermalization and many-body localization [679–682]. Owing to the highly tunable experimental settings it has been possible to engineer Hamiltonian dynamics of closed quantum systems, ranging from integrable to chaotic systems, and measure non-trivial observables, as the entanglement growth following a quantum quench [80, 81, 683, 684] or out-of-time ordered correlators [685, 686]. In typical situations when a system is driven out of equilibrium, any subsystem's RDM evolves non-trivially in time, approaching a stationary state. The evolution of the subsystem density matrix, during this process, can be appropriately characterised in terms of its operator entanglement

(OE), i.e. the entanglement entropy of an operator viewed as a state in operator space [687–690].

The OE is an interesting quantity in a wide variety of situations, and for multiple reasons. Most prominently, in $1d$ systems, the OE is a quantifier of the approximability of a quantum operator by matrix product operators (MPO) [631, 689–694]. Moreover, the OE often captures important universal properties of the dynamics [631,689–691,694–699]. For instance, the OE of the evolution operator $U(t) = e^{-iHt}$ grows linearly in ergodic phases [631, 695], but only logarithmically in localised phases [631,691]. Another example is the OE of a local operator O evolving in Heisenberg-picture, $O(t) = e^{iHt}Oe^{-iHt}$, which grows linearly in systems with chaotic dynamics [695] but only logarithmically for integrable dynamics [697–699]. The time evolution of the OE is also closely related to other fundamental entanglement measurements such as negativity [151, 152, 163, 173], temporal entanglement [700–702], and reflected entropy [703,704] The main operator we will focus on in this Chapter is the RDM of a subsystem. Its OE has been theoretically shown to exhibit an *entanglement barrier* [631, 696, 705]: after a quantum quench from a shortly-correlated state, the OE of the subsystem density matrix initially grows linearly and then decays at longer times, thus displaying a barrier-shaped curve. The initial linear growth is a consequence of the generic linear growth of the (state) entanglement entropy after a quench [44, 47], while the decay at later times reflects the convergence of the RDM towards a simple stationary state, through the standard mechanism of thermalization [706–708] (or relaxation to a Generalised Gibbs ensemble [709–711]) for isolated quantum systems. A similar *barrier* is also observed for the density matrix of the full system when the latter undergoes dissipative evolution [692, 694]. Such *entanglement barriers* have important consequences in terms of the simulability of the dynamics after a quantum quench. Indeed, as any MPO with bond dimension χ has an OE which is at most $\log \chi$ [631, 712], we know that, to approximate a density matrix ρ with OE equal to S, we will need a bond dimension at least as large as e^S. Consequently, a high value of the OE at the top of the *barrier* signals the impossibility to use (low bond dimension) MPO methods to simulate the dynamics of the system.

Inspired by the relevance of the *entanglement barrier*, our goal is to show it can be observed in an experimental quantum many-body system, using the randomised measurement data from trapped ion experiments [80]. The randomised measurement toolbox [558] has enabled measuring state-agnostically properties of the underlying quantum state such as purity and Renyi entanglement entropies [80, 558, 713] negativities [88, 89], state fidelities [714] and scrambling [557] with a lower measurement cost compared to quantum state tomography.

The experimental setup of Ref. [80] also offers a hint to study how the OE is affected by the presence of a $U(1)$ symmetry. This gives us the chance to introduce the notion of symmetry resolution for operator entanglement as it has been done for state entanglement. In this Chapter we start the investigation of decomposition in symmetry sectors of the OE. The first challenge is to identify the most appropriate supercharge operator (i.e. the operator in the space of operators) responsible for a decomposition in symmetry sectors of the OE. Such identification allows us to introduce the notion of symmetry resolved operator entanglement (SROE) [1].

The presence of an entanglement barrier in the different symmetry sectors and its relation with the specifics of the dynamics is uncharted territory and is interesting both from a purely theoretical standpoint and from the point of view of numerical simulations. In general, the intermediate "bumps" characterising the dynamics of OE represent an obstacle for an efficient simulation of the operator. It would be interesting to discover if and in which regime the existence of such a barrier does depend on the symmetry sector, and therefore if, in the case of small entanglement, it is possible to represent the operator as an MPO in any of them.

The Chapter is organised as follows. In Sec. 16.2 we provide a bird's eye view about both

[1] We note, however, that a slightly different definition of SROE, with respect to the one in this Chapter, was already introduced in Ref. [694])

the experimental results from the randomised measurement protocol and the theoretical ones. In Sec. 16.3 we introduce formally the operator entanglement (OE) and its symmetry resolution. In Sec. 16.4, using a combination of CFT and of exact analytical and numerical calculations in critical free fermion chains, we study the SROE of the RDM ρ_{AB} of a subsystem $A \cup B$ after a quantum quench. Finally we draw our conclusions.

16.2 Summary of the main results

Here we provide a short summary of the results about the operator entanglement and its symmetry resolution. The main points are also illustrated in Fig. 16.1. The results are twofold, but in the following sections we will mainly focus on the second point of the following list. More details about the first one can be found in [716].

1. With a new analysis of the published experimental data of *Brydges et al.* [80], we were able to identify and measure for the first time the OE and SROE of a subsystem's density matrix in a many-body quantum system. We employ the *randomised measurements* toolbox [558] and introduce a new efficient method to post-process experimental data in order to extract higher-order density matrix functionals. A schematic of this procedure is shown in Fig. 16.1a). Subsequently, in Fig. 16.1b)-d), we show the experimentally measured OE and SROE, respectively, as in Eq. (16.3.2), which are supported by tensor network simulations modelling the full experiment. Our main observations are summarised here:

   (a) We witness the entanglement barrier for OE and for SROE, in a given symmetry sector, for a bipartite subsystem $A \cup B$ made up of four out of twenty ions. This barrier equally presents bump structures due to finite size effects.

   (b) We provide experimental evidence of the absence of the entanglement barrier when the finite size effects are too large (e.g. for a subsystem of four out of ten ions of the chain).

   (c) We observe a rough qualitative satisfactory agreement of SROE with the numerical results, for some symmetry sectors. The sizeable deviation between theory and experiment are mainly explained because of the small populations in the corresponding symmetry sectors, that we understand using perturbation theory analysis and due to the low measurement statistics performed in the experiment.

2. To gain insights into SROE and into its own entanglement barrier, we provide a thorough theory analysis in chains of non-interacting fermions, which in spite of their simplicity capture the main physical features of OE and SROE. In particular, for these models we obtain the general formula in Eq. (16.4.21), which governs the evolution of the SROE. This formula allows us to uncover three main physical effects, which we expect to appear more generically in chains of qubits, beyond the simple non-interacting fermion ones. These effects are:

   (a) the appearance of a barrier for SROE in *any* charge sector, which resembles the behaviour of the total OE;

   (b) a delay time for the onset of the SROE that grows linearly with the charge sector of the subsystem;

   (c) the effective equipartition in the scaling limit of large time and subsystem size for small charges (see Eq. (16.4.22)), where by equipartition we mean that the SROE is equally distributed among the different symmetry sectors.

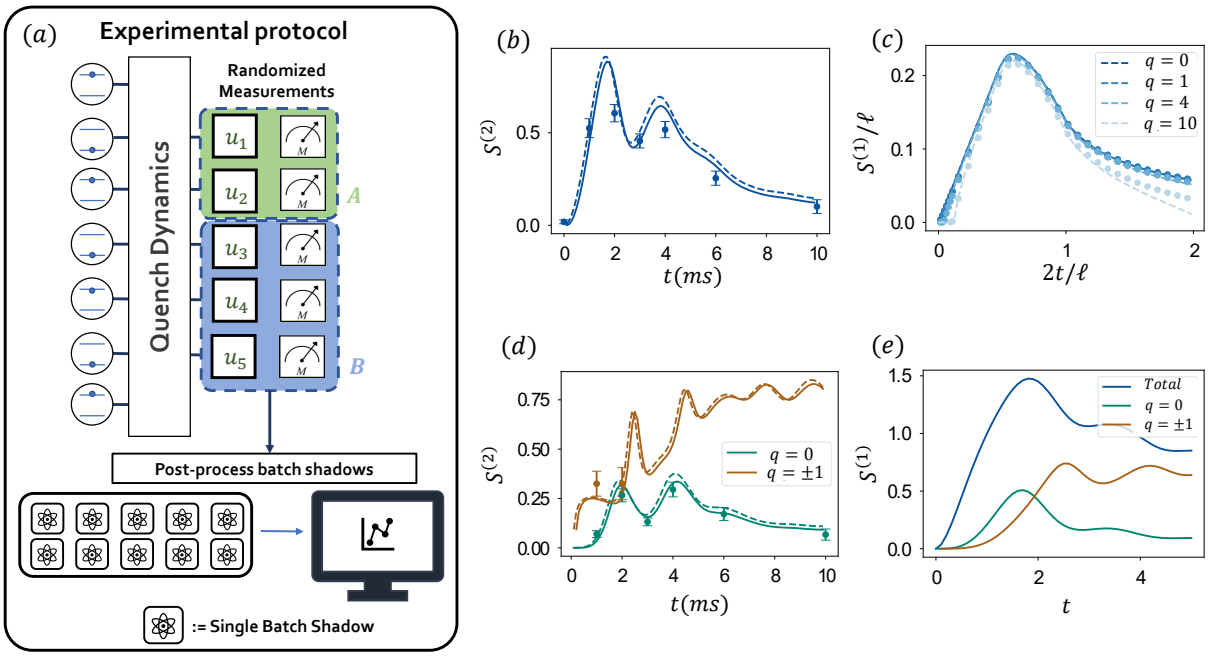

Figure 16.1: Overview of the results: a) Schematic of the method to post-process the experimental data. After the quench dynamics, randomised measurements are performed. The collected bit-strings are used to estimate OE and the SROE with a method we dub *batch shadows estimator*. b)-d) Experimental results for the operator entanglement of the RDM (of 4 ions out of 20) $S^{(2)}(\rho_{AB})$ and its symmetry resolution $S^{(2)}_q(\rho_{AB})$, as in Eqs. (16.3.2)-(16.3.19), after a global quantum quench. The points correspond to the experimental data, the curves are numerical results obtained via tensor network algorithms with (solid) or without (dashed) dissipation considered. The entanglement barrier is visible for the total operator entanglement and the symmetry sector $q = 0$. c)-e) Symmetry resolution of the OE of the RDM after a global quantum quench in a free fermion chain under unitary evolution. c) Numerical data (symbols) with subsystem length $\ell_A = 120$ compared with quasiparticle prediction (16.4.21) (continuous lines). This plot shows the three main features of the SROE in the thermodynamic limit, i.e. the barrier in each sector q, the delay time and the equipartition for small q. e) Symmetry resolution of the OE of the RDM after a global quantum quench, for 4 sites out of a 20 sites chain. Comparing with the experimental results in d), we can spot several qualitative features of OE although the model is short ranged and there is no dissipation.

These effects are visible in Fig. 16.1c). There we plot OE and SROE of the RDM, for a bipartition $A \cup B$, where A and B are of lengths ℓ_A and ℓ_B respectively (here $\ell \equiv \ell_A + \ell_B = 256$). The numerical results are obtained for a quench in the tight-binding model from the Neel state (the calculation is performed in a finite periodic chain of total size $L = 8 \times (\ell_A + \ell_B)$). The solid lines correspond to Eq. (16.4.21).

16.3 Operator entanglement and symmetry resolution

In this section we introduce formally the OE, discuss its connection with mixed state entanglement, and introduce its symmetry resolution in the presence of an additive global conserved charge.

16.3.1 Definition of Operator Entanglement

Let us now introduce the concept of OE for an operator O which acts non trivially in $A \cup B$ and admits the Schmidt decomposition [631]

$$\frac{O}{\sqrt{\mathrm{Tr}(O^\dagger O)}} = \sum_i \lambda_i O_{A,i} \otimes O_{B,i}, \tag{16.3.1}$$

where $\sum_i \lambda_i^2 = 1$, the operators $O_{A,i}$ (same for $O_{B,i}$) obey the orthonormality condition $\mathrm{Tr}[O_{A,i}^\dagger, O_{A,j}] = \delta_{ij}$ and the normalisation factor $\sqrt{\mathrm{Tr}(O^\dagger O)}$ ensures that we deal with properly normalised operators. From this decomposition, we can quantify the entanglement properties of an operator through the definition of the Rényi n-OE

$$S^{(n)}(O) \equiv \frac{1}{1-n} \log \sum_j \lambda_j^{2n}. \tag{16.3.2}$$

whose limit $n \to 1$ gives the OE

$$S(O) \equiv \sum_j -\lambda_j^2 \log \lambda_j^2. \tag{16.3.3}$$

16.3.2 Symmetry resolved operator Entanglement

In the presence of a global symmetry, the total OE of the reduced density splits in different charge sectors, similarly to the SREE. To understand how this happens and the consequent notion of SROE in a system with $U(1)$ symmetry, let us focus first on a minimal illustrative example: a 3-qubits system, whose qubits are labeled A, B and C, in a state of the form ($|\alpha|^2 + |\beta|^2 + |\gamma|^2 = 1$)

$$|\psi\rangle_{ABC} = \alpha\,|001\rangle + \beta\,|010\rangle + \gamma\,|100\rangle\,. \tag{16.3.4}$$

This is an eigenstate of the total charge operator $Q = \sum_{j=A,B,C} Q_j$ with $Q_j = (1 + Z_j)/2$, and Z_j the Pauli Z-operator acting on qubit j. The RDM of the subsystem AB is

$$\rho_{AB} = |\alpha|^2\,|00\rangle\langle 00| + (\beta\,|01\rangle + \gamma\,|10\rangle)(\beta^*\langle 01| + \gamma^*\langle 10|)\,. \tag{16.3.5}$$

Importantly, ρ_{AB} commutes with $Q_A + Q_B$.

We can now vectorise the reduced density matrix in such a way that the first (second) ket contains the degrees of freedom of A (B) in this way (see also Eq. (16.3.9)):

$$\begin{aligned} |\rho_{AB}\rangle = {} & |\alpha|^2\,|00\rangle_A\,|00\rangle_B + |\beta|^2\,|00\rangle_A\,|11\rangle_B + \\ & + |\gamma|^2\,|11\rangle_A\,|00\rangle_B + \beta\gamma^*\,|01\rangle_A\,|10\rangle_B + \\ & + \beta^*\gamma\,|10\rangle_A\,|01\rangle_B\,. \end{aligned} \tag{16.3.6}$$

From this state, it is possible to build the density matrix $|\rho_{AB}\rangle\langle\rho_{AB}|$ and, by tracing it over B, to obtain the reduced density matrix associated to the operator ρ_{AB}, which reads

$$\begin{aligned}\mathrm{Tr}_B\,|\rho_{AB}\rangle\langle\rho_{AB}| &= |\beta|^4\,|00\rangle\langle 00| \\ &+ |\beta|^2|\gamma|^2(|01\rangle\langle 01| + |10\rangle\langle 10|) \\ &+ (|\alpha|^2\,|00\rangle + |\gamma|^2\,|11\rangle)(|\alpha|^2\,\langle 00| + |\gamma|^2\,\langle 11|).\end{aligned} \tag{16.3.7}$$

By reshuffling the elements of the basis, we find out that the matrix has a block-diagonal decomposition as

$$\mathrm{Tr}_B\,|\rho_{AB}\rangle\langle\rho_{AB}| \cong \left(|\gamma|^2|\beta|^2\right)_{q=-1} \oplus \begin{pmatrix} |\beta|^4+|\alpha|^4 & |\alpha|^2|\gamma|^2 \\ |\alpha|^2|\gamma|^2 & |\gamma|^4 \end{pmatrix}_{q=0} \oplus \left(|\beta|^2|\gamma|^2\right)_{q=1}. \tag{16.3.8}$$

It is clear that each block is now labelled by the imbalance between the charge in A and in its copy coming from the vectorization of ρ_{AB}.

Although very neat, the former example does not yet explain how and why in full generality the OE of the reduced density matrix of a symmetric state splits in charge sectors. To show the rationale for a generic many-body system, we can use again the standard notion of vectorised form of an operator for the reduced density matrix ρ_{AB}. This is nothing but the mapping

$$\rho_{AB} = \sum_{ij}(\rho_{AB})_{ij}\,|i\rangle\langle j| \to |\rho_{AB}\rangle = \sum_{ij}(\rho_{AB})_{ij}\,|i\rangle\,|j\rangle, \tag{16.3.9}$$

where $|i\rangle$ is an arbitrary basis in the Hibert space of AB. Now, our goal is to find a supercharge $\mathcal{Q}_{AB}$, i.e. the superoperator commuting with $|\rho_{AB}\rangle\langle\rho_{AB}|$ in terms of which we define the SROE. We exploit the obvious relation for $Q_{AB} = Q_A + Q_B$

$$\begin{aligned}Q_{AB}\rho_{AB} &= \sum_{ij}(\rho_{AB})_{ij}Q_{AB}\,|i\rangle\langle j| \\ &\to \sum_{ij}(\rho_{AB})_{ij}(Q_{AB}\,|i\rangle)\,|j\rangle = Q_{AB}\otimes\mathbb{1}\,|\rho_{AB}\rangle\end{aligned} \tag{16.3.10}$$

and similarly $\rho_{AB}Q_{AB} \to \mathbb{1}\otimes Q_{AB}^T\,|\rho_{AB}\rangle$. Therefore, from the commutation relation $[Q_{AB},\rho_{AB}] = 0$, we naturally define the supercharge operator as

$$\mathcal{Q}_{AB} = Q_{AB}\otimes\mathbb{1} - \mathbb{1}\otimes Q_{AB}^T, \tag{16.3.11}$$

satisfying

$$\mathcal{Q}_{AB}\,|\rho_{AB}\rangle = 0. \tag{16.3.12}$$

The form of this supercharge appears to us far from obvious a priori. As a consequence, being $\mathcal{Q}_{AB}$ Hermitian, we find that

$$[\mathcal{Q}_{AB}, |\rho_{AB}\rangle\langle\rho_{AB}|] = 0, \tag{16.3.13}$$

and exploiting $\mathcal{Q}_{AB} = \mathcal{Q}_A + \mathcal{Q}_B$, by tracing over the subsystem B, we get

$$[\mathcal{Q}_A, \mathrm{Tr}_B\,|\rho_{AB}\rangle\langle\rho_{AB}|] = 0. \tag{16.3.14}$$

This commutation relation implies that $\mathrm{Tr}_B\,|\rho_{AB}\rangle\langle\rho_{AB}|$ has a block diagonal structure with each block corresponding to an eigenvalue q of the supercharge $\mathcal{Q}_A$. The SROE is just the OE in each of these blocks.

After the vectorised form allowed us to simply identify the right quantum number, we can come back to the definition (16.3.2) of the OE in terms of the Schmidt eigenvalues and show how to modify it for the SROE. What we mean by 'symmetry resolved operator Schmidt decomposition' is that the RDM for the subsystem AB is of the general form

$$\frac{\rho_{AB}}{\sqrt{\mathrm{tr}[\rho_{AB}^2]}} = \sum_q \sum_j \lambda_j^{(q)} O_{A,j}^{(q)} \otimes O_{B,j}^{(-q)}, \tag{16.3.15}$$

where

$$\mathrm{Tr}[O_{A,j_1}^{(q_1)} O_{A,j_2}^{(q_2)}] \;=\; \mathrm{Tr}[O_{B,j_1}^{(q_1)} O_{B,j_2}^{(q_2)}] \;=\; \delta_{q_1,q_2}\delta_{j_1,j_2}, \tag{16.3.16}$$

and q is the eigenvalue of $\mathcal{Q}_A$.

Because of the normalization of the l.h.s of Eq. (16.3.15), we have $\sum_q \sum_j (\lambda_j^{(q)})^2 = 1$, so that the coefficients $(\lambda_j^{(q)})^2$ define a certain probability distribution. Since the terms in the Schmidt decomposition are naturally organised into charge subsectors, it is natural to consider the SROE, namely the entropy of the probability distribution conditioned to each of the charge sectors. Defining the probability in the charge sector q as

$$p(q) \equiv \sum_j (\lambda_j^{(q)})^2, \tag{16.3.17}$$

we have

$$S(\rho_{AB}) \;=\; \sum_q p(q) S_q(\rho_{AB}) \;+\; \sum_q -p(q)\log p(q), \tag{16.3.18}$$

where the SROE of ρ_{AB} in the charge sector q is

$$S_q(\rho_{AB}) \;\equiv\; \sum_j -\frac{(\lambda_j^{(q)})^2}{p(q)} \log \frac{(\lambda_j^{(q)})^2}{p(q)}. \tag{16.3.19}$$

and, for a generic Rényi index n, as

$$S_q^{(n)}(\rho_{AB}) \;\equiv\; \frac{1}{1-n} \log \sum_j \frac{(\lambda_j^{(q)})^{2n}}{p(q)^n}. \tag{16.3.20}$$

16.3.3 Operator Entanglement and entanglement criteria

There is a connection between operator entanglement and the more familiar concept of 'state' entanglement where one is interested in showing that ρ_{AB} cannot be written as a convex mixture of product states $\rho_{AB} = \sum_i p_i \rho_A^{(i)} \otimes \rho_B^{(i)}$, $p_i \geq 0$ [715]. Let λ_i be the operator Schmidt decomposition of the operator $O = \rho_{AB}$. According to the realignement/computable cross norm criterion (CCNR) [717, 718] For all separable states (not entangled) states, we have

$$\sum_i \lambda_i \leq 1/\sqrt{\mathrm{tr}\left[\rho_{AB}^2\right]} \tag{16.3.21}$$

The connection between the CCNR criterion and OE, which are the quantities that can accessed experimentally, has been recently discussed in Ref. [719] here we show a slightly weaker but much compact entanglement condition: Using the CCNR criterion, one can prove that the Rényi 2-OE and the Rényi 2-entropy $R^{(2)}$ for a separable system must satisfy the following inequality

$$S^{(2)}(\rho_{AB}) \leq -\log(\mathrm{tr}\left[\rho_{AB}^2\right]), \tag{16.3.22}$$

Conversely, if $S^{(2)}(\rho_{AB}) > -\log(\mathrm{tr}\left[\rho_{AB}^2\right])$, i.e. if ρ_{AB} is more 'operator mixed' than 'state mixed', ρ_{AB} is necessarily entangled.

16.4 Symmetry resolved operator entanglement in free fermionic chains

We have shown in Fig. 16.1 that most of the qualitative features for OE and SROE can be also observed in free-fermion chains under unitary evolution, despite the model is short ranged and there is no dissipation. This connection led us to wonder whether one could extract the main physical treats of the OE and SROE of the RDM by studying the unitary time evolution of free fermions in the thermodynamic limit. Therefore, in this section, we show that in this regime the problem can be tackled analytically, unveiling some interesting properties of the SROE, such as the time delay of the charge sectors or the equipartition.
To achieve our goal, the calculation of the SROE by the definition (16.3.19) is a difficult task, especially for an analytic derivation. Therefore, we can apply a trick similar to what has been done for the standard entanglement resolution, i.e. connecting it with the computation of the charged moments of the RDM. Using the vectorised version of the operator ρ_{AB}, they are defined as

$$Z_n(\alpha) \equiv \frac{1}{(\mathrm{Tr}[\rho_{AB}^2])^n} \mathrm{Tr}[(\mathrm{Tr}_B(|\rho_{AB}\rangle\langle\rho_{AB}|))^n e^{i\alpha\mathcal{Q}_A}], \tag{16.4.1}$$

and their Fourier transform gives

$$\begin{aligned} \mathcal{Z}_n(q) &= \int_{-\pi}^{\pi} \frac{d\alpha}{2\pi} e^{-iq\alpha} Z_n(\alpha), \\ S_q^{(n)}(\rho_{AB}) &= \frac{1}{1-n} \log \frac{\mathcal{Z}_{n,q}(\rho_{AB})}{\mathcal{Z}_{1,q}^n(\rho_{AB})}, \end{aligned} \tag{16.4.2}$$

where q is the eigenvalue of $\mathcal{Q}_A$.

16.4.1 Free-fermion techniques for the OE

For the eigenstates of quadratic lattice Hamiltonians, it is possible to compute the entanglement entropies in terms of the eigenvalues of the correlation matrix of the system. We will show that this trick can be applied also for the computation of the OE and, more in general, of the charged moments (16.4.1).
Let us take a free-fermionic chain of length L with $U(1)$ symmetry, described by the Hamiltonian

$$H = -\frac{1}{2}\sum_{i=1}^{L}(c_{i+1}^\dagger c_i + \text{h.c.}) \tag{16.4.3}$$

where $c_i^\dagger$ (c_i) is the creation (annihilation) operator such that $\{c_i, c_j^\dagger\} = \delta_{ij}$ and $c_{L+1} = c_1, c_{L+1}^\dagger = c_1^\dagger$, i.e. we impose periodic boundary conditions. The reduced density matrix for a subsystem $A\cup B$, ρ_{AB}, where $A\cup B = [1,\ell_A]\cup[\ell_A+1,\ell_A+\ell_B]$ consists of two adjacent intervals, can be put in a diagonal form as

$$\rho_{AB} = \bigotimes_{k=1}^{\ell_A+\ell_B} \frac{e^{-\lambda_k d_k^\dagger d_k}}{1+e^{-\lambda_k}}, \tag{16.4.4}$$

where $e^{-\lambda_k} = \frac{n_k}{1-n_k}$, with n_k the occupation number at a given wave vector k and d_k's are also fermionic operators satisfying $\{d_k, d_{k'}^\dagger\} = \delta_{kk'}$. It is more convenient to write Eq. (16.4.4) as

$$\begin{aligned}\rho_{AB} &= \bigotimes_{k=1}^{\ell_A+\ell_B} \frac{|0\rangle_k \langle 0|_k + e^{-\lambda_k} |1\rangle_k \langle 1|_k}{1+e^{-\lambda_k}} \\ &= \bigotimes_{k=1}^{\ell_A+\ell_B} [(1-n_k) |0\rangle_k \langle 0|_k + n_k |1\rangle_k \langle 1|_k],\end{aligned} \tag{16.4.5}$$

so that by applying the vectorisation trick in Eq. (16.3.9) for ρ_{AB}, we get

$$\begin{aligned}\frac{|\rho_{AB}\rangle}{\sqrt{\mathrm{Tr}[\rho_{AB}^2]}} &= \bigotimes_{k=1}^{\ell_A+\ell_B} \frac{1}{\sqrt{Z_k}}[(1-n_k) |0\rangle_k |0\rangle_{\tilde{k}} + n_k |1\rangle_k |1\rangle_{\tilde{k}}] \\ &= \bigotimes_{k=1}^{\ell_A+\ell_B} \frac{1}{\sqrt{Z_k}}[1-n_k+n_k d_k^\dagger \tilde{d}_k^\dagger] |0\rangle ,\end{aligned} \tag{16.4.6}$$

where $Z_k = n_k^2 + (1-n_k)^2$ and the $\tilde{d}_k^\dagger$'s are new creation operators that anti-commute with all the d_k's, and $|0\rangle$ is the state annihilated by all the d_k's and $\tilde{d}_k$'s. The $2(\ell_A+\ell_B) \times 2(\ell_A+\ell_B)$ correlation matrix of the state $|\rho_{AB}\rangle$ reads

$$\begin{aligned}&\langle \rho_{AB}| \begin{pmatrix} d_k^\dagger \\ \tilde{d}_k \end{pmatrix} \begin{pmatrix} d_{k'} & \tilde{d}_{k'}^\dagger \end{pmatrix} |\rho_{AB}\rangle \\ &= \frac{\delta_{kk'}}{Z_k} \begin{pmatrix} n_k^2 & n_k(1-n_k) \\ n_k(1-n_k) & (1-n_k)^2 \end{pmatrix}.\end{aligned} \tag{16.4.7}$$

In the basis of $d_k, \tilde{d}_k$'s, the supercharge operator takes the form

$$\mathcal{Q} = \sum_k d_k^\dagger d_k - \sum_k \tilde{d}_k^\dagger \tilde{d}_k. \tag{16.4.8}$$

We can collect the operators into the vector $\mathbf{f} = (d_1, \dots d_{\ell_A+\ell_B}, \tilde{d}_1^\dagger \dots \tilde{d}_{\ell_A+\ell_B}^\dagger)^t$ such that $\mathcal{Q}$ reads $\mathcal{Q} = \mathbf{f}^\dagger \mathbf{f} - (\ell_A+\ell_B)$, where $\ell_A+\ell_B$ is an additive constant.

At this point, to evaluate the charged moments in Eq. (16.4.1), we need to focus on the subsystem A, i.e. we can restrict the supercharge operator to $\mathcal{Q}_A$ and the correlation matrix to the subspace corresponding to the subsystem A. Going back to the spatial basis and diagonalising this matrix, we get $2\ell_A$ real eigenvalues ξ_i between 0 and 1.
Therefore, one can compute the charged moments of the RDM built from $|\rho_{AB}\rangle$ in terms of the eigenvalues as

$$Z_n(\alpha) = e^{-i\alpha(\ell_A+\ell_B)} \prod_{a=1}^{2\ell_A} (\xi_a^n e^{i\alpha} + (1-\xi_a)^n). \tag{16.4.9}$$

Using the results in Eq. (16.4.2), we can compute exactly the SROE for the RDM of a free fermionic chain. We mention that this trick also allows the computation of the total OE as

$$S^{(n)}(\rho_{AB}) = \frac{1}{1-n} \sum_{a=1}^{2\ell_A} (\log[\xi_a^n + (1-\xi_a)^n)]. \tag{16.4.10}$$

16.4.2 Charged moments: a quasiparticle picture

Let us now consider a global quantum quench from an initial conformal invariant state with an evolution Hamiltonian given by the continuum limit of Eq. (16.4.3). The emerging quasiparticles will move with one single velocity and, in the space-time scaling limit $t, \ell_A, \ell_B \gg \tau_0$ (with τ_0 an ultraviolet cutoff), the charged moments are given by

$$\log Z_n(\alpha) = \frac{\pi \Delta_n^\alpha}{\tau_0} \left[t - \mathrm{Max}(\mathrm{Min}(\ell_A, \ell_B)/2, t) - \mathrm{Max}(\mathrm{Max}(\ell_A, \ell_B)/2, t) + \mathrm{Max}(t, (\ell_A + \ell_B)/2) \right], \tag{16.4.11}$$

where

$$\Delta_n^\alpha = \frac{1}{12}\left(n - \frac{1}{n}\right) + \frac{1}{n}\left(\frac{\alpha}{2\pi}\right)^2. \tag{16.4.12}$$

From this result valid for a CFT, one can formulate a quasiparticle picture for the charged moments of free fermionic models with global conserved $U(1)$ charge, whose quench dynamics starts from initial states that are also invariant under $U(1)$ symmetry. This is obtained from the CFT result in Eq. (16.4.11) by first replacing $t \to |v(k)|t$, with $|v(k)|$ the velocity of quasiparticles, that for conformal invariant systems is fixed to be $v(k) = 1$. Then we can integrate over the quasiparticles with quasimomentum k, and replace $\pi \Delta_n^\alpha/(\tau_0) \to 2 z_n(k, \alpha)$, which is the density (in momentum space) of the thermodynamic charged moments in the stationary state, obtaining

$$\log Z_n(\alpha) = \int_{-\pi}^{\pi} \frac{dk}{2\pi} 2 z_n(k, \alpha) \Big[t|v(k)| - \\ \mathrm{Max}(\mathrm{Min}(\ell_A, \ell_B)/2, t|v(k)|) - \mathrm{Max}(\mathrm{Max}(\ell_A, \ell_B)/2, t|v(k)|) + \mathrm{Max}(t|v(k)|, (\ell_A + \ell_B)/2) \Big]. \tag{16.4.13}$$

We remind that a similar trick has been used in Chapter 14. In order to have a predictive formula, one has to fix the function $z_n(k, \alpha)$ in Eq. (16.4.13). Here we focus on out-of-equilibrium protocols for free-fermion models, whose time evolution is given by the Hamiltonian in Eq. (16.4.3). In this case $z_n(k, \alpha)$ is determined from the population of the modes n_k of the postquench Hamiltonian in the stationary state [49, 626] and it reads

$$z_n(k, \alpha) = \log[e^{i\alpha} n_k^n + (1 - n_k)^n] - i\alpha/2. \tag{16.4.14}$$

We focus the attention on a quench from the Néel state, for which $n_k = 1/2$ and the quasiparticle picture for the charged moments reads

$$\log Z_n(\alpha) = (2(1-n)\log 2 + 2\log(\cos(\alpha/2))) \int_{-\pi}^{\pi} \frac{dk}{2\pi} \Big[t|v(k)| - \mathrm{Max}(\mathrm{Min}(\ell_A, \ell_B)/2, t|v(k)|) + \\ - \mathrm{Max}(\mathrm{Max}(\ell_A, \ell_B)/2, t|v(k)|) + \mathrm{Max}(t|v(k)|, (\ell_A + \ell_B)/2) \Big], \tag{16.4.15}$$

where $|v(k)| = |\sin(k)|$ and, for the sake of conciseness, we can introduce the function

$$\mathcal{J}(t) = \int_{-\pi}^{\pi} \frac{dk}{2\pi} \Big[t|v(k)| - \mathrm{Max}(\mathrm{Min}(\ell_A, \ell_B)/2, t|v(k)|) + \\ - \mathrm{Max}(\mathrm{Max}(\ell_A, \ell_B)/2, t|v(k)|) + \mathrm{Max}(t|v(k)|, L_A/2) \Big]. \tag{16.4.16}$$

The quasiparticle prediction for the total OE is also easily obtained as

$$S^{(n)}(\rho_{AB}) = \frac{1}{1-n} \log Z_n(0). \tag{16.4.17}$$

16.4.3 Time delay, barrier and equipartition

From the computation of the charged moments done above, the symmetry resolved moments read

$$\mathcal{Z}_n q) = 2^{2(1-n)\mathcal{J}(t)} \int_{-\pi}^{\pi} \frac{d\alpha}{2\pi} e^{-i\alpha q} \left(\cos\frac{\alpha}{2}\right)^{2\mathcal{J}(t)}. \tag{16.4.18}$$

As already pointed out for the usual symmetry resolved entropies in [132, 133], this quantity assumes negative values for $\mathcal{J}(t) < |q|$. This allows us to identify a *delay time* t_D such that the SROE in a given charge sector starts only after t_D. The equation $J(t_D) = |q|$ reads (as long as $v_M t_D < \frac{1}{2}\mathrm{Min}(\ell_A, \ell_B)$ self-consistently and $v_M \equiv \max(v(k)) = 1$)

$$\mathcal{J}(t) = \int_{-\pi}^{\pi} \frac{dk}{2\pi} |\sin(k)| t < |q|, \tag{16.4.19}$$

and we can conclude that $t_D = \pi|q|/2$ for $|q| < \mathrm{Min}(\ell_A, \ell_B)/\pi$. Therefore, the SROE is given by

$$S_q^{(n)}(\rho_{AB}) = \begin{cases} 0, & t \le t_D \\ 2\mathcal{J}(t)\log 2 + \log \mathcal{Z}_1(q) & t > t_D \end{cases} \tag{16.4.20}$$

We remark that this expression does not depend on the replica index n. In the regime $\mathcal{J}(t) > |q|$, for large $\mathcal{J}(t)$, we obtain

$$S_q^{(n)}(\rho_{AB}) = 2\mathcal{J}(t)\log 2 - (\mathcal{J}(t)+q)\log(1+q/\mathcal{J}(t)) - (\mathcal{J}(t)-q)\log(1-q/\mathcal{J}(t)). \tag{16.4.21}$$

The comparison between this formula and the numerical results in the tight-binding model chain is displayed in the top-right panel of Fig. 16.1. The solid lines correspond to the saddle-point approximation in Eq. (16.4.21) for $t > t_D$. The agreement is good and we can also observe that there are some charge sectors with zero entanglement for $t < t_D$. However, for $t > (\ell_A + \ell_B)/2$ the discrepancy between the numerics and the analytical prediction in Eq. (16.4.21) is larger. One explanation could be that at finite ℓ_A and t the data exhibit some small corrections, and our prediction is recovered only in the scaling limit $t, \ell_A, \ell_B \to \infty$ with their ratio fixed.
For $|q| \ll \mathcal{J}(t)$ we find from Eq. (16.4.21)

$$S_q^{(n)}(\rho_{AB}) = \mathcal{J}(t)\left(2\log 2 - \frac{q^2}{\mathcal{J}(t)^2}\right). \tag{16.4.22}$$

This result states that for small $|q|$ there is an effective equipartition of the OE with violations of order $q^2/(\ell_A + \ell_B)$.

We observe that the SROE is small both at short and at large times, so it can be captured by an MPO with small bond dimension. However, it blows up linearly in the transient regime $t \le (\ell_A + \ell_B)/(2)$, preventing efficient simulation using the MPO representation, whose bond dimension would blow up exponentially in that time window. This also happens for the total OE [631]. At short times, the RDM is still very close to the one of the pure state, and one does not gain much by approximating ρ_{AB} instead of the corresponding state; this trick becomes efficient only at later times.
We conclude by commenting the bottom-right panel of Fig. 16.1, obtained through the free-fermion techniques described in Sec. 16.4.1. We show that the dynamics of the SROE in the different charge sectors is affected by the finite size of the system, which is much smaller with respect to the result showed in the panel above of the same Figure. In particular, one can observe the entanglement barrier only in the sector $q = 0$, while for $q = 1$ the data present a plateaux followed by a decrease due do the finite size of the system.

16.5 Closing remarks

This Chapter is devoted to analyse the OE of the RDM after a global quantum quench and its symmetry resolution. These quantities blow up linearly in time, before they decrease and saturate to a finite value. The presence of this barrier is strongly affected by the finite size of the system, as can be demonstrated experimentally. This feature is also visible for free fermionic systems evolving under unitary evolution, which have been our main focus since they fit with the topics/techniques of the previous Chapters of this thesis. However, let us summarise again all the results we have found in [716].

The experimental results, also supported by tensor network simulations, have been obtained by a post-processing method of randomized measurements data that has practical applications to probe non-linear properties of quantum many-body systems. We observe the presence of the entanglement barrier of the RDM of a partition of 4 ions out of $L = 10, 20$ both for the total OE and for the charge sector $q = 0$ and $L = 20$. However, the finite size effects prevent the appearance of such a barrier in the charge sectors $q = \pm 1$ and for $q = 0, L = 10$. When $L = 20$, in the charge sectors $q = \pm 1$, the available statistics only allows us to explore the early time behaviour of the SROE.

For small system sizes L, the phenomenology mentioned above can be also observed in free fermionic systems without dissipation. Therefore, guided by conformal field theory and free-fermion techniques, we show that the semiclassical picture of moving quasiparticles [44] can be adapted in this context, leading to a general conjecture for the charged OEs whose Fourier transform gives the desired SROE. Beyond the barrier, we observe a delay time proportional to the charge sector and an effective equipartition for small q.

Because of this phenomenology, we expect our main physical findings to show up for rather generic quench protocols. However, it would be very interesting to engineer situations in which some of them are absent, e.g. with the entanglement barrier appearing only in given charge sectors, breaking equipartition.

The combination of CFT and exact calculations in critical free-fermion chains allows to compute the SROE of other operators, such as the thermal density matrix ρ_β and the local operators evolving in Heisenberg picture $O = e^{itH} O e^{-itH}$, too. The main trait of the former case is that the leading order term of the SROE corresponds to the total OE, which diverges logarithmically in the the subsystem size, ℓ_A, at low temperatures, i.e. when the RDM is very close to the one of the ground state, while it is bounded (in ℓ_A) at finite temperature β. The fact that the leading term coincides with the total OE resembles the entanglement equipartition for the usual symmetry resolution, and it can be traced back to the conformal invariance of the system also in this case. For the latter operator and free fermion Hamiltonians, one can study the SROE of a Jordan-Wigner string and it turns out that it grows logarithmically in time, while the fermion creation/annihilation operators satisfy the operator area law. These are preliminary steps towards the general understanding of the symmetry resolution of OE, which certainly deserves further investigation.

To conclude, the study of the OE and its interplay with symmetries leave space for further investigations about the connection between entanglement measures and the charge operators defined in the enlarged Hilbert space, as in Eq. (16.3.14). We will come back to this in the conclusions of this thesis.

Chapter 17

Conclusions

Despite each Chapter contains its own conclusions, which are more related to the specific topic we dealt with, here we want to give a more general overview about the possible aspects that could deserve further investigations.

The core of this thesis has been the study of entanglement in theories with global conserved charges. However, it would be natural to ask whether similar procedures could be applied in systems endowed with local symmetries, and, therefore, a possible connection with the study of entanglement in gauge theories. This problem is quite challenging because it turns out that the Hilbert space of physical states, i.e., gauge-invariant states, does not admit a tensor product decomposition in terms of the Hilbert space of states in a region A and its complement. Thus, it is not clear how to compute the entanglement by simply using the definition of reduced density matrix. One possible approach for defining the entanglement entropy was given in [219]: the authors work with gauge-invariant states, and the algebra of operators acting in the region A and its complement B. They argue that this algebra has a non-trivial centre for gauge theories, and this centre is responsible for the space of gauge-invariant states not having a tensor product decomposition. Therefore, by diagonalising the centre and going to sectors where it takes a fixed value, the Hilbert space of gauge-invariant states in each sector does admit a tensor product decomposition, leading to a definition of the density matrix and the entanglement entropy. Another possible approach consists in working on a spatial lattice, embedding the space of gauge-invariant states in a bigger space obtained by taking the tensor product of the Hilbert spaces on each link of the lattice [221, 222]. This admits a tensor product decomposition in terms of the Hilbert spaces for the set of links of interest. It would be interesting if using one of this two approaches, one can use the tools adopted in this thesis, like the charged moments and the approach of Chapter 3, to study this subject.

This idea of enlarging the Hilbert space reminds other possible ways to quantify the entanglement. One of this involves the purification of a mixed state. Let us appeal (for the last time!) to our travel friends Alice and Bob to specify a bit better what we mean by purification, without any details about how this operation can be done. To achieve this goal, we need to introduce a possible third adversary, Eve, such that we start from a pure state $|\Psi\rangle$ living in the Alice's, Bob's and Eve's Hilbert space

$$|\Psi\rangle \in \mathcal{H}_A \otimes \mathcal{H}_B \otimes \mathcal{H}_E. \tag{17.0.1}$$

Then we trace over Eve's Hilbert space, $\mathcal{H}_E$, producing a mixed state ρ_{AB}. The purification is a process which transforms the mixed state ρ_{AB} into pure states, meaning that the final state of Alice and Bob has to be pure and hence not entangled with anything else. The adversary Eve is out of the game, whatever operation and measurements she performs. This procedure allows recovering a pure state starting from a mixed one and can be defined, for example, by properly enlarging

the original Hilbert space of our theory [720–723]. If we introduce an Hilbert space which is the identical copy of the original one, the entanglement entropy computed from the *canonically* purified state living in this doubled Hilbert space provides the *reflected entropy* [703, 704]. Despite this quantity, like the entanglement of purification, has been introduced in the context of AdS/CFT because it posseses an understandable gravity dual, it would be interesting to study what we can learn from it in the presence of a global charge. As done for the negavity, this process would require to understand what is the correct quantum number and, therefore, the charge with respect to which one should perform the resolution.

It should be clear from this work that the investigation of the entanglement in different contexts allows, on one hand, to explore lots of aspects of quantum many-body systems. On the other hand, it also gives the possibility to learn several techniques which are extremely powerful, ranging from the realm of integrability to quantum field theory. We hope that the work collected in this thesis will stimulate future investigations in this fascinating field of research.

Acknowledgments

I am not good at all with words, but I will try to conclude this thesis by acknowledging people who have shared these years with me, without whom this work could not exist.

First of all, I want to express my gratitude to my supervisor, Pasquale, for everything he has taught to me and, above all, for his continuous encouragements. There will be always a reason for saying thanks when I go out from your office.

I thank Jerome, for his sincere advices, and Robert, for the patience he has had with me in these years. Every single page of this thesis could not have been written without the several fruitful collaborations I have had, so I want to thank Paola, Filiberto, Vittorio, Federico, Luca, Lorenzo, Vincenzo, Marcello, Mario, Riccarda. I thank the whole group of Statistical Physics, faculties, students and postdocs, for the stimulating working environment I have found.

The huge SISSA community has been fundamental in these years, from the professors to the technical staff and, last but not least, the friends of leisure, coffees and fun.

Ringrazio la mia famiglia, e soprattutto mamma e papà, per il loro sostegno anche a chilometri di distanza, i miei amici di sempre, ed infine Giuseppe, per quell'incontro fortuito davanti alla 138.

Bibliography

[1] A. Einstein, *B. Podolsky and N. Rosen, Can Quantum-Mechanical Description of Physical Reality Be Considered Complete?*, Phys. Rev. E **47** (1935) 777.

[2] E. Schrödinger, *Discussion of Probability Relations between Separated Systems,* Math. Proc. Camb. Philos. Soc. **31** (1935) 555-563.

[3] E. Schrödinger, *Probability relations between separated systems,* Math. Proc. Camb. Philos. Soc. **32** (1936) 446-452.

[4] M. Born, The Born-Einstein Letters; *Correspondence between Albert Einstein and Max and Hedwig Born from 1916 to 1955*, Walker, New York, 1971.

[5] E. H. Lieb and D. W. Robinson, *The finite group velocity of quantum spin systems*, Commun. Math. Phys. 28 (1972) 251.

[6] A. Peres, D. Terno, *Quantum Information and Relativity Theory*,Rev. Mod. Phys. **76**, 93 (2004).

[7] J. S. Bell, *On the Einstein Podolski Rosen paradox*, Physics, 1, 195-200 (1964)

[8] S. J. Freedman, J. F. Clauser, *Experimental Test of Local Hidden-Variable Theories*, Phys. Rev. Lett **28**, 938 (1972).

[9] A. Aspect, P. Grangier, G. Roger, *Experimental tests of realistic local theories via Bell's theorem*, Phys. Rev. Lett. **47**, 460 (1981).

[10] M. A. Nielsen and I. L. Chuang, *Quantum computation and quantum information*, Cambridge University Press, Cambridge, UK, 10th anniversary ed. (2010).

[11] C. H. Bennett, G. Brassard, C. Crépeau, R. Jozsa, A. Peres, and W. K. Wootters, *Teleporting an unknown quantum state via dual classical and Einstein-Podolsky-Rosen channels* Phys. Rev. Lett. **70**, 1895 (1993).

[12] C. H. Bennett, D. P. Di Vincenzo, J. A. Smolin, and W. K. Wootters, *Mixed-state entanglement and quantum error correction*Phys. Rev. A **54**, 3824 (1996).

[13] L. Amico, R. Fazio, A. Osterloh, and V. Vedral, *Entanglement in many-body systems*, Rev. Mod. Phys. **80**, 517 (2008).

[14] P. Calabrese, J. Cardy, and B. Doyon, *Entanglement entropy in extended quantum systems*, J. Phys. A **42**, 500301 (2009).

[15] J. Eisert, M. Cramer, and M. B. Plenio, *Area laws for the entanglement entropy*, Rev. Mod. Phys. **82**, 277 (2010).

[16] N. Laflorencie, *Quantum entanglement in condensed matter systems*, Phys. Rep. **643**, 1 (2016).

[17] C. Holzhey, F. Larsen, and F. Wilczek, *Geometric and renormalized entropy in conformal field theory*, Nucl. Phys. B **424**, 443 (1994).

[18] C. G. Callan and F. Wilczek, *On Geometric Entropy*, Phys. Lett. B **333**, 55 (1994).

[19] G. Vidal, J. I. Latorre, E. Rico and A. Kitaev, *Entanglement in Quantum Critical Phenomena*, Phys. Rev. Lett. **90** (2003) 227902.

[20] P. Calabrese and J. Cardy, *Entanglement entropy and quantum field theory*, J. Stat. Mech. (2004) P06002.

[21] P. Calabrese and J. Cardy, *Entanglement entropy and conformal field theory*, J. Phys. A **42**, 504005 (2009).

[22] L. Bombelli, R. K. Koul, J. Lee, and R. D. Sorkin, *Quantum source of entropy for black holes*, Phys. Rev. D **34**, 373 (1986).

[23] M. Srednicki,*Entropy and area,* Phys. Rev. Lett. **71**, 666 (1993).

[24] J. D. Bekenstein, *Black Holes and Entropy*, Phys. Rev. D **7**, 2333 (1973).

[25] S. W. Hawking, *Black hole explosions?*, Nature 248, 30 (1974).

[26] S. Ryu and T. Takayanagi, *Holographic Derivation of Entanglement Entropy from the anti-de Sitter Space/Conformal Field Theory Correspondence,* Phys. Rev. Lett. (2006) 181602.

[27] S. Ryu and T. Takayanagi, *Aspects of holographic entanglement entropy*, JHEP **08** (2006) 045.

[28] M. Rangamani and T. Takanayagi, *Holographic Entanglement Entropy*, Lect. Notes Phys. **931** (2017).

[29] T. Nishioka, S. Ryu, and T. Takayanagi, *Holographic entanglement entropy: an overview*, J. Phys. A **42**, 504008 (2009).

[30] D. N. Page, *Average entropy of a subsystem*, Phys. Rev. Lett. **71**, 1291 (1993)

[31] D. N. Page, *Information in black hole radiation*, Phys. Rev. Lett. **71** 3743 (1991).

[32] P. Hayden, D. W. Leung and A. Winter, *Aspects of Generic Entanglement*, Comm. Math. Phys. **265** 95 (2006).

[33] P. Hayden and J. Preskill, *Black holes as mirrors: quantum information in random subsystems,* JHEP **09** (2007) 120.

[34] A. Almheiri, T. Hartman, J. Maldacena, E. Shaghoulian, A. Tajdini, *Replica Wormholes and the Entropy of Hawking Radiation,* JHEP **05** (2020) 013.

[35] G. Penington, S. H. Shenker, D. Stanford, Z. Yang, *Replica wormholes and the black hole interior,* JHEP **03** (2022) 205.

[36] S. Popescu, A. J. Short, A. Winter, *Entanglement and the foundations of statistical mechanics*, Nature Phys. **2** 754 (2006).

[37] C. Gogolin and J. Eisert, *Equilibration, thermalisation, and the emergence of statistical mechanics in closed quantum systems*, Rep. Progr. Phys. **79** 056001 (2016).

[38] A. Kitaev and J. Preskill, *Topological Entanglement Entropy*, Phys. Rev. Lett. **96**, 110404 (2006).

[39] M. Levin and X.-G. Wen, *Detecting Topological Order in a Ground State Wave Function*, Phys. Rev. Lett. **96**, 110405 (2006).

[40] A. Kitaev, *Fault-tolerant quantum computation by anyons*, Ann. Phys. **303** (2003) 2.

[41] R. B. Laughlin, *Anomalous Quantum Hall Effect: An Incompressible Quantum Fluid with Fractionally Charged Excitations*, Phys. Rev. Lett. **50** (1983) 1395.

[42] S. R. White, *Density matrix formulation for quantum renormalization groups*, Phys. Rev. Lett. **69**, 2863 (1992).

[43] J. I. Cirac, F. Verstraete, *Renormalization and tensor product states in spin chains and lattices,* J. Phys. A: Math. Theor. **42**, 504004 (2009).

[44] P. Calabrese and J. Cardy, *Time Dependence of Correlation Functions Following a Quantum Quench*, Phys. Rev. Lett. **96**, 136801 (2006).

[45] P. Calabrese and J. Cardy, *Quantum quenches in extended systems*, J. Stat. Mech. P06008 (2007).

[46] P. Calabrese and J. Cardy, *Evolution of Entanglement Entropy in One-Dimensional Systems*, J. Stat. Mech. P04010 (2005).

[47] V. Alba and P. Calabrese, *Entanglement and thermodynamics after a quantum quench in integrable systems*, PNAS **114**, 7947 (2017).

[48] V. Alba and P. Calabrese, *Entanglement dynamics after quantum quenches in generic integrable systems*, SciPost Phys. **4**, 017 (2018).

[49] P. Calabrese, *Entanglement spreading in non-equilibrium integrable systems, Lectures for Les Houches Summer School on "Integrability in Atomic and Condensed Matter Physics"*, SciPost Phys. Lect. Notes 20 (2020).

[50] M. B. Hastings, *An area law for one-dimensional quantum systems*, J. Stat. Mech. P08024 (2007).

[51] E. Schmidt, *Zur Theorie der linearen und nichtlinearen Integralgleichungen*, Mathematische Annalen **63** (1907) 433.

[52] E. Chitambar, D. Leung, L. Mancinska, M. Ozols and A. Winter, *Everything You Always Wanted to Know About LOCC (But Were Afraid to Ask)*, Commun. Math. Phys. **328** (2014) 303.

[53] M. A. Nielsen, *Conditions for a Class of Entanglement Transformations,* Phys. Rev. Lett. **83** (1999) 436.

[54] C. H. Bennett, H. J. Bernstein, S. Popescu, B. Schumacher, *Concentrating partial entanglement by local operations,* Phys. Rev. A **53**, 2046 (1996).

[55] E. H. Lieb and M. B. Ruskai, *A Fundamental Property of Quantum-Mechanical Entropy,* Phys. Rev. Lett. **30** (1973) 434.

[56] E. H. Lieb and M. B. Ruskai, *Proof of the strong subadditivity of quantum-mechanical entropy,* J. Math. Phys. **14** (1973) 1938.

[57] M. Kormos and Z. Zimboras, *Temperature driven quenches in the Ising model: appearance of negative Rényi mutual information*, J. Phys. A **50**, 264005 (2017).

[58] S. O. Scalet, A. M. Alhambra, G. Styliaris, and J. I. Cirac, *Computable Rényi mutual information: Area laws and correlations*, Quantum **5**, 541 (2021).

[59] A. Peres, *Separability Criterion for Density Matrices* Phys. Rev. Lett. **77**, 1413 (1996).

[60] R. Simon, *Peres-Horodecki Separability Criterion for Continuous Variable Systems*, Phys. Rev. Lett. **84**, 2726 (2000).

[61] W. K. Wootters and W. H. Zurek *A single quantum cannot be cloned*, Nature **299**,802 (1982).

[62] G. Vidal and R. F. Werner, *A computable measure of entanglement*, Phys. Rev. A **65**, 032314 (2002).

[63] M. B. Plenio, *Logarithmic Negativity: A Full Entanglement Monotone That is not Convex*, Phys. Rev. Lett. **95**, 090503 (2005);
J. Eisert, *Entanglement in quantum information theory*, Arxiv:0610253.

[64] X.-S. Ma et al., *Quantum teleportation over 143 kilometres using active feedforward,* Nature 489, 269-273 (2012).

[65] I. Klich, G. Refael and A. Silva, *Measuring entanglement entropies in many-body systems,* Phys. Rev. A 74 (2006) 032306.

[66] I. Klich and L. Levitov, *Quantum Noise as an Entanglement Meter*, Phys. Rev. Lett. **102** (2009) 100502.

[67] H. F. Song, C. Flindt, S. Rachel, I. Klich and K. Le Hur, *Entanglement entropy from charge statistics: Exact relations for noninteracting many-body systems,* Phys. Rev. B **83** (2011) 161408.

[68] H. F. Song, S. Rachel, C. Flindt, I. Klich, N. Laflorencie and K. Le Hur, *Bipartite fluctuations as a probe of many-body entanglement,* Phys. Rev. B **85** (2012) 035409.

[69] H. Häffner, W. Hänsel, C. F. Roos, J. Benhelm, D. Chek-al kar, M. Chwalla et al., *Scalable multiparticle entanglement of trapped ions,* Nature **438** (2005) 643.

[70] R. Blatt and D. Wineland, *Entangled states of trapped atomic ions,* Nature **453** (2008).

[71] M. Steffen, M. Ansmann, R. C. Bialczak, N. Katz, E. Lucero, R. McDermott et al., *Measurement of the Entanglement of Two Superconducting Qubits via State Tomography,* Science **313** (2006) 1423.

[72] C. Song, K. Xu, W. Liu, C.-P. Yang, S.-B. Zheng, H. Deng et al., *10-Qubit Entanglement and Parallel Logic Operations with a Superconducting Circuit*, Phys. Rev. Lett. **119** (2017) 180511.

[73] A. K. Ekert, C. M. Alves, D. K. L. Oi, M. Horodecki, P. Horodecki and L. C. Kwek, *Direct Estimations of Linear and Nonlinear Functionals of a Quantum State,* Phys. Rev. Lett. **88** (2002) 217901.

[74] J. Cardy, *Measuring Entanglement Using Quantum Quenches,* Phys. Rev. Lett. **106** (2011) 150404.

[75] D. A. Abanin and E. Demler, *Measuring Entanglement Entropy of a Generic Many-Body System with a Quantum Switch,* Phys. Rev. Lett. **109** (2012) 020504.

[76] C. Moura Alves and D. Jaksch, *Multipartite Entanglement Detection in Bosons,* Phys. Rev. Lett. **93** (2004) 110501.

[77] A. J. Daley, H. Pichler, J. Schachenmayer and P. Zoller, *Measuring Entanglement Growth in Quench Dynamics of Bosons in an Optical Lattice,* Phys. Rev. Lett. **109** (2012) 020505.

[78] H. Pichler, L. Bonnes, A. J. Daley, A. M. Läuchli and P. Zoller, *Thermal versus entanglement entropy: a measurement protocol for fermionic atoms with a quantum gas microscope,* New J. Phys. **15** (2013) 063003.

[79] A. M. Kaufman, M. E. Tai, A. Lukin, M. Rispoli, R. Schittko, P. M. Preiss, and M. Greiner, *Quantum thermalisation through entanglement in an isolated many-body system*, Science **353**, 794 (2016).

[80] T. Brydges, A. Elben, P. Jurcevic, B. Vermersch, C. Maier, B. P. Lanyon, P. Zoller, R. Blatt, and C. F. Roos, *Probing entanglement entropy via randomized measurements*, Science **364**, 260 (2019).

[81] A. Lukin, M. Rispoli, R. Schittko, M. E. Tai, A. M. Kaufman, S. Choi, V. Khemani, J. Leonard, and M. Greiner, *Probing entanglement in a many-body localized system*, Science **364**, 6437 (2019).

[82] J. H. Bardarson, F. Pollmann, and J. E. Moore, *Unbounded growth of entanglement in models of many-body localization*, Phys. Rev. Lett. **109**, 017202 (2012).

[83] R. Vosk and E. Altman, *Dynamical Quantum Phase Transitions in Random Spin Chains*, Phys. Rev. Lett. **112**, 217204 (2014).

[84] M. Goldstein and E. Sela, *Symmetry-Resolved Entanglement in Many-Body Systems*, Phys. Rev. Lett. **120**, 200602 (2018).

[85] J. C. Xavier, F. C. Alcaraz, and G. Sierra, *Equipartition of the entanglement entropy*, Phys. Rev. B **98**, 041106 (2018).

[86] N. Laflorencie and S. Rachel, *Spin-resolved entanglement spectroscopy of critical spin chains and Luttinger liquids*, J. Stat. Mech. (2014) P11013.

[87] D. Azses, R. Haenel, Y. Naveh, R. Raussendorf, E. Sela, and E. G. Dalla Torre, *Identification of Symmetry-Protected Topological States on Noisy Quantum Computers*, Phys. Rev. Lett. **125**, 120502 (2020).

[88] A. Neven, J. Carrasco, V. Vitale, C. Kokail, A. Elben, M. Dalmonte, P. Calabrese, P. Zoller, B. Vermersch, R. Kueng, and B. Kraus, *Symmetry-resolved entanglement detection using partial transpose moments*, Npj Quantum Inf. **7**, 152 (2021).

[89] V. Vitale, A. Elben, R. Kueng, A. Neven, J. Carrasco, B. Kraus, P. Zoller, P. Calabrese, B. Vermersch, and M. Dalmonte, *Symmetry-resolved dynamical purification in synthetic quantum matter*, SciPost Phys. **12**, 106 (2022).

[90] R. Bonsignori, P. Ruggiero, and P. Calabrese, *Symmetry resolved entanglement in free fermionic systems*, J. Phys. A **52**, 475302 (2019).

[91] S. Fraenkel and M. Goldstein, *Symmetry resolved entanglement: Exact results in 1d and beyond*, J. Stat. Mech. (2020) 033106.

[92] N. Feldman and M. Goldstein, *Dynamics of Charge-Resolved Entanglement after a Local Quench*, Phys. Rev. B **100**, 235146 (2019).

[93] H. M. Wiseman and J. A. Vaccaro, *Entanglement of Indistinguishable Particles Shared between Two Parties*, Phys. Rev. Lett. **91**, 097902 (2003).

[94] H. Barghathi, C. M. Herdman, and A. Del Maestro, *Rényi Generalization of the Accessible Entanglement Entropy*, Phys. Rev. Lett. **121**, 150501 (2018).

[95] H. Barghathi, E. Casiano-Diaz, and A. Del Maestro, *Operationally accessible entanglement of one dimensional spinless fermions*, Phys. Rev. A **100**, 022324 (2019).

[96] H. Barghathi, J. Yu, and A. Del Maestro *Theory of noninteracting fermions and bosons in the canonical ensemble*, Phys. Rev. Res. **2**, 043206 (2020).

[97] M. T. Tan and S. Ryu, *Particle Number Fluctuations, Rényi and Symmetry-resolved Entanglement Entropy in Two-dimensional Fermi Gas from Multi-dimensional bosonisation*, Phys. Rev. B **101**, 235169 (2020).

[98] S. Murciano, G. Di Giulio, and P. Calabrese, *Symmetry resolved entanglement in gapped integrable systems: a corner transfer matrix approach*, SciPost Phys. **8**, 046 (2020).

[99] P. Calabrese, M. Collura, G. Di Giulio, and S. Murciano, *Full counting statistics in the gapped XXZ spin chain*, EPL **129**, 60007 (2020).

[100] S. Murciano, P. Ruggiero, and P. Calabrese, *Symmetry resolved entanglement in two-dimensional systems via dimensional reduction*, J. Stat. Mech. (2020) 083102.

[101] S. Murciano, R. Bonsignori, and P. Calabrese, *Symmetry decomposition of negativity of massless free fermions*, SciPost Phys. **10**, 111 (2021).

[102] F. Ares, S. Murciano, and P. Calabrese, *Symmetry-resolved entanglement in a long-range free-fermion chain*, arXiv:2202.05874.

[103] L. Capizzi, O.E. Castro-Alvaredo, C. De Fazio, M. Mazzoni and L. Santamaria-Sanz, *Symmetry Resolved Entanglement of Excited States in Quantum Field Theory I: Free Theories, Twist Fields and Qubits*, arXiv:2203.12556 (2022).

[104] L. Capizzi, C. De Fazio, M. Mazzoni, M. and L. Santamaria-Sanz and O.E. Castro-Alvaredo, *Symmetry Resolved Entanglement of Excited States in Quantum Field Theory II: Numerics, Interacting Theories and Higher Dimensions*, arXiv:2206.12223 (2022).

[105] Filiberto Ares, Pasquale Calabrese, Giuseppe Di Giulio, Sara Murciano, *Multi-charged moments of two intervals in conformal field theory* , JHEP **09** 051 (2022).

[106] S. Murciano, P. Calabrese and L. Piroli, *Symmetry-resolved Page curve*, Phys. Rev. D **106**, 046015 (2022).

[107] Z. Ma, C. Han, Y. Meir, and E. Sela, *Symmetric inseparability and number entanglement in charge conserving mixed states*, Phys. Rev. A **105**, 042416 (2022).

[108] N. G. Jones, *Symmetry-resolved entanglement entropy in critical free-fermion chains*, arXiv:2202.11728 [quant-ph].

[109] L. Piroli, E. Vernier, M. Collura, and P. Calabrese, *Thermodynamic symmetry resolved entanglement entropies in integrable systems*, arXiv:2203.09158.

[110] LP. H. C. Lau, T. Noumi, Y. Takii and K. Tamaoka, *Page curve and symmetries,* arXiv:2206.09633 (2022)

[111] S. Murciano, G. Di Giulio, and P. Calabrese, *Entanglement and symmetry resolution in two dimensional free quantum field theories*, JHEP **08** (2020) 073.

[112] D. X. Horvath, L. Capizzi, and P. Calabrese, *U(1) symmetry resolved entanglement in free 1+1 dimensional field theories via form factor bootstrap*, JHEP **05** (2021) 197.

[113] D. X. Horvath, P. Calabrese, and O. A. Castro-Alvaredo, *Branch Point Twist Field Form Factors in the sine-Gordon Model II: Composite Twist Fields and Symmetry Resolved Entanglement*, SciPost Phys. **12**, 088 (2022).

[114] D. X. Horvath and P. Calabrese, *Symmetry resolved entanglement in integrable field theories via form factor bootstrap*, JHEP **11** (2020) 131.

[115] L. Capizzi, D. X. Horvath, P. Calabrese, and O. A. Castro-Alvaredo, *Entanglement of the 3-State Potts Model via Form Factor Bootstrap: Total and Symmetry Resolved Entropies*, JHEP **05** (2022) 113.

[116] E. Cornfeld, M. Goldstein, and E. Sela, *Imbalance Entanglement: Symmetry Decomposition of Negativity*, Phys. Rev. A **98**, 032302 (2018).

[117] L. Capizzi, P. Ruggiero, and P. Calabrese, *Symmetry resolved entanglement entropy of excited states in a CFT*, J. Stat. Mech. 073101 (2020) 033106.

[118] H.-H. Chen, *Symmetry decomposition of relative entropies in conformal field theory*, JHEP **07** (2021) 084.

[119] L. Capizzi and P. Calabrese, *Symmetry resolved relative entropies and distances in conformal field theory*, JHEP **10** (2021) 195.

[120] L. Hung and G. Wong, *Entanglement branes and factorization in conformal field theory*, Phys. Rev. D **104**, 026012 (2021).

[121] P. Calabrese, J. Dubail, and S. Murciano, *Symmetry-resolved entanglement entropy in Wess-Zumino-Witten models*, JHEP **10** (2021) 067.

[122] R. Bonsignori and P. Calabrese, *Boundary effects on symmetry resolved entanglement*, J. Phys. A **54**, 015005 (2021).

[123] B. Estienne, Y. Ikhlef, and A. Morin-Duchesne, *Finite-size corrections in critical symmetry-resolved entanglement*, SciPost Phys. **10**, 054 (2021).

[124] H.-H. Chen, *Charged Rényi negativity of massless free bosons*, JHEP **02** (2022) 117.

[125] Z. Ma, C. Han, Y. Meir, and E. Sela, *Symmetric inseparability and number entanglement in charge-conserving mixed states*, Phys. Rev. A **105**, 042416 (2022).

[126] A. Milekhin and A. Tajdini, *Charge fluctuation entropy of Hawking radiation: a replica-free way to find large entropy*, arXiv:2109.03841.

[127] M. Ghasemi, *Universal Thermal Corrections to Symmetry-Resolved Entanglement Entropy and Full Counting Statistics*, 2203.06708.

[128] S. Zhao, C. Northe, and R. Meyer, *Symmetry-Resolved Entanglement in AdS_3/CFT_2 coupled to $U(1)$ Chern-Simons Theory*, JHEP **07** (2021) 030.

[129] K. Weisenberger, S. Zhao, C. Northe, and R. Meyer, *Symmetry-resolved entanglement for excited states and two entangling intervals in AdS_3/CFT_2*, JHEP **12** (2021) 104.

[130] S. Zhao, C. Northe, K. Weisenberger, and R. Meyer, *Charged Moments in W_3 Higher Spin Holography*, JHEP **05** (2022) 166.

[131] S. Baiguera, L. Bianchi, S. Chapman, and D. A. Galante, *Shape Deformations of Charged Rényi Entropies from Holography*, arXiv:2203.15028.

[132] G. Parez, R. Bonsignori, and P. Calabrese, *Quasiparticle dynamics of symmetry resolved entanglement after a quench: the examples of conformal field theories and free fermions*, Phys. Rev. B **103**, L041104 (2021).

[133] G. Parez, R. Bonsignori, and P. Calabrese, *Exact quench dynamics of symmetry resolved entanglement in a free fermion chain*, J.Stat.Mech. **2109** 093102 (2021).

[134] S. Fraenkel and M. Goldstein, *Entanglement Measures in a Nonequilibrium Steady State: Exact Results in One Dimension*, SciPost Phys. **11**, 085 (2021).

[135] G. Parez, R. Bonsignori, and P. Calabrese, *Dynamics of charge-imbalance-resolved entanglement negativity after a quench in a free-fermion mode*, J. Stat. Mech. (2022) 053103.

[136] S. Scopa and D. X. Horvath, *Exact hydrodynamic description of symmetry-resolved Rényi entropies after a quantum quench*, arXiv:2205.02924.

[137] H.-H. Chen, *Dynamics of charge imbalance resolved negativity after a global quench in free scalar field theory*, arXiv:2205.09532.

[138] X. Turkeshi, P. Ruggiero, V. Alba, and P. Calabrese, *Entanglement equipartition in critical random spin chains*, Phys. Rev. B **102**, 014455 (2020).

[139] M. Kiefer-Emmanouilidis, R. Unanyan, J. Sirker, and M. Fleischhauer, *Bounds on the entanglement entropy by the number entropy in non-interacting fermionic systems*, SciPost Phys **8**, 083 (2020).

[140] M. Kiefer-Emmanouilidis, R. Unanyan, J. Sirker, and M. Fleischhauer, *Evidence for unbounded growth of the number entropy in many-body localized phases*, Phys. Rev. Lett. **124**, 243601 (2020).

[141] M. Kiefer-Emmanouilidis, R. Unanyan, M. Fleischhauer, and J. Sirker, *Absence of true localization in many-body localized phases*, Phys. Rev. B **103**, 024203 (2021).

[142] E. Cornfeld, L. A. Landau, K. Shtengel, and E. Sela, *Entanglement spectroscopy of non-Abelian anyons: Reading off quantum dimensions of individual anyons*, Phys. Rev. B **99**, 115429 (2019).

[143] K. Monkman and J. Sirker, *Operational Entanglement of Symmetry-Protected Topological Edge States*, Phys. Rev. Res. **2**, 043191 (2020).

[144] D. Azses and E. Sela, *Symmetry resolved entanglement in symmetry protected topological phases*, Phys. Rev. B **102**, 235157 (2020).

[145] D. Azses, R. Haenel, Y. Naveh, R. Raussendorf, E. Sela, and E. G. Dalla Torre, *Identification of Symmetry-Protected Topological States on Noisy Quantum Computers*, Phys. Rev. Lett. **125**, 120502 (2020).

[146] D. Azses, E. G. Dalla Torre, and E. Sela, *Observing Floquet topological order by symmetry resolution*, Phys. Rev. B **104**, L220301 (2021).

[147] B. Oblak, N. Regnault, and B. Estienne, *Equipartition of Entanglement in Quantum Hall States*, Phys. Rev. B **105**, 115131 (2022).

[148] M. Kiefer-Emmanouilidis, R. Unanyan, M. Fleischhauer, and J. Sirker, *Slow delocalization of particles in many-body localized phases*, Phys. Rev. B **103**, 024203 (2021).

[149] Y. Zhao, D. Feng, Y. Hu, S. Guo, and J. Sirker, *Entanglement dynamics in the three-dimensional Anderson model*, Phys. Rev. B **102**, 195132 (2020).

[150] M. Kiefer-Emmanouilidis, R. Unanyan, M. Fleischhauer, and J. Sirker, *Unlimited growth of particle fluctuations in many-body localized phases*, Ann. Phys. 168481 (2021).

[151] P. Calabrese, J. Cardy, and E. Tonni, *Entanglement negativity in quantum field theory*, Phys. Rev. Lett. **109**, 130502 (2012).

[152] P. Calabrese, J. Cardy, and E. Tonni, *Entanglement negativity in extended systems: a quantum field theory approach*, J. Stat. Mech. (2013) P02008 .

[153] M. Ibanez Berganza, F. C. Alcaraz, and G. Sierra, *Entanglement of excited states in critical spin chains*, J. Stat. Mech. 01016 (2012).

[154] F. C. Alcaraz, M. Ibanez Berganza, and G. Sierra, *Entanglement of Low-Energy Excitations in Conformal Field Theory*, Phys. Rev. Lett. **106**, 201601 (2011).

[155] L. J. Dixon, D. Friedan, E. J. Martinec, and S. H. Shenker, *The Conformal Field Theory Of Orbifolds*, Nucl. Phys. B **282**, 13 (1987).

[156] J. L. Cardy, O. A. Castro-Alvaredo, and B. Doyon, *Form factors of branch-point twist fields in quantum integrable models and entanglement entropy*, J. Stat. Phys. **130**, 129 (2008).

[157] V. Knizhnik, *Analytic fields on riemann surfaces. II*, Comm. Math. Phys. **112**, 567 (1987).

[158] A. Belin, L.-Y. Hung, A. Maloney, S. Matsuura, R. C. Myers, and T. Sierens, *Holographic charged Rényi entropies*, JHEP **12** (2013) 059.

[159] P. Caputa, G. Mandal, and R. Sinha, *Dynamical entanglement entropy with angular momentum and $U(1)$ charge*, JHEP **11** (2013) 052.

[160] P. Caputa, M. Nozaki, and T. Numasawa, *Charged Entanglement Entropy of Local Operators*, Phys. Rev. D **93**, 105032 (2016).

[161] J. S. Dowker, *Conformal weights of charged Rényi entropy twist operators for free scalar fields in arbitrary dimensions*, J. Phys. A **49**, 145401 (2016).

[162] J. S. Dowker, *Charged Rényi entropies for free scalar fields*, J. Phys. A **50**, 165401 (2017).

[163] H. Shapourian, K. Shiozaki, and S. Ryu, *Partial time-reversal transformation and entanglement negativity in fermionic systems*, Phys. Rev. B **95**, 165101 (2017).

[164] H. Shapourian, P. Ruggiero, S. Ryu, and P. Calabrese, *Twisted and untwisted negativity spectrum of free fermions*, SciPost Phys. **7**, 037 (2019).

[165] H. Shapourian, K. Shiozaki, and S. Ryu, *Many-Body Topological Invariants for Fermionic Symmetry-Protected Topological Phases*, Phys. Rev. Lett. **118**, 216402 (2017).

[166] K. Shiozaki, H. Shapourian, and S. Ryu, *Many-body topological invariants in fermionic symmetry protected topological phases: Cases of point group symmetries*, Phys. Rev. B **95**, 205139 (2017).

[167] I. Peschel and M. C. Chung, *Density Matrices for a Chain of Oscillators*, J. Phys. A **32**, 8419 (1999).

[168] M. C. Chung and I. Peschel, *Density-matrix spectra of solvable fermionic systems,* Phys. Rev. B **64** (2001) 064412.

[169] I. Peschel, *Calculation of reduced density matrices from correlation functions*, J. Phys. A **36**, L205 (2003).

[170] M. C. Chung and I. Peschel, *Density-matrix spectra for two-dimensional quantum systems,* Phys. Rev. B **62** (2000) 4191.

[171] I. Peschel and V. Eisler, *Reduced density matrices and entanglement entropy in free lattice models*, J. Phys. A **42**, 504003 (2009).

[172] J. I. Latorre, E. Rico, and G. Vidal, *Ground state entanglement in quantum spin chains*, Quant. Inf. Comp. **4**, 048 (2004).

[173] V. Eisler and Z. Zimborás, *On the partial transpose of fermionic gaussian states,* New J. Phys., **117** 053048, (2015).

[174] M. Fagotti and P. Calabrese, *Entanglement entropy of two disjoint blocks in XY chains*, J. Stat. Mech. (2010) P04016.

[175] O. A. Castro-Alvaredo and B. Doyon, *Bi-partite entanglement entropy in massive 1+1-dimensional quantum field theories*, J. Phys. A **42**, 504006 (2009).

[176] H. Casini, C. D. Fosco, and M. Huerta, *Entanglement and alpha entropies for a massive Dirac field in two dimensions*, J. Stat. Mech. (2005) P07007.

[177] H. Casini and M. Huerta, *Entanglement and alpha entropies for a massive scalar field in two dimensions.* J. Stat. Mech. P12012 (2005).

[178] H. Casini and M. Huerta, *Entanglement entropy in free quantum field theory*, J. Phys. A **42**, 504007 (2009).

[179] R. J Baxter, *Exactly solved models in statistical mechanics*, Academic Press, San Diego (1982).

[180] I. Peschel, M. Kaulke, and O. Legeza, *Density-matrix spectra for integrable models*, Ann. Physik (Leipzig) **8**, 153 (1999).

[181] E. Ercolessi, S. Evangelisti, and F. Ravanini, *Exact entanglement entropy of the XYZ model and its sine-Gordon limit*, Phys. Lett. A **374**, 2101 (2010).

[182] P. Calabrese, J. Cardy, and I. Peschel, *Corrections to scaling for block entanglement in massive spin-chains*, J. Stat. Mech. P09003 (2010).

[183] A. B. Zamolodchikov, *Irreversibility of the Flux of the Renormalization Group in a 2-D Field Theory*, JETP Lett. **43**, 730 (1986).

[184] D. Bianchini O. Castro-Alvaredo, B. Doyon, E. Levi, and F. Ravanini, *Entanglement Entropy of Non Unitary Conformal Field Theory*, J. Phys. A **48**, 04FT01 (2014).

[185] R. Couvreur, J. L. Jacobsen, and H. Saleur, *Entanglement in nonunitary quantum critical spin chains*, Phys. Rev. Lett. **119**, 040601 (2017).

[186] S. N. Solodukhin, *Entanglement entropy, conformal invariance and extrinsic geometry*, Phys. Lett. B **665**, 305 (2008).

[187] S. N. Solodukhin, *Entanglement Entropy in Non-Relativistic Field Theories*, JHEP **04** (2010) 101.

[188] S. N. Solodukhin, *Entanglement entropy of round spheres*, Phys. Lett. B **693**, 605 (2010).

[189] H. Casini, M. Huerta and R. C. Myers, *Towards a derivation of holographic entanglement entropy*, JHEP **05** (2011) 036.

[190] H. Casini, M. Huerta, and J. Rosabal, *Remarks on entanglement entropy for gauge fields*, Phys. Rev. D **89**, 085012 (2014).

[191] C. P. Herzog, *Universal thermal corrections to entanglement entropy for conformal field theories on spheres*, JHEP **10** (2014) 028.

[192] L.-Y. Hung, R.C. Myers and M. Smolkin, *Twist operators in higher dimensions,* JHEP **10** (2014) 178.

[193] H. Casini, M. Huerta, L. Leitao, *Entanglement entropy for a Dirac fermion in three dimensions: vertex contribution*, Nucl. Phys. B **814**, 594 (2009).

[194] H. Casini, M. Huerta, *Universal terms for the entanglement entropy in 2+1 dimensions*, Nucl. Phys. B **764**, 183 (2007).

[195] C. P. Herzog, Tatsuma Nishioka *Entanglement Entropy of a Massive Fermion on a Torus*, JHEP **03** (2013) 077.

[196] S. N. Solodukhin *Entanglement entropy of black holes*, Living Rev. Relativity **14**, 8 (2011).

[197] T. Nishioka, *Entanglement entropy: holography and renormalization group*, Rev. Mod. Phys **90**, 035007 (2018).

[198] D. Bianchini and O. A. Castro-Alvaredo, *Branch Point Twist Field Correlators in the Massive Free Boson Theory*, Nucl. Phys. B **913**, 879 (2016).

[199] O. A. Castro-Alvaredo, *Massive Corrections to Entanglement in Minimal E8 Toda Field Theory*, SciPost Phys. **2**, 008 (2017).

[200] O. A. Castro-Alvaredo, M. Lencses, I. M. Szecsenyi, and J. Viti, *Entanglement Dynamics after a Quench in Ising Field Theory: A Branch Point Twist Field Approach*, JHEP **12** (2019) 79.

[201] E. Cornfeld and E. Sela, *Entanglement entropy and boundary renormalization group flow: Exact results in the Ising universality class*, Phys. Rev. B **96**, 075153 (2017).

[202] G. Mussardo, *Statistical field theory: an introduction to exactly solved models in statistical physics*, 2nd edition, Oxford University Press (2020).

[203] A. O. Gogolin, A. A. Nersesyan, and A. M. Tsvelik, *Bosonization and Strongly Correlated Systems*, Cambridge (1998).

[204] T. Giamarchi, *Quantum physics in one dimension*, Clarendon Press (2003).

P. Ruggiero, E. Tonni, and P. Calabrese, *Entanglement entropy of two disjoint intervals and the recursion formula for conformal blocks*, J. Stat. Mech. (2018) 113101.

[205] P. Calabrese, J. Cardy, and E. Tonni, *Finite temperature entanglement negativity in conformal field theory*, J. Phys. A **48**, 015006 (2015).

[206] P. Calabrese, J. Cardy, and E. Tonni, *Entanglement entropy of two disjoint intervals in conformal field theory*, J. Stat. Mech. (2009) P11001.

[207] M. A. Rajabpour and F. Gliozzi, *Entanglement entropy of two disjoint intervals from fusion algebra of twist fields*, J. Stat. Mech. P02016 (2012);

[208] M. Hoogeveen and B. Doyon, *Entanglement negativity and entropy in non-equilibrium conformal field theory*, Nucl. Phys. B **898**, 78 (2015).

[209] T. Dupic, B. Estienne, and Y. Ikhlef, *Entanglement entropies of minimal models from null-vectors*, SciPost Phys. **4**, 031 (2018).

[210] P. Calabrese, J. Cardy, and E. Tonni, *Entanglement entropy of two disjoint intervals in conformal field theory II*, J. Stat. Mech. (2011) P01021.

[211] M. Headrick, *Entanglement Renyi entropies in holographic theories*, Phys. Rev. D **82**, 126010 (2010).

[212] B. Chen and J. Zhang, *On short interval expansion of Rényi entropy*, JHEP **11** (2013) 164.

[213] B. Chen, J.-B. Wu, and J. Zhang, *Short interval expansion of Rényi entropy on torus*, JHEP **08** 130 (2016).

[214] A. Belavin, A. Polyakov, A. Zamolodchikov, *Infinite conformal symmetry in two-dimensional quantum field theory*, Nucl. Phys. B **241**, 333 (1984).

[215] E. Witten, *Nonabelian Bosonization in Two-Dimensions*, Commun. Math. Phys. **92**, 455 (1984).

[216] J. Wess and B. Zumino, *Consequences of anomalous Ward identities*, Phys. Lett. B **37**, 95 (1971).

[217] A. O. Gogolin, A. Nersesyan, and A. M. Tsvelik, *Bosonization and Strongly Correlated Systems*, Cambridge University Press (2004).

[218] A. M. Tsvelik, *Non Abelian bosonization and WZNW models*, AIP Conference Proceedings 580, 189 (2001).

[219] H. Casini, M. Huerta, and J. A. Rosabal, *Remarks on entanglement entropy for gauge fields*, Phys. Rev. D **89**, 085012 (2014).

[220] M-C. Banuls, K. Cichy, J. I. Cirac, K. Jansen, and S. Kühn, *Efficient Basis Formulation for (1+1)-Dimensional SU(2) Lattice Gauge Theory: Spectral calculations with matrix product states,* Phys. Rev. X **7**, 041046 (2017).

[221] S. Ghosh, R. M. Soni, and S. P. Trivedi, *On The Entanglement Entropy For Gauge Theories,* JHEP **09** 069 (2015) .

[222] R. M. Soni and S. P. Trivedi, *Aspects of Entanglement Entropy for Gauge Theories,* JHEP **01** 136 (2016) .

[223] K. V. Acoleyen, N. Bultinck, J. Haegeman, M. Marien, V. B. Scholz, and F. Verstraete, *The entanglement of distillation for gauge theories,* Phys. Rev. Lett. **117**, 131602 (2016).

[224] S. Aoki, N. Iizuka, K. Tamaoka, and T. Yokoya, *Entanglement Entropy for 2D Gauge Theories with Matters*, Phys. Rev. D **96**, 045020 (2017).

[225] E. Fradkin, *Field Theories of Condensed Matter Physics*, Cambridge University Press (2013).

[226] E. Meckes, *The Random Matrix Theory of the Classical Compact Groups*, Cambridge University Press (2019).

[227] H. Reinhardt, *Emergence of the Haar measure in the standard functional integral representation of the Yang-Mills partition function*, Mod. Phys. Lett. A **11**, 2451 (1996).

[228] Harish-Chandra, *The Plancherel formula for complex semisimple Lie groups*, Trans. Amer. Math. Soc. **76**, 485 (1954).

[229] M. Vergne, *A Poisson-Plancherel formula for semi-simple Lie groups*, Annals of Mathematics **115**, 639 (1982).

[230] H. D. Fegan, *The heat equation on a compact Lie group*, Trans. Amer. Math. Soc. 246, (1978).

[231] I. Affleck, *Exact critical exponents for quantum spin chains, non-linear σ-models at $\theta = \pi$ and the quantum Hall effect*, Nucl. Phys. B **265**, 409 (1986).

[232] I. Affleck, *Critical behavior of two-dimensional systems with continuous symmetries*, Phys. Rev. Lett. **55**, 1355 (1985).

[233] I. Affleck and F. D. M. Haldane, *Critical theory of quantum spin chains*, Phys. Rev. B **36**, 464 (1987).

[234] F. D. M. Haldane, *Exact Jastrow-Gutzwiller resonating-valence-bond ground state of the spin-1/2 antiferromagnetic Heisenberg chain with* $1/r^2$ *exchange,* Phys. Rev. Lett. **60**, 635 (1988).

[235] B. S. Shastry, *Exact solution of an* $S = 1/2$ *Heisenberg antiferromagnetic chain with long-ranged interactions,* Phys. Rev. Lett. **60**, 639 (1988).

[236] C. Gils, E. Ardonne, S. Trebst, D. A. Huse, A. W. W. Ludwig, M. Troyer, Z. Wang, *Anyonic quantum spin chains: Spin-1 generalizations and topological stability,* Phys. Rev. B **87**, 235120 (2013).

[237] L. A. Takhtajan, *The picture of low-lying excitations in the isotropic Heisenberg chain of arbitrary spins,* Phys. Lett. A **87**, 479 (1982).

[238] H. M. Babudjan, *Exact solution of the one-dimensional isotropic Heisenberg chain with arbitrary spins S*, Phys. Lett. A **90**, 479 (1982).

[239] R. Bondesan, J. Dubail, A. Faribault and Y. Ikhlef, *Chiral* $SU(2)_k$ *currents as local operators in vertex models and spin chains,* J. Phys. A **48**, 065205 (2015).

[240] V. Kac, *Infinite dimensional Lie algebras* (Cambridge Univ. Press, 1995).

[241] I. G. Macdonald, *The Volume of a Compact Lie Group*, Inventiones mathematicae 56, (1980).

[242] J. Cardy and E. Tonni, *Entanglement hamiltonians in two-dimensional conformal field theory*, J. Stat. Mech. 123103 (2016) .

[243] J. J. Bisognano and E. H. Wichmann, *On the Duality Condition for a Hermitian Scalar Field*, J. Math. Phys. **16**, 985 (1975).

[244] J. J. Bisognano and E. H. Wichmann, *On the Duality Condition for Quantum Fields*, J. Math. Phys. **17**, 303 (1976).

[245] H. Casini, M. Huerta and R. Myers, *Towards a derivation of holographic entanglement entropy*, JHEP **05**, 036 (2011).

[246] V. Alba, P. Calabrese, and E. Tonni, *Entanglement spectrum degeneracy and Cardy formula in 1+1 dimensional conformal field theories*, J. Phys. A **51**, 024001 (2018).

[247] I. Affleck and A.W.W. Ludwig, *Universal non- integer ground state degeneracy in critical quantum systems*, Phys. Rev. Lett. **67**, 161 (1991).

[248] M. Caraglio and F. Gliozzi, *Entanglement entropy and twist fields*, JHEP **11** (2008) 076.

[249] S. Furukawa, V. Pasquier, and J. Shiraishi, *Mutual Information and Boson Radius in* $c = 1$ *Critical Systems in One Dimension*, Phys. Rev. Lett. **102**, 170602 (2009).

[250] P. Calabrese, L. Tagliacozzo, and E. Tonni, *Entanglement negativity in the critical Ising chain*, J. Stat. Mech. (2013) P05002.

[251] V. Alba, *Entanglement negativity and conformal field theory: a Monte Carlo study*, J. Stat. Mech. P05013 (2013).

[252] A. Coser, E. Tonni, and P. Calabrese, *Towards the entanglement negativity of two disjoint intervals for a one dimensional free fermion*, J. Stat. Mech. (2016) 033116.

[253] F. Ares, R. Santachiara, and J. Viti, *Crossing-symmetric Twist Field Correlators and Entanglement Negativity in Minimal CFTs*, JHEP **10** (2021) 175.

[254] G. Rockwood, *Replicated Entanglement Negativity for Disjoint Intervals in the Ising and Free Compact Boson Conformal Field Theories*, arXiv:2203.04339.

[255] T. Dupic, B. Estienne, and Y. Ikhlef, *Entanglement entropies of minimal models from null-vectors*, SciPost Phys. **4**, 031 (2018).

[256] H. Casini and M. Huerta, *Reduced density matrix and internal dynamics for multicomponent regions*, Class. Quant. Grav. **26**, 185005 (2009)

[257] V. Alba, L. Tagliacozzo, and P. Calabrese, *Entanglement entropy of two disjoint blocks in critical Ising models*, Phys. Rev. B **81**, 060411(R) (2010).

[258] V. Alba, L. Tagliacozzo, and P. Calabrese, *Entanglement entropy of two disjoint intervals in $c = 1$ theories*, J. Stat. Mech. (2011) P06012.

[259] M. Headrick, A. Lawrence, and M. Roberts, *Bose-Fermi duality and entanglement entropies*, J. Stat. Mech. (2013) P02022.

[260] A. Coser, L. Tagliacozzo, and E. Tonni, *On Rényi entropies of disjoint intervals in conformal field theory*, J. Stat. Mech. (2014) P01008.

[261] C. De Nobili, A. Coser, and E. Tonni, *Entanglement entropy and negativity of disjoint intervals in CFT: some numerical extrapolations*, J. Stat. Mech. (2015) P06021.

[262] A. Coser, E. Tonni, and P. Calabrese, *Spin structures and entanglement of two disjoint intervals in conformal field theories*, J. Stat. Mech. (2016) 053109.

[263] P. Ruggiero, E. Tonni, and P. Calabrese, *Entanglement entropy of two disjoint intervals and the recursion formula for conformal blocks*, J. Stat. Mech. (2018) 113101.

[264] A. Bastianello, *Rényi entanglement entropies for the compactified massless boson with open boundary conditions*, JHEP **10** (2019) 141.

[265] A. Bastianello, J. Dubail and J.M. Stéphan, *Entanglement entropies of inhomogeneous Luttinger liquids*, J. Phys. A: Math. Theor. **53**, 155001 (2020).

[266] T. Grava, A. P. Kels, and E. Tonni, *Entanglement of Two Disjoint Intervals in Conformal Field Theory and the 2D Coulomb Gas on a Lattice*, Phys. Rev. Lett. **127**, 141605 (2021).

[267] M. Gerbershagen, *Monodromy methods for torus conformal blocks and entanglement entropy at large central charge*, JHEP **08** (2021) 143.

[268] B.-Q. Jin and V. E. Korepin, *Quantum spin chain, Toeplitz determinants and Fisher-Hartwig conjecture*, J. Stat. Phys. **116**, 79 (2004).

[269] P. Di Francesco, P. Mathieu, and D. Senechal, *Conformal Field Theory*, Springer-Verlag, New York, (1997).

[270] J. D. Fay, *Theta functions on Riemann surfaces*, Springer Notes in Mathematics 352 (Springer, 1973).

[271] E. Verlinde and H. Verlinde, *Chiral Bosonization, Determinants and the String Partition Function*, Nucl. Phys. B, **288**, 357 (1987).

[272] S. Groha, F. H. L. Essler, and P. Calabrese, *Full Counting Statistics in the Transverse Field Ising Chain*, SciPost Phys. **4**, 043 (2018).

[273] V. Enolskii and T. Grava, *Singular $\mathbb{Z}_N$ curves, Riemann-Hilbert problem and modular solutions of the Schlesinger equation*, Int. Math. Res. Not. **32**, 1619 (2004).

[274] V. Enolskii and T. Grava, *Thomae type formulae for singular $\mathbb{Z}_N$ curves*, Lett. Math. Phys. **76**, 187 (2006).

[275] S. Murciano, P. Calabrese, and R. M. Konik, *Generalized entanglement entropies in two-dimensional conformal field theory*, JHEP **05**, 152 (2022).

[276] V. Alba, M. Fagotti, and P. Calabrese, *Entanglement entropy of excited states*, J. Stat. Mech. 10020 (2009).

[277] J. Zhang and M.A. Rajabpour, *Excited state Rényi entropy and subsystem distance in two-dimensional non-compact bosonic theory. Part I. Single-particle states*, JHEP **12**, 160 (2020).

[278] J. Zhang and M.A. Rajabpour, *Universal Rényi Entropy of Quasiparticle Excitations*, J. Stat. Mech. 093101 (2021).

[279] J. Zhang and M. A. Rajabpour, *Excited state Rényi entropy and subsystem distance in two-dimensional non-compact bosonic theory I. Single-particle states*, JHEP **12**, 160 (2020).

[280] J. Zhang and M. A. Rajabpour, *Excited state Rényi entropy and subsystem distance in two-dimensional non-compact bosonic theory II. Multi-particle states*, JHEP **08**, 106 (2021).

[281] J. Zhang and M. A. Rajabpour, *Entanglement of magnon excitations in spin chains*, arXiv:2109.12826.

[282] B. Chen, W.-Z. Guo, S. He, and J. Wu, *Entanglement entropy for descendent local operators in 2D CFTs*, JHEP **10**, 173 (2015).

[283] L. Taddia, F. Ortolani, and T. Pálmai, *Rényi entanglement entropies of descendant states in critical systems with boundaries: conformal field theory and spin chains*, J. Stat. Mech. 093104 (2016).

[284] T. Pálmai, *Entanglement Entropy from the Truncated Conformal Space*, Phys. Lett. B **759**, 439 (2016).

[285] T. Pálmai, *Excited state entanglement in one dimensional quantum critical systems: extensivity and the role of microscopic details*, Phys. Rev. B **90**, 161404 (2014).

[286] F. H. L. Essler, A. M. Läuchli, and P. Calabrese, *Shell-Filling Effect in the Entanglement Entropies of Spinful Fermions*, Phys. Rev. Lett. **110**, 115701 (2013).

[287] P. Calabrese, F. Essler, and A. Läuchli, *Entanglement entropies of the quarter filled Hubbard model*, J. Stat. Mech. 09025 (2014).

[288] Q. Miao, T. Barthel, *Eigenstate Entanglement: Crossover from the Ground State to Volume Laws,* Phys. Rev. Lett. **127**, 040603 (2021)

[289] T. Barthel, Q. Miao, *Scaling functions for eigenstate entanglement crossovers in harmonic lattices,* Phys. Rev. A **104**, 022414 (2021).

[290] Q. Miao, T. Barthel, *Eigenstate entanglement scaling for critical interacting spin chains,* Quantum **6**, 642 (2022)

[291] N. Lashkari, *Modular hamiltonian of excites states in conformal field theory*, Phys. Rev. Lett. **117**, 041601 (2016).

[292] N. Lashkari, *Relative entropies in conformal field theory*, Phys. Rev. Lett. **113**, 051602 (2014).

[293] H. Casini, E. Testé, and G. Torroba, *Relative entropy and the RG flow*, JHEP **03**, 08 (2017).

[294] H. Casini, I. S. Landea, and G. Torroba, *The g-theorem and quantum information theory*, JHEP **10**, 140 (2016).

[295] H. Casini, *Relative entropy and the Bekenstein bound*, Class. Quant. Grav. **25**, 205021 (2008).

[296] D. D. Blanco, H. Casini, L. Y. Hung, and R. Myers, *Relative Entropy and Holography.* JHEP **08**, 060 (2013).

[297] D. L. Jafferis, A. Lewkowycz, J. Maldacena, and S. J. Suh, *Relative entropy equals bulk relative entropy*, JHEP **06**, 004 (2016)

[298] G. Sarosi and T. Ugajin, *Relative entropy of excited states in two dimensional conformal field theories*, JHEP **07**, 114 (2016).

[299] T. Ugajin, *Mutual information of excited states and relative entropy of two disjoint subsystems in CFT*, JHEP **10**, 184 (2017).

[300] G. Sarosi and T. Ugajin, *Relative entropy of excited states in conformal field theories of arbitrary dimensions*, JHEP **02**, 060 (2017).

[301] R. Arias, D. Blanco, H. Casini, and M. Huerta, *Local temperatures and local terms in modular Hamiltonians*, Phys. Rev. D **95**, 065005 (2017).

[302] V. Balasubramanian, J. J. Heckman, and A. Maloney, *Relative Entropy and Proximity of Quantum Field Theories*, JHEP **05**, 104 (2015).

[303] P. Ruggiero and P. Calabrese, *Relative Entanglement Entropies in 1+1-dimensional conformal field theories*, JHEP **02**, 039 (2017).

[304] S. Murciano, P. Ruggiero, and P. Calabrese, *Entanglement and relative entropies for low-lying excited states in inhomogeneous one-dimensional quantum systems,* J. Stat. Mech. 034001 (2019).

[305] A. J. A. James, R. M. Konik, P. Lecheminant, N. J. Robinson, and A. M. Tsvelik, *Non-perturbative methodologies for low-dimensional strongly-correlated systems: From non-Abelian bosonization to truncated spectrum methods* Rep. Progr. Phys. **81**, 046002 (2018).

[306] V. Vedral, *The role of relative entropy in quantum information theory*, Rev. Mod. Phys. **74**, 197 (2002).

[307] K. M. R. Audenaert and J. Eisert, *Continuity bounds on the quantum relative entropy*, J. Math. Phys. **46**, 102104 (2005).

[308] J. Zhang, P. Ruggiero, and P. Calabrese, *Subsystem Trace Distance in Quantum Field Theory*, Phys. Rev. Lett. **122**, 141602 (2019).

[309] J. Zhang, P. Ruggiero, and P. Calabrese, *Subsystem trace distance in low-lying states of* $(1+1)$*-dimensional conformal field theories*, JHEP **10**, 181 (2019).

[310] J. Zhang and P. Calabrese, *Subsystem distance after a local operator quench*, JHEP **02**, 056 (2020).

[311] Y. Nakataa, T. Takayanagia, Y. Takia, K. Tamaoka and Z. Weia, *Holographic Pseudo Entropy*, Phys. Rev. D **103**, 026005 (2021).

[312] A. Mollabashi, N. Shiba, T. Takayanagi, K. Tamaoka, Z. Weia, *Pseudo-Entropy in Free Quantum Field Theories*, Phys. Rev. Lett. **126**, 081601 (2021).

[313] V. P. Yurov and A. B. Zamolodchikov, *Truncated conformal space approach to scaling Lee-Yang model,* Int. J. Mod. Phys. A **05**, 3221 (1990).

[314] V. P. Yurov and A. B. Zamolodchikov, *Truncated fermionic space approach to the critical 2-D Ising model with magnetic field,* Int. J. Mod. Phys. A **06**, 4557 (1991).

[315] S. Murciano, P. Calabrese, and R. M. Konik, *Post-Quantum Quench Growth of Renyi Entropies in Low Dimensional Continuum Bosonic Systems*, Phys. Rev. Lett. **129**, 106802 (2022).

[316] A. Elben, B. Vermersch, M. Dalmonte,I. Cirac and P. Zoller, *Rényi Entropies from Random Quenches in Atomic Hubbard and Spin Models*, Phys. Rev. Lett. **120**, 050406 (2018)

[317] U. Schollwöck, *The density-matrix renormalization group in the age of matrix product states,* Ann. Phys. **326**, 96, (2011).

[318] G. Vidal, *Classical simulation of infinite-size quantum lattice systems in one spatial dimension,* Phys. Rev. Lett. **98**, 070201 (2007).

[319] U. Schollwöck A. J Daley, C. Kollath and G Vidal, *Time-dependent density-matrix renormalization-group using adaptive effective hilbert spaces,* J. Stat. Mech. P0404005 (2004).

[320] S. R. White and A. E. Feiguin, *Real-time evolution using the density matrix renormalization group,* Phys. Rev. Lett. **93** 076401, (2004).

[321] F. Verstraete and J. I. Cirac, *Continuous matrix product states for quantum fields,* Phys. Rev. Lett., **104** 190405, (2010).

[322] J. Haegeman, J. I. Cirac, T. J. Osborne, and F. Verstraete, *Calculus of continuous matrix product states,* Phys. Rev. B, **88** 085118, (2013).

[323] A. Tilloy and J. I. Cirac, *Continuous tensor network states for quantum fields,* Phys. Rev. X **9** 021040 (2019).

[324] J. Voit, *One-dimensional fermi liquids,* Rep. Progr. Phys., **58** 977, (1995).

[325] A. M. Tsvelik, *Quantum Field Theory in Condensed Matter Physics,* Cambridge University Press, 2 edition, (2003).

[326] D. Laroche, G. Gervais, M. P. Lilly, and J. L. Reno, *1d-1d coulomb drag signature of a luttinger liquid,* Science, **343** 631, (2014).

[327] S. Wang, S. Zhao, Z. Shi, F. Wu, Z. Zhao, L. Jiang, K. Watanabe, T. Taniguchi, A. Zettl, C. Zhou and F. Wang, *Nonlinear luttinger liquid plasmons in semiconducting single-walled carbon nanotubes*, Nature Mat., **19** 986, (2020).

[328] J.-S. Caux and P. Calabrese, *Dynamical density-density correlations in the one-dimensional bose gas,* Phys. Rev. A, **74** 031605, (2006).

[329] A. H. van Amerongen, J. J. P. van Es, P. Wicke, K. V. Kheruntsyan, and N. J. van Druten, *Yang-yang thermodynamics on an atom chip,* Phys. Rev. Lett., **100** 090402, (2008).

[330] B.Lake, A. M. Tsvelik, S. Notbohm, D. A. Tennant, T. G. Perring, M. Reehuis, C. Sekar, G. Krabbes, and B. Büchner, *Confinement of fractional quantum number particles in a condensed-matter system,* Nature Phys., **6** 50, (2009).

[331] D. Hirobe, M. Sato, T. Kawamata, Y. Shiomi, K. I. Uchida, R. Iguchi, Y. Koike, S. Maekawa, and E. Saitoh, *One-dimensional spinon spin currents,* Nature Phys., **13** 30, (2016).

[332] X. Dong, *The gravity dual of Rényi entropy,* Nature Comm., **7** 12472, (2016).

[333] M. Ohya and P. Denes, *Quantum Entropy and Its Use*, Springer, (2004).

[334] H. Araki, *Relative Entropy of States of Von Neumann Algebras,* Publ. Res. Inst. Math. Sci. Kyoto, **1976** 809, (1976).

[335] H. Li and F. D. M. Haldane, *Entanglement spectrum as a generalization of entanglement entropy: Identification of topological order in non-abelian fractional quantum hall effect states,* Phys. Rev. Lett., **101** 010504, (2008).

[336] O. A. Castro-Alvaredo and D. X. Horvath, *Branch Point Twist Field Form Factors in the sine-Gordon Model I: Breather Fusion and Entanglement Dynamics,* SciPost Phys., **10** 132, (2021).

[337] AL. B. Zamolodchikov, *Mass scale in the sine-Gordon and its reductions,* Int. J. Mod. Phys. A, **10** 1125, (1995).

[338] M. Kollar, F. A. Wolf, and M. Eckstein, *Generalized gibbs ensemble prediction of prethermalization plateaus and their relation to nonthermal steady states in integrable systems,* Phys. Rev. B, **84** 054304, (2011).

[339] M. Fagotti and P. Calabrese, *Evolution of entanglement entropy following a quantum quench: Analytic results for the xy chain in a transverse magnetic field,* Phys. Rev. A, **78** 010306, (2008).

[340] F. Ravanini, R. Tateo, and A. Valleriani, *Dynkin TBAs,* Int. J. Mod. Phys. A, **8** 1707, (1993).

[341] T. R. Klassen and E. Melzer, *Purely elastic scattering theories and their ultraviolet limits,* Nucl. Phys. B, **338** 485, (1990).

[342] G. Delfino, *Quantum quenches with integrable pre-quench dynamics,* J. Phys. A, **47** 402001, (2014).

[343] M. Kormos, M. Collura, G. Takács, and P. Calabrese, *Real-time confinement following a quantum quench to a non-integrable model,* Nature Phys., **13** 246, (2016).

[344] M. Pigneur, T. Berrada, M. Bonneau, T. Schumm, E.e Demler, and J. Schmiedmayer, *Relaxation to a phase-locked equilibrium state in a one-dimensional bosonic josephson junction,* Phys. Rev. Lett., **120** 173601, (2018).

[345] E. G. Dalla Torre, E. Demler, and A. Polkovnikov, *Universal rephasing dynamics after a quantum quench via sudden coupling of two initially independent condensates,* Phys. Rev. Lett., **110** 090404, (2013).

[346] D. X. Horváth, I. Lovas, M. Kormos, G. Takács, and G. Zaránd, *Nonequilibrium time evolution and rephasing in the quantum sine-gordon model,* Phys. Rev. A, **100** 013613, (2019).

[347] V. Alba and P. Calabrese, *Quench action and Rényi entropies in integrable systems,* Phys. Rev. B, **96** 115421, (2017).

[348] V. Alba and P. Calabrese, *Rényi entropies after releasing the néel state in the xxz spin-chain,* J. Stat. Mech., P113105, (2017).

[349] M. Mestyán, V. Alba, and P. Calabrese, *Rényi entropies of generic thermodynamic macrostates in integrable systems,* J. Stat. Mech., P083104, (2018).

[350] K. Klobas and B.Bertini, *Exact relaxation to gibbs and non-equilibrium steady states in the quantum cellular automaton rule 54*, SciPost Phys., **11** 106, (2021).

[351] I. Peschel, *On the entanglement entropy for a XY spin chain*, J. Stat. Mech. (2004) P12005.

[352] R. Weston, The Entanglement Entropy of Solvable Lattice Models, J. Stat. Mech. L03002 (2006).

[353] E. Ercolessi, S. Evangelisti, and F. Ravanini, *Exact entanglement entropy of the XYZ model and its sine-Gordon limit*, Phys. Lett. A **374**, 2101 (2010).

[354] E. Ercolessi, S. Evangelisti, F. Franchini, and F. Ravanini, *Essential singularity in the Renyi entanglement entropy of the one-dimensional XYZ spin-1/2 chain*, Phys. Rev. B **83**, 012402 (2011);
E. Ercolessi, S. Evangelisti, F. Franchini, and F. Ravanini, *Correlation Length and Unusual Corrections to the Entanglement Entropy*, Phys. Rev. B **85**, 115428 (2012);
E. Ercolessi, S. Evangelisti, F. Franchini, and F. Ravanini, *Modular invariance in the gapped XYZ spin-1/2 chain*, Phys. Rev. B **88**, 104418 (2013).

[355] A. De Luca and F. Franchini, *Approaching the RSOS critical points through entanglement: one model for many universalities*, Phys. Rev. B **87**, 045118 (2013).

[356] D. Bianchini and F. Ravanini, *Entanglement Entropy from Corner Transfer Matrix in Forrester Baxter non-unitary RSOS models*, J. Phys. A **49**, 154005 (2016).

[357] G. B. Mbeng, V. Alba, and P. Calabrese, *Negativity spectrum in 1D gapped phases of matter*, J. Phys. A **50**, 194001 (2017).

[358] E. Levi, O. A. Castro-Alvaredo, and B. Doyon, *Universal corrections to the entanglement entropy in gapped quantum spin chains: a numerical study*, Phys. Rev. B **88**, 094439 (2013)

[359] H. Itoyama and H. B. Thacker, *Lattice Virasoro algebra and corner transfer matrices in the Baxter eight-vertex model*, Phys. Rev. Lett. **58**, 1395 (1987).

[360] T. Nishino, *Density Matrix Renormalization Group Method for 2D Classical Models*, J. Phys. Soc. Jpn. **74**, 3598 (1995).

[361] T. Nishino and K. Okunishi, *Density Matrix and Renormalization for Classical Lattice Models*, Lect. Notes Phys. **478**, 167 (1997).

[362] P. Calabrese and A. Lefevre, *Entanglement spectrum in one-dimensional systems*, Phys. Rev A **78**, 032329 (2008).

[363] I. Peschel and T. T. Truong, *Corner Transfer Matrices for the Gaussian Model*, Ann. Physik (Leipzig) **48**, 185 (1991).

[364] V. Alba, M. Haque, and A. M. Läuchli, *Boundary-Locality and Perturbative Structure of Entanglement Spectra in Gapped Systems*, Phys. Rev. Lett. **108**, 227201 (2012).

[365] V. Alba, M. Haque, and A. M. Läuchli, *Entanglement spectrum of the Heisenberg XXZ chain near the ferromagnetic point*, J. Stat. Mech., P08011 (2012).

[366] I. Peschel, *Entanglement in solvable many-particle models*, Braz. J. Phys. **42**, 267 (2012).

[367] C. Ferreira and J.L. López, *Asymptotic expansions of the Hurwitz-Lerch zeta function*, J. Math. Anal. App. **298**, 210 (2004).

[368] E. T. Whittaker and G. N. Watson, *A course of modern analysis*, 4 ed., Cambridge Mathematical Library, Cambridge University Press, 1996.

[369] A. Botero and B. Reznik, *Spatial structures and localization of vacuum entanglement in the linear harmonic chain*, Phys. Rev. A **70**, 052329 (2004).

[370] A. Holevo, M. Sohma, and O. Hirota, *Capacity of quantum Gaussian channels*, Phys. Rev. A **59**, 1820 (1999).

[371] A. Holevo, *Probabilistic and Statistical Aspects of Quantum Theory*, Publications of the Scuola Normale Superiore (2011).

[372] H. Boos, M. Jimbo, T. Miwa, F. Smirnov, and Y. Takeyama, *Density matrix of a finite sub-chain of the Heisenberg anti-ferromagnet*, Lett. Math. Phys. **75**, 201 (2006).

[373] J. Sato, M. Shiroishi, and M. Takahashi, *Exact evaluation of density matrix elements for the Heisenberg chain*, J. Stat. Mech. P12017 (2006).

[374] J. Sato and M. Shiroishi, *Density matrix elements and entanglement entropy for the spin-1/2 XXZ chain at* $\Delta = 1/2$, J. Phys. A **40**, 8739 (2007)

[375] B. Nienhuis, M. Campostrini, and P. Calabrese, *Entanglement, combinatorics and finite-size effects in spin-chains*, J. Stat. Mech. (2009) P02063.

[376] V. Alba, M. Fagotti, and P. Calabrese, *Entanglement entropy of excited states*, J. Stat. Mech. P10020 (2009).

[377] H. Katsura and I. Maruyama, *Derivation of Matrix Product Ansatz for the Heisenberg Chain from Algebraic Bethe Ansatz*, J. Phys. A **43**, 175003 (2010).

[378] T. Miwa and F. Smirnov, *New exact results on density matrix for XXX spin chain*, Lett. Math. Phys. **109**, 698 (2019).

[379] F. Smirnov, *Exact density matrix for quantum group invariant sector of XXZ model*, arXiv:1804.08974.

[380] F. Gohmann, *Statistical mechanics of integrable quantum spin systems*, arXiv:1909.09967.

[381] V. Alba, M. Haque, and A. M. Laeuchli, *Entanglement spectrum of the two dimensional Bose-Hubbard model*, Phys. Rev. Lett. **110**, 260403 (2013).

[382] S. Wald, R. Arias, and V. Alba, *Entanglement and classical fluctuations at finite-temperature critical points*, arXiv:1911.02575.

[383] S. Hofferberth, I. Lesanovsky, T. Schumm, A. Imambekov, V. Gritsev, E. Demler, and J. Schmiedmayer, *Probing quantum and thermal noise in an interacting many-body system*, Nature Phys. **4**, 489 (2008).

[384] T. Kitagawa, S. Pielawa, A. Imambekov, J. Schmiedmayer, V. Gritsev, and E. Demler, *Ramsey Interference in One-Dimensional Systems: The Full Distribution Function of Fringe Contrast as a Probe of Many-Body Dynamics*, Phys. Rev. Lett. **104**, 255302 (2010).

[385] T. Kitagawa, A. Imambekov, J. Schmiedmayer, and E. Demler, *The dynamics and prethermalization of one-dimensional quantum systems probed through the full distributions of quantum noise*, New J. Phys. **13**, 73018 (2011).

[386] M. Gring, M. Kuhnert, T. Langen, T. Kitagawa, B. Rauer, M. Schreitl, I. Mazets, D. A. Smith, E. Demler, and J. Schmiedmayer, *Relaxation and Prethermalization in an Isolated Quantum System*, Science **337**, 1318 (2012).

[387] J. Armijo, T. Jacqmin, K. V. Kheruntsyan, and I. Bouchoule, *Probing Three-Body Correlations in a Quantum Gas Using the Measurement of the Third Moment of Density Fluctuations*, Phys. Rev. Lett. **105**, 230402 (2010).

[388] T. Jacqmin, J. Armijo, T. Berrada, K. V. Kheruntsyan, and I. Bouchoule, *Sub-Poissonian Fluctuations in a 1D Bose Gas: From the Quantum Quasicondensate to the Strongly Interacting Regime*, Phys. Rev. Lett. **106**, 230405 (2011).

[389] I. Klich and L. Levitov, *Many-Body Entanglement: a New Application of the Full Counting Statistics*, Adv. Theor. Phys. **1134**, 36 (2009).

[390] B. Hsu, E. Grosfeld, and E. Fradkin, *Quantum noise and entanglement generated by a local quantum quench*, Phys. Rev. B **80**, 235412 (2009).

[391] P. Calabrese, M. Mintchev and E. Vicari, *Exact relations between particle fluctuations and entanglement in Fermi gases*, EPL **98**, 20003 (2012).

[392] G. C. Levine, M. J. Bantegui, and J. A. Burg, *Full counting statistics in a disordered free fermion system*, Phys. Rev. B **86**, 174202 (2012).

[393] R. Susstrunk and D. A. Ivanov, *Free fermions on a line: Asymptotics of the entanglement entropy and entanglement spectrum from full counting statistics*, EPL **100**, 60009 (2012).

[394] P. Calabrese, P. Le Doussal, and S. N. Majumdar, *Random matrices and entanglement entropy of trapped Fermi gases*, Phys. Rev. A **91**, 012303 (2015).

[395] Y. Utsumi, *Full counting statistics of information content*, Eur. Phys. J. Spec. Top. 227, 1911 (2019).

[396] R. W. Cherng and E. Demler, *Quantum Noise Analysis of Spin Systems Realized with Cold Atoms*, New J. Phys. **9**, 7 (2007).

[397] M. Bortz, J. Sato, and M. Shiroishi M, *String correlation functions of the spin-1/2 Heisenberg XXZ chain*, J. Phys. A **40**, 4253 (2007).

[398] D. B. Abraham, F. H. L. Essler, and A. Maciolek, *Effective Forces Induced by a Fluctuating Interface: Exact Results*, Phys. Rev. Lett. **98**, 170602 (2007).

[399] A. Lamacraft and P. Fendley, *Order Parameter Statistics in the Critical Quantum Ising Chain*, Phys. Rev. Lett. **100**, 165706 (2008).

[400] D. A. Ivanov and A. G. Abanov, *Characterizing correlations with full counting statistics: Classical Ising and quantum XY spin chains*, Phys. Rev. E **87**, 022114 (2013).

[401] Y. Shi and I. Klich, *Full counting statistics and the Edgeworth series for matrix product states*, J. Stat. Mech. (2013) P05001.

[402] V. Eisler, *Universality in the Full Counting Statistics of Trapped Fermions*, Phys. Rev. Lett. 111, 080402 (2013).

[403] I. Klich, *A note on the Full Counting Statistics of paired fermions*, J. Stat. Mech. (2014) P11006.

[404] M. Moreno-Cardoner, J. F. Sherson and G. De Chiara, *Non-Gaussian distribution of collective operators in quantum spin chains*, New J. Phys. **18**, 103015 (2016).

[405] J.-M. Stéphan and F. Pollmann, *Full counting statistics in the Haldane-Shastry chain*, Phys. Rev. B **95**, 035119 (2017).

[406] M. Collura, F. H. L. Essler, and S. Groha, *Full counting statistics in the spin-1/2 Heisenberg XXZ chain*, J. Phys. A **50**, 414002 (2017).

[407] K. Najafi and M. A. Rajabpour, *Full counting statistics of the subsystem energy for free fermions and quantum spin chains*, Phys. Rev. B **96**, 235109 (2017).

[408] S. Humeniuk and H. P. Büchler, *Full Counting Statistics for Interacting Fermions with Determinantal Quantum Monte Carlo Simulations*, Phys. Rev. Lett. **119**, 236401 (2017).

[409] A. Bastianello, L. Piroli, and P. Calabrese, *Exact local correlations and full counting statistics for arbitrary states of the one-dimensional interacting Bose gas*, Phys. Rev. Lett. **120**, 190601 (2018).

[410] A. Bastianello and L. Piroli, *From the sinh-Gordon field theory to the one-dimensional Bose gas: exact local correlations and full counting statistics*, J. Stat. Mech. (2018) 113104.

[411] G. Perfetto, L. Piroli, and Andrea Gambassi, *Quench action and large deviations: Work statistics in the one-dimensional Bose gas*, Phys. Rev. E **100**, 032114 (2019).

[412] G. Del Vecchio Del Vecchio, A. Bastianello, A. De Luca, G. Mussardo, *Exact out-of-equilibrium steady states in the semiclassical limit of the interacting Bose gas*, SciPost Phys. **9** 002, (2020).

[413] V. Gritsev, E. Altman, E. Demler and A. Polkovnikov, *Full quantum distribution of contrast in interference experiments between interacting one-dimensional Bose liquids*, Nature Phys. **2**, 705 (2006).

[414] V. Eisler and Z. Racz, *Full Counting Statistics in a Propagating Quantum Front and Random Matrix Spectra*, Phys. Rev. Lett. **110**, 060602 (2013).

[415] I. Lovas, B. Dora, E. Demler, and G. Zarand, *Full counting statistics of time of flight images*, Phys. Rev. A **95**, 053621 (2017).

[416] M. Collura and F. H. L. Essler, *How order melts after quantum quenches*, Phys. Rev. B **101**, 041110 (2020).

[417] M. Collura, *Relaxation of the order-parameter statistics in the Ising quantum chain*, SciPost Phys. **7**, 072 (2019).

[418] M. Arzamasovs and D. M. Gangardt, *Full Counting Statistics and Large Deviations in a Thermal 1D Bose Gas*, Phys. Rev. Lett. **122**, 120401 (2019).

[419] M. N. Najafi and M. A. Rajabpour, *Formation probabilities and statistics of observables as defect problems in the free fermions and the quantum spin chains*, arXiv:1911.04595.

[420] M. Collura, A. De Luca, P. Calabrese, and J. Dubail, *Domain-wall melting in the spin-1/2 XXZ spin chain: emergent Luttinger liquid with fractal quasi-particle charge*, Phys. Rev. B **102** 180409(R), (2020).

[421] F. Ares, M. A. Rajabpour, J. Viti, *Exact full counting statistics for the staggered magnetization and the domain walls in the XY spin chain* Phys. Rev. E 103, 042107 (2021)

[422] G. Vidal, *Efficient simulation of one-dimensional quantum many-body systems*, Phys. Rev. Lett. **93**, 040502 (2004).

[423] T. Barthel, M.-C. Chung, and U. Schollwöck, *Entanglement scaling in critical two-dimensional fermionic and bosonic systems,* Phys. Rev. A **74**, 022329 (2006).

[424] D. Gioev and I. Klich, *Entanglement entropy of fermions in any dimension and the Widom conjecture,* Phys. Rev. Lett. **96**, 100503 (2006)

[425] M. M. Wolf, *Violation of the Entropic Area Law for Fermions*, Phys. Rev. Lett. **96**, 010404 (2006).

[426] W. Li, L. Ding, R. Yu, T. Roscilde, and S. Haas, *Scaling Behavior of Entanglement in Two- and Three-Dimensional Free Fermions,* Phys. Rev. B **74**, 073103 (2006).

[427] P. Calabrese, M. Mintchev, and E. Vicari. Entanglement entropies in free fermion gases for arbitrary dimension, EPL **97**, 20009 (2012).

[428] R. C. Helling, H. Leschke and W. L. Spitzer, *A special case of conjecture by Widom with implications to fermionic entanglement entropy*, Int. Math. Res. Not. **2011**, 1451 (2011).

[429] S. Farkas and Z. Zimboras, *The von Neumann entropy asymptotics in multidimensional fermionic systems*, J. Math. Phys. **48**, 102110 (2007).

[430] B. Swingle, *Renyi entropy, mutual information, and fluctuation properties of Fermi liquids*, Phys. Rev. B **86**, 045109 (2012).

[431] M. B. Plenio, J. Eisert, J. Dreissig, and M. Cramer, *Entropy, entanglement, and area: analytical results for harmonic lattice systems,* Phys. Rev. Lett. **94**, 060503 (2005).

[432] M. Cramer, J. Eisert, M. B. Plenio, and J. Dreissig, *An entanglement-area law for general bosonic harmonic lattice systems,* Phys. Rev. A **73**, 012309 (2006).

[433] M. Cramer, J. Eisert, and M.B. Plenio, *Statistics dependence of the entanglement entropy,* Phys. Rev. Lett. **98**, 220603 (2007)

[434] H. Ju, A. B. Kallin, P. Fendley, M. B. Hastings, and R. G. Melko, *Entanglement scaling in two-dimensional gapless systems*, Phys. Rev. B **85**, 165121 (2012).

[435] X. Chen, W. Witczak-Krempa, T. Faulkner, and E. Fradkin, *Two-cylinder entanglement entropy under a twist,* J. Stat. Mech. 043104 (2017).

[436] A. J. A. James and R. M. Konik, *Understanding the entanglement entropy and spectra of 2d quantum systems through arrays of coupled 1d chains*, Phys. Rev. B **87**, 241103 (R) (2013).

[437] F. Kolley, S. Depenbrock, I. P. McCulloch, U. Schollwöck, and V. Alba, *Entanglement spectroscopy of SU(2)-broken phases in two dimensions*, Phys. Rev. B **88**, 144426 (2013).

[438] J.-M. Stephan, H. Ju, P. Fendley, and R. G. Melko, *Entanglement in gapless resonating-valence-bond states*, New J. Phys. **15**, 015004 (2013).

[439] S. Inglis and R. G. Melko, *Entanglement at a two-dimensional quantum critical point: a $T = 0$ projector quantum Monte Carlo study*, New J. Phys. **15**, 073048 (2013).

[440] J. McMinis and N. M. Tubman, *Renyi entropy of the interacting Fermi liquid*, Phys. Rev. B **87**, 081108(R) (2013).

[441] J. E. Drut and W. J. Porter, *Hybrid Monte Carlo approach to the entanglement entropy of interacting fermions*, Phys. Rev. B **92**, 125126 (2015).

[442] M. A. Metlitski, C. A. Fuertes, and S. Sachdev, *Entanglement Entropy in the O(N) model*, Phys. Rev. B **80**, 115122 (2009).

[443] S. Whitsitt, W. Witczak-Krempa, and S. Sachdev, *Entanglement entropy of the large N Wilson-Fisher conformal field theory*, Phys. Rev. B **95**, 045148 (2017).

[444] W. Ding, A. Seidel, and K. Yang, *Entanglement Entropy of Fermi Liquids via Multidimensional Bosonization*, Phys. Rev. X **2**, 011012 (2012).

[445] P. Calabrese and F. H. L. Essler, *Universal corrections to scaling for block entanglement in spin-1/2 XX chains*, J. Stat. Mech. P08029 (2010).

[446] J. I. Latorre and A. Riera, *A short review on entanglement in quantum spin systems*, J. Phys. A **42**, 504002 (2009).

[447] D. Vodola, L. Lepori, E. Ercolessi, A. V. Gorshkov, and G. Pupillo, *Kitaev chains with longrange pairing*, Phys. Rev. Lett. **113**, 156402 (2014).

[448] F. Ares, J. G. Esteve, F. Falceto, and A. R. de Queiroz, *Entanglement in fermionic chains with finite-range coupling and broken symmetries*, Phys. Rev. A **92**, 042334 (2015).

[449] D. Vodola, L. Lepori, E. Ercolessi, A. V. Gorshkov, and G. Pupillo, *Long-range Ising and Kitaev models: phases, correlations and edge modes*, New J. Phys. **18**, 015001 (2016).

[450] F. Ares, J. G. Esteve, F. Falceto, and A. R. de Queiroz, *Entanglement entropy in the long-range Kitaev chain*, Phys. Rev. A **97**, 062301 (2018).

[451] F. Ares, J. G. Esteve, F. Falceto, and Z. Zimborás, *Sublogarithmic behaviour of the entanglement entropy in fermionic chains*, J. Stat. Mech. 093105 (2019).

[452] N. Defenu, T. Donner, T. Macri, G. Pagano, S. Ruffo, and A. Trombettoni, *Long-range interacting quantum systems*, arXiv:2109.01063 [cond-mat.quant-gas].

[453] M. Saffman, T. G. Walker, and K. Molmer, *Quantum information with Rydberg atoms*, Rev. Mod. Phys. **82**, 2313 (2010).

[454] C. Monroe, W. C. Campbell, L.-M. Duan, Z.-X. Gong, A. V. Gorshkov, P. W. Hess, R. Islam, K. Kim, N. M. Linke, G. Pagano, P. Richerme, C. Senko, and N. Y. Yao, *Programmable quantum simulations of spin systems with trapped ions*, Rev. Mod. Phys. **93**, 025001 (2021).

[455] F. Mivehvar, F. Piazza, T. Donner, H. Ritsch, *Cavity QED with Quantum Gases: New Paradigms in Many-Body Physics*, Advances in Physics **70**, 1 (2021).

[456] A. Elben, R. Kueng, H.-Y. Huang, R. van Bijnen, C. Kokail, M. Dalmonte, P. Calabrese, B. Kraus, J. Preskill, P. Zoller, and B. Vermersch, *Mixed-state entanglement from local randomized measurements*, Phys. Rev. Lett. **125**, 200501 (2020).

[457] A. J. Heeger, S. Kivelson, J. R. Schrieffer, and W. P. Su, *Solitons in conducting polymers*, Rev. Mod. Phys. **60**, 781 (1988).

[458] W. P. Su, J. R. Schrieffer, and A. J. Heeger, *Solitons in Polyacetylene*, Phys. Rev. Lett. **42** 1698 (1979).

[459] S. Ryu and Y. Hatsugai, *Topological Origin of Zero-Energy Edge States in Particle-Hole Symmetric Systems*, Phys. Rev. Lett. **89**, 077002 (2002).

[460] X.-C. Wen, *Symmetry protected topological phases in non-interacting fermion systems*, Phys. Rev. B **85**, 085103 (2012).

[461] J. K. Asbóth, L. Oroszlány, and A. Pályi, *A Short Course on Topological Insulators: Band-structure topology and edge states in one and two dimensions*, Lect. Notes Phys. 919 (2016).

[462] S. Ryu and Y. Hatsugai, *Entanglement entropy and the Berry phase in the solid state*, Phys. Rev. B **73** 245115 (2006).

[463] J. Sirker, M. Maiti, N.P. Konstantinidis, and N. Sedlmayr, *Boundary Fidelity and Entanglement in the symmetry protected topological phase of the SSH model* J. Stat. Mech. P10032 (2014).

[464] V. Eisler, G. Di Giulio, E. Tonni, and I. Peschel, *Entanglement Hamiltonians for non-critical quantum chains,* J. Stat. Mech. 103102 (2020).

[465] T. Micallo, V. Vitale, M. Dalmonte, and P. Fromholz, *Topological entanglement properties of disconnected partitions in the Su-Schrieffer-Heeger model*, SciPost Phys. Core **3**, 012 (2020).

[466] S.-L. Zhang, Q. Zhou, *Two-leg Su-Schrieffer-Heeger chain with glide reflection symmetry*, Phys. Rev. A **95**, 061601(R) (2017).

[467] B. Pérez-González, M. Bello, A. Gómez-León, and G. Platero, *SSH model with long-range hoppings: topology, driving and disorder*, arXiv:1802.03973 [cond-mat.mes-hall].

[468] B. Pérez-González, M. Bello, A. Gómez-León, and G. Platero, *Interplay between long-range hopping and disorder in topological systems*, Phys. Rev. B **99**, 035146 (2019).

[469] N. Ahmadi, J. Abouie, and D. Baeriswyl, *Topological and non-topological features of generalized Su-Schrieffer-Heeger models*, Phys. Rev. B **101**, 195117 (2020).

[470] H.-C. Hsu and T.-W. Chen, *Topological Anderson insulating phases in the long-range Su-Schrieffer-Heeger model*, Phys. Rev. B **102**, 205425 (2020).

[471] E. L. Basor and C. A. Tracy, *The Fisher-Hartwig conjecture and generalizations*, Physica A **177** 167 (1991).

[472] E. L. Basor and K. E. Morrison *The Fisher-Hartwig conjecture and Toeplitz eigenvalues*, Linear Algebr. Appl. **202**, 129 (1994).

[473] F. W. J. Olver, A. B. Olde Daalhuis, D. W. Lozier, B. I. Schneider, R. F. Boisvert, C. W. Clark, B. R. Miller, and B. V. Saunders (ed), *NIST Digital Library of Mathematical Functions*, (Gaithersburg: National Institute of Standards and Technology) (http://dlmf.nist.gov/)

[474] M. E. Fisher and R. E. Hartwig, *Toeplitz determinants, some applications, theorems and conjectures*, Adv. Chem. Phys. **15**, 333 (1968).

[475] E. L. Basor, *A localization theorem for Toeplitz determinants*, Indiana Math. J. **28**, 975 (1979).

[476] H. Widom, *Asymptotic behavior of block Toeplitz matrices and determinants*, Adv. in Math. **13**, 284 (1974).

[477] F. Ares, J. G. Esteve, and F. Falceto, *Entanglement of several blocks in fermionic chains,* Phys. Rev. A **90**, 062321 (2014).

[478] H. Shapourian and S. Ryu, *Entanglement negativity of fermions: monotonicity, separability criterion, and classification of few-mode states*, Phys. Rev. A **99**, 022310 (2019).

[479] H. Shapourian and S. Ryu, *Finite-temperature entanglement negativity of free fermions*, J. Stat. Mech. 043106 (2019).

[480] S. Pappalardi, P. Calabrese, and G. Parisi, *Entanglement entropy of the long-range Dyson hierarchical model*, J. Stat. Mech. (2019) 073102.

[481] C. Monthus, *Properties of the simplest inhomogeneous and homogeneous Tree-Tensor-States for Long-Ranged Quantum Spin Chains with or without disorder*, Physica A **576**, 126040 (2021).

[482] L.D'Alessio, Y. Kafri, A. Polkovnikov, and M. Rigol, *From quantum chaos and eigenstate thermalization to statistical mechanics and thermodynamics, Adv. Phys.* **65** *239, (2016).*

[483] L. Vidmar and M. Rigol, *Entanglement entropy of eigenstates of quantum chaotic hamiltonians,* Phys. Rev. Lett., **119** 220603, (2017).

[484] Y. O Nakagawa, M. Watanabe, H. Fujita, and S. Sugiura, *Universality in volume-law entanglement of scrambled pure quantum states,* Nature Comm., **9** 1, (2018).

[485] H. Fujita, Y. O Nakagawa, S. Sugiura, and M. Watanabe, *Page curves for general interacting systems,* JHEP, **12** (2018) 112.

[486] T.-C. Lu and T. Grover, *Renyi entropy of chaotic eigenstates,* Phys. Rev. E, **99** 032111, (2019).

[487] E. Bianchi, L. Hackl, M. Kieburg, M. Rigol, and L. Vidmar, *Volume-law entanglement entropy of typical pure quantum states,* arXiv:2112.06959 (2021).

[488] F. GSL Brandao, A. W Harrow, and M. Horodecki, *Local random quantum circuits are approximate polynomial-designs,* Comm. Math. Phys., 346 **397**, 2016.

[489] E. Onorati, O. Buerschaper, M. Kliesch, W. Brown, A. H. Werner, and J. Eisert, *Mixing properties of stochastic quantum hamiltonians,* Comm. Math. Phys., **355** 905, (2017).

[490] S. Lloyd and H. Pagels, *Complexity as thermodynamic depth,* Ann. Phys., **188** 186, (1988).

[491] E. Lubkin and T. Lubkin, *Average quantal behavior and thermodynamic isolation,* Int. J. Theor. Phys., **32** 933, (1993).

[492] S. K. Foong and S. Kanno, *Proof of page's conjecture on the average entropy of a subsystem,* Phys. Rev. Lett., **72** 1148, (1994).

[493] J. S.-Ruiz, *Simple proof of page's conjecture on the average entropy of a subsystem,* Phys. Rev. E, **52** 5653, (1995).

[494] S. Sen, *Average entropy of a quantum subsystem,* Phys. Rev. Lett., **77** 1, (1996).

[495] K. Zyczkowski and H.-J. Sommers, *Induced measures in the space of mixed quantum states,*, J. Phys. A: Math. Gen., **34** 7111, (2001).

[496] V. Cappellini, H.-J. Sommers, and K. Zyczkowski, *Distribution of G-concurrence of random pure states,* Phys. Rev. A, **74** 062322, (2006).

[497] O. Giraud, *Distribution of bipartite entanglement for random pure states,* J. Phys. A: Math. Theor., **40** 2793, (2007).

[498] P. Vivo, M. P. Pato, and G. Oshanin, *Random pure states: Quantifying bipartite entanglement beyond the linear statistics,* Phys. Rev. E, **93** 052106, (2016).

[499] L. Wei, *Proof of Vivo-Pato-Oshanin's conjecture on the fluctuation of von Neumann entropy,* Phys. Rev. E, **96** 022106, (2017).

[500] Eugenio Bianchi and Pietro Doná, *Typical entanglement entropy in the presence of a center: Page curve and its variance,* Phys. Rev. D, **100** 105010, (2019).

[501] P. Facchi, U. Marzolino, G. Parisi, S. Pascazio, and A. Scardicchio, *Phase transitions of bipartite entanglement,* Phys. Rev. Lett., **101** 050502, (2008).

[502] C. Nadal, S. N. Majumdar, and M. Vergassola, *Phase transitions in the distribution of bipartite entanglement of a random pure state,* Phys. Rev. Lett., **104** 110501, (2010).

[503] C. Nadal, S. N Majumdar, and M. Vergassola, *Statistical distribution of quantum entanglement for a random bipartite state,* J. Stat. Phys., **142** 403, (2011).

[504] A. De Pasquale, P. Facchi, G. Parisi, S. Pascazio, and A. Scardicchio, *Phase transitions and metastability in the distribution of the bipartite entanglement of a large quantum system,* Phys. Rev. A, **81** 052324, (2010).

[505] Y. Chen, D.-Z. Liu, and D.-S. Zhou, *Smallest eigenvalue distribution of the fixed-trace Laguerre beta-ensemble,* J. Phys. A: Math. Theor., **43** 315303, (2010).

[506] P. Facchi, G. Florio, G. Parisi, S. Pascazio, and K. Yuasa, *Entropy-driven phase transitions of entanglement,* Phys. Rev. A, **87** 052324, (2013).

[507] P. Facchi, G. Parisi, S. Pascazio, A. Scardicchio, and K. Yuasa, *Phase diagram of bipartite entanglement,* J. Phys. A: Math. Theor., **52** 414002, (2019).

[508] Y. Nakata and M. Murao, *Generic entanglement entropy for quantum states with symmetry,* Entropy, **22** 684, (2020).

[509] S. C. Morampudi, A. Chandran, and C. R. Laumann, *Universal entanglement of typical states in constrained systems,* Phys. Rev. Lett., **124** 050602, (2020).

[510] M. Znidaric, *Entanglement of random vectors,* J. Phys. A: Math. Theor., **40** 105, (2006).

[511] S. N. Majumdar, O. Bohigas, and A. Lakshminarayan, *Exact minimum eigenvalue distribution of an entangled random pure state,* J. Stat. Phys., **131** 33, (2008).

[512] F. D. Cunden, P. Facchi, G. Florio, and S. Pascazio, *Typical entanglement,* Eur. Phys. J. Plus, **128** 48, (2013).

[513] A. De Pasquale, P. Facchi, V. Giovannetti, G. Parisi, S. Pascazio, and A. Scardicchio, *Statistical distribution of the local purity in a large quantum system,* J. Phys. A: Math. Theor., **45** 015308, (2011).

[514] K. Hejazi and H. Shapourian, *Symmetry protected entanglement in random mixed states,* arXiv:2112.00032, (2021).

[515] H. Shapourian, S. Liu, J. Kudler-Flam, and A. Vishwanath, *Entanglement negativity spectrum of random mixed states: A diagrammatic approach,* PRX Quantum, **2** 030347, (2021).

[516] J. K. Basak, D. Basu, V. Malvimat, H.Parihar, and G. Sengupta, *Page Curve for Entanglement Negativity through Geometric Evaporation,* SciPost Phys., **12** 4, (2022).

[517] M. Afrasiar, J. Basak, C. Chandra, and G. Sengupta, *Islands for Entanglement Negativity in Communicating Black Holes,* , arXiv:2205.07903, (2022).

[518] D. Basu, H.d Parihar, V. Raj,and G. Sengupta, Gautam, *Defect extremal surfaces for entanglement negativity,* , arXiv:2205.07905, (2022).

[519] J. Basak, D. Basu, V. Malvimat, H. Parihar and G. Sengupta, *Reflected Entropy and Entanglement Negativity for Holographic Moving Mirrors,* , arXiv:2204.06015 (2022).

[520] J. Kudler-Flam, V. Narovlansky, and S. Ryu, *Negativity spectra in random tensor networks and holography,* JHEP **02** (2022) 076.

[521] L. Vidmar, L. Hackl, E. Bianchi, and Marcos Rigol, *Entanglement entropy of eigenstates of quadratic fermionic hamiltonians,* Phys. Rev. Lett., **119** 020601,(2017).

[522] L. Vidmar, L. Hackl, E. Bianchi, and M. Rigol, *Volume law and quantum criticality in the entanglement entropy of excited eigenstates of the quantum ising model,* Phys. Rev. Lett., **121** 220602, (2018).

[523] L. Vidmar and M. Rigol, *Entanglement entropy of eigenstates of quantum chaotic hamiltonians,* Phys. Rev. Lett., **119** 220603, (2017).

[524] L. Hackl, L. Vidmar, M. Rigol, and E. Bianchi, *Average eigenstate entanglement entropy of the xy chain in a transverse field and its universality for translationally invariant quadratic fermionic models,* Phys. Rev. B, **99** 075123, (2019).

[525] P. Łydżba, M. Rigol, and L. Vidmar, *Eigenstate entanglement entropy in random quadratic hamiltonians,* Phys. Rev. Lett., **125** 180604, (2020).

[526] P. Łydżba, M. Rigol, and L. Vidmar, *Entanglement in many-body eigenstates of quantum-chaotic quadratic hamiltonians,* Phys. Rev. B, **103** 104206, (2021).

[527] E.Bianchi, L. Hackl, and M. Kieburg, *Page curve for fermionic gaussian states,* Phys. Rev. B, **103** 241118, (2021).

[528] Chunxiao Liu, Xiao Chen, and Leon Balents. Quantum entanglement of the sachdev-ye-kitaev models. *Phys. Rev. B*, 97:245126, Jun 2018.

[529] P. Zhang, C. Liu, and X. Chen, *Subsystem Rényi entropy of thermal ensembles for syk-like models,* SciPost Phys., **8** 94, (2020).

[530] D. Bernard and L. Piroli, *Entanglement distribution in the quantum symmetric simple exclusion process,* Phys. Rev. E, **104** 014146, (2021).

[531] A. Altland, D. A. Huse, and T. Micklitz, *Maximum entropy quantum state distributions,* arXiv:2203.12580 (2022).

[532] T. Rakovszky, F. Pollmann, and C. W. von Keyserlingk, *Diffusive hydrodynamics of out-of-time-ordered correlators with charge conservation,* Phys. Rev. X, **8** 031058, (2018).

[533] V. Khemani, A. Vishwanath, and D. A. Huse, *Operator spreading and the emergence of dissipative hydrodynamics under unitary evolution with conservation laws,* Phys. Rev. X, **8** 031057, (2018).

[534] L. Piroli, C. Sünderhauf, and X.-L. Qi, *A random unitary circuit model for black hole evaporation,* JHEP, **04** (2020) 063.

[535] L. C. Malacarne, R. S. Mendes, and E. K. Lenzi, *Average entropy of a subsystem from its average tsallis entropy,* Phys. Rev. E, **65** 046131, (2002).

[536] M. Fagotti, P. Calabrese, and J. E. Moore, *Entanglement spectrum of random-singlet quantum critical points* Phys. Rev. B, **83** 045110, (2011).

[537] S. Bravyi, *Lagrangian representation for fermionic linear optics,* Quantum Inf. and Comp., **5** 216, (2005).

[538] H. Touchette, *The large deviation approach to statistical mechanics,* Phys. Rep., **478** 1-69, (2009).

[539] P. J Forrester, *Log-gases and random matrices,* Princeton University Press, 2010.

[540] S. N. Majumdar and G. Schehr, *Top eigenvalue of a random matrix: large deviations and third order phase transition,* J. Stat. Mech., P01012, (2014).

[541] P. Vivo, S. N. Majumdar, and O. Bohigas, *Distributions of conductance and shot noise and associated phase transitions,* Phys. Rev. Lett., **101** 216809, (2008).

[542] P. Vivo, S. N. Majumdar, and O. Bohigas, *Probability distributions of linear statistics in chaotic cavities and associated phase transitions,* Phys. Rev. B, **81** 104202, (2010).

[543] K. Damle, S. N. Majumdar, V. Tripathi, and P. Vivo, *Phase transitions in the distribution of the andreev conductance of superconductor-metal junctions with multiple transverse modes,* Phys. Rev. Lett., **107** 177206, (2011).

[544] P. J Forrester, *Large deviation eigenvalue density for the soft edge Laguerre and Jacobi β-ensembles,* J. Phys. A: Math. Theor., **45** 145201, (2012).

[545] H. M. Ramli, E. Katzav, and I. P. Castillo, *Spectral properties of the jacobi ensembles via the coulomb gas approach,* J. Phys. A: Math. Theor., **45** 465005, (2012).

[546] M. Bauer, D. Bernard, and T. Jin, *Equilibrium fluctuations in maximally noisy extended quantum systems,* SciPost Phys., **6** 45, (2019).

[547] M. Bauer, D. Bernard, and T. Jin, *Stochastic dissipative quantum spin chains (i) : Quantum fluctuating discrete hydrodynamics,* SciPost Phys., **3** 033, (2017).

[548] D.Bernard, Fabian H. L. Essler, L. Hruza, and M. Medenjak, *Dynamics of fluctuations in quantum simple exclusion processes,* SciPost Phys., **12** 42, (2022).

[549] Filiberto Ares, S. M. and Pasquale Calabrese, *Entanglement asymmetry as a probe of symmetry breaking*, arXiv:2208.xxxxx.

[550] E. Lieb, T. Schultz, and D. Mattis, *Two soluble models of an antiferromagnetic chain*, Ann. Phys. **16**, 407 (1961).

[551] R. Balian and E. Brezin, *Nonunitary Bogoliubov transformations and extension of Wick's theorem*, Il Nuovo Cimento B **64**, 37 (1969).

[552] M. Fagotti, M. Collura, F. H. L. Essler, P. Calabrese, *Relaxation after quantum quenches in the spin-1/2 Heisenberg XXZ chain*, Phys. Rev. B **89**, 125101 (2014).

[553] L. Piroli, E. Vernier, and P. Calabrese, *Exact steady states for quantum quenches in integrable Heisenberg spin chains*, Phys. Rev. B **94**, 054313 (2016).

[554] J.-M. Stéphan, *Emptiness formation probability, Toeplitz determinants, and conformal field theory*, J. Stat. Mech. (2014) P05010.

[555] A. Kumar and J. Bechhoefer, *Exponentially faster cooling in a colloidal system*, Nature **584**, 64 (2020).

[556] B. Bertini, K. Klobas, V. Alba, G. Lagnese, and P. Calabrese *Growth of Rényi Entropies in Interacting Integrable Models and the Breakdown of the Quasiparticle Picture*, arXiv:2203.17264.

[557] B. Vermersch, A. Elben, L. M. Sieberer, N. Y. Yao, and P. Zoller, *Probing scrambling using statistical correlations between randomized measurements,* Phys. Rev. X **9**, 021061 (2019).

[558] A. Elben, S. T. Flammia, H.-Y. Huang, R. Kueng, J. Preskill, B. Vermersch, and P. Zoller, *The randomized measurement toolbox,* arXiv:2203.11374.

[559] S. Murciano, V. Vitale, M. Dalmonte and P. Calabrese, *The Negativity Hamiltonian: An operator characterization of mixed-state entanglement,* Phys. Rev. Lett. **128**, 140502 (2022).

[560] C. Kokail, B. Sundar, T. V. Zache, A. Elben, B. Vermersch, M. Dalmonte, R. van Bijnen, and P. Zoller, *Quantum variational learning of the entanglement hamiltonian,* Phys. Rev. Lett., **127** 170501, (2021).

[561] C. Kokail, R. van Bijnen, A. Elben, B. Vermersch, and P. Zoller, *Entanglement hamiltonian tomography in quantum simulation,* Nature Physics, **17** 8, (2021).

[562] W. Zhu, Z. Huang, and Y.-C. He, *Reconstructing entanglement hamiltonian via entanglement eigenstates,* Phys. Rev. B, **99** 235109, (2019).

[563] P. Ruggiero, V. Alba, and P. Calabrese, *Negativity spectrum of one-dimensional conformal field theories,* Phys. Rev. B, **94** 195121, (2016).

[564] A. W. Sandvik and J. Kurkijärvi, *Quantum monte carlo simulation method for spin systems,* Phys. Rev. B, **43** 5950, (1991).

[565] J. Eisert, V. Eisler, and Z. Zimborás, *Entanglement negativity bounds for fermionic Gaussian states,* Phys. Rev. B, **97** 165123, (2018).

[566] H. J. Borchers and J. Yngvason, *Modular groups of quantum fields in thermal states,* J. Math. Phys., **40** 2, (1999).

[567] G. Wong, I.Klich, L. A. Pando Zayas, and D. Vaman, *Entanglement temperature and entanglement entropy of excited states,* JHEP, **12** (2013) 20.

[568] R. E. Arias, H. Casini, M. Huerta, and D. Pontello, *Entropy and modular hamiltonian for a free chiral scalar in two intervals,* Phys. Rev. D, **98** 125008, (2018).

[569] Mihail Mintchev and Erik Tonni, *Modular hamiltonians for the massless dirac field in the presence of a boundary,* JHEP, 2021 **03** (2021) 204.

[570] R. Longo, P. Martinetti, and K.-H. Rehren, *Geometric modular action for disjoint intervals and boundary conformal field theory,* Rev. Math. Phys., **22** 03, (2010).

[571] M. Mintchev and E. Tonni, *Modular hamiltonians for the massless dirac field in the presence of a defect,* JHEP, **03** (2021) 205.

[572] S. Hollands, *On the Modular Operator of Mutli-component Regions in Chiral CFT,* Comm. Math. Phys. **384** 785 (2021).

[573] I. Klich, D. Vaman, and G. Wong, *Entanglement hamiltonians for chiral fermions with zero modes,* Phys. Rev. Lett., **119** 12, (2017).

[574] P.Fries and I. A. Reyes, *Entanglement spectrum of chiral fermions on the torus,* Phys. Rev. Lett., **123** 21, (2019).

[575] M. Dalmonte, B.Vermersch, and P. Zoller, *Quantum simulation and spectroscopy of entanglement hamiltonians,* Nat. Phys., **14** 8, (2018).

[576] G. Giudici, T. Mendes-Santos, P. Calabrese, and M. Dalmonte, *Entanglement hamiltonians of lattice models via the bisognano-wichmann theorem,* Phys. Rev. B, **98** 134403, (2018).

[577] J. Zhang, P. Calabrese, M. Dalmonte, and M. A. Rajabpour, *Lattice Bisognano-Wichmann modular Hamiltonian in critical quantum spin chains,* SciPost Phys. Core, **2** 007, (2020).

[578] V. Eisler and I. Peschel, *Analytical results for the entanglement hamiltonian of a free-fermion chain,* J. Phys. A, **50** 284003, (2017).

[579] V. Eisler and I. Peschel, *Properties of the entanglement hamiltonian for finite free-fermion chains,* J. Stat. Mech., 104001 (2018).

[580] G. Di Giulio and E. Tonni, *On entanglement hamiltonians of an interval in massless harmonic chains,* J. Stat. Mech., 033102 (2020).

[581] J. Kudler-Flam, H. Shapourian, and S. Ryu, *The negativity contour: a quasi-local measure of entanglement for mixed states,* SciPost Phys., **8** 063, (2020).

[582] G. Di Giulio, R. Arias, and E. Tonni, *Entanglement hamiltonians in 1d free lattice models after a global quantum quench,* J. Stat. Mech., 123103 (2019).

[583] V. Eisler, E. Tonni, and I. Peschel, *On the continuum limit of the entanglement hamiltonian,* J. Stat. Mech., 073101 (2019).

[584] F.Parisen Toldin and F. F. Assaad, *Entanglement hamiltonian of interacting fermionic models,* Phys. Rev. Lett., **121** 20, (2018).

[585] F. Rottoli, S. Murciano, E. Tonni and P. Calabrese *Entanglement and negativity Hamiltonians for the boundary massless Dirac field,* in preparation.

[586] S. Murciano, V. Aba and P. Calabrese *Quench dynamics of Rényi negativities and the quasiparticle picture,* arXiv:2110.14589 (2021).

[587] J. Gray, L. Banchi, A. Bayat, and S. Bose, *Machine Learning Assisted Many-Body Entanglement Measurement*, Phys. Rev. Lett. **121**, 150503 (2018).

[588] E. Cornfeld, E. Sela, and M. Goldstein, *Measuring fermionic entanglement: Entropy, negativity, and spin structure*, Phys. Rev. A **99**, 062309 (2019).

[589] V. Alba and P. Calabrese, *Quantum information dynamics in multipartite integrable systems,* EPL **126**, 60001 (2019).

[590] A. Coser, E. Tonni, and P. Calabrese, *Entanglement negativity after a global quantum quench,* J. Stat. Mech. P12017 (2014).

[591] X. Wen, P.-Y. Chang, and S. Ryu, *Entanglement negativity after a local quantum quench in conformal field theories*, Phys. Rev. B **92**, 075109 (2015).

[592] C.-M. Chung, V. Alba, L. Bonnes, P. Chen, and A. M. Lauchli, *Entanglement negativity via replica trick: a Quantum Monte Carlo approach*, Phys. Rev. B **90**, 064401 (2014).

[593] K.-H. Wu, T.-C. Lu, C.-M. Chung, Y.-J. Kao, and T. Grover, *Entanglement Renyi negativity across a finite temperature transition: a Monte Carlo study*, Phys. Rev. Lett. **125**, 140603 (2020).

[594] T.-C. Lu and T. Grover, *Entanglement transitions as a probe of quasiparticles and quantum thermalization*, Phys. Rev. B **102**, 235110 (2020).

[595] E. Wybo, M. Knap, and F. Pollmann, *Entanglement dynamics of a many-body localized system coupled to a bath*, Phys. Rev. B **102**, 064304 (2020).

[596] B. Bertini, E. Tartaglia, and P. Calabrese, *Quantum Quench in the Infinitely Repulsive Hubbard Model: The Stationary State*, J. Stat. Mech. (2017) 103107.

[597] B. Bertini, E. Tartaglia, and P. Calabrese, *Entanglement and diagonal entropies after a quench with no pair structure*, J. Stat. Mech. (2018) 063104.

[598] A. Bastianello and P. Calabrese, *Spreading of entanglement and correlations after a quench with intertwined quasiparticles*, SciPost Phys. **5**, 033 (2018).

[599] A. Bastianello and M. Collura, *Entanglement spreading and quasiparticle picture beyond the pair structure*, SciPost Phys. **8**, 045 (2020).

[600] L. Piroli, B. Pozsgay, and E. Vernier, *What is an integrable quench?*, Nucl. Phys. B **925**, 362 (2017).

[601] P. Calabrese, F. H. L. Essler, and G. Mussardo, *Introduction to "Quantum Integrability in Out of Equilibrium Systems"*, J. Stat. Mech. 064001 (2016).

[602] L. Vidmar and M. Rigol, *Generalized Gibbs ensemble in integrable lattice models*, J. Stat. Mech. 064007 (2016).

[603] F. H. L. Essler and M. Fagotti, *Generalized Gibbs ensemble in integrable lattice models*, J. Stat. Mech. 064002 (2016).

[604] L. Bonnes, F.H.L. Essler, and A. M. Läuchli, *Light-cone dynamics after quantum quenches in spin chains*, Phys. Rev. Lett. **113**, 187203 (2014).

[605] M. Mestyan, B. Bertini, L. Piroli, and P. Calabrese, *Exact solution for the quench dynamics of a nested integrable system*, J. Stat. Mech. (2017) 083103

[606] L. Piroli, E. Vernier, P. Calabrese, and B. Pozsgay, *Integrable quenches in nested spin chains I: the exact steady states*, J. Stat. Mech. (2019) 063103.

[607] L. Piroli, E. Vernier, P. Calabrese, and M. Rigol, *Correlations and diagonal entropy after quantum quenches in XXZ chains*, Phys. Rev. B **95**, 054308 (2017)

[608] R. Modak, L. Piroli, and P. Calabrese, *Correlations and entanglement spreading in nested spin chains*, J. Stat. Mech. (2019) 093106.

[609] K. Klobas, B. Bertini, and L. Piroli, *Exact thermalization dynamics in the "Rule 54" Quantum Cellular Automaton*, Phys. Rev. Lett. **126**, 160602 (2021).

[610] K. Klobas and B. Bertini, *Entanglement dynamics in Rule 54: Exact results and quasiparticle picture*, arXiv:2104.04513.

[611] V. Alba and P. Calabrese, *Quantum information scrambling after a quantum quench*, Phys. Rev. B **100**, 115150 (2019).

[612] R. Modak, V. Alba, and P. Calabrese, *Entanglement revivals as a probe of scrambling in finite quantum systems*, J. Stat. Mech. 083110 (2020).

[613] O. A. Castro-Alvaredo, B. Doyon, and T. Yoshimura, *Emergent Hydrodynamics in Integrable Quantum Systems Out of Equilibrium*, Phys. Rev. X **6**, 041065 (2016).

[614] B. Bertini, M. Collura, J. De Nardis, and M. Fagotti, *Transport in Out-of-Equilibrium XXZ Chains: Exact Profiles of Charges and Currents*, Phys. Rev. Lett. **117**, 207201 (2016)

[615] V. Alba, *Towards a Generalized Hydrodynamics description of Rényi entropies in integrable systems*, Phys. Rev. B **99**, 045150 (2019).

[616] V. Alba, *Entanglement and quantum transport in integrable systems*, Phys. Rev. B **97**, 245135 (2018).

[617] V. Alba, B. Bertini, and M. Fagotti, *Entanglement evolution and generalised hydrodynamics: interacting integrable systems*, SciPost Phys. **7**, 005 (2019).

[618] B. Bertini, M. Fagotti, L. Piroli, and P. Calabrese, *Entanglement evolution and generalised hydrodynamics: noninteracting systems*, J. Phys. A **51**, 39LT01 (2018).

[619] M. Mestyán and V. Alba, *Molecular dynamics simulation of entanglement spreading in generalized hydrodynamics*, SciPost Phys. **8**, 055 (2020).

[620] V. Alba, B. Bertini, M. Fagotti, L. Piroli, and P. Ruggiero, *Generalized-Hydrodynamic approach to Inhomogeneous Quenches: Correlations, Entanglement and Quantum Effects*, J. Stat. Mech. (2021) 114004.

[621] V. Alba, *Unbounded entanglement production via a dissipative impurity*, SciPost Phys. **12**, 011 (2022).

[622] V. Alba and F. Carollo, *Spreading of correlations in Markovian open quantum systems*, Phys. Rev. B **103**, 020302 (2021).

[623] F. Carollo and V. Alba, *Emergent dissipative quasi-particle picture in noninteracting Markovian open quantum systems*, arXiv:2106.11997.

[624] V. Alba and F. Carollo, *Hydrodynamics of quantum entropies in Ising chains with linear dissipation*, J. Phys. A: Math. Theor. **55** 074002 (2022).

[625] B. Bertini and P. Calabrese, *Prethermalisation and Thermalisation in the Entanglement Dynamics*, Phys. Rev. B **102**, 094303 (2020)

[626] P. Calabrese, *Entanglement and thermodynamics in non-equilibrium isolated quantum systems*, Physica A **504**, 31 (2018).

[627] F. Igloi and I. Peschel, *On reduced density matrices for disjoint subsystems*, EPL **89**, 40001 (2010).

[628] P. Calabrese, F. H. L. Essler, and M. Fagotti, *Quantum Quench in the Transverse-Field Ising Chain*, Phys. Rev. Lett. **106**, 227203 (2011).

[629] P. Calabrese, F. H. L. Essler, and M. Fagotti, *Quantum Quench in the Transverse Field Ising chain I: Time evolution of order parameter correlators*, J. Stat. Mech. P07016 (2012).

[630] K. Shiozaki, H. Shapourian, K. Gomi, and S. Ryu, *Many-body topological invariants for fermionic short-range entangled topological phases protected by antiunitary symmetries*, Phys. Rev. B **98**, 035151 (2018).

[631] J. Dubail, *Entanglement scaling of operators: a conformal field theory approach, with a glimpse of simulability of long-time dynamics in 1+1d*, J. Phys. A **50**, 234001 (2017).

[632] E. Leviatan, F. Pollmann, J. H. Bardarson, D. A. Huse, and E. Altman, *Quantum thermalization dynamics with Matrix-Product States*, arXiv:1702.08894.

[633] C. Jonay, D. A. Huse, and A. Nahum, *Coarse-grained dynamics of operator and state entanglement*, arXiv:1803.00089.

[634] L. Capizzi, S. Murciano and P. Calabrese, *Rényi entropy and negativity for massless Dirac fermions at conformal interfaces and junctions,* JHEP **08** (2022) 171.

[635] J. L. Cardy, *Conformal Invariance and Surface Critical Behaviour*, Nucl. Phys. B **240**, 514 (1984).

[636] J. Cardy, *Boundary conditions, fusion rules and the Verlinde formula*, Nucl. Phys. B **324**, 581 (1989).

[637] J. Cardy, *Boundary Conformal Field Theory*, arXiv:hep-th/0411189.

[638] H. Saleur, *Lectures on Non Perturbative Field Theory and Quantum Impurity Problems*, arXiv:cond-mat/9812110.

[639] I. Affleck, *Conformal Field Theory Approach to the Kondo Effect*, Acta Phys. Polon. B **26**, 1869 (1995).

[640] J. Polchinski, *TASI Lectures on D-Branes*, arXiv:hep-th/9611050.

[641] C. Bachas, J. de Boer, R. Dijkgraaf, and H. Ooguri, *Permeable conformal walls and holography*, JHEP 06 (2002) 027.

[642] C. L. Kane and M. P. A. Fisher, *Transmission through barriers and resonant tunneling in an interacting one-dimensional electron gas*, Phys. Rev. B **46**, 15233 (1992).

[643] J. Zhao, I. Peschel, X. Wang, *Critical entanglement of XXZ Heisenberg chains with defects*, Phys. Rev. B 73, 024417 (2006).

[644] M. Collura and P. Calabrese, *Entanglement evolution across defects in critical anisotropic Heisenberg chains*, J. Phys. A **46**, 175001 (2013).

[645] K. Sakai and Y. Satoh, *Entanglement through conformal interfaces*, JHEP **12** (2008) 001.

[646] E. Brehm and I. Brunner, *Entanglement entropy through conformal interfaces in the 2D Ising model*, JHEP **09** (2015) 80.

[647] C. Bachas, I. Brunner, and D. Roggenkamp, *Fusion of Critical Defect Lines in the 2D Ising Model*, J. Stat. Mech. (2013) P08008.

[648] I. Peschel, *Entanglement entropy with interface defects*, J. Phys. A: Math. Gen. **38**, 4327 (2005).

[649] V. Eisler and I. Peschel *Solution of the fermionic entanglement problem with interface defects*, Ann. Phys. (Berlin) **522**, 679 (2010).

[650] P. Calabrese, M. Mintchev, and E. Vicari, *Entanglement Entropy of Quantum Wire Junctions*, J. Phys. A **45**, 105206 (2012).

[651] I. Peschel and V. Eisler *Exact results for the entanglement across defects in critical chains*, J. Phys. A **45**, 155301 (2012).

[652] V. Eisler and I. Peschel, *On entanglement evolution across defects in critical chains*, EPL **99**, 20001 (2012).

[653] J. Frohlich, J. Fuchs, I. Runkel, and C. Schweigert, *Kramers-Wannier Duality from Conformal Defects*, Phys. Rev. Lett. **93**, 070601 (2004).

[654] J. Frohlich, J. Fuchs, I. Runkel, and C. Schweigert, *Duality and defects in rational conformal field theory*, Nucl. Phys. B **763**, 354 (2007).

[655] D. Aasen, R. S. K. Mong, and P. Fendley, *Topological Defects on the Lattice I: The Ising model*, J. Phys. A **49**, 354001 (2016).

[656] E. Brehm, I. Brunner, D. Jaud and C. Schmidt-Colinet, *Entanglement and topological interfaces*, Fortsch. Phys. **64**, 516 (2016).

[657] D. Jaud, *Topological Defects in Conformal Field Theories, Entanglement Entropy and Indices*, PhD Munich U. (2017).

[658] A. Roy and H. Saleur, *Entanglement Entropy in the Ising Model with Topological Defects*, Phys. Rev. Lett. **128**, 090603 (2022).

[659] D. Rogerson, F. Pollmann, and A. Roy, *Entanglement entropy and negativity in the Ising model with defects*, arXiv:2204.03601.

[660] C. Nayak, M. P. A. Fisher, A. W. W. Ludwig, and H. H. Lin, *Resonant multilead point-contact tunneling*, Phys. Rev. B 59, 15694 (1999).

[661] C. Chamon, M. Oshikawa, and I. Affleck, *Junctions of Three Quantum Wires and the Dissipative Hofstadter Model*, Phys. Rev. Lett. **91**, 206403 (2003).

[662] M. Oshikawa, C. Chamon, and I. Affleck, *Junctions of three quantum wires*, J. Stat. Mech. P02008 (2006).

[663] B. Bellazzini and M. Mintchev, *Quantum Fields on Star Graphs*, J. Phys. A **39**, 11101 (2006).

[664] B. Bellazzini, M. Mintchev and P. Sorba, *Bosonization and Scale Invariance on Quantum Wires*, J. Phys. A **40**, 2485 (2007).

[665] C.-Y. Hou and C. Chamon, *Junctions of three quantum wires for spin-1/2 electrons*, Phys. Rev. B **77**, 155422 (2008).

[666] B. Bellazzini, P. Calabrese, and M. Mintchev, *Junctions of anyonic Luttinger wires*, Phys. Rev. B **79**, 085122 (2009).

[667] B. Bellazzini, M. Mintchev and P. Sorba, *Quantum wire junctions breaking time-reversal invariance*, Phys. Rev. B **80**, 245441 (2009).

[668] V. Caudrelier, M. Mintchev, and E. Ragoucy, *Quantum Wire Network with Magnetic Flux*, Phys. Lett. A **377**, 1788 (2013).

[669] P. Calabrese, M. Mintchev, and E. Vicari, *The entanglement entropy of one-dimensional gases*, Phys. Rev. Lett. **107**, 020601 (2011).

[670] P. Calabrese, M. Mintchev, and E. Vicari, *Exact relations between particle fluctuations and entanglement in Fermi gases*, EPL **98**, 20003 (2012).

[671] M. Gutperle and J. D. Miller *Entanglement entropy at CFT junctions*, Phys. Rev. D **95**, 106008 (2017).

[672] M. Gruber and V. Eisler, *Time evolution of entanglement negativity across a defect*, J. Phys. A **53**, 205301 (2020).

[673] K. Ohmori and Y. Tachikawa, *Physics at the entangling surface*, J. Stat. Mech. (2015) P04010.

[674] C. Bachas, I. Brunner, and D. Roggenkamp, *A worldsheet extension of $O(d, d : Z)$*, JHEP **10** (2012) 039.

[675] G. Del Vecchio Del Vecchio, A. De Luca, A. Bastianello, *Transport through interacting defects and lack of thermalisation*, SciPost Phys. **12**, 060 (2022).

[676] P. Calabrese, M. Mintchev, and E. Vicari, *The entanglement entropy of 1D systems in continuous and homogenous space*, J. Stat. Mech. P09028 (2011).

[677] E. Vicari, *Quantum dynamics and entanglement of a 1D Fermi gas released from a trap*, Phys. Rev. A **85**, 062324 (2012).

[678] P. Ruggiero, P. Calabrese, T. Giamarchi, L. Foini, *Electrostatic solution of massless quenches in Luttinger liquids,* arXiv:2203.06740.

[679] R. Blatt and C. F. Roos, *Quantum simulations with trapped ions*, Nature Physics **8**, 277 (2012).

[680] C. Monroe, W. C. Campbell, L. M. Duan, Z. X. Gong, A. V. Gorshkov, P. Hess, R. Islam, K. Kim, N. M. Linke, G. Pagano, et al., *Programmable quantum simulations of spin systems with trapped ions,* Rev. Mod. Phys. **93**, 025001 (2021).

[681] A. Browaeys and T. Lahaye, *Many-body physics with in- dividually controlled rydberg atoms*, Nature Physics **16**, 132 (2020).

[682] L. K. Joshi, A. Elben, A. Vikram, B. Vermersch, V. Galitski, and P. Zoller, *Probing many-body quantum chaos with quantum simulators,* Phys. Rev. X **12**, 011018 (2022).

[683] Vovrosh and J. Knolle, *Confinement and entanglement dynamics on a digital quantum computer*, Sci. Rep. **11**, 1 (2021).

[684] P. Sierant, G. Chiriacó, F. M. Surace, S. Sharma, X. Turkeshi, M. Dalmonte, R. Fazio, and G. Pagano, *Dissipative floquet dynamics: from steady state to measurement induced criticality in trapped-ion chains,* Quantum **6**, 638 (2022).

[685] J. Li, R. Fan, H. Wang, B. Ye, B. Zeng, H. Zhai, X. Peng, and J. Du, *Measuring out-of-time-order correlators on a nuclear magnetic resonance quantum simulator,* Phys. Rev. X **7**, 031011 (2017).

[686] M. K. Joshi, A. Elben, B. Vermersch, T. Brydges, C. Maier, P. Zoller, R. Blatt, and C. F. Roos, *Quantum information scrambling in a trapped-ion quantum simulator with tunable range interactions,* Phys. Rev. Lett. **124** 240505 (2020).

[687] P. Zanardi, C. Zalka and L. Faoro, *Entangling power of quantum evolutions*, Phys. Rev. A. **62** 030301.

[688] P. Zanardi, *Entanglement of quantum evolutions*, Phys. Rev. A. **63** 040304.

[689] I. Pižorn, T. Prosen, *Operator space entanglement entropy in a transverse Ising chain*, Phys. Rev. A **76** 032316 (2007).

[690] I. Pižorn, T. Prosen, *Operator space entanglement entropy in XY spin chains*, Phys. Rev. B **79** 184416 (2009).

[691] T. Zhou and D. J. Luitz, *Operator entanglement entropy of the time evolution operator in chaotic systems,* Phys. Rev. B **95**, 094206 (2017).

[692] K. Noh, L. Jiang, and B. Fefferman, *Efficient classical simulation of noisy random quantum circuits in one di- mension,* Quantum **4**, 318 (2020).

[693] T. Rakovszky, C. von Keyserlingk, and F. Pollmann, *Dissipation-assisted operator evolution method for capturing hydrodynamic transport,* Phys. Rev. B **105**, 075131 (2022).

[694] D. Wellnitz, G. Preisser, V. Alba, J. Dubail, and J. Schachenmayer, *The rise and fall, and slow rise again, of operator entanglement under dephasing,* arXiv:2201.05099 (2022).

[695] C. Jonay, D. A. Huse, and A. Nahum, *Coarse-grained dynamics of operator and state entanglement,* arXiv:1803.00089 (2018).

[696] H. Wang and T. Zhou, *Barrier from chaos: operator entanglement dynamics of the reduced density matrix,* JHEP **12**, 020 (2019).

[697] V. Alba, J. Dubail, and M. Medenjak, Operator entanglement in interacting integrable quantum systems: The case of the rule 54 chain, Phys. Rev. Lett. **122**, 250603 (2019).

[698] B. Bertini, P. Kos, and T. Prosen, *Operator Entanglement in Local Quantum Circuits I: Chaotic Dual-Unitary Circuits,* SciPost Phys. **8**, 67 (2020).

[699] B. Bertini, P. Kos, and T. Prosen, *Operator entanglement in local quantum circuits ii: Solitons in chains of qubits,* SciPost Physics **8**, 068 (2020).

[700] A. Lerose, M. Sonner, and D. A. Abanin, *Influence matrix approach to many-body floquet dynamics,* Phys. Rev. X 11, 021040 (2021).

[701] M. Sonner, A. Lerose, and D. A. Abanin, *Influence func- tional of many-body systems: temporal entanglement and matrix-product state representation,* Ann. Phys. **431**, 168552 (2021).

[702] G. Giudice, G. Giudici, M. Sonner, J. Thoenniss, A. Ler- ose, D. A. Abanin, and L. Piroli, *Temporal entanglement, quasiparticles, and the role of interactions,* Phys. Rev. Lett. **128**, 220401 (2022).

[703] S. Dutta and T. Faulkner, *A canonical purification for the entanglement wedge cross-section,* JHEP **03**, 178 (2021).

[704] P. Bueno and H. Casini, *Reflected entropy, symmetries and free fermions,* JHEP **05**, 103 (2020).

[705] I. Reid and B. Bertini, *Entanglement barriers in dual-unitary circuits,* Phys. Rev. B **104**, 014301 (2021).

[706] M. Rigol, V. Dunjko, and M. Olshanii, *Thermalization and its mechanism for generic isolated quantum systems,* Nature 452, 854 (2008).

[707] T. Mori, T. N. Ikeda, E. Kaminishi, and M. Ueda, *Thermalization and prethermalization in isolated quantum systems: a theoretical overview,* J. Phys. B **51**, 112001 (2018).

[708] K. Mallayya, M. Rigol, and W. De Roeck, *Prethermalization and thermalization in isolated quantum systems,* Phys. Rev. X 9, 021027 (2019).

[709] A. Polkovnikov, K. Sengupta, A. Silva, and M. Vengalattore, *Colloquium: Nonequilibrium dynamics of closed interacting quantum systems,* Rev. Mod. Phys. 83, 863 (2011).

[710] M. Cramer and J. Eisert, *A quantum central limit the- orem for non-equilibrium systems: exact local relaxation of correlated states,* New Jour. Phys. **12**, 055020 (2010).

[711] M. Rigol, V. Dunjko, V. Yurovsky, and M. Olshanii, *Relaxation in a completely integrable many-body quantum system: An ab initio study of the dynamics of the highly excited states of 1d lattice hard-core bosons,* Phys. Rev. Lett. **98**, 050405 (2007).

[712] N. Schuch, M. M. Wolf, F. Verstraete, and J. I. Cirac, *Entropy scaling and simulability by matrix product states,* Phys. Rev. Lett. 100, 030504 (2008).

[713] A. Rath, R. van Bijnen, A. Elben, P. Zoller, and B. Vermersch, *Importance sampling of randomized measurements for probing entanglement,* Phys. Rev. Lett. **127**, 200503 (2021).

[714] A. Rath, C. Branciard, A. Minguzzi, and B. Vermersch, *Quantum fisher information from randomized measurements,* Phys. Rev. Lett. **127**, 260501 (2021).

[715] O. Gühne and G. Tóth, *Entanglement detection,* Phys. Rep. **474**, 1 (2009).

[716] A. Rath, V. Vitale, S. Murciano, M. Votto, J. Dubail, C. Branciard, R. Kueng, P. Calabrese, B. Vermersch, *Entanglement barrier and its symmetry resolution: theory and experiment,* in preparation.

[717] O. Rudolph, *Further results on the cross norm criterion for separability,* Quant. Inf. Proc. **4**, 219 (2005).

[718] K. Chen and L.-A. Wu, *A matrix realignment method for recognizing entanglement,* Quant. Info. Comput. **3**, 193 (2003).

[719] Z. Liu, Y. Tang, H. Dai, P. Liu, S. Chen, and X. Ma, *Detecting entanglement in quantum many-body systems via permutation moments,* arXiv:2203.08391 (2022).

[720] B. M. Terhal, M. Horodecki, D. W. Leung and D. P. DiVincenzo, *The entanglement of purification*, J. Math. Phys. **43**, 4286 (2002).

[721] T. Takayanagi and K. Umemoto, *Entanglement of purification through holographic duality,* Nature Phys. 14, 573 (2018)

[722] P. Nguyen, T. Devakul, M. G. Halbasch, M. P. Zaletel and B. Swingle, *Entanglement of purification: from spin chains to holography*, JHEP **01** 098 (2018).

[723] A. Bhattacharyya, T. Takayanagi and K. Umemoto, *Entanglement of Purification in Free Scalar Field Theories*, JHEP **04**, 132 (2018).